ACTA TECHNICA

ACADEMIAE SCIENTIARUM HUNGARICAE

REDIGIT: M. MAJOR

TOMUS 68
FASCICULI 1—2

AKADÉMIAI KIADÓ, BUDAPEST 1970

ACTA TECHNICA

Az *Acta Technica* angol, francia, német és orosz nyelven közöl értekezéseket a műszaki tudományok köréből.

Az *Acta Technica* változó terjedelmű füzetekben jelenik meg, több füzet alkot egy kötetet.

A közlésre szánt kéziratok a következő címre küldendők:

Acta Technica
Budapest V., Münnich Ferenc u. 7.

Ugyanerre a címre küldendő minden szerkesztőségi és kiadóhivatali levelezés.

Megrendelhető a belföld számára az „Akadémiai Kiadó"-nál (Budapest V., Alkotmány utca 21. Bankszámla 05-915-111-46), a külföld számára pedig a „Kultúra" Könyv- és Hírlap Külkereskedelmi Vállalatnál (Budapest I., Fő utca 32. Bankszámla: 43-790-057-181) vagy annak külföldi képviseleteinél és bizományosainál.

Die *Acta Technica* veröffentlicht Abhandlungen aus dem Bereiche der technischen Wissenschaften in deutscher, englischer, französischer und russischer Sprache.

Die *Acta Technica* erscheint in Heften wechselnden Umfanges. Vier Hefte bilden einen Band.

Die zur Veröffentlichung bestimmten Manuskripte sind an folgende Adresse zu senden:

Acta Technica
Münnich Ferenc u. 7.
Budapest V.,
Ungarn

An die gleiche Anschrift ist auch jede für die Schriftleitung und den Verlag bestimmte Korrespondenz zu richten. Abonnementspreis pro Band: $ 16.00.

Bestellbar bei dem Buch- und Zeitungs-Außenhandels-Unternehmen »Kultura« (Budapest I., Fő utca 32. Bankkonto Nr. 43-790-057-181) oder bei seinen Auslandsvertretungen und Kommissionären.

ACTA TECHNICA

TOMUS 68

INDEX

ACTA TECHNICA

ACADEMIAE SCIENTIARUM HUNGARICAE

REDIGIT: M. MAJOR

TOMUS 68

AKADÉMIAI KIADÓ, BUDAPEST 1970

Acta Technica Academiae Scientiarum Hungaricae; Tomus 68 (1—2), pp. 3—8 (1970)

PEAK LOAD POWER STATION FED FROM LONG DISTANCE GAS PIPELINE

A. FONÓ
CORRESPONDING MEMBER OF THE HUNGARIAN ACADEMY OF SCIENCES

[Manuscript received June 13, 1969]

Peak load power station can be fed from gas stored in a long distance pipeline in which the gas is stored by increasing its average pressure by interconnecting a compressor in the last line section. The overpressure thus caused can be utilized at the end of the line for power production during offpeak periods. The thus produced energy is so much more than that needed for boosting the pressure that from the gain the necessary investments can be amortised in a short time. By this means the storing of the gas does not cost any money.

Peak power stations are needed for equalizing the fluctuations of the demand. Corresponding to the character of the load the *peak power station* has to be started daily at least once. It is essential to be able to put full load on it in a very short time after its starting. The yearly running time being short it can only support low investment costs. In the last years jet-stream driven gas turbines are used in many places for this purpose as this type fulfils well these wanted conditions.

Peak load has to be covered by stored energy or by energy produced from stored energy bearer. A gas turbine producing peak power has to be fed from stored gas, as it is not economical to build a pipeline with dimensions also suitably for peak load. Gas can be stored without extra costs for its storing by increasing the average pressure in the pipeline feeding the peak power station.

The pressure in the pipeline can be increased by interconnecting a compressor between the last compressor station and the end of the line. Thus boosting the pressure it will also be higher at the end of the line. The overpressure above that needed by the consumer can be utilized for energy production by expansion of the gas. The energy produced at the end of the line is considerably more than the energy consumption of the interconnected compressor. The gain in energy corresponds to the reduction of the flow resistance in the pipeline section in consequence of the higher average pressure and with it of the diminished flowing speed.

Increasing the pressure in the pipeline in the said manner is so economical that the recuperated energy will pay the necessary investments in a short time. Consequently storing gas in the pipeline by this means does not cost

any money. The general scheme is shown in Fig. 1, the variations of the pressure on the line on diagram Fig. 2. Taking out stored gas from the pipeline the pressure has to be diminished at the outlet.

When the pressure at the end of the line suddenly drops from p_{e1}, corresponding to the fully charged line to p_{e2} which is the pressure needed regularly by the consumers and which was the end pressure before inserting a compressor, then gas suddenly starts streaming out with a great velocity causing a pressure drop. The distance l from the outlet to the place of starting pressure-drop

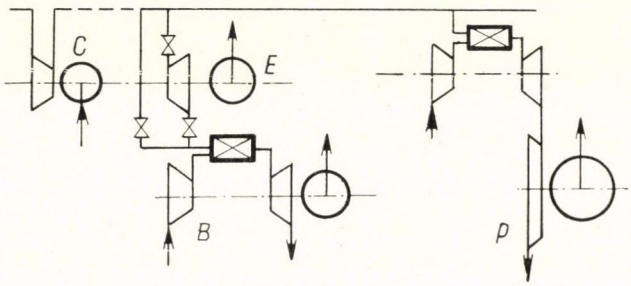

Fig. 1. General scheme

Denotations: Compressor *C*, expander *E*, basic load *B*, peak load *P*

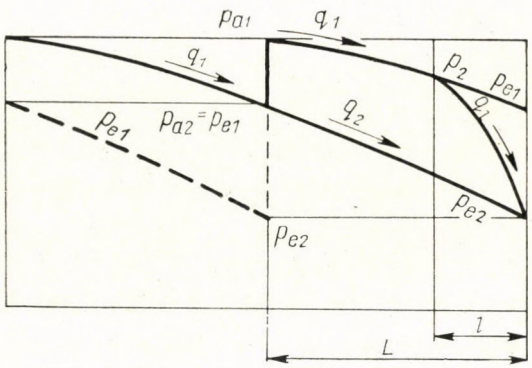

Fig. 2. Pressure conditions on the line

increases until L is reached which corresponds to the maximal stored gas quantity which can be extracted.

The pressure on the line — as shown in Fig. 2 — is dropping from the pressure p_{a1} before inserting a compressor to p_{e2}, and after recompression from p_{a1} to p_{e1} at the same flowing quantity of q_1, further it may flow with a pressure drop to p_{e2} with the increased flowing quantity of q_1. After dropping the pressure at the end of the line from p_{e1} to p_{e2}, the place of the beginning pressure drop — proceeds in the direction of the place with the pressure p_{a1} — and when it reached the distance l where the pressure is p_l, then the pressure drops from p_l to p_{a2} delivering q_l Nm^3/h gas.

The quantity of gas which can be extracted from the stored in the line section of length l is ΔQ_l. The maximum stored quantity corresponding to the distance L is ΔQ_L. From earlier publications [1]

$$\Delta Q_l = Q - Q_l = \frac{2}{3}\frac{d^2\pi}{4p_0} l \frac{p_{a1}^3 - p_{e1}^3 - p_{a2}^3 + p_{e2}^3}{p_{a1}^2 - p_{e1}^2} \text{ Nm}^3. \quad (1)$$

The quantity flowing above the normal from the stored [2]

$$\Delta q = q_l - q_1 = \left(q_1^2 + p_{e1}^2 \frac{c}{l}\right)^{1/2} - q_1 \text{ Nm}^3/\text{h} \quad (2)$$

corresponding to the signs in Fig. 2 and Fig. 3.

In the usual case of interconnecting a compressor in the middle of the last line section at a distance of Lm:

$$\Delta q = q_l - q_1 = q_1 \left[\left(1 + \frac{L}{l}\right)^{1/2} - 1\right] \text{Nm}^3/\text{h}.$$

The expressions (1) and (2) are valid for stationary conditions. The difference between two values of Q belonging to two close enough values of l and the corresponding average value of q can be considered to give with good approximation the time elapsing between these two nearby states. The flowing quantity diminishes the stored gas quantity from $Q(l - \Delta l/2)$ to $Q(l + \Delta l/2)$ by $\Delta Q_{\Delta l}$. The time needed for it is

$$\Delta t = \frac{\Delta Q}{q}.$$

The sum of the so calculated time-sections is the total time t needed to reach the conditions characterized by $\Delta Q_{l\max}$ and $q_{l\max}$.

On an *example* shown in Fig. 3a $q_{\max}$ [Nm³/h] and in Fig. 3b $\Delta Q_{\max}$ [Nm³] are traced as a function of t h, the time since the start of dropping the pressure from p_{e1} to p_{e2}. If the extracted gas quantity q is less than the marked $q_{\max}$, then the time of extracting the stored quantity will be longer. This q quantity can only be extracted as long as the extracted $\Delta Q_{\max}$ quantity reaches the value corresponding to that which could be extracted by $q_{\max}$. After that time $q_{\max}$ is the highest rate available. This can be seen on the treated examples in the diagrams.

On the treated *Example 1* the gas extraction increases linearly at a steepness marked with tan α, until consuming the available quantity ΔQ_1.

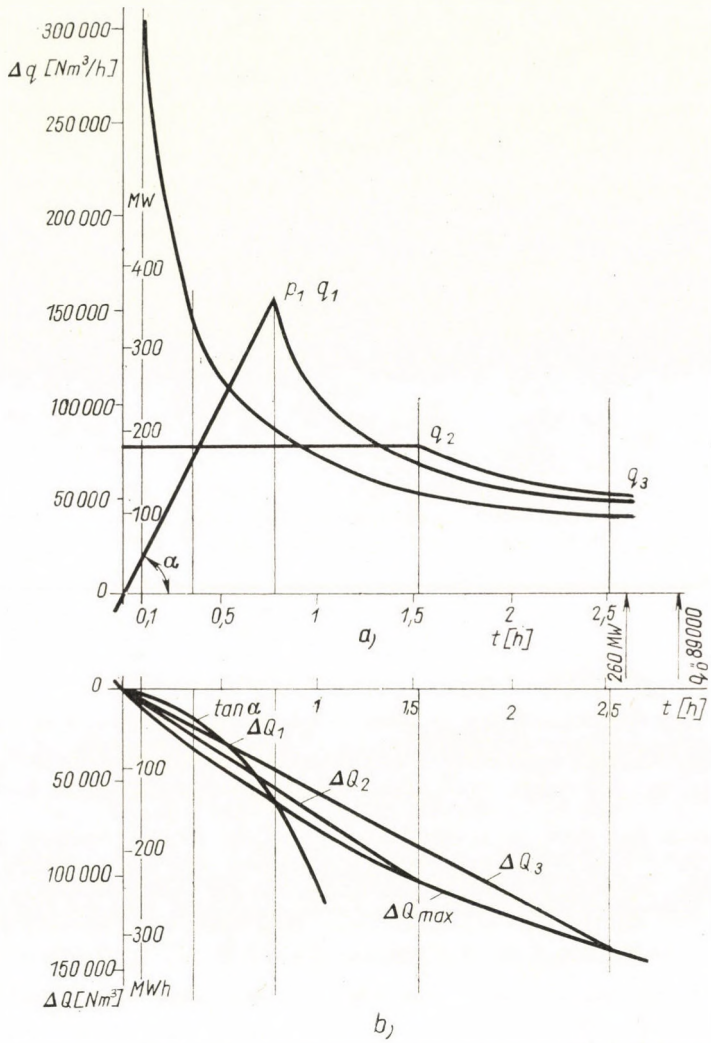

Fig. 3. An example to show the change of $q_{\max}$ [Nm³/h] (*a*) and of $Q_{\max}$ [Nm³] (*b*) as a function of t [h]

This ΔQ_1 is in Fig. 3b the intersection of the curve ΔQ_1 — a quadratically increasing curve — with that of $\Delta Q_{\max}$. After reaching the peak at p_1 the q line follows conform to its original shape the $q_{\max}$ line.

On *Example 2* the constant load q_2 reaches $q_{\max}$ at the intersection of the straight ΔQ_2 with $\Delta Q_{\max}$; behind this point of intersection the quantity which can be extracted corresponds to $q_{\max}$ and similarly q_3 corresponding to the maximal quantity disposable: $\Delta Q_{\max}$.

The smallest $q_{\max}$ quantity corresponding to q_L may be at our disposition for a longer time in case of utilizing the quantity stored in the next line

section behind the interconnected compressor — as marked on the diagram with broken lines. For this purpose the interconnected compressor should be able to deal with a pressure ratio of p_a/p_{e2}. If the interconnected compressor halved the distance behind the last compressor station, then the so stored quantity will double the stored one. The consumption of energy for compression will be in the case of the treated examples less than that produced by the expansion during offload hours.

The diagrams 3a and 3b can be used for following the possible working conditions of a peak load gas turbine. The treated diagram deals with gas quantities. The quantity of gas needed for energy production depending on the quality of the gas, of the kind, the size and the quality of the gas turbogenerator set, is calculated in the following example with 3 kWh/Nm³ for normal load and with 2,2 kWh/Nm³ for peak load. The corresponding MW-s and MWh-s are marked on the diagrams. The normally flowing gas quantity q_0 Nm_3/h is also marked on diagram 3a with the base load performance of the turbo set fed by it.

Numerical example: On a pipeline at 220 km distance from its end was a compressor station. Before inserting a compressor at half of this distance the pressure behind the compressor station started with $p_a = 600\,000$ kg/m² and dropped before the consumer to 200 000 kg/m². The flowing quantity through the pipe of 0,365 m inner diameter was 89 000 Nm³/h. After inserting a compressor at 110 km distance the pressure of the gas arriving with $p_{e1} = 44{,}8$ atm will be increased to 60 atm and the pressure at the end of the line would rise from $p_{e2} = 20$ atm to $p_{e1} = 44{,}8$ atm with unchanged streaming quantity of $q_0 = 89\,000$ Nm³/h.

The work needed for compressing this q_0 quantity to a pressure ratio of $p_a/p_{e1} = 60/44{,}8$ would be 1000 kW. Inserting an expander at the end of the line to utilize the overpressure (dropping the pressure in relation of p_{e1}/p_{e2}) it would produce 1700 kW.

Heating the gas before expansion the heat would be utilized with good economy.

The stored quantity in the last line section would be 140 000 Nm³, the minimal rate of q_{max} extraction 56 000 Nm³/h. The shortest time of extracting the stored gas quantity would be 2,5 hours, from the last line section.

The stored quantity could be doubled utilizing the quantity stored in the section behind the interconnected compressor if this compressor could deal with the pressure ratio of p_a/p_{e2}. This compressor would consume 2400 kW during 2,5 hours needed to extract additional 140 000 Nm³ at the rate of 56 000 Nm³/h. The compressor would consume during 2,5 hours 1 MW and during another 2,5 hours 2,4 MW. The expander would produce 1,7 MW during 19 hours. The daily overproduction would consequently be 24 MWh.

Corresponding to this example if the total supplied gas quantity would be utilized for power production, then the base load turbogenerator set could be of 260 MW size and the size of the peak load turbine, may — corresponding to the shape of the peak load development — be similar.

REFERENCES

1. *Acta Techn. Hung.* **27** (1959), 66—67.
2. *Acta Techn. Hung.* **34** (1961), 440.

Gasturbinen Spitzenkraftwerk. In einer Ferngasleitung kann der mittlere Druck durch zwischengeschalteten Verdichter erhöht werden. Die durch Druckerhöhung vergrößerte Gasmenge kann als aufgespeicherte Menge zur Speisung einer Spitzenkraftwerk-Gasturbine benützt werden. Der Überdruck am Ende der Gasleitung kann während der Zeit zwischen den Spitzenlasten zur Energieerzeugung nutzbar gemacht werden. Die erzeugte Energiemenge ist bedeutend mehr als die von dem Verdichter verbrauchte, wodurch die für Spitzendeckung benötigte Gasmenge unentgeltlich gespeichert werden kann.

Газотурбиная электростанция пиковой нагрузки, работающая на захраненном в газопроводе газа *(А. Фоно)*. Среднее давление можно повышать дополнительным устройством для сжатия газа в газопроводе. Избытное количество газа, соответствующее повышенному среднему давлению, является захранённым газом, с которым можно питать газотурбинную электростанцию пиковой нагрузки. Вне времени пиковой нагрузки повышенное в конце газопровода давление можно использовать для выработки энергии. Выработанная энергия больше чем энергия, требуемая для сжатия газа, таким образом хранение газа в качестве носителя энергии являестя бесплатным.

Acta Technica Academiae Scientiarum Hungaricae; Tomus 68 (1—2), pp. 9—14 (1970)

ON THE SPECTRUM FACTORIZATION
PART II

F. CSÁKI
CORRESPONDING MEMBER OF THE HUNGARIAN ACADEMY OF SCIENCES
and
P. FISCHER

[Manuscript received February 7, 1969]

As a direct continuation of a previously published paper, the necessary and sufficient conditions as well as procedures of factorizing pulsed-data matrices are now given here.

I. Introduction

The z-transformation is one of the best of the transformation methods used in the theory of the sampled-data systems. Let $f(t)$ be a function of a real variable, if $t \geqq 0$. Its z-transformation, $F(z)$ is defined by the following relation:

$$F(z) = \sum_{n=0}^{\infty} f(nT)\, z^{-n}, \tag{1}$$

where z is the complex variable, if this function exists, and T is the time of the sampling period.

It is obvious that the domain of the convergence of the function $F(z)$ is always on the outside of a circle, and according to the Cauchy—Hadamard theorem the radius of this circle is defined by the relationship

$$M = \overline{\lim_{n\to\infty}} \sqrt[n]{|f(nT)|}.$$

That is, the z-transform exists, if and only if

$$|f(nT)| \leqq e^{an}$$

beginning from some n.

Similarly to the continuous-data systems, the optimum statistical design procedure of WIENER [1, 2] can be generalized for strictly digital or pulsed-data single-variable and multi-variable systems, respectively. In the latter case the inputs and outputs are assumed as being pulsed-data stationary ergodic stochastic processes. The optimization criterion is the least sum of the mean-square errors between the sets of actual and ideal outputs. For obtain-

ing explicit solution formulae one of the main problems is the spectrum factorization of power-density-spectrum matrices. In a previous paper [3] the authors have proposed some factorization procedures for continuous-data power-density-spectrum matrices of rank n as well as of rank $r < n$. As a direct continuation of the paper mentioned [3], now we will take up the treatise of the factorization procedures of pulsed-data power-density-spectrum matrices.

In the following we shall give an exact definition of this problem and two solutions for the factorization of certain types of matrices will be presented which appear sufficient for the practice.

II. Definitions and theorems

Further on the matrix will be indicated by a bold-face capital letter, its elements by the same lower case letter and by an approximate index. Let $\mathbf{A}$ be an arbitrary matrix. Then $\mathbf{A}^T$, $\overline{\mathbf{A}}$, $\mathbf{A}^*$, $\mathbf{A}^{-1}$ and $|\mathbf{A}|$ denote the transpose in succession, the complex conjugate, the adjoint, the inverse and the determinant of the matrix. $\mathbf{I}$ denotes the unity matrix and $\mathbf{I}_n$ the $n \times n$ unity matrix, the frequency ω denotes an arbitrary real quantity, $j = \sqrt{-1}$, and s is a complex variable. A matrix is called a rational matrix if each of its elements is a rational fractional-function.

The para-transform of a matrix $\mathbf{A}(z)$ is the following [it is denoted by $\mathbf{A}^*_*(z)$]:

$$\mathbf{A}^{\ddagger}(z) = \overline{\mathbf{A}^T\left(\frac{1}{\bar{z}}\right)}. \tag{2}$$

A rational matrix is a para-transformed-hermitian, if its para-transform is equal to itself. That is

$$\mathbf{A}^*_*(z) = \mathbf{A}(z). \tag{3}$$

On the unit circle a para-transformed-hermitian matrix is a hermitian matrix in the usual sense, because

$$\frac{1}{\bar{z}} = z, \quad \text{if} \quad |z| = 1$$

so,

$$\mathbf{A}(z) = \overline{\mathbf{A}^T\left(\frac{1}{\bar{z}}\right)} = \overline{\mathbf{A}^T(z)}. \tag{4}$$

It is easy to verify that the following relations hold:

$$\mathbf{A}_*^*(z)_*^* = \mathbf{A}(z) \tag{5}$$

and

$$[\mathbf{A}(z)\ \mathbf{B}(z)]_*^* = \mathbf{B}_*^*(z)\ \mathbf{A}_*^*(z). \tag{6}$$

If the coefficients of the elements of a rational matrix are real, the relation (2) can be written in the following form:

$$\mathbf{A}(z) = \mathbf{A}^T\left(\frac{1}{z}\right). \tag{7}$$

There is the following relation between the elements of a para-transformed-hermitian matrix:

$$a_{kl}(z) = \overline{a_{lk}\left(\frac{1}{\bar{z}}\right)}. \tag{8}$$

If the coefficients of the elements of $\mathbf{A}(z)$ are real, then the relation (8) will be the following:

$$a_{kl}(z) = a_{lk}\left(\frac{1}{z}\right). \tag{9}$$

Theorem 1

The necessary and sufficient condition of the factorization of the rational matrix $\mathbf{A}(z)$ in the form

$$\mathbf{A}(z) = \mathbf{A}_-(z)\ \mathbf{A}_+(z) \tag{10}$$

— where matrices $\mathbf{A}_-(z)$ and $\mathbf{A}_+(z)$ have the following properties:

a) $\mathbf{A}_-(z)$ and $\mathbf{A}_+(z)$ are also rational matrices and $[\mathbf{A}_-(z)]_*^* = \mathbf{A}_+(z)$;

b) if the rank of $\mathbf{A}(z)$ is r, the $\mathbf{A}_-$(resp. $\mathbf{A}_+$) is $n \times r$ (resp. $r \times n$) matrix;

c) $\mathbf{A}_-$(resp. $\mathbf{A}_+$) matrix possesses a left (resp. right) inverse;

d) all the poles of $\mathbf{A}_-(z)$ [resp. $\mathbf{A}_+(z)$] are in the domain $|z| \geq 1$ (resp. $|z| \leq 1$), the matrix is analytic in the domain $|z| < 1$ (resp. $|z| > 1$) and there exists its left (resp. right) inverse of the same properties —

is that the matrix $\mathbf{A}(z)$ is a paratransformed-hermitian and positive semi-definite on the unit circle. This theorem is a special case of the following more general theorem:

Theorem 2

Let us give an arbitrary circle or line of the complex plan, then the necessary and sufficient condition of the factorization $\mathbf{A}(z)$ in the form (10) — where matrices $\mathbf{A}_-(z)$ and $\mathbf{A}_+(z)$ have the following properties:

a) $\mathbf{A}_-(z)$ and $\mathbf{A}_+(z)$ are also rational matrices and we obtain $\mathbf{A}_+(z)$ from $\mathbf{A}_-(z)$ if we replace z by the inversion of z to the circle or to the line;

b) if the rank of $\mathbf{A}(z)$ is r, the $\mathbf{A}_-(z)$ resp. $\mathbf{A}_+(z)$ is $n \times r$ (resp. $r \times n$) matrix;

c) $\mathbf{A}_-(z)$ resp. $\mathbf{A}_+(z)$ matrix possesses a left (resp. right) inverse;

d) let $f(z) = 0$ be the equation of the circle or one of the line, then all the poles of $\mathbf{A}_-(z)$ [resp. $\mathbf{A}_+(z)$] are in the domain $f(z) \geqq 0$ [resp. in the domain $f(z) \leqq 0$], the matrix is analytic in the domain $f(z) < 0$ [resp. $f(z) > 0$] and there exists its left (resp. right) inverse of the same properties —

is that the matrix is invariant to the transformation replacing z by the inversion of the z to the circle or line and is positive semidefinite on the given circle or line. This theorem easily follows from the theorem of YOULA [4].

Remark: It is obvious that *Theorem 2* contains as a special case the theorem of YOULA and *Theorem 1.* The utilization of the bi-linear transformations

$$w = \frac{z+1}{z-1} \tag{11}$$

and

$$z = \frac{w+1}{w-1} \tag{12}$$

gives a method to obtain from the arbitrary transformation method a new one in the field of the z-transformation matrix [6].

III. Summary of the proposed method

In the following we note the steps of our modified algorithm, which are:

1. Elimination and factorization of denominators.
2. Determination of the rank.

2.1 The rank r is equal to the order. Then

2.1.1 calculation and decomposition of the determinant;

2.1.2 decrease of the degree of the polynomial of the determinantal expansion by means of matrices $\mathbf{B}_{\alpha i}(z)$ and $\mathbf{C}_{ai}(z)$;

2.1.3 after the multiple repetition of the cycle we obtain an elementary polynomial matrix;

2.1.4 the reduction of elementary polynomial matrices: row and column transformation according to the given rules, the decrease of the degree of the highest power of the determinantal expansion by two, by means of $\mathbf{\Delta}(z)$ and $\mathbf{F}(z)$ matrices;

2.1.5 after the multiple repetition of the cycle we obtain a positive definite hermitian matrix of constant elements;

2.1.6 decomposition of the positive definite hermitian matrix of constant elements to the product of two matrices where the factors are para-conjugates of each other;

2.1.7 substitution of corresponding matrices T_i to, (17) and division with, the factorized denominator.

2.2 The rank $r < n$.

The definitions of the matrices can be seen in [3].

IV. An illustrative example

Let us consider the following example

$$\mathbf{A}(z) = \begin{bmatrix} \dfrac{2(1-e^{-2T})}{(1-ze^{-T})(1-z^{-1}e^{-T})} & \dfrac{2A}{3} \cdot \dfrac{(1-e^{-3T})}{(1-ze^{-T})(1-z^{-1}e^{-2T})} \\ \dfrac{2A}{3} \dfrac{(1-e^{-3T})}{(1-ze^{-2T})(1-z^{-1}e^{-T})} & \dfrac{1}{4} \cdot \dfrac{(1-e^{-4T})}{(1-ze^{-2T})(1-z^{-1}e^{-2T})} \end{bmatrix} =$$

$$= \begin{bmatrix} \dfrac{1}{1-ze^{-T}} & \\ & \dfrac{1}{1-ze^{-2T}} \end{bmatrix} \begin{bmatrix} 2(1-e^{-2T}) & \dfrac{2A}{3}(1-e^{-3T}) \\ \dfrac{2A}{3}(1-e^{-3T}) & \dfrac{1}{4}(1-e^{-4T}) \end{bmatrix} \begin{bmatrix} \dfrac{1}{1-z^{-1}e^{-T}} & \\ & \dfrac{1}{1-z^{-1}e^{-2T}} \end{bmatrix}$$

and

$$\begin{bmatrix} 2(1-e^{-2T}) & \dfrac{2A}{3}(1-e^{-3T}) \\ \dfrac{2A}{3}(1-e^{-3T}) & \dfrac{1}{4}(1-e^{-4T}) \end{bmatrix} =$$

$$= \begin{bmatrix} \sqrt{2(1-e^{-2T})} & 0 \\ \dfrac{2A}{3} \dfrac{1-e^{-3T}}{\sqrt{2(1-e^{-2T})}} & \dfrac{\sqrt{\dfrac{1}{4}(1-e^{-4T})(1-e^{-2T}) - \dfrac{2A^2}{9}(1-e^{-3T})^2}}{\sqrt{1-e^{-2T}}} \end{bmatrix} \times$$

$$\begin{bmatrix} \sqrt{2(1-e^{-2T})} & \dfrac{2A}{3} \dfrac{(1-e^{-3T})}{\sqrt{2(1-e^{-2T})}} \\ 0 & \dfrac{\sqrt{\dfrac{1}{4}(1-e^{-4T})(1-e^{-2T}) - \dfrac{2A^2}{9}(1-e^{-3T})^2}}{\sqrt{1-e^{-2T}}} \end{bmatrix}$$

if $$0 \leq A < \sqrt{\frac{9}{8} \frac{(1-e^{-4T})(1-e^{-2T})}{(1-e^{-3T})^2}},$$

then the factorization of $\mathbf{A}(z)$ is the following:

$$\mathbf{A}_{-}(z) = \begin{bmatrix} \sqrt{2(1-e^{-2T})}\ \dfrac{1}{1-ze^{-T}} & 0 \\ \dfrac{2A}{3}\ \dfrac{1-e^{-3T}}{\sqrt{2(1-e^{-2T})}(1-ze^{-2T})} & \dfrac{\sqrt{\dfrac{1}{4}(1-e^{-4T})(1-e^{-2T}) - \dfrac{2A^2}{9}(1-e^{-3T})^2}}{\sqrt{(1-e^{-2T})}\,(1-ze^{-2T})} \end{bmatrix}$$

If

$$A = \frac{3}{2\sqrt{2}}\ \frac{\sqrt{(1-e^{-4T})(1-e^{-2T})}}{1-e^{-3T}}\ ,$$

then

$$\mathbf{A}_{-}(z) = \begin{bmatrix} \dfrac{\sqrt{2(1-e^{-2T})}}{1-ze^{-T}} \\ \dfrac{\sqrt{1-e^{-4T}}}{2\,(1-ze^{-2T})} \end{bmatrix}.$$

If

$$A > \frac{3}{2\sqrt{2}}\ \frac{\sqrt{(1-e^{-4T})}\sqrt{(1-e^{-2T})}}{1-e^{-3T}}\ ,$$

then such $\mathbf{A}_{-}(z)$ matrix does not exist.

REFERENCES

1. Csáki, F.: Simplified Derivation of Optimum Transfer Functions for Digital Stochastic Processes. *Periodica Polytechnica* (Electrical Engineering) **9** (1965), 237.
2. Csáki, F.: Optimum Pulse-Transfer Functions for Multivariable Digital Stochastic Processes. *Periodica Polytechnica* (Electrical Engineering) **9** (1965), 353.
3. Csáki, F.—Fischer, P.: On the Spectrum Factorization. *Acta Techn. Hung.* **58** (1967), 145—168.
4. Youla, D. C.: On the Factorization of Rational Matrices. *IRE Transactions on Information Theory* **15** (1961); Part 7, 172—189.
5. Davis, M. C.: Factoring the Spectral Matrix. *IEEE Transactions on Automatic Control* (1963), 296—305.
6. Tuel, W. G.: Computer Algorithm for Spectral Factorization of Rational Matrices. *IBM Journal of Research and Development.* **12** (1968); No. 2, 163—176.

Spektrale Faktorisierung, Teil II. Als unmittelbare Fortsetzung eines früher erschienenen Artikels sind hier die notwendigen und hinreichenden Bedingungen sowie die Algorithmen der spektralen Faktorisierung von Matrizen für Abtastsysteme gegeben.

Спектральное разложение, II (*Ф. Чаки и П. Фишер*). Как непосредственное продолжение опубликованного раньше сообщения, в настоящей работе представлены как необходимые и достаточные условия, так и алгоритмы спектрального разложения матриц для импульсных систем.

Acta Technica Academiae Scientiarum Hungaricae; Tomus 68 (1—2), pp. 15—28 (1970)

IMPROVEMENT OF THE PROCESS "HIGH-GRADE IONIZATION IN COLD GAS"

D. HALÁSZ

DOCTOR OF TECHN. SC.

and

K. SZENDY

CORRESPONDING MEMBER OF THE HUNGARIAN ACADEMY OF SCIENCES

[Manuscript received September 9, 1968]

The authors and other contributors made several proposals for the non-equilibrium ionization in MHD generators which have been presented and discussed at various MHD symposiums. None of these suggestions have come so far up to expectations. In a new method propounded in the present paper, recombination is expected to be impeded by photons emitted by glowing grains introduced into the working gas. Numerical relations have still to be determined by further examinations and experiments. Any MHD generator, especially its open-cycle version, will only become feasible, if the working gas is kept at moderate temperatures (1200 to 1800° K), where the proposed ionization effect may be useful.

I

At the *MHD Symposium* at *Stanford* in 1967 the authors published a process permitting the attainment of required conductivity of the working gas in MHD generators operated at relatively low temperatures (150 to 500°C) [1]. With due regard to the advanced knowledge of ionization gained in the meantime, new ideas and proposals have become known, it was found to be appropriate to reconsider the problem and to perform the examinations and experiments still required.

II

By way of introduction it must be stated that neither our previous proposal, nor other suggestions published in the international literature aimed at facilitating ionization, have led to practicable results. Thus, no feasible method for obtaining non-equilibrium ionization could be considered as available for the time being [2]. Yet, especially a closed-cycle system — under the present conditions — can by no means be implemented without solving the problem of non-equilibrium ionization.

III

The proposal in its initial shape, as formulated in the sixties, by several contributors almost simultaneously, was presented by the authors at the *MHD Symposium* held in *Paris* in 1964 [3]. According to this proposal, particles

of a material of low work function (e.g. fine grains of BaO generally assumed in literature as having diameters of 5×10^{-8} m) are blown into the working gas at the beginning of the generator channel. Under the effect of elevated temperature free electrons are released from the particles. In the presence of these free electrons the working gas becomes conductive to a certain extent. Numerical conditions are shown by the differential equation (6) deduced in the paper. By means of this equation and with the simplifying assumption of considering the specific charge constant, the expectable average charge density, i.e. the number of electrons per sq.cm, and the specific conductivity can be determined for different parameters.

Let the following values be assumed:

work function of BaO 1,68 eV;
weight ratio of BaO to working fluid, 2×10^{-2};
grain diameter of BaO particles assumed to be spherical 10^{-6} cm.

For different temperatures the specific values listed in Table 1 are obtained.

Table I

T [°K]	q_R [coulomb/sq. cm]	$n\left[\frac{1}{\text{sq.cm}}\right]$	Electric conductivity, σ [mho/cm]
1300	$2{,}25 \times 10^{-7}$	$1{,}4 \times 10^{12}$	$0{,}055 \times 10^{-3}$
2000	$5{,}20 \times 10^{-7}$	$3{,}24 \times 10^{12}$	$0{,}18 \times 10^{-3}$
3000	$6{,}6 \times 10^{-7}$	$4{,}12 \times 10^{12}$	$0{,}283 \times 10^{-3}$

According to the figures given in the table, the steady-state specific charge (q_R), the number of free electrons, consequently the conductivity is low and increases very slowly and almost proportionally with temperature. At low temperatures (e.g. to ensure the initial value required for magnetically excited ionization) this method is applicable; at high temperatures, however, the ionization thus obtained is by orders of magnitude lower than that achieved by potassium salting, hence it is impracticable.

IV

The purpose of the procedure mentioned in Chapter I was to obtain, by salting with BaO, a similar degree of ionization as if the working gas temperature were equal to the much higher temperature of BaO particles: we assumed that the electron emission of a BaO grain did not depend on the temperature of the gas, but on that of the grain.

It clearly emerges from Chapter I that the results that could thus be obtained would be rather limited. The advantage of keeping the working gas cold would be preserved, but the degree of ionization would remain too low to be of any use. This situation was not even changed by the fact that the number of electrons increased by about four orders of magnitude in the immediate vicinity of the particle (between 1300 and 3000°K). In spite of all this, any marked increase in the average electron density was prevented by the space charge.

Some improvement nevertheless becomes apparent from the fact that, with otherwise equal percentage of salting, the distance between two BaO grains was reduced in proportion to the 1/3 power of temperature. As a result of this effect at 3000°K, a charge density of about 16×10^{-7} was obtained, instead of $6{,}6 \times 10^{-7}$ indicated in the Table.

After all, the proposed procedure remained impracticable.

V

It may become clear from the investigations briefly outlined in the foregoing that the rapid increase of ionization which was expected to set in with increasing temperature failed to take place. Hence, the space charge was to be decreased, which — as is known — could be approached by introducing positive ions into the space occupied by the electrons.

A procedure of introducing the salting material may be chosen, making out an overall of 2 per cent, in a proportion of, say, 1 per cent in the form of potassium salts and another of 1 per cent in that of BaO. A certain degree of thermal ionization is produced by the potassium salts, and, in the space concerned, beside electrons (emitted partly by the BaO and partly produced by thermal ionization) positive ions will also be present.

As demonstrated by an approximative numerical investigation, the result will not be decisive, not even under favourable conditions, thus neither can this method be considered as viable.

VI

A method similar in principle to the former has been described by E. C. LARY and others [4], who have suggested the use of compound grains, e.g. tungsten particles partly coated with caesium and suspended in a working fluid containing caesium in a gaseous form. Electrons will be emitted from the caesium coating of tungsten, while positive caesium ions will be released from the free (uncoated) tungsten surface by surface ionization. Thus, the working fluid will be, in the most favourable case, quasi-neutral, and the deteriorating effect of the space charge described in Chapter IV will not be effective. With

a quasi-neutral working fluid, high conductivity values are easily obtainable. E.g., with the data included in the Table, the conductivity at 1300°K would be by two orders of magnitude higher, and would increase rapidly with increasing temperature.

The proposal is extremely ingenious. It would, however, be required to verify the feasibility of stabilizing the unstable quasi-neutral state under practical conditions, and to see whether the expensive salting material and its by no means simple technology could at all be made economical.

VII

According to the investigations made so far, the diameter of BaO particles should be chosen to be very small ($\sim 5 \times 10^{-8}$ m). The production of such particles can be considered as practically solved (by condensing BaO vapour); it has turned out, however, that rapid coagulation of particles takes place in the generator under the effect of mass forces, causing the growth of particle diameters. At the *MHD Symposium* held in *Warsaw*, interesting and valuable experiments on this subject were described by B. WALDIE and J. FELLS [5]. According to the experiments and deduced formulae it may be expected that, during the 0,85 sec time the working fluid is passed through the steam boiler, the diameter of BaO particles, in a 500 MW closed-cycle generator, grows fivefold, while the conductivity of the gas drops to 1/20.

When judging the different procedures, this factor should be borne in mind.

VIII

All attempts made so far have led to the conclusion that by blowing hot BaO particles into the cold working fluid the required degree of ionization is unattainable and the average degree of ionization varies but very slightly when increasing the temperature of BaO particles.

The procedure, however, has but one marked result: If in some way or other, the required degree of ionization is ensured at the inlet end of the generator for whatever short period, by the glowing BaO (generally a ceramic substance, or possibly carbon particles), will prevent the *recombination and disappearance of electrons*, this recombination being the main trouble encountered in all kinds of, but particularly of the non-equilibrium ionization.

The electrons immediately tend to recombine in cold gas, each electron falling into a positive ion and carrying with itself the entire ionization potential. As long as the energy corresponding to the ionization potential is not fully transferred through radiation, from the ion to its surroundings, collision, etc., the components of the positive ion get into the state of self-oscillation; they

are in an anomalous motion, in a quasi-excited state. The glowing of BaO grain continuously emits photons. Although the cross-sectional area of ions is small as compared to that of the photons, in the instant of recombination, viz. *in statu nascendi*, the conditions are anomalous:

a) The ionization potential is very low in the first moment (the ionization potential is carried by the electron);

b) the effective cross-sectional area increases because of self-oscillation of ion components;

c) several successive excited states are produced.

The equilibrium of renewed electron emission and recombination will take place at a lower specific electron density than the original. In Chapter IX an investigation will be made to find the condition for obtaining acceptable resultant electron density.

IX

In connection with the method proposed in the preceding Chapter VIII a few important phenomena are still to be examined:

1. The cooling of grains in the colder working fluid, during their passage through the generator channel;

2. coagulation of small-diameter solid grains;

3. effect of radiated heat (released photons) of the glowing grains on recombination.

1

The cooling of grains in the working fluid is discussed in Chapters III V, VI and XI of paper [1]. As stated in Chapter XI, with $d = 10^{-8}$ m diameter, the heat-transfer coefficient is $\alpha = 8{,}6$ kcal/m²h°K. According to Equ. (2) of Chapter III of paper [1], the time required for a grain to cool from T_0 (e.g. 3000°K) to T_2 (e.g. 2800°K), if the gas temperature is T_1 (e.g. 900°K), is given by the following formula:

$$t = \frac{d\gamma c(T_0 - T_2)\,3600}{3\left(\frac{T_0+T_2}{2} - T_1\right)\alpha} \text{ [sec]}. \tag{1}$$

With the values given for γ and c in Chapter X of the present paper, the time is about $1{,}04 \times 10^{-3}$ sec.

It should be briefly noted that monatomic and diatomic gases exhibit a favourable behaviour. Triatomic gases (H_2O, CO_2) are less favourable, because heat from solid grains is dissipated by these gases also through radiation, in addition to conduction. This gas radiation is selective and is the smaller, the lower is the partial pressure of gases. The available calculation methods are

hardly applicable to practical conditions and, hence, experiments can only decide whether or not these triatomic gases would cause a too rapid cooling of the solid grains.

Conditions may be improved, if so required, by

a) building into the generator channel a second, third, etc. radiation belt in which the cooled solid grains are heated again;

b) applying high, ultrasonic flow velocities cutting down the transit times;

c) blowing carbon grains (instead of BaO particles) into the working fluid, by which the grain temperature is maintained by burning of the grains;

d) adopting grain diameters not smaller than necessary. Heat accumulated by a particle is proportional to the volume, i.e. to the third power of grain diameter, while the heat loss is proportional to the surface and to the second power of the diameter. In the course of our subsequent explications (see item 3) it will become clear that as *the grain diameter is small it ceases to be a decisive factor*, and there is a way of applying particle diameters ($\sim$1 micron) that will practically prevent coagulation.

2

Mention has already been made of a recent paper [5] dealing with coagulation. Experimental results do not preclude the assumption that the hazard of coagulation is reduced by the repelling force acting between particles of identical polarity where both the temperature and charge of particles are high and the staying time is negligible due to the high transit velocity. The situation is different in the heat recovery equipment of a supplementary power plant, where both the temperature and charge are low and the staying time is short, due to the low transit velocity. According to the example presented in the paper, the staying time in the generator channel is 0,13, and in the steam boiler 0,85 sec. Under these conditions, as stated by the experimenter, it is probable that coagulation would give rise to intolerably large diameters in the "supplementary" equipments, independently of the behaviour in the generator channel.

In the arrangement proposed in the present paper, the working fluid acts in the generator channel *only*, and there is no supplementary power plant. Although the temperature of the working fluid is not higher than in the flue ducts of the steam boiler, *the particle temperature remains high* and repulsion keeps on acting. Thus, coagulation causes no trouble whatsoever.

3

The glowing particles continuously emit radiating energy (photons) towards the positive ions. The ions, before recombination is started, reflect this radiation, while the thermal energy content of particles does not decay.

As soon as recombination is started, the electron falls into the ion, taking along the entire ionization potential; the components of the ion start to oscillate and, in this state, *in statu nascendi*, the effective cross-sectional area of the ion exposed to the photons suddenly increases and takes over the energy of the photon. In the first instant of collision, the ionization potential is apparently zero. But the collision energy of the electron is gradually irradiated by the ion. The entire collision energy having been irradiated, the electron is tied up to the electron by the entire ionization potential.

It is known that a photon is capable of ionizing, if

$$h\nu \geqq eU_i\,, \tag{2}$$

where h Planck constant [Ws²];
ν oscillation frequency of the photon [1/sec];
e charge of the electron [As];
U_i ionization voltage [V].

As long as the ionization voltage remains below the value $h\nu/e$, as stated in Equ. (2), the photon will be capable of preventing recombination. Depending on the temperature of the particle, the ionization potential of the salting material and other factors, a state of equilibrium will set in between the states of full recombination and the absence of recombination. By properly selecting the conditions, the aim is to bring this state of equilibrium as close as possible to that of the absence of recombination.

As regards numerical relations the following statements apply.

According to the experiments, if coagulation has started at all — which is probably inevitable — the BaO particle is of loose structure, similar to hoar-frost. Since hoar-frost developing in this way is a "black" body, black radiation may be reckoned with in case of BaO particles as well.

The maximum intensity of black radiation, according to Wien's law will be

$$\left|\frac{c}{\nu}\right|_{\max} = \frac{0{,}00288}{T}\ [\mathrm{m}], \tag{3}$$

where c velocity of light [m/sec];
ν oscillation frequency [1/sec];
T temperature [°K].

Considering Equ. (2), the ionization potential at which a photon is capable of ionizing at temperature T [°K], under the most favourable conditions, will be

$$U_i = \frac{h}{e}\,\frac{cT}{0{,}00288} = 0{,}431\times 10^{-3}\,T \text{ volt}. \tag{4}$$

It should be emphasized that, *here, T is not the temperature of the working fluid, but that of the particle.*

Ionization is, of course, possible not only at the frequency corresponding to the radiation of highest intensity, but also at a frequency lower than that, especially, if also excitation voltages lower than the ionization voltage exist, or if such a voltage is artificially produced, e.g. by dosing in addition to K other substances, at which a low excitation voltage is known.

It is a hopeless task to numerically determine in advance as to what ionization level would set in under certain conditions. In order to reach this goal, *performance of experiments and generalization of their results would be required.*

The intensity of heat radiated by a glowing particle is proportional to the surface of the particle. The summed-up surface of several smaller particles is larger than that of a large particle of identical mass. The intensity, i.e. the number of photons emitted in a second, has no direct effect on ionization, the latter being in principle dependent on the frequency. An indirect effect will, however, be observable, because at low intensity the probability of the encounter of a photon and an ion is reduced. Considering that the photons travel with the velocity of light and, in addition, the entire system is confined by well-reflecting surfaces having a multiplying effect on collisions, this hazard will cease to prevail at a diameter difference of a few orders of magnitude.

Thus, there is no weighty reason of making the particle diameter as small as possible. Particle diameters in the vicinity of, say, 1 micron, which are technologically easily obtainable and non-coagulating, may be used. This will have substantial advantages mainly with the closed-cycle process.

X

In the described proposal a decisive role is played by the reflection of heat rays. It should be premised that "reflection" here is not meant as an optical phenomenon. The heat rays are not required to be reflected in a regular way (this would not even be desirable), but rather *the rays should be prevented from transforming into heat on the reflection surface.* A smooth plane surface is not required. The phenomenon should better be termed as dispersion of heat rays, requiring a "white" surface instead of a "smooth" one, thus the *microstructure* of the surface is also an important factor.

According to the available experimental data [6], at 900°K, 98 per cent is reflected by Ag, 95 per cent by Al and 93 per cent by Mo, the given figures being about inversely proportional with increasing temperature values. It is probable that for dispersion the corresponding figures would be even better or, in other words, these figures could be improved by proper metallurgical and technological methods.

Adhering to the reflection figures known at present, let us find at what rate and within what time would a particle of diameter d [m], specific gravity γ[kp/cu.m], specific heat c [Kcal/kp°K] and temperature T [°K] lose

its heat content through radiation. Let the calculation be based on the assumption that one k-th part of the heat emitted will be regained by the particle and, in fact, only one $(1—k)$-th part will be eradiated.

The heat lost by the particle at a temperature drop of dT is

$$dQ_1 = -\frac{d^3\pi}{6}\gamma c dT \quad \text{[Kcal/particle]}, \tag{5}$$

where

d particle diameter [m];
γ specific gravity of the particle [kp/sq.m];
c specific heat of the particle [Kcal/kp °K].

The heat emitted by the particle during a period of dt [s] is

$$dQ_2 = d^2\pi\frac{\sigma}{3600}(T^4-\vartheta^4)(1-k)\,dt \quad \text{[Kcal/particle]} \tag{6}$$

where

$\sigma = 4{,}96\times10^{-8}$ [Kcal/sq.m.h. °K⁴];
ϑ constant temperature of the reflecting wall of the confined space; and
t time [sec].

By making the two relations equal, the connection between temperature and time is found:

$$\frac{dT}{T^4-\vartheta^4} = -\underbrace{\left[\frac{6\,\sigma\,(1-k)}{d\,3600\,\gamma c}\right]}_{A}dt. \tag{7}$$

In the numerator on the left side, the term ϑ^4 is neglected beside T^4. The error introduced thereby and its correction will be assessed later. After integration

$$-\frac{1}{3T^3} = -At + C_1. \tag{8}$$

If $t = 0$, then $T = T_0$. Finally

$$T = \frac{1}{1{,}44\left[\frac{1}{3T^3} + At\right]^{1/3}}. \tag{9}$$

This formula indicates how the temperature of the particle decreases in the function of time. In practice, the main item to be considered is to find the rate of temperature drop suffered by the particle through radiation while staying in the generator channel.

Let the data be e.g.:

$$T_0 = 3000\ ^\circ\text{K};\ \vartheta = 900\ ^\circ\text{K};\ d = 5\times10^{-8}\ \text{m};$$
$$\gamma_{BaO} = 5{,}3\times10^{3}\ \text{kp/cu.m};\ C_{BaO} = 0{,}25$$
$$\text{Kcal/kp}\ ^\circ\text{K};\ k = 0{,}98 \text{ and } t = 2\times10^{3}\ \text{sec.}$$
$$A = 2{,}5\times10^{-8}$$

and

$$T = \frac{1}{1{,}44\left[\frac{1}{3(3\times10^{3})^{3}} + 2{,}5\times10^{-8}\times2\times10^{-3}\right]^{1/3}} = 1750\ ^\circ\text{K}.$$

The temperature has dropped considerably. Due to the neglection, the correction will hardly help. It is assumed that $T^4 - \vartheta^4 \sim T^4$, the value of β is calculated for $T_0 = 3000\ ^\circ$K and $T = 1750\ ^\circ$K and their mean value is taken $T_k = 0{,}96$:

$$T_k = \frac{1750}{0{,}96} = 1825\ ^\circ\text{K}.$$

Such a cooling is, of course, not permissible. The easiest countermeasure is to increase the particle diameter to e.g. 10^{-6} m. In this case $A = 1{,}25\times10^{-9}$ and

$$T = \frac{1}{1{,}44\left[\frac{1}{3(3\times10^{3})^{3}} + 1{,}25\times10^{-9}\times2\times10^{-3}\right]^{1/3}} = 2820\ ^\circ\text{K}.$$

The correction will modify this result to 2943 °K as the temperature of the particle after cooling.

The calculation presented above serves only for giving a rough information on the expectable conditions. A few shortcomings of the investigation are immediately apparent:

a) It is impossible that an increase of the particle diameter monotonously improves the conditions. Let us consider the case when the entire salting material is concentrated into a single sphere. The calculation would give good results as long as recombination took place practically unhindered. The method fails to take into account the effect of particle distribution.

b) Radiation and re-radiation take place according to intricate laws which, as far as we know, have not been examined yet, for the case of dispersed small-diameter particles. Usually, adopted methods are based on assuming "closely-spaced walls" or "confined radiating materials"; the calculation presented is based on the former assumption.

c) The magnitude of re-radiation coefficient of confining walls will vary according to the various temperatures, in particle operation.

d) What the time will be while the particle stays in the generator channel, etc.

Any deeper analysis could only be possible by simultaneous experiments. In any case, the following statements can be made:

The problem is neither simple nor easy; it is important to produce and select the most suitable materials and apply optimum conditions;

the necessary, optimum limits should not be overstepped in decreasing the particle diameter;

suitable limits should be maintained in increasing the particle temperature and in decreasing the wall temperature.

The particle material should also be an item to be considered. E.g., at very high temperatures, at which BaO would melt, carbon particles may prove to be better than BaO, their combustion compensating for the radiated heat. For information the following figures are to be considered: the heat supplied by a BaO particle of $d = 10^{-6}$ m diameter, at a heat drop of 200°K, is $1{,}39 \times 10^{-13}$ Kcal.

A carbon particle also of $d = 10^{-6}$ m diameter would furnish an amount of heat equal to $2{,}20 \times 10^{-11}$ Kcal, when burnt, i.e. by two orders of magnitude more heat than BaO. The work function of C (4,39 eV) is much higher than that of BaO (1,67 eV), but this is of no importance according to the present proposition.

The question remains, however, whether the carbon particle would be capable of burning during the very short period of staying in the generator channel. In the generator channel there is but very little O_2 left (or none in closed-cycle operation), and the combustion of the carbon particle would take place either very slowly or not at all. The carbon particle should, therefore, be employed in combination with another substance containing the required O_2, e.g. with BaO_2 (barium peroxide) or with some other substance emitting O_2 at high temperature.

XI

In this chapter, the methods for open- and closedcycle MHD generators will be tested separately, since the phenomena occurring in the two systems have to be judged differently.

1. Open-cycle MHD generator

In order to obtain high thermal efficiency, in the combustion chamber of the generator a high temperature is to be kept, by which the required degree of ionization is ensured by equilibrium thermal ionization. In the nozzle the working fluid adiabatically expands until the generator temperature is reached. This may not be lower than 1000°C, otherwise the combustion air could not be preheated sufficiently to obtain a temperature within the combustion chamber without oxygen enrichment. The BaO (or other) solid particles will assume the high temperature prevailing in the latter. The walls of the nozzle and generator channel have to be lined with a reflecting material, provided with reduced

cooling, if required. It is in the generator channel where heat energy is transformed into electric energy, in accordance with efficiency.

By applying this procedure it is to be expected that

the desired lower degree of ionization will be obtained in the generator channel even at low working-fluid temperature;

the service life of the electrodes and walls will become acceptably long;

the heat losses introduced by the walls will be moderate and, thus, low-capacity generators of high efficiency can also be built;

air preheating can be achieved by means of recuperation;

the expensive and relatively low-efficiency supplementary power plant increasing the specific investment cost and decreasing overall efficiency can be dispensed with and, last but no least, the plant efficiency will considerably increase, to about 65 per cent.

2. Closed-cycle generator

The basic task is to ensure the required degree of ionization, as an initial state, in the working fluid. There are several known methods available for reaching this aim, *e.g.* d.c. and a.c. electric fields, electro-magnetic radiation, injection of charged or uncharged particles, thermionic emission with substances of low work function, etc.

Referring to one of the methods listed above, mention should be made of the procedure applied by B. KARLOVITZ in a test rig of the *Westinghouse Electric Corporation* as early as in 1938: the ionization with a high-velocity electron beam [7]. As is known, the method has failed to become useful. This was commented by B. KARLOVITZ in the following words: "*Powerful electron beams were produced and introduced in the gas stream, but no voltage or current was generated. Later it was realized that stray magnetic fields deflected the electron beams to the walls and, consequently, the resulting ionization was very weak and not uniformly distributed.*"

These difficulties can be avoided now. Ionization by electron beams should be performed outside the generator, in a space protected from stray fields, in a tube having a wall not absorbing electrons and containing pure potassium gas. If the degree of ionization is very high in the potassium gas, the uneven distribution loses its meaning. It is the potassium ions and free electrons that are to be injected into the working fluid. The method described above is only one example from among the many possible ways from which the most practicable one should always be selected.

The required high temperature should be transferred to the BaO or other ceramic particles, in this or another way, outside the generator channel, and the particle should be injected together with the electrons into the gener-

ator channel. With reflecting walls the degree of ionization will not be reduced considerably.

The temperature of the working fluid in the generator can be made as low as required. This is an essential feature not only for extending the service life of constructional parts, but in case of closed-cycle operation, where the initial temperature is relatively low, for increasing the thermal efficiency.

Of course, the conventional supplementary plant may also be omitted in this case, efficiency will increase, and the MHD generator will become competitive with a gas turbine, with respect to both cost and efficiency.

It should be mentioned that this method also opens the way for designing a high-efficiency MHD compressor, which is desirable with a view to both the closed-cycle and open-cycle operation.

XII

In conclusion, in the light of the method described, a brief survey is given below of the present stand of MHD development, as may be found from relevant publications and papers presented at the various symposions. The picture obtained is not encouraging.

The *open-cycle* MHD generator seems technically solved, but its feasibility is questionable due to the following facts:

It can be used in units of such very high capacities that have not yet been tested;

the expectable efficiency — 45 to 50 per cent — fails to considerably supersede that of conventional units;

the high stresses — imposed especially on the electrodes and generator channel — will unfavourably influence service life and maintenance costs;

there is no proof, and neither is it probable, that a substantial advantage would be provided by this method, or, even, whether it could be made competitive at all;

the only remaining advantage, though important for future potentialities, is its suitability for building very large-capacity units.

The *closed-cycle* MHD generator is very backward with respect to the open-cycle version. From among its problems only one is worth mentioning: the non-equilibrium ionization required at relatively low working-fluid temperature is not solved yet.

*

Thus, the feasibility of the MHD system has become questionable. At any rate, development work would again be hopeful, if by means of further theoretical research and experiments, the method proposed would prove fully or partly practicable.

REFERENCES

1. HALÁSZ, D.—SZENDY, CH.: High-Grade Ionization in Cold Gas. *Acta Techn. Hung.* **58** (1967), 169—180.
2. *Status Report* on MHD Electrical Power Generation Nuclear Fusion; **7** (1967), 279.
3. HALÁSZ, D.—SZENDY, CH.—KOVÁCS, CH. P.: Electron Emission in MHD generators. International Symposium on Magnetohydrodynamic Electrical Power Generation (Paris) 1964.
4. LARY, E. C. et al. *U. S. Patent* 3, 139, 551 (1964).
5. WALDIE, B.—FELLS, J.: Experimental and Theoretical Studies of Gaseous Suspensions; Thermionic Emitting Particles for Use as MHD Working Fluids. Symposium on MHD, Warsaw 1968; Vol. II, 1173.
6. SCHMIDT,H.—FURTHMAN, F.: Über die Eigenstrahlung fester Körper. *Mitt. Kais. Wilch. Inst. Eisenforschung* (Düsseldorf) **10** (1928), 225.
7. Engineering Aspects of Magnetohydrodynamics. *Proceedings of the Third Symposium* 1962 (GORDON and BREACH), New York 1962; 196.

Weiterentwicklung des Verfahrens »Hochgradige Ionisation in kaltem Gas«. Für die Ionisation außerhalb des Gleichgewichts in MHD-Generatoren haben die Verfasser und andere mehrere Vorschläge gemacht, die auf verschiedenen MHD-Symposien diskutiert worden waren. Bis jetzt hat kein Vorschlag die daran geknüpften Erwartungen erfüllt. Nach einem neueren Vorschlag können ins Arbeitsgas eingebrachte, von glühenden Körnern emittierte Photone die Rekombination verringern. Die zahlenmäßigen Zusammenhänge müssen durch weitere theoretische Untersuchungen und Versuche bestimmt werden. Der MHD-Generator, insbesondere die Variante mit offenem Kreisprozeß wird praktisch dann verwirklicht werden können, wenn im Generator das Arbeitsgas auf mittlerer Temperatur (1200 ÷ 1800 °K) gehalten werden kann, wobei der vorgeschlagene Ionisationseffekt nützlich sein kann.

Усовершенствование метода «Высокой ионизации в холодном газе» *(Д. Халас и К. Сенди).* Авторами данной статьи и другими авторами в отношении ионизации вне равновесия в МГД генераторах представлено ряд предложений, которые были обсуждены на различных симпозиумах по МГД генераторам. До сих пор еще ни одно из представленных преложений не оправдало себя. На основе последнего нового предложения рекомбинация может быть снижена фотонами, эмиттированными из накаленных частиц, проникших в рабочий газ. Числовые зависимости должны быть определены на основе дальнейшего теоретического и экспериментального анализа. МГД генератор, а в особенности его вариант с открытым контуром практически может быть решен только в том случае, если в генераторе рабочий газ можно будет держать при средней температуре (1200 ÷ 1300° К), т. е. когда предлагаемый эффект ионизации может оказать помощь.

Acta Technica Academiae Scientiarum Hungaricae; Tomus 68 (1—2), pp. 29—49 (1970)

DEPENDENCE OF CATHODE PROPERTIES ON NEON DOPING AND DISCHARGE CURRENT

J. F. BITÓ
CAND. OF TECHN. SC.
RESEARCH INSTITUTE FOR ELECTRONICS, BUDAPEST

[Manuscript received November 5, 1968]

Up to the present time no experimental data have been published concerning the influence of neon-gas doping on the cathode properties of mercury vapour–argon discharges. In the course of our experiments it was possible to demonstrate the dependence of cathode fall, cathode spot temperature, length of cathode side spaces, the field strength of the positive column, the voltage drop and power consumption of the discharge tube on the partial pressure of neon. Furthermore the dependence of cathode properties on the discharge current has also been determined. The relationships obtained in the experiments have been interpreted in terms of the known plasmaphysical data.

I. Introduction

In the improvement of light utilisation (efficacy) of fluorescent lamps, and in increasing their specific power consumption (power on unit discharge path), neon is almost exclusively employed in addition to argon as a dope gas, in a suitable per cent to meet the particular requirements [1]. As has been demonstrated [1], neon has the capacity of increasing the share of positive column in the total power consumption of the discharge [1]. Among others this accounts for the fact that today neon is employed as a dope gas. However, the effects on the cathode side associated with its uses have as yet not been elucidated. The literature [1—3] contains only so much information that the life of the cathode coating and hence the life of the discharge tube as a whole, is reduced considerably with increasing amounts of neon doping added. BERNIER and GUNGLE [4] also carried out probe measurements in the vicinity of the cathode providing some information on the influence of neon doping on cathode fall and on the ion current (under conditions not fully elucidated). They wished to establish from the investigations the influence of filament voltage on the cathode in an argon-neon gas atmosphere, by employing a special electrode structure. Their objective was to utilise the results of investigations in the design of a new cathode structure. Published in the same source [4], those authors tried to establish relationships between the arcover stresses in argon and in neon-argon discharges and the cathode fall. However, no author has so far published information, for instance, on the unequivocal influence on cathode fall — a point of great significance for the usefulness of neon gas.

II. Experimental conditions, methods of investigation

The experiments were carried out with mercury-vapour/argon discharges of 1100 mm discharge path in hard glass discharge tubes of 36 mm inside diameter. During the tests, d.c. and a.c. arc discharges were produced (in a space containing 3 torr argon and 6×10^{-3} torr mercury vapour) between treble-filament oxide cathodes of identical construction. The effects of the neon doping were studied at an arc current of 430 mA. Ohmic and inductive current limiting was applied with d.c. and a.c. discharges, respectively. The method of investigation was a special cathode-side diagnostic system developed by us [7]. It has the following components: d.c. and a.c. probe measurements, measurement of emission and work function, pyrometric and electronic measurements of average cathode temperature and spot temperature, cathetometric determination of spot area, stoboscopic measurement of the dimensions of cathode space, scanning of the positive column by means of a double probe.

III. Results

1. Influence of the neon dope on the cathode

In our investigations, efforts were made to find fundamental relationships that would make the interpretation of the cathode-end influences possible. Fig. 1 shows the dependence of cathode fall V_c on the neon doping. As is

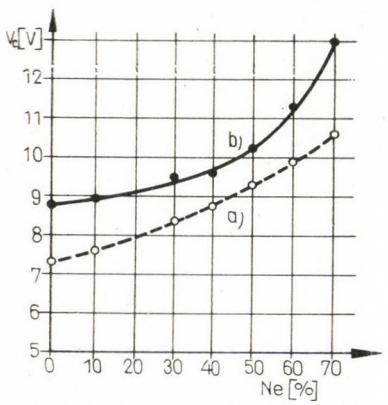

Fig. 1. Dependence of cathode fall V_c on neon doping, in d.c. (*a*) and a.c. (*b*) discharges

evident from the figure, the relationship found in former experiments [5] between d.c. and a.c. cathode falls remains unchanged, and a percentual increase in the amount of neon leads, in both cases, to increased cathode falls. The increment tends to be higher with increasing neon content.

Neon has a first ionization potential (21,47 V) higher than that of argon (15,69 V); on the other hand, its mass (20,18 amu) is only half that of argon

(39,94 amu). Both gases have ionization potentials by far exceeding that of mercury (10,38 V); on the other hand, their masses are much smaller than that of mercury atoms (200,61 amu). These properties determine the way in which they take part in the discharge processes; among other things, those properties give an account of the nature of special fundamental phenomena associated with the discharge processes. The experimental results to be described below have all been obtained in argon, at a pressure of 3 torr, at a discharge current of 430 mA, under the conditions described in the Introduction.

With reference to the ionization potentials and atomic weights mentioned above, it is evident from the experimental conditions that the electrons try above all to ionize the mercury atoms (this applies to excitations as well); accordingly, a direct participation of neon in the discharge process is not expectable. However, it may have an indirect influence on the discharge processes (as can be seen in Fig. 1). When, with the given gas pressure maintained, part of the argon atoms are substituted by neon atoms, dual influence will be exerted. The number of ionizations due to high-energy electrons will be reduced in the cathode space. This is because electrons which have a sufficient energy for the ionization of argon atoms are certainly not capable of ionizing neon atoms as well. Thus, a decrease in the ion current of inert gas (playing an important role comparable to that of mercury ions) may be assumed. However, that decrease has probably a lesser influence than the second effect associated with the appearance of neon atoms. As has earlier been pointed out neon atoms have masses smaller than that of argon atoms; accordingly, their collision cross-sections (in respect to electrons as well as positive ions) are far below those of argon atoms.

Having a lower probability of colliding with primary electrons emitted by the cathode, those neon atoms give, on account of their high ionization potentials, a small number of ions to the discharge process — less than that provided by argon atoms until they were, in part, substituted by neon atoms. As a result, the number of ions striking the cathode will be slightly reduced leading to a lower cathode temperature; this, in turn, will involve a drop in the emission current and a rise in the cathode fall.

Taking into consideration the fact that neon atoms involved in the discharge have masses (and, hence, probability of collision) lower than those of argon or mercury atoms, a further cathode-end process can be deduced which tends to increase the efficiency of the above mentioned ionization processes — also by detracting ions from the cathode face. The use of neon atoms produces an effect simulating a reduction in the diameter of the discharge tube (thus increasing the wall dissipations). This is because neon atoms, on account of their smaller collision cross-sections, impose a lesser restriction on the diffusion to the wall of the positive ions migrating towards the cathode. As a result, the wall dissipation increases and, moreover, fewer positive ions

reach the cathode, too, as compared with previous conditions of discharge in a pure argon atmosphere. Thus, again, the cathode-spot temperature decreases involving a drop of the emission current leaving the cathode; which following from the foregoing, the cathode fall must rise.

Accordingly, the use of neon as a doping brings about an indirect increase in the cathode fall through several by-effects, too, thus compensating for — and producing — the surplus ion current lost for the discharge on account of the presence of neon doping.

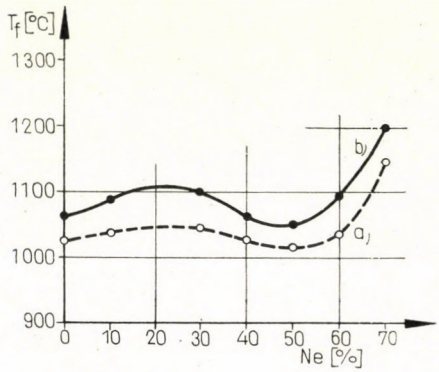

Fig. 2. Dependence of spot temperature T_f on neon doping, in d.c. (*a*) and a.c. (*b*) discharges

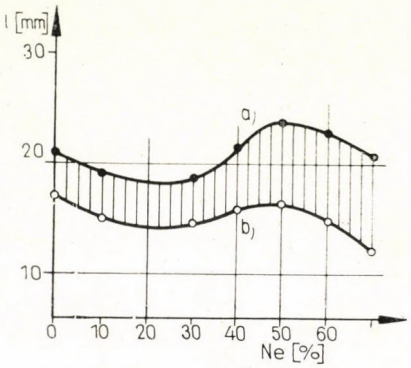

Fig. 3. Dependence of the length (*l*) of the Faraday dark space (*a*) and of the negative glow (*b*) on neon doping, in a.c. discharge

If, now, one considers Fig. 2 illustrating the cathode-spot temperature (T_f) plotted versus the percentual content of neon component related to argon, the relationship differs from that expectable on the basis of Fig. 1. Fig. 1 pointed to the conclusion that, with increasing quantity of neon doping, the cathode-spot temperature would fall, presenting a relationship between cathode-spot temperature and cathode fall, as that obtained with pure argon. To find an interpretation of the difference, one must again proceed from the assumption that the cathode maintains the discharge together with the cathodic spaces, and that their effects cannot be studied separately. In case of argon, an analysis of its pressure variations yielded relatively simple relationships; as evidenced in Figs 1 and 2, the influence of neon doping is more difficult to analyse. Yet, considering Fig. 3 illustrating the neon-dependence of cathodic spaces, some relationship can be demonstrated between the cathode-spot temperature and variations in the boundaries of cathodic spaces, similar to the above relationships concerning pure argon. In this instance, too, variations in the boundaries of cathodic spaces follow variations in cathode temperature. Fig. 3 relates to an a.c. discharge, but similar characteristics were obtained with d.c. discharges as well. The total dimensions of the spaces exceeded in each case the neon dependence, too, the dimensions obtained with a.c. discharges — i.e. the relationship found and

discussed in connection with argon [5] remained valid in this instance, too. Similarly, the relationship found previously between d.c. and a.c. cathode-spot temperatures [2] remained valid.

In our opinion, the relationship between Figs 1 and 2 is obscured by the fact that — as could be assumed with reference to the cathetometric spot-area measurements — the area of the cathode spot did not remain constant at different neon components; moreover, local discharges also occurred between the filament turns — introducing appreciable modifications of the cathode-spot properties (primarily its temperature). That interfering phenomenon, which, of course, affected the measurement of spot temperature as well, could not be eliminated even by the most careful precautions. Accordingly, whereas the experiments associated with discharges in pure argon atmosphere involved nearly constant cathode-spot areas, those made with neon doping involved variations in the cathode-spot area, too.

In the course of those experiments, though several repetitions of temperature measurements gave correct results, one parameter which was previously well controlled — the cathode-spot area — could not be kept under control. The cathode-spot area exhibited variations in the course of neon-dependence investigations that could be given an unequivocal interpretation. Though detectable, those variations could not be described in an unambiguous manner on account of the cathode construction. They probably involved a change in the number of electrons leaving the cathode but this phenomenon had presumably no influence on the velocity of emitted electrons.

If this assumption is accepted, it will be possible to give an interpretation to the unchanged relationship between the spot temperature measured and the cathodic spaces. This is because the dependence of cathodic spaces on the cathode spot must remain if it is assumed that, at a given spot temperature, variations in the cathode-spot area affect, in the first approximation, only the number of electrons emitted by the cathode, leaving their initial kinetic energy unaffected. This is because the cathodic spaces perform above all the functions of an appropriate acceleration and, subsequently, homogenization, of the electrons emitted by the cathode. It is only the cathode fall and the cathodic dark space (situated in the corresponding negative glow) which take part in the active production of electrons by ensuring the positive space charge (composed of ions) and the ion current impacting on the cathode. Thus, if our initial assumption is correct, variations in the cathode-spot area are primarily responsible for the alteration of the relationship between the cathode fall and the cathode-spot temperature.

If it were possible to determine the dimensions of the cathodic dark space, the lack of knowledge on the actual cathode-spot area (and its variations) would probably introduce a factor of error in those measurements as well. In this instance, the measurement cannot even be carried out on account of

the filament structure. A much simpler case is presented e.g. by flat-cathode tubes permitting variations in the cathode spot to be followed in a much more convenient manner. Regardless of all these points, neon — which has thermal conductivity properties superior to those of argon — influences the cathode-spot temperature and area and, hence, the energy equilibrium, in a manner not yet elucidated. This phenomenon, which is partly beyond our control, is not discussed here in detail because, in the lack of knowledge on a fundamental parameter (spot area), only approximative assumptions could be made which cannot be controlled and checked.

As regards their character, the cathodic spaces shown in Fig. 3 vary with the cathode-spot temperature; however, in this case, even the spot-dependence of cathodic spaces does not provide a straight line. It is a descending quadratic curve. Since a comparison of Figs 2 and 3 will reveal that relationship (which was discussed in detail in the foregoing), the function is not presented here (it can be easily reconstructed from the curves). However, it is worth noting that the hachured area in Fig. 3 (representing the axial dimension of the Faraday dark space) tends to increase with the percentual content of neon doping. Accordingly, the more argon atoms are substituted by neon atoms, the longer Faraday dark space will be necessary. This, again, points to the conclusion that the homogenization function of the Faraday dark space cannot be fulfilled by neon atoms as adequately as was fulfilled by argon atoms. In other words, the energetical homogenization of electrons can be ensured by argon atoms even along a shorter space. This, again, may be attributed to different probabilities of collision (resulting from the different masses of atoms of the two inert gases).

With reference to Fig. 3 (taking into account the data of Figs 1 and 2 as well), an optimum neon quantity can be selected that is useful for the discharge but will not increase the cathode dissipations appreciably and, at the same time, will not adversely affect the economy of discharge through the dimensions of the cathodic spaces. Since the cathode fall exhibits a monotonously increasing trend, and the cathodic spaces have a minimum at a neon doping of 20%, it is useful to employ a small neon content provided that the emission coating of the cathode (the emitter) is so constructed as to withstand severe stresses and high spot temperatures without damages. Fortunately, the rise in the temperature of the cathode spot is as low as about 50 °C upon addition of 20% of neon doping. Accordingly, if neon is to be used in the discharge tube as a doping, the introduction of about 20% of neon would seem to be practical, with a view to minimum cathode-end dissipations. Observing the cathode-end dissipations alone, the use of neon in an amount greater than that would considerably impair the economy of the discharge tube.

Apart from influencing the cathode end, neon affects the field strength of the positive column as well. Fig. 4 shows the neon-dependence of field

strength values E measured in a.c. and d.c. discharges. That relationship is not linear, the a.c. field strengths being again higher than the d.c. values. The curve representing d.c. discharge conditions is not a new discovery. It has already been studied by LEMAIGRE-VOREAUX [6] who plotted field strengths versus the ionization potentials and atomic weights of various inert gases, yielding a straight line. Furthermore, he studied binary mixtures as well, but could not find any typical relationship. However, the a.c. field strength curve shown in Fig. 4 has so far not been published in the literature.

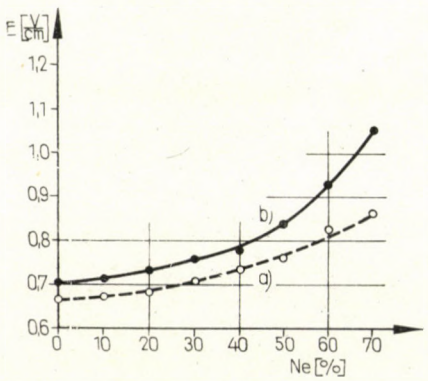

Fig. 4. Dependence of field strength E of the positive column on neon doping, in d.c. (*a*) and a.c. (*b*) discharges

To give an interpretation of those curves, one must proceed from the assumption that the interactions involved in the discharge are altered by substituting part of the argon atoms by neon atoms. Similar to the cathodic space, neon atoms do not take part directly in the discharge in the positive column either — or, at least, their direct influence is negligible compared with their indirect influence. A considerable part of the ions moving in the positive column avoid reaching the wall and, hence, recombination on the wall, at the expense of elastic collisions and the accompanying energy dissipations. Neutral mercury and argon atoms are the collision partners. If the probability of collisions is reduced (e.g. as a result of reduced size of the collision partner), the number of ions reaching the wall of the discharge tube will grow. However, charges lost as a result of wall diffusion ion migration has to be supplied in some way. Those dissipations are compensated for by the positive column by upsetting the equilibrium conditions (increasing the field strength).

As a result, the number of ionizations will increase, to a certain extent compensating wall dissipations. On the other hand, owing to the increased field strength, the drift velocity of positive ions migrating towards the cathode will also increase, resulting in a lower wall diffusion current. Those two effects together produce the condition that the discharge is maintained with the

discharge current determined by the external electric circuit. This means that the increase in field strength is a "defensive action" by the positive column, whereby it compensates for the losses in charge carriers caused by the substitution of neon atoms for a part of the argon atoms.

In the Introduction it was mentioned that the use of neon imposes a hard stress on the cathode coating as well. This effect can also be deduced from the above mechanism. Neon atoms staying in the vicinity of the cathode offer a less adequate protection against ions striking at the cathode than that

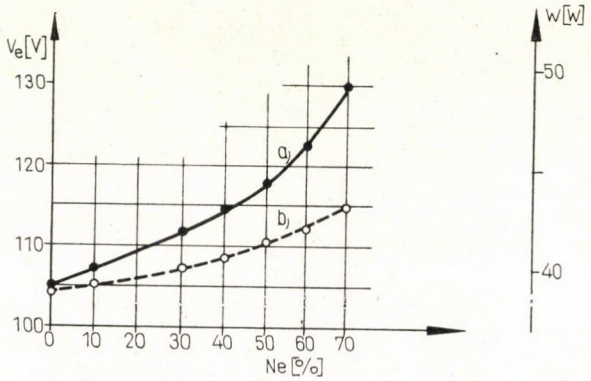

Fig. 5. Dependence of the voltage drop V_e (*a*) and power consumption W (*b*) of the discharge tube on neon doping, in a.c. discharge

provided by argon atoms (heavier in weight and having larger diameters). As a result, the presence of neon doping simulates a condition in which the pressure of pure argon atmosphere has been reduced. Both factors lead to the same result — a rapid consumption of the cathode coating both thermally (evaporation) and mechanically (powdering).

The two curves of Fig. 5 show the neon-dependence of the burning potential (V_e) and power consumption (W) of the discharge tube. Both curves represent a.c. discharge conditions (more useful from a practical point of view); besides, the courses of the curves are the same in d.c. discharge conditions as well. Anyway, in this instance, some principal components of the burning potential exhibit an identical type of dependence so that the curve representing their sum total exhibits the expected course. Our supplementary measurements have shown the anode fall to increase with the percentual share of the neon component in both a.c. and d.c. discharge conditions. The power curve, also shown in Fig. 5, follows the course of the burning-potential curve since the discharge current was maintained at a constant level during the measurements.

Comparing the results obtained with pure argon [5] and with a neon-argon gas mixture, it may be stated that — though the presence and influence

of neon could be detected fairly well — the discharge conditions are altered e.g. by varying the spot area to such an extent that a description thereof based on the fundamental relationships and their correlation was difficult to present. Although the studies of the applicability of neon and the related fundamental knowledge and relationships are also of great significance from an industrial point of view, yet their theoretical (and especially experimental) investigations are confronted with serious difficulties, requiring an extremely large-scale apparatus coupled with continuous multilateral checkup. According to our knowledge, nobody has yet undertaken a theoretical investigation of the role of neon under the discharge conditions here described (bearing great significance from a practical point of view as well). The relationships and interpretations given by us in the foregoing may now form a basis for more detailed calculations concerning cathode dimensioning which can be best made by proceeding from the equilibrium conditions of the cathode.

2. Current dependences

Apart from the pressure dependences of cathode-end parameters (and their influence by means of neon doping), remarkable findings are expectable (from both scientific and practical points of view) from their investigation as the function of discharge current.

The experiments were carried out under discharge conditions associated with 40-watt fluorescent tubes (providing the invariable reference standards), using several tubes the same time. The measurement was aimed at extending our knowledge on cathode-end parameters to other discharge currents (in addition to the nominal discharge current of 430 mA specified for 40-watt fluorescent lamps). Accordingly, the investigations were made in a spectral-pure argon atmosphere at 3 torr and 25 $\pm$ 1°C determining the pressure of mercury vapour in the discharge tube.

Prior to the commencement of the measurements, investigations were made by cathetometric measurements to check whether the cathode-spot area varies in the range of the discharge current studied by us (250 to 600 mA). While it was difficult to locate the spot in the previous investigations associated with neon dependence, this time we were able to clearly establish its constant dimensions as well. Since the spot temperature could be measured well in the course of the investigations also carried out in argon, which was found to be independent of gas pressure, too, the conclusion may be drawn that the presence of neon upsets the argon-mercury equilibrium of the cathode spot (established in the discharge) by its specific properties assumed in the foregoing. This may manifest itself not only in variations of the cathode-spot area but also in blurring of the spot boundaries, as if they were due to a secondary local discharge process caused by the neon gas alone. On the other hand, the dimen-

sions of the cathode spot are, in this instance, independent of variations in both the argon pressure and in the discharge current throughout the range mentioned above.

It may be stated with reference to the above conclusion that the location, dimensions and temperature of the cathode spot observe a "minimum" rule. Of course, external parameters (gas pressure, location of emitter, quality of coating etc.) have a contribution to this process, but the function performed by the discharge current is nonetheless important. According to the results

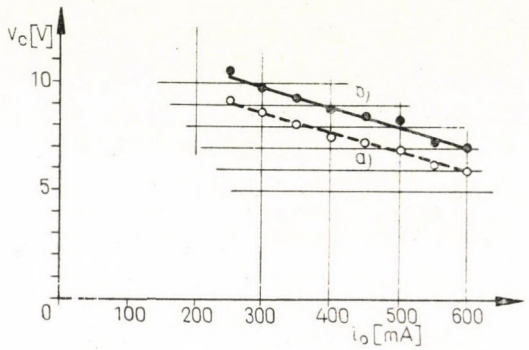

Fig. 6. Dependence of cathode fall V_c on discharge current i_0, in d.c. (*a*) and a.c. (*b*) discharges

of preliminary experiments mentioned in the Introduction, the changes in pressure or the increase of the discharge current will not alter the spot dimensions — rather its temperature and surface current density, thus adapting cathode-end conditions to a mode of operation better suited to the new discharge conditions. Accordingly, in an argon-mercury vapour discharge, no changes in pressure or in discharge current have an influence on the spot dimensions (in the range studied by us); a more powerful, decisive influence is exerted by the location and physical parameters of the emission coating (emitter).

In determining the current dependence of cathode-end parameters, the course of the cathode-fall curve is presented in the first place (shown in Fig. 6 for d.c. and a.c. discharge conditions). As evidenced by the figure, the a.c. cathode fall again represents a higher value, supporting the qualitative interpretation offered in the first discussion.

As was expected, the cathode fall tends to decrease with increasing discharge current i_0. As the tube operates in the arc discharge range of negative characteristic, this means that the cathode fall actually follows the burning-potential characteristic.

Another remarkable feature of the relationship of Fig. 6 is its linearity, permitting relatively simple relationships to be sought for. Thus already two data are available concerning the cathode behaviour in this instance. It is

a known fact that the cathode end provides the electrons required for an increase in the current without altering the dimensions of the cathode spot (even when the cathode fall is decreasing). Presumably, the increase in the surface current density of the cathode is primarily limited to the cathode spot; as a result, an increase in the cathode-spot temperature is also expectable. This assumption is confirmed by the current dependence of the cathode-spot temperature shown in Fig. 7. As will be seen in the Figure, the a.c. discharge again has a higher cathode-spot temperature than the d.c. discharge. The

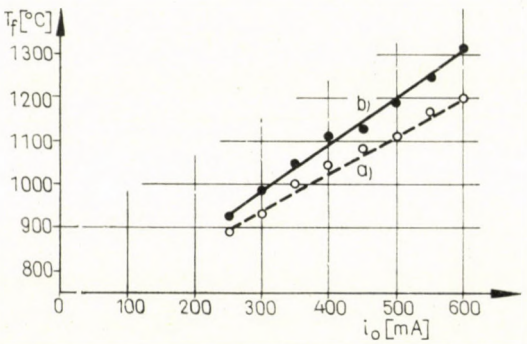

Fig. 7. Dependence of spot temperature T_f on discharge current i_0, in d.c. (*a*) and a.c. (*b*) discharges

increase in the discharge current involves, in both cases, a rise in the cathode-spot temperature. A comparison of the curves in Figs 6 and 7 shows an increase in the spot temperature which is sufficient for producing the increase in current (it will be seen that the cathode fall decreases with increasing spot temperature at different discharge currents).

As compared with the relationships presented so far, the current dependences have a radically different character. Whereas, in the previous experiments the constant level of the discharge current was invariably a fixed point of reference, now it is just this parameter that will be varied. Although the cathode-spot area was found to be constant, nevertheless — since a majority of electrons introduced in the discharge by the cathode are supplied by the cathode spot — its surface current density also tends to increase nearly in proportion with increasing discharge current. Thus, those investigations are aimed at finding common characteristic features of the current producing processes of the cathode surface at different discharge currents (cathode-surface current densities).

The possibilities associated with the increase in current density are given in scalar relationship

$$j = n \times e \times v \qquad (1)$$

where j absolute value of current density (distribution function);
n concentration of charged particles (distribution function);
e elementary charge;
v velocity of charged particles (distribution function).

Hence, it is evident that the current density may be increased in one of two ways: by increasing the number of charge carriers produced in unit time or, simultaneously or independently, increasing the velocity of charge carriers. Transferring this statement to the cathode-end processes of discharges, it may be stated in first approximation (ignoring the volumetric and wall dissipations) that the increasing discharge current imposes double requirements on the cathode — more electrons, and at a higher velocity, must be fed from the cathode to the positive column. This is because the increase in current is — unless accounted for by some external factor — ensured by the discharge through varying more than one parameter. Accordingly, an increase in the emission current of the cathode is expectable — but so is an increase in the length of the accelerating space (cathode fall region). As is evident from Figs 6 and 7, the discharge had to increase considerably the cathode-spot temperature (in addition to producing a decrease in cathode fall) in order to permit a current determined by the external circuit of the discharge tube to flow between the electrodes. However, this does not give a complete description of the relationship between the discharge and the cathodic spaces. The accelerating effect of the cathode end also depends on the length of accelerating spaces. Fig. 8 shows, at various discharge currents, the locations and dimensions of the cathodic spaces of oxide-cathode discharges under the conditions of d.c. and a.c. discharges. In this instance, too, the filament coil is arranged at point $l = 0$.

The statement also applies to various discharge currents that the positive-end boundaries of the cathodic spaces are located farther from the cathode in a.c. discharges than in d.c. discharges.

Fig. 8 reveals a remarkable relationship between the location of the cathodic-space boundaries and the discharge current. The boundary of the negative glow is recessing from the cathode with increasing discharge current (in both a.c. and d.c. discharges), whereas the boundary of the Faraday dark space draws closer to the cathode filament. This means that, of the cathodic spaces, the axial dimensions of the Faraday dark space tend to decrease with increasing axial dimensions of the negative glow.

To give an account for this phenomenon, one must proceed again from the function of the cathodic spaces. The potential drop (cathode fall) occurs in the cathodic dark space included in the negative glow; that potential drop will accelerate the electrons emitted by the cathode; moreover, in regions close to the negative glow space, it will also indirectly supply the losses of those spaces (by aid of multiplication processes). The Faraday dark space

following it has no electron producing function — its primary function being the energetical homogenization mentioned in the foregoing.

Now again considering relationship (1) and accepting the interpretation giving a good approximation in connection with it, it may be stated that the generation of charge (in this instance, electron emission and volumetric ionization) is performed by the cathode and by part of the cathodic dark space, whereas the acceleration of the charges produced (electrons) is performed by the cathodic dark space as a whole. Accordingly, the Faraday dark space performs no direct function in ensuring the rise in current. As has already

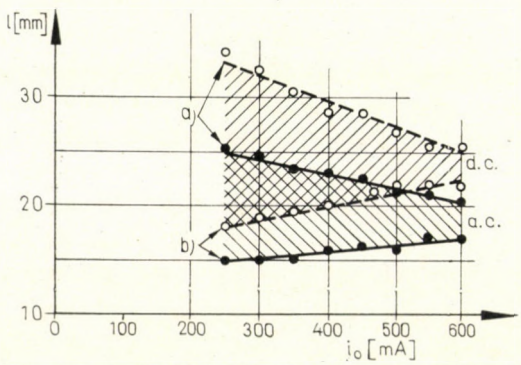

Fig. 8. Dependence of the length (l) of the Faraday dark space (a) and of the negative glow (b) on discharge current i_0, in d.c. and a.c. discharges

been mentioned, the cathode end ensures the adaptation to the new conditions presumably by means of one way of increasing the current density but, by adjustment of all available facilities, produces electrons in the required number and with the desired velocity in accordance with an energy-minimum requirement. This is also made evident by the experimental results: the cathode fall decreases with increasing discharge current (Fig. 6) but the cathode-spot temperature rises (Fig. 7) accompanied by an expansion of the axial dimensions of the negative glow including the cathodic dark space (Fig. 8). Accordingly, two parameters of cathode mechanism studied by us (and regarded as fundamental ones) exhibited simultaneous variations. The remarkable feature of this phenomenon is further increased by the fact that all the three fundamental parameters — which are inseparable from each other — are in a linear relationship with the discharge current.

In this instance, too, it would be possible to specify a linear dependence of cathode fall on spot temperature; however, on account of the varying current density on the cathode face, this would be a mere comparison. The curves of cathode fall plotted with reference to the data of Figs 6 and 7 exhibit a descending trend with increasing spot temperature. Even the possibility of interconnecting some of those points is disputable since they pertain to

different discharge currents. The only common characteristic in both cases is the constant spot area. This, however, as was earlier pointed out, is typical of the proper ties and location of the emission coating of the cathode (the emitter) rather than of the cathode-space mechanism. The discharge processes have a decisive influence on the stress of the cathode through the cathode spot; a two-way transmission of that influence is performed primarily by the electron emission and the positive ion current. Thus, no constant cathode stress may be conceived on the part of the discharge unless the current density at the cathode face is maintained constant. This, of course, is again a statement of limited accuracy, whose approximative nature can be judged by the energy-equilibrium calculations already mentioned several times.

The constant current density at the cathode face was, to a good approximation, taken for granted in the relationships concerning the pressure dependences (presented at the beginning of the experimental section). In the studies on the effects of neon doping, no constant current density at the cathode face (or in the cathode spot) could be conceived on account of variations in the cathode-spot area (although the discharge current was maintained at a constant level). On the other hand, in connection with the current dependence at present under test, the current density at the cathode face again cannot be regarded as constant on account of the type of studies and the constancy of the cathode spot. In lack of comparability, this prevents the establishing in connection with cathode fall, spot temperature and cathodic spaces. Accordingly, it would be erroneous to draw any conclusion e.g. on cathode fall and cathode-spot temperature from the data of Figs 6 and 7. This is the reason why no detailed analysis was given, at the time of studying the function of the neon component, to the relationship between the cathode fall and the cathode-spot temperature. While, in that case, the cathode-spot area was the variable factor, here its current was varied in accordance with the particular type of experiment.

Taking the relationships between the three fundamental cathode-end parameters together, only the following statement can be made. Changes in the discharge due to increased current simultaneously affect all the three fundamental parameters. The cathode performs its functions with an emission current increased in proportion with the rise in cathode-spot temperature but with decreasing cathode fall; on the other hand, the range of the cathode fall increases. Based on the foregoing, the conclusion may be drawn that the emission current of the cathode increases with rising spot temperature (or with rising average cathode temperature). This is because the assumption appears to be true (which cannot, however, be checked) that the dimensions of the negative glow are primarily determined by the range of the cathode fall, the dark space, and the changes in axial dimensions, found by us, are due approximately to changes in the dimensions of the cathode-fall region. This

assumption appears to be acceptable with reference to the parameters of the cathodic spaces [5] as well.

Maintained at a constant level, the current density at the cathode face must provide a fundamental point of reference for both the dimensional investigations of cathodic spaces and the search of relationships concerning the phenomena taking place on the cathode as well as on the cathode face. The relationships shown in Fig. 8 (dependence of cathodic spaces on the discharge current) also have the remarkable feature that each point of the straight lines (giving approximative relationships for cathodic spaces) pertains to a different discharge current. This means that the electron current as well as the ion current striking the cathode vary from point to point (in terms of the curve). Again, proceeding from the statement [7] made on the energy balance, it may be stated in relation to the simplest case (d.c. discharge) that the ion current represents the principal component of the positive energy transport to the cathode. Of course, its magnitude is directly related with the electron current (under given discharge conditions) and, owing to its very nature, changes in the latter represent the more decisive factor determined — under given discharge conditions — by the cathode structure as well as by the properties and location of the emission coating.

The interaction range between the electron current and the ion current is the space extending from the cathode as far as the end of the negative glow space toward the positive end; the most important link is the discharge mechanism of the cathodic dark space (within that, primarily the space charge distribution determining both the cathode fall and the ionization processes). Hence, a relationship may be assumed to exist between changes in the ion current and in the discharge current. The ion current is also directly typical of the cathode mechanism and the nature of electron production; its magnitude depends not only on the type of discharge processes taking place in the cathodic dark space but also on the particular mode of cathode operation, on the particular typical emission current range (saturation region or the current range limited by the space charge). Our observations have shown the cathode to be characterized in this instance by the electron production limited by the space charge. The same space charges, located right at the cathode face, influence the positive ion current striking the cathode as well.

All things considered, information should be gained on the phenomena of ion currents, fundamental for cathode operation. Probe measurements would appear to be the most practical means to this end, but for knowledge of interfering effects of oxide-coated cathodes. This manifests itself above all in some particles of the emitter coating impacting on the probe located in the neighbourhood of the cathode followed by condensation of those particles on the probe; as a result, the surface properties of the probe and, hence, its work function are altered, preventing accurate measurements. Thus these

means cannot be applied. On the other hand, it has been ascertained that the positive energy transport associated with the bombardment of positive ions is an important component of the energy equilibrium. Proceeding from this statement, the assumption was made (regarded as a satisfactory one) that, under given discharge conditions, a relationship exists between the ion current and the cathode-spot temperature, considering the two parameters to be proportional and co-varying under various influences. This could be made without any difficulty in the case of d.c. discharge because some calculations based on approximative energy equilibrium conditions (not to be discussed here in detail) also pointed to the conclusion that, upon attainment of equilibrium conditions, a proportionality did actually exist between the ion current and the spot temperature. But that relationship can be transferred to a.c. discharge conditions as well (on the basis of functional relationships discussed earlier), although in that type of discharge the energy transport during the anodic half cycle (primarily the electron current) does not demonstrate this relationship too clearly; under such conditions, even the approximative calculations based on the energy equilibrium do not give such unequivocal results. However, it was obvious that the spot temperature varies in an a.c. discharge in a manner similar to d.c. discharge — but, owing to phenomena taking place during the anodic half cycle, in a temperature range always higher than that associated with d.c. discharge. Taking this for granted, it may be stated that a cathodic parameter was found in both d.c. and a.c. discharge conditions that is directly related with the ion current arriving at the cathode and proportional to it in magnitude — under the conditions of a given cathode construction and emitter properties (this is a fundamental specification). This is the cathode-spot temperature which, of course, provides information not only on the magnitude of ion current but also includes several parameters whose variations were eliminated for the present discussion by keeping them at a constant level.

With good approximation, this consideration may be applied to the pressure dependence of cathode parameters as well. No detailed discussion of this problem will be presented here because, at this point, we have to analyse the highly important functions performed by the electron-current and ion-current components in connection with the investigation of current dependences. Even thus far, the relationship to be presented below has been tacitly utilized; instead of probe measurements (which are practically impossible to carry out unequivocally and in a well reproducible manner), the spot temperature was used as a basis of conclusions concerning all phenomena in which ion current performs a function. Thus, through elimination of an uncertain measurement, a parameter has been found that provides information not only on ion current but also permits relationships to be established for a number of other parameters. It should be added here that, in the course of the

work to be described here, our main concern was the relationship between the fundamental parameters, not the values of micro-parameters taking part in the formation of the fundamental parameters (being undeterminable anyway).

Accordingly, in the course of investigations on current dependences, the ion-current component increased proportionally with the discharge current (with reference to Fig. 7); furthermore, that process was responsible above all for the generation of the adequate quantity of electrons required for the discharge, too.

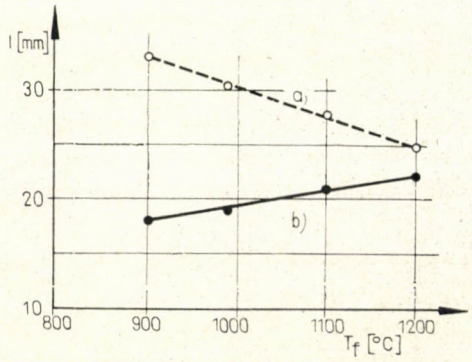

Fig. 9. Dependence of the length (l) of the Faraday dark space (a) and of the negative glow (b) on spot temperature T_f, in d.c. discharge

Considering all these points, in the dimensional studies of cathodic spaces, one must make a distinction between the cathodic dark space (ensuring the cathode fall), including the negative glow, and the Faraday dark space. Although the curves of Fig. 9 representing the dependence on spot temperature of cathodic spaces in d.c. discharges contain points, each of which pertains to a different current density, yet — for the above considerations in connection with ion currents — those curves give a somewhat clearer picture than Fig. 8. It follows from the foregoing that an increase in the ion-current component (in proportion with the rise in spot temperature) will not only permit a decrease in cathode fall (Fig. 6) but will also increase the range of cathode fall which, based on the foregoing considerations, is regarded as the most active region of the negative-glow space section, determining the dimensions of other factors involved. Similarly, there are multiple relationships between the ion current, the ion concentration and the cathode fall on one hand, and the cathode-fall ranges on the other. The magnitude of ion current is influenced by the cathode fall and, through the ion concentration, by the axial length of the cathodic dark space as well. Through a feedback mechanism, the ion current and, hence, other cathodic parameters (spot temperature, cathode fall) are set at a value — in accordance with the electron emission and further electron

generation in the cathodic space — which is ultimately determined by the external circuit by limiting the discharge current.

In the course of the experiments here described, the discharge current was varied systematically. Accordingly, both the cathode-surface phenomena and the volumetric phenomena in front of the cathode responded jointly to the current variations. Fig. 9. shows that, in respect to the cathodic spaces, the negative-glow region plays a decisive role in both charge-carrier generation and acceleration, whereas the importance of the Faraday dark space is gradually declining with increasing current density. Nor was it expected, on the basis of our previous knowledge concerning the cathodic spaces, that the dimensions of the dark space would be influenced by an increase in the ion-current component. The spot temperature shown in Fig. 9 is proportional to the dependence on ion current (in harmony with our previous statements); on the other hand, Fig. 8 shows the cathodic dark space plotted versus the entire discharge current. In both cases the function of that region decreases with increasing current. From the viewpoint of ion current, the function of that region may indeed decline since from that region only few positive ions even reach normally the cathode (through the cathode-fall range), and the flow of positive ions is determined — as far as the centre of the negative glow region — by the diffusion processes. With the discharge current increasing, more and more positive ions are required, and the diffusion processes contribute to their generation to a declining extent — primarily on account of the space-change conditions and, secondarily, by the nature of diffusion processes.

The generation of electron current is performed by the emitter of the cathode and, secondly, by the cathodic dark space. As has been pointed out in the foregoing, of the cathodic spaces both the negative glow space and the Faraday dark space are primarily associated with the energetical homogenization of the electrons. As is evident from Figs 8 and 9, this function gradually becomes less important with increasing discharge current; it is conceivable that the energy spectrum of electrons entering the positive column not only increases in an average sense but also becomes more co-ordinated, representing a closer approximation to an energy spectrum that may be described with the Maxwell–Boltzmann distribution.

Fig. 10 shows the current dependence of potential gradient E measured in the positive column. Like the current dependence of the cathode fall (Fig. 6), it can also be characterized by a straight line of negative slope. According to supplementary measurements, the current dependence of the anode fall can also be described by a similar function. Hence, it appears to be natural that the burning potential V_e of the discharge tube also exhibits an increasing trend with increasing discharge current (shown, together with power consumption W, in Fig. 11). Despite the decrease in burning potential, the power-consumption curve steeply ascends with increasing discharge current.

The potential-gradient curves of Fig. 10 intersect one another in the discharge current range of 500 to 600 mA in each discharge tube tested. Beyond that point, the field strength of the positive column in a d.c. discharge exceeds that obtained in an a.c. discharge.

It is evident from the relationships presented so far that both the ion current and the electron current increase with the discharge current. As the

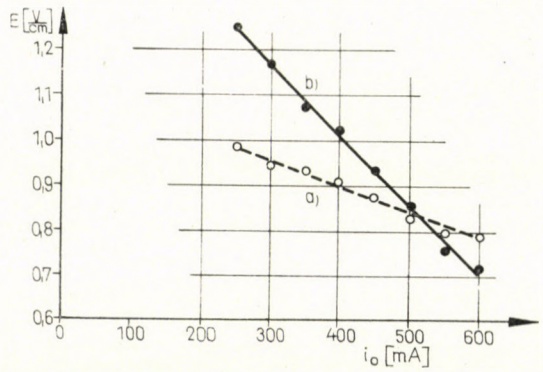

Fig. 10. Dependence of field strength E of the positive column on discharge current i_0, in d.c. (*a*) and a.c. (*b*) discharges

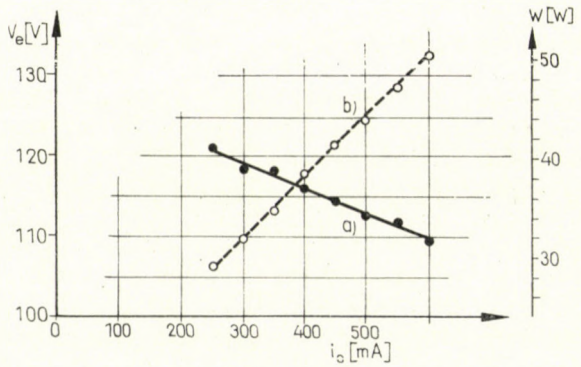

Fig. 11. Dependence of voltage drop V_e (*a*) and power consumption W (*b*) of the discharge tube on discharge current i_0, in a.c. discharge

increase in the ion-current component is closely related with the increase in the electron-current component, the quotient of the two currents is, under given discharge conditions, closely related again with the emission properties of the cathode. Under the conditions of a d.c. discharge, it may be stated with a reasonable degree of approximation that — if the quotient of electron current and ion current is small (essentially, this quotient is, in a figurative sense, obtained from factor γ_i integrated for the number of ions arriving at the cathode face and allowing of interpretation in a similar manner) — this will point to poor emission properties of the cathode because the secondary

emission (the fundamental process of thermal ion generation) has a low efficiency; therefore, at a given cathode fall and discharge condition, too many ions have to strike the cathode to the quantity of electrons required for the discharge.

In connection with this statement, the term "given discharge conditions" refers above all to a constant cathode fall, length of cathodic dark space and dimensions of cathode spot. In the change here discussed (associated with the current increase), the increasing ion current caused a rise in the cathode-spot temperature and the resulting higher electron concentration dispensed with the need of a great cathode fall. On the other hand, however, the requirement of increasing ion currents necessitated an increase in the axial dimensions of the negative glow (in accordance with the relationships presented). In the arc-discharge current range, it is at those current densities that the cathode actually becomes a thermionic cathode; at that point, the role played by the cathode coating becomes predominant (in self-sustaining discharges). This is why, in this instance, the emission current of the cathode is far from the saturation range — demonstrated by actual experiments with the same tubes. On the other hand, this means that the electron current emitted by the cathode tends to increase linearly with temperature along the small section investigated by us. This accounts for the fact that the functions of cathode fall, cathode spot and emission current presented so far (representing rather simple conditions) can be described with a straight line. Although, as has been mentioned in the Introduction, the field strength in front of the cathode may contribute to the emission by the cathode (Schottky effect), this effect remains apparently negligible compared with the thermionic effect in the cases studied by us (where linear relationships were obtained).

The results of experiments with neon doping could not be expressed as linear relationships — presumably because of the reasons mentioned there. However, in all the three cases, emission processes arose with the cathode, limited by the space charge and located outside the saturation current range. According to approximative calculations, the field strength in front of the cathode did not exceed in any of the cases 10—50 V/cm (in the average) — a fact pointing to the subordinated role of the Schottky effect. On the other hand, this brings about evidence of the high-grade construction of cathodes in those fluorescent lamps. By the use of a cathode coating enhancing the electron emission the work function of the cathode is reduced and the cathode operation is made more economic. In this way, the high accelerating field in front of the cathode and the great cathode fall will be dispensed with. It is evident from the foregoing that the electron emitter coating of useful properties has made possible a direct reduction of the cathode fall. However, as has been pointed out earlier, the dimensions of the cathodic spaces, and the cathode fall proper, are dependent — in addition to the properties of the

emitter and the construction of the cathode filament — on the cathode-spot temperature (as a fundamental parameter) as well as on the gas pressure, the neon doping and the magnitude of discharge current. Although no investigation has so far been made on the effects of auxiliary electrodes in the cathode space, their presence is also likely to influence both the fundamental parameters and their relationships.

REFERENCES

1. Summary Report of Bródy Laboratory of "HIKI", Department No. 114; 1965.
2. Van Boort, H. J. J.: *Philips Technische Rundschau* (1963/64), 90.
3. Van Boort, H. J. J.—Kolkman, D.: *Philips Technische Rundschau* **20** (1958), 1.
4. Bernier, C. J.—Gungle, W. C.: *Ill. Eng.* **53** (1958), 32.
5. Bitó, J.: Candidate Dissertation; 1966.
6. Lemaigre-Voreaux, P.: *Bull. de la Soc. Franç. Électr.* **4** (1963), 42/2.
7. Bitó, J.: Doctorate dissertation; 1968.

Die Abhängigkeit katodischer Eigenschafter von dem Neon Zusatz und von dem Entladungsstrom. Bisher wurden keine solche Daten von Experimenten behandelt, die den Einfluß des Neon-Zusatz-Gases auf die katodischen Eigenschaften der Quecksilberdampf—Argon Entladungen angegeben hätten. Als Resultat unserer Experimente haben wir nachgewiesen, daß der Katodenfall, die Brennflecktemperatur, die Länge der katodischen Gebiete sowie die Feldstärke der positiven Säule, der Spannungsabfall und die Leistungsaufnahme der Entladungsröhre von dem partialen Druck des Neons abhängen. Die Abhängigkeit der katodischen Eigenschaften von dem Entladungsstrom wurde ebenfalls festgelegt. Die Zusammenhänge wurden mit Anwendung der bisher gekannten plasmaphysikalischen Daten interpretiert.

Зависимость катодных свойств от добавки неона и от разрядного тока *(Й. Ф. Бито.)*. Экспериментальные данные, описывающие влияние разрядов добавочного неонного газа и ртутных паров — аргона на катодные свойства, до сих пор еще не были опубликованы. Зависимость падения напряжения на катоде, температуры катодного пятна, длины катодных пространств, а также электрического градиента положительного столба, далее падения напряжения разряда и ее мощности от парциального давления неона показана, как результат наших исследований. Зависимость катодных свойств от разрядного тока определена таким же образом. Найденные соотношения интерпретированы использованием плазменно-физических данных, известных до сих пор.

Acta Technica Academiae Scientiarum Hungaricae; Tomus 68 (1—2), pp. 51—72 (1970)

ANALYTIC CALCULATION OF DIRECT OR COUNTERFLOW HEATING OF SOLID CHARGES

K. SEITZ and J. FÜLÖP

[Manuscript received May 9, 1967]

The paper deals with the calculation of the heating of a solid charge by direct or counter current. The partial differential equation systems describing the physical processes examined in the paper are solved by the help of a new method called "non-orthogonal" extension. With the above outlined calculating method the mathematical description of such heating processes becomes possible in the course of which — owing to the interaction of the two media — the temperature of the heat transporting medium changes continuously.

Symbols

$T = T(x, y)$	temperature of the charge depending on its location [°C];
$T' = T'(x, y)$	temperature of the heat transfer medium [°C];
T_0	homogeneous temperature of the heat absorbing medium at entry [°C];
T_0'	temperature of the heat transfer medium at entry [°C];
v	rate of travel of the heat absorbing medium [m/h];
v'	flow velocity of the heat transfer medium [m/h];
α	coefficient of convective heat transfer [kcal/m²h °C];
λ	coefficient of heat conductance of the heat absorbing medium [kcal/mh °C];
c	specific heat of the heat absorbing medium [kcal/kp °C];
γ	bulk density of the heat absorbing medium [kp/m³];
c'	specific heat of the heat transfer medium [kcal/kp °C];
γ'	specific gravity of the heat transfer medium [kp/m³].

I. Introduction

Heating with a continuously varying temperature of the heat transfer medium, due to the interaction of the two media, is frequent in industrial processes. In what follows heating will refer to heating or cooling. Such processes include, for instance, heating in industrial furnaces or chemical equipment, where the temperature of both the heat absorbing and the heat transfer media continuously varies in function of the length of the equipment, according to their respective heat capacities. The temperature of the heat transfer medium would, namely, remain constant throughout the process only if its heat capacity would be "infinitely large" in relation to that of the heat absorbing medium. Since, however, no such extreme dimensions occur in industrial processes, the temperature of the heat transfer medium cannot be regarded as being nearly constant and a temperature which varies due to the interaction of the two media must be determined.

When such realistic conditions are being considered, the mathematical model of the heating process can no longer be expressed by a single partial differential equation, but another equation must be found which expresses the law of interaction of the two media while they are heated up.

II. The purpose of the calculation, assumptions

The example on Fig. 1 will be studied to elucidate the case. In the channel with the cross section $EFGH$ a charge of the cross section $ABCD$ (heat absorbing medium) travels at a velocity of v, in the channel with the cross section $ABLK$ and $MCDN$ the heat transfer medium proceeds at a velocity of v' in the direction of the positive axis y.

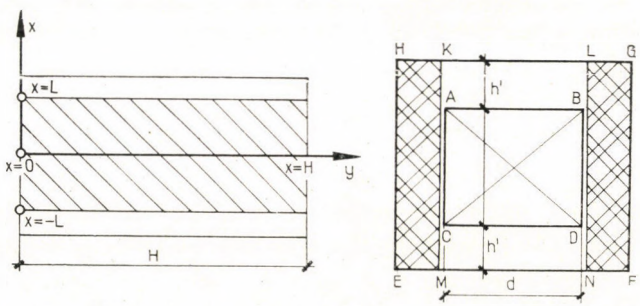

Fig. 1

For the formulation of the mathematical model, the following assumptions have been made:

a) Since the charge of the cross section $ABCD$ has no thermal losses over the surfaces AC and BD, heat flux in it takes place only in the direction of y;

b) there is no heat conduction in the charge in the direction of y;

c) the channel of the cross section $ENGF$ has no heat loss to any external medium;

d) the mathematical model holds true for the steady state only, in which constant temperatures are set in time to any given cross section of the channel;

e) the temperature of the heat transfer medium is the sole function of T^* (i.e. complete mixing is assumed to take place in the heat transfer medium, and the thus attained mean temperature is used in the calculation).

The *geometry* of the system is shown in Fig. 2.

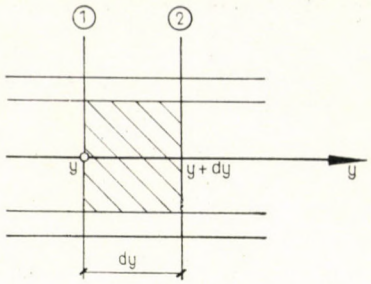

Fig. 2

III. The general principle of the calculation

For the formulation of the system of differential equations of the mathematical model, let us study the heat balance along a differential section of the channel. To do this, we shall set out from the most general form of the equation of transport:

$$\frac{\partial \Phi}{\partial t} + \operatorname{div} I + q = 0 \tag{1}$$

in which the first member, obviously, stands for the variations of the local density with time, the second for the divergence of the flux and the third for the source, or sink, respectively.

Being no source in our model, the process under review is stationary and the first and third members of the transport equation are equal to zero. The shorter form which characterizes the process in hand is:

$$\operatorname{div} I = \operatorname{div} (\lambda \operatorname{grad} \Phi - v\Phi) = 0. \tag{1a}$$

Substituting the temperature T for the general variable and referring the equation only to two spatial directions according to the model (since in the model conductance takes place in the direction x and the charge travels in the direction y, from the gradient the derivative according to x and from the convective member the velocity in the direction of y will remain), we obtain the following equation:

$$\frac{\partial T}{\partial y} = \frac{\lambda}{vc\gamma} \cdot \frac{\partial^2 T}{\partial x^2}, \tag{1b}$$

while equation (3) will yield the heat balance of the differential element of the charge.

For the location-dependent temperature of the charge the Fourier law holds true:

$$\frac{\partial T}{\partial y} = a \frac{\partial^2 T}{\partial x^2},$$

where

$$a = \frac{\lambda}{vc\gamma}.$$

Secondly let us write down the heat balance of the heat transfer medium. The quantity of heat entering through the cross section 1 is equal to:

$$dq_B = 2\, h'\, dv'\, c'\, \gamma'\, T^*(y). \tag{2}$$

Part of it escapes across cross section 2:

$$d_{k1} = 2h'\, dv'\, c'\, \gamma'\, [T^*(y) + dT^*(y)], \tag{3}$$

while the difference between the two is transmitted to the charge:

$$q_{k2} = 2\, d\, dy\, \alpha\, [T^*(y) - T(L, y)]. \tag{4}$$

Substituting the relations (2), (3) and (4) into the relationship:

$$q_B = q_{k1} + q_{k2}, \tag{5}$$

then reducing and simplifying, we arrive at the differential equation:

$$\frac{dT^*}{dy} = -\frac{\alpha}{h'\, \gamma'\, c'\, v'} [T^*(y) - T(L, y)]. \tag{6}$$

The Newtonian boundary condition holds true for two surfaces of the charge:

$$\frac{\partial}{\partial x} T(L, y) = h\, [T^*(y) - T(L, y)], \tag{7}$$

$$\frac{\partial}{\partial x} T(-L, y) = -h\, [T^*(y) - T(-L, y)]. \tag{8}$$

The starting conditions were:

$$T(x, 0) = T_0, \tag{9}$$

$$T^*(0) = T_0^* \tag{10}$$

and the above equations, together:

$$\frac{\partial T(x,y)}{\partial y} = a \frac{\partial^2 T(x,y)}{\partial x^2}, \tag{11}$$

$$\frac{dT^*(y)}{dy} = -b[T^*(y) - T(L,y)], \tag{12}$$

$$\frac{\partial}{\partial x} T(-L,y) = -h[T^*(y) - T(-L,y)], \tag{13}$$

$$\frac{\partial}{\partial x} T(L,y) = h[T^*(y) - T(L,y)], \tag{14}$$

$$T(x,0) = T_0, \tag{15}$$

$$T^*(0) = T_0^* \tag{16}$$

yield the system of differential equations for the above problem of heating up.

Let us now solve the system of differential equations (11) and (12) under the conditions determined by (13), (14), (15) and (16). Let us introduce the function

$$F(x,y) = T(x,y) - T^*(y) \tag{17}$$

which will make equation (1) assume the following form:

$$a F_{xx} = F_t + T^{*\prime}(y). \tag{18}$$

The criteria (13), (14) and (15) can now be written in the following form:

$$F(x,0) = T_0 - T_0^*, \tag{19}$$

$$F_x(L,y) = -hF(L,y), \tag{20}$$

$$F_x(-L,y) = hF(-L,y). \tag{21}$$

According to (12) and (17), the differential equation (18) can be put into the following form:

$$aF_{xx}(x,y) = F_t(x,y) - bF(L,y). \tag{22}$$

The solution of the partial differential equation (22) can be found in the form:

$$R(x,y) = \sum_{k=0}^{\infty} X_k(x)(x) e^{-a\mu_k^2 y}. \tag{23}$$

Collating the relations (22) and (23) we obtain

$$\sum_{k=1}^{\infty} [aX_k''(x)+a\mu_k^2 X_k(x)-bX_k(L)]\, e^{-a\mu_k^2 z}=0. \tag{24}$$

Accordingly, owing to (20), (21), (23) and (24):

$$aX_k''(x)+a\mu_k^2 X_k(x)-bX_k(L)=0; \tag{25}$$

$$X_k'(L)=-hX_k(L), \tag{26}$$

$$X_k'(-L)=hX_k(-L). \tag{27}$$

The general solution of the differential equation (25) is as follows:

$$X_k(x)=\frac{b}{a\mu_k^2}X_k(L)+A_k\cos\mu_k x+B_k\sin\mu_k x. \tag{28}$$

According to the equality (28):

$$X_k(L)=\frac{b}{a\mu_k^2}X_k(L)+A_k\cos\mu_k L+B_k\sin\mu_k L, \tag{29}$$

$$X_k(L)=\frac{a\mu_k^2}{a\mu_k^2-b}(A_k\cos\mu_k L+B_k\sin\mu_k L). \tag{30}$$

Substituting into the equality (28) the right side of (30) instead of $X_k(L)$:

$$X_k(x)=A_k\left(\cos\mu_k x+\frac{b}{a\mu_k^2-b}\cos\mu_k L\right)+B_k\left(\sin\mu_k x+\frac{b}{a\mu_k^2-b}\sin\mu_k L\right). \tag{31}$$

Deriving both sides of the equality (28):

$$X_k'(x)X_k'|x|=-A_k\mu_k\sin_k x+B_k\mu_k\cos\mu_k x. \tag{32}$$

With the relations (26), (30) and (32):

$$A_k\left(\frac{ha\mu_k^2}{a\mu_k^2-b}\cos\mu_k L-\mu_k\sin\mu_k L\right)+\left(\mu_k\cos\mu_k L+\frac{ha\mu_k^2}{a\mu_k^2-b}\sin\mu_k L\right)B_k=0. \tag{33}$$

Similarly to equation (33), according to (27), (31) and (32):

$$\left(\mu_k\sin\mu_k L-\frac{ha\mu_k^2}{a\mu_k^2-b}\cos\mu_k L\right)A_k+\left(\mu_k\cos\mu_k L+h\frac{a\mu_k^2-2b}{a\mu_k^2-b}\sin\mu_k L\right)B_k=0. \tag{34}$$

The system consisting of equations (33) and (34) will have a solution which differs from the trivial only when the system's determinant is 0. This, however, holds true only if the μ_k quantities were determined from the following equation:

$$ha\mu_k^2 \cos^2 \mu_k L - \mu_k (-b + a\mu_k^2 - h^2 a) \sin_k L \cos \mu_k L - \\ - h(a\mu_k^2 - b) \sin^2 \mu^2 \mu_k L = 0. \tag{35}$$

Accordig to the relationships (19) and (23):

$$\sum_{k=1}^{\infty} X_k(x) = T_0 - T_0^* \tag{36}$$

and, obviously, owing to the equality of (31) and (36):

$$B_k = 0. \tag{37}$$

Accordingly, in consideration of (23), (31) and (37):

$$F(x, y) = \sum_{k=1}^{\infty} A_k \left(\cos \mu_k x + \frac{b}{a\mu_k^2 - b} \cos \mu_k L \right) e^{-a\mu_k^2 y}. \tag{38}$$

If (37) holds true then, owing to (20), (21) and (38) μ_k, instead of (35), must satisfy the eigenvalue equation:

$$\tan \mu_k L = \frac{ha^2 \mu_k}{a\mu_k^2 - b}. \tag{39}$$

After the derivation of both sides of the (17) equality according to x' then substituting L for x, we arrive at:

$$T_x(L, y) = F_x(L, y). \tag{40}$$

Owing to (14) and (40)

$$\frac{1}{h} F_x(L, y) = T^*(y) - T(L, y). \tag{41}$$

From the relations (12) and (41) it follows that

$$\frac{dT^*(y)}{dy} = -\frac{b}{h} F_x(L, y). \tag{42}$$

From the above equation, according to (16):

$$T^*(y)=T_0^* - \frac{b}{h}\int_0^y F_x(L,y)\,dy. \tag{43}$$

From the relations (38) and (43) we obtain the equality:

$$\begin{aligned} T^*(y) &= T_0^* + \frac{b}{h}\int_0^y \sum_{k=1}^{\infty} \mu_k A_k \sin \mu_k L \cdot e^{-a\mu_k^2 y}\,dy = \\ &= T_0^* - \frac{b}{ah}\sum_{k=1}^{\infty} A_k \frac{\sin \mu_k L}{\mu_k}\left(e^{-a\mu_k^2 y} - 1\right). \end{aligned} \tag{44}$$

According to (17) and (44):

$$T(x,y) = F(x,y) + T_0^* - \frac{b}{ah}\sum_{k=1}^{\infty} A_k \frac{\sin \mu_k L}{\mu_k}(e^{-a\mu_k^2 y} - 1). \tag{45}$$

Substituting into (45) the right side of (38) for $F(x, y)$ we obtain

$$\begin{aligned} T(x,y) = T_0^* &+ \sum_{k\neq 1}^{\infty} A_k \left(\cos \mu_k x + \frac{b}{a\mu_k^2 - b}\cos \mu_k L\right) e^{-a\mu_k^2 y} - \\ &- \frac{b}{ah}\sum_{k=1}^{\infty} A_k \frac{\sin \mu_k L}{\mu_k}(e^{-a\mu_k^2 y} - 1). \end{aligned} \tag{46}$$

In consideration of the eigenvalue equation (39), (46) may also be written in the following form:

$$T(x,y) = T_0^* + \frac{b}{ah}\sum_{k=1}^{\infty} A_k \frac{\sin \mu_k L}{\mu_k} + \sum_{k=1}^{\infty} A_k \cos \mu_k x\, e^{-a\mu_k^2 y}. \tag{47}$$

The coefficients A_k of the equality (47) are determined from the equation:

$$\sum_{k=1}^{\infty} A_k \left(\cos \mu_k x + \frac{b}{a\mu_k^2 - b}\cos \mu_k L\right) = T_0 - {}_0^*{} \tag{48}$$

obtained by the combination of the relations (36) and (38).

Since the functions in brackets on the left side of the equation (48) do not yield an orthogonal system of functions in the interval $(-L\,;\,L)$, the A_k coefficients cannot be determined according to the methods used in the Fourier expansion.

In the following, the coefficients A_k will be determined by a "non-orthogonal" expansion in series. Writing down the differential equation (25) for $X_k(x)$ and $X_l(x)$, then multiplying the first equation by $X_l(x)$ and the second one by $X_k(x)$, we obtain the following system of equations:

$$aX_k''(x)\,X_l(x)+a\mu_k^2\,X_k(x)\,X_l(x)-bX_k(L)\,X_l(x)=0\,, \tag{49}$$

$$aX_l''(x)\,X_k(x)+a\mu_l^2\,X_k(x)\,X_l(x)-bX_l(L)\,X_k(x)=0\,. \tag{50}$$

Deducting (50) from (49), subsequently integrating both sides of the thus obtained equation from $-L$ to $+L$:

$$\begin{aligned} a\int_{-L}^{L}[X_k''(x)\,X_l(x)-X_l''(x)\,X_k(x)]\,dx+a\,(\mu_k^2-\mu_l^2)\int_{-L}^{L}X_k(x)\,X_l(x)\,dx- \\ -bX_k(L)\int_{-L}^{L}X_l(x)\,dx+bX_l(L)\int_{-L}^{L}X_k(x)\,dx=0\,. \end{aligned} \tag{51}$$

Combining the relations (26) and (27) with (51) we arrive at the equality:

$$a(\mu_k^2-\mu_l^2)\int_{-L}^{L}X_k(x)\,X_l(x)\,dx=bX_k(L)\int_{-L}^{L}X_l(x)\,dx-bX_l(L)\int_{-L}^{L}X_k(x)\,dx. \tag{52}$$

Let $f(x)$ be a continuous function in the interval of $(-L, L)$. Now let us expand $f(x)$ into a progressive series according to the functions $X_k(x)$:

$$\sum_{k=1}^{\infty}A_k\,X_k(x)=f(x). \tag{53}$$

Multiplying both sides of (53) equality with $X_l(x)$ and integrating them from $-L$ to L:

$$\int_{-L}^{L}f(x)X_l(x)\,dx=\sum_{k=1}^{\infty}{}^{*}\,A_k\int_{-L}^{L}X_k(x)X_l(x)\,dx+A_l\int_{-L}^{L}X_l^2(x)\,dx. \tag{54}$$

$\sum_{k=1}^{\infty}{}^{*}$ in the relation (44) indicates that the summation index k_1 in the summation may assume each value along the $(1, 2, 3, \ldots, l-1, l+1, l+2, \ldots)$. From the equations (52) and (54) it follows that

$$\begin{aligned} \int_{-L}^{L}f(x)\,X_l(x)\,dx=\sum_{k=1}^{\infty}{}^{*}\,A_k\left[\frac{b}{a(\mu_k^2-\mu_l^2)}\,X_k(L)\int_{-L}^{L}X_l(x)\,dx=\right. \\ \left.=\frac{b}{a(\mu_k^2-\mu_l^2)}\,X_l(L)\int_{-L}^{L}X_k(x)\,dx\right]+A_l\int_{-L}^{L}X_l^2(x)\,dx. \end{aligned} \tag{55}$$

In consideration of the equalities (31) and (37) we arrive at the equalities

$$\int_{-L}^{L} X_k(x)\,dx = 2(Lb+ha)\frac{\sin \mu_k L}{ha\,\mu_k}, \tag{56}$$

$$X_k(L) = \frac{\mu_k}{h}\sin \mu_k L. \tag{57}$$

Accorging to (56) and (57):

$$\int_{-L}^{L} X_k(x)\,dx = \frac{2(ha+Lb)}{a\mu_k^2} X_k(L). \tag{58}$$

According to (57) and (58):

$$\begin{aligned} bX_k(L)\int_{-L}^{L} X_l(x)\,dx - bX_l(L)\int_{-L}^{L} X_k(x)\,dx = \\ = \frac{2b}{a}(ha+Lb)\frac{\mu_k^2-\mu_l^2}{\mu_k^2\cdot\mu_l^2} X_k(L)\,X_l(L). \end{aligned} \tag{59}$$

Accordingly, combining (55) and (59) we shall obtain:

$$\int_{-L}^{L} f(x)\,X_l(x)\,dx = \frac{2b}{a^2}(ha+Lb)\sum_{k=1}^{\infty} A_k \frac{1}{\mu_k^2\,\mu_l^2} X_k(L)\,X_l(L) + A_l\int_{-L}^{L} X_l^2(x)dx. \tag{60}$$

In view of the equality (56):

$$\int_{-L}^{L} f(x)\,dx = \frac{2}{a}(ha+Lb)\sum_{k=1}^{\infty} A_k \frac{1}{\mu_k^2} X_k(L). \tag{61}$$

With relations (60) and (61):

$$\begin{aligned} \int_{-L}^{+L} f(x)\,X_l(x)\,dx = \frac{b}{a}\,\frac{1}{\mu_l^2} X_l(L)\int_{-L}^{L} f(x)\,dx - \\ - \frac{2b}{a^2}(ha+Lb)\frac{1}{\mu_l^4} A_l\,X_l^2(L) + A_l\int_{-L}^{L} X_l^2(x)\,dx. \end{aligned} \tag{62}$$

After rearrangement:

$$\begin{aligned} \int_{-L}^{L} f(x)\,X_l(x)\,dx - \frac{b}{a}\,\frac{1}{\mu_l^2} X_l(L)\int_{-L}^{L} f(x)\,dx = \\ = A_l\left[\int_{-L}^{L} X_l^2(x)\,dx - \frac{2b}{a^2}(ha+Lb)\frac{1}{\mu_l^4} X_l^2(L)\right]. \end{aligned}$$

From equation (63):

$$A_l = \frac{\int_{-L}^{L} f(x)\, X_l(x)\, dx - \dfrac{b}{a\mu_l^2} X_l(L) \int_{-L}^{L} f(x)\, dx}{\int_{-L}^{L} X_l^2(x)\, dx - \dfrac{2\, b(ha+Lb)}{a^2\, \mu_l^4} X_l^2(L)} \tag{64}$$

which completes the determination of the coefficients A_l.

It is evident that

$$f(x) = T_0 - T_0^* \tag{65}$$

and

$$A_l = (T_0 - T_0^*) \frac{2\, ah\mu_l \sin \mu_l L}{aLh\mu_l^2 + (a\mu_l^2 + b) \sin^2 \mu_l L} \,. \tag{66}$$

With the equalities (44), (47) and (66):

$$\frac{T_0^* - T(x,y)}{T_0^* - T_0} = \sum_{k=1}^{\infty} \frac{2ah\mu_k \sin \mu_k L}{aLh\mu_k^2 + (a\mu_k^2 + b) \sin^2 \mu_k L} \cos \mu_k x\, e^{-a\mu_k^2 y} + \\ + \sum_{k=1}^{\infty} \frac{2\, b \sin^2 \mu_k L}{aLh\mu_k^2 + (a\mu_k^2 + b) \sin^2 \mu_k L} \tag{67}$$

and

$$\frac{T^*(y) - T_0^*}{T_0 - T_0^*} = \sum_{k=1}^{\infty} \frac{2\, b \sin^2 \mu_k L}{aLh\mu_k^2 + (a\mu_k^2 + b) \sin^2 \mu_k L} (1 - e^{-a\mu_k^2 y}). \tag{68}$$

By heating in counterflow, the heat transfer medium enters at the cross section v—H and the two media (heat transmitting and heat absorbing) flow in opposite directions. The mathematical model of this heating pattern will be obvious from what has been shown above:

$$\frac{\partial T(x,y)}{\partial y} = a \frac{\partial^2 T(x,y)}{\partial^2 x}, \tag{69}$$

$$\frac{dT^*(y)}{dy} = b\,[T^*(y) - T(L,y)]\,; \tag{70}$$

$$T_x(L,y) = h\,[T^*(y) - T(L,y)]\,, \tag{71}$$

$$T_x(-L,y) = -h[T^*(y) - T(-L,y)]\,; \tag{72}$$

$$T(x,0) = T_0, \tag{73}$$

$$T^*(H) = T_0^*. \tag{74}$$

To solve the example, let us first solve the system of differential equations

$$a\frac{\partial^2 T(x,y)}{\partial x^2}=\frac{\partial T(x,y)}{\partial y} \tag{75}$$

and

$$\frac{dT^*(y)}{dy}=b\,[T^*(y)-T(L,y)] \tag{76}$$

under the following starting and boundary conditions:

$$T(x,0)=T_0, \tag{77}$$

$$T^*(0)=T_v^*, \tag{78}$$

$$T_x(L,y)=h\,[T^*(y)-T(L,y)]\,, \tag{79}$$

$$T_x(-L,y)=-h\,[T^*(y)-T(-L,y)]. \tag{80}$$

The solution of (75), (76), (77), (78), (79) and (80) will evidently be the same as that of the system composed of the equations (11), (12), (13), (14), (15) and (16), provided that b is replaced by $-b$ in (12). However, care must be taken that in this particular case the μ_k eigenvalues, instead of the equation (39), must be determined from the equation

$$\tan \mu L=\frac{ha\mu}{a\mu^2+b}\,. \tag{81}$$

Unlike (39), the equation (81) has an imaginary root, too. This latter is such that when substituted for μ_1 in the equations (67) and (68), the first members of the series will become real, like all other members. Accordingly, taking into consideration the equations (67) and (68), we shall have:

$$\frac{T_v^*-T(x,y)}{T_v^*-T_0}=\sum_{k=1}^{\infty}\frac{2ah\mu_k\sin\mu_k L}{aLh\mu_k^2+(a\mu_k^2-b)\sin^2\mu_k L}\cos\mu_k x\,e^{-a\mu_k^2 y}- \\ -\sum_{k=1}^{\infty}\frac{2\,b\sin^2\mu_k L}{aLh\mu_k^2+(a\mu_k^2-b)\sin^2\mu_k L}\,, \tag{82}$$

$$\frac{T^*(y)-T_v^*}{T_0-T_v^*}=\sum_{k=1}^{\infty}\frac{2\,b\sin^2\mu_k L}{aLh\mu_k^2+(a\mu_k^2-b)\sin^2\mu_k L}(e^{-a\mu_k^2 y}-1). \tag{83}$$

Although the value of T_v^* is not known in advance in the counterflow problem, it can be determined from the equation $T^*(H)=T_0^*$ in possession of T_0^*. Namely, in consideration of (83):

$$\frac{T_0^* - T_v^*}{T_0 - T_v^*} = \sum_{k=1}^{\infty} \frac{2\,b \sin^2 \mu_k L}{aLh\mu_k^2 + (a\mu_k^2 - b)\sin^2 \mu_k L} \left(e^{-a\mu_k^2 H} - 1\right), \tag{84}$$

whence, denoting the right side of equation (84) by $k(H)$, we obtain:

$$T_v^* = \frac{k(H)T_0 - T_0^*}{k(H) - 1} . \tag{85}$$

Substituting T_v^* and (83) by the right side of (85) in the relation (82), we arrive at the solution of the counterflow problem.

Both the direct and counterflow solutions can be rendered more clear and easier to survey by introducing the criterion of similarity, as is usual in thermodynamics. The Nusselt number is

$$Nu = \frac{\alpha L}{\lambda} \tag{86}$$

and the modified Fourier member:

$$F_{0y} = \frac{ay}{L^2} . \tag{87}$$

The ratio of heat capacities entering during the unit of time is

$$p = \frac{2\,vc\gamma L}{2\,v'c'\gamma' h'} = \frac{vc\gamma L}{v'c'\gamma' h'} . \tag{88}$$

Taking into consideration the equations (86), (87) and (88), the direct flow solution of (67) and (68) will appear in the following form:

$$\frac{T_0^* - T(x,y)}{T^* - T_0} = \sum_{k=1}^{\infty} \varphi_k' \left[\delta_k \frac{\cos \delta_k \overline{x/L}}{\sin \delta_k} e^{-F_{0y}\delta_k^2} + p \right], \tag{89}$$

$$\frac{T_0^* - T^*(y)}{T^* - T_0} = \sum_{k=1}^{\infty} p\varphi_k' (1 - e^{-F_{0y}\delta_k^2}), \tag{90}$$

$$\varphi_k' = \frac{2 \sin^2 \delta_k}{\delta_n^2 + \delta_k \sin \delta_k \cos \delta_k + 2p \sin^2 \delta_k} . \tag{91}$$

The equation which corresponds to equation (39) is the transcendent equation:

$$\tan \delta_k = \frac{\delta_k}{\frac{\delta_k^2}{Nu} - p} . \tag{92}$$

Making use o equation (89) and

$$\overline{T}(y) = \frac{1}{2L}\int_{-L}^{+L} T(x, y)\,dx \tag{93}$$

the mean temperature of the heat absorbing medium will be:

$$\frac{T_0^* - \overline{T}(0, y)}{T_0^* - T_4} = \sum_{k=1}^{\infty} \varphi_k' (e^{-F_{0y}\delta_k^2} + p), \tag{94}$$

while the following core temperature will arise in the heat absorbing medium if $x = 0$ is substituted into the equation (89):

$$\frac{T_0^* - T(y)}{T_0^* - T_0} = \sum_{k=1}^{\infty} \varphi_k' \left(\frac{\delta_k}{\sin \delta_k} e^{-F_{0y}\delta_k^2} + p \right). \tag{95}$$

To obtain the surface temperature of the heat absorbing medium, $x = \pm L$ is substituted into equation (89):

$$\frac{T_0^* - T(L, y)}{T_0^* - T_0} = \sum_{k=1}^{\infty} \varphi_k' (\delta_k \cot \delta_k\, e^{-F_{0y}\delta_k^2} + p). \tag{96}$$

Accordingly, the relations (94), (95) and (96) can be used to advantage in the calculation of heating problems with a direct flow.

The solution of the counterflow heating problem, on the other hand, is as follows:

$$\frac{T_0^* - T(x, y)}{T_0^* - T_0} = \sum_{k=1}^{\infty} \varphi_k \left(\delta_k \frac{\cos \delta_k x/L}{\sin \delta_k} e^{-F_{0y}\delta_k^2} - p \right), \tag{97}$$

$$\frac{T_0^* - T^*(y)}{T_0^* - T_0} = \sum_{k=1}^{\infty} p\varphi_k \left(e^{-F_{0y}\delta_k^2} - 1 \right), \tag{98}$$

where

$$\varphi_k = \frac{2 \sin^2 \delta_k}{\delta_k^2 + \delta_k \sin \delta_k \cos \delta_k - 2p \sin^2 \delta_k},$$

while the outlet temperature of the gas is T_0^*. Although this is unknown, it can be obtained from the relationship

$$T^*(H) = T_0', \tag{99}$$

since

$$\frac{T_0^* - T_0'}{T_0^* - T_0} = \sum_{k=1}^{\infty} p\varphi_k (e^{-F_{0y}\delta_k^2} - 1) \tag{100}$$

which readily enables the determination of T^*. According to the relationship (81) we have:

$$\tan \delta_k = \frac{\delta_k}{\frac{\delta_k^2}{Nu} + p} . \tag{101}$$

As per the above, in possession of T_0^* the mean temperature of the heat absorbing medium is

$$\frac{T_0^* - \bar{T}(y)}{T_0^* - T_0} = \sum_{k=1}^{\infty} \varphi_k (e^{-F_{0y} \delta_k^2} - p) \tag{102}$$

and the core temperature:

$$\frac{T_0^* - T(0, y)}{T_0^* - T_0} = \sum_{k=1}^{\infty} \left(\frac{\delta_k}{\sin \delta_k} e^{-F_{0y} \delta_k^2} - p \right). \tag{103}$$

The surface temperature:

$$\frac{T_0^* - T(\pm L, y)}{T_0^* - T_0} = \sum_{k=1}^{\infty} \varphi_k (\delta_k \cot \delta_k e^{-F_{0y} \delta_k^2} - p) . \tag{104}$$

Direct and/or counterflow heating problems, in addition to the analytic solution, can be solved also by approximation. From among the known approximation solutions, we have chosen the relaxation method and do not seek for the temperature distribution in the material and in the gas as a continuous function of place. For this purpose, we cover the system with a mesh having Δx and Δy spacing, and calculate the temperatures at the mesh points.

The values of the first and second derivates in the system of equations can be determined from the formula of the Taylor series. Let us denote the mesh points in the direction of x by m, and those in the direction of y by the index n (Fig. 3). According to the Taylor formula, in the direction of x we obtain

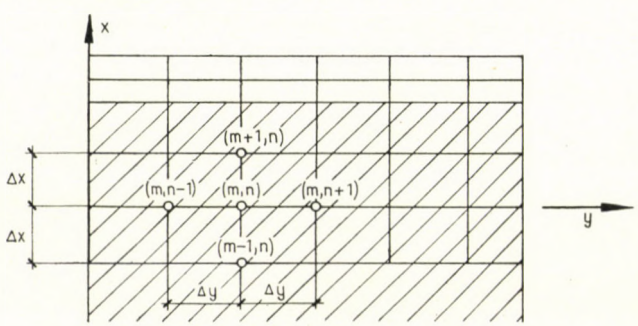

Fig. 3

$$T_{m+1,n} \cong T_{m,n} + \Delta x \left(\frac{\partial T}{\partial x}\right)_{m,n} + \frac{1}{2} \Delta x^2 \left(\frac{\partial^2 T}{\partial_x^2}\right) \tag{105}$$

and

$$T_{m-1,n} \cong T_{m,n} - \Delta x \left(\frac{\partial T}{\partial x}\right)_{m,n} + \frac{1}{2} \Delta x^2 \left(\frac{\partial^2 T}{\partial_x^2}\right)_{m,n} . \tag{106}$$

Adding the two equations, we arrive at

$$\left(\frac{\partial^2 T}{\partial x^2}\right)_{m,n} \cong \frac{T_{m+1,n} + T_{m-1,u} - 2T_{m,n}}{\Delta x^2} . \tag{107}$$

In the same way, in the direction of y

$$T_{m,n+1} \cong T_{m,n} + \Delta y \left(\frac{\partial T}{\partial y}\right)_{m,n} , \tag{108}$$

whence

$$\left(\frac{\partial T}{\partial y}\right)_{m,n} \cong \frac{T_{m+n+1} - T_{m,n}}{\Delta y} . \tag{109}$$

Substituting the relations (107) and (108) into the Fourier equation

$$\left(\frac{\partial T}{\partial y}\right)_{m,n} = a \left(\frac{\partial^2 T}{\partial x^2}\right)_{m,n}$$

we obtain:

$$T_{m,n+1} = \frac{a\Delta y}{\Delta x^2} (T_{m+1,n} + T_{m-1,n}) + \left(1 - \frac{2a\Delta y}{\Delta x^2}\right) T_{m,n} \tag{110}$$

which holds true for both the direct and the counterflow systems.

IV. Direct flow system

In a direct flow system both the heat transfer and the heat absorbing media proceed in the direction of the y axis. In such a case both media enter the system at the cross section $x = 0$. The mathematical model of the direct flow system is illustrated in equations (11)—(16); their transformation into difference equations will yield the relaxation equations for the problem studied.

The difference equation (110) corresponding to (11) is

$$T_{m,n+1} = \frac{a\Delta y}{\Delta x^2} (T_{m+1,n} + T_{m-1,n}) + \left(1 - \frac{2a\Delta y}{\Delta x}\right) T_{m,n} , \tag{111}$$

while the boundary condition as per (14) is

$$\frac{\partial T(L,y)}{\partial t} = h\,[(T^*(y) - T(L,y)]\,,$$

which yields the picture seen in Fig. 4. Transforming also the differential equation for the heat transfer medium (12):

$$\frac{T_{F,n} - T_{F-1,n}}{\Delta x} \cong h\,(T_n^* - T_{F,n})\,,$$

$$T_{F,n} = \frac{T_{F-1,n} + h\Delta x T_n^*}{1 + h\Delta x}\,. \tag{112}$$

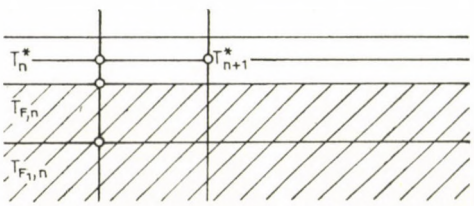

Fig. 4

Transforming also the differential equation for the heat transfer medium (12)

$$\frac{dT^*}{dt} = b\,[T^*(y) - T(L,y)]$$

into a difference equation

$$\frac{T_{n+1}^* - T_n^*}{\Delta y} = -b\,(T_n^* - T_{F,n}),$$

i.e.

$$T_{n+1} = (1 - b\Delta y)\cdot T_n^* + b\Delta y T_{F,n}. \tag{113}$$

Equations (111), (112) and (113) will yield the relaxation solutions, together with the original stipulations

$$T(x, 0) = T_0, \tag{114}$$

$$T^*(0) = T_0^*. \tag{115}$$

Through these equations it is possible to calculate the temperatures of the cross section with the index $(n + 1)$, provided that the temperature of the heat absorbing medium in a cross section with the index n is known. Since

the temperatures corresponding to the index $n = 0$ are given by (114) and (115), the problem is, in fact, solved.

It should be noted here that the boundary condition (14), symmetric with that of (13), has not been taken into consideration since, by dint of the character of the problem, the temperature distribution of the heat absorbing medium is symmetric to the y axis. This fact, in the relaxation equations, was taken into account partly by calculating the positive x domain of the heat absorbing medium only (due to the symmetry) and partly by setting the criterion that the mesh point temperatures immediately above the axis y be identical with the temperature immediately below the axis y.

V. Counterflow system

The relaxation programme of the counterflow system is by and large similar to that of the direct flow arrangement, since the two differential equation systems also bear many similarities. The differences lie in the point of entry of the heat transmitting medium and the sign of the parameter b in the differential equation relating to the heat transfer medium. As a result, the formulas for relaxation will be as follows:

$$T_{m,n+1} = \frac{a\Delta y}{\Delta x^2}(T_{m+1,n}+T_{m-1,n}) + \left(1 - \frac{2a\Delta y}{\Delta x}\right) T_{m,n}\,, \tag{116}$$

$$T_{F.n} = \frac{T_{F-1,n}+h\Delta x T_n^*}{1+h\Delta x}\,, \tag{117}$$

$$T_{n+1}^* = (1+b\Delta y)\,T_n^* - b\Delta y\,T_{F,n}\,, \tag{118}$$

$$\begin{aligned} T(x, 0) &= T_0, \\ T^*(L) &= T_0^*. \end{aligned} \tag{119}$$

When using the equations, certain difficulties will arise from the fact that, while the temperature of the entering heat transfer medium is known in the cross section $y = L$, the temperature of the entering heat absorbing medium is known in the point $x = 0$. The recurrent use of the relaxation formula requires the knowledge of both the heat transfer and the heat absorbing media in the cross section $x = 0$. If this requirement is satisfied, the relaxation formulas transform into such a system of equations in which each mesh point temperature is the function of the heat transfer medium leaving at the point $x = 0$.

Arriving to the cross section $x = L$ where the temperature of the entering heat transfer medium is known, the mesh point temperatures can be numeri-

cally determined. For computer programming, it is more rational to assume the temperature of the heat transfer medium leaving at $x = 0$ in advance, and vary it until the temperature of the medium entering at the point $x = L$, and recalculated with the assumed value, equals the one assumed to be in the boundary condition.

VI. Example

To compare the two methods, a numerical problem was elaborated for the counterflow case. The *material constants of the heat absorbing medium (solid)* are as follows: Coefficient of heat conductivity $\lambda = 0{,}4$ kcal/m h °C, specific heat $c = 0{,}2$ kcal/kg °C, bulk density $\gamma = 1500$ kg/m^3;

the *constants of the heat transfer medium:* specific heat $c' = 0{,}24$ kcal/kg °C, specific gravity $\gamma' = 1{,}3$ kp/m^3, velocity of the heat absorbing medium $v = 8$ m/h, velocity of the heat transfer medium $v' = 4300$ m/h, coefficient of convective heat transfer $\alpha = 100$ kcal/m h °C;

furnace constants: $H = 10$ m, $h' = 0{,}10$ m , $h = 0{,}15$ m;

initial temperatures: $T(x, 0) = 0$, T_δ 1000 °C.

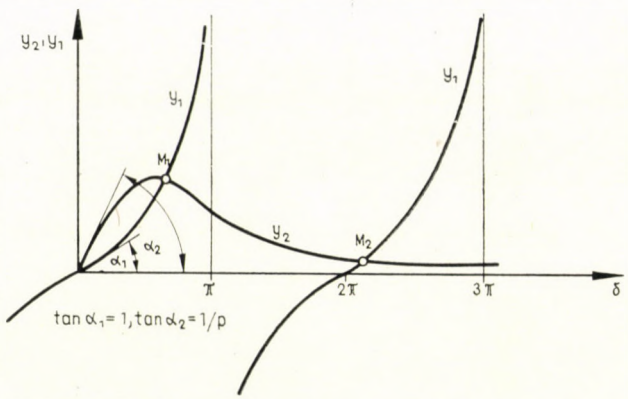

Fig. 5

Before performing the numerical calculation of the analytic solution, it is worthwhile to study the transcendent equation which yields the roots. Corresponding to equation (101):

$$\tan \delta_k = \frac{\delta_k}{\frac{\delta_k^2}{Nu} + p} .$$

The roots δ_k sought for are obtained from the points of intersection of the curves

$$y_1 = \tan\delta \tag{120}$$

and

$$y_2 = \frac{\delta}{\frac{\delta^2}{Nu} + p} \tag{121}$$

(see also Fig. 5). Provided that $1/p > 1$, viz. $p < 1$, then the root δ_1 falls to the interval $(0; \pi)$. Should $p > 1$, the first root will fall to the interval $(2\pi; 3\pi)$.

Apparently, provided that $p > 1$, equation (101) has a unique pure imaginary solution. Namely, let

$$\delta_k = i\beta_k,$$

where $i = \sqrt{-1}$. In this case equation (101) assumes the following form:

$$\tan h\, \beta_k = \frac{\beta_k}{-\frac{\beta_k^2}{Nu} + p}\,.$$

The β_k root to be determined (we shall later on see that there is only one such root) is yielded by the point of intersection of the curves

$$y_1 = \tan h\, \beta$$

and

$$y_2 = \frac{\beta}{-\frac{\beta^2}{Nu} + p}\,.$$

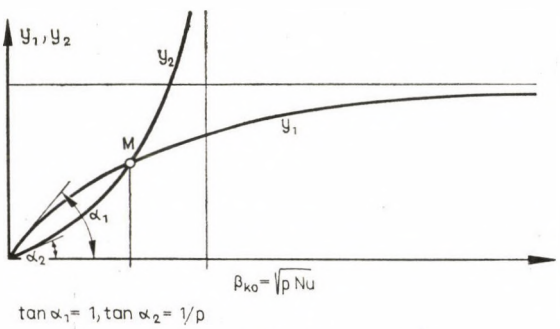

Fig. 6

(see also Fig. 6). The curves y_1 and y_2 have an intersection M only, provided that $1 > 1/p$, i.e. $p > 1$. Accordingly, if $p > 1$, then

$$\delta = i\beta$$

(without index, there being no more β solutions), where

$$0 \leq \beta < \sqrt{pNu}\,.$$

In a case with $p = 1$,

$$\delta_1 \equiv 0.$$

The relation

$$\varphi_1 = \frac{\delta \sin^2 \delta_k}{\delta_k^2 + \delta_k \sin \delta_k \cos \delta_k - 2p \sin^2 \delta_k}$$

after the substitution $\delta_1 = i\beta$ (provided that $p > 1$) transforms into

$$\varphi_1 = \frac{2 \sinh^2 \beta}{\beta^2 + \beta \sinh \beta \cosh \beta - 2p \sinh^2 \beta}$$

where, obviously, y_1 is real.

Making use of the constants: $F_{0H} = 0{,}296$; $Nu = 18{,}75$ and $p = 1{,}3416$ the following roots are obtained: $\delta_1 = 0{,}964$ and $\delta_2 = 4{,}215$. In what follows, we shall calculate with the first two members of the series and point out where this satisfies the requirements and where it does not satisfy them.

Using the given constants: $\varphi_1 = 3{,}0733$ and $\varphi_2 = 0{,}0885$, the temperature of gas at exit (T_0^*), on the basis of

$$\frac{T_0^* - T_0'}{T_0^* - T_0} = p\varphi_1 (e^{-F_{0H}\delta_1^2} - 1) + p\varphi_2 (e^{-F_{0H}\delta_2^2} - 1),$$

where $T_0 = 0$, is

$$T_0^* = 412{,}3\ ^\circ\mathrm{C}\,.$$

This value, as a result of the relaxation calculation, becomes

$$T_{0\,\mathrm{re}}^* = 419{,}2\ ^\circ\mathrm{C}\,.$$

In possession of T_0^*, the core temperature $T(0, H)$ at the point of exit of the heat absorbing medium, on the basis of

$$\frac{T_0^* - T(0, H)}{T_0^* - T_0} = \varphi_1 \left(\frac{\delta_1}{\sin \delta_1} e^{-F_{0H}\delta_1^2} - p \right) + \varphi_2 \left(\frac{\delta_2}{\sin \delta_2} e^{-F_{0H}\delta_2^2} - p \right)$$

will be

$$T(0, H) = 198\ ^\circ\mathrm{C}$$

obtained through the relaxation calculation:

$$T_{\mathrm{re}}(0, H) = 227{,}4\ ^\circ\mathrm{C}\,.$$

At the point $x = H$, in possession of T_0^*, the mean temperature of the heat absorbing medium will be

$$T(H) = 430\ ^\circ\mathrm{C}$$

on the basis of

$$\frac{T_0^* - \overline{T}(H)}{T_0^* - T_0} = \varphi_1 (e^{-F_{0H}\delta_1^2} - p) + \varphi_2 (e^{-F_{0H}\delta_2^2} - p)$$

and the same value through relaxation calculation will be

$$T_{\mathrm{ee}}(H) = 457\ ^\circ\mathrm{C}\,.$$

The heat balance, on the basis of either one of the two calculations, may be checked through the relationship:

$$T_0' - T_0^* = p\overline{T}(H)\,.$$

From the analytic solution, we obtained:

$$p\overline{T}(H) = 576{,}9$$

and

$$T_0' - T_0^* = 587{,}7\,.$$

Along relaxation calculation, we arrive at

$$p\overline{T}_{\mathrm{re}}(H) = 613{,}1$$

and

$$T_0' - T_0^* = 581\,.$$

As will be apparent, in spite of the fact that only two members of the infinite series are taken into consideration, the heat balance of the analytic solution shows a better agreement than that of the approach along relaxation. The results of another analytic solution may, naturally, be rendered more accurate by taking more members of the infinite series into consideration. The advantages of the approximation through relaxation give less calculation work and its applicability for even more complex cases, in which the analytic approach would become excessively involved.

ACKNOWLEDGEMENT

The authors wish to express their thanks to Mr. G. SASVÁRI for proposing the idea of the problem dealt with and for his most important advices.

Analytische Berechnung der Erwärmung einer festen Ladung durch Gegenstrom oder durch Gleichstrom. Die Arbeit befaßt sich mit der Berechnung der Erwärmung einer festen Ladung durch Gegenstrom oder Gleichstrom. Die partialen Differentialgleichungen, durch welche die in der Arbeit geprüften physikalischen Prozesse beschrieben werden, können mit Hilfe einer neuen Methode, der sogenannten »nicht orthogonalen« Reihebildung, gelöst werden. Mit Hilfe der oben erwähnten Rechenmethode wird die mathematische Wiedergabe von Heizungsprozessen ermöglicht, bei welchen die Temperatur des wärmeübertragenden Mediums während des Prozesses infolge der Wechselwirkung der zwei Media sich fortwährend ändert.

Аналитический расчет нагрева твердого заряда встречным или постоянным током *(К. Шейтц и Й. Фюлеп).* В статье рассматривается расчет нагрева твердого заряда встречным или постоянным током. Система дифференциальных уравнений с частной производной, описывающая физические явления, исследованные в данной работе, решается с помощью нового метода, называемого «неортогональным» разложением. Указанный выше метод расчета позволяет математически описать те процессы нагрева, во время которых температура теплопередающей среды непрерывно меняется за счет взаимодействия двух сред.

Acta Technica Academiae Scientiarum Hungaricae; Tomus 68 (1—2), pp. 73—85 (1970)

BESTIMMUNG DER UNBEEINFLUSSTEN EINSCHWINGSPANNUNG MIT EINEM OPERATORENRECHENVERFAHREN AUS VORBERECHNETEN GLEICHUNGEN BEI DEN VERTEILTE PARAMETER ENTHALTENDEN NETZEN

T. MIHÁLKOVICS
FORSCHUNGSINSTITUT FÜR ELEKTRISCHE ENERGIE, BUDAPEST

Eine Bestimmungsmethode der auf einem gegebenen Netzpunkt auftretenden Einschwingspannung ist das auf dem Thévénin-Prinzip basierende Operatorenrechnungsverfahren. Für die Netze, die mit den konzentrierten nicht ersetzbare Elemente mit verteilten Parametern (z. B. Freileitungen) enthalten, sind die für die Rechnung zugrunde gelegten charakteristischen Gleichungen ziemlich kompliziert. Damit die Betriebsingenieure diese Rechnungen nicht ableiten müssen, hat HAMMARLUND die Rechnungen für zahlreiche Stromkreise durchgeführt. Die Erfahrungen des Verfassers haben aber erwiesen, daß es über die von HAMMARLUND abgeleiteten Stromkreise hinaus in einigen Fällen notwendig ist, die Ableitungen auch für neue, mehr komplizierte Stromkreise durchzuführen. Der Verfasser teilt über die Beschreibung der Methode sowie praktische Beispiele hinaus solche für neue Stromkreise abgeleitete Ergebnisse samt Hammarlunds Stromkreisen in Tafeln mit.

I. Einleitung

Es ist bekannt, daß eine erfolgreiche Unterbrechung außer dem unterbrochenen Kurzschlußstrom und der Wiederkehrspannung auch von der nach der Unterbrechung auftretenden Schalt-Überspannung, der sog. Einschwingspannung abhängt. Die Charakteristiken der Einschwingspannung werden durch die Netzparameter und den Leistungsschalter zusammen bestimmt.

Die von dem Leistungsschalter nicht beeinflußte, sog. unbeeinflußte Einschwingspannung (im weiteren U.E.S.) auf dem gegebenen Netzpunkt muß bekannt sein. Die Typenprüfung des Leistungsschalters an den Hochleistungs-Prüffeldern läuft bei gewissen vorgeschriebenen U.E.S. Parametern ab. Ob der Leistungsschalter auf dem gegebenen Netzpunkt eingebaut oder nicht eingebaut werden kann, ergibt sich aus dem Vergleich der für den Leistungsschalter garantierten U.E.S. Parameter mit denen der U.E.S. auf dem vorliegenden Netzpunkt. Die von dem Leistungsschalter nicht beeinflußte Einschwingspannung bildet also im weiteren das Thema unserer Untersuchungen. Wir setzen also eine ideale Unterbrechung voraus (Abschnitt II. c).

Das auf dem Thévéninschen Prinzip basierende Operatorenrechnungsverfahren der U.E.S. hat eingehend zuerst HAMMARLUND [1] untersucht und die Ergebnisse für zahlreiche Stromkreise gegeben. (Diese Stromkreise kommen in der Literatur unter der Bezeichnung *A 1*, *A 2*, . . .; *B 1* . . .; *C 1* . . . usw. vor.)

In unserer Praxis hat das untersuchte Netz oft irgendeinem von HAMMARLUND abgeleiteten Stromkreis entsprochen, aber bei einigen komplizierteren Netzen war es notwendig, die Rechnungen auch für neue Stromkreise abzuleiten. (Die Stromkreise *M1*, *M2*, *M3*, *M4*, *M6*.) Ein gewisser Teil dieser neuen Stromkreise berücksichtigt beispielsweise, daß man unter inländischen Umständen in vielen Fällen keine unendliche Speisung voraussetzen kann. Untersucht man kompliziertere Stromkreise, d. h. nimmt die Zahl von Netzelementen zu, so werden die zugrundegelegten charakteristischen Gleichungen der Rechnung immer komplizierter. Die Rechnungen sind wegen der zunehmenden Gradzahl und der in ihnen vorkommenden Tangentenfunktionen zweckmäßig mit Rechenmaschinen durchzuführen.

II. Grundbedingungen der Rechnungen

a) Messungen und theoretische Überlegungen zeigen, daß der erstlöschende Pol des dreipoligen Kurzschlusses ohne Erdberührung die größte Steilheit von U.E.S. sowie die höchste Wiederkehrspannung ergibt, die im allgemeinen das 3/2-fache der Phasenspannung beträgt. Deshalb wird im weiteren dieser Fall untersucht.

b) In unseren Rechnungen werden die verlustlosen Netze in Betracht gezogen; die Dämpfung wird also nicht berücksichtigt, die Netzelemente werden nur mit ihren Induktivitäten und Kapazitäten abgebildet. Diese Bedingung vereinfacht die Rechnungen bedeutend, macht aber die Verwendbarkeit unserer Ergebnisse nicht schlechter. Für den Leistungsschalter ist der Ablauf der Schwingung nur bis zur ersten oder zweiten Spitze — im allgemeinen bis zum Zeitpunkt der maximalen Amplitude — von entscheidender Bedeutung, in diesem Zeitbereich ist aber die Dämpfung ziemlich klein, wie aus den Bildern 5 bis 8 des Zahlenbeispiels hervorgeht.

c) Wir setzen also eine ideale Ausschaltung voraus, der Leistungsschalter schaltet also im Nulldurchgang aus, die Lichtbogenspannung ist Null und nach der Ausschaltung ist der Widerstand der Schaltstrecke unendlich.

III. Verwendung der auf dem Thévéninschen Prinzip basierenden Operatorenrechnungsmethode in den Stromkreisen mit verteilten Parameterelementen

1. Prinzipielle Grundlagen der Methode

Die bei der Ausschaltung des Kurzschlußstromes auftretende U.E.S. kann im Sinne des Thévéninschen Prinzips berechnet werden [2]. Sind die operatorische Impedanzfunktion des von dem Kontakt her des Leistungsschalters betrachteten Netzes $Z(p)$ und die Laplacesche Transformation des

Kurzschlußstromes $I(p)$, so ergibt die Transformation der U. E. S. die Gleichung (1):

$$U_v(p) = I(p) \cdot Z(p) \,. \tag{1}$$

Die Linearnetze mit konzentriertem Parameter beschreibenden Kirchoff-Gesetze sind Linear-Integro-Differentialgleichungen mit konstanten Koeffizienten. In diesem Fall ist Gl. (1) ein rationaler algebraischer Bruch. Bei der Rücktransformation solcher Bruchfunktionen ist es höchst zweckmäßig, den Entwicklungssatz von Heaviside zu verwenden, welcher die Kenntnis der Pole von Bruchfunktion voraussetzt. Bei den rationalen Bruchfunktionen sind die Pole die einzigen singulären Punkte und deren Zahl ist endlich.

Betrachten wir weiterhin die Netze mit verteilten Parametern. Das bedeutet in erster Linie solche Netze, in denen die den Ablauf der U.E.S. entscheidend beeinflussenden Freileitungen vorhanden sind, deren Substitution durch π oder T-Glied einen groben Fehler verursacht. Bei diesen Netzen mit verteilten Parametern ist die Impedanzfunktion $Z(p)$ transzendent und die Polenzahl kann unendlich sein. Diese Impedanzfunktionen sind gewöhnlich Meromorphfunktionen, haben also auf der ganzen Ebene keine andere Singularität als die Pole. Bei der Gruppe der Meromorphfunktionen, denen wir bei der Lösung von Stromkreisen mit Freileitungen begegnen, kann der Heavisidesche Entwicklungssatz hier auch verwendet werden, wie es DAHR [3] aufgrund der Mittag—Lefflerschen Theorie von Zerlegung auf einfache Brüche dargestellt hat.

Im weiteren werden die aus der verschiedenen Kombination der Systeme mit konzentrierten und verteilten Parametern gebildeten Stromkreise untersucht. Die bearbeiteten Stromkreise können meist in der Praxis verwendet werden. Die Methode sowie ihre praktische Durchführung wird durch Beispiele dargestellt, damit der Leser auch die Aufgabe lösen kann, die auf keinen der im weiteren dargestellten Stromkreise zurückgeführt werden kann.

2. *Darstellung der Methode am einfachen Stromkreis mit Freileitung (Stromkreis A1)*

Betrachten wir den Stromkreis nach Bild 1. Der Leistungsschalter ist am Ende der Freileitung, die Speisung erfolgt von dem am anderen Ende der Freileitung für konzentriert angesehenen Generatortransformatorblock mit Induktivität L_0.

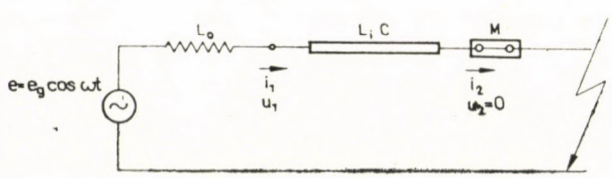

Bild 1. Einphasiger Stromkreis

Der Theorie der homogenen Leitungen entsprechend gibt die nachstehende Gl. (2) die eintretende Impedanzfunktion der mit der Impedanz $Z_0 = pL_0$ abgeschlossenen Freileitung von Induktivität L und Kapazität C

$$Z_b = Z \frac{Z \tanh \gamma l + Z_0}{Z + Z_0 \tanh \gamma l}, \tag{2}$$

wobei $Z = \sqrt{L/C}$ den Wellenwiderstand der Freileitung,
γ die Fortpflanzungskonstante,
l die Länge der Freileitung

bedeuten.

Aus der Theorie der homogenen Leitungen ist es bekannt, daß $\gamma l = p\sqrt{LC}$ ist. Gehen wir auf die relativen Einheiten über, betrachten wir die Angaben der Freileitung als Grundgröße, ist also $L = 1$. $C = 1$, so erhalten wir:

$$Z = \sqrt{L/C} = 1, \quad p\sqrt{LC} = p .$$

Führen wir die nachstehende Bezeichnung ein:

$$L/L_0 = 1/L_0 = m . \tag{3}$$

An Hand der Gl. (3) ist:

$$Z_0 = pL_0 = p/m .$$

Dadurch vereinfacht sich Gl. (2) wie folgt:

$$Z_b = \frac{m \tanh p + p}{m + p \tanh p} . \tag{4}$$

Betrachten wir nun den Kurzschlußstrom mit der Darlegung der Gleichungen der homogenen Leitungen:

$$\begin{aligned} u_1 &= i_2 Z \sinh (j\omega\sqrt{LC}) = e_g \cos \omega t - i_1 j\omega L_0 , \\ i_1 &= i_2 \cosh (j\omega\sqrt{LC}) \end{aligned} \tag{5}$$

Aus Gl. (5) ergibt sich

$$i_2 = \frac{e_g \sin \omega t}{\sqrt{L/C} \sin(\omega\sqrt{LC}) + \omega L_0 \cos(\omega\sqrt{LC})} .$$

Führen wir die folgenden Bezeichnungen ein:

$$\tau = t/\sqrt{LC},$$

$$\beta = \omega\sqrt{LC},$$

wobei ω die Kreisfrequenz der Generatorspannung mit dem Scheitelwert e_g ist.

Der Kurzschlußstrom ist:

$$i = i_2 = \frac{e_g \sin \beta\tau}{\omega\left(\frac{L \sin \beta}{\beta} + L_0 \cos \beta\right)} . \tag{6}$$

Da β gewöhnlich klein ist (für eine Freileitung von 100 km: $\beta \approx 0{,}1$), kann man $\cos \beta \approx 1$ und $\sin \beta \approx \beta$ nehmen. So erhalten wir:

$$i \approx \frac{e_g \sin \beta\tau}{\omega(L_0 + L)} . \tag{7}$$

Die Gleichung (7) ergibt sich auch aus der gewöhnlichen Starkstrombetrachtung ohne die Anführung der Gleichungen der homogenen Leitungen. In relativer Einheit ist die Grundspannung e_g.

In relativer Einheit ist der Grundstrom

$$\frac{e_g}{\sqrt{L/C}} .$$

Der Kurzschlußstrom ergibt sich in relativer Einheit aus der Gleichung (6) zu:

$$i_{v,e} = \frac{m \cdot \sin \beta\tau}{\beta\left(\cos \beta + m \frac{\sin \beta}{\beta}\right)} . \tag{8}$$

Mit der Transformation der Gleichung (8) erhält man:

$$I(p) = \frac{m}{\cos \beta + m \frac{\sin \beta}{\beta}} \cdot \frac{1}{p^2 + \beta^2} . \tag{9}$$

Die Transformation von U.E.S. wird:

$$U_v(p) = I(p) \cdot Z(p) = \frac{m}{\cos \beta + m \frac{\sin \beta}{\beta}} \cdot \frac{1}{p^2 + \beta^2} \cdot \frac{m \tanh p + p}{m + p \tanh p} . \tag{10}$$

Die charakteristische Gleichung wird:

$$m + p \tanh p = 0 . \tag{11}$$

Statt hyperbolischer Funktionen erhält man im verlustlosen Fall — d. h. wenn die Wurzeln keine reelle Komponente haben — trigonometrische Funktionen; wir erhalten also mit der Substitution von $p = j\gamma$ aus Gl. (11) die Gl. (12)

$$m - \gamma \tan \gamma = 0 . \tag{12}$$

Die Wurzeln der Gleichung (12) sind:

$$\gamma = \pm\gamma_1; \pm\gamma_2; \ldots; \pm\gamma_k; \ldots \quad .$$

Die Zerlegung in einfache Brüche ist wie folgt:

$$U_v(p) = H \cdot \frac{A(p)}{B(p)} . \tag{13}$$

$$\left.\begin{aligned} A(p) &= p + m \tanh p \,, \\ B(p) &= (p^2 + \beta^2)\,(m + p \tanh p) \,, \\ H &= \frac{m}{\cos\beta + m\dfrac{\sin\beta}{\beta}} \end{aligned}\right\} \tag{14}$$

$$U_v(p) = H\left\{\left[\frac{A(p)}{B'(p)}\right]_{p=j\beta} \cdot \frac{1}{p - j\beta} + \left[\frac{A(p)}{B'(p)}\right]_{p=-j\beta} \cdot \right.$$
$$\left. \cdot \frac{1}{p + j\beta} + \Sigma\left[\frac{A(p)}{B'(p)}\right]_{p=P_K} \cdot \frac{1}{p - P_K}\right\}, \tag{15}$$

wobei P_K die Wurzeln der Gleichung (11) sind.

Es sei $$B(p) = C(p) \cdot D(p) \,, \tag{16}$$

$$\left.\begin{aligned} C(p) &= p^2 + \beta^2 \,, \\ D(p) &= m + p \tanh p \end{aligned}\right\} ; \tag{17}$$

$$C(p)\,|_{p=\pm j\beta} = 0 \,; \qquad D(p)\,|_{p=P_K} = 0 \,.$$

So ergibt sich:

$$B'(p)\,|_{p=\pm j\beta} = [C'(p)\,D(p) + C(p)\,D'(p)]_{p=\pm j\beta} = [C'(p)\,D(p)]_{p=\pm j\beta} \,,$$
$$B'(p)\,|_{p=P_K} = [C(p) \cdot D'(p)]_{p=P_K} \,.$$

Auf Grund des Voranstehenden kann die Gl. (15) auf folgende Form gebracht werden:

$$U_v(p) = H\left\{\left[\frac{A(p)}{C'(p)\,D(p)}\right]_{p=j\beta} \frac{1}{p - j\beta} + \left[\frac{A(p)}{C'(p) \cdot D(p)}\right]_{p=-j\beta} \cdot \right.$$
$$\left. \cdot \frac{1}{p + j\beta} + \Sigma\left[\frac{A(p)}{C(p)\,D'(p)}\right]_{p=P_K} \cdot \frac{1}{p - P_K}\right\} . \tag{18}$$

Im vorliegenden Beispiel ist: $C'(p) = 2p$

$$D'(p) = \tanh p + p(1 - \tanh^2 p) .$$

$$\left[\frac{A(p)}{C'(p)\,D(p)}\right]_{p=j\beta} = \left[\frac{A(p)}{C'(p)\,D(p)}\right]_{p=-j\beta} = \frac{\beta + m\tan\beta}{2\beta(m - \beta\tan\beta)} .$$

$$\left[\frac{A(p)}{C(p)\,D'(p)}\right]_{p=j\gamma k} = \left[\frac{A(p)}{C(p)\,D'(p)}\right]_{p=-j\gamma k} =$$

$$= \frac{\gamma_k + m\tan\gamma_k}{(\beta^2 - \gamma_k^2)\,[\tan\gamma_k + \gamma_k(1 + \tan^2\gamma_k)]} .$$

Wird der Wert von $\tan\gamma_k$ aus Gleichung (12) ausgedrückt und in Gl. (18) gesetzt, so erhalten wir:

$$U_v(p) = H\left\{\frac{\beta + m\tan\beta}{2\beta(m - \beta\tan\beta)}\,\frac{2p}{p^2 + \beta^2} + \right.$$

$$\left. + \Sigma\,\frac{\gamma_k^2 + m^2}{(\beta^2 - \gamma_k^2)[m + \gamma_k^2 + m^2]}\,\frac{2p}{p^2 + \gamma_k^2}\right\} .$$

Mit der Rücktransformation von $U_v(p)$ erhält man die Gleichung (19) wie folgt:

$$u = \frac{m}{m\cos\beta - \beta\sin\beta}\cos\beta\tau - \frac{m}{\cos\beta + m\dfrac{\sin\beta}{\beta}} \cdot$$

$$\cdot\,\Sigma\,2\,\frac{\gamma_k^2 + m^2}{m^2 + m + \gamma_k^2}\,\frac{1}{\gamma_k^2 - \beta^2}\cos\gamma_k\tau . \tag{19}$$

Da β gewöhnlich klein ist ($\cos\beta \approx 1$; $\sin\beta \approx \beta$), wird:

$$u \approx \frac{m}{m - \beta^2}\cos\beta\tau - \frac{m}{1 + m} \cdot \Sigma\,2\,\frac{\gamma_k^2 + m^2}{m^2 + m + \gamma_k^2}\,\frac{1}{\gamma_k^2 - \beta^2}\cos\gamma_k\tau . \tag{20}$$

Die Frequenz der Teilschwingungen kann man in relativer Einheit aus der charakteristischen Gleichung berechnen, die U.E.S. ergibt sich aber aus Gl. (19) bzw. (20). Aus den relativen Einheiten können die Istwerte in Kenntnis der Grundeinheiten berechnet werden. Die Grundeinheiten sind wie folgt:

Induktivität, L (Induktivität der Freileitung);
Kapazität, C (Kapazität der Freileitung);
Widerstand, $\sqrt{L/C}$;
Zeit, $\sqrt{LC}$ ($\tau = t/\sqrt{LC}$);
Kreisfrequenz, $1/\sqrt{LC}$ ($\beta = \omega\sqrt{LC}$);
Spannung, e_g (Scheitelwert von Generatorspannung);
Strom, $e_g/\sqrt{L/C}$.

3. Anwendung des Berechnungsverfahrens für den dreipoligen Kurzschluß

Die Gleichung (19) bzw. (20) ergibt also im wesentlichen die U.E.S. eines einphasigen Kreises (Bild 1). Es stellt sich die Frage, wie dieses Verfahren in einem Drehstromnetz verwendet werden kann.

Wendet man die Methode der symmetrischen Komponenten auf den erstlöschenden Pol eines dreipoligen Kurzschlusses an (Abschnitt II.a), so ergibt sich die Laplacesche Transformation von U.E.S. aus Gleichung (21) [4]:

$$U_v(p) = I(p) \cdot \frac{3}{2} Z_1(p). \tag{21}$$

Bild 2 stellt im Falle eines dreipoligen ungeerdeten Kurzschlusses die von dem erstlöschenden Pol des Leistungsschalters aus betrachtete Impedanz dar (Z_1 ist die Impedanz im Mitsystem, Z_2 im Gegensystem).

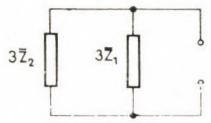

Bild 2. Impedanz betrachtet von dem erstlöschenden Pol des Leistungsschalters im Falle eines dreipoligen ungeerdeten Kurzschlusses (wenn $\bar{Z}_0 = \infty$)

Da $\bar{Z}_1 = \bar{Z}_2$ ist, genügt es nach dem Zusammenhang (21), nur das Mitsystem als ein einphasiges abzubilden. Die auf den einphasigen Stromkreis abgeleiteten Ergebnisse können also sinngemäß auf den erstlöschenden Pol des dreipoligen Kurzschlusses angewendet werden.

4. Durchführung von Berechnungen auf Grund vorher angegebener Gleichungen

Die Gleichungen der abgeleiteten Stromkreise enthält die Tafel I. In der Tafel sind die Bedeutung der für die verschiedenen Stromkreise verwendeten Konstanten (m, n, a usw.), die Werte von $I(p)$, $Z(p)$, die charakteristische Gleichung und endlich die Einschwingspannung u zusammengestellt. Der Einfachheit halber geben wir in der Tafel den Wert der Transformation von Einschwingspannung $U_v(p) = I(p) \cdot Z(p)$ nicht an.

Entspricht der Prüfstromkreis beispielsweise dem Bild 3, so ergibt sich dieser Stromkreis aus *M1*, falls $L_1 = \infty$ ist. Wir gewinnen also aus den abgeleiteten Gleichungen des Stromkreises *M1* durch die Substitution $n = 0$ die entsprechenden Gleichungen für den Stromkreis in Bild 3. Betreffs der Tafel I möchten wir bemerken, daß die Gleichungen des Kreises *A4* zwar aus den Gleichungen des Stromkreises *M2* des Verfassers durch Vereinfachung gewonnen werden können, trotzdem sind sie separat angegeben. Bei einigen

Tafel I

Gleichungen der abgeleiteten Stromkreise

Bezeichnung	Schaltungsschema des Stromkreises	Bezeichnungen	$I(p) = H\,\frac{1}{p^2+\beta^2}$ $(\cos\beta\approx 1;\ \sin\beta\approx\beta)$	Impedanzfunktion $Z(p)$	Charakteristische Gleichung	Einschwingspannung
B5	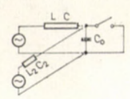	$m = \frac{L_2}{L}$ $n = \frac{C_2}{C}$ $a = \frac{C_0}{C}$	$H = \frac{m+1}{m}$	$\frac{\tanh p \cdot \tanh mp}{a\,p\tanh p \cdot \tanh mp + \tanh p + \tanh mp}$	$\tan\gamma + \tan m\gamma - a\gamma\tan\gamma \cdot \tan m\gamma = 0$	$u = \frac{m+1}{m+1-am\beta^2}\cos\beta\tau - H\Sigma\,\frac{2\tan^2\gamma_k}{E\tan^2\gamma_k - F\tan\gamma_k + m + 1}\cdot\frac{\cos\gamma_k\tau}{\gamma_k^2-\beta^2}$ $E = ma^2\gamma_k^2 + m + a + 1$ $F = 2\,ma\gamma_k$
B8	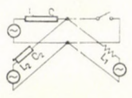	$m = \frac{L_2}{L} = \frac{C_2}{C}$ $a = \frac{L}{L_1}$	$H = \frac{1+m+am}{m}$	$\frac{p\tanh p \cdot \tanh mp}{p\tanh mp + p\tanh p + a\tan h\,p\cdot\tanh mp}$	$\gamma(\tan m\gamma + \tan\gamma) + a\tan\gamma\cdot\tan m\gamma = 0$	$u = \cos\beta\tau - H\Sigma\,\frac{2\gamma_k^2\tan^2\gamma_k}{E\tan^2\gamma_k + F\tan\gamma_k + \gamma_k^2(m+1)}\cdot\frac{\cos\gamma_k\tau}{\gamma_k^2-\beta^2}$ $E = (m+1)\gamma_k^2 + a(1+am)$ $F = 2ma\gamma_k$
C2		$m = \frac{L}{L_0}$ $n = \frac{C}{C_0}$ $a = \frac{C_2}{C}$	$H = \frac{m+1}{m}$	$n\,\frac{(ap^2+m)\tanh p + p}{(p^2a + amn + m)p\tanh p + p^2 + mn}$	$-(mna + m - \gamma^2 a)\,\gamma\tan\gamma - \gamma^2 + mn = 0$	$u = \frac{mn}{m+1}\,\frac{m - a\beta^2 + 1}{mn + \beta^2(\beta^2 a - m - mna - 1)}\cos\beta\tau - H\Sigma\,\frac{2m^2n^2}{\gamma_k^6a^2 + \gamma_k^4 E + \gamma_k^2 F + G}\cdot\frac{\cos\gamma_k\tau}{\gamma_k^2-\beta^2}$ $E = a + 1 - 2am - 2mna^2$ $F = 2m^2na + m^2n^2a^2 + m^2 + m - 2mna - 2mn$ $G = m^2n^2a + m^2n^2 + m^2n$
M1	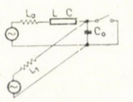	$m = \frac{L}{L_2}$ $n = \frac{L}{L_1}$ $a = \frac{C_0}{C}$	$H = \frac{m+n(m+1)}{m+1}$	$\frac{p(m\tanh p + p)}{(p^2am + p^2 + mn)\tanh p + p^3a + p(m+n)}$	$(-\gamma^2am - \gamma^2 + mn)\tan\gamma - \gamma^3a + \gamma(m+n) = 0$	$u = \frac{m+n(m+1)}{m+n(m+1) - \beta^2(am+a+1)}\cos\beta\tau - H\Sigma\,\frac{2\gamma_k^2(m^2+\gamma_k^2)}{\gamma_k^6a^2 + \gamma_k^4E + \gamma_k^2F + G}\cdot\frac{\cos\gamma_k\tau}{\gamma_k^2-\beta^2}$ $E = a^2m^2 + a^2m + a + 1 - 2an$ $F = m^2 + n^2 + am^2 + m + n - 2am^2n - 2amn$ $G = m^2n^2 + m^2n + mn^2$
A4	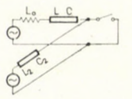	$m = \frac{L_2}{L} = \frac{C_2}{C}$ $a = \frac{L}{L_0}$	$H = \frac{ma+a+1}{m(a+1)}$	$\frac{(p + a\tanh p)\tanh pm}{p + a\tanh p + (a + p\tanh p)\cdot\tanh pm}$	$\gamma + a\tan\gamma + (a - \gamma\tan\gamma)\tan\gamma m = 0$	$u = \frac{a+1+ma}{a+1+m(a-\beta^2)}\cos\beta\tau - H\Sigma\,\frac{2(\gamma_k + a\tan\gamma_k)^2}{(1+\tan^2\gamma_k)\,E}\cdot\frac{\cos\gamma_k\tau}{\gamma_k^2-\beta^2}$ $E = \gamma_k^2(m+1) + a(ma+a+1)$
M2	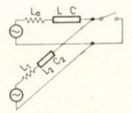	$m = \frac{L_2}{L} = \frac{C_2}{C}$ $a = \frac{L}{L_0}$ $b = \frac{L}{L_1}$	$H = \frac{b+ab+a+mab}{1+a+bm+abm}$	$\frac{EF}{E(p\tanh pm + b) + F(a + p\tanh p)}$ $E = a\tanh p + p$ $F = b\tanh pm + p$	$(a\tan\gamma + \gamma)(b - \gamma\tan\gamma m) + (b\tan\gamma m + \gamma)(a - \gamma\tan\gamma) = 0$	$u = \frac{b+ab+a+mab}{(a+1)(b-\beta^2m) + (bm+1)(a-\beta^2)}\cos\beta\tau - H\Sigma\,\frac{2(a\tan\gamma_k+\gamma_k)(b\tan\gamma_km+\gamma_k)}{G+K+L+M}\cdot\frac{\gamma}{\gamma_k^2-\beta^2}$ $G = (\gamma_k\tan\gamma_k\,m - b)(a + a\tan^2\gamma_k + 1)$ $K = (a\tan\gamma_k + \gamma_k)(\tan\gamma_km + \gamma_km + \gamma_km\tan^2\gamma_km)$ $L = (b\tan\gamma_k\,m + \gamma_k)(\tan\gamma_k + \gamma_k + \gamma_k\tan^2\gamma_k)$ $M = (\gamma_k\tan\gamma_k - a)(bm + bm\tan^2\gamma_k\,m + 1)$
M3	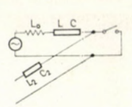	$m = \frac{L_2}{L} = \frac{C_2}{C}$ $a = \frac{L}{L_0}$	$H = \frac{a}{a+1}$	$\frac{p + a\tanh p}{(p + a\tanh p)\tanh pm + a + p\tanh p}$	$-(\gamma + a\tan\gamma)\tan\gamma m + a - \gamma\tan\gamma = 0$	$u = \frac{a}{a - \beta^2(am+m+1)}\cos\beta\tau - H\Sigma\,\frac{2(\gamma_k + a\tan\gamma_k)^2}{(1+\tan^2\gamma_k)\cdot E}\cdot\frac{\cos\gamma_k\tau}{\gamma_k^2-\beta^2}$ $E = \gamma_k^2(m+1) + a(ma+a+1)$
M4	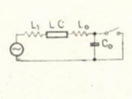	$m = \frac{L}{L_0}$ $n = \frac{C}{C_0}$ $a = \frac{L}{L_1}$	$H = \frac{ma}{ma+a+m}$	$n\,\frac{mE + pF}{pmE + (p^2+nm)F}$ $E = p + a\tanh p$ $F = a + p\tanh p$	$-\gamma^2(m+a) + nma - (ma + nm - \gamma^2)\gamma\tan\gamma = 0$	$u = \frac{man}{ma+a+m}\,\frac{m+a+ma-\beta^2}{nma - \beta^2(m+a+ma+nm-\beta^2)}\cos\beta\tau - H\Sigma\,\frac{2m^2n^2(\gamma_k^2+a^2)}{\gamma_k^6+G\gamma_k^4+K\gamma_k^2+L}\cdot\frac{\cos\gamma_k\tau}{\gamma_k^2-\beta^2}$ $G = m^2 + a^2 - 2mn + a + n$ $K = m^2a + m^2n + ma^2 - 2nma + m^2a^2 + n^2m^2 - 2nma^2$ $L = nm^2a^2 + n^2m^2a + n^2m^2a^2$
M6	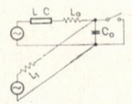	$m = \frac{L}{L_0}$ $n = \frac{C}{C_0}$ $a = \frac{L}{L_1}$	$H = \frac{ma+m+a}{m+1}$	$n\,\frac{p^2 + pm\tanh p}{p(p^2+an+mn) + (p^2+na)\,m\tanh p}$	$-\gamma^3 + \gamma(an+mn) + m(na - \gamma^2)\tan\gamma = 0$	$u = \frac{(ma+m+a)n}{(ma+m+a)n - \beta^2(m+1)}\cos\beta\tau - H\Sigma\,\frac{2\gamma_k^2m^2n^2}{\gamma_k^6 + E\gamma_k^4 + F\gamma_k^2 + G}\cdot\frac{\cos\gamma_k\tau}{\gamma_k^2-\beta^2}$ $E = m^2 + m - 2an - 2mn$ $F = a^2n^2 + m^2n^2 + 2amn^2 + m^2n - 2nma - 2m^2na$ $G = a^2n^2m + m^2n^2a + m^2n^2a^2$

Stromkreisen wurde bei den Berechnungen vorausgesetzt, daß das Verhältnis der Induktivitäten und Kapazitäten von Fernleitungen gleich ist (z. B. bei dem Kreis *A4* ist $L_2/L = C_2/C$). Diese Annäherung entspricht der Wirklichkeit. Man muß sich dessen bewußt sein, daß bei den Berechnungen Induktivitäten der Hauptnetzelemente (Generator, Transformator, Fernleitung, Drossel), die sog. »Hochfrequenzinduktivität« verwendet werden soll. Ihre Größen sind aus der Literatur und auch aus unseren Messungen bekannt.

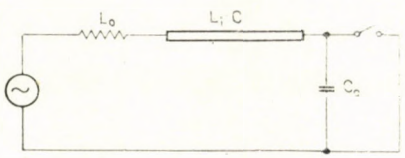

Bild 3. Prüfstromkreis

Ist die Größe dieser »Hochfrequenzinduktivität« für das vorliegende Netzelement nicht bekannt, so kann sie mit guter Annäherung auf folgende Weise berechnet werden:

$$\left.\begin{aligned} L_g^x &= 0{,}7 \cdot L_d'', \\ L_{\text{trf}}^x &= 0{,}85 \cdot L_s, \\ L_f^x &= 0{,}85 \cdot L_f, \\ L_v^x &= L_v \end{aligned}\right\}. \tag{22}$$

Die mit dem Index^x bezeichneten Größen ergeben die »Hochfrequenzinduktivität« des Generators, Transformators, der Drossel und Freileitung. Dabei sind:

L_d'' leitungsgerichtete subtransiente Induktivität des Generators;
L_s Streuinduktivität des Transformators;
L_f Induktivität der Drossel;
L_v Induktivität der Freileitung.

5. *Berechnungsbeispiel*

Betrachten wir die Berechnung von U.E.S. des in Bild 4 angegebenen, dem Stromkreis *M4* entsprechenden Netzes. Die Berechnungen sollen mit dem auf ein Spannungsniveau reduzierten Wert durchgeführt werden; er möge in unserem Beispiel 35 kV betragen. Die »Hochfrequenzinduktivität« des Transformators *Tr 1* beträgt nach den Messungen

$$L_1^x = 17{,}38 \text{ mH/Phase}.$$

Die Streuinduktivität ergibt sich zu:

$$L_{s1} = 0{,}081 \cdot \frac{35^2}{16 \cdot \omega} = 19{,}8 \text{ mH/Phase},$$

$$L_1^x = 0{,}878 \cdot L_{s1}.$$

Das liegt dem empfohlenen Wert 0,85 nahe [Gl. (22)].

Die »Hochfrequenzinduktivität« des Transformators *Tr 2* beträgt $L_2^x = 28{,}6$ mH/Phase:

$$L_2^x = 0{,}895 L_{S2};$$

$$m = \frac{L}{L_0} = \frac{\frac{3}{2} \cdot 50}{\frac{3}{2} \cdot 28{,}6} = 1{,}75;$$

$$n = \frac{C}{C_0} = \frac{\frac{2}{3} \cdot 380}{\frac{2}{3} \cdot \left(\frac{10{,}5}{35}\right)^2 \cdot 78{,}8} = 53{,}6;$$

$$a = \frac{L}{L_1} = \frac{\frac{3}{2} \cdot 50}{\frac{3}{2} \cdot 17{,}38} = 2{,}88.$$

Die Tafel II enthält die sich mit der Lösung der charakteristischen Gleichung des Netzes nach Bild 4 ergebenden Wurzeln γ_k und dementsprechend die Frequenzen der Schwingungen von U.E.S. sowie ihre Amplituden.

Die Messung der U.E.S. des Netzes nach Bild 4 wurde an dem Netzanalysator des *Forschungsinstitutes für Elektrische Energie* durchgeführt. Der Netzanalysator zur Messung der

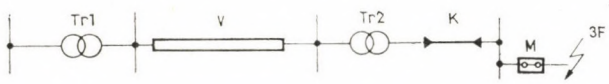

Bild 4. Stromkreis *M4* entsprechendes Netz (Daten einzelner Netzelemente: *Tr 1 Transformator* zu 120/35 kV, 16 MVA, $\varepsilon = 8{,}1\%$; *V Freileitung* $l = 40$ km, $L_v = 50$ mH/Phase, $C_v = 380$ nF/Phase; *Tr 2 Transformator* zu 35/10, kV 5, 12 MVA, $\varepsilon = 9{,}8\%$; *Kapazität positiver Reihe des Kabels* im Mitsystem $C_0 + 3C = 78{,}8$ nF)

Tafel II

Ergebnis des Berechnungsbeispiels

γ_k	Schwingung von U.E.S.	
	Frequenz [Hz] $f_k = \gamma_k / 2\pi \sqrt{CL}$	Amplitude [in e_g Einheiten]
1,164	1344	0,6006
3,72	4297	0,08882
6,485	7492	0,06805
8,912	10293	0,1498
10,52	12150	0,08316
13,072	15097	0,00763

Einschwingspannung ist dem reellen Netz vollständig äquivalent und modelliert es mit hoher Genauigkeit. Die gemessenen U.E.S.-Kurven werden in den Bildern 5 und 6 im Maßstab von 0,5 msec/Teilung und 0,1 msec/Teilung dargestellt. Die aufgrund der Tafel II berechnete U.E.S. zeigen die Bilder 7 und 8 in einem dem Bild 5 bzw. 6 entsprechenden Zeitmaß.

Das Oszillographieren der den berechneten Schwingungen entsprechenden U.E.S. erfolgte auf folgende Weise. Wir haben mit den Verhältnissen der Amplitude von Tafel II entsprechenden Induktivitäten parallel Kondensatoren geschaltet. Mit diesen Kondensatoren haben wir die den Wurzeln γ_k entsprechenden Einschwingungen eingestellt, dann bei der Schaltung der Schwingkreise nach Bild 9 zwischen die Punkte $A—B$ Stromhalbwellen eingeprägt, und dort läßt sich die U.E.S. oszillographieren. Die Dämpfung von U.E.S. in den Bildern 7 und 8 kann mit der kleinen Dämpfung der Schwingkreise nach Bild 9 erklärt werden.

Durch den Vergleich der Bilder 5 bis 8 wird es klar, daß die gemessenen und berechneten U.E.S. Kurven sehr gut übereinstimmen.

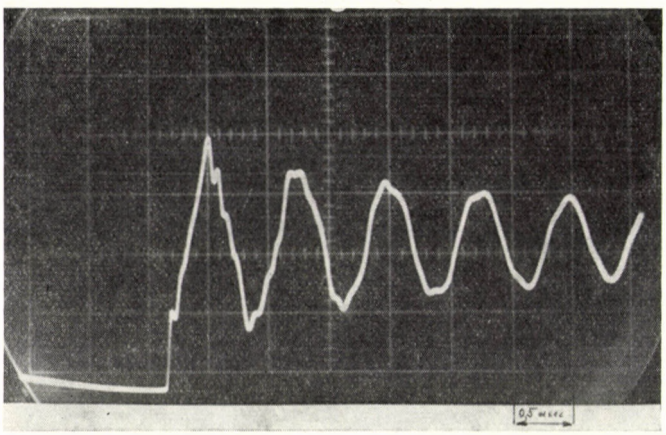

Bild 5. Gemessene U.E.S. Kurve, Maßstab 0,5 msec/Teilung

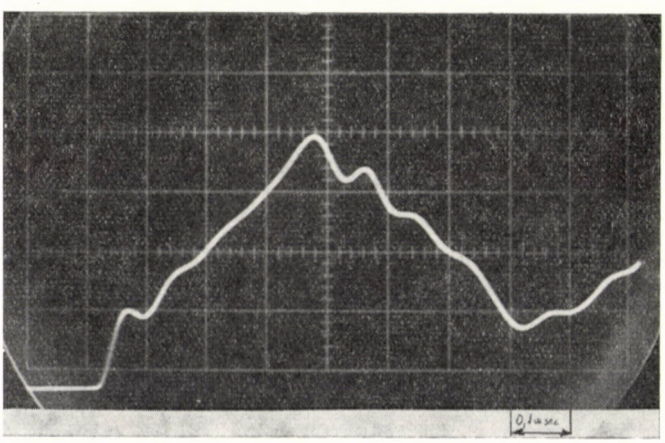

Bild 6. Gemessene U.E.S. Kurve, Maßstab 0,1 msec/Teilung

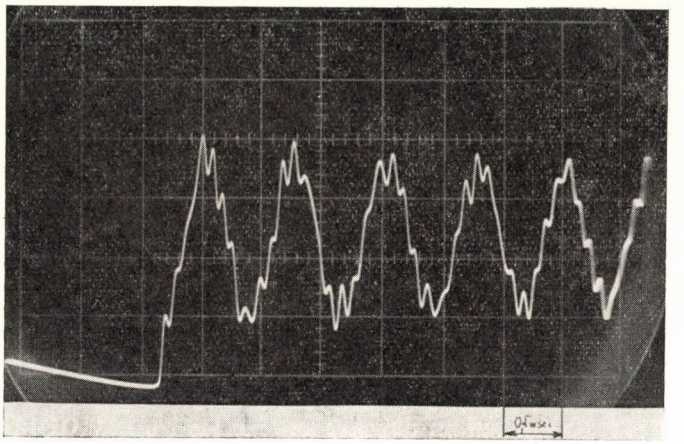

Bild 7. Berechnete U.E.S. Kurve, Maßstab 0,5 msec/Teilung

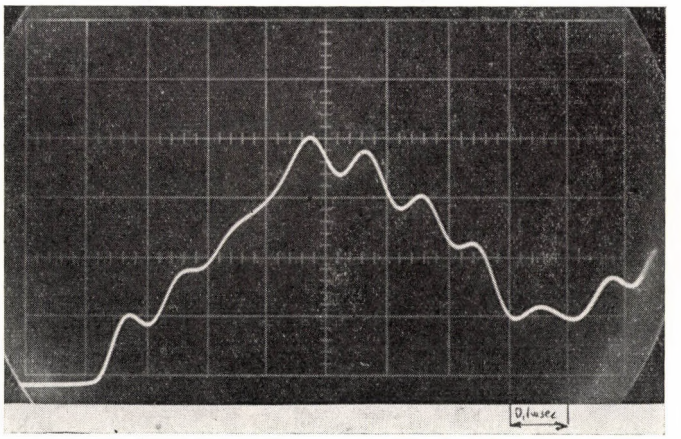

Bild 8. Berechnete V.S.F. Kurve, Maßstab 0,1 msec/Teilung

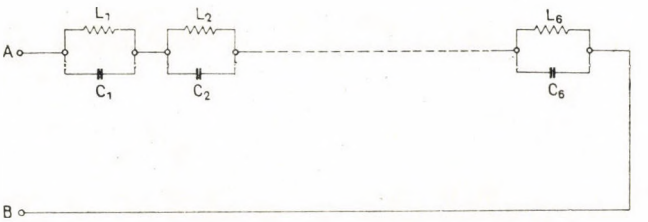

Bild 9. Schaltung zum Oszillographieren von berechneter U.E.S.

SCHRIFTTUM

1. HAMMARLUND, P.: Transient recovery voltage subsequent to short-circuit interruption; Stockholm 1946.
2. GESZTI, P. O.: Villamosművek III (Elektrizitätswerke III). Tankönyvkiadó, Budapest 1963.
3. DAHR, K.: Integrational and operational calculus; Stockholm 1935.
4. SZABÓ-BAKOS, R.: A független V. S. F. paramétereinek vizsgálata 35 kV-os távvezetékek kistávolságú zárlatai esetén (Untersuchung der Parameter von unbeeinflußter Einschwingspannung im Falle von Abstandskurzschlüssen in 35 kV Netzen). *VILLENKI*, Budapest 1961.
5. *Акодис—Корзун—Хлюпин*: Восстанавливающееся напряжение на контактах выключателя. Изв. вузов СССР энергетика, Москва 1967; № 7.
6. MIHÁLKOVICS, T.: A hálózati független visszaszökőfeszültség számítási módszerei (Rechnungsmethoden der unbeeinflußten Einschwingspannung). VEIKI, Budapest 1968.

Determination of the Independent Restriking Voltage on Circuit Breaker Contacts by Operator Calculus, From Equations Calculated in Advance, for Networks with Distributed Parameters. One method for calculating the restriking voltage arising in a given network point is the operator calculus based on Thévénin's theorem. In the case of networks containing elements with distributed parameters, not replaceable by elements with lumped constants (e.g. transmission lines), the characteristic equations forming the base of the calculation are rather complicated. To save plant engineers these calculations, HAMMARLUND [1] carried out the calculations for a considerable number of circuits. But the experience of the author has proved that over and above the circuits analyzed by HAMMARLUND, in certain cases it is necessary to carry out the calculations also for new, more complicated circuits. The author presents the method and its application to a numerical example, and furthermore he tabulates results deduced for such new circuits, together with those for the circuits of HAMMARLUND.

Определение операторным вычислительным методом независимого восстанавлибающегдся напряжения на контактах выключателя в случае сетей, содержащих элементы с распределенными параметрами, на основе заранее вычисленных уравнений *(Т. Михалкович)*. Одним из методов определения восстанавлидающегося напряжения, возникающего в данной сетевой точке, является операторный вычислительный метод, основывающийся на принципе Тевинина. В случае таких сетей, которые содержат элементы с распределенными параметрами (например, линии электропередачи), не замещаемые концентрированными, представляющие основу вычислений характеристические уравнения являются довольно сложными. Чтобы инженерам-производственникам не потребовалось выполнять эти вычисления, HAMMARLUND [1] для значительного числа цепей выполнил эти вычисления. Однако, опыт автора показал, что сверх цепей, выведенных HAMMARLUND, в отдельных случаях необходимо, чтобы вычисления были бы выполнены и для новых, более сложных цепей. Автор сверх изложения и демонстрировании на практическом примере предлагаемого метода приводит полученные для таких новых цепей результаты в табличной форме, совместно с цепями HAMMARLUND.

Acta Technica Academiae Scientiarum Hungaricae; Tomus 68 (1—2), pp. 87—115 (1970)

STRESSES IN THE VESSEL OF A PRESSURIZED WATER REACTOR DURING STOPPING

F. KOLONITS

OFFICE FOR POWER STATION AND NETWORK DESIGN, BUDAPEST

[Manuscript recieved March 27, 1968]

The present work analyzes the stresses in the vessel of a pressurized water reactor in case of quick stopping. The results obtained are evaluated numerically for the pressured vessel of a reactor of the "Voroniesh" type. This study is a part of the investigations made in 1967 by the author at the *Institute of Thermal Power Stations, Technical University, Budapest.*

Symbols

q intensity of the thermal source [kcal/cm³ s];
x wall thickness coordinate (its value is zero at the inner surface) [cm];
μ factor of energy absorption [1/cm];
δ wall thickness of the vessel [cm];
r radial coordinate in the wall of the vessel [cm];
$R_{b,k}$ the inner and outer radius of the wall of the vessel [cm];
T temperature (the reference point of the calibration is the temperature of the cooling water at the inlet, 250 °C);
A parameter characterizing the rate of the change in temperature [°C/s];
ϱ stress [kp/cm²];
t time [s, on an "adjusted" scale °C];
λ thermal conductivity [kcal/cm s °C];
α heat transfer coefficient [kcal/cm² s °C];
ϑ interval in which the temperature of the cooling water falls [°C];
t_h time by which the minimal temperature of the cooling water is reached (time-limit);
a thermal diffusivity [cm²/s];
φ_i root of the equation of the series expansion;
γ denotes λ/α;
H error;
m the half width of the active zone;
s denotes $\pi/(2\ m)$;
$\varkappa$ exponent of the exponential disappearance of the thermal source.

I. The outline of the problem

In the atomic power station planned to be built in our country according to the plans, reactors of the "Voroniesh" type would operate. The reactor of this kind is a typical representative of the group of the so-called "tank-type" PWR pressurized water reactors (Fig. 1).

The cooling medium which is at the same time a moderator as well as a reflector, is natural water. It enters the vessel at a temperature of 250 °C, streams along the wall (in the meantime its temperature is practically unchanged), then it goes upwards through the reactor and here it is heated

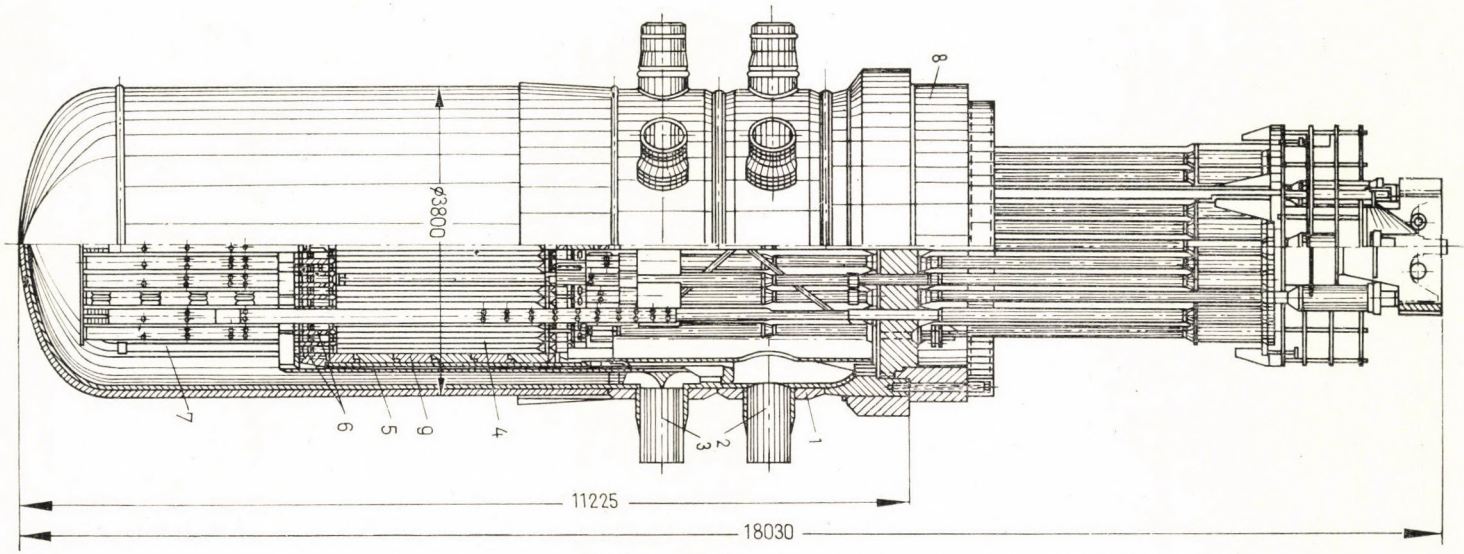

Fig. 1. The "Voroniesh" so-called "tank-type" pressurized water reactor

Denotations: Body of the vessel *1*; cooling water outlet *2*; cooling water inlet *3*; active zone of the reactor *4*; reactor well *5*; raisable basket *6*; drain tube *7*; hold-down ring *8*; thermal protection (according to STERMAN [5]).

up to a temperature of 278 °C. Having departed from the vessel it becomes colder, to a temperature of 250 °C, while producing saturated steam for the secondary circuit.

In case of PWR reactors it is necessary to apply a high pressure (in the present case 120 ata) to prevent evaporation in the primary circuit. In case of a tank-type reactor it loads the vessel; the difficulties are evidently the greater as the dimensions of the reactor and consequently of the vessel increase. The wall thickness of the vessel considered is $\delta = 12$ cm. It limits the value of pressure, consequently the temperature of the cooling water; in this way it limits the characteristics of the live steam produced for the cycle attached.

Owing to this fact, the pressure and temperature of the live steam are far from the values regarded as up-to-date in case of power stations with fossile fuel which has a bad influence on the thermal efficiency of the secondary cycle.

On the other hand, the saturated live steam will be extremely damp at the end of the expansion and it will cause problems of water breaking and erosion. As a result the efficiency of the thermal cycle becomes worse.

These are but the "essential limits" of the PWR reactors which may be regarded as being developed and which are competitive with other types applicable in the industry. Moreover, there are methods by which the characteristics can be improved in a given case but the grounds must be investigated by a complex technical-economic analysis. One of these possibilities is the fossile superheating of the saturated steam obtained from the steam-generator [17]. Naturally, this method has its drawbacks, too, besides its evident advantages (e.g. a specially constructed furnace is necessary, etc.). Moreover, problems will occur in the connected operation of the equipments having different characters.

It may occur that for some reason load relief may happen at the reactor-side (e.g. emergency stop). In this case the connected control system will begin to stop the superheating furnace immediately, but for certain time its surfaces must be cooled further. There is a possible method which uses the thermal capacity of the primary circuit to take steam off at a definite rate from the steam generator by lowering the pressure and protecting the superheating surfaces with it. As a consequence the temperature of the primary circuit will decrease in time according to a rule determined by the circumstances in the secondary circuit: the greater the steam consumption, the greater is the rate of cooling. It has, of course, an influence on the temperature of the reactor parts and above a certain rate thermal stresses of not permissible magnitude may arise.

One of the most important parts affected is the vessel of the reactor which is heavily loaded by the high pressure and the steady-state thermal

stresses. If the vessel is insulated from outside (as the type of "Voroniesh" is), the temperature increases in the wall towards the outer surface, for the wall is heated by the radiations absorbed and the heat can depart only toward the inside of the vessel. If this heating is ended (the reactor stops working) the wall is cooled to the temperature of the cooling water; the differences in the temperature decrease (with the maximum inside, at the place of maximum heat-flux). If the temperature of the cooling water decreases, meanwhile the wall gives more heat into the cooler surroundings, the heat-flux is more intensive at the inner surface of the wall, the differences in the temperature increase and the thermal stresses are higher. These exceed the steady-state values except for cases of an extremely low rate of cooling.

The analysis of the stresses in the vessel under various operating conditions was given as a diploma work at the *Institute of Thermal Power Stations, Technical University Budapest.* In the present paper a part of this analysis concerning the above problem will be explained.

II. The simplifying assumptions

The considerations involve a number of simplifying assumptions. These are explained in detail and reasons are given in [4]. Some of the statements concern only the steady state, but they be adopted in the present computations.

Summarized, the section of the vessel at the half-height of the active zone will be considered. The pattern of temperature will be determined as a plain wall which is perfectly isolated on one side. This side corresponds to the outer surface of the cylinder. The heat-source will be regarded as being distributed by the rule $q = q_0 \exp(-\mu x)$, where x is the distance measured from the inner fibre, and μ is the reduced factor of energy absorption for the radiations loading the wall. Owing to the various kinds of radiation exponential functions of various exponents should have been used but these can be replaced by one favourable exponential function. An actual consideration yielded a value of 0,1797 [1/cm]. q_0 is the intensity of the thermal source at the inner surface. No close data being available it was determined by assumption that the total allowable reduced stress (it is 3030 kp/cm^2 on the basis of the data in the Soviet literature, assuming a value of $\sigma_{0,2} = 5000$ kp/cm^2), will occur in steady state (in permanent work). Hence a value of $q_0 = 2{,}46 \cdot 10^{-4}$ kcal/cm^3 is obtainable.

Only a radial heat-flow in the wall is considered. Having determined the temperature distribution in this way, the thermal stresses are calculated on the basis of formulae concerning the thick-wall pipes:

$$\sigma_r = \frac{E}{1-\nu}\left[-\frac{1}{r^2}\int_{R_b}^{r} \alpha T r dr + \frac{r^2 - R_b^2}{r^2(R_k^2 - R_b^2)}\int_{R_b}^{R_k} \alpha T r dr\right],$$

$$\sigma_a = \frac{E}{1-\nu}\left[\frac{2}{R_k^2 - R_b^2}\int_{R_b}^{R_k} \alpha T r dr - \alpha T\right], \tag{1}$$

$$\sigma_t = \frac{E}{1-\nu}\left[\frac{1}{r^2}\int_{R_b}^{r} \alpha T r dr + \frac{r^2 + R_b^2}{r^2(R_k^2 - R_b^2)}\int_{R_b}^{R_k} \alpha T r dr - \alpha T\right],$$

where α is the coefficient of thermal expansion, E is the modulus of elasticity and ν is the Poisson number [16]. The stresses caused by the internal pressure can be calculated from the known formulae for thick-wall pipes. The axial change in the temperature-field in the wall of the vessel, mainly caused by the axial change in the intensity of the radiation emitted by the active zone of the reactor, will not be taken into consideration. (Contrary to the steady-state case now the temperature of the cooling water changes in the axial direction due to the varying temperature of the entering cooling water. But the magnitude of this change is small according to the expected flow velocity; it can be neglected.)

A fall of 100 °C is assumed in the temperature of the primary circuit and two possible ways of operation are considered:

The change in the temperature is linear in time

$$T = 250 - At, \tag{2a}$$

the change is quadratic

$$T = 250 - At + \frac{A^2}{400}t^2 \tag{2b}$$

from 250 °C to 150 °C, where A [°C/s] is a constant characterizing the rate of change.

In the detailed examinations the power of the reactor and thus the heating of the wall of the vessel are assumed to fall abruptly to zero. This is a good approximation because the process is quick in reality, too, though not abrupt.

III. General notes

The differential equation to be solved is

$$\frac{\partial^2 T}{\partial x^2} = \frac{1}{a}\frac{\partial T}{\partial t} - \frac{q}{\lambda}. \tag{3}$$

Boundary conditions (with the notation $\gamma = \lambda/\alpha$):

$$\left.\frac{\partial T}{\partial x}\right|_{x=\delta} = 0\,; \quad \gamma \left.\frac{\partial T}{\partial x}\right|_{x=0} = T\Big|_{x=0} - T_0(t)\,, \tag{4}$$

where $T_0(t)$ is one of the functions of (2). Initial condition:

$$T(x, 0) = T_{\text{Steadystate}} \quad . \tag{5}$$

If 250 °C is chosen as the reference point of the temperature calibration the terms $+250$ will be eliminated and

$$T_{\text{Steadystate}} = \frac{q_0}{\lambda_\mu}\left[\gamma(1-e^{-\mu\delta}) + \frac{1}{\mu}(1-e^{-\mu x}) - e^{-\mu\delta}x\right] \tag{6}$$

(for deduction see [4]).

The unsteady processes are essentially characterized by the T_0 time-function of the boundary condition. But every time-function can be written in the form of $T_0(At)$ as well. If the substitution $z = At$ is introduced, A is eliminated from the boundary condition.

Similarly substituting into Equ. (3) one obtains

$$\frac{\partial^2 T}{\partial x^2} = \frac{1}{a/A}\,\frac{\partial T}{\partial z} - \frac{q}{\lambda}\,.$$

As the measuring units and calibrations of the individual physical quantities are only conventions, the quantity a/A [cm²/°C] can again be denoted by a and At [°C] by t. Then the original differential equation to be solved will be returned formally, but some quantities will be measured in a special system, which will be adjusted to the present problem.

Choosing the time-calibration in this way is important because thus the advance-stage of the processes expressed by a boundary condition is chosen as the measure of the time (instead of an "absolute" unit). The comparison of the processes of various velocities but of identical character seems to be more realistic on this basis.

Let the boundary conditions be rewritten for an arbitrary fall ϑ in cooling water temperature instead of 100 °C. Linear

$$T_0 = \begin{cases} -t\,, & \text{if} \quad t < \vartheta\,, \\ -\vartheta\,, & \text{if} \quad t \geqslant \vartheta\,. \end{cases} \tag{7a}$$

The temperature of the cooling water decreases linearly to $-\vartheta$ and becomes steady at this temperature. For a quadratic change in the temperature of the cooling water it can similarly be written:

$$T_0 = \begin{cases} -t + \dfrac{t^2}{4\vartheta}, & \text{if } t < 2\vartheta, \\ -\vartheta, & \text{if } t \geqslant 2\vartheta. \end{cases} \tag{7b}$$

Let the moment when the desired temperature-fall is reached, be called time-limit (t_h). According to the statements above, this will be ϑ for the linear case and 2ϑ for the quadratic case.

IV. Determination of temperature fields

As the equation to be solved and the boundary conditions are linear, the principle of superposition may be adopted. The considered temperature field can be obtained by adding to one another the solutions in the following two fundamental problems.

a) Cooling from an even zero initial temperature, the temperature of the cooling water decreases linearly or quadraticaly to $-\vartheta$ and then becomes steady;

b) vanishing of a temperature field of arbitrary distribution (for the present case this field is that of the steadystate) by identically zero temperature of cooling water in time.

1. Effect of the change in the temperature of the cooling water

The method of operator-computation based on Laplace-transformation will be applied [5]—[10]. The differential equation to be solved

$$a \frac{\partial^2 T}{\partial x^2} = \frac{\partial T}{\partial t}.$$

Initial condition

$$T(x, 0) \equiv 0.$$

Boundary conditions

$$\left.\frac{\partial T}{\partial x}\right|_{x=\delta} = 0; \quad \gamma \left.\frac{\partial T}{\partial x}\right|_{x=0} = \left. T \right|_{x=0} - T_0.$$

Let us form the Laplace transform of the equation and the conditions with respect to time. Let its variable be p. Let it furthermore be:

$$T \circ\!\!-\!\!\bullet\, \tau; \; T_0 \circ\!\!-\!\!\bullet\, \tau_0; \; s^2 = p/a.$$

The equation (having applied the initial condition) will be

$$\frac{d^2 \tau}{dx^2} - s^2 \tau = 0.$$

Boundary conditions are

$$\left.\frac{d\tau}{dx}\right|_{x=\delta} = 0\,; \quad \gamma \left.\frac{d\tau}{dx}\right|_{x=0} = \tau\Big|_{x=0} - \tau_0\,.$$

The solution is

$$\tau = \tau_0 \frac{p \cosh s(\delta - x)}{(\cosh s\delta + \gamma s \sinh s\delta)\, p} = \tau_0\, pm(p). \tag{8}$$

First of all let us determine the inverse transform of $m(p)$, namely $M(t)$.

Though $s = \sqrt{p/a}$ is double-valued being the inverse of the even function $p = as^2$ ($p = 0$ is the point of divergence), it is represented in $m(p)$ involved in even functions — $\cosh(ks)$, $s \sinh(ks)$ — which eliminate this kind of singularities. All the singularities of $m(p)$ are the poles at the zero places of the denominator. If these are determined the expansion-theorem may be formally applied.

One root of the denominator is $p = 0$. The others with the substitution $s = j\varphi$ are

$$\cos \delta\varphi - \gamma\varphi \sin \delta\varphi = 0\,,$$

$$\cot \delta\varphi = \gamma\varphi\,. \tag{9}$$

The function cot having branches of infinite number is intersected by the straight line $\gamma\varphi$ at points of infinite number on both the positive and negative half-plane. Let the points on the positive half-plane be denoted by φ_i. The p values corresponding to them are

$$p_i = -a\varphi_i^2.$$

The φ-s on the negative half plane give the same roots.

The derivative of the denominator is

$$(\cosh s\delta + \gamma s \sinh s\delta) + p\left(\frac{\delta+\gamma}{2\,sa} \sinh s\delta + \frac{\gamma\delta}{2a} \cosh s\delta\right).$$

This is 1 at $p = 0$. At $p_i = -a\varphi_i^2$ the first term is 0. For the second term being 0, the equation with the substitution $s = \gamma\psi$ must be satisfied

$$\cot \delta\psi = -\frac{\delta+\gamma}{\delta\gamma\psi}\,.$$

This also gives $\pm$ solutions of infinite number. But $\delta\varphi_i$ is in the interval $[i\pi; i\pi + \pi/2]$ and $\delta\psi_i$ is in $[i\pi + \pi/2; (i+1)\pi]$, thus substituting $s = \varphi_i$, the

derivative will not become zero; the corresponding p_i solutions are simple ones.

On the basis of all these

$$m(p) \circ\!-\!\bullet M(t) = 1 - \sum_{i=0}^{\infty} \frac{2 \cos \varphi_i (\delta - x)}{\varphi_i^2 \cos \varphi_i \delta \left(\frac{\delta + \gamma}{\gamma \varphi_i^2} + \delta \gamma \right)} \; e^{-a \varphi_i^2 t}.$$

On the basis of the equation of series expansion (9)

$$\cos \delta \varphi_i = (-1)^i \frac{\gamma \varphi_i}{\sqrt{1 + \gamma^2 \varphi_i^2}} .$$

It can be seen that $\cos \delta \varphi_i$ is the minimum when $i = 0$, $\gamma \varphi_i$ being also minimum. Summarized: the infinite series involved is "majorized" term-by-term in an absolute value by the series

$$\sum_{i=0}^{\infty} \frac{2}{\varphi_i^2 \, \delta \gamma \cos \varphi_0 \delta} .$$

But evidently if $i\pi < \delta \varphi_i$, then even the latter series is "majorized" by the series

$$\frac{2}{\gamma \delta \cos \varphi_0 \delta} \left(\frac{1}{\varphi_i^2} + \sum_{i=1}^{\infty} \frac{\delta^2}{i^2} \right).$$

This series being convergent and "majorizing" the original series in the entire domain $(x; t)$, the latter is absolutely and uniformly convergent (according to Weierstrass's theorem [11]). $p\tau_0$ is the transform of dT_0/dt considering $T_0(0) = 0$. Therefore, in convolution-form

$$T = M * \frac{dT_0}{dt} .$$

The series of M being absolutely convergent the convolution can be formed term-by-term. In case of $t > t_h$ it must be taken into account that beyond t_h

$$\frac{d\tau_0}{dt} \equiv 0 .$$

At last for quadratic change

$$t < t_h, \; T = -t + \frac{t^2}{4\vartheta} +$$

$$+ \sum_{i=0}^{\infty} \frac{2 \cos \varphi_i (\delta - x) \left[\left(1 + \frac{1}{2\vartheta a \varphi_i^2} \right) (1 - e^{-a \varphi_i^2 t}) - \frac{t}{2 \vartheta a \varphi_i^2} \right]}{a \varphi_i^4 \cos \varphi_i \delta \left(\frac{\gamma + \delta}{\gamma \varphi_i^2} + \gamma \delta \right)} , \tag{10}$$

$$t > t_h,\ T = -\vartheta + \\ + \sum_{i=0}^{\infty} \frac{2\cos\varphi_i(\delta - x)\left[\left(1 + \frac{1}{2\vartheta a\varphi_i^2}\right)(1 - e^{-a\varphi_i^2 t_h}) - \frac{t_h}{2\vartheta a\varphi_i^2}\right]}{a\varphi_i^4 \cos\varphi_i\,\delta\left(\frac{\gamma+\delta}{\gamma\varphi_i^2} + \gamma\delta\right)} e^{-a\varphi_i^2(t-t_h)}.$$

In a linear case there are no terms involving ϑ in the infinite series and in case of $t < t_h$ the corresponding linear formula has to be added to the series.

2. *Disappearance of an arbitrary temperature pattern in time (the effect of the initial condition)*

Now the Fourier method of separation will be applied. The differential equation to be solved is

$$a\frac{\partial^2 T}{\partial x^2} = \frac{\partial T}{\partial t}.$$

Initial condition is $T(x; 0) = f(x)$. Boundary conditions

$$\left.\frac{\partial T}{\partial x}\right|_{x=\delta} = 0\,;\quad \gamma\left.\frac{\partial T}{\partial x}\right|_{x=0} = \left. T\right|_{x=0}.$$

Let us seek for the solution in the form $T = u(x)v(t)$. Rewritten in a favourable form (differentiation with respect to its own argument is indicated by a comma) it can be separated

$$\frac{u''}{u} = \frac{1}{a}\frac{v'}{v}.$$

As the temperature can only decrease in time, the constant of separation is negative. The equations are

$$u'' + \varphi^2 u = 0\,,$$
$$v' + a\varphi^2 v = 0\,.$$

The solution $T = u \cdot v$ satisfying the boundary condition No. 1 is

$$T = k\cos\varphi(\delta - x)\,e^{-a\varphi^2 t}. \qquad (11)$$

This satisfies the boundary condition No. 2 if

$$\gamma\varphi \sin \varphi\delta = \cos \varphi\delta ,$$

$$\cot \varphi\delta = \gamma\varphi .$$

This agrees with the equation of series expansion (9) obtained during the solution of the previous fundamental problem.

As it is represented in (11), only in even functions the negative φ_i-s do not increase the group of the fundamental solutions.

Now only the initial condition remains to be satisfied; it is necessary that

$$f(x) = \sum_{i=0}^{\infty} k_i \cos \varphi_i(\delta - x). \tag{12}$$

The function system $\cos \varphi_n(\delta - x)$ is orthogonal in the interval $[0; \delta]$ this can be proved in case of $n = m$

$$\int_0^{\delta} \cos \varphi_n(\delta - x) \cdot \cos \varphi_m(\delta - x)\, dx = \frac{\sin \varphi_n \delta \cdot \cos \varphi_n \delta}{2\varphi_n} + \frac{\delta}{2} \tag{13}$$

and for $n \neq m$ it is 0.

The question of completeness will not be considered here, we only refer to the deep analogy of the considered function system and the well-known complete elementary trigonometric systems (multitude, etc.).

Consequently it is possible to expand a function into series according to the function-system considered. The formula of coefficients is

$$A_n = \frac{\int_0^{\delta} f(x) \cos \varphi_n(\delta - x)\, dx}{\int_0^{\delta} \cos^2 \varphi_n(\delta - x)\, dx} .$$

The denominator was determined in Equ. (13). In the evaluation of the numerator the Laplace transformation is a useful aid. The integral is a convolution if δ is regarded as variable. If $f(\delta) \circ\!\!-\!\!\bullet\, W\, F(p)$ the integral is

$$\mathfrak{L}^{-1}\left[\frac{pF(p)}{p^2+\varphi_n^2}\right].$$

If $f(x)$ is the steady-state plane-formula (6), then having determined the expansion according to (12), the whole solution can be regarded as a sum of the fundamental solutions obtained according to (11).

$$T = \frac{q_0}{\lambda} \sum_{i=0}^{\infty} \frac{2 \cos \varphi_i(\delta - x)\left[1+\gamma\mu - \dfrac{\gamma\mu\, e^{-\mu\delta}}{\cos \delta\varphi_i}\right]}{(\mu^2+\varphi_i^2)\,\varphi_i^2 \cos \delta\varphi_i \left(\dfrac{\gamma+\delta}{\gamma\varphi_i^2} + \delta\gamma\right)} \; e^{-a\varphi_i^2 t}. \tag{14}$$

This is absolutely and uniformly convergent in its entire domain.

V. Computational technics

1. Solution of the equation of series expansion

Having adopted the substitution $\delta\varphi_i = x_i$

$$\cot x_i = \frac{x_i}{k},$$

where $k = \delta/\gamma$. If x_{n-1} is known, hence x_n can be determined approximately, for (see Fig. 2):

$$\begin{aligned} \cot(x_{n-1} - \lambda_n) &= \cot x_n, \\ \cot x_n - \cot x_{n-1} &= \frac{\pi - \lambda_n}{k}. \end{aligned} \tag{15}$$

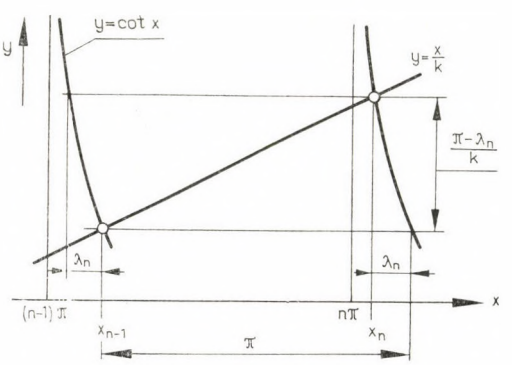

Fig. 2

Having adopted the substitution

$$\cot \lambda_n \approx \frac{1}{\lambda_n}$$

(the first term of its expansion [12]) and using the equation of series expansion after reduction from the system of Equs (15), it follows that

$$x_{n-1}\lambda_n^2 - [k(k+1)+x_{n-1}(x_{n-1}+\pi)]\lambda_n+\pi k = 0.$$

Since λ_n is small but k and x_{n-1} are relatively great, the quadratic term may be neglected. Thus,

$$\lambda_n = \frac{\pi k}{k(k+1)+x_{n-1}(x_{n-1}+\pi)} .$$

Hence ($\pi^* = \pi/\delta$)

$$\varphi_n = \varphi_{n-1}+\pi^* - \frac{\pi^* k}{k(k+1)+\delta^2\,\varphi_{n-1}(\varphi_{n-1}+\pi^*)} . \tag{16}$$

The smaller values (where the approximation is inaccurate) are tabulated in the literature [5, 13]. In our case the formula (16) yielded an approximation equivalent to the tables referred to already at relatively small serial numbers.

For a more accurate determination of the roots, iteration will be applied combined with the tangent-method [14]. Let ψ_i be an approximation to the root φ_n. The equation of series expansion can be rewritten in the form

$$\psi_{i+1} = \frac{1}{\delta}\left[\left(n+\frac{1}{2}\right)\pi - \operatorname{arc\,tan}\,\gamma\psi_i\right] = F(\psi_i). \tag{17}$$

The pure iteration is convergent, since

$$M = \left|\frac{dF}{d\psi}\right| = \frac{\gamma}{\delta}\,\frac{1}{1+\gamma^2\psi^2} < 1 .$$

F and M decrease monotonously and F is convex from below.

The application of the tangent-method is favourable, the derivative formula being more simple than a step of iteration. This is shown by the common representation of iteration on Fig. 3.

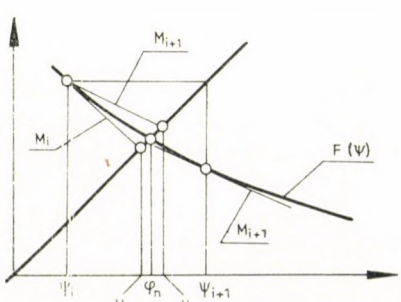

Fig. 3

The approximation is from both sides (as the derivative is negative); ψ_i and ψ_{i+1} fall on different sides of φ_n; let their distance be Δ. Let the M of the individual approximations be M_i and M_{i+1}. The approximative values $(u; v)$ shown in the figure are also on different sides of φ_n and if their arithmetic mean is taken, the half of their difference will be the maximum possible error. If

$$S_i = \frac{\Delta}{1+M_i},$$

then

$$\varphi_n \approx \psi_i + \frac{1}{2}(S_{i+1}+S_i); \qquad H < \frac{1}{2}(S_{i+1}-S_i). \tag{18}$$

One can go on with the process to the desired accuracy.

In our computations the first step was already found to be satisfactory; the value of $\cos \delta\varphi_i$ calculated directly from the result deviated from that calculated from the equation of series expansion by a trigonometric formula only in the sixth to seventh decimal-figure.

2. Completed analyses: the method of computations

The formulae employed are not adequate for manual calculations, therefore, the problem was programmed for the computer of type *Elliot 803/B* of the *Ministry of Heavy Industries* in the programming language *Autocode A 103.*

The program can be divided into four parts from a functional point of view

a) feeding of data;

b) computing and printing subroutines;

c) segments organizing the course of solution;

d) modification of data, emergency print.

Part *a)* reads in and stores all fundamental data necessary for the computation.

Part *b)* includes:

The root generator. There is the first solution to the equation of series expansion $\delta\varphi_0$ among the fundamental data. The subroutine is able to determine the following φ from this. Moreover, it computes a number of quantities depending on φ which are frequently used in series expansions and stores all these values.

The rest of the program uses these stored data. If a root of higher serial number is needed it uses the root-generator.

The subroutines for the computation of temperature distribution. These evaluate the solutions of various fundamental problems (among them those explained here), taking into consideration the given fundamental data and the given limit of error. They can take into consideration 30 members of expansions in case of $t < t_h$ and beyond this limit 25 members. The expansion corresponding to $t = 0$ is stored by the first calculation and furthermore the exponential multiplicators corresponding to the various points of time are to be calculated only.

Subroutine for calculation of stresses. It evaluates the components of stress on the basis of formulae (1). It evaluates the integrals by means of the Simpson method. It determines the reduced stresses according to Hencky—Huber—Mises and prints the results.

The segments of part *c)* use the subroutines of part *b)* in a suitable sequence. All individual segments solve one certain problem, correspondingly superpose several patterns of temperature. The control can be transmitted to the individual segments from the keyboard or from a tape. There is a segment which is able to print the results of every subroutine. The tapes obtained or an arbitrary temperature distribution can be re-read by another segment which summarizes them and then the subroutine for calculation of stresses can be called by another segment.

The segments of part *d)* placed at various parts of the program assure its elastic and economic applicability. Some fundamental data can be modified; results calculated and stored (e.g. the roots of the equation of series expansion) can be printed on tape and can be re-read with their aid. It may have importance if a lengthy computation must be carried out in several parts, due to the little time when the computer would be available.

The computation corresponding to the problem to be solved must be built of these constituent parts by means of suitable organization from keyboard or tape control transfers, triggers in a favourable sequence.

3. *Completed analyses: Calculations*

The characteristics of the material are calculated for 250 °C [15]; $\alpha =$ $= 18\,270$ kcal/m²h°C [4]. We analyzed the temperature and stress patterns to the moment $t = 250$ by the values $A = 10, 20, 50, 100$ °C/min for linear and for quadratic changes in temperature. The results obtained for $A = 20$ °C/min are plotted in Figs 4—9 (for other values of A, curves of a similar character can be obtained). The maximum always occurs at the inner surface (resulting from tensile stresses).

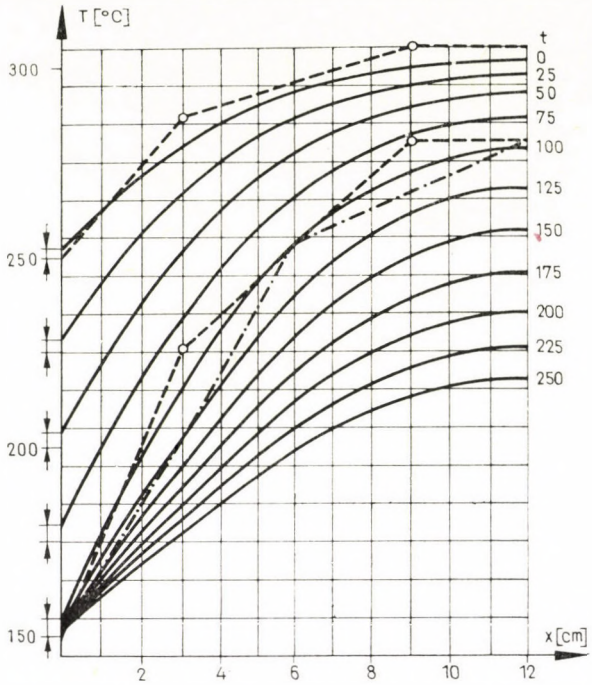

Fig. 4. Temperature diagram: Linear cooling, $A = 20$ °C/min, $q_0 = 0{,}000246$ kcal/cm³s (Dashed and dotted line: approximative methods; see Appendix)

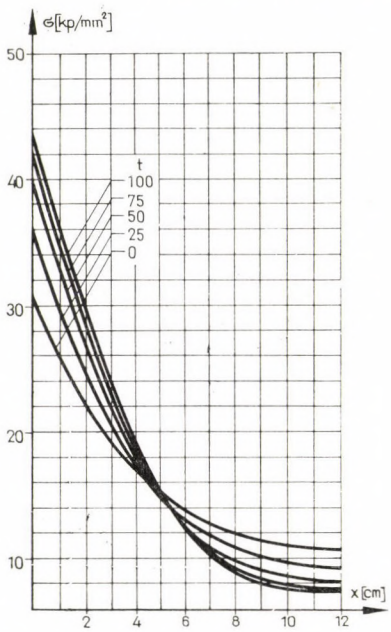

Fig. 5. Stress diagram: Linear cooling, $A = 20$ °C/min, $q_0 = 0{,}000246$ kcal/cm³s, $t = 0-100$

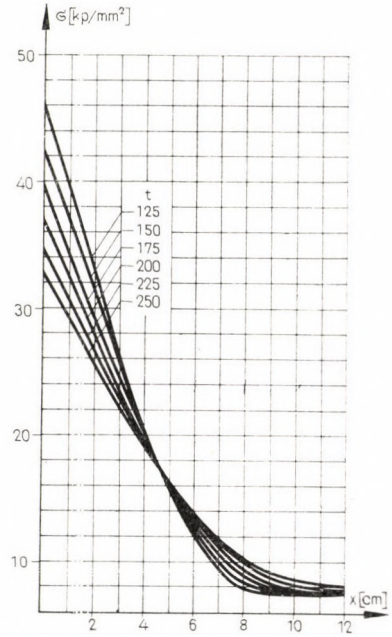

Fig. 6. Stress diagram: Linear cooling, $A = 20$ °C/min, $q_0 = 0{,}000246$ kcal/cm³s, $t = 125-250$

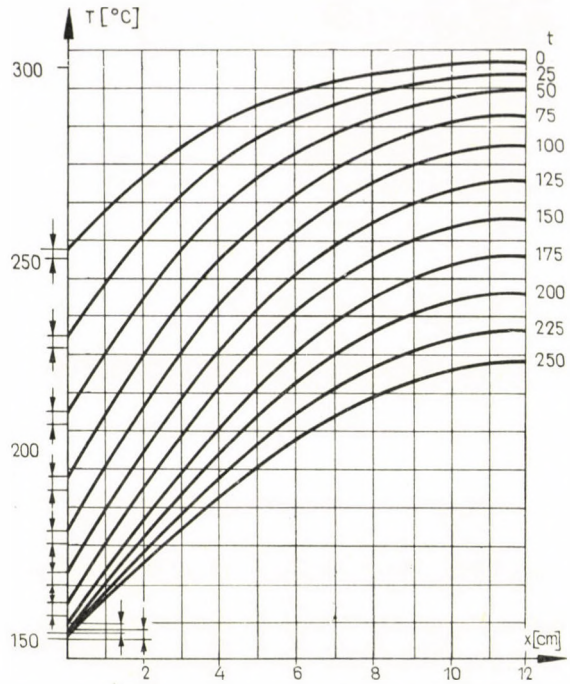

Fig. 7. Temperature diagram: Quadratic cooling, $A = 20$ °C/min, $q_0 = 0{,}000246$ kcal/cm³s

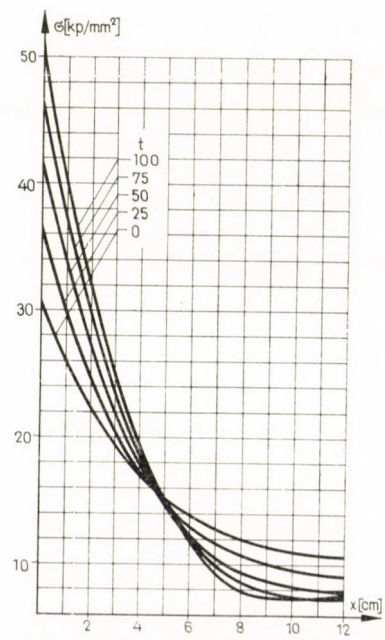

Fig. 8. Stress diagram: Quadratic cooling, $A = 20$ °C/min, $q_0 = 0{,}000246$ kcal/cm³s, $t = 0-100$

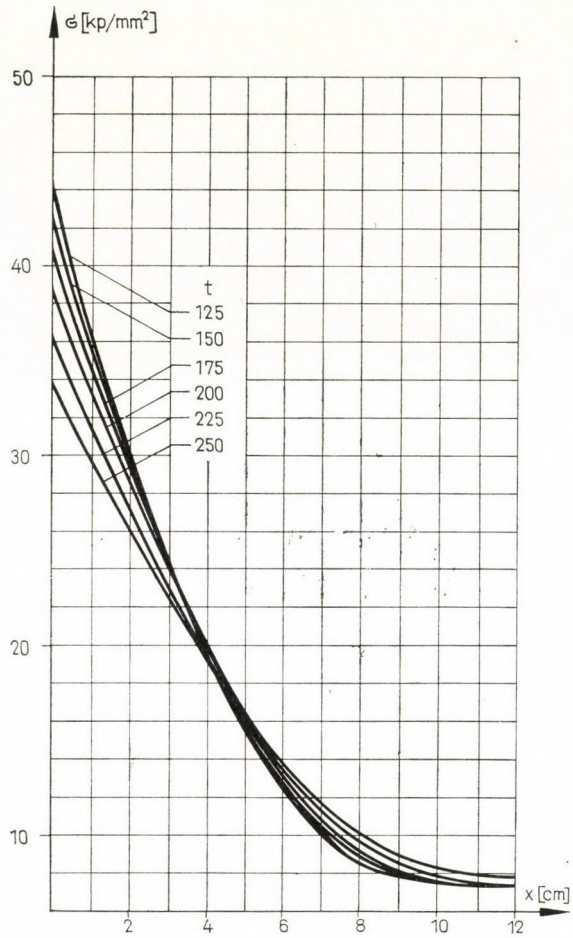

Fig. 9. Stress diagram: Quadratic cooling, $A = 20$ °C/min, $q_0 = 0{,}000246$ kcal/cm³ s, $t = 125-250$

The critical rate of cooling will be determined from the following conditions:

Peaks of stresses will occur only temporarily due to cooling. The quick stopping evidently cannot be a frequent state of operation. For these reasons the total $\sigma_{0,2}$ is considered to be the limit.

From the previous results the zone where the excess of this limit was to be expected could be seen. Further calculations have been carried out at points of the needed number in this zone. For a linear case the values of σ_{max} listed in Table I are valid.

The maximum stress always occurs at $t = 100$. This is in accordance with the physical meaning; the diminuation of temperature of the cooling water increases the gradient at the wall up to $t = 100 = t_h$, then this effect ends

Table I

Values of σ_{max} [kp/cm²] *for a linear case*

A [°C/s]	t				
	90	95	100	105	110
0,330	4826,2	4905,7	4983,6	4905,4	4822,0
0,333	4834,2	4914,2	*4992,6*	4914,9	4832,0
0,338	4847,1	4928,0	*5007,2*	4930,5	4848,3
0,340	4852,2	4933,4	5012,9	4936,6	4854,7

and equalization begins. If a parabola were drawn in the neighbouring values of t, it would give a maximum close to 100.

The results are nearly linear as a function of A: having interpolated, the critical rate is

$$A_{crit,1} = 0{,}33553\ °C/s \doteq 20{,}1318\ °C/min.$$

The temperatures and stresses existing in the moment $t = 100$ (i.e. when the maximum thermal stress occurs) are shown in diagrams of Figs 10—11 by various values of A in order to illustrate its effect. In diagram of Fig. 12 the stress components existing when $t = 100$ and $A = 20$ °C/min are shown; the latter is close to the critical value.

Table II

Values of σ_{max} [kp/cm²] *for a quadratic case*

A [°C/s]	t				
	134	142	150	158	166
0,65	4957,0	*4968,3*	*4969,0*	*4960,0*	4940,9
0,70	5014,2	*5028,9*	*5033,3*	*5027,6*	5011,8
0,75	5065,0	*5082,9*	*5090,5*	*5087,7*	5075,1
0,80	5110,3	5131,3	5141,8	5141,8	5131,9

The case of quadratic cooling of the cooling water has been considered in the zone of Table II. The maximum time depends here on the rate of change. Having drawn a parabola in the neighbouring values, the value and time of the maximum have been determined (Table III).

Table III

Value and time of the maximum

A [°C/s]	The maximum's	
	value [kp/cm²]	time
0,65	4969,888	146,578
0,70	5027,623	149,485
0,75	5090,853	151,850

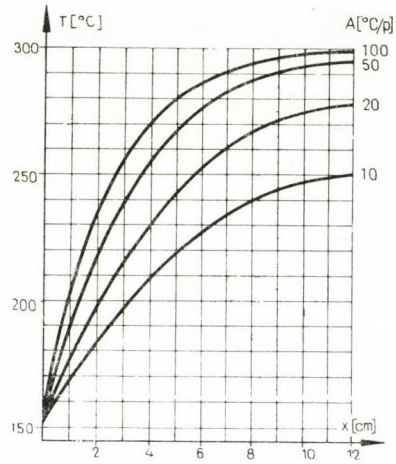

Fig. 10. Temperature diagram: Linear cooling, $t = 100$ (in case of σ_{max}), $q_0 = 0{,}000246$ kcal/cm³s

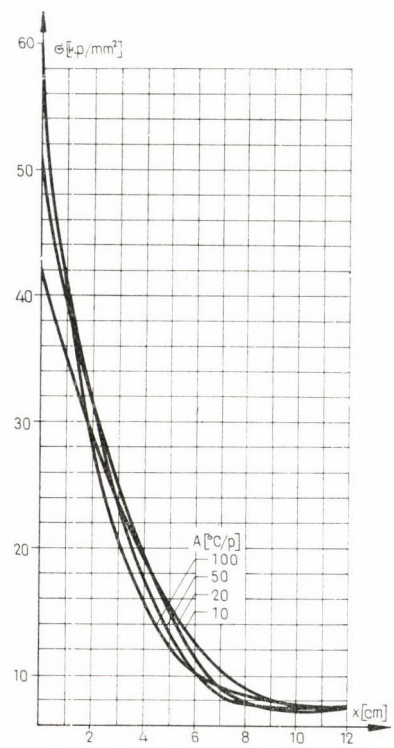

Fig. 11. Stress diagram: Linear cooling, $t = 100$ (in case of σ_{max}), $q_0 = 0{,}000246$ kcal/cm³s

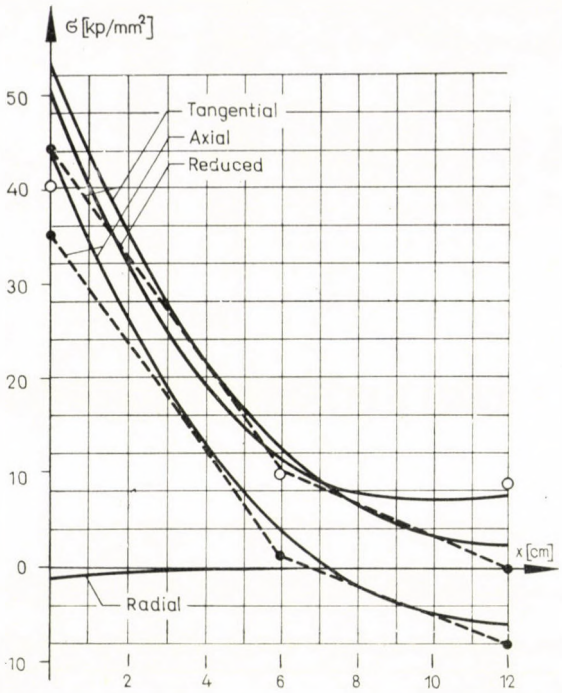

Fig. 12. Stress diagram: Linear cooling, $A = 20$ °C/min, $t = 100$ (in case of σ_{max}), $q_0 = 0{,}000246$ kcal/cm³ s (dashed line: stresses, ○: reduced stress calculated with the approximative method)

It can be seen that both place and value of the maximum grow with the rate. The values of A and the time corresponding to 5000 kp/cm² were determined with the aid of parabolic interpolation (in the function of A):

$$A = 0{,}67728\ °C/s \div 40{,}6368\ °C/min$$

and

$$t = 148{,}099$$

(linear interpolation would yield 0,6761 °C/s and 148,094).

An interesting result can be obtained by examining the minimal time of cooling necessary in case of different methods of operation. These are in the relative time-scale 100 and 200, respectively. Having converted them into the actual time by means of the critical rate parameters determined above, 4,97 and 4,925 min are obtained, the difference 0,91%. From this viewpoint the two methods of operation are practically equivalent.

VI. Additional considerations

All our calculations were based on the assumption that the heating of the wall comes to an end abruptly. It is a rather good approximation because the protective device, if it works properly, must have a very quick effect.

The secondary radiation sources are of a much lower intensity (and also disappear in time). For the sake of completeness let us look at the question more closely.

The heating evidently depends considerably on the power of the reactor and this on the neutron-flux. The flux diminishes according to a rather complicated exponential rule in a sub-critical state. For the purposes of our informative considerations it is replaced by one exponential disappearance $\exp(-\varkappa t)$.

The conditions in the axial direction and along the thickness of the wall will be examined separately with the approximating assumptions explained in [4] and also applied here.

1. Examination in the axial direction

Let be cut out a 1 cm segment of the vessel wall in the axial direction and let the axial heat-flow and the differences in the temperature along the wall-thickness be neglected (so the approximative model applied in [4] is obtained).

The heating is assumed to be cosinusoidally distributed along the width of the active zone ($2m = 250$ cm) and its intensity is assumed to be q_0 in the middle. Having introduced the notation $\pi/(2\,m) = s$ and regarding $\varphi(t)$ as the time-function of the disappearance, the equilibrium of heat generated, departing into the surroundings of temperature $T_0(t)$ and used for the heating of the wall, can be written in the form

$$q_0\,\delta dx dt \varphi(t) \cos sx = (T - T_0, \alpha dx dt + \varrho c \delta dx \frac{dT}{dt}\,dt\,,$$

where c is the specific heat; ϱ is the density of the material of the wall. With the notation $\alpha/\varrho c\delta = k$

$$\frac{dT}{dt} + kT = \frac{\delta k}{\alpha}\,q_0\,\varphi(t) \cos sx + kT_0.$$

Having varied the constants one obtains

$$T = \frac{\delta k}{\alpha}\,q_0 \cos sx\, e^{-kt} \int_{t_0}^{t} e^{kt}\varphi(t)\,dt + ke^{-kt} \int_{t_0}^{t} e^{kt}\,T_0\,dt \quad (t_0 = \text{const.}).$$

In a steady-state case [4]

$$T = \frac{\delta}{\alpha}\,q_0 \cos sx,\; T_0(0) = 0\,.$$

This is the initial condition of the problem. Hence

$$T = \frac{\delta k}{\alpha} q_0 \cos sx\, e^{-kt}\left[\int_0^t e^{kt}\varphi(t)\,dt + \frac{1}{k}\right] + k\, e^{-kt}\int_0^t e^{kt} T_0\,dt. \tag{19}$$

All these only concern the heated section; there is no change in the unheated part. The axial gradient depends on φ with the following factor of proportionality

$$S = e^{-kt}\left[\int_0^t e^{kt}\varphi(t)\,dt + \frac{1}{k}\right].$$

It is minimal if the values of $\varphi(t)$ are the possibly lowest ones, namely, in case of abrupt stop. In all other cases it is higher; written specially for the exponential disappearance mentioned above

$$S = \frac{e^{-kt} - e^{-\varkappa t}}{\varkappa - k} + \frac{e^{-kt}}{k}.$$

It is always positive and decreases monotonously with time, it has no local extreme value and decreases with the increase of $\varkappa$.

It can be seen that in case of non-abrupt disappearance of the heat source higher gradients and so higher thermal stresses will arise in the same moments. In case of exponential disappearance there is no peak-value in time, though the term additional to that for the skiplike case (the first part of S) at first it grows from zero and disappears only later.

2. *Examination in radial direction*

One more temperature distribution is to be superposed to the solution on the fundamental problem treated in IV. 2. The $q(t)$ which we wished to obtain is shown in Fig. 13a and that assumed previously, in Fig. 13b. The temperature pattern being the difference of them is shown in Fig. 13c and it can be calculated as

$$q(t) = 1(t)\, e^{-\varkappa t}.$$

The equation is

$$\frac{\partial^2 T}{\partial x^2} = \frac{1}{a}\frac{\partial T}{\partial t} - \frac{q_0}{\lambda} e^{-\mu x}\, 1(t)\, e^{-\varkappa}.$$

Initial and boundary conditions are

$$T(x, 0) \equiv 0;$$

$$\left.\frac{\partial T}{\partial x}\right|_{x=\delta} = 0; \quad \gamma \left.\frac{\partial T}{\partial x}\right|_{x=0} = T\Big|_{x=0}.$$

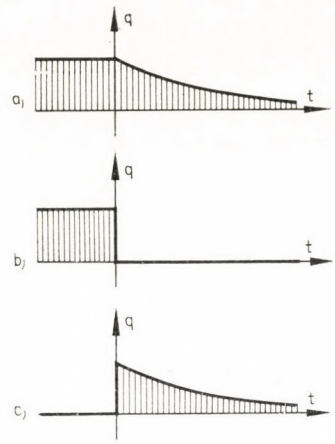

Fig. 13

Its Laplace-transform is ($s = \sqrt{p/a}$)

$$\frac{d^2\tau}{dx^2} - s^2\tau = = \frac{q_0}{\lambda(p+\varkappa)} e^{-\mu x},$$

where

$$T(x, t) \circ\!-\!\bullet \tau(x, p).$$

Boundary conditions

$$\left.\frac{d\tau}{dx}\right|_{x=\delta} = 0\,; \quad \gamma \left.\frac{d\tau}{dx}\right|_{x=0} = \tau\Big|_{x=0}.$$

Solution

$$\tau = \frac{aq_0}{\lambda} \cdot \frac{1}{(p+\varkappa)(p-a\mu^2)} \left[e^{-\mu x} - \right.$$

$$\left. - \frac{\mu e^{-\mu\delta}\left(\frac{\sinh sx}{s} + \gamma \cosh sx\right) - (1+\gamma\mu)\cosh s(\delta - x)}{\cosh s\delta + \gamma s \sinh s\delta} \right].$$

Re-transformed and superposed on the fundamental problem IV. 2

$$T = \frac{q_0}{\lambda} \sum_{i=0}^{\infty} \frac{2\cos\varphi_i(\delta - x)\left[1 + \gamma\mu - \frac{\gamma\mu\, e^{-\mu\delta}}{\cos\delta\varphi_i}\right]}{(\mu^2 + \varphi_i^2)\varphi_i^2 \cos\delta\varphi_i \left(\frac{\gamma+\delta}{\gamma\varphi_i^2} + \delta\gamma\right)} \cdot \frac{\varkappa e^{-a\varphi_i^2 t} - a\varphi_i^2 e^{-\varkappa t}}{\varkappa - a\varphi_i^2} \cdots . \qquad (20)$$

The multiplier dependent on t (and partly independent of $\varkappa$) can be written in the form

$$a\varphi_i^2\left[\frac{e^{-a\varphi_i^2 t}-e^{-\varkappa t}}{\varkappa-a\varphi_i^2}+\frac{e^{-a\varphi_i^2 t}}{a\varphi_i^2}\right]$$

which is a perfect analogue of S. The conclusions are the same. The part additional to the gradient (the first term) decreases with the growth of $\varkappa$.

The considerations can be carried out even in this case similarly to the previous one for an arbitrary $\varphi(t)$ time-function of disappearance. Let then $\varphi_{\circ-\bullet}\Phi$ be the Laplace transform of the solution (20) which has to be multiplied by $(p+\varkappa)\Phi$. And since

$$(p+\varkappa)\Phi_{\circ-\bullet}\varphi'(t)+\varphi(-0)\delta(t)+\varkappa\varphi$$

(δ is the Dirac pulse), the temperature-field sought for will be the convolution of this and Equ. (20), it is to be superposed on the field assuming abrupt disappearance.

If $\varphi(t)$ is a skip, $\varphi(-0)=1$ and $\varphi'(t)$ is $-\delta(t)$, the third term is identically zero, there is really no field to be superposed being there because one member of the convolution being zero. But in every other case it exists and it increases the gradients and thermal stresses compared to the abrupt case.

APPENDIX

Approximative method for calculation

The considerations explained above needed a rather complicated mathematical apparatus; to the application of the method a digital computer is necessary. The question may be raised whether a "more practical" method could be constructed by means of suitable approximations which, though it is not exact, gives approximative informations about the conditions.

For the determination of the temperature pattern let the wall be separated into two layers of a thickness of 6 cm. The total heat generated in steady state in a layer (of 1 cm^2 crosssectional area) between certain x_1 and x_2 coordinates is

$$Q=\int_{x_1}^{x_2} q_0\, e^{-\mu x}=\frac{q_0}{\mu}\left(e^{-\mu x_1}-e^{-\mu x_2}\right). \tag{21}$$

On the basis of this equation the heat generated in the layer at the cooling water is $Q_1 = 0{,}903$ cal/s and that in the outer layer $Q_2 = 0{,}3075$ cal/s. From the viewpoint of the heat-conduction between the layers let be considered as determinants the temperatures of the fibres in the middle T_1^* and T_2^* and let it be assumed that the temperature of the inside wall is equal to that of the cooling water, i.e. 250 °C in steadystate. As all the generated heat departs into the cooling water, it can be written as:

$$\begin{aligned}\frac{\lambda(T_2^*-T_1^*)}{\delta/2}&=Q_2\,,\\ \frac{\lambda(T_1^*-250)}{\delta/4}&=Q_1+Q_2\,.\end{aligned} \tag{22}$$

Hence $T_1^* = 287{,}17$ °C, $T_2^* = 306{,}06$ °C. The function of temperature can be replaced by a dashed line drawn across these points (it goes horizontally towards the outside wall according to the condition grad $T = 0$). In the temperature diagram of Fig. 4 this approximation is indicated by a dotted line.

The problem for unsteady state has been solved by turning to a difference-equation of the form:

$$\Delta T_t \cong a\Delta t(\Delta^2 T/\Delta x^2)\,. \tag{23}$$

For the second difference ratios it can be shown that

$$\left[\frac{\Delta^2 T}{\Delta x^2}\right]_1 = \frac{4}{\delta^2}(T_2^* - 3T_1^* + 2T_0)\,,$$
$$\left[\frac{\Delta^2 T}{\Delta x^2}\right]_2 = \frac{4}{\delta^2}(T_1^* - T_2^*)\,. \tag{24}$$

According to the simplified pattern the temperature of the fibre is in the middle $T_1 = (T_1^* + T_2^*)/2$, at the outside $T_2 = T_2^*$. The results of the computations are tabulated (Table IV). Linear change in temperature was assumed during the calculations carried out for every 75 seconds till the end of change in temperature (in the diagram it is $t = 100$). For the sake of comparison the values given by the computer, and the errors are written at the values of T_0, T_1 and T_2. The rate of cooling of the cooling water is 20 °C/min.

Table IV

Time [s]		T_0 [°C]	T_1^* [°C]	T_1 [°C]	$T_2 = T_2^*$ [°C]
0		250	287,17	296,61	306,06
75		225	276,35	289,36	302,37
150		200	261,38	279,34	297,30
225		175	244,42	267,31	290,29
300	calculated	150	226,28	253,81	281,33
	given by the computer	154,82	—	253,51	279,22
Error [%]		−3,112	—	+0,118	+0,756

In spite of the very rough model a rather good approximation was obtained at the two sides, and in the middle of the wall (dotted line in the temperature diagram of Fig. 4).

The stresses can be calculated like for shells, as the wall thickness is small compared to the other dimensions of the vessel [18].

TIMOSHENKO assumes a steady change in temperature between the two fibres at the sides of the wall. He states that the simple plate would become spherical if it were freely deformed. If the plate cannot become deformed freely, stresses will arise to keep it in the "operating form" instead of the stress-free spherical form. A cylindrical shell would remain cylindrical even after heating, if the temperature pattern is symmetrical; the form of the shell remains unchanged apart from the radial growth. The stresses can be calculated similarly to clamped simple plates.

This treatment, as in general the theory of shells, neglects the radial stresses. It does not cause any trouble in our case, as the radial stresses are low in comparison with the others.

But the temperature pattern cannot be regarded as being linear and, therefore, we shall try to make the method more accurate according to TIMOSHENKO.

The wall will be separated into two layers, as during the calculation of the temperature field and the temperature differences between the outside fibres of the layers will be taken into consideration. So the distribution indicated by a dotted line in the diagram of Fig. 4 will be considered as a rough approximation but not as rough as if the total change were to be regarded as linear.

If the individual layers became deformed freely, they would form spheres of the radius

$$R_i = \frac{\delta}{2\alpha \Delta T_i} \; ; \tag{25}$$

the radius would be smaller at the inside, i.e. the radius of layer 1.

Let moments act in both dimensions of the plate in order to bend the two spherical surfaces to have the same mean radius R. One of the spheres has to be bent outwards and the other in the opposite direction by the moment of the same magnitude in order to produce the same stresses and strains in the outside fibres. In this way the two layers can be joined into one plate; in one cross-section the sum of the moments will be zero, no outer force is needed to sustain the form. The spherical surface of the radius R will be the "force-free form" of the plate, only the internal thermal stresses will act. The stresses produced by the partial moments are

$$\begin{aligned} \sigma_1 &= \frac{E\delta}{4(1-\nu)} \cdot \left(\frac{1}{R_1} - \frac{1}{R}\right), \\ \sigma_2 &= \frac{E\delta}{4(1-\nu)} \cdot \left(\frac{1}{R} - \frac{1}{R_2}\right). \end{aligned} \tag{26}$$

From the condition $\sigma_1 = \sigma_2$

$$\frac{2}{R} = \frac{1}{R_1} + \frac{1}{R_2} \, . \tag{27}$$

The internal stress existing in the outside fibres (tensile) and in the middle (compressive) having substituted the values of the curvatures is

$$\sigma = \frac{E\alpha}{4(1-\nu)} \cdot (\Delta T_1 - \Delta T_2) \, , \tag{28}$$

in the present case 786 kp/cm^3. The "force-free" curvature

$$\frac{1}{R} = \frac{\alpha}{\delta} (\Delta T_1 + \Delta T_2) \tag{29}$$

is the same as if it resulted from the effect of a linear change in temperature between the two outside fibres; $\Delta T_1 + \Delta T_2$ is the same, but now even internal additional stresses exist. The stress needed to eliminate this curvature is

$$\sigma_0 = \frac{E\alpha}{2(1-\nu)} \cdot (\Delta T_1 + \Delta T_2) \tag{30}$$

which is in the present case 2602 kp/cm^2. Having taken the temperature field to be linear in the whole width of the wall, only this stress could have been obtained. The rate of the internal additional stress to this is 30,2% which cannot be neglected. The membrane stresses arising from the internal pressure have to be added to the thermal stresses, too. They are in the axial direction σp = 912,3 kp/cm^2, in the tangential direction twice as much. The total stresses are

$$\begin{aligned} &\text{at the inner surface} \quad \sigma_0 + \sigma + k \cdot \sigma_p, \\ &\text{in the middle} \quad\quad\quad\quad - \sigma + k \cdot \sigma_p, \\ &\text{in the outer fibre} \quad - \sigma_0 + \sigma + k \cdot \sigma_p. \end{aligned} \tag{31}$$

In axial direction $k = 1$, in the tangential direction $k = 2$. They are tabulated and so are the reduced stresses calculated according to Hencky—Huber—Mises. The latter are compared to the results of the exact calculation (everywhere in kp/cm²) in Table V.

Table V

	Inner fibre	Middle	Outer fibre
Axial	3514,5	126,5	−903,5
Tangential	4427	1039	9
Reduced	4040	982	908
Exact reduced	4993,4	1145,1	762,72
Error [%]	−19,1	−15,63	+19,03

The change in the component stresses is linear according to the approximation. They are indicated by dashed lines in the diagram of Fig. 12 and the reduced stresses in the three considered fibres are also indicated.

To sum up the results it can be stated that the approximation in spite of the significant neglections gives a pattern of the stresses. But it underestimates the stresses with a great error just at the place of the maximum, therefore, it is not adequate for dimensioning.

REFERENCES

1. Lévai, A.: Atomtechnika IV (Nuclear Technics IV). Tankönyvkiadó, Budapest 1964 (manuscript).
2. *Стерман, Л. С.:* Тепловая часть атомных электростанций. Госатомиздат, Москва 1963.
3. *Крамеров, А. Я.:* Некоторые пути развития реакторов ВВЭР. *Атомная Энергия* **17** (1964), 6.
4. Kolonits, F.: Steady-state Thermal Stresses in the Vessel of a Pressurized Water Reactor. *Acta Techn. Hung.* **62** (1968), 351—374.
5. Fodor, Gy.: A Laplace-transzformáció műszaki alkalmazása (Technical Application of the Laplace Transformation). Műszaki Könyvkiadó, Budapest 1962.
6. Doetsch, G.: Handbuch der Laplace-Transformation. Verlag Birkhäuser, Basel 1950—1956.
7. Mikusinski, J.: Operátorszámítás (Operator Calculus). Műszaki Könyvkiadó, Budapest 1961.
8. Kármán, T.—Biot, M.: Matematikai módszerek (Mathematical Methods). Műszaki Könyvkiadó, Budapest 1967.
9. Freud, G.: Parciális differenciálegyenletek (Partial Differential Equations). Tankönyvkiadó, Budapest 1968.
10. Fenyő, I. — Frey, T.: Matematika villamosmérnökök számára (Mathematics for Electrical Engineers). Műszaki Könyvkiadó, Budapest 1964—1965.
11. Rothe, G.: Matematika gépészmérnökök számára (Mathematics for Mechanical Engineers). Műszaki Könyvkiadó, Budapest 1960.
12. Pattantyús, Á. G.: Gépész- és villamosmérnökök kézikönyve (Handbook for Mechanical and Electrical Engineers), I. Műszaki Könyvkiadó, Budapest 1959.
13. Carslaw, H. S.—Jaeger, J. C.: Conduction of Heat in Solids, 2nd edition. Clarendon Press, Oxford 1959.
14. Kolonits, F.: Calculation of Gear Correction by Iteration. *Acta Techn. Hung.* **56** (1966), 320.
15. *Имбрицкий, М. И.-Никитин, А. П.:* Справочник по трубопроводам арматуре для тепловых электрических станций. Госэнергоиздат, Москва 1962.
16. Ponomarjov, Sz. D.: Szilárdsági számítások a gépészetben (Strength Calculations in Mechanical Engineering), III. Műszaki Könyvkiadó, Budapest 1965.
17. Heller, L.: New Viewpoints and Possibilities of the Thermodynamics of Atomic Power Stations. *Acta Techn. Hung.* **14** (1956), 137—164.
18. Timoshenko, S.—Woinowsky-Krieger, S.: Lemezek és héjak elmélete (Theory of Plates and Shells). Műszaki Könyvkiadó, Budapest 1966.

Beanspruchung eines Reaktorgefäßes beim Abstellen. Die Arbeit untersucht die Beanspruchung des Reaktorgefäßes eines Druckwasserreaktors (Pressurized Water Reactor) bei schnellem Abstellen. Die erhaltenen Ergebnisse werden auch für das Druckgefäß eines Reaktors vom 'Woronesh' Typ zahlenmäßig ausgewertet. Die Untersuchungen sind ein Teil der 1967 am Lehrstuhl für Wärmekraftwerke der Budapester Technischen Universität ausgearbeiteten Diplomarbeit des Verfassers.

Нагрузка реакторного сосуда при останове *(Ф. Колонич).* В работе анализируется нагрузка реакторного сосуда в случае реактора на сжатой воде при быстром останове. Полученные результаты анализируются также численно в отношении для работающего под давлением реакторного сосуда реактора типа воронежского. Излагаемый анализ является одной частью дипломного проекта, разработанного автором в 1967 года на Кафедре теплоэлектростанций Будапештского политехнического института.

Acta Technica Academiae Scientiarum Hungaricae; Tomus 68 (1—2), pp. 117—119 (1970)

ON MICROINHOMOGENEITIES IN GaAs CRYSTALS

A. LŐRINCZY, T. NÉMETH, M. SALLAY-NÉMETH

RESEARCH INSTITUTE FOR TECHNICAL PHYSICS OF THE HUNGARIAN ACADEMY OF SCIENCES, BUDAPEST

and

J. ŚWIDERSKI

INSTITUTE OF FUNDAMENTAL TECHNICAL PROBLEMS, WARSAW

[Manuscript received November 5, 1968]

Microinhomogeneity was detected on GaAs crystals (mono- and polycrystals) by means of electrolytic etching and using photovoltaic effect. The presence of microinhomogeneity going through without breaking the grain boundaries of crystals cannot be explained by the well-known mechanisms of formation.

The present paper deals with the results obtained with GaAs crystals. The aim of our investigations is to demonstrate the microinhomogeneity of GaAs mono- and polycrystals prepared by the Czochralski technique and the Bridgman method. The investigated samples polished both mechanically and chemically were exposed to pulse anodic etching, then the selective etch patterns were examined by microscope. The 5—10% aqueous solution of KOH was used as an electrolyte at room temperature. The electrolytic etching was carried out by a special high power pulse, the short duration of which considerably increased the selectivity. The observed periodical impurity distribution was checked on the samples by photovoltage measurements. The results obtained by the two different methods showed good agreement within the limits of the experimental error (Figs 1, 2).

Regarding the distance between the periodicities of single crystals, the results agreed with those obtained on polycrystals cut out from the same crystal. The observations made with samples of polycrystals are of special interest. As recorded on the photo, the "striations" grow through the polycrystalline boundaries without changing their direction, although in the vicinity of the boundary the selective appearance of striations does not occur. This latter is probably due to the diffusion processes in the vicinity of the boundaries. The neighbouring crystal grains showed an orientation difference of about 10°.

In lack of an adequate theory, it is impossible to determine the difference of the period and direction of the microinhomogeneity lines. The growth without changing the direction, however, cannot be explained by theories worked out so far, trying to explain the origin of microinhomogeneities [4, 5]. It is known that a crystal growing freely from a melt follows a special custom, characteristic for the material, i.e. the growth rates of the crystal plates con-

siderably differ. This phenomenon is caused by the energy difference (depending on the orientation), needed for the formation and growth of the two-dimensional surface nucleus (characterized in practice by the orientation dependent value of the constitutional supercooling) [6]. The experimental results proving that the segregation constant of the impurities depends on the crystal orientation, on the growth rate, on the temperature etc., are well known, too [7, 8].

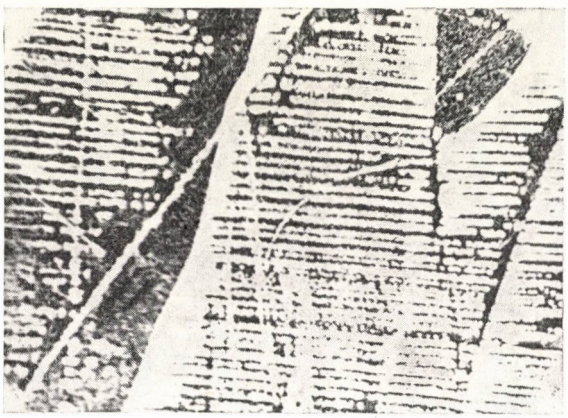

Fig. 1. Striations on GaAs crystal (×200)

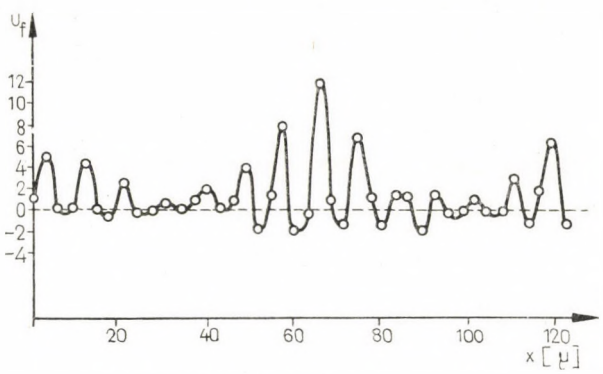

Fig 2. Photovoltaic effect on striations

Based on the above it might be expected that on polycrystalline samples the orientation of the growing surfaces has an essential influence on the building in and distribution regularities of the impurities, depending on the orientation. The same refers to the distance of periodicity and amplitude of the microinhomogeneities.

Our results do not seem to prove the phenomena expected to be valid according to those mentioned above, since the dependence on orientation of

the segregation coefficient of impurities and the degree of supercooling of the solid—liquid interface is not realized. For proving our above-mentioned results, investigations were carried out on simple semiconductors as well. In case of Ge polycrystals the results agreed well with those observed on GaAs polycrystals.

In our opinion the growth conditions should conceal parameters, besides the well-known supercooling, segregation and orientation. This unknown parameter might have a more important role at certain experimental conditions than the above-mentioned ones. Among others, our experiments prove that the inhomogeneity of the distribution and building in of contaminations during crystal growth is a usual phenomenon.

REFERENCES

1. Lőrinczy, A.—Németh, T.—Szebeni, P.: *Acta Physica* **16** (1963), 63.
2. Morizane, K.—Will, A.—Gatov, H. C.: *J. Electrochem. Soc.* **114** (1967), 738.
3. Cronin, G. R.: *J. Electrochem. Soc.* **113** (1966), 292.
4. Plaskett, T. S.: *J. Electrochem. Soc.* **112** (1965), 954.
5. Landau, A. I.: *FMM* **6** (1959), 148.
6. LeMay, C. S.: *J. Appl. Phys.* **34** (1963), 439.
7. Hall, R. N.: *J. Phys. Chem.* **57** (1963), 836.
8. Willardson, R. K.—Allred, W. P.: Symp. on GaAs 1966, 35.

Über Mikroinhomogenitäten in GaAs-Kristallen. Es werden Mikroinhomogenitäten in GaAs-Kristallen (Einkristalle und Polykristalle) mittels elektrolytischer Ätzung und Messung der Photospannung nachgewiesen. Die Anwesenheit der über die Kristallgrenzen kontinuierlich hinüberreichenden Mikroinhomogenitäten kann mit den bekannten Entstehungsmechanismen nicht erklärt werden.

О микроннеоднородностях на кристаллах арсенида галлия *(А. Лэринци, Т. Немет* и *М. Шаллаи-Немет)*. Выявлены микронеоднородности на кристаллах арсенида галлия (монокристаллы и поликристаллы) электролитическим травлением и измерением фото эдс. Присутствие микронеоднородностей переходящих через кристаллические грани без перелома не может быть объяснено знакомыми механизмами возникновения.

Acta Technica Academiae Scientiarum Hungaricae; Tomus 68 (1—2), pp. 121—130 (1970)

DIAGNOSTIC SYSTEM FOR THE EXAMINATION OF THE CATHODE SIDE OF ARC DISCHARGES WITH OXIDE COATED CATHODES

J. F. BITÓ
CAND. OF TECHN. SC.
RESEARCH INSTITUTE FOR ELECTRONICS, BUDAPEST

[Manuscript received November 28, 1968]

For the dynamic characterization of the arc discharges with oxide coated cathode on the cathode side, a diagnostic system, containing 10 experimental methods, was worked out. The system was constructed so that the measuring methods constituting it should make possible a manifold control, a simultaneous measurement and a relatively small perturbation. The formation of the diagnostic system became necessary on account of the strong microphysical heterogeneity of the cathode side. With the application of the system of the briefly characterized measuring methods we succeeded e.g. in establishing the cathode side model of the arc discharges with oxide coated cathodes.

I. Introduction

The microparameters of cathode spaces of arc discharges with oxide coated cathode and the interaction between the cathode and cathode space formed there, further the behaviour of the oxide cathode itself can be examined only by a several times controlled diagnostic system [1, 2]. One reason for this is the vicinity of the oxide cathode, the other one is the strong heterogeneity in the microphysical sense of the word. The former excludes the direct adaptability of the probe measurements, which proved to be good at the discharges by plasmaphysical examinations and by the examination of positive columns, on account of the influence exerted on the work function of the atoms with cathode coating, striking into the probe surface. The strong heterogeneity of the spaces — e.g. the irregularity of the energy distribution of the electrons — excludes not only the application of probe measurements as an independent experimental system, but also reduces the number of those experimental methods which could be taken into account.

The interaction between the cathode and cathode spaces, further the more detailed examination of the cathode function and of the single space complexes made necessary the formation of such an experimental system, the single elements of which gave with a certain overlapping and good reproducibility the values of the basic parameters, inevitably necessary for further calculations and a complete characterization.

One point of view in the formation of this system was that the function of the cathode should be characterized together with the gas space, in inter-

action with it, so to say dynamically, with the indication of the time dependences. Therefore, our aim was not the detailed and thorough analysis of the semiconducting properties of the cathode coating, but for the time being only the setting up of an experimental system describing its behaviour. In possession of the thus acquired data the measuring system will be improved later on, in order to establish the interesting data of the cathode and of the plasma as well.

The diagnostic system of the cathode side described below — first in international relations — essentially serves the registration of the most important functional characteristics and the registration of the macro-and microparameters as well.

It consists of the following elements:

probe measurements;

the determination of the length of the cathodic spaces;

measurements of the cathode spot temperature;

the measurement of the emission current and the calculation of the work function (in gas);

the non-pyrometrical determination of the spot temperature and of the average temperature of the cathode;

the determination of the surface of the cathode spot;

interferometric electron concentration measurements with a laser beam;

microwave transmission measurements;

measurements of cathode damage;

oscillation and striation control with photomultipliers.

Altough the measuring system was worked out for a more detailed examination of d.c. and a.c. low-pressure mercury-argon discharges [1, 2], on the basis of its structure it is, however, also adequate for the examination of high pressure discharges and for the examination of the cathode side of discharge systems in the field without arc discharges.

II. The applied experimental methods

1. Probe measurements

The measurement of the electronic parameters — first of the plasma potentials — are carried out with the aid of the probe measurement system [3] which was well applicable at our previous examinations with d.c. and a.c. The block diagram of the electronic system applied by this method is shown in Fig. 1.

The measuring principle and system of Langmuir is also applied by this probe measurement method; however, it also makes possible the determination of some parameters of a.c. discharges, beside the probe measurements with d.c. In the case of determinations of plasma potential the system worked out by us could theoretically be applied also in the cathode space, the measure-

ments however gave, because of the vicinity of the oxide cathode, uncertain results and so they could not be taken into consideration for the evaluation of the results. For the sake of further safety the probe measurements are to be carried out on probes protruding into the positive column [1—3], e.g. with the application of cylindrical nickel probes having a small surface.

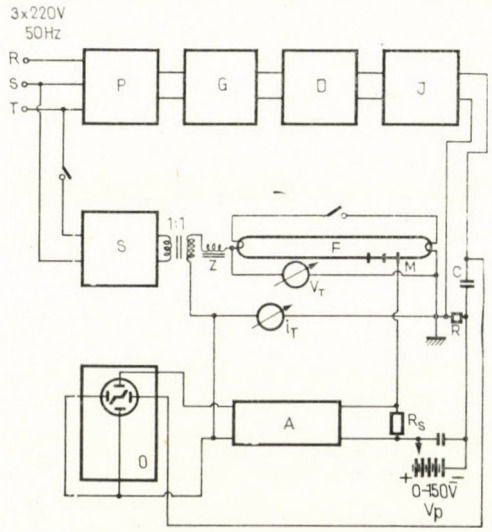

Fig. 1. Block diagram of the electronic system of probe measurements: the sign of generator G, controlled by phase shifter P is pointed out by differentiator D and through it moves the impulse generator I; so a probe voltage-impulse of a wanted shape arrives to probe M and to oscilloscope O; the probe current is amplified by a difference amplifier A; the discharge tube F is supplied by a stabilizator S; the discharge current is limited by ballast Z; the voltage drop on probe circuit resistance R is amplified and the probe is supplied by voltage source V_p; the probe impulse and the tube voltage are examined by the double-beam oscilloscope K at the same time

The sign of the square-wave generator G controlled by the phase shifter P, and shown in the block diagram in Fig. 1 is pointed by differentiator D, and through it moves the impulse generator I to the emission of saw-tooth impulses of positive polarity, with changeable duration and amplitude. This impulse of max. 80 V amplitude of a short transit time, in general of 250 μsec, falls partly to the probe of the discharge tube — the voltage of the probe is given by this — it appears on the other part as a sweep sign on the horizontal plates of the oscilloscope O. Under the influence of the probe voltage, which may be formed at any time, and which is variable in size and space of time, according to the probe characteristics, discovered by LANGMUIR, the probe current will flow through the probe from the discharge and this current will produce a voltage drop on the probe circuit resistance R_p.

This voltage drop will be carried and gained by the difference amplifier A on the vertical plates of oscilloscope O. Consequently under the influence of

every probe voltage-impulse an adequately amplified probe current appears on the screen of the oscilloscope O, in the function of the probe voltage, belonging to it — that is to say the Langmuir probe characteristic sought for — from which the discharge parameter can be calculated in the usual way. The plasma potentials (in this case) necessary for us are given by the position of the knee, formed by the section characterizing the electron energy distribution and the saturation section of the electron current [3].

With the help of phase shifter P through the probe circuit, constructed to the cathode, the momentary value of the plasma potential appearing in the place of the applied probes could be given within each half period.

Being aware of this and after the definition of the boundaries of the Faraday dark space, the axial potential distribution of the discharge can be constructed graphically in each phase, and consequently also the cathode and anode fall can be calculated. As in case of oxide cathode discharges on behalf of the presence of the complex cathode light, the cathode dark space cannot be separated from the negative glow, it is advisable to take the edge of the cathode fall space at the positive column in each case, up to the well observable boundary of the given glow space and Faraday dark space.

The potential fall, arising here and extending until the cathode, can be determined by extrapolation. As from the approximative calculations it has turned out that the length of the negative glow space did not change considerably, in general we have found that the eventual error, resulting from our previous assumptions did not exceed the inaccuracy, otherwise occurring by our measurements. On the measurements of the anode fall the length of the anodic dark space was neglected according to the practice so far.

The voltage impulse falling to the probe and the tube voltage of the discharge are examined with the aid of the double beam oscilloscope K. The probe circuit voltage supply V_p, shown in Fig. 1, served the coordination and establishment of the momentary function of the examined half period and of the selected electrode. With the aid of this voltage source the probe took up electron current only in one half period when a suitable voltage difference was chosen and it was applied as a pre-voltage falling to the probe. It can so be established in which half period of the tube voltage curve, appearing on the screen of the double beam oscilloscope K, does the examined electrode play the function of the cathode or of the anode. The measurements are carried out after the establishment of this, on the basis of the degrees on the phase shifter at each 10° phase angle of the 180° half period. In the course of the measurements on the screen of the double beam oscilloscope K, the moment can be established when the tube voltage has a characteristic change, e.g. breaks down, at the time when the voltage impulse falls on the probe. Also the starting time of the measurement can be chosen in this way.

Before the beginning of each measurement the surface of the active part

of the probe must be carefully cleaned from the accumulated impurities, and in the measurements the basic experimental requirements, to be kept up by probe measurements [3—5], must be assured.

The inaccuracy of the measuring method already previously determined, reached in case of potential measurements $\pm 0{,}2$ V, the greatest time resolution was 10^{-5} sec [3].

2. *The determination of the length of cathodic spaces*

The examination of cathodic spaces of d.c. discharges is by far a simpler task. In this case the distances between the cathode light, space complex, being constant in time and the Faraday dark space, further between the boundary of the Faraday dark space at the positive column and the cathode spiral may be read off with the help of a mm scale, placed behind the above-mentioned discharge spaces. The exactness of these measurements was determined by the applied optical system and by the scale.

On the examinations of 50 cps a.c. discharges a stroboscopic method, controlled by a phase shifter, was developed for the determination of the spaces. A disc of adequate diameter, supplied with slots, was turned by a synchron motor. Its drive was controlled by a phase shifter, and in this way with the application of the mm division, applied at d.c. measurements, the space dimensions resulting from the different phase angles and from the changes of limits could be given with an accuracy mentioned previously. We succeeded e.g. in the establishment of the formation in time of the meniscus on the cathode side of the positive column. The measurements were carried out by the application of an adequate background in a properly darkened room.

3. *Measurements of spot temperature*

The temperatures of the cathode and of the cathode spot are measured with a pyrometer. As can be seen from our previous experiments [1, 2], the average temperature of the cathode follows the changes of the cathode spot temperature. Taking into account the fact that a considerable part of the electrons emitted from the cathode are produced by the cathode spot, which means that its temperature has a determining character from the point of view of the emission, it is advisable to look for the interactions in relation to the cathode spot temperature and according to it, in the course of the experiments, the spot temperature must be measured directly.

If the temperature measurement is carried out by an optical pyrometer, then the measured values must be corrected on account of the emission coating, according to the correction curve $E = 0{,}35$ belonging to the correction diagram of emissivity, published in No. 170 of the *U.S. Bureau of Standards*

Technologic Papers. Before the experiments also the measurements of the cathode mean temperature were carried out on the basis of the variation of resistance of the tungsten spiral. This method proved more reliable than the average temperature obtained on the basis of the optical pyrometric temperature measurements, carried out on more spots of the cathode surface.

4. Emission measurement and the calculation of the work function

For the characterization of the thermionic emissivity of the cathode the already previously applied [2] Cayless measuring method developed by us, was applied. The tungsten spiral is applied for the coupling of the oscillations, indicating the appearance or presence of the positive space charge before the cathode, thus for the measurements a special tube need not be constructed or other elements protruding into the discharge space and there producing disturbances. In the sense of this method during a constant cathode heating (of d.c. or a.c.) in case of d.c. arc discharge with changeable current intensity, from the disappearance of the characteristic oscillations of the positive space charge formed of positive ions before the cathode, we may draw a conclusion about the disappearance of the positive ion cloud, that is to say, about the formation of a state without space charge (zero field) before the cathode.

This state can easily be found, if beside a given cathode heating the discharge current intensity is changed. In this way the discharge current intensity can be established, for the maintenance of which without cathode fall enough electrons are supplied by the externally heated cathode. With the change of the discharge current also a positive space charge and a negative space charge field can be formed in the space before the cathode. This discharge current, at which the positive space charge before the cathode disappears, and which essentially constitutes the electron current emitted thermionically from the cathode, can be looked upon as the emission current of the cathode, characteristic in the given circumstances.

The method reacts sensitively on the cathode changes and can be well applied at the different measurements.

The course of the measuring is the following: heating the cathode spiral with a 550 mA heating current (with application of a sort of current stabilization) a d.c. discharge is brought about between the two electrodes so that the electrode which is to be examined should be the cathode. With the change of the discharge current that state is looked for, when before the cathode the so-called zero field will be formed: that is to say, the space charge consisting of positive ions will cease to exist. This could be observed with the aid of an oscilloscope, so that we looked for the moment of the disappearance of the space charge oscillations, picked up at the formation of the zero field with a spiral — applied as an aerial — and carried on to the oscilloscope.

If that discharge current is chosen — at a heating current held at a constant value — by which the oscillation stops, we get a current value, characteristic for the thermionic emissivity of the cathode. Our measurements can be carried out with an inaccuracy of $\pm 10\%$.

The measurement of the emission current, together with the measurement of the spot temperature and the determination of the spot surface, was used also for the determination of the work function of the cathode. The Speros and Buccili method for the measurement of the work function was taken as a completion and control.

5. *The non-pyrometric determination of the spot temperature and average temperature of the cathode, with cathodes of double outlets and spiral structure*

For the completeness of the system of cathode investigations such measuring methods were sought for, which could be applied at any moment of the discharge, without notable disturbing interference. We started out from two further observations, which were the following:

a) The dependence on the cathode temperature of the voltage difference between the ends of the cathode spiral;

b) the dependence on the cathode temperature of the voltage peak of re-ignition.

With the more detailed analysis of the first observation it was proved that the average temperature of the cathode is proportional, on one side, to the temperature of the cathode spot, on the other side to the emission current of the cathode, if the cathode structure and the weight of the emission coating coincide with good approximation.

We succeeded in this way — in a special case — in taking back both the spot temperature measurement and the measurement of the average temperature to a simple measurement of the voltage difference.

In the course of a more detailed analysis and verification of this method it turned out that the value of the voltage difference between the ends of the cathodes — measured in case of a stationary discharge — is disturbed to a certain extent by the divergence (a low-current glow discharge) in the glow space, existing between the cathode ends. Therefore, for the sake of increasing the accuracy of the measurement both the cathode emission and the cathode temperature belonging to it — measured in the above-mentioned way — were also detected at such an external cathode heating current, where glow discharge had not been formed yet.

After this we turned to the determination by a tube voltmeter of the voltage difference impulse. This way the average temperature of the half period of the cathode and the anode as well could have been determined with-

out a perturbation in the discharge. With the calibration curves the temperature of the cathode could have been characterized also in °C.

By employing this measuring method we did not find it necessary to examine with a diagnostic purpose the re-ignition peak voltage, also characteristic for the cathode temperature [2].

6. The determination of the cathode spot surface

In general, on the cathode of arc discharges a cathode spot of a temperature higher than that of the whole cathode is formed, by the position and surface of which the emission phenomena are considerably influenced. The surface and the position of the spot are changed in many cases already during the measurements, without any external perturbations. For the registration of this change a cathetometric system was applied [1], which, after an adequate enlargement, made the projection of this section of the cathode possible. The size of the spot can be given by this method with an accuracy depending on the position and on the degree of enlargement of the cathode spot, further on the structure of the cathode surface.

7. Measurements of electron concentrations by laser beam

For the establishment of electron concentrations of the cathode spaces and the time dependence of this parameter such an interferometric refractometer is to be applied, by which a He—Ne gas laser serves as radiation source [8]. The accuracy of the measurement, assumed by us, carried out in the infrared, but detected in the red, was 10^{10} electron/cm^3 [8]. A more detailed analysis of the measuring method is not given here, it was published in a previous paper of the author, with the indication of the theoretical and experimental bases and possibilities of its applications as well [8]. The measurement can easily and rapidly be carried out and makes a time resolution of 10^{-8} sec possible, which offers at the examinations in the cathode space a unique possibility, reached so far.

8. Transmission measurements by microwaves

For the determination of the electron concentration also a microwave technique — to a certain extent more complicated — may be applied, which can be looked upon as one element of the well-known microwave diagnostic system [9]. Control measurements can be carried out with this method only then, if the auxiliary control of striations and oscillations to be outlined in item 10 does not indicate instabilities and oscillations in the cathode space, which may be ascribed to the application of this method.

9. Measurements of the cathode damages

Because of the damaging effect exerted by the ions striking into the cathode, the oxide cathode systems are characterized by an evaporation and by a pulverization process. For the registration of these processes the cathode damage measurement, already applied by KÜHL [10] and proved several times by us [11], seems to be appropriate. A detailed analysis of this method is not given here.

10. Oscillation and striation control with photomultipliers

The cathode space can be characterized by an oscillation sensitivity of a very high and large frequency range [9]. Therefore, simultaneously with the application of the single measuring method it must be found to what degree does the disturbance, caused by the measurement — e.g. oscillation — influence the phenomena to be measured. The photomultiplier detecting the oscillations brought about in the cathode space which can be applied as an indirect detecting, the method which was earlier used by the author [9, 12], seemed suitable for this purpose. In the latter case, by the demonstration of the standing or moving striation, appearing in the plasma of the positive column and caused by the oscillations or by the change of the striation parameters, a conclusion may be drawn about the character of the influence of the measurements carried out in the plasma space. This striation process is, namely, very sensitive to the changes in the cathode space [9] and, therefore, it may eventually be applied later, after certain refinements, as an indirect experimental method of the cathode space.

For this the wave length of the formed striation, its distribution velocity and the intensity of the single light maxima — of the excitation fronts — must be measured, e.g. with the application of the methods described by us previously [9, 12].

With the application of the diagnostic system on the cathode side, briefly outlined above, we succeeded in the determination of the most important cathodic and cathode space characteristics of the low-pressure arc discharge of oxide cathode, and of their correlations as well [2].

The cathode side model, characteristic for the examined case, was formed with the application of this system of correlations.

The advantage of this diagnostic system consists in the providing of a multiple, independent control system, the good time resolution, further the good reproducibility, resulting from the facts reported above.

REFERENCES

1. BITÓ, J. F.: Cand. Thesis; Budapest 1966.
2. BITÓ, J. F.: Ph. D. Thesis; Budapest 1968.
3. BITÓ, J. F.—SZEMZŐ, E.: *Tungsram Technische Mitteilungen* **12** (1964), 495.

4. BITÓ, J. F.: *Magyar Fizikai Folyóirat* **14** (1966), 185.
5. BITÓ, J. F.: *Magyar Fizikai Folyóirat* **14** (1966), 297
6. SPEROS, D. M.— BUCCILI, P. R.: *J. Electrochemical Society* **109** (1962), 940.
7. SPEROS, D. M.— BUCCILI, P. R.: *Journal of Electrochemical Society* **110** (1963), 7.
8. BITÓ, J. F.: *Acta Techn. Hung.* (under publication).
9. BITÓ, J. F.: Introduction to the Experimental Plasma Physics. Mérnöki Továbbképző Intézet, Budapest 1967.
10. KÜHL, B.: *Technisch-wissenschaftliche Abhandlungen der Osram Gesellschaft* **7** (1958), 84.
11. LAKATOS, G.—BITÓ, J. F.: *British Journal of Applied Physics* **15** (1964), 189.
12. LAKATOS, G.—BITÓ, J. F.: *Nature* (1965), 445.

Diagnostisches System für die Prüfung der Bogenentladungen mit Oxydkathoden an der Kathodenseite. Für die dynamische Charakterisierung der kathodenseitigen Bogenentladungen mit Oxydkathode wurde ein diagnostisches System ausgearbeitet, welches 10 Prüfmethoden enthält. Das System wurde so ausgebaut, daß durch die Prüfverfahren eine mehrfache Kontrolle, simultane Messungen und eine relativ kleine Perturbation ermöglicht werden. Die Ausgestaltung des diagnostischen Systems wurde wegen der starken mikrophysikalischen Heterogenität der Kathodenseite notwendig. Durch Anwendung des Systems der kurz dargelegten Meßmethoden ist es uns z. B. gelungen, das kathodenseitige Modell der Bogenentladungen mit Oxydkathode festzustellen.

Диагностическая система для исследования дугового разряда оксидногдо катода на катодной стороне (*Й. Ф. Бишо*). Для динамической характеристики дуговых разрядов с оксидными катодами на катодной стороне разработан метод, состоящий из 10 экспериментальных методов. Система построена таким образом, чтобы измерительные методы, из которых она состоит, способствовали бы многократному контролю, одновременному измерению и относительно малой пертурбации. Оформление диагностической системы стало необходимым из-за сильной микрофизической гетерогенности катодной стороны. Применяя систему кратко охарактеризованных измерительных методов, нам удалось, например, определить модель дуговых разрядов с оксидными катодами на катодной стороне.

Acta Technica Academiae Scientiarum Hungaricae; Tomus 68 (1—2), pp. 131—144 (1970)

STABILITY RANGE OF FEEDBACK CONTROL SYSTEMS

S. KERESZTÉLY

HUNARIAN ACADEMY OF SCIENCES, BUDAPEST
RESEARCH INSTITUTE FOR AUTOMATION

[Manuscript received December 21, 1968]

The parameters of a controlled plant may change within a given range. The criterion is determined, which is to be satisfied by the loop gain of the rated system, in order to keep the feedback control system stable over the whole range of the parameter changes. The calculation may be carried out with a computer. By generalizing the method the fulfillment of stricter demands than stability may be prescribed with practically the same amount of calculation work.

I. Requirements

In practice, the values of the components building up a feedback control system are only more or less accurately known. In addition, these elements may change their values during use, due to wear or ageing which may, in turn, depend on external factors (such as temperature). A feedback system is required to operate, within the specified range of these variations, in a satisfactory manner. The problem is represented, from practical aspects, by the variation of the elements within the controlled plant, as the design of the compensator makes it possible, providing for the necessary accuracy and stability. Therefore, investigations will be restricted to the case when variations occur only in the controlled plant. In the $G(s, \lambda_1, \lambda_2, \ldots \lambda_n)$ transfer function of the controlled plant, these variations affect the values of the λ_i parameters (which mean time constant, damping factor, gain, delay). The variation range of the individual parameters can be determined on the basis of the following considerations:

a) Deviation of the value of a built-in element from the rated value (maximum deviation) is generally specified (accuracy of resistors and condensers, tolerance of mechanical parts), wherefrom the range of the parameter variations thereby caused can be readily calculated.

b) the effect of external factors (such as temperature) can similarly be taken into consideration by the dependence of the value of individual elements (such as the temperature coefficient of the resistor). The possible range of the external factor in question (for example operational temperature range) must, of course, be known;

c) when calculating the variation due to wear, the life required from the component concerned must be specified. On the basis of calculated or experimental data, the rate of wear and, thereby, the maximum variation can be determined;

d) variations due to ageing can only be described statistically. Here the range to be tolerated can be determined on the basis of a specified error probability, if the statistical features of the component are known.

According to the above considerations, the $G(s, \lambda_1, \lambda_2, \ldots \lambda_n)$ transfer function of the controlled section may have the pertaining variation range of the individual parameters determined:

$$\begin{aligned} &\lambda_1 \in \Lambda_1 , \\ &\lambda_2 \in \Lambda_2 , \\ &\text{---------} \\ &\lambda_n \in \Lambda_n . \end{aligned} \tag{1}$$

Generally, however, in the n-dimensional parameter space the range of the possible values of parameter vector

$$\bar{\lambda} = \begin{bmatrix} \lambda_1 \\ \lambda_2 \\ \vdots \\ \lambda_n \end{bmatrix} \tag{2}$$

is not the n-dimensional cube described by Equ. (1), as it is only part of the former. This is because the maximum variations of the different parameters cannot be associated, as each may occur only in a certain combination of the variations causing the parameter variations proper. Thus the possible value range of the parameters can be characterized by the

$$\bar{\lambda} \in \bar{\Lambda} \tag{3}$$

relation. Range $\bar{\Lambda}$ is known

to represent a continuous range in the n-dimensional space;

to be located inside of the n-dimensional cube characterized by Equs (1), and

to have a form easy to determine accurately, in theory, from the variations of the elements the controlled plant consists of.

The foregoing findings lead to the following question: under what conditions will the feedback control system remain stable if, in the $G(s, \bar{\lambda})$ transfer function of the controlled plant, $\bar{\lambda}$ is anywhere in the range $\bar{\Lambda}$. The rated value of the controlled plant parameters is $\bar{\lambda}_0$ which is within the range $\bar{\Lambda}$.

II. A survey of the methods generally used to provide for a stability range

The most well-known method to maintain the feedback control system stable in a certain vicinity of the $\bar{\lambda}_0$ rated parameter value is to provide for gain and phase margins. Definition of these two ideas in a simple case is illustrated by Fig. 1 showing loop gain A in the function of frequency. Gain margin a_0 and phase margin φ_0 are intended to keep the Nyquist diagram as far as possible from the "dangerous" (—1 ; 0) point. Their values, however, do not

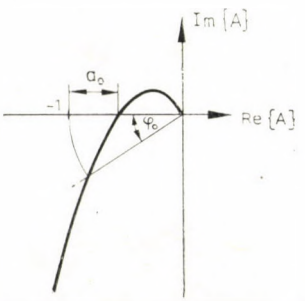

Fig. 1. Definition of the gain and phase margin

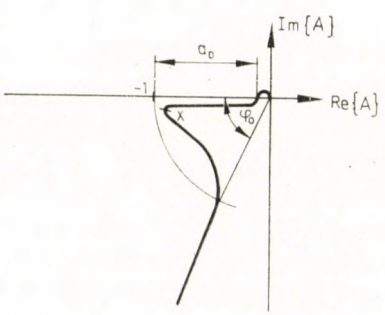

Fig. 2. Narrow stability range system

give information on the stability range magnitude within the $\bar{\lambda}$ parameter space, nor permit the qualitative statement according to which more amplification and phase reserves would ensure a wider stability range. A good example is the Nyquist diagram presented in Fig. 2 which is hardly stable in spite of its excessive gain and phase reserves, and where an insignificant joint gain and phase increase at point x, that is, a minor $\bar{\lambda}_0$ variation in the proper direction, would cause instability.

It is much more reassuring to study the maximum of the absolute value of feedback gain. The locus of the identical values over the plane A forms a

circle, and the stability margin is characterized by the parameter of the circle, the Nyquist diagram is tangential to (Fig. 3). Unfortunately, it cannot be stated here unconditionally either that a lower M value would have a wider stability range associated in the parameter area, although this might be true in many cases. Moreover, the question cannot even be raised what an M value would be required to provide for the stability of the feedback control system within a given $\bar{A}$ range.

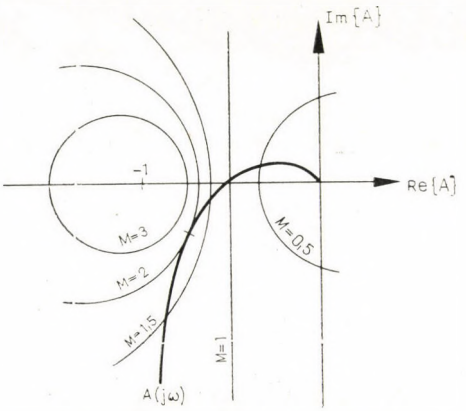

Fig. 3. Maximum feedback gain

On the extent of the stability range some conclusions may be arrived at from the location of the poles of the closed system on the complex plane; the pole located near to the imaginary axis on plane s is considered dangerous since it may be displaced, upon the effect of even minor parameter variations, to the other side of the axis whereby the system would become unstable. It is very difficult, however, to arrive at numerical conclusions, as the rate of pole movement depends on the location of all the poles and zeros. A good example is a sampled data control system having a finite settling time, that is, where each pole of the closed system is at the point $z = 0$. Accordingly, the real part of each pole in plane s is $-\infty$. This might indicate extremely high stability but, in fact, such systems would exhibit a rather narrow stability range. This could be attributed to the fact that the poles concentrated into a single point would travel at an extremely fast rate over the complex plane.

The root-locus method accurately follows the pole travel in the function of a single parameter variation (generally that of the gain factor). This method has not been extended to study the simultaneous variation of several parameters and, since the curve might turn into a planar range in case of even two parameters, this might not be expected either.

III. Stability condition within the $\bar{A}$ range

The following paragraphs aim at the determination of the requirements to be satisfied by the loop gain designed for rated parameters, in order to maintain the feedback control system stable, if the values of the plant parameters are characterized by any point of the $\bar{A}$ range.

In case of continuous systems, the condition of stability is to have the roots [here $A(s, \bar{\lambda})$ is the loop gain] of equation

$$1 + A(s, \bar{\lambda}) = 0 \tag{4a}$$

satisfying the condition

$$\mathrm{Re}\{s_i\} < 0. \tag{5a}$$

In case of sampled data control systems, the stability requirement is

$$1 + A(z, \bar{\lambda}) = 0, \tag{4b}$$

$$|z_i| - 1 < 0 \tag{5b}$$

where $z = e^{sT}$. When introducing substitution $w = (z-1)/(z+1)$

$$1 + A(w, \bar{\lambda}) = 0, \tag{4c}$$

$$\mathrm{Re}\{w_i\} < 0. \tag{5c}$$

The above equations are identical in form for complex variables s, z, and w and, in order to save parallel presentation, hence the variable ξ will be written instead of all these variables [naturally, $A(\xi, \bar{\lambda})$ indicates another functionality in each case within the same system].

$$1 + A(\xi, \bar{\lambda}) = 0, \tag{4}$$

$$f(\xi_i) < 0. \tag{5}$$

In Equ. (4), loop gain $A(\xi, \bar{\lambda})$ is expressed by loop gain $A(\xi, \bar{\lambda}_0)$ encountered in the $\bar{\lambda}_0$ case of the rated parameters, and the transfer function at the rated and changed parameter values of the controlled plant:

$$A(\xi, \bar{\lambda}) = A(\xi, \bar{\lambda}_0) \frac{G(\xi, \bar{\lambda})}{G(\xi, \bar{\lambda}_0)}. \tag{6}$$

Equ. (4) will thereby be

$$1 + A(\xi, \lambda_0) \frac{G(\xi, \bar{\lambda})}{G(\xi, \bar{\lambda}_0)} = 0 \tag{7}$$

and transposed:

$$A(\xi, \bar{\lambda}_0) = -\frac{G(\xi, \bar{\lambda}_0)}{G(\xi, \bar{\lambda})} . \tag{8}$$

The criterion of stability is to have condition (5) to hold for each ξ_i root of Equ. (8), if $\bar{\lambda} \in \bar{\Lambda}$. Now let us study the meaning of each side of Equ. (8) at a fixed ξ_0, for which

$$f(\xi_0) = 0. \tag{9}$$

Equs (5a)—(5c) show that $A(\xi_0, \bar{\lambda}_0)$ is a point of the Nyquist diagram of a system with rated parameter values. The right hand side of the equation, $-G(\xi_0, \bar{\lambda}_0)/G(\xi_0, \bar{\lambda}_0)$, describes a continuous range on the complex plane, at a fixed ξ_0, if $\bar{\lambda} \in \bar{\Lambda}$, since $\bar{\Lambda}$ is a continuous range. Let us indicate this range with $\Gamma(\xi_0)$.

If the rated system ($\bar{\lambda} = \bar{\lambda}_0$) is stable, and the equation order of the transfer function of the controlled plant does not vary in the $\bar{\Lambda}$ range, the criterion of stability has to satisfy for each ξ_0 value satisfying Equ. (9), the following condition:

$$A(\xi_0, \bar{\lambda}_0) \notin \Gamma(\xi_0) \tag{10}$$

that is, to prevent the Nyquist diagram from entering range $\Gamma(\xi_0)$.

This statement can be simply verified in the following manner. If the equation order of the $G(\xi, \bar{\lambda})$ transfer function of the controlled plant does not vary, the ξ_i roots of Equ. (8) will continuously change, starting from the value assumed at $\bar{\lambda} = \bar{\lambda}_0$, which is characteristic of the rated system. If this is stable, the roots of Equ. (8) satisfy, at rated parameter values, Equ. (5). The solutions of Equ. (9) separate the complex plane into two ranges.

Thus, the continuously changing roots can be displaced from range $f(\xi) < 0$ to range $f(\xi) > 0$ only by crossing the line $f(\xi) = 0$ at $\bar{\lambda}_j \in \bar{\Lambda}$. This, however, would mean that in case of $\bar{\lambda} = \bar{\lambda}_j$ the relation $\xi_i = \xi_0$ would hold and, in Equ. (8):

$$A(\xi_0, \bar{\lambda}_j) = -\frac{G(\xi_0, \bar{\lambda}_0)}{G(\xi_0, \bar{\lambda}_j)} \in \Gamma(\xi_0) \tag{11}$$

which contradicts the requirement (10). Thus, if the requirement (10) is satisfied, the roots of Equ. (8) satisfy the condition (5) within the entire $\bar{\Lambda}$ range, that is, the control system will remain stable, if $\bar{\lambda} \in \bar{\Lambda}$.

The solutions of Equ. (9) can be described by the complex function of a real variable which, in the cases discussed, has a simple form:

$$s = \xi_0 = j\omega , \quad -\infty < \omega < \infty ; \tag{12a}$$

$$z = \xi_0 = e^{j\omega T}, \quad -\frac{\pi}{T} \leqslant \omega \leqslant \frac{\pi}{T}; \tag{12b}$$

$$w = \xi_0 = jv = j \tan \frac{\omega T}{2}; \; -\infty < v < \infty, \; -\frac{\pi}{T} \leqslant \omega \leqslant \frac{\pi}{T}. \tag{12c}$$

Combining into a single equation:

$$\xi_0 = \varphi(\omega). \tag{12}$$

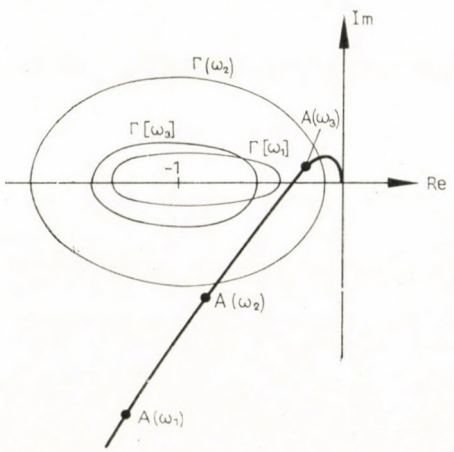

Fig. 4. Prohibited range and Nyquist diagram at some ω values

$A[\varphi(\omega), \bar{\lambda}_0]$ is the Nyquist diagram of the control system at rated parameter values, and $\Gamma[\varphi(\omega)]$ is the range where, to assure stability in the entire $\bar{\Lambda}$ range, the Nyquist diagram must not enter. Naturally, part of the range of the complex plane, forbidden by $\Gamma[\varphi(\omega)]$ at a fixed ω_1 value may be permitted for the Nyquist diagram at another ω_2 value (Fig. 4).

In the complex number plane, the range includes the (—1 ; 0) point at any ω value because, at $\bar{\lambda} = \bar{\lambda}_0$,

$$-\frac{G(\xi_0, \bar{\lambda}_0)}{G(\xi_0, \bar{\lambda})} = -1.$$

The stability requirement described by Equ. (10) can be presented by the $\mathrm{Re}\{A\} = a$; $\mathrm{Im}\{A\} = b$; ω three-dimensional illustration. The $\Gamma[\varphi(\omega)]$ prohibited ranges form a body here (Fig. 5) where the Nyquist diagram expanded to a space curve by the ω variable must not enter, but has to be by-passed, in case of an unstable plant by the Nyquist curve counter-clockwise. Thus, the $\Gamma[\varphi(\omega)]$ body takes over the duty of the (—1 ; 0) point of the Nyquist curve and defines, in a frequency selective manner, the distance the Nyquist diagram must run from the critical (—1 ; 0) point, depending on its direction,

in order to maintain the control system stable within the entire $\bar{A}$ range.

The significance of the stability condition defined in Equ. (10) is represented by its reducing the dimension number of the stability problem, regardless of the dimension number of $\bar{A}$, always to 2, and relating the loop gain at rated parameters with a quantity depending on nothing but the controlled plant and its parameters. It may offer a guidance for the synthesis as well since, if the rated loop gain is sought for in case of a given controlled plant, a trial

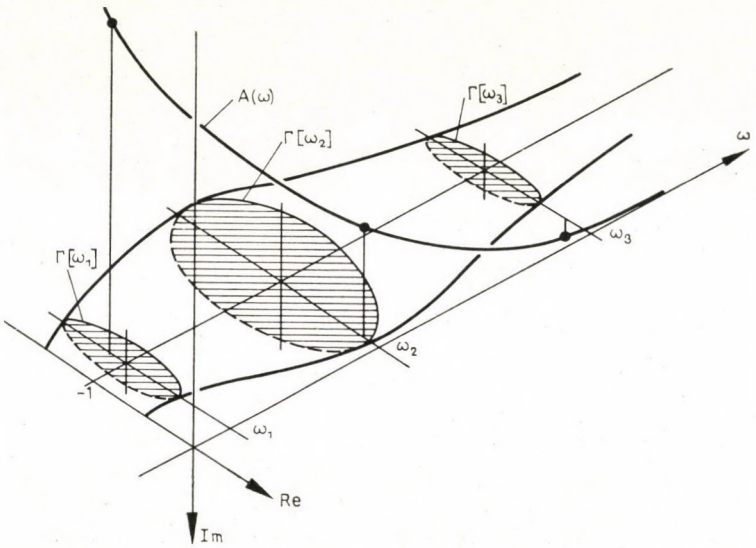

Fig. 5. Three-dimensional illustration of the prohibited range and the Nyquist diagram

with an $A(\xi, \bar{\lambda}_0)$ loop gain can detect on the basis of Equ. (10) the ω range, as compared to this equation, where the loop gain should be modified, and in which direction.

Determination of the $\Gamma[\varphi(\omega)]$ body surface equation is a hopeless attempt even in simple cases. A realistic possibility is represented by the numerical method whereby in the range, where the Nyquist diagram might approach the body, the points should be determined in a suitable close spacing.

Since the equations of both the loop gain and the controlled plant are finite, and generally of a low order, neither the Nyquist diagram nor the $\Gamma[\varphi(\omega)]$ body may contain several peaks and, therefore, an acceptable result might be obtained by checking only a comparatively low number of points. And since the $\Gamma[\varphi(\omega)]$ range always includes the (—1 ; 0) point, it is best to calculate in a polar coordinate system built around this point.

$$a = \varrho \cos \vartheta - 1 , \tag{13a}$$

$$b = \varrho \sin \vartheta . \tag{13b}$$

With an ω_i resp. ϑ_j value fixed, the value defining a point of the surface will be given by the solution of the following problem:

$$\varrho = \max |1-Y(\bar{\lambda})| \; ;$$
$$Y(\bar{\lambda}) = \frac{G[\varphi(\omega_i), \bar{\lambda}_0]}{G[\varphi(\omega_i), \bar{\lambda}]} \, , \tag{14}$$
$$\bar{\lambda} \in \bar{\Lambda} \; ;$$
$$\text{arc} \; \{1-Y(\bar{\lambda})\} = \vartheta_j .$$

With more maxima given, the minima between each two must also be found, as they represent further points of the surface.

Testing whether a given $A[\varphi(\omega), \bar{\lambda}_0]$ loop gain is acceptable, for each ω value the calculation on not more than a single ϑ value must be performed:

$$\vartheta_j = \text{arc} \{1+A \, [\varphi(\omega_i) \, , \, \bar{\lambda}_0]\} \, . \tag{15}$$

IV. Satisfaction of the requirements stricter than stability in the $\bar{\Lambda}$ range

Through the investigations covered by the previous chapter, conditions for the stability of the feedback control system with a $\bar{\Lambda}$ range of the controlled plant parameters have been determined. Determination of the $\Gamma[\varphi(\omega)]$ range

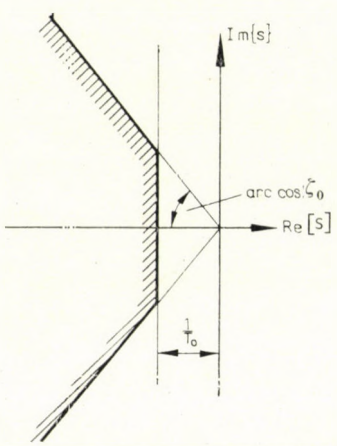

Fig. 6. Permitted range of the characteristic equation roots on the s plane

prohibited for the Nyquist diagram of the rated system, however, requires much feasible calculation, in practice, only by using a digital computer. With this in mind, on the other hand, it seems permissible to design the control system against a slight increase of the computation work, in addition to stability, for the satisfaction of refined quality requirements as well, if a possibility can be found for this purpose.

Let it be required from the control system to have no time constant of its transfer function exceed a predetermined T_0 value in the $\bar{A}$ range of the parameters. Satisfaction of this requirement protects it against an excessive reduction of the working speed.

As another requirement, the damping factor of the oscillating members in the transfer function should reach a minimum ζ_0 value.

The control system will satisfy these two conditions, if the roots of its characteristic equation are located within the range illustrated by Fig. 6.

The limit equation of the range permissible for the roots is:

$$s = \xi_0 = \begin{cases} -\dfrac{1}{T_0} + j\omega\,, & |\omega| \leqslant \dfrac{\sqrt{1-\zeta_0^2}}{T_0\,\zeta_0}\,; \\ -\dfrac{\zeta_0|\omega|}{\sqrt{1-\zeta_0^2}} + j\omega\,, & |\omega| \geqslant \dfrac{\sqrt{1-\zeta_0^2}}{T_0\,\zeta_0}\,. \end{cases} \tag{16a}$$

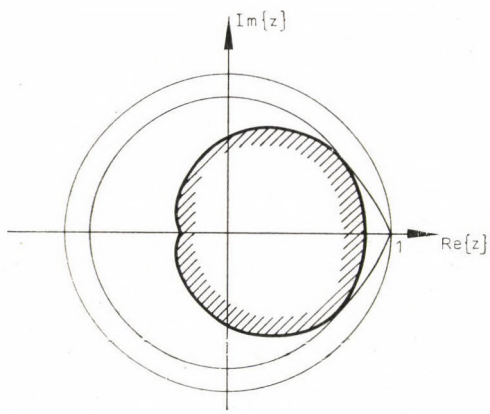

Fig. 7. Permitted range of the characteristic equation roots on the z plane

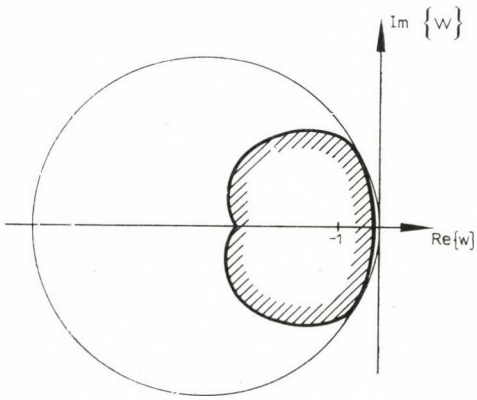

Fig. 8. Permitted range of the characteristic equation roots on the w plane

In case of sampled data control systems, the roots of the characteristic equation of the closed system must be located in the z plane within the range of the form illustrated by Fig. 7, and in the w plane within that shown by Fig. 8 to make the control system satisfy the above requirements.

The equation of the range limit is:

$$z = \xi_0 = \begin{cases} e^{-\frac{T}{T_0} + j\omega T}\,, & |\omega| \leqslant \dfrac{\sqrt{1-\zeta_0^2}}{T_0\,\zeta_0}\,; \\ e^{-\frac{T\zeta_0|\omega|}{\sqrt{1-\zeta_0^2}} + j\omega T}\,, & \dfrac{\sqrt{1-\zeta_0^2}}{T_0\,\zeta_0} \leqslant |\omega| \leqslant \dfrac{\pi}{T} \end{cases} \tag{16b}$$

and

$$w=\xi_0=\begin{cases}\tanh\left(-\dfrac{T}{2T_0}+j\omega\dfrac{T}{2}\right), & |\omega|\leqslant\dfrac{\sqrt{1-\zeta_0^2}}{T_0\zeta_0};\\[2ex] \tanh\left(-\dfrac{T\zeta_0|\omega|}{2\sqrt{1-\zeta_0^2}}+j\omega\dfrac{T}{2}\right), & \dfrac{\sqrt{1-\zeta_0^2}}{T_0\zeta_0}\leqslant|\omega|\leqslant\dfrac{\pi}{T}.\end{cases}\tag{16c}$$

The boundary line equation can be written in each of the three cases as the complex function of the real variable, that is, generally

$$\xi_0=\psi(\omega).\tag{16}$$

The roots of the characteristic equation of the feedback control system are given by the solution of Equ. (8). If the complex variable ξ is replaced at each side of this equation by the boundary line equation described by Equs (16)

$$A(\xi,\bar{\lambda}_0)=A[\psi(\omega),\bar{\lambda}_0]\tag{17}$$

then the modified Nyquist diagram of the rated system will be obtained, and

$$-\frac{G(\xi,\bar{\lambda}_0)}{G(\xi,\bar{\lambda})}=-\frac{G[\psi(\omega),\bar{\lambda}_0]}{G[\psi(\omega),\bar{\lambda}]}\tag{18}$$

describes a range on the complex plane, in case of a fixed ω, while $\bar{\lambda}\in\bar{\Lambda}$. This range is indicated by $\Gamma[\psi(\omega)]$. If

a) each pole of the transfer function of the rated system is within the specified range;

b) the eventually compensated poles or zeros of the transfer function of the controlled plant are within the specified range (i.e. those roots of the characteristic equation of the rated system which do not represent transfer function poles);

c) the equation order of the controlled plant transfer function does not vary within the $\bar{\Lambda}$ range, then the condition of having the feedback control system satisfy the specified requirements in the entire $\bar{\Lambda}$ range is to prevent the modified Nyquist diagram from entering the $\Gamma[\psi(\omega)]$ range, in a manner identical to Equ. (10), that is

$$A[\psi(\omega),\bar{\lambda}_0]\notin\Gamma[\psi(\omega)].\tag{19}$$

This statement can be verified in a manner identical with the argumentation under paragraph III.

Range $\Gamma[\psi(\omega)]$ always includes point (—1 ; 0) and, similarly to the body shown in Fig. 4, represents a prohibited range for the modified Nyquist diagram. This body is by-passed by the modified Nyquist diagram as many times in a counter-clockwise manner, as many poles loop gain A_0 has outside of the range illustrated in Figs 6—8.

Equs (13)—(15) can be used for exact calculations with the modification, however, that instead of the function $\varphi(\omega)$ described by Equs (12) function $\psi(\omega)$ given by Equs (16) must be made use of in Equs (14) and (15).

V. Variation of the controlled section equation order

For reasons of simplicity, the previous investigations have categorically excluded those cases when the equation order of the controlled plant transfer function would vary. In case of equation order variations the roots of the characteristic equation will not vary continuously and may, without crossing the limit curve [$\varphi(\omega)$ and/or $\psi(\omega)$], be transferred into the forbidden range. Since, in practice, the equation order of the controlled plant transfer function may actually vary, it must be determined when this might be permitted.

The first case to be studied is when, by a special combination of the parameter values, both the numerator and the denominator of the controlled plant transfer function have the same root. This will occur in a $\bar{A}_1$ range of the parameter values which always has a lower number of dimensions than the $\bar{A}$ range. It is easy to realize that, in the differential environment of the $\bar{A}_1$ range, the characteristic equation has a root different from that simultaneously present one in both the numerator and denominator, within that range, only differentially. An equation order variation of this type, therefore, cannot cause any difficulties if the common root is within the specified range, but if it is outside, the requirements are impossible to satisfy.

If the nominal system is characterized by $\bar{\lambda}_0 \in \bar{A}_1$ (which is true in every case where a pole or zero of the controlled plant transfer function is compensated), then the roots of the characteristic equation of the closed control system represent not only the solutions of equation $A(\xi, \bar{\lambda}_0) + 1 = 0$, but also the compensated poles and zeros. This is why paragraph IV includes stipulation *b)*.

In the other case to be studied, the equation order of the controlled plant transfer function will increase if certain parameters exceed a limit value. This occurs in sampled data control systems because of delay or sampling period variations. However, the new root will always enter here at $z = 0$ (whereas the others keep changing continuously) and, therefore, this is always permissible.

VI. Further tasks

In the foregoing paragraphs only the first approximation of the problem raised, that is, behaviour of the control system in case of the variation of the controlled plant parameters within a given range, has been carried out. The most important problems left to be solved are as follows:

a) Algorithmization of the problem presented by Equ. (14). Here some difficulties may be encountered as, in certain cases, several extreme values will exist, whereas sometimes the range will include the ∞ point of the complex number plane and, consequently, at a certain range of ϑ will not include any extreme value.

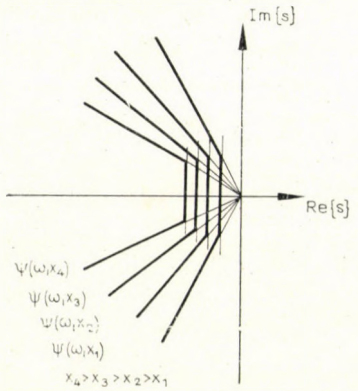

Fig. 9. Shape of the $\psi(\omega, x)$ function set on the s plane

b) Algorithmization of the synthesis of a loop gain corresponding to the requirements set. In rather simple cases the $\psi(\omega)$ function can be fixed at a given $G(\xi, \bar{\lambda})$ and $\bar{A}$, respectively, and the nominal system may be optimized on the basis of any optional criterion, in the course of the determination of the $A(\xi, \bar{\lambda}_0)$ loop gain. The result will depend on the $\bar{\lambda}_0$ value. In other cases only one $\psi(\omega, x)$ function set is fixed at a given $G(\xi, \bar{\lambda})$ and $\bar{A}$, where x is a parameter which, if increased, will represent stricter quality requirements (as an example, Fig. 9 illustrates such a function set in the s plane). In the course of the synthesis, the maximum x value (and the pertaining loop gain) whereat the problem can still be solved should be sought for. Here the results will not depend on the $\bar{\lambda}_0$ value. The value of this method can be argued, as the maximum time constant does not characterize unequivocally the operation speed of the system.

Über den Stabilitätsbereich von rückgekoppelten Regelsystemen. Die Parameter einer Regelstrecke können sich innerhalb eines gegebenen Bereichs ändern. Das Kriterium wird bestimmt, dem die Schleifenverstärkung des nominellen Systems Genüge leisten muß, damit das rückgekoppelte Regelsystem im gesamten Bereich der Parameteränderungen stabil bleibt.

Die Berechnungen können mit einem Computer durchgeführt werden. Durch Verallgemeinerung der Methode kann auch die Erfüllung von höheren Anforderungen als die der Stabilität vorgeschrieben werden, wobei der Rechenaufwand praktisch derselbe bleibt.

О диапазоне устойчивости регулирующих систем с обратной связью *(Щ. Керестель)*. Параметры некоторого регулируемого участка могут изменяться в заданном диапазоне. Определяется тот критерий, который должен быть удовлетворен передаточной функцией разомкнутой системы для сохранения устойчивости регулирующей системы с обратной связью во всем диапазоне изменений параметров. вычисления можно Выполнить при помощи ЭВМ. Обобщениен данного метода можно добиться удовлетворения также условий более строгой устойчивости практически при идентичной по объему вычислительной работе.

Acta Technica Academiae Scientiarum Hungaricae; Tomus 68 (1—2), pp. 145—160 (1970)

SOME QUESTIONS OF IDENTIFICATION ON THE BASIS OF FREQUENCY RESPONSE

J. GYÜRKI

RESEARCH INSTITUTE FOR AUTOMATION OF THE HUNGARIAN ACADEMY OF SCIENCES

[Manuscript received December 30, 1968]

An iterative least-square approximation method is presumed in the article for the identification of linear, dynamical control systems on the basis of the frequency response. The main concept of the method is described and two special questions are intensively investigated, namely, the weighting problem and the decision about the structure of the identified transfer function. To the background of the theoretical part the proposed method was programmed on a MINSK—22 digital computer and the results of the practical investigation summarized. A numerical example is presented, too.

I. Introduction

The practical identification procedures, based on different measurement data are essentially data of processing methods, inverting the functional connection which exist between the measured values and the mathematical description of the system. The frequency response appears in the classical control theory as one of the important characteristics and sufficient description of the system. Its points can be measured directly (sinusoidal test) or derived indirectly from other measured functions (impulse test data, step response, impulse response) with the aid of the Fourier transformation. In this way the identification based on frequency response has great significance.

STROBEL [1] has given a good survey on this kind of identification methods. In our paper we will extend and generalize the least-square method of the frequency response identification, which was first proposed by LEVY [2] and improved by SANATHANAN–KOERNER [3] and STROBEL [1]. We will deal with the identification problem from a practical point of view, especially with the weighting problem and the decision about the structure of the computed transfer function. Our investigations are based on digital computer programmes.

II. The computing method

Let the experimental frequency response of the system under investigation be given as

$$G_E(j\omega_i) = P(\omega_i) + jQ(\omega_i); \quad i = 1, 2, \ldots N. \tag{1}$$

The aim of the identification is to compute the parameters of a rational-fractional function, which approximates in a prescribed sense the experimental frequency response:

$$G(j\omega) = \frac{\sum_{k=1}^{m} a_k (j\omega)^k}{1 + \sum_{k=1}^{n} b_k (j\omega)^k} . \tag{2}$$

The idea on the computation of the parameters of Equ. (2) on the basis of data (1) is the error square minimalization in a discrete case, namely:

$$\sum_{=1}^{N} \varepsilon_i^2 = \sum_{i=1}^{N} |G_E(j\omega_i) - G(j\omega_i)|^2 = \sum_{i=1}^{N} \left| P(\omega_i) + jQ(\omega_i) - \frac{\alpha(\omega_i) + j\beta(\omega_i)}{\gamma(\omega_i) + j\delta(\omega_i)} \right|^2 = \min. \tag{3}$$

The minimalization of the preceding expression concludes in a multidimensional nonlinear regression, because of the special form of the frequency response (2). To avoid the problems of the nonlinear regression let us define a modified error [2]:

$$\sum_{i=1}^{N} \varepsilon_i'^2 = \sum_{i=1}^{N} \varepsilon_i^2 \cdot [\gamma^2(\omega_i) + \delta^2(\omega_i)] . \tag{4}$$

The minimalization of the modified error square with the usual procedure already concludes in a linear regression. The matrix form of the equations, which arises at the computation, is:

$$\underset{n \times (m+1)}{\begin{bmatrix} \lambda_0 & 0 & -\lambda_2 & 0 & \lambda_4 \dots \\ 0 & \lambda_2 & 0 & -\lambda_4 & 0 \dots \\ \lambda_2 & 0 & -\lambda_4 & 0 & \lambda_6 \dots \\ 0 & \lambda_4 & 0 & -\lambda_6 & 0 \dots \\ \vdots & \vdots & \vdots & \vdots & \vdots \\ T_1 & -S_2 & -T_3 & S_4 & T_5 \dots \\ S_2 & T_3 & -S_4 & -T_5 & S_6 \dots \\ T_3 & -S_4 & -T_5 & S_6 & T_7 \dots \\ S_4 & T_5 & -S_6 & T_7 & S_8 \dots \\ \vdots & \vdots & \vdots & \vdots & \vdots \end{bmatrix}}
\underset{n \times n}{\begin{bmatrix} T_1 & S_2 & -T_3 & -S_4 & T_5 \dots \\ -S_2 & T_3 & S_4 & -T_5 & -S_6 \dots \\ T_3 & S_4 & -T_5 & -S_6 & T_7 \dots \\ -S_4 & T_5 & S_6 & -T_7 & -S_8 \dots \\ \vdots & \vdots & \vdots & \vdots & \vdots \\ U_2 & 0 & -U_4 & 0 & U_6 \dots \\ 0 & U_4 & 0 & U_6 & 0 \dots \\ U_4 & 0 & -U_6 & 0 & U_8 \dots \\ 0 & U_6 & 0 & -U_8 & 0 \dots \\ \vdots & \vdots & \vdots & \vdots & \vdots \end{bmatrix}}
\cdot
\begin{bmatrix} a_0 \\ a_1 \\ a_2 \\ a_3 \\ \vdots \\ a_m \\ \hline b_1 \\ b_2 \\ b_3 \\ b_4 \\ \vdots \\ b_n \end{bmatrix}
=
\begin{bmatrix} S_0 \\ T_1 \\ S_2 \\ T_2 \\ \vdots \\ \hline 0 \\ U_2 \\ 0 \\ U_4 \\ \vdots \end{bmatrix} \tag{5}$$

where

$$\lambda_k = \sum_{i=1}^{N} \omega_i^k ;$$

$$S_k = \sum_{i=1}^{N} \omega_i^k P(\omega_i) ; \tag{6}$$

$$T_k = \sum_{i=1}^{N} \omega_i^k \, Q(\omega_i) \, ;$$

$$U_k = \sum_{i=1}^{N} \omega_i^k [P^2(\omega_i) + Q^2(\omega_i)] .$$

The solution of Equ. (5) gives the parameters of the frequency response (2), and the decision on the structure appears as a decision on the order of submatrices. The problem of the structure will be investigated in the following.

III. The weighting problem

The weighting factor in Equ. (4) has many disadvantages, as it depends on the unknown parameters and frequency, too. For real physical systems the parameters a_i, b_i are positive numbers, so the weighting factor grows tremendously at higher frequencies, and causes "greater weight" for the points of the experimental frequency response in this interval. The high frequency part of the data determines the whole course of the computed frequency response. It is not advantageous, because the error term is in general greater at higher frequencies, and the low frequency part contains more useful information about the system.

The disadvantages of the modified error term are evitable with the reserve of the advantages of the linear regression, if the results of the modified error minimalization are considered as intermediate results. Let the weighting factor at the second minimalization be:

$$p_2(\omega_i) = \frac{\gamma_2^2(\omega_i) + \delta_2^2(\omega_i)}{\gamma_1^2(\omega_i) + \delta_1^2(\omega_i)} \, . \tag{7}$$

The weighting factor is characterized by the differences between the denominators of the first and second approximations. In general, the weighting factor at the k-th iteration will be:

$$p_k(\omega_i) = \frac{\gamma_k^2(\omega_i) + \delta_k^2(\omega_i)}{\gamma_{k-1}^2(\omega_i) + \delta_{k-1}^2(\omega_i)} \, . \tag{8}$$

The limit value of the expression (8) tends to $p_k(\omega_i) \equiv 1$, and gives the opportunity to stop the iterative procedure.

In many practical cases the weighted error square minimalization is preferable, because the available "a priori" information suggests that some points of the frequency response have greater significance, or the error is less at an interval. Another situation, which appears essentially as a weighting

problem is the minimalization of the relative error square instead of the absolute error given by Equ. (3). In the latter case the weighting term is the reciprocal value of the experimental frequency response:

$$p_r(\omega_i) = \frac{1}{\sqrt{P^2(\omega_i)+Q^2(\omega_i)}} \,. \tag{9}$$

The practical identification, according to the preceding considerations, concludes in one of the four possible weighting situations, depending on the "a priori" information about the system and the error on the measured data. The weighting factors for these situations at the k-th iterative step are:

First case: absolute error minimalization with identical weight,

$$p_{ak} = \frac{\gamma_k^2(\omega)+\delta_k^2(\omega)}{\gamma_{k-1}^2(\omega)+\delta_{k-1}^2(\omega)}; \tag{10}$$

second case: absolute error minimalization with external weight,

$$p'_{ak} = \frac{\gamma_k^2(\omega)+\delta_k^2(\omega)}{\gamma_{k-1}^2(\omega)+\delta_{k-1}^2(\omega)} \cdot p_m^2(\omega); \tag{11}$$

third case: relative error minimalization with identical weight,

$$p_{rk} = \frac{\gamma_k^2(\omega)+\delta_k^2(\omega)}{\gamma_{k-1}^2(\omega)+\delta_{k-1}^2(\omega)} \cdot \frac{1}{P^2(\omega)+Q_2(\omega)}; \tag{12}$$

fourth case: relative error minimalization with external weight,

$$p'_{rk} = \frac{\gamma_k^2(\omega)+\delta_k^2(\omega)}{\gamma_{k-1}^2(\omega)+\delta_{k-1}^2(\omega)} \cdot \frac{p_m^2(\omega)}{P^2(\omega)+Q^2(\omega)} \,. \tag{13}$$

The weighting expressions (10)—(13) refer to the square error, and $p_m(\omega)$ is the external weighting factor.

The computation of the matrix element for the iterative linear regression procedure changes according to the four weighting situations. Instead of Equs (6), the following expressions hold:

$$\begin{aligned} \lambda_k &= \sum_{i=1}^{N} \omega_i^k \, q(\omega_i); \\ S_k &= \sum_{i=1}^{N} \omega_i^k \, P(\omega_i) \, q(\omega_i); \end{aligned} \tag{14}$$

$$T_k = \sum_{i=1}^{N} \omega_i^k \, Q(\omega_i) \, q(\omega_i) ;$$

$$U_k = \sum_{i=1}^{N} \omega_i^k [P^2(\omega_i) + Q^2(\omega_i)] \, q(\omega_i).$$

The $q(\omega_i)$ factors are in simple relation with the expressions (10)—(13):

First case:

$$q_{ak} = \frac{1}{\gamma_{k-1}^2(\omega) + \delta_{k-1}^2(\omega)} ; \tag{15}$$

second case:

$$q'_{ak} = \frac{p_m^2(\omega)}{\gamma_{k-1}^2(\omega) + \delta_{k-1}^2(\omega)} ; \tag{16}$$

third case:

$$q_{rk} = \frac{1}{\gamma_{k-1}^2(\omega) + \delta_{k-1}^2(\omega)} \cdot \frac{1}{P^2(\omega) + Q^2(\omega)} ; \tag{17}$$

fourth case:

$$q'_{rk} = \frac{p_m^2(\omega)}{\gamma_{k-1}^2(\omega) + \delta_{k-1}^2(\omega)} \cdot \frac{1}{Q^2(\omega) + P^2(\omega)} . \tag{18}$$

IV. The decision problem about the structure

For every regression methods have also to present a discussion about the accuracy and correctness of the regression curve. In many cases the "a priori" information gives a correct decision on the structure of the curve, and the only problem is the estimation of the variances belonging to the computed numerical parameters. In the identification procedure, however, the structural decision is very important and appears as a fundamental problem.

It is known from the literature [4] that the methods and concepts of the mathematical statistics present a possibility of investigating the quality characteristics of the regression curve. The confidence intervals and significance levels at the hypothesis test give a basis for the decision on the correctness of the results. The structural decision appears in our identification procedure as a decision on the degrees (n and m) of the frequency response (2), respectively, about the order of submatrices in Equ. (5).

In general, there are many possibilities in the field of system identification to perform a structural decision. These ideas depend mainly on the inherent properties of the actual procedure. Here we shall present two concepts which are adaptable to our method and to the digital computer program in a simple manner.

If the "a priori" information or another knowledge is available for the structural decision, then the following tests appear as a control of our information concerning the structure.

1. Decision on the basis of the statistical test

In this paper we do not deal with the details and methods of the mathematical statistics concerning the statistical test mentioned. We restrict ourselves to cite the principal idea of the decision only and refer to the literature [4].

We will compute the empirical variance at the end of the iterative procedure for every structure, which is given by:

$$S^2 = \frac{\sum_{i=1}^{N} |G_E(j\omega_i) - G(j\omega_i)|^2}{2N-(m+n+1)} \,. \tag{19}$$

The analysis of the empirical variances belonging to the different structures takes place with the χ^2 and t hypothesis tests. Had this been started from the highest possible structure and the degrees of the numerator and denominator were systematically decreased, then the proper structure was reached when the empirical variance and the significance levels suddenly changed by the decrease of the numerator and/or the denominator degree by one.

The basis of the decision is acceptable from a practical consideration, too. Namely, if the experimental frequency response originates from a realistic linear system, which is characterized by a well defined m and n pair, but is perturbed by noise, then the approximation belonging to a greater m and n than the proper ones cannot be better than the approximation which is produced by the proper structure. But the approximation in pure mathematical sense suddenly becomes worse if the structure is improper either in the numerator or the denominator. It has to be emphasized that the preceding considerations hold if the system is really a linear, time invariant one (or approximately is of such a kind) and the error term is a sample of a stochastic signal with a zero mean value. In the opposite case, as was expressed by STROBEL [1], the decrease of the structure by one causes such a change on the frequency response, which is in the magnitude of the error itself.

2. Decision on the basis of pole-zero configurations

The transfer function belonging to the frequency response (2) can be written in another form, too:

$$G(s) = \frac{\sum_{k=1}^{m} a_k s^k}{1 + \sum_{k=1}^{n} b_k s^k} = \frac{a_0 \prod_{k=1}^{m} \frac{1}{\alpha_k}(s-\alpha_k)}{\prod_{k=1}^{n} \frac{1}{\beta_k}(s-\beta_k)} . \tag{20}$$

Let us assume that the poles and zeros are distinct, but real or conjugate complex roots are allowed.

The investigation of the pole-zero configurations of different structures which approximate the same experimental data shows that the structures of higher degree than the proper one do not give better results because of pole-zero compensations and of appearance poles and zeros with a negligible effect.

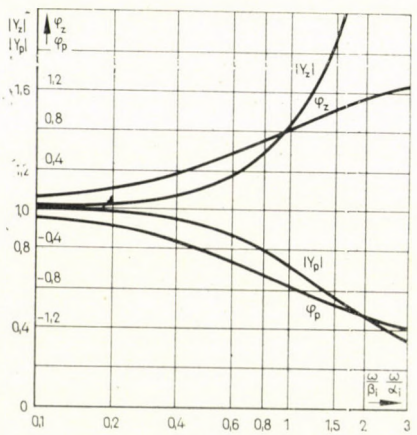

Fig. 1

If a pole and a zero agree in Equ. (20), the reduction of the structure is obvious. However, if a pole-zero pair or a set of them appear, which cause an effect on the frequency response only in a restricted interval and the effect is negligible, then the simplification will be allowed by practical considerations. An effect caused by a pole-zero set, which is in the magnitude of the error term, can be considered as negligible.

The possible pole-zero configurations which are significant for the structure reduction can be discussed by its Bode-plot. The neglected part appears as a multiplicative factor in Equ. (20), and so its effect can be characterized by the absolute value and the phase.

a) Single pole or zero far from the frequency interval on which the experimental data are available. The neglected part in this case is:

$$G_z(s) = \frac{1}{\alpha_i}(s-\alpha_i) \quad \text{or} \quad G_p(s) = \frac{\beta_i}{s-\beta_i} . \tag{21}$$

The Bode-plot of this element is plotted in Fig. 1. The effect of the single-root element is negligible in the interval $0 \leq \omega \leq \alpha_i$ (resp. $0 \leq \omega \leq \beta_i$), and can

be omitted if the break point $\omega_B = \alpha_i$, resp. $\omega_B = \beta_i$ is outside the interval of the experimental data.

b) Pole-zero pair. The neglected part in this case is:

$$G_{zp}(s) = \frac{\beta_i}{\alpha_i} \frac{s-\alpha_i}{s-\beta_i} . \tag{22}$$

The Bode diagram of this element is plotted in Fig. 2. The amplitude error and the maximum of the phase depend on the ratio β_i/α_i. The maximum value of the phase is:

$$\tan \varphi_{\max} = \frac{1}{2} \left(\sqrt{\frac{\beta_i}{\alpha_i}} - \sqrt{\frac{\alpha_i}{\beta_i}} \right). \tag{23}$$

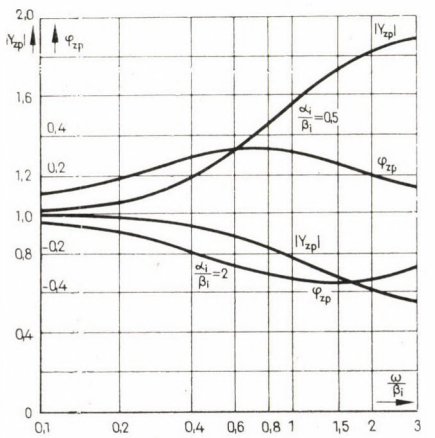

Fig. 2

The phase error is limited to a finite interval, but the absolute value error tends to a constant if ω tends to infinity. If the break points (α_i and β_i) lie beyond the important interval of the experimental frequency response, then the effect of the element (22) is negligible. If they lie in the important interval, it can be cancelled when the ratio β_i/α_i is near to one. The allowed value of this ratio depends on the error level, too.

c) Two pairs of pole-zero. The neglected part in this case is:

$$G_{zp}(s) = \frac{\alpha_i b_i}{\beta_i a_i} \frac{s-\alpha_i}{s-\beta_i} \cdot \frac{s-a_i}{s-b_i} . \tag{24}$$

We shall restrict ourselves now to the situation, when the conditions hold:

$$\beta_i < \alpha_i < a_i < b_i \quad \text{or} \quad \alpha_i < \beta_i < b_i < a_i$$

and

$$\frac{\beta_i b_i}{\alpha_i a_i} = 1 .$$

The Bode-plot of the transfer element (24) with the preceding restrictions is plotted in Fig. 3. Both the amplitude and the phase errors are restricted to a finite interval. The maximum (or minimum) of the amplitude error appears at the frequency:

$$\omega_M = \sqrt{\beta_i b_i} = \sqrt{\alpha_i a_i}$$

and the magnitude of it is:

$$\left|G_{zp}(j\omega)\right|_{\substack{\max \\ \min}} = \frac{\alpha_i}{\beta_i} \frac{\frac{a_i}{\alpha_i} + 1}{\frac{b_i}{\beta_i} + 1} = \frac{a_i}{b_i} \frac{\frac{\alpha_i}{a_i} + 1}{\frac{\beta_i}{b_i} + 1} . \tag{25}$$

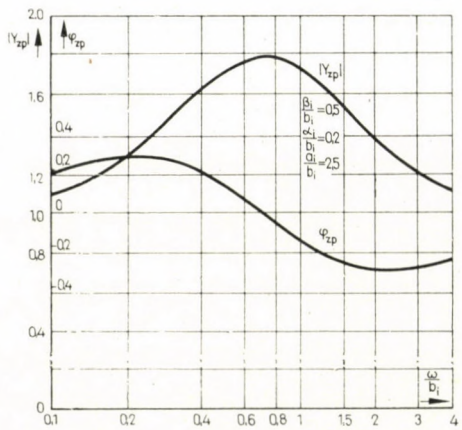

Fig. 3

The preceding three pole-zero combinations represent the simplest configurations and we were restricted to real roots only. There are a lot of other possible pole-zero sets with conjugate complex poles and zeros, which are possibilities regarding the structure reduction. But the decision on the simplification is more difficult in these situations.

The legality of the structure simplification on the basis of pole-zero compensation is assisted by the investigations performed by UNBEHAUEN [5]. The effect of different distortions was discussed in his paper, which can appear on the measured time functions, caused by measurement errors, noises and drift. The errors of the numerical computation of the frequency response with the aid of the Fourier transformation also conclude in such distortions. It was shown that the effect of these distortions appears on the frequency response in a finite interval, and the mathematical and graphical form of these error functions closely agree with the Bode-diagram of the simplest pole-zero configurations, which were discussed in the preceding part.

V. The digital computer program

The concepts and the detailed algorithm of the identification procedure which was described in the preceding sub-paragraphs would have been collected into a digital computer program. The main characteristics and properties of this program will be summarized in the following.

After taking in the data of the experimental frequency response (real and imaginary part) and the starting value of m and n, the first iteration step is performed on the basis of the modified error term (4). But the following steps are based on the expression (8). There is a possibility to choose one of the four available weighting situations. The external weighting factor $p_m(\omega)$ is also needed as input data. The twofold iterative action is controlled partly automatically, partly by special input information. The first iteration which tries to nullify the unwanted properties of the modified error will be stopped automatically by the asymptotic properties of the expression (8). The second iterative action, namely, the systematic decrease of the degrees of the numerator and the denominator, starts from the highest possible structure (m and n). The highest structure which can occur in the identification appears as a weak "a priori" information about the experimental frequency response. The systematic decrease of the structure can be performed in three ways:

a) The degree of the numerator is fixed and the degree of the denominator will be decreased till an end value;

b) the denominator degree is fixed and the numerator degree will be decreased;

c) both the denominator and the numerator degrees will be decreased.

The decision about the structure of the identified transfer function can be performed with the aid of some extra computation. The statistical test of the empirical variance and the computation of the variances of the computed parameters $a_0, a_1, \ldots a_m; b_1, b_2, \ldots b_n$ need the computation of the sum (19) and the inverse of matrix (5). These data are available after each iterative step, if it is wanted. The second concept, the comparison of the pole-zero configurations, needs the computation of the roots of the numerator and denominator polynomials. To perform it a root-solving subroutine is matched to the whole procedure, which works on the base of the modified Newton-iteration algorithm.

VI. Example

Numerous investigations in connection with the digital computer procedure and the identification method were performed. Different transfer elements and their indirect measurement were simulated on a digital computer and the results prepared for the identification method. The points of the "experimental"

frequency response were generated on the basis of the indirect measurement (impulse test and step response) with the aid of Fourier-transformation. The error term arised partly from the simulation, partly because of the Fourier-transformation, but in some cases it was applied to the exact frequency response points in the form of random numbers with known statistics. The results of our investigations are summarized in the conclusions.

To illustrate the results of our investigations and to show the merits of the digital computer procedure let us look at the results of a particular system. The exact transfer function of the investigated system was:

$$Y(s) = 90\,\frac{1 + 2s + 4s^2}{(s^2 + 0{,}4s + 1)\,(s^2 + 3s + 9)} = \frac{10 + 20s + 40s^2}{1 + 0{,}73333s + 1{,}24444s^2 + 0{,}3777\,s^3 + 0{,}1111\,s^4}\,. \tag{26}$$

The exact frequency response is plotted in Fig. 4 and the error terms of the experimental frequency responses which were generated from the step response and from an impulse test (half sine wave input signal $T = 3{,}6$ sec duration) are plotted in Fig. 5 (A and B curves respectively). The results of the identification with absolute error minimalization on the bases of the two experimental frequency responses at the correct structure are summarized in Table I.

Table I

1. Computed parameters belonging to different kinds of data

	a_0	a_1	a_2	b_1	b_2	b_3	b_4
Exact	10	20	40	0,73333	1,24444	0,37777	0,11111
Step response	10,013	19,971	40,091	0,73444	1,24558	0,37869	0,11132
Impulse test data	9,939	20,029	39,7015	0,72842	1,24316	0,37396	0,11197
$S_1 = \pm 0{,}25$	9,972	19,997	39,847	0,73103	1,24255	0,37608	0,1110
$S_2 = \pm 2$	10,005	19,5963	40,1485	0,7360	1,25075	0,38076	0,11236
$S_3 = \pm 5$	9,237	21,594	38,425	0,71448	1,22743	0,35975	0,10824

2. Poles and zeros of the computed transfer functions

	Poles		Zero
Exact	$-1{,}5 \pm j\,2{,}5981$	$-0{,}2 \pm j\,0{,}9798$	$-0{,}25 \pm j\,0{,}43301$
Step response	$-1{,}5008 \pm j\,2{,}5954$	$-0{,}20014 \pm j\,0{,}97947$	$-0{,}24907 \pm j\,0{,}43662$
Impulse test data	$-1{,}4702 \pm j\,2{,}60123$	$-0{,}19959 \pm j\,0{,}98002$	$-0{,}25225 \pm j\,0{,}43243$
$S_1 = \pm 0{,}25$	$-1{,}49438 \pm j\,2{,}60122$	$-0{,}19967 \pm j\,0{,}9804$	$-0{,}250921 \pm j\,0{,}43277$
$S_2 = \pm 2$	$-1{,}49453 \pm j\,2{,}58997$	$-0{,}19992 \pm j\,0{,}97746$	$-0{,}24405 \pm j\,0{,}4355$
$S_3 = \pm 5$	$-1{,}46264 \pm j\,2{,}6509$	$-0{,}19924 \pm j\,0{,}98397$	$-0{,}28099 \pm j\,0{,}4018$

The experimental variances belonging to the step response data are shown in Table II, as the function of the first iterative process and the structure. The pole-zero configurations of the different structures are summarized here, too.

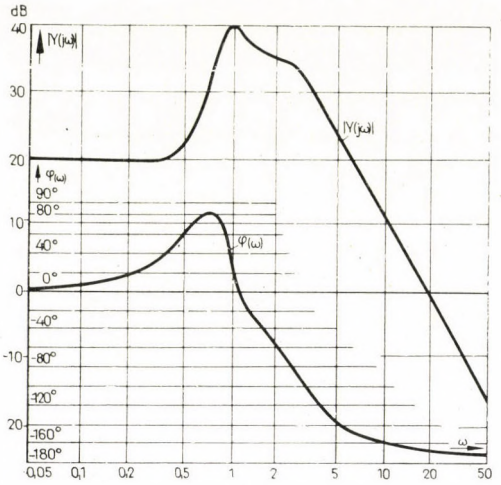

Fig. 4

Table II

1. Experimental variances belonging to the step response data

n	m	Iterative steps		
		1	2	3
5	6	,5763402 +03	,1732926 +00	,2590243 −01
	5	,2586710 +03	,5638554 −01	,2559036 −01
	4	,2609285 +03	,5488095 −01	,2529761 −01
	3	,2776470 +03	,7840000 −01	,2502352 −01
	2	,5786279 +03	,6747674 −01	,2473255 −01
	1	,5874597 +03	,1364252 +03	,7915747 +02
	0	,5984965 +03	,5040795 +03	,5108522 +03
4	6	,6050759 +03	,1684337 +00	,2584337 −01
	5	,5977226 +03	,1409523 +00	,2529761 −01
	4	,5811647 +03	,1176470 +00	,2500000 −01
	3	,5906279 +03	,8081395 −01	,2473255 −01
	2	,6034712 +03	,1942528 +00	,2445977 −01
	1	,6060340 +03	,1475340 +03	,1086886 +03
	0	,5900865 +03	,4981685 +03	,5139797 +03
3	6	,5943333 +03	,1539523 +03	,1161904 +03
	5	,5871647 +03	,1517882 +03	,1145011 +03
	4	,5725930 +03	,1503720 +03	,1130465 +03
	3	,5942758 +03	,1540643 +03	,1134022 +03
	2	,6028977 +03	,1577727 +03	,1127954 +03
	1	,6494494 +03	,1764000 +03	,1140337 +03
	0	,5930000 +03	,5032555 +03	,5004555 +03

2. Pole-zero configurations belonging to the step response data

n	m		
	5	4	3
3	$-0{,}24913 \pm j\,0{,}4333$ $+1148{,}6$	$-0{,}24913 \pm j\,0{,}4333$ $-6073{,}6$	$-0{,}04007$ $+3{,}3663 \pm j\,11{,}6626$
	$-0{,}200117 \pm j\,0{,}97947$ $-1{,}49998 \pm j\,2{,}595$ $+964{,}27$	$-0{,}200112 \pm j\,0{,}979464$ $-1{,}49999 \pm j\,2{,}59506$	$-0{,}34396 \pm j\,1{,}24696$ $-75{,}403$
2	$-0{,}24912 \pm j\,0{,}4333$	$-0{,}24907 \pm j\,0{,}436622$	$-0{,}4023$ $+23{,}180$
	$-0{,}200115 \pm j\,0{,}97945$ $-1{,}50013 \pm j\,2{,}5969$ $-6137{,}9$	$-0{,}20014 \pm j\,0{,}97947$ $-1{,}50077 \pm j\,2{,}5954$ $-1{,}50077 \pm j\,2{,}5954$	$+0{,}092565 \pm j\,2{,}5196$ $-2{,}1918$
	$-0{,}04145$	$-0{,}038027$	$-0{,}05466$
	$-0{,}28533 \pm j\,1{,}1733$ $-0{,}66472 \pm j\,4{,}1424$ $+6{,}8895$	$-0{,}33715 \pm j\,1{,}253$ $-0{,}60814 \pm j\,5{,}11974$	$-0{,}33647 \pm j\,1{,}2423$ $-28{,}41$

Table I also contains the results of the identification, when the exact frequency response points were perturbed by random numbers equally distributed on a finite interval. The chosen interval of the perturbing random numbers were: $S_1 = \pm 0{,}25$; $S_2 = \pm 2$; $S_3 = \pm 5$. The empirical variances and the pole-zero configurations belonging to the noise interval $S_2 = \pm 2$ are summarized in Table III.

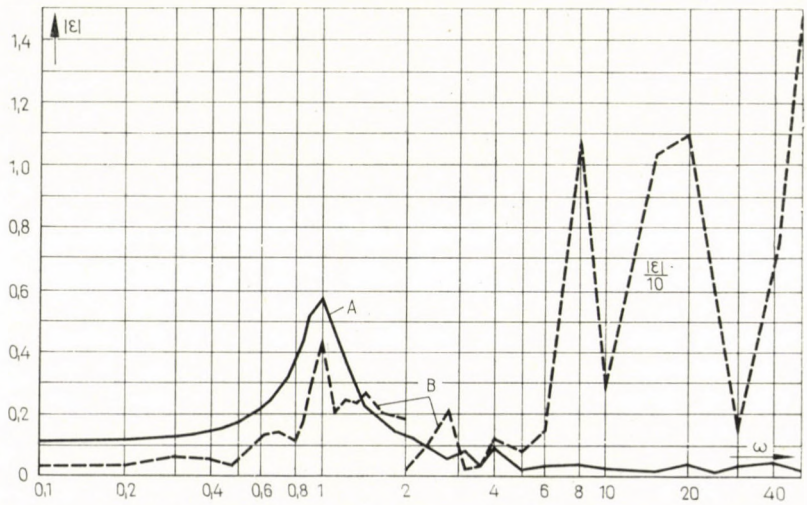

Fig. 5

Table III

1. Experimental variances belonging to $S_2 = \pm 2$

n	m	Iterative steps				
		1	2	3	4	5
5	6	,7235263 +03	,1561276 +03	,8220921 +02	,1528552 +01	,1369210 +01
	5	,2712818 +03	,1138636 +03	,3767532 +01	,1351948 +01	,1350649 +01
	4	,5885512 +03	,1608423 +03	,1152564 +03	,3660256 +01	,1333333 +01
	3	,6710379 +01	,1895632 +03	,1146405 +03	,4388607 +01	,1345569 +01
	2	,6391437 +03	,2074087 +03	,1150887 +03	,5300000 +01	,1328750 +01
	1	,6312530 +03	,2055802 +03	,1150753 +03	,8944197 +02	,7925925 +02
	0	,6213890 +03	,5373012 +03	,5415609 +03	,5268780 +03	,5232682 +03
4	6	,7140207 +03	,1558116 +03	,7502467 +02	,1469220 +01	,1351948 +01
	5	,7047692 +03	,1536371 +03	,7284743 +02	,1442692 +01	,1333333 +01
	4	,6553974 +03	,2077974 +03	,1187215 +03	,9469620 +01	,1320253 +01
	3	,6646487 +03	,2066112 +03	,9794999 +01	,1868749 +01	,1327500 +01
	2	,6309530 +03	,2220197 +03	,9460123 +02	,1533333 +01	,1313580 +01
	1	,6221317 +03	,2352414 +03	,1153024 +03	,9882317 +02	,1019256 +03
	0	,6174698 +03	,5529722 +03	,5524337 +03	,5250481 +03	,5342168 +03
3	6	,6836538 +03	,2050717 +03	,1230512 +03	,1097179 +03	,1069602 +03
	5	,6750253 +03	,2012253 +03	,1214886 +03	,1083025 +03	,1055784 +03
	4	,7512625 +03	,2156112 +03	,1191625 +03	,1078237 +03	,1050124 +03
	3	,7387740 +03	,2145098 +03	,1200962 +03	,1067518 +03	,1038543 +03
	2	,7041341 +03	,2925487 +03	,1216768 +03	,1077158 +03	,1025524 +03
	1	,6987192 +03	,3745060 +03	,1293891 +03	,1086927 +03	,1019096 +03
	0	,7096452 +03	,5567535 +03	,5309404 +03	,5274095 +03	,5287583 +03

VII. Conclusions

a) The modified error term minimalization [Equ. (4)] is not a successful procedure if noise is present. The noise part of the high frequency interval determines the whole course and the parameters of the approximate frequency response almost independently of the chosen structure and the course of the experimental frequency response at lower frequencies. The experimental variance is very high in this case, and great errors appear on the low frequency interval.

b) The iterative procedure for eliminating the unwanted properties of the modified error has good convergence properties, if the signal/noise ratio is greater than one at higher frequencies. The speed of the convergence depends on the noise level. If there are some "a priori" information that the experimental frequency response has low signal/noise ratio at higher frequencies,

2. Pole-zero configurations belonging to $S_2 = \pm 2$

m	n		
	5	4	3
5			$-0{,}030863$ $+8{,}9847$ $-12{,}868$ $+ 1{,}8639 \pm j\, 22{,}6337$ $- 0{,}3236 \pm j\, 1{,}232$ $-91{,}984$
3	$-0{,}24517 \pm j\, 0{,}4360$ $-316{,}79$ $-0{,}19972 \pm j\, 0{,}9774$ $-1{,}4835 \pm j\, 2{,}585$ $-1508{,}1$	$-0{,}245015 \pm j\, 0{,}43578$ $-516{,}21$ $-0{,}19960 \pm j\, 0{,}9775$ $-1{,}4835 \pm j\, 2{,}5866$	
2	$-0{,}24491 \pm j\, 0{,}43595$ $-0{,}19982 \pm j\, 0{,}97737$ $-1{,}4866 \pm j\, 2{,}5852$ $+454{,}499$	$-0{,}24405 \pm j\, 0{,}43548$ $-0{,}19992 \pm j\, 0{,}97746$ $-1{,}49453 \pm j\, 2{,}58997$	
1	$-0{,}036335$ $-0{,}2874 \pm j\, 1{,}1851$ $-0{,}79596 \pm j\, 4{,}6197$ $+8{,}9366$	$-0{,}005594$ $-0{,}30239 \pm j\, 1{,}21116$ $-0{,}71550 \pm j\, 5{,}5846$	

it is practical to omit these points to increase the speed of convergence and the accuracy of the identification. If there are many points with low signal/noise ratio at higher frequencies the iterative procedure will be unable to converge to the "equal weight" situation, especially when the approximate transfer function has more free parameters than the correct one, and so there is a possibility to exactly approximate (in a pure mathematical sense) the noisy data. The experimental variance is high in this situation, and it remains at this level in the course of the iterative procedure.

c) The results of the identification are consistent, when the noise term has a zero mean. This is true at a high noise level, too. Unfortunately the indirect system measurements lead sometimes to non-zero expectation in the noise term existing on the computed frequency response due to drift and other types of errors.

d) The results of the iterative least-square method are independent of the noise statistics, the only demand is the zero mean value of the noise.

e) The decision about the structure of the frequency response on the basis of the statistical test of the experimental variance is effective if the noise term on the experimental data is not high.

f) The knowledge of the pole-zero configurations belonging to different structures gives us a good possibility for the whole supervision of the frequency response, the noise term and the identification. This test signs some drifting part of the frequency response, but if there are no "a priori" information available for the proper structure the reduction of the structure on the basis of the recognized pole-zero pairs is sometimes a doubtful action.

g) The relative error minimalization will be effective and the procedure properly convergent if the error term has really such a character that the relative error is approximately constant on the whole frequency interval. The weighting factor at the relative error minimalization in the "equal relative weight" situation has the same character as the "automatic" weighting term at the absolute error minimalization, if the investigated transfer element is a physically realizable one. The determining role of the high frequency interval is far stronger and it can be suppressed only in that case, if indeed the relative error is constant.

REFERENCES

1. STROBEL, H.: On a New Method of Determining the Transfer Function by Simultaneous Evaluation of the Real and Imaginary Parts of the Measured Frequency Response. 3rd IFAC Conference, London 1966; Session 1, Paper 1. F.
2. LEVY, E. C.: Complex Curve Fitting. *IRE Trans. on Automatic Control* (1959), May.
3. SANATHANAN, C. K.— KOERNER, I.: Transfer Function Synthesis as a Ratio of Two Complex Polynomials. *IEEE Trans. on Automatic Control* **AC-9** (1963); January, 56—58.
4. PRÉKOPA, A.: Valószínűségelmélet (The theory of probability). Műszaki Könyvkiadó, Budapest 1962.
5. UNBEHAUEN, H.—SCHLEGEL, G.: Estimation of the Accuracy in the Identification of Control Systems Using Deterministic Test Signals. Preprints of the IFAC Symposium, Prague 1967; June.

Einige Probleme der Kennwertermittlung aufgrund des Frequenzganges. Im Artikel wird für die Kennwertermittlung linearer, dynamischer Regelsysteme aufgrund des Frequenzganges eine iterative Methode der kleinsten Quadrate vorgeschlagen. Nebst Beschreibung der grundlegenden Konzeption der Methode werden zwei besondere Probleme eingehend untersucht, namentlich das Problem der Gewichtsverteilung und die Feststellung der Struktur der identifizierten Übertragungsfunktion. Aufgrund des theoretischen Teils wurde die Methode für den Digitalrechner MINSK—22 programmiert und die Resultate der praktischen Untersuchung werden zusammengefaßt. Die Arbeit enthält auch ein Zahlenbeispiel.

Некоторые вопросы идентификации, проведенной на основе частотной функции *(Й. Дьюрки)*. Для идентификации на основе частотной функции линеарных динамических систем регулирования предлагается итеративный метод наименьших квадратов. Наряду с описанием основной концепции предлагаемого метода детально рассматривается два специальных случая, а именно проблема взвешивания и определение структуры идентифицированной переносной функции. На основе теоретической части метод программирован для ЦЭВМ МИНСК—22 и дано обобщение результатов практического анализа. В работе приведен также числовой пример.

Acta Technica Academiae Scientiarum Hungaricae; Tomus 68 (1—2), pp. 161—178 (1970)

A LASER BEAM METHOD FOR THE EXAMINATION OF CATHODE SPACES

J. F. BITÓ

CAND. OF TECHN. SC.

RESEARCH INSTITUTE FOR ELECTRONICS, BUDAPEST

[Manuscript received November 26, 1968]

With the cathode side application of the traditional experimental methods, adapted so far, the plasma microparameters of these spaces cannot be determined with a satisfactory accuracy. In this paper an interferometric method with laser beams is demonstrated, with the aid of which the value of the electron concentration in the cathode spaces, its time dependence and axial distribution can be determined in a simple way, with an accuracy of $\pm 10^{10}$ electron/cm^3. The highest time resolution which can be reached is 10^{-8} sec.

I. Introduction

The experimental analysis of the discharge plasma in the cathode spaces has not yet been resolved completely [1]. One reason for this is that in contrast to the positive column of the cold plasmas of low pressure, the cathode spaces cannot be examined by classical methods exactly on account of the vicinity of the cathode. The other difficulty is that the spaces may be looked upon as the "fore-ground" of the positive column. Therefore, neither the electrons nor the ions have the distributions, which can easily be examined, e.g. the Maxwell–Boltzmann, or Druyvesteyn type distribution. The latter makes e.g. the application of the classical probe measurements in the cathode spaces dubious.

The idea of such an examination was already put forward much earlier, in case of which a monoenergetic electron beam was transmitted through the cathode space to be analysed [2]. While the perturbation by electron or ion beams of the plasma systems of high temperature does not bring about a notable change in the examined system, so in the case of cold plasmas this intervening essentially alters the conditions to be examined. Therefore, the application of this method has not been taken into account here.

Because neither the probe measurements nor the electron beam—plasma interaction have given satisfactorily exact and well reproducible results, also the plasma spectroscopic methods were tried out in the cathode space [3]. The great advantage of these methods manifests itself exactly at extreme field strength, that is to say in the case of a great electric or magnetic field strength. The electric field strength in the cathode spaces of the discharges can attain only in the cathode fall space such an order of magnitude, which

causes a significant and noticeable alteration of the spectral lines. For lack of a magnetic field neither this observation offers sufficient data about the plasma microparameters.

The microwave methods, which make the measurement of electron-concentrations of 10^{14} electron/cm^3 possible, cannot be applied on account of the oscillations caused by them in the cathode space. Besides, nearly every characteristic oscillation process of the discharges can be observed in the cathode space. From the microwave measuring methods the transmission measurements without external magnetic field might be taken into account, but in the course of this probing not the really negligible small sounding power, but the periodical disturbance, carried into the microwave range gives difficulties.

Even the weak disturbances can be considerably amplified by the cathode space in an appropriate frequency range with the aid of electron groups, emerging from the cathode, and similar to a divergent electron beam. While the plasma, in general, performs the function of a selective amplifier, that is to say, it amplifies the disturbances carried into it in a relatively narrow band, so the cathode space, on account of its inhomogeneities and in consequence of its characteristic "inclination" for oscillation in a wide band, can easily be influenced with the aid of an external disturbance. This causes in many cases on the other hand the shift of the whole cathode mechanism.

Because the probe measurements, the electron beam soundings, the spectroscopic observations and the application of microwave methods in the cathode space were not successful either, we could get informations about the phenomena occurring in the cathode spaces only by means of indirect measurements; by diagnostic systems, not based on the measurements of microparameters, or by means of theoretical calculations of a doubtful value and of approximative character.

In the following an interferometric method with laser beam is described with the aid of which the value of electron concentration in the cathode space, its time dependence and axial distribution can be determined in a simple way.

II. Interferometrical measurement of the plasma refractivity

The optical refractive index n of the neutral, not extremely dense gases can be characterized [3—5] by the dispersion equation:

$$(n-1) = \frac{2\pi \cdot e^2 N}{m} \sum_k \frac{f_k}{\omega_k^2 - \Omega^2}, \tag{1}$$

where f_k oscillator strength;
m mass of the gas atom;
ω_k frequency belonging to the corresponding level;
N concentration of the gas atoms.

On the selection of the sounding frequency [Ω] we must take into consideration the term-scheme of the examined gas, unless the irradiation should occur on the resonance wave length. From this point of view the 1066,7 and the 1043,3 Å resonance lines must be excluded by argon. Neglecting these lines and maintaining only the second order approximation, further concretizing the deduction only to argon, we get the following well-known Cauchy-equation [5]:

$$(n-1) = 27{,}92 \cdot 10^{-3} + \frac{1{,}56 \cdot 10^{14}}{\lambda^2}, \tag{2}$$

where λ is the wave length of the sounding light.

Taking into account the well-known fact that the refractive index changes at low pressure in a linear way with the variation of pressure [6], we get the equation

$$(n-1) = \left(1{,}3 \cdot 10^{-23} + 0{,}58 \cdot 10^{-33} \cdot \frac{1}{\lambda^2}\right) \cdot N_A, \tag{3}$$

where α_A is the concentration of the argon atoms.

For the sake of a later examination it is worth-while to take into consideration the well applicable Gladstone–Dale formula, which also shows an interaction between the refractive index and the particle density:

$$(n-1) \approx 2\pi N_A - \alpha_A^{\circ}, \tag{4}$$

where α_A° is the polarizability.

Let us now consider the case when the originally neutral argon gas becomes ionized to a certain degree (x) under an external effect in such a way that the so formed plasma contains only single charged positive ions and negative ions do not occur at all in it. This latter condition does not mean a serious restriction in the case of argon, by other gases, however, such as oxygen and nitrogen it means a serious restriction. The refractive component may be looked upon in this case as such a gas-complex of three components, the single components of which are the following:

a) The neutral argon atoms, the N_A° density of which can be given with the aid of ionization degree x in the form

$$N_A^{\circ} = N_A(1-x), \tag{5}$$

where N_A means the concentration of the neutral atoms before the ionization;

b) the ionized argon atoms, the N_A^{+} density of which is given by the connection:

$$N_A^{+} = x \cdot N_A; \tag{6}$$

c) the electrons, which appear in the equilibrium case in concentration

$$N_e = N_A^+ = x \cdot N_A \tag{7}$$

with the assumption of the total neutrality.

Each of these gas components has some kind of refractivity and polarizability corresponding to it. When there are no permanent dipoles, then the polarizability corresponds to the susceptibility. It can be shown [7] that in each case, when there are no great field strengths and the density of the gas components has not an extremely high value, the components of the susceptibility are summarized and thus the resulting susceptibility of the gas compound is given by their elementary mathematical sum.

Maintaining the restrictions and taking into account the linear connection between the refractive index and polarizability, characterized by the Gladstone–Dale formula, for the plasma containing the components *a*, *b*, *c*, described in the above enumeration, the following connection can be given for the refractive index:

$$(n_p - 1) = (n_A^\circ - 1) + (n_A^+ - 1) + (n_e - 1)\,, \tag{8}$$

where n_p refractive index of the plasma;
n_A° refractive index of the neutral argon gas;
n_A^+ refractive index of the single ionized argon atoms, of positive charge;
n_e refractive index of the electron gas.

Following the forming of this model dynamically, we must take into account that the initial concentration of the argon atoms has diminished during the course of the ionization and in addition two new components, electrons and ions, appeared in the system with a well defined supplementary refractivity.

The refractivity of the single ionized argon atoms cannot naturally be determined in a direct way. Calculations were made however [6] concerning the value of the quotient, obtained by the polarizability of the argon ions and neutral argon atoms. According to this the following relation

$$0{,}34 < \frac{\alpha_A^+}{\alpha_A^\circ} < 0{,}72 \tag{9}$$

is valid, where α_A^+ means the polarizability of the single charged argon ions and α_A° the polarizability of the neutral argon atoms.

With the repeated application of the Gladstone–Dale formula we obtained a connection also for the refractivity; the refractive index of the ions is only about 34—72% of the refractive index of the neutral gas atoms of the

same concentrations. The plasma however also contains a third component, the electron gas, the refractive index of which may be calculated from the dielectric constant of the plasma starting out from the assumption that the refractive index of the electron gas coincides with that of the plasma [3].

If we start at the characterization of the plasma from the model, consisting of two fluids — of electron gas and of ion gas — then the following basic equations can be obtained:

$$\varrho_0 \frac{\partial \mathbf{v}}{\partial t} = \frac{1}{c}[\mathbf{j}\mathbf{H}_0] - \nabla p, \tag{10}$$

$$\frac{m}{N_e \cdot e^2}\frac{\partial \mathbf{j}}{\partial t} = \mathbf{E} + \frac{1}{c}[\mathbf{v}\mathbf{H}_0] + \frac{1}{e \cdot N_e}\Delta p_e - \frac{1}{e \cdot N_e c}[\mathbf{j} \cdot \mathbf{H}_0] - \frac{\mathbf{j}}{\sigma}, \tag{11}$$

$$\frac{\partial \varrho}{\partial t} + \varrho \operatorname{div} \mathbf{v} = 0, \tag{12}$$

$$p = F(\varrho, \tau); \tag{13}$$

where m mass of the electron;
e charge of the electron;
j current density;
t time;
E electric field strength;
c velocity of light;
v velocity of volume elements;
ϱ_0 average value of the charge density;
ϱ charge density;
H_0 strength of the static external magnetic field;
p pressure of the plasma;
p_e pressure of the electron gas;
σ electrical conductivity of the plasma;
T temperature of the plasma.

If we assume that the external electric field has no influence on the plasma ($\mathbf{E}_0 \equiv 0$), and regard its own internal magnetic field of plasma as negligibly small, compared to the external static magnetic field strength, with the consideration of the relation

$$|\mathbf{H}| \ll |\mathbf{H}_0| \tag{14}$$

then the Maxwell-equations take the forms

$$\operatorname{rot} \mathbf{H} = \frac{4\pi}{c}\mathbf{j} + \frac{1}{c}\frac{\partial \mathbf{D}}{\partial t}, \tag{15}$$

$$\operatorname{rot} \mathbf{E} = \frac{1}{c}\frac{\partial \mathbf{H}}{\partial t}; \tag{16}$$

$$\operatorname{div} \mathbf{D} = 4\pi\mathbf{q}, \qquad \operatorname{div} \mathbf{H} = 0; \tag{17}$$

$$\left(\frac{\mathbf{B}_0}{\mathbf{H}_0} = \mu = 1\right). \tag{18}$$

where q is the charge density determined by the polarization processes.

Neglecting the own pressure of the plasma beside the magnetic pressure and taking into account our above-mentioned conditions, Equs (10), (11) and (12) can be brought to the forms

$$\varrho_0 \frac{\partial \mathbf{v}}{\partial t} = \frac{1}{c}[\mathbf{j} \cdot \mathbf{H}_0], \tag{19}$$

$$\frac{m}{N_e \cdot e^2} \cdot \frac{\partial \mathbf{j}}{\partial t} = \mathbf{E} + \frac{1}{c}[\mathbf{v}\mathbf{H}_0] - \frac{1}{e \cdot N_e \cdot c}[\mathbf{j} \cdot \mathbf{H}_0] - \frac{\mathbf{j}}{\sigma}, \tag{20}$$

$$\frac{\partial \varrho}{\partial t} + \varrho \operatorname{div} \mathbf{v} = 0. \tag{21}$$

If an electromagnetic wave of angular frequency, travelling in direction k arrives to the boundary of the plasma, the processes arising there can be described with the aid of these equations. By the description the characteristic plasma frequencies must be taken into account. These are the following:

a) The cyclotron frequency of the electrons (ω_e)

$$\omega_e = \frac{e \cdot |\mathbf{H}|}{m \cdot c}; \tag{22}$$

b) the cyclotron frequency of the ions of m_i mass (ω_i)

$$\omega_i = \frac{e \cdot |\mathbf{H}_0|}{m_i \cdot c}; \tag{23}$$

c) the plasma frequency of the electrons and ions (ω_{0e}, ω_{0i})

$$\omega_{0e} = \left(\frac{4\pi \cdot N_e \cdot e^2}{m}\right)^{1/2}, \tag{24}$$

$$\omega_{0i} = \left(\frac{4\pi n_i \cdot e^2}{m_i}\right)^{1/2}; \tag{25}$$

d) the effective impact frequency ν_{ei} between the electron and ions

$$\nu_{ei} = \frac{\alpha_{ei} n_i + \alpha_{ne} \cdot n_n}{m}, \tag{26}$$

where n_i ion concentration;
n_n concentration of the neutral atoms;
m_e mass of the electron;
α_{ei} coefficient depending on the electron and ion velocities;
α_{re} coefficient depending on the velocity of the neutral particles and electrons.

In consideration of all these, the general dispersion equation can be deducted, the parts of which may be discussed according to the character of the arising oscillations. In case of waves travelling perpendicularly to the external magnetic field direction, we get a well arranged dispersion equation if the current density vector of the plasma is perpendicular to the direction of wave propagation [3]:

$$\Omega^2 = \frac{w_{0e}^2 \cdot \Omega^2}{\Omega^2 - \mathbf{k}^2 c^2}, \tag{27}$$

from this the refractive index is

$$n^2 = \frac{\mathbf{k}^2 \cdot c^2}{\Omega^2} = 1 - \frac{w_{0e}^2}{\Omega^2}. \tag{28}$$

If the plasma is not influenced by an external static magnetic field, that is to say $\mathbf{H}_0 = 0$, then we get the same dispersion relation. If the current density $\mathbf{j}$ is not perpendicular to the direction of the wave propagation, the dispersion equation has a more complicated character:

$$n^2 = 1 - \frac{\omega_{0e}^2}{\Omega^2 \left(1 - \frac{\boldsymbol{w}_i \cdot \boldsymbol{w}_e}{\Omega^2} + \frac{\omega_e^2}{\omega_{0e}^2 + \Omega^2 + \omega_i \omega_e}\right)}. \tag{29}$$

On the basis of the dispersion equations, with the aid of the connection

$$n^2 \equiv \varepsilon \tag{30}$$

also the dielectric constant ε can be given, which may be divided into a real and an imaginary part:

$$\varepsilon = \varepsilon_r + i\varepsilon_i = \left(\frac{\mathbf{k} \cdot \boldsymbol{c}}{\Omega}\right)^2 = n^2; \tag{31}$$

from which

$$|\mathbf{k}| = \frac{\Omega}{c} (\varepsilon_r + i\varepsilon_i)^{1/2}, \tag{32}$$

$$|\mathbf{k}| = \frac{\Omega}{c} \left(\frac{\varepsilon_r + |\varepsilon|}{2}\right)^{1/2} + i\,\Omega \left(\frac{|\varepsilon| - \varepsilon_r}{2}\right). \tag{33}$$

The dielectric constant of the plasma will be positive or negative depending on the sign of the quadrate of the refractive index, which at the same time makes also the distinction of the interaction phenomena possible [3].

The dielectric constant may also be connected with the characteristic plasma oscillations. On this basis the connection (31) will take the form

$$\varepsilon = \frac{1}{4\pi}\left(1 - \frac{\omega_{0e}}{\nu_{ei}^2+\Omega^2} + i\,\frac{\omega_{0e}^2 - \frac{\nu_{ei}}{r}}{\nu_{ei}^2+\Omega^2}\right) \tag{34}$$

which is often simplified by the fact that in consideration of

$$\left(\frac{\nu_{ei}}{\Omega}\right)^2 \ll 1 \tag{35}$$

an approximation is applied.

Consequently, the refractive index is unambiguously connected with the dielectric constant and with the electron concentration. Its value can be given starting from the basic equations, outlined above, in the most simple case, by the application of the Maxwell long wave approximation in the form

$$n = \sqrt{\varepsilon} = \left[1 - \left(\frac{\omega_{0e}}{\Omega}\right)^2\right]^{1/2} \tag{36}$$

which may be in some cases simplified further, with the application of approximation

$$n \approx 1 - \frac{1}{2}\left(\frac{\omega_{0e}}{\Omega}\right)^2 \tag{37}$$

if condition

$$\omega_{0e} \ll \Omega \tag{38}$$

is fulfilled.

Taking into account the value of the plasma frequency, defined by connection (24), Equ. (36) may be transformed into a more usual, explicit form:

$$(n-1) = -\frac{2\pi N_e \cdot e^2}{m_e \cdot \Omega^2}\,. \tag{39}$$

The same expression — the classical dispersion formula — is also given for the refractive index of the electron gas, measured in the optical frequency range [11]. In case of inert gases the expression (39) is positive and that which belongs to its absolute value is because of the absorption lines to be found in the Schuman range, essentially lower than in case of free electron

gas. If we apply e.g. the green mercury line of 5460 Å wavelength for sounding by argon gas of N_A° concentration, the connection

$$(n-1) = +1{,}046 \cdot 10^{-23} N_A^\circ \tag{40}$$

for free electrons of N_e concentration

$$(n-1) = -1{,}3 \cdot 10^{-22} N_e \tag{41}$$

connections may be deduced.

On the basis of Equs (40) and (41) the conception is obvious that the measurement of the refractive index should be carried out in a relative manner by the determination of the decrease of the refractive index, caused by the partial ionization of the neutral gas. Consequently, if in the examined discharge space there is a neutral atom cloud of $N_A^\circ = 10^{16}$ atom/cm^3 concentration to be found at the beginning, then the refractive index of this gas is

$$n_A \sim 1{,}046 \cdot 10^{-7}.$$

If in this gas a plasma of $N_e \sim 10^{16}$ electron/cm^3 concentration is formed, then, according to our previous remarks and conclusions, this manifests itself in the refractive index of the plasma with an additive of $-6{,}4 \cdot 10^{-7}$ order of magnitude. The influence of the ions was neglected in this case, but according to the calculations [3], the mistake arising from this was only of 1%.

On the basis of similar assumptions it can be proved that the mistake, deriving from the neglecting of the ion-effect is, in case of an ionization of 100% much smaller than by an ionization of 10%. This can be attributed to the fact, that the electron gas component plays the main role in the forming of the refractive index. By further refining of these estimations [8] usually the influence of the local microfields is also taken into account, which cause an essential increase of polarization, concerning both the electrons and ions. The exact and systematic estimation of this effect has not succeeded so far, although these examinations wouldcertainly offer interesting data and further improvements for the measurements of the refractive index, which were carried out at different optical wave lengths.

With the help of this method it would be possible e.g. to separate the changes of the refractive index caused by the neutral atoms, by the ion gas and the electron gas. The separation can be carried out on the basis that the neutral and ion refractive indices are in case of an examination with a sounding beam of changing λ wavelength the slowly altering functions of $1/\lambda^2$, the refractive index of the electron gas on the other hand changes proportionally to λ^2.

Taking all this into account and accepting a difference not higher than 2% between the real and the calculated or estimated values, it may be assumed that the changes of the refractive index of plasma are proportional to its

changes of electron concentration. Consequently in case of a plasma the Δn_p change of the refractive index can be characterized on the basis of connection

$$\Delta n_p = \Delta(n_p - 1) = \frac{1}{2}\left(\frac{\omega_{0e}}{\Omega}\right)^2. \tag{42}$$

This can be given with the introduction of the δ optical path on the basis of

$$\delta = n_p \cdot d\,, \tag{43}$$

where d is the thickness of the investigated and sounded plasma column, which may be given in the following form:

$$\Delta\delta = \Delta n_p \cdot d\,. \tag{44}$$

Assuming that there is a constant d plasma thickness, this form serves not only for the estimation of the error occurring in the determination of the optical path, but it gives at the same time a classical possibility for the measurement of the refractive index and also for the determination of the difference in the optical path. The difference of the optical path is, however, measured in this case by comparing it to the neutral gas or to the plasma with a known refractive index. By the examination of the plasma of the cathode spaces the refractive index of the neutral gas may serve as a basis of comparison.

For the characterization of the change in the optical paths the easily manageable, but approximative connection

$$\Delta\delta = (\Delta n)\cdot d \approx 4 \cdot 10^7 \frac{\lambda^2}{c^2} N_e \cdot d$$

may also be applied, in general, which is usually given [3] in case of a non-uniform plasma (e.g. in case of the cathode space plasmas) in the form:

$$\Delta\delta = 4 \cdot 10^7 \frac{\lambda^2}{c^2} \int_{-d/2}^{+d/2} N_e(z)\, dz\,, \tag{45}$$

which, with the assumption of an electron distribution to be characterized e.g. by a cos-type form assumes the following shape:

$$\int_{-d/2}^{+d/2} N_{e_{\max}} \cdot \cos\left(\frac{\pi}{2} \cdot \frac{z - \frac{d}{z}}{\frac{d}{2}}\right) dz\,. \tag{46}$$

This can easily be transformed to the form

$$\int_0^d N_{e_{\max}} \cdot \sin\left(\frac{\pi \cdot z}{d}\right) dz\,, \tag{47}$$

from which we get in the end the form:

$$\Delta\delta = 4 \cdot 10^7 \frac{\lambda^2}{c^2}\left(\frac{2}{\pi}\right) N_{e_{\max}} \cdot \alpha\,. \tag{48}$$

It is worth while carrying out the measurement of the refractive index by a laser beam in the red or infrared spectral ranges, taking into account the diminishing possibility of the background noises.

On the basis of the interferometric experiments carried out by ASHBY and collaborators [9] it is suitable to use helium-neon laser, applying both lines of this laser, the 5328 Å line in the red and the 33,910 Å line in the infrared spectral range. With the aid of this laser, however, only such plasmas can be examined, the average electron concentration $\mathbf{N}_e$ of which are [3]:

$$\mathbf{N}_e \geq 3{,}3 \cdot 10^{16} \cdot \frac{1}{d}, \tag{49}$$

where d is the thickness of the plasma taken along the beam. Our calculations can be made on the basis of equation

$$S = \left(\frac{\omega_0}{\Omega}\right)^2 \cdot \frac{L}{\lambda}, \tag{50}$$

derived from connection

$$S = 8{,}9 \cdot 10^{-14} N_e \cdot L \cdot \lambda \tag{51}$$

which creates a direct connection between the shift of the interference bands (S) and the electron concentration of the plasma.

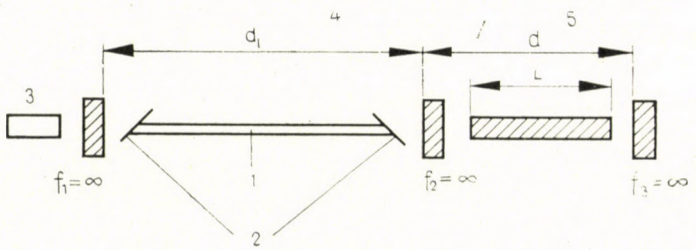

Fig. 1. Scheme for the measurement of the refractive index by a flat mirror laser beam system (*1* laser, *2* laser mirrors, *3* photomultiplier, *4* laser cavity, *5* plasma cavity)

The design of the measuring system suitable for the examinations in the cathode space can be seen in Fig. 1. The beam emitted from the helium-neon laser passes through the plasma placed in the optical cavity resonator and is reflected from the so-called external end mirror, and an interference arises between the emitted radiation and the cavity oscillations. The original intensity of the laser radiation of course considerably depends on the phase of the reflected beams. The intensity of the laser beam is modulated in this way and, therefore, the changes in the different optical paths can easily be given with the counting of the maxima and the minima to be found in the intensity of the laser. The cycle of the modulation corresponds to the usual interferometer stripes and rings. If the change of the optical path is slow, then the stripes, that is to say the modulating changes in the light intensity of the laser, can be followed even with the naked eye. At higher frequencies

usually a photomultiplier method is applied for this purpose, with the placing of the photomultiplier at the free end of the laser, in the manner illustrated in Fig. 1.

The helium-neon laser is extremely suitable for such experiments, its two characteristic lines are, namely, of symmetric excitation. Interferometric experiments can be carried out with both lines, but the detection of the red line in the visible spectral range is essentially easier than in the infrared range. As both wave lengths have a common upper energy level — neon 3 s_2 —, there is a coupling between the intensities of these two wave lengths. Therefore, any modulation of 33,910 Å laser beam causes e.g. an additional modulation also in the intensity of the 6328 Å radiation. This gives an opportunity for the utilization of the higher sensitivity, however keeping the possibility of the detection in the visible spectral range to be carried out without any difficulty.

The observation in the infrared of the modulation taking place on the red, that is to say, the observation of the reciprocal effect could not be carried out so far. Presumably a coupling of this kind is very weak [10], but from the point of view of the measuring techniques this has no importance.

III. Time resolution

The time resolution can also be carried out with the usual, classical method, with a rotating mirror [9]. It can be proved that with the application of the infrared line of the helium-neon laser the velocity of the changes occurring in the electron concentration and still detectable, can be given in $cm^{-3} \cdot \cdot sec^{-1}$ units in the form:

$$\frac{dN_e}{dt} \approx \frac{10^{23}}{d} . \tag{52}$$

By the indication of this upper limit not the parameters of the detector, but the laser qualities have a determining character. In case of an interference, produced in the infrared, the upper frequency-limit corresponds to 3 MHz, by the examinations carried out in the red, it corresponds approximately to 100 kHz.

In case of an interference in the infrared, for the determination of the intensity of the infrared beam, generally an indium antimonide detector is used [3].

If we mark the two characteristic intensities, belonging to the above-mentioned red and infrared lines of the helium-neon laser by I_1 and I_2, then a coupled differential equation system, consisting of two equations may be written:

$$\frac{dI_1}{dt} = a_1 I_1 + b_1 I_1^2 + c_1 I_1 \cdot I_2 , \tag{53}$$

$$\frac{dI_2}{dt} = a_2 I_2 + b_2 I_2^2 + c_2 I_1 \cdot \mathbf{I}_2 ; \tag{54}$$

where a_1 and a_2 show the combined effect of the stimulated emission, the absorbtion loss and the loss on the mirrors, the factors b_1 and b_2 characterize the change in the population inversion, following the increase in the radiation intensity, the factors c_1 and c_2 characterize the transverse connection, that is the cross coupling, which is characteristic of the depopulation, taking place on identical upper level at different wave lengths.

For the laser processes it is necessary that

$$a_1, a_2 > 0.$$

For the equilibrium intensities I_{10} and I_{20} — on the basis of the previous considerations — the equations

$$\mathbf{I}_{10} = \frac{(a_2 \cdot c_1 - a_1 b_2)}{(b_1 \cdot b_2 - c_1 \cdot c_2)}, \tag{55}$$

$$\mathbf{I}_{20} = \frac{(a_1 c_2 - a_2 b_1)}{(b_1 \cdot b_2 - c_1 \cdot c_2)} \tag{56}$$

are given. Let us assume that the interference occurs in case of a red line (index 1) and the optical path changes in such a way that the interference stripes appear at $\omega/2\pi$ frequency. In this case the modulated intensity I_1 may be received by a linearized analytical perturbation method, with the assumption that the a_1 has also a small oscillation factor, in absolute value, that is to say a factor as e.g.:

$$a_1 \sim \tilde{a}_1 \exp(i\omega t).$$

On the basis of our previous considerations

$$\tilde{I}_1 \left[(i\omega - b_1 I_{10}) - \frac{c_1 c_2 I_{10} I_{20}}{(i\omega - b_2 I_{20})} \right] = \tilde{a}_1 I_{10} \tag{57}$$

or with similar assumption for the infrared line, with the observation of the interference in the red:

$$\tilde{I}_1 \left[(i\omega - b_1 I_{10}) - \frac{c_1 c_2 \cdot I_{10} I_{20}}{(i\omega - b_2 I_{20})} \right] = \frac{\tilde{a}_2 c_1 I_{10} I_{20}}{(i\omega - b_2 I_{20})} . \tag{58}$$

As in both cases there is a coupling, among real experimental conditions it can be claimed that

$$\omega \ll b_2 \cdot I_{20} \tag{59}$$

leads to a common frequency characteristic, which with the introduction of expression

$$\omega_0 = \frac{a_1 b_2 - a_2 c_1}{b_2}$$

can be characterized in the form:

$$\frac{\tilde{I}_\omega}{\tilde{I}_{\omega=0}} = \frac{1}{1 + \frac{i\omega}{\omega_0}} \tag{60}$$

that is to say

$$\frac{\tilde{I}_\omega}{\tilde{I}_{\omega=0}} = \frac{1}{\left[1 + \left(\frac{\omega}{\omega_0}\right)^2\right]^{1/2}} . \tag{61}$$

If $\omega \ll \omega_0$ is valid, then the proportion of P_1 and P_2, resulting in case of infrared interference, that is the proportion of the modulation at infrared and red line, is the following:

$$\left(\frac{P_1}{P_2}\right)_{irir} = \frac{c_2 I_{20}}{b_1 I_{10}} \tag{62}$$

by interference in the infrared

$$\left(\frac{P_1}{P_2}\right)_{r} = \frac{b_2 I_{20}}{c_2 I_{10}} . \tag{63}$$

According to the experiments the value of the quotient in Equ. (62) is near one, that of the quotient in connection (63) is far greater than one, so

$$\frac{c_1 I_{20}}{b_1 I_{10}} \approx 1 , \tag{64}$$

$$\frac{b_2 I_{20}}{c_2 I_{10}} \gg 1 . \tag{65}$$

The two inequalities, deriving from an experimental control with the consideration of Equs (53) and (54) show that the cross coupling is insignificant in the case of infrared, in the case of the red line, however, it can be compared in importance to the direct, nonlinear expression. If the infrared itself is applied for the detection of the interference, arising at the infrared line, the connection

$$\tilde{I}_2 \left[(i\omega - b_2 I_{20}) - \frac{c_1 c_2 I_{10} I_{20}}{(i\omega - b_1 I_{20})} \right] = \tilde{a}_2 I_{20} \tag{66}$$

is given, from which with the application of Equs (60), (65) and (66) the following connection can be gained:

$$\frac{(\check{I}_2)_\omega}{(\check{I}_2)_{\omega=0}} \approx 1. \tag{67}$$

On the basis of all this the very important experimental fact can be established that the frequency characteristics are restricted by this interferometric method only by the qualities of the red channel. A notable increase in the frequency resolution can be ensured only by the complete

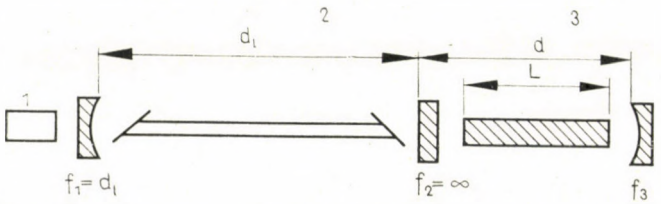

Fig. 2. Scheme of the interferometer equipped with a spherical mirror proposed by GERARDO and VERDEYEN (*1* photomultiplier, *2* laser cavity, *3* plasma cavity)

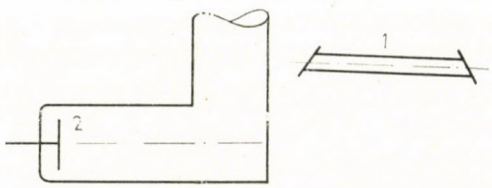

Fig. 3. Discharge tube construction, suitable for the taking of the radial distribution of the electron concentration, to be applied by laser beam measurements (*1* laser, *2* cathode)

passing over to the infrared light. In this case, however, the modulation of the infrared light must be observed and measured in a direct way. QUINN has already tried this [3] and he has extended the upper limit of the resolution until 1 MHz.

GERARDO and collaborators have increased the sensitivity of the laser interferometer in such a manner that they applied a concave mirror at the closing of the plasma cavity, as shown in Fig. 2.

The increase of the sensitivity was reached by the use of the transverse modes. The change in the optical path, caused by the plasma placed in the reference cavity was determined in such a way — shown previously — from the modulation of the outgoing light of the laser [1]. Consequently the modulation comes about because the reflexion coefficient which the laser "detects" through the mirror with f_2 focus depends on the optical path of the reference and the plasma cavity. As it can be seen from the previously shown equations, the reflexion coefficient is minimal in that case, when the laser beam has a resonance in the cavity and vice versa.

The applicability of the laser to time resolution examinations is to a certain degree limited. The reason for this can be deduced from the laser rate-equations:

$$\frac{\partial n_{2i}}{\partial t} = k_2 - \frac{B}{\Delta\nu_N} \varrho_{\nu i}(n_{2i} - n_{1i}), \tag{68}$$

$$\frac{\partial n_{1i}}{\partial t} = \frac{B}{\Delta\nu_N} \varrho_{\nu i}(n_{2i} - n_{1i}) - \frac{n_{1i}}{\tau}, \tag{69}$$

$$\frac{\partial \varrho_{\nu i}}{\partial t} = \left[h\nu \frac{B}{\Delta\nu_N}(n_{2i} - n_{1i}) - \mathfrak{B}\frac{c}{d_l} \right] \varrho_{\nu i}; \tag{70}$$

where $\varrho_{\nu i}$ energy density of the radiation of ν_i frequency;
k_2 excitation constant;
B Einstein's coefficient of induced transition, for the transition from level *2* to level *1*;
n_{2i} concentration of the atoms in state *2*;
n_{1i} concentration of the atoms in state *1*;
$n_{2i}(n_{1i})$ concentration of the atoms in the *2*(*1*) state within the natural $\Delta\nu_N$ line width, at ν_i laser frequency;
τ radiative lifetime of the transition;
c light velocity;
$\mathfrak{B}$ $= 1/2 \cdot (T_1 + T_{2r}) + F_2$, the loss factor;
F absorption and dispersion loss, arising in the laser cavity;
T_1 transmission of the mirror with focus distance f_1;
T_{2r} transmission of the plasma cavity.

By the construction of Equs (68), (69) and (70), the spontaneous emission was neglected. The loss factor $\mathfrak{B}$ in Equ. (70) depends on the optical path of the reference cavity. For the characterization of the upper limit of the time resolution, the $\partial\varrho_{\nu i}/\partial t$ speed characterizing the change of radiation density must be determined, which makes even the formation of a quasi steady radiation density state possible — of the equilibrium state — in the function of the quick changes of $\mathfrak{B}$. But as the system of the outlined basic equations is not linear, their solving encounters serious difficulties. Therefore, starting out from these equations with the application of approximations, we can get acceptable estimations.

The time resolution which can be reached by the laser beam interferometer is on the basis of the previously shown connections max. 10^{-8} sec. This is sufficient for the observation of the cathode side phenomena of discharges, with a time constant of 10^{-6} sec in general.

The reflected laser beam applied for the measurement is divergent, its cross section is about one hundred times larger than the emitted beam. So, for the increase of the sensitivity an additional optical cavity must be applied. It is characteristic for the measuring method outlined here that the applied laser is not only a light source, but at the same time it performs the interference detecting too. This can be reached in a very simple way, by adjusting the mirror on an optical bank.

IV. The establishment of the space dependence of the electron concentration

The radial dependence of the measured parameters can be established by this method only in an indirect way, by the application of Equs (44)—(48), under the assumption of an acceptable radial distribution function. The determination in this way of the radial dependence cannot be looked upon as sufficiently exact.

In the sense of another supposition the cathode space should be formed in a discharge tube, bent twice at a right angle and in this case the performance of the radial sounding does not encounter any difficulty. If these measurements are performed by some discharge types, then some assumption can be made concerning the radial distribution functions.

The axial dependences, that is to say, the sounding in the different discharge cross sections can be carried out without any difficulties.

V. Some characteristic parameters of the electron concentration measurements

The here outlined measuring method can be applied in the case if the electron concentration of the examined cathode space reaches at least the 10^{11} electron/cm^3 value. The error of the measurements is namely $\pm 10^{10}$ electron/cm^3 [3]. The value of the electron concentrations occurring in the cathode space of arc discharges is even in case of a discharge of low pressure between 10^{11}—10^{12} electron/cm^3, which makes the application of this method reasonable.

The resonance condition of the experimental apparatus shown in Fig. 1 is the following:

$$n \cdot d = \frac{q \cdot \lambda}{2}, \tag{71}$$

where n refractive index of the plasma;
d length of the cavity containing the plasma;
λ sounding wave length;
q integral value characteristic for the scheme [3].

From this the value of the electron concentration N_e can be given with the aid of equation

$$N_e = \frac{1{,}14 \cdot 10^{13}}{\lambda \cdot L}, \tag{72}$$

where L is the thickness of the plasma column in the cathode space.

With the application of the Gerardo–Verdeyen measuring system by spherical mirror, the electron concentrations can be given by the connection:

$$N_e = 1{,}14 \cdot 10^{13} \frac{1}{\lambda \cdot L} \left[\frac{1}{2\pi} \cos^{-1} \left(1 - \frac{2d}{f_3} \right) \right] \tag{73}$$

where f_3 is the focal distance of the mirror, closing the optical cavity and the other sign coincides with those applied in the previous calculations.

In the latter case a resonance arises both in the axial and in the transverse methods. These can be evaluated also separately from each other [11].

REFERENCES

1. BITÓ, J. F.: Ph. D. Thesis, Budapest 1968.
2. BITÓ, J. F.: *Magyar Fizikai Folyóirat* **10** (1962), 411—417.
3. BITÓ, J. F.: Introduction to the Experimental Plasma Physics. Mérnöki Továbbképző Intézet, Budapest 1967.
4. BROWN, M.—WOLF, E.: Principles of Optics. Pergamon Press, New York 1959.
5. JENKINS, F. A.—WHITE, H. E.: Fundamentals of Optics. McGraw-Hill Book Co., New York 1957.
6. ASCOLI-BARTOLI, U.—DEANGELIS, A.—MARTELUCCI, S.: *Il Nuovo Cimento* **17** (1960), 6.
7. HIRSCHFELDER, K.—CURTIS, I.—BIRD, J.: Molecular Theory of Gases and Liquids. John Whiley and Sons, New York 1954.
8. ALPHER, R. A.—WHITE, D. R.: *Phys. Fluids* **2** (1959), 2.
9. ASHBY, D. E.—JEPHCOTT, D. F.—MALEIN, A.—RAYNER, F. H.: *Journal of Applied Physics* **36** (1965); No. 1, 29.
10. BLOOM, A. L.—BELL, W. E.—REMPEL, R. E.: *Applied Optics* **2** (1963), 317.
11. GERARDO, J. B.—VERDEYEN, J. T.—GUSINOW, M. A.: *Journal of Applied Physics* **36** (1965); No. 7, 2146.

Methode mit Laser-Strahl für die Prüfung von Kathodengebieten. Durch Verwendung in dem Katodenraum der bisher angewandten Prüfungsmethoden, die im allgemeinen als traditionell betrachtet werden können, konnten die Mikroparameter des Plasmas nicht mit der nötigen Genauigkeit bestimmt werden. Hier wird eine interferometrische Methode durch Anwendung von Laser-Strahl bekannt gemacht, mit deren Hilfe der Wert der Elektronenkonzentration im Katodenraum, deren Zeitabhängigkeit wie auch die axiale Raumabhängigkeit in einer einfachen Weise mit einer Genauigkeit von $\pm 10^{10}$ Elektron/cm^3 bestimmbar sind. Die erreichbare maximale Zeitauflösung ist 10^{-8} sec.

Метод для исследования катодных пространств с помощью лазерного луча *(Й. Ф. Бито)*. Используя в катодном пространстве экспериментальные методы, применявшиеся до сих пор и считавшиеся в общем традиционными, микропараметры плазмы этих пространств не могут быть определены с удовлетворительной точностью. Изложен интерферометрический метод с лазерным лучем, с помощью которого величина электронной концентрации в катодном пространстве, ее временная зависимость и аксиальная зависимость от места могут быть определены просто с точностью порядка $+ 10^{10}$ *электрон/см*^{3}. При этом достигается максимальное временное разложение порядка 10^{-8} *сек*.

Acta Technica Academiae Scientiarum Hungaricae; Tomus 68 (1—2), pp. 179—189 (1970)

KINETICS OF THE LAST RECOVERY STAGE IN COLD WORKED TUNGSTEN*

KAMEL A. EL-DEHEMY**

RESEARCH INSTITUTE FOR TECHNICAL PHYSICS OF THE HUNGARIAN ACADEMY OF SCIENCES, BUDAPEST

[Manuscript received December 19, 1968]

The recovery of the dislocation network was investigated by means of electrical resistivity measurements on severely cold worked undoped powder metallurgical tungsten wires. The decrease of the dislocation density during annealing follows the same kinetics in doped and undoped samples. The activation energy in both cases is close to that of self-diffusion. The detailed mechanism of the decrease of the dislocation density is still unknown. The inhomogeneity of the samples makes it impossible to determine the activation energy without a detailed assumption of the annealing kinetics.

I. Introduction

On powder metallurgical and zone refined tungsten wires, which were cold worked at room temperature, two recovery stages have been found for electrical resistivity [1—4]. The first one takes place at about 600—800°K and the second one continuously extends from 800°K to the recrystallization temperature. The first stage was attributed to the annealing out of the extra vacancies produced by the room temperature deformation, whereas the second one seems to be connected with the annihilation and redistribution of dislocations, since according to Koo [6] the hardness also decreases in this temperature region. The activation energy of the second stage depends strongly on the purity of the samples: in zone refined tungsten, SCHULTZ [2] found an activation energy of $76 \pm 2{,}5$ Kcal/mol and in doped powder metallurgical tungsten, KOVÁCS–CSETÉNYI [5] found an activation energy of 110 ± 10 Kcal/mol. SCHULTZ [2] has assumed that the recovery in zone refined tungsten obeys a MEECHAN–BIRKMAN type kinetics [7], and KOVÁCS–CSETÉNYI [5] have assumed that the recovery kinetics in the doped powder metallurgical tungsten is analogous to that proposed by KUHLMANN-WILSDORF [8].

The aim of the present paper is to investigate the kinetics of the second recovery stage on powder metallurgical undoped tungsten wires.

* Part of the thesis submitted for the Candidate Degree of Science.
** On leave from *Higher Technical Institute, Cairo (U.A.R.).*

II. Experimental

The specimens were drawn at constantly decreasing temperatures from sintered and forged rods. The final drawing was made at about 600°C and the final diameter of the wires was 0,12 mm. The chemical analysis is given in Table I.

Table I

Analysis of pure (undoped) tungsten by the spectroscopical method

Element	Amount [wt. %]	Element	Amount [wt. %]
Fe	$1 \cdot 10^{-3} - 10^{-4}$	Si	$1 \cdot 10^{-3} - 5 \cdot 10^{-4}$
Ni	$5 \cdot 10^{-3} - 1 \cdot 10^{-4}$	Ti	$1 \cdot 10^{-3}$
Cr	$1 \cdot 10^{-4}$	K	$2 \cdot 10^{-3}$
Al	$1 \cdot 10^{-4} - 1 \cdot 10^{-5}$	Na	10^{-3}
Mo	$5 \cdot 10^{-3} - 1 \cdot 10^{-4}$		

The carbon lubricant was removed from the wires in a warm 30% NaOH solution. The annealing was made in a vacuum of 10^{-4} Torr by self-resistance heating. The temperature was determined from the measured heating current by means of the *Langmuir tables* [9]. The resistivity was measured on the 6 cm long middle part of the annealed 25 cm long specimen to eliminate the cooling effect of the grips [10]. The measured resistance values were determined by the *Poggendorf compensating method* at two temperatures: at 298°K and at 77°K (in liquid N_2).

The resistivity ratio

$$Z = \frac{\varrho_{77°K}}{\varrho_{298°K}} \simeq \frac{r_{77°K}}{r_{298°K}}$$

was calculated from resistance values corrected for a nominal thermostat temperature. The deviation between the nominal and actual thermostat temperature was determined by a dummy. In order to have different specimen lengths for the resistivity measurement and for annealing, the potential leads were sharp edges, pressed mechanically to the sample. (The potential leads of the dummy were spot welded.) The experimental values represent the average of two independent measurements. The error amounted to $\pm 0{,}5\%$, when the measurement was repeated on different specimens from the same stock. The isochronal annealing was made on separate samples, and at the isothermal annealing for a given temperature one sample was used.

III. Results

The results of the isochronal and isothermal annealing are shown in Figs 1 and 2. In Fig. 1, only one wide stage appears extending from 800°K to 1300°K. The annealing curves do not show any expected anomaly due to the change from recovery to recrystallization kinetics (Figs 1, 2). When the

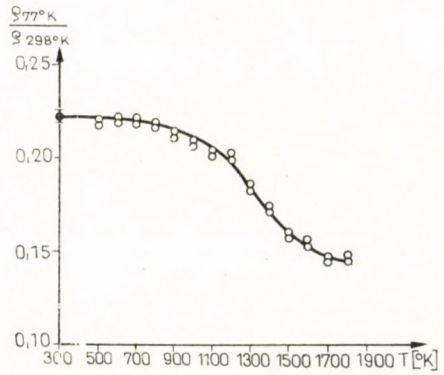

Fig. 1. Resistivity change in undoped tungsten during isochronal annealing (annealing time 30 min)

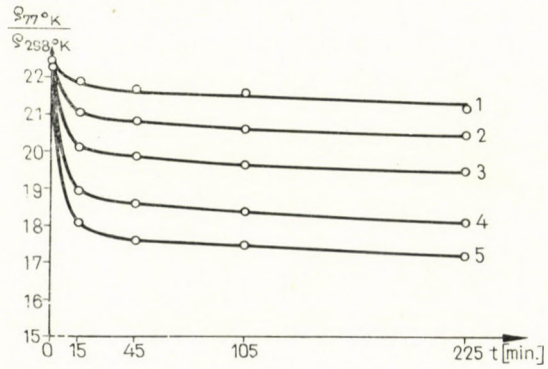

Fig. 2. Resistivity change in undoped tungsten during isothermal annealing (curve *1:* 800° K; curve *2:* 950°K; curve *3:* 1150°K; curve *4:* 1300° K; curve *5:* 1400°K)

samples were heated for one hour in 100°K steps, the *Debye—Scherrer rings* showed a spotty appearance, first at 1100°K (Fig. 3). Since spotty Debye—Scherrer rings are characteristic for fine grained recrystallized matrices [26], we can conclude that recrystallization begins* between 1000°K and 1100°K. In the cold drawn state the Debye—Scherrer rings were, of course, continuous as is shown in Fig. 4.

* Since X-ray diffraction takes place in a quite thin surface layer on the wires, this recrystallization temperature is characteristic only for this layer.

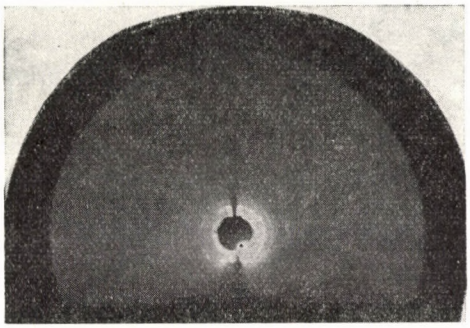

Fig. 3. X-ray reflection photographs taken on tungsten wire annealed at 1100°K for one hour

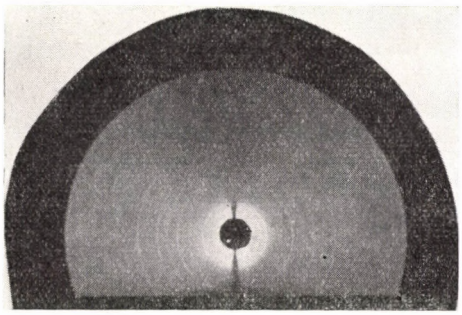

Fig. 4. X-ray reflection photographs taken on the cold drawn tungsten wire by using unfiltered Ag microbeam at 50 kV and 350 μA

IV. Discussion

KOVÁCS—CSETÉNYI [5] used the following kinetics for the evaluation of the activation energy

$$\frac{dx(t)}{dt} = -A \cdot \exp\left[\frac{Q - Bx(t)}{RT}\right], \tag{1}$$

where

$$x(t) = \frac{Z(t) - Z_r}{Z_w - Z_r};$$

$Z(t)$ resistivity ratio at a certain temperature and time;
Z_w, Z_r resistivity ratios measured in the cold worked and in the recrystallized states;
Q activation energy of the process;
A, B constants.

The solution of (1) is

$$x(t) = 1 - \frac{RT}{B} \log\left(1 + \frac{t}{t_0}\right), \tag{2}$$

where t_0 is determined by the equation

$$1 = -\frac{RT}{B} \log \frac{B \cdot t_0}{RT} \cdot A \cdot \exp \frac{-Q}{RT} \tag{3}$$

and so for $t \gg t_0$, Equ. (2) may be written in the simplified form:

$$x(t) = 2 + \log \frac{B}{RT} A \cdot \exp\left(\frac{-Q}{RT}\right) - \frac{RT}{B} \log(t). \tag{4}$$

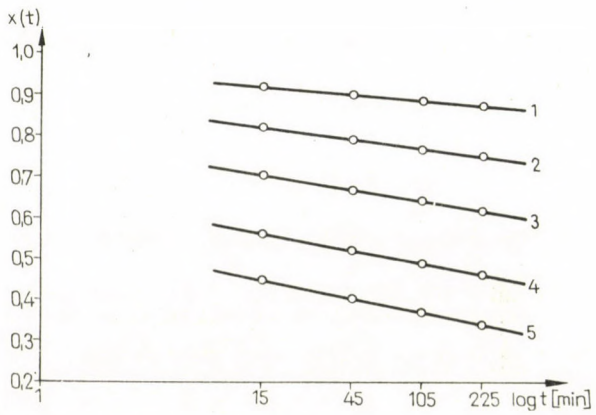

Fig. 5. Normalized kinetical curves according to Equ. (1) [curve *1:* 800°K; curve *2:* 950°K curve *3:* 1150°K; curve *4:* 1300°K; curve *5:* 1400°K]

Isothermal annealing curves plotted according to Equ. (4) are shown in Fig. 5. The activation energy turns out to be between 110 and 150 Kcal/mol (see Table II). This is not far from the activation energy of self-diffusion in tungsten (see Table III) and so it seems to be in a certain agreement with Kovács—Cseténvi's results on doped powder metallurgical tungsten.

Table II

Calculated activation energy of recovery

Temperature range [°K]	Activation energy [Kcal//mol] calculated from		
	Equ. (1)	Equ. (8)	Equ. (9)
800—950	110	215	9
950—1150	118	240	4
1150—1300	137	269	12
1300—1400	146	264	19

Table III

Activation energy of self-diffusion

Author	Q [Kcal/mol]	Method
DANNEBERG [21], 1961	120,5	Direct
SCHNITZEL [22], 1959	125	Indirect
VAN LIEMPT [23], 1945	140	Indirect
VASILEV and CHERNOMORCHENKO [24], 1956	146	Direct
ANDELIN et al. [25], 1965	153,1	Direct

Let us discuss the process underlying (1). The resistivity ratio $r_{77°K}/r_{2998°K}$ would be 0,100 for ideally pure and defect-free tungsten [27]. This ratio amounts to 0,22 in the cold worked state on our samples and after an annealing for 15 min at 2600°K, resistivity ratios between 0,130 and 0,105 were found [27] on comparable samples. Therefore, the high resistivity ratio found in cold worked matrix is, certainly, not caused by solved impurities. This high resistivity ratio cannot be associated with vacancies, since the drawing and annealing were made above the temperature of annealing-out of vacancies. Therefore, the observed high resistivity ratio is due to the presence of dislocations,* and thus according to [15],

$$X(t) \simeq \beta N, \tag{5}$$

where N is the dislocation density and β is a constant.

We have now to emphasize that (1) is not the recovery kinetics suggested by KUHLMANN-WILSDORF, since it was assumed that the rate of recovery of the flow stress (σ) obeys the equation:

$$\frac{d\sigma}{dt} = -A \exp\left(-\frac{Q - B \cdot \sigma}{RT}\right). \tag{6}$$

Such kinetics were observed on strongly cold worked copper, aluminium and silver at relatively low temperatures [11—13]. Equations (1) and (6) are equivalent when σ and x are proportional. But there is no reason for such an assumption. On the contrary it is well known [14] that in cold worked metals

$$\sigma = \sigma_0 + \alpha G b^2 \sqrt{N}, \tag{7}$$

* The supposition that in the investigated annealing stage, the decrease of the resistivity ratio is due to the decrease of dislocation density, had also been supported by the measurements of KOO [6], who found a pronounced decrease of yield stress in this annealing stage.

where σ_0 is the so-called frictional stress;
α is a constant about 0,3;
G is the rigidity modulus;
b is the Burgers vector;
N is the dislocation density.

Inserting Equs (5) and (7) into Equ. (6), we arrive at the following:

$$\frac{d}{dt}\left[x^{\frac{1}{2}}(t)\right] = -A \exp\left[-\frac{Q - Bx^{\frac{1}{2}}(t)}{RT}\right]. \tag{8}$$

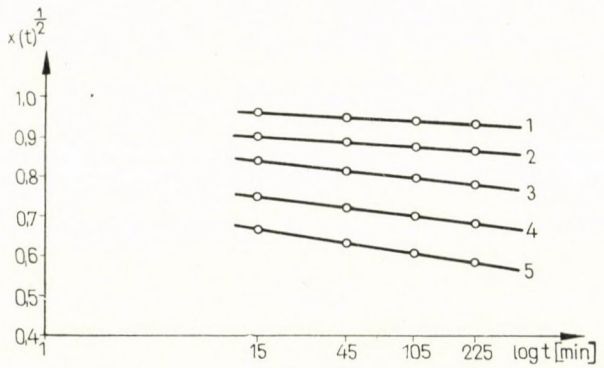

Fig. 6. Normalized kinetical curves according to Equ. (8) [curve *1*: 800° K; curve *2*: 950° K; curve *3*: 1150° K; curve *4*: 1300° K; curve *5*: 1400° K]

The isothermal annealing curves were plotted according to the solution of (8) in Fig. 6. The activation energies calculated from these plots are listed in Table II.

In Equ. (5), Q ought to be the activation energy of cross slip or of climb. These are namely the two thermally activated processes by which the dislocation density may decrease during recovery (see e.g. [16]). The activation energy of these processes cannot be larger than that of self-diffusion. The activation energies obtained from (8) are thus unreasonably high. This means that the fitting seen in Fig. 6 may be the consequence of the "too many free parameters" in (8).

The mutual annihilation of dislocations governed by stress-induced climb may also obey the following kinetics [16, 17]:

$$\frac{d\sigma}{dt} = -A \cdot \sigma^3 \cdot \exp -\frac{Q}{RT}. \tag{9}$$

Such kinetics were observed in aluminium at higher recovery temperatures [18—20].

The isothermal annealing curves were plotted according to (9) in Fig. 7. Table II shows the corresponding activation energies which are unreasonably low, since the activation energy of the climb is the activation energy of self-diffusion.

This discussion shows that our results may be fitted into a kinetics of some unknown nature (1), which gives a reasonable activation energy; but unreasonable activation energies are obtained when the results are fitted to recovery kinetics (8) or (9), which were experimentally verified in FCC

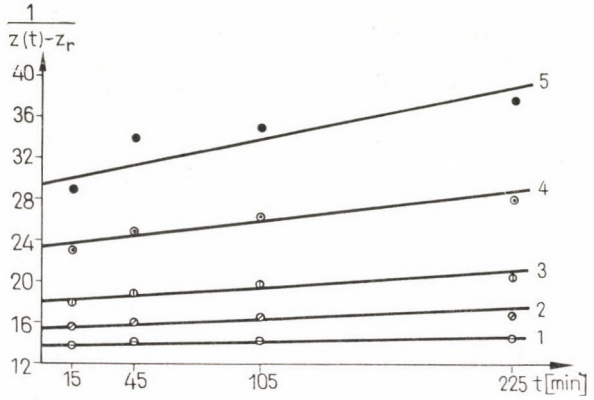

Fig. 7. Isothermal annealing curves according to equation (9) [curve *1:* 800° K; curve *2:* 950° K; curve *3:* 1150° K; curve *4:* 1300° K; curve *5:* 1400° K]

metals. Equs (1) and (6) have to be considered as different kinetics since there are no published results supporting a proportionality betwe en σ and x. We have thus to say in agreement with SCHULTZ [1, 2] that the detailed mechanism of the recovery stage between 800°K and 1300°K in tungsten is still unknown.

One question remains. Is the activation energy of the discussed recovery stage in zone refined and powder metallurgical tungsten comparable? The activation energy obtained certainly "depends" on the type of annealing kinetics to which the experimental data are fitted. This difficulty can be solved, if we use the method of MEECHAN and BIRKMAN [17]. This method has two suppositions:

The kinetics is described by an equation

$$\frac{dx}{dt} = F(x) \cdot \exp - \frac{Q}{RT} \tag{10}$$

where $F(x)$ is an arbitrary monotonous function of x. (Each discussed kinetics was from this type.)

The initial state of each specimen is the same and at a given temperature the isothermal annealing is made on the same sample, whereas in the isochronal

measurements, different samples were used. The results of the application of (10) are plotted in Fig. 8, which shows, beside the experimental points, three full straight lines *A*, *B* and *C*, corresponding to the activation energies: 76 (SCHULTZ), 110 (CSETÉNYI) and 128 Kcal/mol from this work, respectively. To the experimental points of Fig. 8, no straight line can be fitted. This has two possible explanations:

a) The observed recovery process is not governed by a single activation energy;

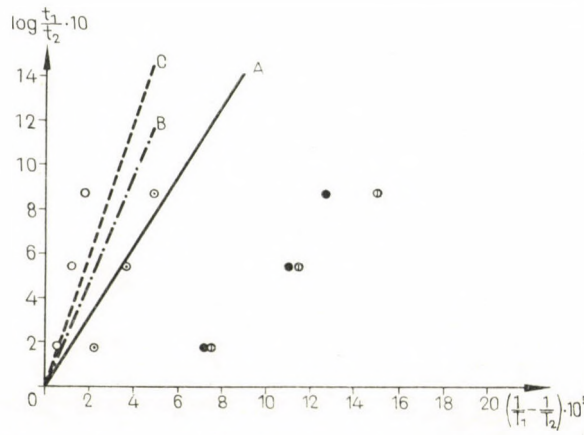

Fig. 8. Annealing kinetic curves using the Meechan—Birkman method: beside the experimental points, there are three straight lines *A*, *B* and *C* which correspond to the activation energies 76 (SCHULTZ), 110 (CSETÉNYI) and 128 Kcal/mol (from this work) respectively

Denotations: ① $T_1 = 800°K$, $t_2 = 30$ min.; ● $T_1 = 950°K$, $t_2 = 30$ min.; ⊙ $T_1 = 1150°K$, $t_2 = 30$ min.; ○ $T_1 = 1300°K$, $t_2 = 30$ min.

b) the samples are too inhomogeneous for the Meechan—Birkman method. The explanation *a)* is somewhat supported by Table II, which gives the activation energies derived from different data in different temperature intervals. The inhomogeneity of the samples may be seen from Table IV, where the resistivity ratios of the used samples are listed.

Table IV

Inhomogeneity of the samples taken from the stock A and B

Specimen	Resistivity ratio, Z_w	Specimen	Resistivity ratio, Z_w
1 *A*	0,2240	1 *B*	0,2249
2 *A*	0,2215	2 *B*	0,2248
3 *A*	0,2242	3 *B*	0,2233
4 *A*	0,2223	4 *B*	0,2235

V. Conclusions

The kinetics of the decrease of dislocation density during annealing may be described to doped and undoped powder metallurgical wires with the same kinetic equation (1). The activation energy is close to that of self-diffusion. The process underlying this kinetics is still unknown. The determination of the activation energy without a detailed assumption of the annealing kinetics by the Meechan—Birkman method is difficult, since the samples made from powder metallurgical tungsten wires have quite different resistivity ratios even when they were cut from the same stock.

*

Acknowledgement

The author wishes to express his thanks to Dr. I. S. SZÁNTÓ for his interest in this work. It is a pleasure for him to thank also Dr. I. GAÁL and Mr. L. URAY for valuable discussions.

REFERENCES

1. SCHULTZ, H.: *Z. Naturforschung* **142** (1959), 361.
2. SCHULTZ, H.: *Acta Met.* **12** (1964), 649.
3. NEIMARK, L. A.—SWALIN, R. A.: *Trans. Met. Soc. AIME* **218** (1960), 82.
4. KOO, R. C.: Reactive Metals. Interscience Publishers, New York—London 1958, 265.
5. KOVÁCS—CSETÉNYI: *Acta Phys. Hung.* **18** (1964), 11.
6. KOO, R. C.: *Less-Common Metals* **3** (1961), 412.
7. MEECHAN, C. J.—BIRKMAN, J. A.: *Phys. Rev.* **103** (1956), 1193.
8. KUHLMAN-WILSDORF, D.: *Proc. Phys. Soc.* **A64** (1951), 140.
9. JONES, H. A.—LANGMUIR, I.: *General Electric Review* **30** (1927), 6.
10. CARSLAW, H. S.—JAEGER, J. C.: Conduction of Heat in Solids. Clarendon Press, Oxford 1959; 154.
11. BORELIUS, G.: L'état solide; Brussels 1952.
12. ASTRÖM, H. V.: *Arkiv för Fysik* **13** (1957), 69.
13. BAILEY, J. E.—HIRSCH, P. B.: *Phil. Mag.* **5** (1960), 485.
14. NABARRO, F. R.—BASINSKI, Z. S.—HOLT, D. B.: *Adv. in Phys.* **13** (1964), 193.
15. ZIMAN, J. M.: Electrons and Phonons. Clarendon Press, Oxford 1960; 350.
16. FRIEDEL, J.: Dislocations. Pergamon Press, Oxford 1964; 278.
17. LI, J. C. M.: In Recrystallization, Grain Growth and Textures (ed. Margolin). *ASM Metals* (1966), 59.
18. BETTERIDGE, W.: *J. Inst. Met.* **82** (1954), 149.
19. BETTERIDGE, W.: Teddington Conference on Creep and Fractures (Nat. Phys. Lab.) 1956.
20. PERRYMAN, E. C. W.: *J. Met.* **7** (1955), 1053.
21. DANNEBERG, W.: *Metall* **15** (1961), 977.
22. SCHNITZEL, R. H.: *J. Appl. Phys.* **30** (1959), 2011.
23. VAN LIEMPT, J. A. M.: *Rec. Trav. Chim.* **64** (1945), 239.
24. *Василев, В. П.—Черноморченко, Ш. Г.: Заводская Лаборатория* **22** (1956), 688.
25. ANDELIN, R. L.—KNIGHT, J. D.—KAHN, M.: *Trans. Met. Soc. AIME* **233** (1965), 19.
26. TAYLOR, A.: X-Ray Metallography. John Wiley and Sons Inc., New York—London 1961.
27. URAY, L.—GAÁL, I.: *Acta Techn. Hung.* **65** 1969, 139.

Kinetik der letzten Erholungsstufe in kaltverformtem Wolfram. In stark kaltverformten pulvermetallurgischen, zusatzfreien Wolframdrähten wurde mittels elektrischer Widerstandsmessung die Erholung des Versetzungsnetzes untersucht. Sowohl in den zusatzfreien pulvermetallurgischen Wolframdrähten als auch in denjenigen mit Zusätzen folgt die Verringerung der Versetzungsdichte während der Wärmebehandlung derselben Kinetik. Die Aktivierungsenergie ist in beiden Fällen nahe der Aktivierungsenergie der Selbstdiffusion. Der genaue Mechanismus der Verringerung der Versetzungsdichte ist unbekannt. Die Inhomogenität der Probekörper erlaubt es nicht, die Aktivierungsenergie ohne Hypothesen über die Kinetik der Erholung zu bestimmen.

Кинетика последней фазы восстановления вольфрама холодной обработки *(К. А Эл-Дехеми)*. Исследовано восстановление дислокационной цепи измерением электрического сопротивления на полученной методами порошковой метал лургии проволоке вольфрамовой без добавок, подвергнутой сильной холодной деформации. Снижение дислокационной плотности в случае полученной методами порошковой металлургии вольфрамовой проволоки с добавкой и без нее имеет одну и ту же кинетику в процессе термообработки. Энергия активации в обоих упомянутых выше случаях лежит близко к энергии активации самодиффузии. Неизвестен детальный механизм снижения дислокационной плотности. Неоднородность образцов не делает возможным произвести определение без предположений, сделанных относительно кинетики восстановления.

Acta Technica Academiae Scientiarum Hungaricae; Tomus 68 (1—2), pp. 191—193 (1970)

SWITCHING PHENOMENA IN GERMANIUM-OXIDE FILMS

A. LŐRINCZY and M. NÉMETH-SALLAY

RESEARCH INSTITUTE FOR TECHNICAL PHYSICS OF THE HUNGARIAN ACADEMY OF SCIENCES

[Manuscript received February 17, 1969]

In the course of the conductivity and dielectric strength measurements on GeO_2 films, it was found that at a well-defined bias U_k, a sandwich structure (MOS) metal — GeO_2 — Ge, which has a d.c. resistance of more than 1000 megohms, "turns on", i.e. the metal and the semiconductor have been brought into connection (diode-characteristics). A short current pulse in the right direction could "turn off" the device (10—50 V, 5—6 μF condenser) into the high resistance position. With proper caution the cycle could be repeated a few ten times, or so. The used *n*-type germanium had high resistance. The oxide layer prepared by sedimentation (from solution) has a thickness of about 10 μm, the metal was an evaporated gold spot or a metal needle; in the majority of cases the latter was used.

These experiments were carried out by an a.c. bias with a series resistance as a limiter. Typical value of dielectric strength was 7.10^7 V/m. At the first switching the "switch on" voltage U_k depends on the oxide thickness, at the subsequent operations it remained nearly constant, its values, however, slightly differed from specimen to specimen.

At the small values of the series resistance — high switching current — the "switched on" condition had a linear voltage-current relationship. The "switching on" and the "switching off" were accompanied by small sparklings well visible in the darkness. By the sparkling the oxide layer, and even the surface of the semiconductor were destroyed in a crater-shaped way (Fig. 1).

Because of the considerable crater formation, the switching mechanism of [1] (a metal filament development) does not seem to be directly applicable taking the remaining "switch on" voltage values into consideration. In [1] the "switch off" is interpreted by a fusing element analogy, in our case this could not be compared with the phenomenon that occasionally the "switch off" was established by touching the two terminals of the device.

It was observed that in the course of the sparklings the needle was matted by a black layer. On a metal sheet the so coated needle behaved as a switching device. Since the insulator layer on it was not thicker than a few thousands Å, the "switch on" voltage became lower. After this experience

we started using oxide deposited copper needles. The sedimentation procedure consists of 5 gr of 99,999% GeO_2 dissolved in 1 l of water (the water has a resistivity higher than 2 megohmcm and the metal contamination lower than 10^{-3} gr/l). This solution was distilled to 0,3 l, thus it became a supersaturated solution. This was poured into a quartz vessel and the copper needles (semiconductor plates) were immersed in it for the time depending on the layer thickness wanted.

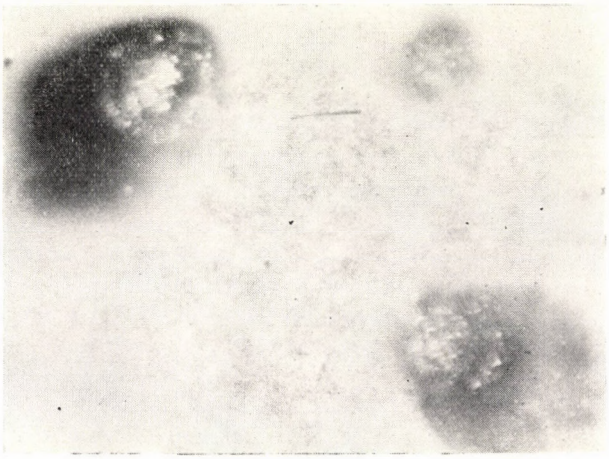

Fig. 1

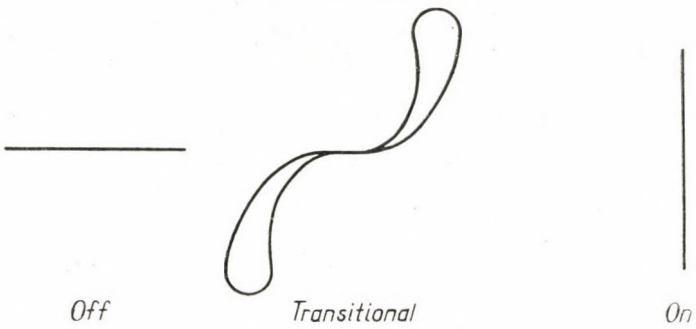

Fig. 2

The switching phenomenon appearing on the screen of an oscilloscope is shown in Fig. 2 according to which at the switching a negative current-voltage characteristic appears. When preparing the devices a copper needle coated with an oxide layer (10 μm thick) was touched by a copper plate. In these cases no sparkling could be observed. The "switch on" was performed by discharging a condenser charged up to 250 V through a series resistance. The "switch off" was established by touching the terminals with a battery

of 1,5 V for a moment. This arrangement might serve as a real device; its resistance being only a few ohms it could be used for switching a considerable power. It should be noted that the subsequent operations need increasing switching power consumption.

In some cases the "switch off" current pulse was not high enough, and after a few seconds the device turns on automatically. D. R. LAMB [2] described a switching phenomenon on SiO_2 in a small current range and proved that it is due to sodium contamination and not to filament. It might be assumed that in our case the injected contamination is ionized or activated in another way. Much to our regret a correct temperature dependence of the "switch on" resistance could not be obtained. Recently reversible memory phenomena in insulator films have been described [3], without clearly explaining its mechanism.

REFERENCES

1. GIBBONS, J. F.—BEADLE, W. E.: Switching Properties of Thin NiO Films. *Solid State Electronics* **7** (1964), 785.
2. LAMB, D. R.—RUNDLE, P. C.: A Non-Filamentary Switching Action in Thermally Grown SiO_2 Films. *British J. Appl. Phys.* **18** (1967), 29.
3. SIMMONS, J. G.—VERDERBER, R. R.: New Conduction and Reversible Memory Phenomena in Thin Insulating Films. *Proc. Roy. Soc.* **A 301** (1967), 77.

Über ein neues Schaltungsphänomen an dünnen GeO_2-Schichten. Es wird ein neues Schaltungsphänomen beschrieben, das an dünnen Germaniumdioxidschichten gefunden worden ist. Die MOS (Metall-Oxid-Halbleiter)-Struktur hat bei kleinen Gleichspannungen einen großen Widerstand. Bei einer bestimmten Schwellenspannung klappt sie um und besitzt dann einen kleinen Widerstand, der auch nach der Verminderung der Spannung erhalten bleibt. Ein kurzer Stromimpuls bewirkt von neuem ein Umklappen, demzufolge die Struktur wieder gleichbleibend hochohmig wird. Der Zyklus kann wiederholt werden.

Явление переключения в илёнках GeO_2 *(А. Лэринци и М. Немет Шаллаи).* Описывается явления переключения, обнаруженное в тонких слоях двуокиси германия. На постоянном токе структуре МОП (металл-окись-полупроводник) имеет большое сопротивление при низких напряжениях. При достижении напряжения порога происходит перескакивание на маленькое значение сопротивления, которое сохраняется и после понижения напряжения. Под действием короткого импульса тока структура снова переходит в стабильное положение с большим значением сопротивления. Цикл повторимый.

Acta Technica Academiae Scientiarum Hungaricae, Tomus 68 (1—2), pp. 195—197 (1970)

ON THE TIME DEPENDENCE OF THE PARAMETERS ON THE CATHODE SIDE

J. F. BITÓ

CAND. OF TECHN. SC.

RESEARCH INSTITUTE FOR ELECTRONICS, BUDAPEST

[Manuscript received July 17, 1969]

The time dependence of the cathode fall, anode fall and plasma potential of the a.c. oxide cathode discharge was experimentally determined by the author with the aid of an adequate diagnostic system. With the analysis of the time dependence of the cathode spaces he refers to an interesting and characteristic contraction of column in the vicinity of the plasma.

I. Experimental conditions, methods

Our measurements were carried out with glass discharge tubes of 1200 mm length and 38 mm diameter. Electrodes, made of tungsten triplespiral and having an emission coating, carried on it, were built into these tubes. The examinations were carried out at 430 mA discharge current, by $6 \cdot 10^{-3}$ mm Hg mercury vapour pressure — that is to say at 25 ± 1°C ambient temperature — with the application of argon ground gas, bringing about an a.c. current discharge of 50 cps frequency. External cathode heating, auxiliary electrodes and external magnetic field were not used. Our experimental methods were the following [1]: probe measurement, pyrometric and electronic temperature measurement, emission measurement, stroboscopic determination of the cathode space-lengths and cathode spot examination by cathetometer.

II. Results

The probe measurements were carried out at each 10° phase angle in the half period, corresponding to the 180° phase angle, and the cathode fall was determined by extrapolation on the basis of the measured plasma potentials. The starting point for the measurement was the moment, when it was characteristic for the peak value of the tube voltage. The half period in our case begins at about 0.55 msec before the closing of the half period.

The time dependence curve of the cathode fall follows the formation the tube in time of voltage. In order to manage the time dependence more easily, it is advisable in general to give the average values of the cathode fall, calculated from the momentary values and integrated for the half period.

From the plasma potential measurements, carried out at different moments on the probes, protruding into the different points of the positive column aware of the distance between the probes, the time dependence of the potential gradient of the positive column was determined within

a half period. The field strength of the positive column changes, corresponding to the tube voltage. The time dependence of the anode fall corresponds as regards its character to the curve, describing the time dependence of the cathode fall [2]. For the sake of control we determined the momentary tube voltage of the discharge tube at a deliberately chosen time, and examined whether the result of our calculation coincided with the momentary tube voltage value to be gained experimentally, in an additive way. With the application of the connection

$$V_T(t_1) = V_K(t_1) + V_A(t_1) + l_p(t_1) \cdot E_p(t_1), \tag{1}$$

where $V_T(t_1)$ tube voltage in the moment t_1;
$V_K(t_1)$ cathode fall in the moment t_1;
$V_A(t_1)$ anode fall in the moment t_1;
$l_p(t_1)$ length of the positive column in the moment t_1;
$E_p(t_1$f) ield strength of the positive column, measured in the moment t_1.

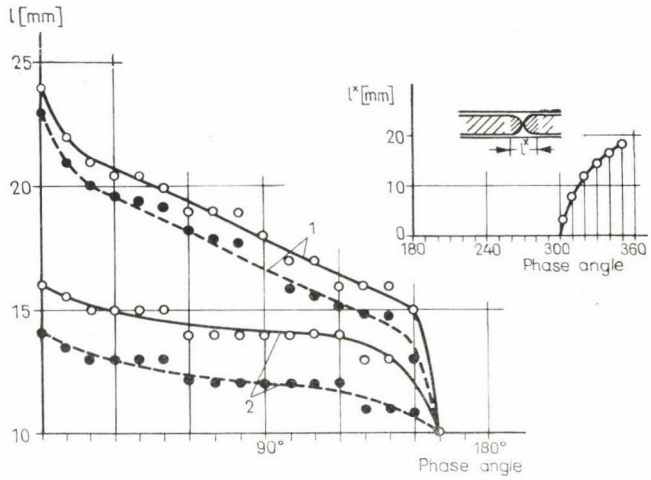

Fig. 1. The time dependence of the axial length of the cathode light and of the Faraday dark space with (- - - - -) and without (———) auxiliary electrodes (*1* Faraday dark space, *2* cathode light; *l** anodic half period)

As the measurements were extended, apart from the Faraday dark space to all discharge spaces, if they were right, then also the connection (1) must have been valid. According to the controls, performed at different times [1], the right side of the equation was, in general, by 0,5—1,5 V less than the tube voltage. This was attributed to the neglected transient spaces and to the inaccuracy in the measurement.

With the aid of a stroboscopic measurement [1] it would be shown that the boundaries of the cathode spaces were not constant, further we have taken the time dependence of the axial dimension of the two cathode spaces, characteristic for the arc discharges with oxide coated cathodes. The results are shown in Fig. 1.

The distances of these spaces from the cathode axis are given on the vertical axis of the coordinate system, and the time of the different measurements on the horizontal axis. From the four curves, in the middle of Fig. 1 the dotted ones give, in case of applying plane auxiliary electrodes having spiral end potentials, the time dependence of the cathode light and of the boundary at the positive column of the Faraday dark space; the full ones indicate the same, for relations without auxiliary electrodes. The boundary of the Faraday dark space is, at the 0° phase angle, the farthest from the cathode. The change in the axial length of the Faraday dark space is given by the difference of the boundary of the cathode light and of the boundary of the Faraday dark space at the positive column (the distance of the positive column from the cathode). After the breakdown the dimensions of this field gradually diminish. The dimension of the cathode light, containing the cathode dark space, lighting spaces and negative glow space, decreases more slowly. With the applied stroboscopic measuring method it could have been shown that in the last third of the anodic half period in the otherwise homogeneous positive column, extending to the anode, an infolding appeared along the walls in the form of a contraction.

This infolding gradually becomes more effective and although the positive column is not broken off, nevertheless it seems so, as if the two convex lenses were connected to each other by their domed sides, perpendicularly to the discharge axis. The time dependence of this process is shown in the corner of Fig. 1: the curve indicates the time dependence of the distance near the wall, arising at the reopening of the narrowing positive column. This separation begins at 300° phase angle and it strengthens up till 350°, where the decay of the discharge can be observed. This instability appears from time to time also at other places in the positive column, appearing regularly in the a.c. discharge near the electrodes which function as anodes. At the decay of the discharge the remaining discharge thread is already sufficient for the conduction of the abruptly diminishing discharge current.

REFERENCES

1. Bitó, J. F.: Ph. D. Thesis; Budapest 1968.
2. Bitó, J. F.: Cand. Thesis; Budapest 1966.

Die Zeit-Abhängigkeit der katodenseitigen Parameter. Der Verfasser bestimmt experimentell mit Hilfe eines geeigneten dyagnostischen Systems die Zeit-Abhängigkeit des Katodenfalls, Anodenfalls und Plasmapotentials der Wechselstromentladung mit Oxydkatode. Er analysiert die Zeit-Abhängigkeit der Dimension der Kathodenräume und weist auf eine interessante und charakteristische Kontraktion der Säule in der Nähe der Katode hin.

Временная заиисимость параметров катодной стоноы *(Я, Ф. Бито)*. Автор экспериментальным путем с помощью подходящей диагностической системы определяет временную зависимость катодного и анодного падений и потенциала плазмы разряда переменноготока оксидного катода. Анализом временной зависимости катобных пространств автор показываел очень интерерную и характерную контракцию столба вблизи катода.

Acta Technica Academiae Scientiarum Hungaricae; Tomus 68 (1—2), pp. 199—213 (1970)

INVESTIGATIONS ON THE DAMAGED SURFACE LAYER STRUCTURE OF SEMICONDUCTOR SINGLE CRYSTALS

LAPPING EFFECT

E. RÓZSA and V. STEFÁNIAY*

INDUSTRIAL RESEARCH INSTITUTE FOR ELECTRONICS, BUDAPEST

[Manuscript received March 4, 1969]

The report deals with the investigation of the structure and depth of the damaged surface layer of semiconductor single crystals resulting from lapping and with the methods adapted for measuring. Applying X-ray diffraction methods the structure and the depth of the damaged layer of [111] oriented germanium and silicon wafers are investigated. The degree of the flexure of the bent wafers due to mechanical stresses is measured as well. A relation is shown between the radius of curvature and the quality of the lapping process.

I. Introduction

For producing semiconductor devices with advantageous electronic parameters monocrystalline wafers of given thickness and crystallographic orientation and with damage-free surface are needed. The basic material being available in the shape of large-sized crystalline ingots, the final form is produced by slicing and applying a sequence of mechanical operations resulting in a proper surface finish suitable for device fabrication.

Considering that the semiconductor crystals are hard and brittle materials, the mechanical shaping is only feasible by using abrasive methods. The realization of the respective techniques — slicing, lapping and polishing — is different, but characteristic for the whole process is that the mechanical shaping is made step by step with decreasing sized abrasive grains.**

The aim of the lapping, the intermediate stage of the mechanical shaping process is to reduce the damage due to the slicing and simultaneously to produce a planparallel slice.

The diameter of the lapping abrasives is of mediocre size, in the range of 5—15 microns; the mean diameter of diamond grits suitable for the inner diameter (I. D.) slicing is between 60—70 microns and the polishing abrasives are generally smaller than 0,5 micron.

* Mr. V. STEFÁNIAY is now with United Incandescent Lamp and Electrical Co. Ltd. Budapest.

** We refer to the work of E. MENDEL and E. W. JENSEN [1] in connection with the different abrasive materials and to the reports of W. P. PHARO [2] and E. MENDEL [3] in connection with the adapted shaping methods.

The lapping, a preliminary or intermediate operation, takes a prominent part in attaining the ideal perfect surface finish. The requirements are strict, since the occasionally occurring mechanical damage might adversely influence the result of the surface preparation process or even that of the semiconductor device technology.

To produce up-to-date semiconductor devices characterized by a steadily increasing component density (the number of diodes, transistors and resistors per square millimetre) mechanical shaping processes of excellent quality are needed and this fact emphasized the investigation of the lapping procedure as well.

This report deals with the investigations of the structure and depth of the damaged monocrystalline semiconductor surface layer resulting from lapping and with the methods adapted for measuring and controlling. A brief recapitulation of the literature on the subject is indispensable for the detailed discussion of the results, as the numerous data published are contradictory.

The structure and the depth of the damaged layer of [111] oriented germanium and silicon wafers is investigated by X-ray methods. Applying these methods the degree of the flexure of the bent wafers due to mechanical stresses is measured as well. A relation is shown between the radius of curvature and the quality of the lapping process.

II. Structure and methods

1. Structure of the surface layer

Due to the mechanical shaping performed — i.e. lapping — the surface of the semiconductor crystals becomes distorted. The resulting layer has a complex structure; Fig. 1 showing a simplified outline may be interpreted as follows.

The surface is covered with polycrystalline debris combined with abrasive grains (Fig. 1; *1*) [4], below which a presumably monocrystalline layer of brittled structure can be found (Fig. 1; *2*) [4, 5]. Due to the effect of the cracks and that of the inserted grains the surface volume becomes increased and this results, below a critical thickness, in bending the wafer [6—8]. This phenomenon is dealt with in detail further on. A plastically deformed layer is developed below the brittled layer (Fig. 1; *3*) [9]. In the transition region between the damaged layer and the bulk material dislocations and microcracks were observed [10—12].

Deep scratches manifoldly surpassing the depth of the damaged layer are developed in case of a defective lapping technique (Fig. 2 and Fig. 3).

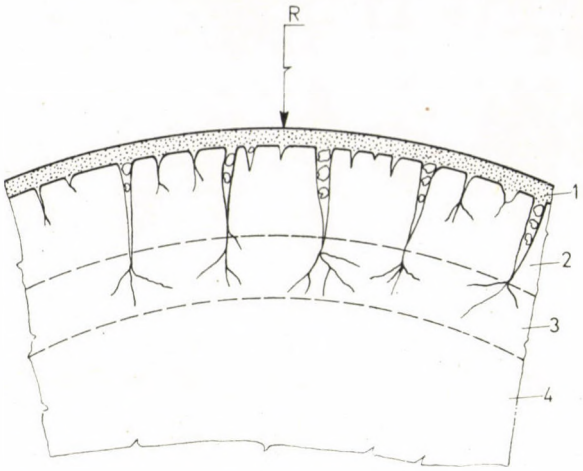

Fig. 1. Simplified outline of the structure of lapped monocrystalline surface (*1* polycrystalline debris; *2* brittled layer; *3* plastically deformed layer; *4* perfect crystalline material; *R* is the radius of curvature)

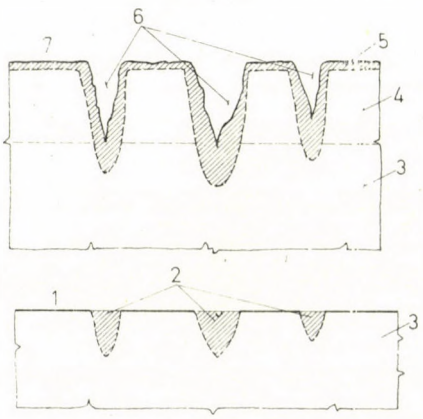

Fig. 2. Lattice defects due to deep scratches (*1* polished surface; *2* damaged crystlline parts; *3* bulk crystal; *4* the layer removed by polishing; *5* damaged layer; *6* scratches; *7* lapped surface)

2. Methods for measuring the depth of the damaged layer

The depth of damage is affected by several parameters which are hardly reproducible. The many contradictory data in the literature referring to the depth of that layer are interpreted by these. The deviations may be attributed rather to the different technological methods used, than to the various measuring principles [13].

The following processes were adapted for the investigations:

a) Optical methods (interference and phase contrast microscopy) are fast, rather widespread and the required investment is low. The observations may be preceded by a slight chemical etching [3, 12—17].

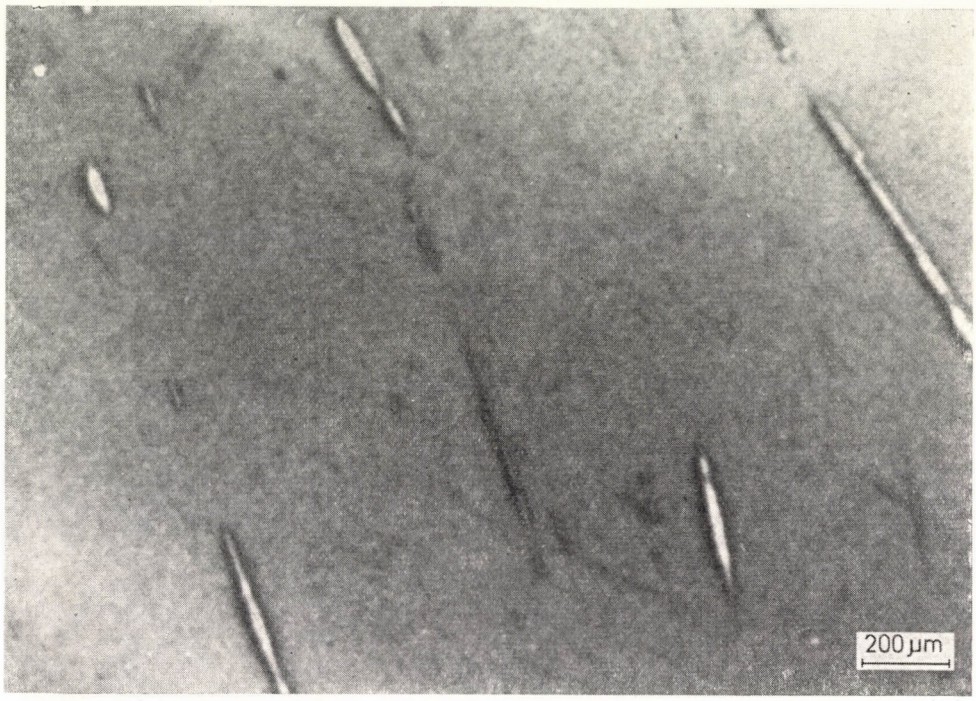

Fig. 3. Lattice defects due to lapping on polished germanium surface [surface reflexion topo graph Cu $K_{\alpha 1}$; Ge (333)]

b) Most informations on the structure of the crystal lattice are available by applying *diffraction methods*. The excellent resolving power renders the *electron-diffraction methods advantageous* [4, 5, 20].

The X-ray diffraction methods are relatively fast and being non-destructive are suitable as an in-process control in semiconductor technology [9, 21—24].

c) Investigating different *physical effects* data characterizing the depth of damage may be obtained. The measurement of electrical parameters, for instance, that of the recombination rate of minority carriers is used [25].

d) Plotting *the change of the etch rate* as a function of the removed damaged layer thickness is characteristic. The reproducibility of the method is about 2 per cent and its correspondence with other methods is fairly good [10, 14, 16, 26].

e) The surface quality of the lapped wafer may be characterized by determining the *radius of curvature*. The measurement can be performed optically [6, 7, 31], or by applying X-ray diffraction methods [8, 27, 28].

III. Experimental

X-ray diffraction methods were used to provide a detailed survey on lapped semiconductor surfaces, Lang's X-ray topography especially for detecting singular imperfections. Investigations concerning X-ray topographical methods are described in detail elsewhere [8, 30]. In this report, too, we should like to emphasize the sensitivity of the method, as single dislocations may be detected with relatively simple means as well. The surface quality of the lapped specimen can be evaluated by measuring the flexure of the wafer due to the damaged layer. An X-ray diffraction method was adapted instead of the generally accepted optical or mechanical methods [28].

The essential part of the method summarized is that exposing a correctly oriented crystal slab to a wide, but nearly parallel X-ray beam, the characteristic components are reflected as narrow beam of rays. The reflection angle fixed and translating the wafer parallel to its plane, the position of the reflected beam remains unaltered, if the orientation of the reflected planes is unaltered along the line of translation as well. Having a misorientation the reflecting lines migrate proportionally. The misorientation angle (ε) within the distance of translation (h) is referred to the known angular resolution of the $K_{\alpha 1,2}$ components. The image is recorded on a photographic plate in a fixed position. (This is a dissimilarity e.g. to Lang's topography.)

If the misorientation on the crystal slab is continuous, the wafer is bent along a spherical surface and the radius of curvature equals $R = h/\varepsilon$. The accuracy of the method is mediocre, but rather fast and entirely non-destructive. The exposure, together with the evaluation, takes only 5—10 minutes. Contrary to the optical and mechanical methods the accuracy of the measurement is not affected by the surface finish of the wafers.

Adapting the described method a misorientation of 10 seconds of arc can be detected on a wafer of 20 mm diameter; this corresponds to a 200 m radius of curvature. The radius of curvature due to the lapping of wafers with 200—300 micron thickness is considerably less: $R = 1 \sim 3$ m.

The photographs taken for the measurement of flexure provide further data characterizing the crystalline surface. The separation of the characteristic lines, or their displacement, respectively, are typical for the flexure and the width of the lines may be attributed to the quality of the crystal lattice.

The exposures were taken by using a *Philips* X-ray tube of 1×1 mm effective focal spot size. The tube operates at 50 kV and 20 mA. The distance between the focus and the specimen is 1300 mm, that between the specimen and the plate is 10 mm in case of diffraction topographs and about 60 mm in curvature measurements.

The reflecting planes for (111) specimen are the (110) planes perpendicular to the surface. The images are recorded on *Ilford* nuclear plates — type *L 4/100*, or on *Gaevert* plates — type *D—7* and *D—4*, respectively.

IV. Experimental results

Single crystal [111] oriented germanium and silicon wafers were available for the experiments. The effect of different lapping procedures and that of different abrasive grains were investigated in separate measuring sequences. If (111) silicon wafers are lapped with a water slurry of 600 mesh α-alumina on fixed stainless steel plate, applying a light hand pressure, the depth of damage is about 6—8 microns.

Table I

The flexure of lapped silicon wafers

Lapping procedure	Lapping abrasive		Radius of curvature, R [m]
	material	size (mesh)	
"Lapmaster" technique*	SiC	600	2,0
	SiC	800	2,9
Lapping by hand on rotating steel plate	SiC	600	1,45
Lapping by hand on fixed steel plate	SiC	600	1,8
	SiC	800	1,5
	α-Al_2O_3	500	1,3
	α-Al_2O_3	800	1,1

* Lapmaster flat lapping machine made by *Payne Prod. Int. Lim.* (England). According to the lapmaster principle three or four conditioning rings ride on a horizontal circular lap plate of cast iron. The rings are held in position by yokes, which allow them to revolve on the lapping surface. The parts to be lapped are placed inside the rings; abrasive compound is fed continuously onto the lapping plate.

The measured radii of curvature of the 250 micron thick (111)Si wafers are presented in Table I. These specimens are lapped on both sides and one side is chemically etched thereafter. The measured radii of curvature of Ge wafers 500 micron thick, on both sides lapped and on one side etched are outlined in Table II.

Table II

The flexure of lapped germanium wafers

Lapping procedure	Lapping abrasive		Radius of curvature, R [m]
	material	size (mesh)	
"Lapmaster" technique	SiC	500	2,5
	SiC	600	3,0
	SiC	800	3,7
Lapping by hand on fixed steel plate	SiC	500	2,5
	SiC	600	3,0
	SiC	800	3,0

V. Discussion

Lattice defects due to lapping can be detected as a continuous diffraction contrast on the topograph (Fig. 4). The damaged layer disappears after chemically etching the wafer and the dislocation network of the bulk material appears (Fig. 5). The lapping process is generally qualified by measuring the depth of

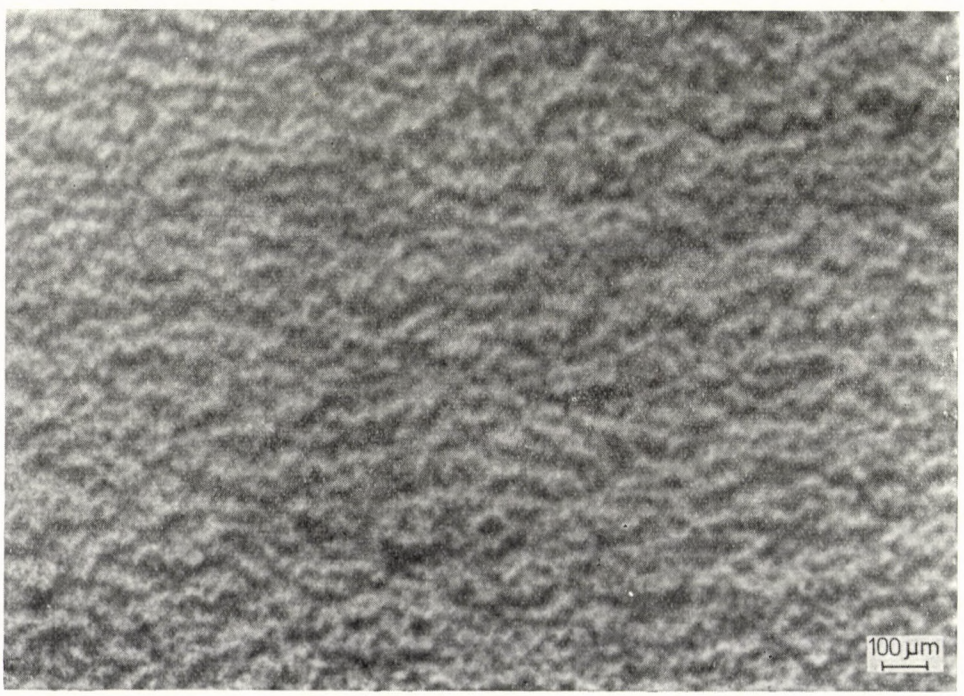

Fig. 4. Transmission topograph of the lapped crystalline wafer [$MoK_{\alpha 1}$; Si ($\bar{2}20$)]

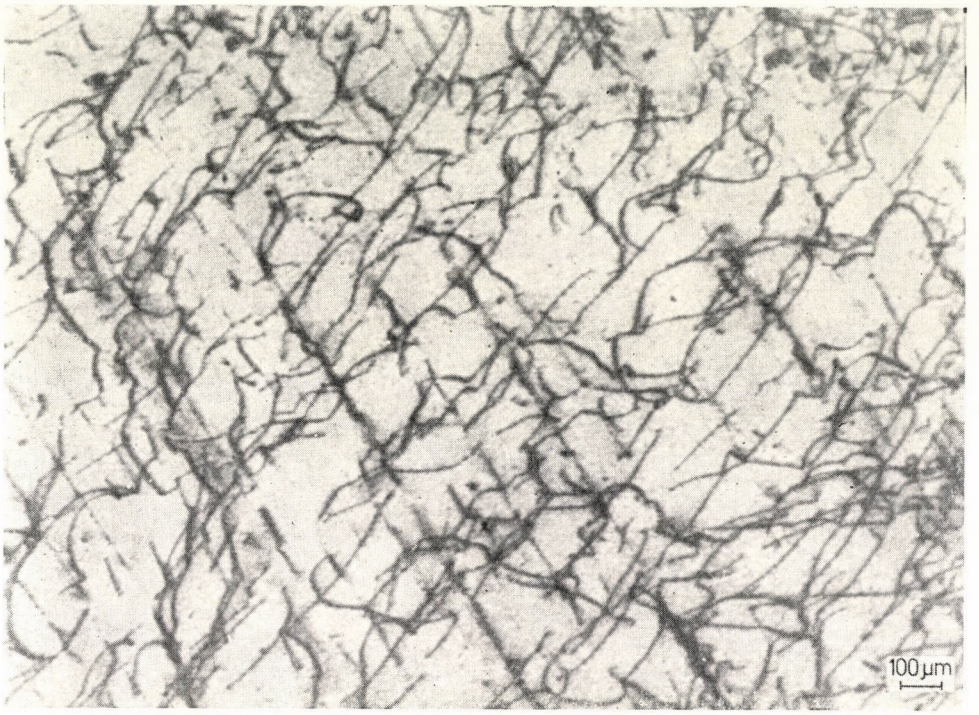

Fig. 5. Topograph of the wafer seen in Fig. 4 after removal of the damaged layer the continuous diffraction contrast due to the lattice defects disappears and the dislocation network of the bulk material is to be seen [$MoK_{\alpha 1}$; Si ($\bar{2}20$)]

the damaged layer. The determination of the flexure of the silicon wafer also gives useful informations.

Crystalline slices lapped on both sides do not show any flexure, as the two opposite effects equalize each other. Removing the distorted layer, e.g. applying chemical-mechanical polishing, the wafer becomes elastically deformed. Investigations were generally performed on specimens pretreated in that way, and this is the initial state of the monocrystalline slices used nowadays in the semiconductor planar technology. Having etched both sides, the bent wafer regains its original plane character.

The results represented in Table I and Table II are in good agreement with the findings of G. WENCZEL [6] and with that of W. DASH [31]. The radius of curvature detected by the former expert was 2,5 m obtained on wafers lapped with grains of 12 micron average diam., and W. DASH measured a value of 1,2 m optically.

More time is needed to obtain a smooth surface on wafers lapped with smaller abrasive grains on fixed stainless steel plate by applying a light hand pressure. The apparent contradiction that abrasive grains of smaller average diam. render smaller radius of curvature, is due to this fact.

The depth of the damaged layer formed on germanium is larger, but in the case described the wafers being thicker the radius of curvature is also of larger value. The experimental data, however, show that the differently sized abrasive grains induce a smaller flexure of the wafers, as the thicker distorted layer suppresses te effect issuing from the different average diameters of the grains.

Knowing the radius of curvature and the depth of the damaged layer, respectively, an approximation was used to determine the average strain (σ) in the surface layer taking the flexure's rotation paraboloid character into consideration [32]. The calculation was based on the following relation:

$$\sigma_{\text{film}} \cong \frac{E}{3(1-\nu)} \cdot \frac{(t_{\text{substr.}})^2}{t_{\text{film}}} \cdot \frac{1}{2R},$$

if

$$t_{\text{substr.}} \gg t_{\text{film}};$$

where E Young modulus of the substrate;
ν Poisson number;
$t_{\text{substr.}}$ thickness of the bulk material;
t_{film} depth of the damaged layer;
R radius of curvature.

The first term of the product is $7{,}684 \cdot 10^{11}$ dyn/cm^2, assuming a circular (111) silicon wafer. Taking the following parameters further in account:

$$t_{\text{substr.}} = 220\ \mu\text{m},$$
$$t_{\text{film}} = 6\ \mu\text{m},$$
$$R = 2\ \text{m},$$

on the basis of the described equation:

$$\sigma_{\text{film}} = 1{,}5 \cdot 10^9\ \text{dyn/cm}^2.$$

The average strain approaches the value — $\sigma_{\max} = 6 \cdot 10^9$ dyn/cm^2 — measured by J. R. Patel and A. R. Chaudhuri [29], which is closely the room-temperature yield point of silicon. The local stress peaks may obtain even greater values than the typical one and they can attain the above mentioned maximum as well.

Knowing the radius of curvature or more exactly the spread of misorientation within a given distance, some conclusions may be drawn in regard to the crystallographic misorientation among the singular blocks. In the calculation it was assumed that the blocks are of the same dimensions and the orientation divergence is uniformly distributed. On the X-ray topographs available the

width of the blocks may be evaluated to 100 microns. If the radius of curvature is $R = 1$ m, the average orientation divergence between the singular blocks is 0.5 minute of arc. Taking into consideration the width of the diffraction lines, deviations of 3 minutes of arc were measured, which are larger than the average divergence. The difference may be attributed to the fact that the spread of misorientation is not uniform among the blocks. Just because of

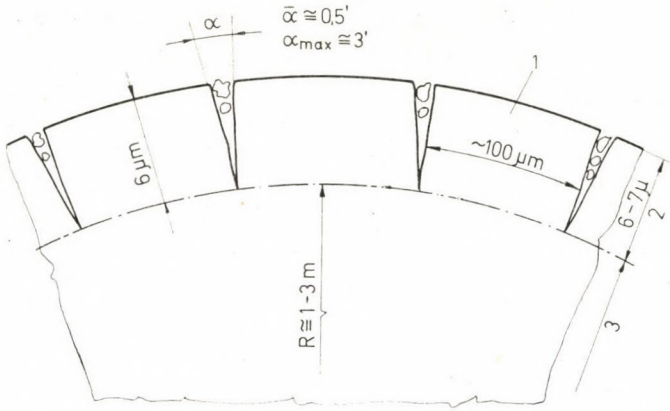

Fig. 6 Misoriented blocks due to the lapping effect are developed

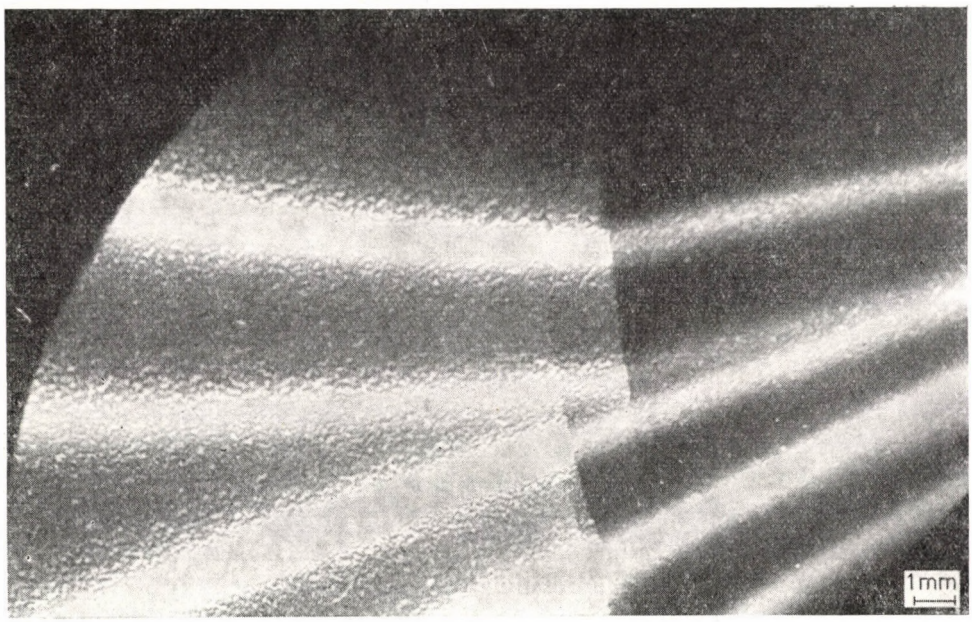

Fig. 7. The characteristic lines are enlarged at the edges of the wafer; it shows that the depth of the damaged layer is inhomogeneous; one part of the wafer is not covered by the damaged layer (photographic negative)

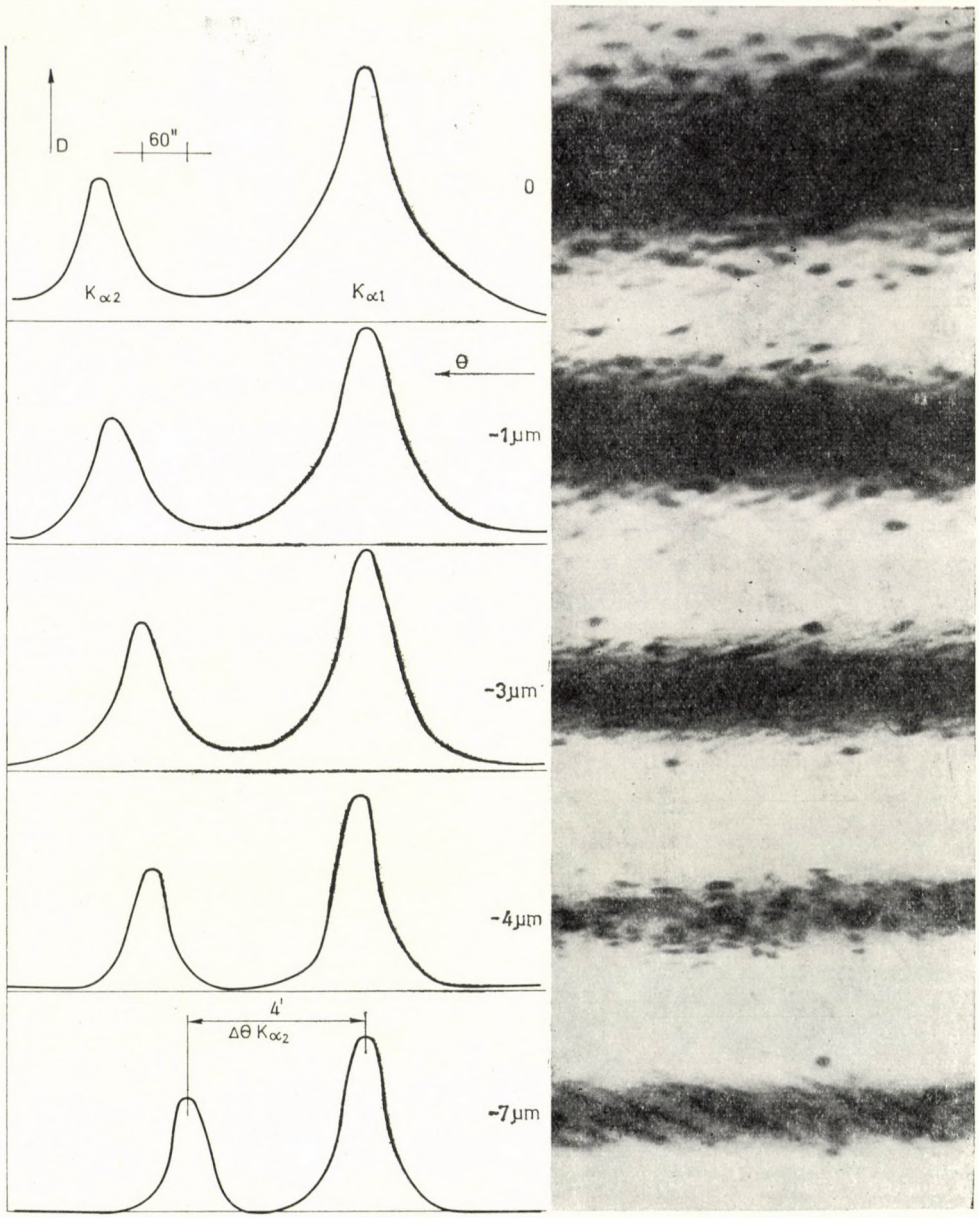

a) *b)*

Fig. 8. The damaged layer progressively removed the distance between the characteristic lines and their width decreases proportionally; in the figure the photometric graphs of the characteristic lines *(a)* and one part of the photographic negative of the $K_{\alpha 1}$ component *(b)* are to be seen

this, it is emphasized that the outline presented in Fig. 6 gives a model and it serves for the illustration of the phenomenon only.

Valuable informations on the structural defects of the crystalline surfaces are available from X-ray topographs measuring the flexure. Fig. 7 is a topograph of a silicon wafer with different surface quality regions. The back side of the specimen is of nearly perfect structure; on one part of the investigated surface the distorted lattice region can be detected, the other part is defectless. The width of components $K_{\alpha 1}$ and $K_{\alpha 2}$ reflected from the perfect surface is determined by the divergence of the X-ray beam, by the spectral width of the lines and by the quality of the crystal lattice. Having a high degree of perfectness on the surface and a negligibly small spectral width of the lines, the range of the components is principally determined by the divergence of the beam. On damaged regions, where the crystal lattice is distorted, the line width is increased. The effect appears to be even stronger at the edges of the wafers, though the defects due to mechanical shaping are more numerous. (Geometrical or other diffraction effects cannot produce this, since the defectless regions are free from broadening.) The edge-effect is well known, it is caused either by the abrasive grains or even more by the edge-chipping of the crystalline wafer.

The surface quality of the lapped silicon wafers may be investigated at different bulk depths, applying progressive etching on the same surface. The result of the etching process is presented in Fig. 8.

The characteristic lines bridge etched steps of 0, 1, 3, 4, 7 microns, respectively. For quantitative evaluation the lines were measured with a fast response photometer made by Zeiss and the results were graphically plotted. On the horizontal axis the relative changes of the reflecting angle and on the vertical axis the blackening are recorded. Simultaneously with the photo-

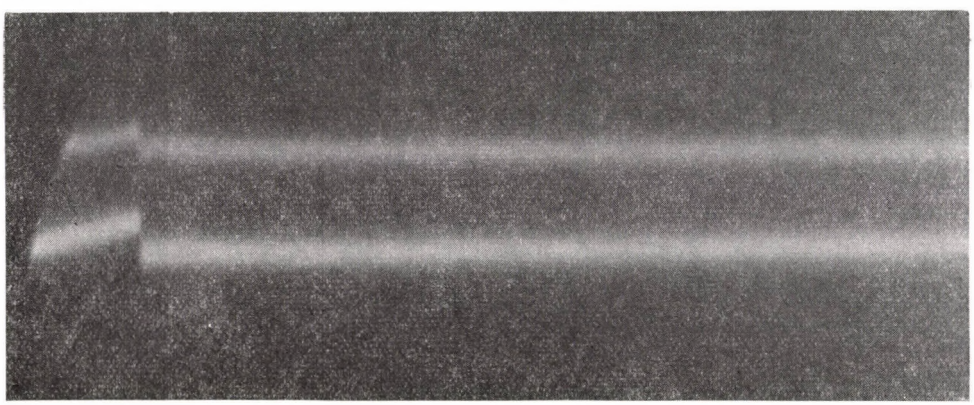

Fig. 9. The $K_{\alpha 1,2}$ components are distorted in the range of the microcracks. The displacement is proportional to the orientation divergence (photographic negative)

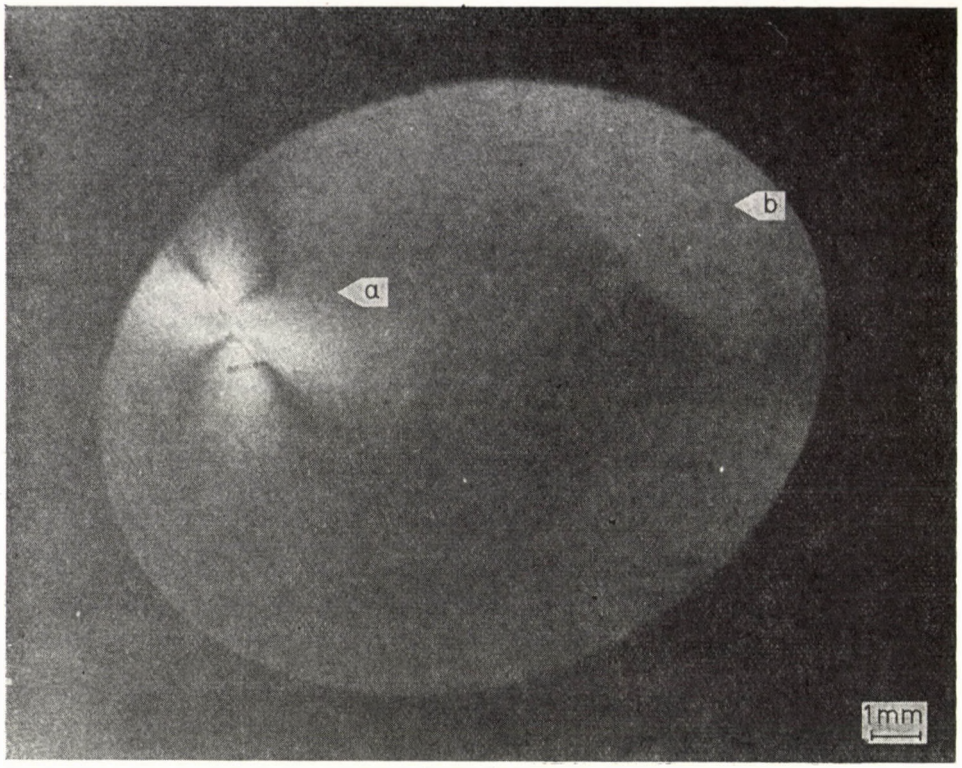

Fig. 10. The strain field due to the microcrack is detectable on the exposure made by the "white" components of the X-ray beam; one part of the monocrystalline wafer is covered by the damaged layer (photographic negative)

metric graphs the diffraction image of one of the characteristic lines ($K_{\alpha 1}$) is presented.

Removed at about 4 microns the continuous damaged layer disappears, but the remaining pointlike lattice defects refer to local disturbances (chipped pits). The observation is confirmed by the sudden diminution of the background level. After removal of 7 microns, most of the pits disappear and the original dislocation network of the bulk material is revealed, the crystalline surface may be considered "perfect". The distances between the lines (slope) diminish as well, and at 7 microns step the theoretically justified value of plane crystalline surface ($K_{\alpha 12} = 4$ minutes of arc) is achieved Si ($\bar{2}20$) reflexion, $MoK_{\alpha 1}$ radiation].

On the topographs performed for the curvature measurements, unvisible microcracks are to be detected from time to time. The microcracks are due to a non-perfect lapping procedure. The strain field around the microcracks could be detected from the distortion of the characteristic lines (Fig. 9) or from the raising of the background level; i.e. the diffracted image of the strain field

appears on the topograph (Fig. 10). Evaluating such topographs the dislocation density of the bulk material can be estimated, the image resolution is, of course, worse than that of the Lang method.

VI. Conclusions

Comparing the data of the literature on the subject and that of our investigations the conclusion can be drawn that the qualification of the lapping methods is possible only for surface shapings of a given technology, which are hardly or not at all reproducible by others. Performing the single processes, i.e. the lapping — proper testing methods are to be developed instead of making mechanical use of the data published in the literature. The control process may be achieved by optical methods or by more exact diffraction methods. It cannot be limited, however, for the determination of a single characterizing parameter — i.e. the average depth of the damaged layer. The investigations are to be extended for studying the homogeneity of the depth of the damaged layer, the effect of the different local disturbances, i.e. scratches and the interaction of the substrate and the distorted layer including the work performed on the flexure of the wafer.

As a result of the investigations the control methods for the qualification of the lapped semiconductor surfaces were determined and beside the parameters, such as the depth and homogeneity of the damaged layer, the flexure of the wafer was taken into consideration as well.

Acknowledgments

The authors wish to thank Dr. I. C. SZÉP and Dr. P. GADÓ for their council and many stimulating discussions and they are indebted to Mr. J. ZOLTAI for the experimental cooperation in the investigations.

REFERENCES

1. MENDEL, E.—JENSEN, E. W.: *Semicon. Prod.* **8** (1965), 29.
2. PHARO, W. P.: *US Gov. Res. Rept.* **AD—264249**.
3. MENDEL, E.: *Solid-State Techn.* **10** (1967), 10.
4. POSER, H.: *I.H.T. Mitteilungen* **2** (1963), 62.
5. STICKLER, R.—BOOKER, G. R.: *Phil. Mag.* **8** (1963), 852.
6. WENCZEL, C. H.: *SCP and SST* **10** (1967), 40.
7. PRUSSIN, S. A.: Metallurgy of Semiconductor Materials (Ed. J. B. SCHROEDER). Interscience Publ., New York 1962.
8. RÓZSA, E.—STEFÁNIAY, V.: X-Ray Topographic Investigation on Mechanically Treated Silicon Wafers. Paper presented at the Fourth Hungarian Conference on X-Ray Diffraction, Esztergom, 1968.
9. RENNINGER, M.: Crystallography and Crystal Perfection (Ed. G. N. RAMACHANDRAN). Academic Press, New York 1963, 145.
10. FAUST, J. W.: *Electrochem. Techn.* **2** (1964), 339.
11. FAUST, J. W.: *Surface Science* **13** (1969), 60.
12. PUGH, E. N.—SAMUELS, L. E.: *J. Electrochem. Soc.* **111** (1964), 1431.
13. STICKLER, R.—FAUST, J. W.: *Electrochem. Techn.* **4** (1966), 399.
14. MENDEL, E.—JACOBSON, H. R.: *Semicond. Prod.* **8** (1965), 38.
15. BOGENSCHÜTZ, A. F.—LANGHEINRICH, W.—MESSINGER, W.: *Metalloberfläche* **18** (1964), 193.

16. Buck, F. M.—McKim, F. S.: *J. Electrochem. Soc.* **103** (1957), 539.
17. Gutsche, H. W.: Surface Damage in Si. Paper presented at the IEEE Symposium, Clayton, Miss. 1967.
18. Noggle, T. S.—Stiegler, J. O.: *J. Appl. Phys.* **30** (1959), 1279.
19. Bogenschütz, A. F.—Mendel, E.—Meieran, E. S.: *J. Appl. Phys.* **36** (1965), 2544.
20. Stickler, R.—Meieran, E. S.: *Trans AIME* **242** (1968), 413.
21. Saccocio, E. J.—McKeown, W.: *J. Appl. Phys.* **38** (1967), 2702.
22. Knudsen, J. F.: Advances in X-Ray Analysis. Plenum Press, New York 1964; Vol. **7**, 159.
23. Aoki, H.—Maruyama, S.: *J. Phys. Soc. Japan* **20** (1965), 1731.
24. Kato, I.—Shinozaki, T.—Goto, K.: *Toshiba Rev.* **19** (1964), 1272.
25. McKelvey, J. P.—Longini, R. L.: *J. Appl. Phys.* **25** (1954), 634.
26. Gatos, H. C. et al.: *J. Electrochem. Soc.* **108** (1961), 645.
27. Wolfson, R. G. et al.: *Int. J. Electronics* **21** (1966), 37.
28. Stefániay, V.: *Mérés és Automatika* **14** (1969), 217.
29. Patel, J. R.—Chaudhuri, A. R.: *J. Appl. Phys.* **34** (1963), 2788.
30. Rózsa, E.—Stefániay, V.: *Tungsram Techn. Mitt.* (in press).
31. Dash, C. V.: *J. Appl. Phys.* **29** (1958), 228.
32. Glanc, R.—Holmwood, R. A.—Rosenfeld, R. L.: *Rev. Sci. Instr.* **36** (1965), 7.

Strukturuntersuchungen am gestörten Oberflächenbereich der Halbleitereinkristalle. Einfluß des Schleifens. Die Struktur des durch den Einfluß des Schleifens gestörten Oberflächenbereichs der Halbleitereinkristalle wird untersucht und die Eindringstiefe der Gitterstörung wird bestimmt. Die Untersuchungen sind mit der Röntgenstrahlbeugungsmethode an [111] orientierten Germanium und Siliziumplatten durchgeführt. Der Krümmungsradius der geschliffenen Platte wird gemessen. Es wird festgestellt, daß die Krümmung durch die Qualität des Schleifens — da ein Zusammenhang zwischen der Krümmung und der mechanischen Beanspruchung besteht — charakterisiert werden kann.

Исследование структуры поврежденных поверхностных слоев полупроводниковых монокристаллов *(Е. Рожа* и *В. Штефаниаи)*. Авторы занимаются структурой, распространенностью и методами исследования поврежденных слоев, образовавшихся после шлифовки на поверхности полупроводниковых монокристаллов. Приводятся результаты рентгеноструктурых исследований, в тенчении которых рассматривались структура и толщина поврежденных слоев на монокристаллических пластинах германия и кремния ориентации [111]. Подобным образом измерялась степень искривленности, образовавщейся на астплинах в результате механических воздействий, и авторами была найдена зависимость между радиусом кривизны и качеством примененного метода шлифовки.

Acta Technica Academiae Scientiarum Hungaricae; Tomus 68 (1—2), pp. 215—243 (1970)

WAVE PROPAGATION IN INHOMOGENEOUS LINEAR MEDIA

CS. FERENCZ

[Manuscript received September 29, 1969]

In the paper, first, the propagation of electromagnetic waves in slightly inhomogeneous media is examined, when the medium is stationary, its parameters change with time and when, finally, it is flowing. In this connection the author points out that the theory permits the uniform treatment of many known results and also permits the exact investigation of the propagation phenomena in flowing media. Afterwards the method for the determination of the complete wave form by the addition of the 'inhomogeneous basic modes' is shown for arbitrary inhomogeneities. The deduction of the "quadruple and multiple refraction-reflection law" is presented. On this basis the ray-tracing programs are revised and the basic scheme of the "modified ray-tracing" programs is given. Finally, it is shown that the homogeneous and the inhomogeneous characteristics of the medium are not identical, and using as an example the electron-polarized medium, the inhomogeneous permittivity is determined. The method for determining the wave image, the "mutual action tensor" and—as an example—the "modified Eikonal equation" are presented.

I. Introduction

The necessity of a rigorous treatment of wave propagation in linear media characterized by medium parameters of the form of highly general functions emerged in consequence to the development of very accurate measurements in space research and of special instruments, particularly in microwave technics. The wave propagation in homogeneous media is very precisely known. Gradually generalizing the research methods developed for the homogeneous case, in this paper a new method will be found for the exact investigation of the field existing in the most general inhomogeneities. On the other hand, it will be seen that in this way one can settle the limits of validity of the formerly used methods (e.g. ray-optical equivalent).

II. Weakly inhomogeneous stationary media

In the first step, let us assume that the medium is free of flows and is electrically neutral, that is $\varrho = 0$. Furthermore, the medium parameters are assumed to be "slowly" varying. A solution for the Maxwell equations is sought for in the following form [1]:

$$\bar{E} = \bar{E}_0(\bar{r}, t)\, e^{j[\omega_0 t - \varphi(\bar{r},t)]}, \tag{1}$$

where $\bar{E}_0(\bar{r}, t)$ is the amplitude, ω_0 is the excitation angular frequency and φ is the phase function.

Introducing the symbols $\bar{\bar{\mu}}(\bar{r}, t)$ and $\bar{\bar{\varepsilon}}(\bar{r}, t)$ for relative permeability and permittivity, respectively, where ε also includes the conductivity terms in the well-known manner, the Maxwell equations are

$$\begin{aligned} \operatorname{curl} \bar{H} &= \frac{\partial}{\partial t}(\varepsilon_0 \bar{\bar{\varepsilon}} \bar{E}), \\ \operatorname{curl} \bar{E} &= -\frac{\partial}{\partial t}(\mu_0 \bar{\bar{\mu}} \bar{H}), \\ \operatorname{div}(\mu_0 \bar{\bar{\mu}} \bar{H}) &= 0, \\ \operatorname{div}(\varepsilon_0 \bar{\bar{\varepsilon}} \bar{E}) &= 0, \\ \bar{D} &= \varepsilon_0 \bar{\bar{\varepsilon}} \bar{E} \quad \text{and} \quad \bar{B} = \mu_0 \bar{\bar{\mu}} \bar{H}, \end{aligned} \tag{2}$$

where ε_0 and μ_0 are the permittivity and permeability of free space, respectively, $\bar{E}$ and $\bar{H}$ are the electric and magnetic field intensities, respectively, $\bar{r}$ is the position vector, t is time.

1

After differentiating in Equs (2) we obtain terms of the following type:

$$\left(\frac{1}{a_{ik}} \frac{\partial a_{ik}}{\partial x_i} + \frac{1}{E_{0k}} \frac{\partial E_{0k}}{\partial x_i} - j \frac{\partial \varphi}{\partial x_i} \right) a_{ik} E_k , \tag{3}$$

where $E_i = E_{0i} e^{j(\omega_0 t - \varphi)}$, E_{0i} and a_{ik} are the components of amplitude and medium parameters, respectively, x_i is an independent variable.

In homogeneous medium Term (3) leads to the well-known relation:

$$(0 + 0 - jk_i)\, a_{ik} E_k = -jk_i\, a_{ik} E_k , \tag{4}$$

where $k_i = \dfrac{\partial \varphi}{\partial x_i} = \text{const.}$

Let the variation of the medium parameters be small for the distance of the wavelength λ. Then

$$\Delta a_{ik} = \frac{\partial a_{ik}}{\partial x_i} \lambda \sim \eta , \tag{5}$$

where η is an infinitesimally small quantity. Multiplying (3) by λ, the order of magnitude of the terms can be estimated:

$$\left(\frac{1}{a_{ik}}\frac{\partial a_{ik}}{\partial x_i}\lambda+\frac{1}{E_{0k}}\frac{\partial E_{0k}}{\partial x_i}\lambda-j\frac{\partial\varphi}{\partial x_i}\lambda\right)a_{ik}E_k. \tag{6}$$

Considering (4) as a limit value, the assumption that the amplitude or the phase does not change either more quickly or slowly, respectively, than the medium parameters, can be justified. Further let $\partial\varphi/\partial x_i = k_i + \Delta k_i$, where $\Delta k_i \neq$ const. So this (6) can be rewritten:

$$(6)\sim\left[\frac{\eta}{a_{ik}}+\frac{\eta}{E_{0k}}-j(k_i\lambda+\Delta k_i\lambda)\right]a_{ik}E_k\cong-j(k_i+\Delta k_i)\lambda a_{ik}E_k\sim-jk_i\lambda a_{ik}E_k. \tag{7}$$

From (7) it can be seen, that in case of weak inhomogeneities the wave propagation vector $K_i = k_i + \Delta k_i$ may be used as a generalization of the homogeneous wave propagation vector, in describing the wave pattern, while in case of strong inhomogeneities also the derivatives of the amplitude E_0 must be taken into account.

2

Let us introduce the

$$\overline{K} = \overline{\text{grad}\,\varphi}$$

and

$$\omega = \omega_0 - \frac{\partial\varphi}{\partial t} \tag{8}$$

generalized propagation vector and generalized angular frequency, respectively. If the medium is weakly inhomogeneous, that is, using (7), the following conditions

$$\frac{1}{E_{0i}}\frac{\partial E_{0i}}{\partial x_j} \ll \frac{\partial\varphi}{\partial x_j}$$

and

$$\frac{1}{a_{ij}}\frac{\partial a_{ij}}{\partial x_i} \ll \frac{\partial\varphi}{\partial x_i} \tag{9}$$

hold, then Maxwell's equations can be rewritten in the following form:

$$\begin{aligned}
\overline{K}\times\overline{H} &= -\omega\varepsilon_0\overline{\overline{\varepsilon}}\overline{E}\,,\\
\overline{K}\times\overline{E} &= \omega\mu_0\overline{\overline{\mu}}\overline{H}\,;\\
\mu_0\overline{K}\overline{\overline{=}}\overline{H} &= 0\,,\\
\varepsilon_0\overline{K}\overline{\overline{\varepsilon}}\overline{E} &= 0
\end{aligned} \tag{10}$$

which are in every respect equivalent to Equs (2). The form of Equs (10) corresponds to the one of wave equation of plane waves propagating inhomogeneous, time invariant media. Thus, the solution method which is usually applied there, will be followed. Forming the vectorial product of $\overline{K}$ with the first or second equation of (10), and substituting the other one into the right side and using the following symbols:

$$\begin{aligned} \overline{\overline{\Lambda}} \ldots &= \overline{K} \times (\overline{K} \times \ldots) , \\ \overline{\overline{P}}^* \ldots &= \overline{K} \times \overline{\overline{e}} \ldots , \\ \overline{\overline{M}}^* \ldots &= \overline{K} \times \overline{\overline{m}} \ldots \\ \overline{\overline{\varepsilon}} &= \overline{\overline{1}} + \overline{\overline{e}} , \\ \overline{\overline{\mu}} &= \overline{\overline{1}} + \overline{\overline{m}} \end{aligned} \tag{11}$$

the following set of homogeneous, linear equations can be obtained:

$$\begin{aligned} (\overline{\overline{\Lambda}} + \omega^2 \varepsilon_0 \mu_0 \overline{\overline{\mu}}) \overline{H} + \omega \varepsilon_0 \overline{\overline{P}}^* \overline{E} &= 0 , \\ - \omega \mu_0 \overline{\overline{M}}^* \overline{H} + (\overline{\overline{\Lambda}} + \omega^2 \varepsilon_0 \mu_0 \overline{\overline{\varepsilon}}) \overline{E} &= 0 . \end{aligned} \tag{12}$$

A non-trivial solution of Equs (12) exists if the determinant equals zero. This condition may be written in two completely equivalent forms. These two possible forms of the "generalized dispersion equation" follow, using the shortening $\alpha^2 = \omega^2 \varepsilon_0 \mu_0$, as:

$$\left| \left(\frac{\overline{\overline{\Lambda}}}{\alpha} + \alpha \overline{\overline{\varepsilon}} \right) + \overline{\overline{M}}^* \left(\frac{\overline{\overline{\Lambda}}}{\alpha} + \alpha \overline{\overline{\mu}} \right)^{-1} \overline{\overline{P}}^* \right| = 0 , \tag{13}$$

$$\left| \left(\frac{\overline{\overline{\Lambda}}}{\alpha} + \alpha \overline{\overline{\mu}} \right) + \overline{\overline{P}}^* \left(\frac{\overline{\overline{\Lambda}}}{\alpha} + \alpha \overline{\overline{\varepsilon}} \right)^{-1} \overline{\overline{M}}^* \right| = 0 . \tag{14}$$

The solution of one of the above equations — taking the boundary conditions into consideration — gives the phase function $\varphi(\bar{r}, t)$ of the propagating wave, further the time t and the corresponding propagation path $\bar{r}$ which can be defined as the trajectory, normal to the surfaces $\varphi(\bar{r}, t) = \text{const}$. Again substituting $\varphi(\bar{r}, t)$ into (10) and using the boundary conditions, the now inevitably existing $\overline{E}$ and $\overline{H}$ fields can be obtained.

3

It requires further investigations to decide what type of quantities and functions may be allowed for together [2] $\overline{\overline{\varepsilon}}$ and $\overline{\overline{\mu}}$, and the former results must also be re-examined, based on the detailed analysis of the inhomogeneous medium parameters (Chapter VI).

4

The derivative in Equs (2) with respect to time plays a far more simple role than the ones with respect to place. Thus, only in case of much time variations, each result of *2* can be employed to find the individual primary modes composing the complete wave pattern, unless using the symbols

$$\begin{aligned} \bar{\bar{\varepsilon}} &= \bar{\bar{\varepsilon}} - j\frac{1}{\omega}\frac{\partial \bar{\bar{\varepsilon}}}{\partial t} = \bar{\bar{1}} + \bar{\bar{e}}^*, \\ \bar{\bar{M}} &= \bar{\bar{\mu}} - j\frac{1}{\omega}\frac{\partial \bar{\bar{\mu}}}{\partial t} = \bar{\bar{1}} + \bar{\bar{m}}^* \end{aligned} \tag{15}$$

in (13) and (14) the following changes take place:

$$\begin{aligned} &\bar{\bar{\varepsilon}} \text{ instead of } \bar{\bar{\varepsilon}}, \\ &\bar{\bar{M}} \text{ instead of } \mu, \\ &\bar{P}^* \ldots = \bar{\bar{K}} \times \bar{\bar{e}}^* \ldots \text{ instead of } \bar{P}^* \ldots = \bar{\bar{K}} \times \bar{\bar{e}} \ldots, \\ &\bar{M}^* \ldots = \bar{\bar{K}} \times \bar{\bar{m}}^* \ldots \text{ instead of } M^* \ldots = \bar{\bar{K}} \times \bar{\bar{m}} \ldots . \end{aligned} \tag{16}$$

The manner of composing the complete wave pattern will be seen later in Chapter IV.

5

The preceding results can be generally applied as was shown in detail in [1]. Taking account of the following, it is advisable to show here the dispersion equation for stationary, isotropic, inhomogeneous media, as a special form of (13).

Then $\bar{\bar{\varepsilon}} = \varepsilon(\bar{r}) \cdot \bar{\bar{1}}$, $\bar{\bar{\mu}} = \bar{\bar{1}}$ and they are constant in time. It can be justified that (13) takes the form of

$$| \bar{\bar{A}} + \omega_0^2 \varepsilon_0 \mu_0 \varepsilon(\bar{r}) \cdot \bar{\bar{1}} | = 0 . \tag{17}$$

Developing this, the well-known Eikonal equation, which is considered as the basis of geometrical optics, can be obtained:

$$\left(\frac{\partial \varphi}{\partial x_1}\right)^2 + \left(\frac{\partial \varphi}{\partial x_2}\right)^2 + \left(\frac{\partial \varphi}{\partial x_3}\right)^2 = \omega_0^2 \varepsilon_0 \mu_0 \varepsilon(x_1, x_2, x_3). \tag{18}$$

6

As another example, the propagation of a wave traversing through the ionosphere between a satellite and the ground can also be investigated. If the tensor $\bar{\bar{\varepsilon}}$ of the electrically neutral plasma [3] is transformed into magnetic

dipole coordinates, using the dipole approximation of the Earth's magnetic field [4] and during the time interval of satellite's passage, the ionosphere is assumed to be independent of longitude (λ_g), then it can be shown that

$$\varphi = \gamma \cdot \lambda_g + f(r, \vartheta); \qquad \gamma = \text{const}, \tag{19}$$

where r is the geocentric distance and ϑ is the magnetic dipole latitude. Further, the partial differential equation for determining the function f follows as:

$$\begin{aligned} & a_1 \left(\frac{\partial f}{\partial r}\right)^4 + \frac{1}{r^4} a_2 \left(\frac{\partial f}{\partial \vartheta}\right)^4 + \frac{1}{r^2} a_3 \left(\frac{\partial f}{\partial r}\right)^2 \left(\frac{\partial f}{\partial \vartheta}\right)^2 + \\ & + 2 a_4 \left[\frac{1}{r} \left(\frac{\partial f}{\partial r}\right)^3 \left(\frac{\partial f}{\partial \vartheta}\right) + \frac{1}{r^3} \left(\frac{\partial f}{\partial r}\right) \left(\frac{\partial f}{\partial \vartheta}\right)^3\right] - \\ & - k_0^2 \left(a_5 - \frac{1}{k_0^2} \frac{\gamma^2}{r^2 \sin^2 \vartheta} a_9\right) \left(\frac{\partial f}{\partial r}\right)^2 - k_0^2 \left(\frac{1}{r^2} a_6 - \right. \\ & \left. - \frac{1}{k_0^2} \frac{\gamma^2}{r^4 \sin^2 \vartheta} a_{10}\right) \left(\frac{\partial f}{\partial \vartheta}\right)^2 - 2 k_0^2 \left(\frac{1}{r} a_7 - \right. \\ & \left. - \frac{1}{k_0^2} \frac{\gamma^2}{r^3 \sin^2 \vartheta} a_4\right) \left(\frac{\partial f}{\partial r}\right) \left(\frac{\partial f}{\partial \vartheta}\right) + \\ & + k_0^4 \left(a_8 - \frac{1}{k_0^2} \frac{\gamma^2}{r^2 \sin^2 \vartheta} a_{11} + \frac{1}{k_0^4} \frac{\gamma^4}{r^4 \sin^4 \vartheta} a_{12}\right) = 0 , \end{aligned} \tag{20}$$

where $\overline{\overline{\mu}}$ is assumed to be the identity tensor, a_i-s are the known functions of the components of $\overline{\overline{\varepsilon}}$ and $k_0^2 = \omega^2 \varepsilon_0 \mu_0$. The value of γ is prescribed by the excitation as a boundary condition. In case of a passage along the magnetic meridian $\gamma = 0$.

III. Weakly inhomogeneous, moving medium

W. P. BIRKEMEIER et al. published in 1968 their measuring results concerning the Doppler shift, coming into existence at about 900 MHz in tropospheric propagation, as a consequence of winds [6]. This effect may be important in Doppler-methods applied in several fields of space research and in its applications. Since the study [6] uses for this investigating effect a mechanical model, the following analysis is based on a new idea differing from the preceding one.

Assuming in the following that the flow is laminar or quasi-laminar the turbulent scattering will be neglected. For electromagnetic waves the Doppler phenomenon can be deduced, based on the theory of special relativity

[7], which in case of homogeneous media moving with a constant velocity v leads to

$$\omega' = \omega_0 \sqrt{1 - \frac{v^2}{c^2}} \frac{1}{\left(1 + \frac{v \cdot \cos \alpha'_v}{c} \cdot n\right)} \tag{21}$$

where the symbol (′) means the quantities that can be measured by an observer moving together with the medium (S' coordinate system), c is the light velocity in free space, α_v is the angle between the wave propagation vector and the velocity of the moving medium in system S' (!) and n is the refractive index also in system S' (!).

Expanding Equ. (21) for the case of $v \ll c$, the so-called "classical" Doppler formula is obtained, in which terms proportional to $(v/c)^i$, $i \geq 2$ may not be included [4]:

$$\Delta\omega = -\omega_0 \frac{v}{c/n} \cos \alpha_v . \tag{22}$$

Using Equ. (4), after well-known transformations

$$\Delta\omega = -\bar{k} \cdot \bar{v} . \tag{23}$$

1. Optical approximation

The electromagnetic wave itself has "experience" only on the change of motion velocity of the medium. Taking into account the manner of excitation exerted on the particles of the consecutive layer by the incident wave with a velocity different from the preceding one, the phenomena at the boundary of the successive layers can be studied by a set of receivers fixed parallel to the boundary in the layer of the changed velocity.

In case of optical approximation let it be assumed that entering the new layer the propagation vector $\bar{K}$ will not change, i.e.

$$\bar{K} = \bar{K}_{st} , \tag{24}$$

where $\bar{K}_{st}$ is the stationary propagation vector, which is the solution for (13) or (14).

As for the change of velocity in the medium it can be written in the form of

$$\overline{\Delta v} = \overline{\overline{\mathrm{Grad}}\, \bar{v}} \cdot \overline{\Delta s} \tag{25}$$

therefore — the total frequency shift along the phase-path P, defined in Chapter II, point 2 — is

$$\Delta\omega = -\int_p \overline{\mathrm{grad}\, \varphi_{st}} \cdot \overline{\overline{\mathrm{Grad}}\, \bar{v}} \cdot d\bar{s} . \tag{26}$$

2

It can be shown that by using the above approximation in a homogeneous case $\Delta\omega \equiv 0$, while if the propagation takes place in inhomogeneous medium, $\Delta\omega \neq 0$. Furthermore, it also appears that the mechanical model applied in [6] is equivalent to another version of this approximation, in which it is assumed that there is a total propagation symmetry and there are winds with $\bar{v} = \text{const}$ velocity between transmitter and receiver which are fixed with respect to the ground.

3. *Discussion according to the wave theory*

It immediately follows from the preceding considerations that in case of an exact treatment Equ. (24) may not hold. However, it is known that at the boundary of the two layers

$$\omega(\bar{r} + d\bar{r}) = \omega(\bar{r}) + \overline{\text{grad}}\ \omega \cdot \text{d}\bar{r} \,. \tag{27}$$

Using Equs (23) and (25) it appears from (27) that

$$\overline{\text{grad}}\ \omega = -\bar{K} \cdot \overline{\overline{\text{Grad}}}\ \bar{v} \,, \tag{28}$$

where the definitions (8) are valid. Examining Maxwell's equations on the base is of Equs (9) and (28), it can be shown that, if

$$\bar{E} = \bar{E}_0\, e^{j[\omega_0 t + \Delta\omega \cdot t - \varphi]},$$

$$\Delta\omega = \Delta\omega(\bar{r}, t),$$

then

$$\text{div}\,(\bar{\bar{\varepsilon}}\bar{E}) = -j(\bar{K} + \bar{K} \cdot \overline{\overline{\text{Grad}}}\ v \cdot \text{t})\bar{\bar{\varepsilon}}E \,, \tag{29}$$

$$\text{curl}\ \bar{H} = -j(\bar{\text{K}} + \bar{K}\ \overline{\overline{\text{Grad}}}\ \bar{v} \cdot t)\bar{H} \,.$$

Thus, generalizing the concept of the propagation vector

$$\overline{\mathfrak{K}} = \bar{K} + (\bar{K}\ \overline{\overline{\text{Grad}}}\ \bar{v})t = \overline{\text{grad}}\ \varphi - \overline{\text{grad}}\ \omega \cdot t \tag{30}$$

can be obtained, where $\omega = \omega_0 + \Delta\omega$. Solving Equs (10) in the original form with the aid of Equs (30), and here substituting $\overline{\mathfrak{K}}$ instead of $\bar{K}$, one arrives at the approximation of quasi-wave-theory.

Examination of (30) shows that assuming the form $\bar{E} = \bar{E}_0 e^{j\Phi}$,

$$\overline{\mathfrak{K}} = -\overline{\text{grad}}\,\Phi\,,$$
$$\omega = \frac{\partial \Phi}{\partial t} \tag{31}$$

(it can also be suitable to apply the symbols $\Phi = \omega_0 t - \psi$, $\psi = -\Delta\omega \cdot t + \varphi$).

Using these notations the Maxwell equations can be rewritten into a form, the solution of which was shown in Chapter II:

$$\begin{aligned}
&\overline{\mathfrak{K}} \times \bar{H} = -\varepsilon_0 \omega \bar{\varepsilon} \bar{E}\,,\\
&\overline{\mathfrak{K}} \times \bar{E} = \mu_0 \omega \bar{\mu} \bar{H}\,;\\
&\mu_0 \overline{\mathfrak{K}} \bar{\mu} \bar{H} = 0\,,\\
&\varepsilon_0 \overline{\mathfrak{K}} \bar{\varepsilon} \bar{E} = 0\,.
\end{aligned} \tag{32}$$

Expanding the generalized dispersion equation which comes from the solution of Equs (32), the conditional equation

$$\overline{\text{grad}}\,\frac{\partial \Phi}{\partial t} = \overline{\text{grad}}\,\Phi \cdot \overline{\text{Grad}}\,\bar{v} \tag{33}$$

must be used, as the generalized form of (28). In this way the electromagnetic wave pattern may exactly be given for a moving medium.

4

If velocity changes are great, and an accurate analysis is wanted, then a relativistic treatment must be followed.

5

Finally, it must be pointed out — based on the results of the theory of relativity — that those ways of treating the propagation in moving media, where the refractive index will be transformed into different possible manners from the "moving" system S' into the system S "at rest" — e.g. [8] and many others — are principally unjustified: The medium at rest for an electromagnetic wave is always the one in which its propagation takes place at the moment. A meaning to the refractive index can be given only in coordinate systems moving together with the medium ([7], [9] etc.). In those explanations where the transformation of the refractive index is made, a closer examination of the applied procedure reveals that the authors have not taken into account the

fact that the phase velocity c/n of the wave will be transformed in a different way from the one which is called the velocity summing of Einstein ([7] etc.). Finally, the results of measurements published in [6] do not follow from the previous "transformation" theory.

For example, the frequency shift mentioned above may be of importance by using geodetical Doppler measurements, as for $\Delta\omega/\omega \sim A \cdot \Delta v/c$, where A is a function of variation in the refractive index, the direction of propagation, etc. By average or great velocities of winds (3—30 m/s), $10^{-11} \leqq \Delta\omega/\omega \leqq 10^{-7}$, a measurable effect may occur.

6

The zero point shift appearing in measurements [6] can be explained in the same way as seen in Chapter III, point 3.

IV. Wave propagation in arbitrarily inhomogeneous media

In the following, a method for treating the propagation in arbitrary, linear media is to be found based on the results of the preceding two parts. The consideration will be applied from two points of view:

a) it is known that the propagating wave must not be of purely sinusoidal form in strong inhomogeneities;

b) combining the propagating methods determinable in homogeneous media, very good results have been achieved.

1

Now it is to be examined, whether the superposition of the solutions of Equs (10) and (32)—(33) will satisfy Maxwell's equations or not. If the set of $\bar{H}_i$ satisfies the mentioned equation system and $b_i = \text{const}$, then it can be obtained that

$$\operatorname{curl}\left(\sum_i b_i \bar{H}_i\right) = -j \sum_i b_i \bar{\mathfrak{K}}_i \times \bar{H}_i ,$$

$$\operatorname{div}\left(\bar{\mu} \sum_i b_i \bar{H}_i\right) = -j \sum_i b_i \bar{\mathfrak{K}}_i \bar{\mu} \bar{H}_i ,$$

$$\frac{\partial \sum_i b_i \bar{H}_i}{\partial t} = j \sum_i b_i \omega_i \bar{H}_i .$$

Thus in the weakly inhomogeneous case

$$\bar{H} = \sum_i b_i \bar{H}_{i0} \, e^{j(\omega_0 t - \psi_i)}$$

is a solution of Maxwell's equations.

On the other hand, Equs (10) and (32)—(33) form a linear equation system, thus substituting into $a_i(\bar{r}, t)\bar{H}_i$ instead of $\bar{H}_i$ corresponds only to a multiplication of both sides by $a_i(\bar{r}, t)$.

Finally it is clear that while

$$\bar{H} = \sum_i b_i \bar{H}_{i0} e^{j(\omega_0 t - \varphi_i)}$$

is periodic,

$$\bar{H} = \sum_i a_i(\bar{r}, t) \bar{H}_{i0} e^{j(\omega_0 t - \varphi_i)}$$

is not a periodic but an almost-periodic function.

2. *The general propagation equations*

Considering the remarks above, let the solution of Maxwell's equations be sought for in the form of a sum consisting of the products of the primary modes and combining functions, that is

$$\bar{E} = \sum_{i=1}^{n} a_i(\bar{r}, t) \bar{E}_{i0} e^{j(\omega_0 t - \varphi_i)}, \tag{34}$$

where the individual primary modes is

$$\bar{E}_i = \bar{E}_{i0} e^{j(\omega_0 t - \varphi_i)}.$$

Let the solution be

$$\begin{aligned}
&\overline{\mathfrak{K}}_i \times \bar{H}_i = -\varepsilon_0 \omega_i \bar{\bar{\varepsilon}} \bar{E}_i, \\
&\overline{\mathfrak{K}}_i \times \bar{E}_i = \mu_0 \omega_i \bar{\bar{\mu}} \bar{H}_i; \\
&\mu_0 \overline{\mathfrak{K}}_i \bar{\bar{\mu}} \bar{H}_i = 0, \\
&\varepsilon_0 \overline{\mathfrak{K}}_i \bar{\bar{\varepsilon}} \bar{E}_i = 0; \\
&\frac{\partial \overline{\mathfrak{K}}_i}{\partial t} = \overline{\mathfrak{K}}_i \cdot \overline{\overline{\operatorname{Grad}}\, \bar{v}}(\bar{r}).
\end{aligned} \tag{32a}$$

That is the solution of Equs (32)—(33), or in case of $\overline{\overline{\operatorname{Grad}}\, \bar{v}} = \bar{\bar{0}}$ that of Equs (10) with no regard of the fact that in strong inhomogeneities Equs (32a) are not longer identical with Maxwell's equations. It is obvious that

$$\overline{\mathfrak{K}}_i = \overline{\operatorname{grad} \psi_i} = -\overline{\operatorname{grad} \Phi_i}$$

and

$$\omega_i = \omega_0 - \frac{\partial \psi_i}{\partial t} = \frac{\partial \Phi_i}{\partial t}.$$

Keeping in mind all the above, let Maxwell's equations be investigated. Then

$$\operatorname{curl} \bar{H} = \operatorname{curl} \sum_i a_i \bar{H}_i = \sum_i \left(- j a_i \overline{\Re}_i \times \bar{H}_i + \overline{\operatorname{grad} a_i} \times \bar{H}_i + a_i \overline{\overline{\nabla}}_{TH_{0i}} \bar{H}_i \right), \quad (35)$$

where

$$\overline{\overline{\nabla}}_{TH_{0i}} = \begin{bmatrix} 0 & -\dfrac{\partial \ln H_{2i0}}{\partial x_3} & \dfrac{\partial \ln H_{3i0}}{\partial x_2} \\ \dfrac{\partial \ln H_{1i0}}{\partial x_3} & 0 & -\dfrac{\partial \ln H_{3i0}}{\partial x_1} \\ -\dfrac{\partial \ln H_{1i0}}{\partial x_2} & \dfrac{\partial \ln H_{2i0}}{\partial x_1} & 0 \end{bmatrix} \quad (36)$$

and it is known that $\overline{\overline{\nabla}}_{TH_{0i}}$ comes after solving (32a). In a similar manner

$$\operatorname{div} \bar{\mu} \bar{H} = \operatorname{div} \left(\bar{\mu} \sum_i a_i \bar{H}_i \right) = \sum_i \left(\langle \overline{\overline{S}}_{mTi} \bar{H}_i \rangle + a_i \langle \overline{\overline{\nabla}}_{\mu i} \bar{H}_i \rangle - j a_i \overline{\Re}_i \bar{\mu} \bar{H}_i \right), \quad (37)$$

where $\overline{\overline{S}}_{mTi}$ and $\overline{\overline{\nabla}}_{\mu i}$ are known from the solution of (32a) and are of the following form:

$$S_{mTi} = \begin{bmatrix} \dfrac{\partial a_i \, \mu_{11}}{\partial x_1} & \dfrac{\partial a_i \, \mu_{12}}{\partial x_1} & \dfrac{\partial a_i \, \mu_{13}}{\partial x_1} \\ \dfrac{\partial a_i \, \mu_{21}}{\partial x_2} & \dfrac{\partial a_i \, \mu_{22}}{\partial x_2} & \dfrac{\partial a_i \, \mu_{23}}{\partial x_2} \\ \dfrac{\partial a_i \, \mu_{31}}{\partial x_3} & \dfrac{\partial a_i \, \mu_{32}}{\partial x_3} & \dfrac{\partial a_i \, \mu_{33}}{\partial x_3} \end{bmatrix} \quad (38)$$

and

$$\overline{\overline{\nabla}}_{\mu i} = \begin{bmatrix} \mu_{11} \dfrac{\partial \ln H_{1i0}}{\partial x_1} & \mu_{12} \dfrac{\partial \ln H_{2i0}}{\partial x_1} & \mu_{13} \dfrac{\partial \ln H_{3i0}}{\partial x_1} \\ \mu_{21} \dfrac{\partial \ln H_{1i0}}{\partial x_2} & \mu_{22} \dfrac{\partial \ln H_{2i0}}{\partial x_2} & \mu_{23} \dfrac{\partial \ln H_{3i0}}{\partial x_2} \\ \mu_{31} \dfrac{\partial \ln H_{1i0}}{\partial x_3} & \mu_{32} \dfrac{\partial \ln H_{2i0}}{\partial x_3} & \mu_{33} \dfrac{\partial \ln H_{3i0}}{\partial x_3} \end{bmatrix}. \quad (39)$$

The symbol $\langle \; \rangle$ means the scalar sum of the individual components. Finally the derivative with respect to time:

$$\frac{\partial \bar{\mu} \bar{H}}{\partial t} = \frac{\partial}{\partial t} \left(\sum_i a_i \bar{\mu} \bar{H}_i \right) = \sum_i \left[\overline{\overline{S}}_{mTi} \bar{H}_i + a_i \left(\bar{\mu} \overline{\overline{\nabla}}_{tH_{0i}} \right) \bar{H}_i + j a_i \omega_i \bar{\mu} \bar{H}_i \right], \quad (40)$$

where $\overline{\overline{S}}_{mTi}$ and $\overline{\overline{\nabla}}_{TH_{0i}}$ follow from the solution of (32a) and have the form

$$\overline{\overline{S}}_{mTi} = \begin{bmatrix} \frac{\partial a_i \mu_{11}}{\partial t} & \frac{\partial a_i \mu_{12}}{\partial t} & \frac{\partial a_i \mu_{13}}{\partial t} \\ \frac{\partial a_i \mu_{21}}{\partial t} & \frac{\partial a_i \mu_{22}}{\partial t} & \frac{\partial a_i \mu_{23}}{\partial t} \\ \frac{\partial a_i \mu_{31}}{\partial t} & \frac{\partial a_i \mu_{32}}{\partial t} & \frac{\partial a_i \mu_{33}}{\partial t} \end{bmatrix} \tag{41}$$

and

$$\overline{\overline{\nabla}}_{TH_{0i}} = \begin{bmatrix} \frac{\partial \ln H_{1i0}}{\partial t} & 0 & 0 \\ 0 & \frac{\partial \ln H_{2i0}}{\partial t} & 0 \\ 0 & 0 & \frac{\partial \ln H_{3i0}}{\partial t} \end{bmatrix}. \tag{42}$$

The tensors in regard to $\overline{E}$ may be derived in an analogous way.

Using the formulas (35)—(42), Maxwell's equations can be written in the following form:

$$\begin{aligned} &\sum_{i=1}^{n} [\overline{\operatorname{grad} a_i} \times \overline{H}_i + a_i \overline{\overline{\nabla}}_{TH_{0i}} \overline{H}_i] - j \sum_{i=1}^{n} (a_i \overline{\mathfrak{K}}_i \times \overline{H}_i) = \\ &\quad = j\varepsilon_0 \sum_{i=1}^{n} (a_i \omega_i \overline{\overline{\varepsilon}} \overline{E}_i) + \varepsilon_0 \sum_{i=1}^{n} [\overline{\overline{S}}_{eti} \overline{E}_i + a_i (\overline{\overline{\varepsilon}} \overline{\overline{\nabla}}_{tE0i}) \overline{E}_i], \\ &\sum_{i=1}^{n} [\overline{\operatorname{grad} a_i} \times \overline{E}_i + a_i \overline{\overline{\nabla}}_{TE_{0i}} \overline{E}_i] - j \sum_{i=1}^{n} (a_i \overline{\mathfrak{K}}_i \times \overline{E}_i) = \\ &\quad = -j\mu_0 \sum_{i=1}^{n} (a_i \omega_i \overline{\overline{\mu}} \overline{H}_i) - \mu_0 \sum_{i=1}^{n} [\overline{\overline{S}}_{mti} \overline{H}_i + a_i (\overline{\overline{\mu}} \overline{\overline{\nabla}}_{tH0i}) \overline{H}_i]; \\ &\mu_0 \sum_{i=1}^{n} [\langle \overline{\overline{S}}_{mTi} \overline{H}_i \rangle + a_i \langle \overline{\overline{\nabla}}_{\mu i} \overline{H}_i \rangle] - j\mu_0 \sum_{i=1}^{n} (a_i \overline{\mathfrak{K}}_i \overline{\overline{\mu}} \overline{H}_i) = 0, \\ &\varepsilon_0 \sum_{i=1}^{n} [\langle \overline{\overline{S}}_{eTi} \overline{E}_i \rangle + a_i \langle \overline{\overline{\nabla}}_{ei} \overline{E}_i \rangle] - j\varepsilon_0 \sum_{i=1}^{n} (a_i \overline{\mathfrak{K}}_i \overline{\overline{\varepsilon}} \overline{E}_i) = 0. \end{aligned} \tag{43}$$

The terms in Equs (43) multiplied by j written in a new equation give an automatical set of equations, as a consequence of the choice of the modes, since it leads to the sum of the terms of Equ. (32a) multiplied by a_i.

Thus Maxwell's equations will be satisfied if the primary modes obtained from Equs (32a) will be combined with the functions a_i that can be determined from Equs (44) remaining from the set of Equs (43).

$$\sum_{i=1}^{n} [\overline{\text{grad}}\, a_i \times \bar{H}_i + a_i \bar{\bar{\nabla}}_{TH0i} \bar{H}_i] = \varepsilon_0 \sum_{i=1}^{n} [\bar{\bar{S}}_{eti} \bar{E}_i + a_i (\bar{\bar{\varepsilon}} \bar{\bar{\nabla}}_{tE0i}) \bar{E}_i] ,$$

$$\sum_{i=1}^{n} [\overline{\text{grad}}\, a_i \times \bar{E}_i + a_i \bar{\bar{\nabla}}_{TE0i} \bar{E}_i] = \mu_0 \sum_{i=1}^{n}{}' [\bar{\bar{S}}_{mti} \bar{H}_i + a_i (\bar{\bar{\mu}} \bar{\bar{\nabla}}_{tH0i}) \bar{H}_i], \tag{44}$$

$$\mu_0 \sum_{i=1}^{n} [\langle \bar{\bar{S}}_{mTi} \bar{H}_i \rangle + a_i \langle \bar{\bar{\nabla}}_{\mu i} \bar{H}_i \rangle] = 0 ,$$

$$\varepsilon_0 \sum_{i=1}^{n} [\langle \bar{\bar{S}}_{eTi} \bar{E}_i \rangle + a_i \langle \bar{\bar{\nabla}}_{\varepsilon i} \bar{E}_i \rangle] = 0 .$$

Thus by means of the functions $a_i(\bar{r}, t)$ determinable from Equs (44) and the inhomogeneous primary modes the complete propagating wave field can be described. If the variations in the amplitudes of the primary modes are small, then in (44) every tensor $\bar{\bar{\nabla}}$ can be substituted by $\bar{\bar{0}}$.

3

It is required in some cases to decide whether the separation of (43) to (32a) and (44) will give the complete solution system, that is whether any boundary condition can be satisfied or not. If all the medium parameters are ideal, and real in a mathematical sense, then it is clear that the solution system will be complete. Other remarks can be made only if $\bar{\bar{\varepsilon}}$ and $\bar{\bar{\mu}}$ are known. With respect to the fact that in inhomogeneous case $\bar{\bar{\varepsilon}}_{INH}$ and $\bar{\bar{\mu}}_{INH}$ are not identical with the medium parameters of the homogeneous case, and its form most often is not clarified, it is not worth while drawing further conclusion for the moment.

4

An important result is that the wave pattern in the most general case will be composed of minimally $n = 8$ primary modes as it is clear from Equs (44). Naturally, one may use more modes than 8, and this is often required by the boundary conditions as well. As special cases, the well-known mode-numbers describing the propagation in homogeneous media ($n = 1$, 2, or 4) also present themselves.

5

Based on the preceding, the non-relativistic Doppler equation [4, 5] for the propagation between satellite and ground station can also be given, which takes into consideration the general, multipath propagation and moving media, too.

V. A re-examination of "ray-tracing" programs

Before examining the "ray-tracing" programs let the refraction and reflection conditions on the boundary surface of two layers be considered. To do this, it is sufficient to make use only of simple medium parameters.

1. Law of "quadruple refraction-reflection"

Let the boundary surface between the layers ① and ② be the $y = 0$ plane. Further $\bar{\bar{\varepsilon}} = \varepsilon \cdot \bar{\bar{1}}$ be varying only along the y-coordinate and let this be $\bar{\bar{\mu}} = \bar{\bar{1}}$.

Let the media ① and ② be weakly inhomogeneous. (Then

$$\frac{\partial H_{i0}}{\partial x_j} \ll \frac{\partial \varphi}{\partial x_j}$$

and the terms referring to H_{i0} may be omitted from (44).) As for the classical ray-tracing method considering the medium as a sequence of homogeneous layers, let the numerical procedure be

$$\begin{aligned} \varepsilon(y) &= [1 - 1(y)]\varepsilon_1 + 1(y)\varepsilon_2 \,, \\ \varepsilon_2 - \varepsilon_1 &= \Delta\varepsilon \,. \end{aligned} \tag{45}$$

Then the requirements against the propagation vectors in the two layers are as follows:

$$\begin{aligned} K_{1i} &= k_0 \sqrt{\varepsilon_1} \\ \text{and} \qquad & \qquad (46) \\ K_{2i} &= k_0 \sqrt{\varepsilon_2} \,. \end{aligned}$$

By using these it can be shown that both in ① and in ② there are two possible modes. If $i = 1$ and $i = 2$ mean the forward and backward propagating waves, respectively, then these can be given as

$$\begin{aligned} \varphi_1 &= k_0 \sqrt{\varepsilon_1}\,(x \sin \alpha_{11}\, \bar{i} + y \cos \alpha_{11}\, \bar{j}) \,, \\ \varphi_2 &= k_0 \sqrt{\varepsilon_1}\,(x \sin \alpha_{12}\, \bar{i} + y \cos \alpha_{12}\, \bar{j}) \,, \\ \varphi_3 &= k_0 \sqrt{\varepsilon_2}\,(x \sin \alpha_{21}\, \bar{i} + y \cos \alpha_{21}\, \bar{j}) \,, \\ \varphi_4 &= k_0 \sqrt{\varepsilon_2}\,(x \sin \alpha_{22}\, \bar{i} + y \cos \alpha_{22}\, \bar{j}) \,, \end{aligned} \tag{47}$$

where α is the angle between the wave vector and y-axis (angle of incidence).

It can be shown that already three modes are sufficient, of the 4, to satisfy the boundary conditions [5]. That leads to the known law of refraction-reflection and that also formed the base of the former ray-tracing programs [10].

However, one can draw a rather more adequate picture with the aid of the method outlined in Chapter IV. Not affected by the fact whether homogeneous or weakly inhomogeneous layers are connected, the complete or "quadruple" laws of refraction-reflection — also involving the multiple reflections — can be determined by using (44), even if the individual layers are characterized by arbitrary medium parameter types.

(In case of more complicated boundary conditions it may be required to use a mode number $n > 4$ also, that leads to the multiple refraction laws.)

Let us evaluate this for the previous simple case: the non-disappearing operators:

$$\overline{\overline{S}}_{mTi} = \begin{bmatrix} 0 & 0 & 0 \\ 0 & \partial a_i/\partial y & 0 \\ 0 & 0 & 0 \end{bmatrix}$$

and

$$\overline{\overline{S}}_{eTi} = \begin{bmatrix} 0 & 0 & 0 \\ 0 & \dfrac{\partial a_i}{\partial y}\left[\varepsilon_1 + 1(y)\Delta\varepsilon\right] + a_i \Delta\varepsilon\,\delta(y) & 0 \\ 0 & 0 & 0 \end{bmatrix}, \tag{48}$$

where $1(y)$ is the unit step distribution, $\delta(y)$ is Dirac's delta-function. Due to the fact that the used distributions are particularly simple, the task can be solved with the function-theory. The Equs (44) will take the following form:

$$\begin{gathered} \sum_{i=1}^{n} \frac{\partial a_i}{\partial y} H_{iz} = 0\,, \\ \sum_{i=1}^{n} \frac{\partial a_i}{\partial y} E_{ix} = 0\,, \\ \sum_{i=1}^{n} \left\{ \left[\varepsilon_1 + 1(y)\Delta\varepsilon\right] \frac{\partial a_i}{\partial y} + a_i\, \Delta\varepsilon\, \delta(y) \right\} E_{iy} = 0\,, \\ 0 = 0\,. \end{gathered} \tag{49}$$

Let one mode more than it is minimally necessary be taken ($n = 4$) and considering the relations that follow from (10):

$$\begin{aligned} H_{iz0} &= H_{i0}\,, \\ E_{iy0} &= \sin \alpha_{ji}\, E_{i0}\,, \\ E_{ix0} &= -\cos \alpha_{ji}\, E_{i0}\,, \\ \frac{E_{i0}}{H_{i0}} &= \sqrt{\frac{\mu_0}{\varepsilon_0}} \frac{1}{\sqrt{\varepsilon_j}} = \frac{Z_0}{\sqrt{\varepsilon_j}}\,. \end{aligned} \tag{50}$$

Let us choose the combining functions, assuming a propagation in the (x, y)-plane, as:

$$\begin{aligned} a_1 &= A_1[1 - 1(y)], \\ a_2 &= A_2[1 - 1(y)], \\ a_3 &= A_3\, 1(y), \\ a_4 &= A_4\, 1(y). \end{aligned} \tag{51}$$

Developing and solving Equ. (49):

$$\begin{aligned} \sqrt{\varepsilon_1} \sin \alpha_{11} &= \sqrt{\varepsilon_2} \sin \alpha_{21}, \\ \alpha_{12} &= \pi - \alpha_{11}, \\ \alpha_{22} &= \pi - \alpha_{21}. \end{aligned} \tag{52}$$

Further, introducing the notation $B_i = A_i H_{i0}$, the relation for the amplitudes

$$\begin{aligned} B_1 &= \frac{1}{2}\left[(B_3 + B_4) + \frac{\sqrt{\varepsilon_1}\cos\alpha_{21}}{\sqrt{\varepsilon_2}\cos\alpha_{11}}(B_3 - B_4)\right], \\ B_2 &= \frac{1}{2}\left[(B_4 + B_3) + \frac{\sqrt{\varepsilon_1}\cos\alpha_{21}}{\sqrt{\varepsilon_2}\cos\alpha_{11}}(B_4 - B_3)\right], \end{aligned} \tag{53}$$

where the values of two amplitudes and one angle must be known from the boundary conditions.

Similarly can this law be derived for more complicated "refractive indices" too. Moreover, this method makes possible not only to separate the medium into homogeneous layers, but also even to weakly inhomogeneous layers.

2. Block diagram of modified ray-tracing

It can be settled on the basis of the preceding that the ray-tracing programs used up till now, running from transmitter to receiver, had not the ability to take the effect of multiple reflections into account. Thus, the phenomenon equivalent to the "resulting impedance" effect, due to the multiple reflections, in determining the input impedance and reflection index of transmission lines consisting of different sections was neglected [10].

Thus, if the medium will be decomposed into homogeneous or weakly inhomogeneous layers, one has to proceed according to the "modified ray-tracing programs", as follows:

a) The assumed exit direction and intensity of the ray departing from the receiver or the inhomogeneity will be assumed. Thus, B_4 or the correspond-

ing reflected ray will be zero, if the inhomogeneity has been left behind;

b) in the first layer — the one next to the transmitter — the incident and the reflected ray will be constructed on the base of the former triple refraction law and aware of the forward travelling part;

c) starting from the receiver backwards to the transmitter from layer to layer, using the laws of quadruple or multiple refractions, the incident and reflected ray can be determined;

d) after reaching the transmitter taking the final errors in direction and amplitude, the assumed starting values may be corrected and the whole procedure repeated.

Note: b) and *c)* may further be successive approximating subroutines.

Three essential differences can be seen with regard to the programs used up till now:

First, the refraction law must be modified; second, the procedure is carried out by starting from the receiver to the transmitter, opposite to the ray direction, instead of going from the transmitter towards the receiver; third, the adjacent layers need not necessarily be homogeneous, but strong inhomogeneities are excluded. Thus, the determination of reflective attenuation involves small errors only.

VI. Parameters of inhomogeneous media

Having found a method for determining the wave pattern not only in the step-by-step equivalent — seen in Chapter V — but in the inhomogeneous media themselves as well, let us try to find the primary modes and combining functions assuming a continuous $\varepsilon(\bar{r})$ and using the results of Chapter IV.

1

For solving the task, the phase function $\varphi(\bar{r})$, can be determined from the Eikonal equation (18), if $\bar{\bar{\varepsilon}} = \varepsilon(y)\bar{\bar{1}}$, $\bar{\bar{\mu}} = \bar{\bar{1}}$. Assuming that the propagation takes place in the $z = 0$-plane, which does not mean any restriction on the generality, the solutions of (18) are:

$$\begin{aligned} \varphi_1 &= k_0 \left[\gamma_1 x + \int \sqrt{\varepsilon(y) - \gamma_1^2}\, dy\right], \\ \varphi_2 &= k_0 \left[\gamma_2 x - \int \sqrt{\varepsilon(y) - \gamma_2^2}\, dy\right]. \end{aligned} \tag{54}$$

Similarly as in Chapter V, point 1 and using

$$\frac{E_{xi}}{H_{zi}} = \mp Z_0 \frac{\sqrt{\varepsilon(y) - \gamma_i^2}}{\varepsilon(y)};$$
$$\frac{E_{yi}}{H_{yi}} = Z_0 \frac{\gamma_i}{\varepsilon(y)} \tag{55}$$

it follows that $\gamma_1 = \gamma_2$.

However, the most important result is that if $\varepsilon(y)$ is a continuous function instead of the step function used in Chapter V, the determination of a_i leads to such an identity from which a_i cannot be evaluated. Because of $\gamma = \text{const}$, it follows that the number of available modes is not enough.

This contradiction can be solved only in a single way. In the preceding the medium parameters $\bar{\bar{\varepsilon}}$ and $\bar{\bar{\mu}}$ derived for homogeneous media have been used. The complete wave pattern — or more exactly the step-by-step *equivalent* of it — could be obtained if the medium was taken as being composed of homogeneous or quasi-homogeneous sections. At the same time, using these functions to describe the medium properties, it was impossible to obtain all the modes existing in the actual inhomogeneities. Thus, the medium parameters of the inhomogeneous and homogeneous media differ from each other, that is:

$$\bar{\bar{\varepsilon}}_{HOM} \neq \bar{\bar{\varepsilon}}_{INH},$$
$$\bar{\bar{\mu}}_{HOM} \neq \bar{\bar{\mu}}_{INH}. \tag{56}$$

2. *Permittivity of in-time stationary, electropolarized media*

With the aim of determining the actually arising electromagnetic wave in inhomogeneous media, and looking for possible new effects, which cannot be examined with the aid of the homogeneous modes, one has first to determine the medium parameters for an inhomogeneous case.

Taking $\bar{p} = q\bar{x}$ for the dipole arising from the displacement of the electron in homogeneous case [11], the equation of motion is

$$m \frac{d^2 \bar{x}}{dt^2} = -a\bar{x} - s \frac{d\bar{x}}{dt} + q\bar{E}_0 e^{j\omega t} \tag{57}$$

from which $\bar{x}$ can be determined, thus

$$\bar{p} = q\bar{x} = q \frac{\frac{q}{m} \bar{E}_0}{\left(\frac{a}{m} - \omega^2\right) + j\omega \frac{s}{m}} e^{j\omega t} = c_H \bar{E}, \tag{58}$$

$$\bar{D} = \varepsilon_0 \bar{E} + \bar{P}$$

and $$\bar{P} = N\bar{p}\,, \quad \bar{D} = \varepsilon_0 \varepsilon_H \bar{E}$$

give: $$\varepsilon_H = 1 + \frac{Nc_H}{\varepsilon_0}\,. \tag{59}$$

By the simultaneous examination of Maxwell's equations and the equation of motion, the effect caused by the inhomogeneities can be settled by using the self-consistent field-method. In the equation of motion one can find the elastic retaining force, the frictional retarding force, and the total excitation force (the effect of wave and inhomogeneity) that is, in a given place of the medium

$$m\frac{d^2\bar{x}}{dt^2} = -a\bar{x} - s\frac{d\bar{x}}{dt} + \bar{E}_g\,. \tag{60}$$

The problem now arises to obtain the component $\bar{F}_{g\,INH}$ of the force $\bar{F}_g = \bar{F}_{gE} + \bar{F}_{g\,INH}$. During the solution process the following scheme must be followed:

$\bar{\bar{\varepsilon}}_{INH} \rightarrow \varphi(\bar{r}) \rightarrow$ Maxwell's equations $\rightarrow a_i \rightarrow$ complete wave field

$\bar{E}_i, \bar{H}_i$

↓

equations of motion:

$\bar{P}$ total polarization vector

↓

$\bar{\bar{\varepsilon}}_{INH}\,(\bar{r}, \varphi, \omega)$

↓

Maxwell's equations

Owing to the fact that all the steps before establishing the equation of motion are justified, let this equation be considered in the following way.

3. *The "interaction tensor"*

As an effect of external excitation in electron polarized media, oscillating dipoles come into existence within the material. Thus, the investigation of the interaction between adjacent particles will be started by examining the field of the oscillating dipole.

The examination of the interaction between the particles will be carried out in a right angle or spherical coordinate system fixed with its z-axis or $\vartheta = \varphi_s = 0$-axis, respectively, to the dipole axis. That is, the z-axis is parallel to $\bar{x}$.

In this case, as is known [12], assuming a dipole moment $\bar{p} = \bar{p}_0 \, e^{j\omega t}$ and using the spherical coordinate system $(r, \vartheta, \varphi_s)$ above it arrives to:

$$
\begin{aligned}
E_r &= j \frac{\omega p_0}{4\pi} \left(\sqrt{\frac{\mu_0}{\varepsilon_0}} \frac{2}{r^2} - j \frac{2}{\omega \varepsilon_0 r^3} \right) \cos \vartheta \, e^{j(\omega t - kr)} , \\
E_\vartheta &= j \frac{\omega p_0}{4\pi} \left(j \frac{\omega \mu_0}{r} - j \frac{1}{\omega \varepsilon_0 r^3} + \sqrt{\frac{\mu_0}{\varepsilon_0}} \frac{1}{r^2} \right) \sin \vartheta \, e^{j(\omega t - kr)} , \\
E_{\varphi s} &= 0 , \\
H_r &= 0 , \\
H_\vartheta &= 0 , \\
H_{\varphi s} &= j \frac{\omega p_0}{4\pi} \left(j \frac{k}{r} + \frac{1}{r^2} \right) \sin \vartheta \, e^{j(\omega t - kr)} .
\end{aligned}
\tag{61}
$$

In the treatment of the interaction, considering that the effect according to the preceding arises in case of strong inhomogeneities, let the following be assumed: The scattering from the individual particles is fundamentally of another type, as there the sizes of the particles, and the distances between the particles are of the order of λ; thus let possibly be a meaning given to the density even at distances which are much smaller than the wavelength λ.

Let the distance between the domain investigated and the adjacent ones be $\Delta r \ll \lambda$, that is, very small in the unit system being used. The terms depending on distance in the field components for the adjacent domains are:

$$
\frac{1}{\Delta r} \ll \frac{1}{\Delta r^2} \ll \frac{1}{\Delta r^3} , \tag{62a}
$$

while for those farther off

$$
\frac{1}{2} \, \frac{1}{\Delta r} \ll \frac{1}{4} \, \frac{1}{\Delta r^2} \ll \frac{1}{8} \, \frac{1}{\Delta r^3} \quad \text{etc.} \tag{62b}
$$

It is to be seen from (62) that it is sufficient to investigate the terms proportional to $1/r^3$ and not each of them, but only the effect of the adjacent domains.

In the point under consideration the dipole moment is given by

$$
p(\bar{r}) = qN(\bar{r})\bar{x}(\bar{r}) \cdot \Delta V , \tag{63}
$$

where the origin of the spherical coordinate system fixed to $\bar{x}$ is the point $\bar{r}$. Thus

$$\bar{p}(\bar{r} + \Delta\bar{r}) = q[N(\bar{r}) + \overline{\text{grad}}\, N \cdot \Delta\bar{r}]\bar{x}(\bar{r} + \Delta\bar{r})\Delta V \tag{64}$$

$$\Delta V = \Delta r^3 \sin\vartheta\, \Delta\vartheta\, \Delta\varphi_s\,. \tag{65}$$

The field of this dipole moment, which is of interest, is given by

$$\bar{E} = \frac{q}{4\pi\varepsilon_0}(N + \overline{\text{grad}}\, N \cdot \Delta\bar{r})\{3[\bar{x}(\bar{r}+\Delta\bar{r})\,\bar{e}_{\Delta r}]\,\bar{e}_{\Delta r} - \bar{x}(\bar{r} + \Delta\bar{r})\} \cdot \sin\vartheta\, d\vartheta\, d\varphi_s\,, \tag{66}$$

where $\bar{e}_{\Delta r}$ is the unit vector pointing towards the direction of $\Delta\bar{r}$.

The total field generated by the adjacent domains will be obtained from summarizing $\bar{E}$ in the $0 \leqq \vartheta \leqq \pi/2$ and $0 \leqq \varphi_s \leqq \pi$ range of angles, after having reduced the four $\bar{E}$-s belonging to the four conjugated directions. The conjugated direction are

$$\begin{aligned} &\Delta\bar{r} && \vartheta\,,\ \varphi_s\,:\\ &-\Delta\bar{r} && (\pi-\vartheta),(\pi+\varphi_s)\,;\\ &\Delta\bar{r}^* && (\pi-\vartheta),\ \varphi_s\,;\\ &-\Delta\bar{r}^* && \vartheta\,,(\pi+\varphi_s)\,. \end{aligned} \tag{67}$$

Further, using $\bar{x}(\bar{r} + \Delta\bar{r}) = \bar{x}(\bar{r}) + \overline{\overline{\text{Grad}}\,\bar{x}}\,\Delta\bar{r}$ and writing Equ. (66) for all four directions, each expression of field intensity can be divided into four parts:

I. Stationary term — independent of $\overline{\text{grad}}\, N$ and $\overline{\overline{\text{Grad}}\,\bar{x}}$;

II. term depending on the wave — depends on $\overline{\overline{\text{Grad}}\,\bar{x}}$;

III. term proportional to the gradient — depends on $\overline{\text{grad}}\, N$;

IV. inhomogeneous term — proportional to the product of $\overline{\text{grad}}\, N$ and $\overline{\overline{\text{Grad}}\,\bar{x}}$.

The terms II and III compensate each other, thus neither the inhomogeneous excitation caused by the propagating wave in homogeneous medium, nor the inhomogeneity at static or quasistationary excitations has any effect at all. The sum of the stationary terms $\sim \bar{x}$, that is it has no moment on the dipole but only effects the coefficient of the elastic retaining force in Equ. (60). The sum of the inhomogeneous terms which play an important role:

$$\bar{E}_{\text{IV}} = \frac{q \sin\vartheta\, d\vartheta\, d\varphi_s}{2\pi\varepsilon_0}\{\overline{\text{grad}}\, N \cdot \overline{\Delta r}\ [3(\overline{\overline{\text{Grad}}\,\bar{x}} \cdot \overline{\Delta r}\ \cdot \bar{e}_{\Delta r})\,\bar{e}_{\Delta r} - \overline{\overline{\text{Grad}}\,\bar{x}} \cdot \overline{\Delta r}] + \overline{\text{grad}}\, N \cdot \overline{\Delta r}^*[3(\overline{\overline{\text{Grad}}\,\bar{x}} \cdot \overline{\Delta r}^* \cdot \bar{e}_{\Delta r^*})\,\bar{e}_{\Delta r^*} - \overline{\overline{\text{Grad}}\,\bar{x}} \cdot \overline{\Delta r}^*]\}\,. \tag{68}$$

Investigating the value of $\overline{\Delta r}$, one can see that as the density determines the average distance of the particles, therefore:

$$\overline{\Delta r} = \delta N^{-1/3} \bar{e}_{\Delta r}\,, \tag{69}$$

where δ is a constant characterizing the structure of the medium. As a consequence of examining the directions, it follows that

$$e_{\Delta r}{}^{*} = \bar{e}_{\Delta r} - \frac{\sqrt{2(1+\cos 2\vartheta)}}{x}\,\bar{x}. \tag{70}$$

Further, in the system fixed to $\bar{x}$, let $\overline{\mathrm{Grad}}\;\bar{x} = (g_{ik})$.

Developing $\bar{E}_{\mathrm{IV}}$ and then integrating in ϑ and φ_s, one can find that the field arising because of the existence of the inhomogeneity

$$\bar{E}_{INH} = \frac{q}{60\,\varepsilon_0}\,\frac{\delta^2}{\sqrt[3]{N^2}}\,(\bar{\bar{A}}\,\overline{\mathrm{Grad}}\,N), \tag{71}$$

where $\bar{\bar{A}}$ is the "interaction tensor". In a coordinate system fixed to $\bar{x}$, it may be written:

$$\bar{\bar{A}} = \begin{bmatrix} (59g_{11} + 33g_{22} - 12g_{33}) & (33g_{21} - 7g_{12}) & (8g_{13} - 12g_{31}) \\ (33g_{12} - 7g_{21}) & (33g_{11} + 59g_{22} - 12g_{33}) & (8g_{23} - 12g_{32}) \\ (-52g_{31} - 12g_{13}) & (-52g_{32} - 12g_{23}) & (-12g_{11} - 12g_{22} + 56g_{33}) \end{bmatrix}. \tag{72}$$

4. *Equation of motion*

Considering that in a coordinate system which is at rest with respect to the observer (laboratory), the vector $\bar{x}$ has a complicated motion, it is expedient to carry out the further computations, not in the system fixed to $\bar{x}$, but in a Cartesian system, fixed to the laboratory. Thus, the equation of motion at a given point of the material is:

$$m\,\frac{\partial^2 \bar{x}}{\partial t^2} = -a\bar{x} - s\,\frac{\partial \bar{x}}{\partial t} + q\bar{E}_0\,e^{j[\omega_0 t - \psi(\bar{r}} + \frac{q^2\,\delta^2}{60\,\varepsilon_0\,N^{2/3}}\,(\bar{\bar{A}}\,\overline{\mathrm{grad}}\,N). \tag{73}$$

In order to develop this equation the tensor $\bar{\bar{A}}$ must be transformed into the laboratory system, and there it must be placed under a closer examination. Let the coordinate systems be fixed to $\bar{x}(S')$ and that fixed to the laboratory (S) closed to each other in such manner that the x'-axis should be in the $x - z'$ plane. (This means an uncertainty in transformation if the x-axis is perpendicular to the z' axis.) Furthermore, from Equ. (73) it can be seen that at the transformation the computational laws of three-dimensional space defined on

the complex number-body must be used. Among these it must be emphasized hat the norm of a vector in this system is:

$$v^2 = \bar{v} \cdot \bar{v}^*$$

or more exactly

$$v^2 = \bar{v}^T \bar{v}^*,$$

where the symbol (*) means the complex conjugated quantity in the following, and the upper index T means the transposed tensor related to the original one.

It can be shown, based on (73), that the solution is needed for the following form:

$$\bar{x} = \bar{x}_0 (\bar{r})\, e^{j[\omega_0 t - \psi(\bar{r})]}.$$

Further, the equation holds at the domain in question and to its closest, adjacent ones. This means an area much smaller in its dimensions than λ, according to the preceding. Thus, it is correct to assume that

$$\frac{1}{x_{i0}} \frac{\partial x_{i0}}{\partial x_j} \ll \frac{\partial \psi}{\partial x_j}. \tag{74}$$

Here it should be noted that the boundary surface of dielectrics and gases or the front surface of shock waves, etc. can be described with the aid of a step function $-1(\bar{r})$ — just because of this restriction, after determining the laws of multiple refraction for inhomogeneous layers, as was seen in Chapter V.

From (74) it can be deduced that in the system S

$$\overline{\overline{\mathrm{Grad}}}\, \bar{x} = -j \bar{x}\, \overline{\mathrm{grad}}^T \psi = -j \bar{x} \bar{K}^T. \tag{75}$$

Making use of all the above outlined it can be shown that

$$\bar{\bar{A}} = 52\, j (\bar{x}\bar{K}^T) + 12\, j (\bar{x}\bar{K}^T)^T - 120\, j (\bar{x}^T \bar{K}) \frac{\bar{x}\bar{x}^T}{x^2} + \bar{\bar{F}} + \bar{\bar{G}}, \tag{76}$$

where

$$\bar{\bar{F}} = 12\, j \frac{(\bar{x}^{T*} \bar{K})}{x_2^2 + x_3^2} \begin{bmatrix} 0 & 0 & 0 \\ 0 & x_3^2\, e^{j2\varphi_3} & -x_2 x_3\, e^{j(\varphi_2+\varphi_3)} \\ 0 & -x_2 x_3\, e^{j(\varphi_2+\varphi_3)} & x_2^2\, e^{j2\varphi_2} \end{bmatrix} \tag{77}$$

and

$$\bar{\bar{G}} = 12\, j \frac{(\bar{x}^T \bar{x})\,(\bar{x}^T \bar{K})}{x^4 (x_2^2 + x_3^2)} \begin{bmatrix} (x_2^2+x_3^2)^2 & -(x_2^2+x_3^2)\, x_1 x_2\, e^{j(\varphi_1-\varphi_2)} & -(x_2^2+x_3^2)\, x_1 x_3\, e^{j(\varphi_1-\varphi_3)} \\ -(x_2^2+x_3^2)\, x_1 x_2\, e^{j(\varphi_1-\varphi_2)} & x_1^2 x_2^2\, e^{j2(\varphi_1-\varphi_2)} & x_1^2 x_2 x_3\, e^{j(2\varphi_1-\varphi_2-\varphi_3)} \\ -(x_2^2+x_3^2)\, x_1 x_3\, e^{j(\varphi_1-\varphi_3)} & x_1^2 x_2 x_3\, e^{j(2\varphi_1-\varphi_2-\varphi_3)} & x_1^2 x_3^2\, e^{j2(\varphi_1-\varphi_3)} \end{bmatrix} \tag{78}$$

further

$$\bar{x}_0 = x_1 e^{jq_1} \bar{e}_1 + x_2 e^{jq_2} \bar{e}_2 + x_3 e^{jq_3} \bar{e}_3. \tag{79}$$

After the appropriate reductions the final form of the equation of motions:

$$\begin{aligned} q\bar{E}_0 = & \left[(a - m\omega^2) + j\left(s\omega - \frac{13}{15} B\bar{K}^T \overline{\operatorname{grad} N}\right)\right] \bar{x} + j2B \frac{(\bar{x}^T \bar{K})(\bar{x}^{T*} \overline{\operatorname{grad} N})}{x^2} \bar{x} - \\ & - j\frac{1}{5} B(\bar{x}^T \overline{\operatorname{grad} N}) \bar{K} + j\frac{1}{5} B \frac{1}{x_2^2 + x_3^2} \left\{(\bar{x}^{T*} \bar{K})[\bar{x} \times (\bar{x} \times \overline{\operatorname{grad} N})_1 \bar{e}_1] - \right. \\ & \left. - (\bar{x}^T \bar{K}) \frac{\bar{x}^T \bar{x}}{x^2} [\bar{x}^* \times (\bar{x} \times \overline{\operatorname{grad} N})]_1 \frac{\bar{x} \times (\bar{e}_1 \times \bar{x}^*)}{x^2}\right\}, \end{aligned} \tag{80}$$

where

$$B = \frac{q^2 \delta^2}{\varepsilon_0} N(r)^{-2/3}.$$

5. *The "modified Eikonal equation"*

According to the solution method outlined in Chapter VI, point 2, now the medium parameters can be determined by the development of Equ. (80) together with Maxwell's equations.

As a first approximation, let the last two terms in Equ. (80) be neglected. Thus

$$q\bar{E}_0 = \left\{(a - m\omega^2) + j\left[s\omega - \frac{13}{15} B\bar{K}^T \overline{\operatorname{grad} N} + 2B \frac{(\bar{x}^T \bar{K})(\bar{x}^{T*} \overline{\operatorname{grad} N})}{x^2}\right]\right\} \bar{x} \tag{81}$$

that is

$$q\bar{E}_0 = \beta \bar{x}\,.$$

Thus, introducing the unit vector $\bar{e}_0 = \bar{E}_0 / E_0$, where $E_0 = \sqrt{\bar{E}_0^T \bar{E}_0^*}$, it is clear that ε_{INH} is a scalar quantity, and

$$\varepsilon_{INH} = 1 + \frac{q^2}{\varepsilon_0} N \frac{1}{(a - m\omega^2) + j\left[s\omega - \frac{13}{15} B(\bar{K}^T \overline{\operatorname{grad} N}) + 2B(\bar{e}_0^T \bar{K})(\bar{e}_0^{T*} \overline{\operatorname{grad} N})\right]}. \tag{82}$$

In this case that part of Maxwell's equations, which is applicable for determining the primary modes — (10) — has the following form:

$$\begin{aligned} & \bar{K} \times \bar{H} = -\varepsilon_0 \omega \varepsilon_{INH} \bar{E}\,, \\ & \bar{K} \times \bar{E} = \mu_0 \omega \bar{H}\,; \\ & \mu_0 \bar{K} \bar{H} = 0\,, \\ & \varepsilon_0 \bar{K} \varepsilon_{INH} \bar{E} = 0 \end{aligned} \tag{83}$$

as for $\bar{\bar{\mu}} = \bar{\bar{1}}$ and $\bar{\bar{\varepsilon}} = \varepsilon_{INH}\bar{\bar{1}}$. From this it can be seen that

$$\bar{K}\bar{E} = \bar{K}\bar{E}_0 = 0$$

that is $(\bar{e}_0^T \bar{K}) = 0$. Therefore,

$$\varepsilon_{INH} = 1 + \frac{1}{\varepsilon_0} \frac{q^2 N}{(a - m\omega^2) + j\left[s\omega - \frac{13}{15} D(\bar{K}\,\overline{\text{grad}}\, N)\right]} . \tag{84}$$

As a further example, let the generalized dispersion equation belonging to Equ. (84) be examined. Using (59) it gives:

$$\varepsilon_{INH} = \varepsilon_H - \frac{(1-\varepsilon_H)^{4/3}(\bar{K}\,\overline{\text{grad}}\,\varepsilon_H)}{c_1\,\varepsilon_H + c_2(1-\varepsilon_H)^{1/3}(\bar{K}\,\overline{\text{grad}}\,\varepsilon_H)} . \tag{85}$$

It can often be assumed, e.g. in troposphere, etc., that $(1 - \varepsilon_H) \ll 1$, thus in many cases the second term of the denominator is negligible, that is:

$$\varepsilon_{INH} \cong \varepsilon_H - c\frac{1-\varepsilon_H}{\varepsilon_H}\sqrt[3]{1-\varepsilon_H}\,(\bar{K}\,\overline{\text{grad}}\,\varepsilon_H), \tag{86}$$

where c_1, c_2 and c are constants, resulting from the preceding and

$$\varepsilon_H = 1 + \frac{c_H}{\varepsilon_0} N(\bar{r}) = \varepsilon_H(\bar{r}).$$

Writing the dispersion equation belonging to (83), the *modified* Eikonal-equation can be obtained:

$$\overline{\text{grad}}\left[\overline{\text{grad}}\varphi - j\omega^2\,\varepsilon_0\,\mu_0\,c\,\frac{1-\varepsilon_H(\bar{r})}{\varepsilon_H(\bar{r})}\sqrt[3]{1-\varepsilon_H(\bar{r})}\,\overline{\text{grad}}\,\varepsilon_H(\bar{r})\right] = \omega^2\,\varepsilon_0\,\mu_0\,\varepsilon_H(\bar{r}) \tag{87}$$

which differs from the commonly used Eikonal equation. Equ. (87) gives the commonly used form of Eikonal equation (18), if $\overline{\text{grad}}\ \varepsilon_H = 0$:

$$\text{grad}^2\varphi = \omega^2\varepsilon_0\mu_0\varepsilon_H(\bar{r}) .$$

6

The tensor $\bar{\bar{\varepsilon}}_{INH}$ can be simply derived, also by neglecting the last term of Equ. (80). Thus Equ. (80) can be written in the form of

$$q\bar{E} = \bar{\bar{P}}\bar{x} , \tag{88}$$

where

$$p_{11} = (a - m\omega^2) + j\left[s\omega - \frac{1}{15} Б(16K_1 \operatorname{grad}_1 N + 13K_2 \operatorname{grad}_2 N + 13K_3 \operatorname{grad}_3 N)\right],$$

$$p_{12} = -j\frac{1}{5} БK_1 \operatorname{grad}_2 N,$$

$$p_{13} = -j\frac{1}{5} БK_1 \operatorname{grad}_3 N,$$

$$p_{21} = -j\frac{1}{5} БK_2 \operatorname{grad}_1 N,$$

$$p_{22} = (a - m\omega^2) + j\left[s\omega - \frac{1}{15} Б(13K_1 \operatorname{grad}_1 N + 16K_2 \operatorname{grad}_2 N + 13K_3 \operatorname{grad}_3 N)\right],$$

$$p_{23} = -j\frac{1}{5} БK_2 \operatorname{grad}_3 N, \tag{89}$$

$$p_{31} = -j\frac{1}{5} БK_3 \operatorname{grad}_1 N,$$

$$p_{32} = -j\frac{1}{5} БK_3 \operatorname{grad}_2 N,$$

$$p_{33} = (a - m\omega^2) + j\left[s\omega - \frac{1}{15} Б(13K_1 \operatorname{grad}_1 N + 13K_2 \operatorname{grad}_2 N + 16K_3 \operatorname{grad}_3 N)\right].$$

Based on this

$$\bar{\bar{\varepsilon}}_{INH} = \bar{\bar{1}} + \frac{q^2 N}{\varepsilon_0} \bar{\bar{P}}^{-1}. \tag{90}$$

7

A general examination shows that Equ. (80) cannot be developed in a simple manner. The solution method outlined in Chapter VI, point 2 is applicable even in this case, but the role of the generalized dispersion equation is overtaken by the equation of motion. Making use of the former example, and combining Equ. (80) with the part of Maxwell's equations concerning the primary modes, the following conditional equation will be obtained:

$$q\bar{E}_0 + \frac{\beta}{\alpha} \bar{\bar{\Gamma}}\bar{E}_0 + j2\frac{Бk_0^2}{\alpha} \frac{(\bar{K}_T \bar{E}_0)(\bar{G}^T(\bar{\bar{\Gamma}}\bar{E}_0)^*)}{(\bar{\bar{\Gamma}}\bar{E}_0)^T(\bar{\bar{\Gamma}}\bar{E}_0)^*} \bar{\bar{\Gamma}}\bar{E}_0 - j\frac{Б}{5\alpha}(\bar{G}^T \bar{\bar{\Gamma}}\bar{E}_0)\bar{K} -$$

$$- j\frac{Б}{5\alpha}\left\{\frac{(\bar{\bar{\Gamma}}\bar{E}_0)^T(\bar{\bar{\Gamma}}\bar{E}_0)}{(\bar{\bar{\Gamma}}\bar{E}_0)^T(\bar{\bar{\Gamma}}\bar{E}_0)^*} \cdot \frac{[(\bar{\bar{\Gamma}}\bar{E}_0)^* \times (\bar{\bar{\Gamma}}\bar{E}_0 \times \bar{G})]_1}{(\bar{\bar{\Gamma}}\bar{E}_0)^T(\bar{\bar{\Gamma}}\bar{E}_0)^*} \cdot \right.$$

$$\left. \cdot \frac{\bar{\bar{\Gamma}}\bar{E}_0 \times [\bar{e}_1 \times (\bar{\bar{\Gamma}}\bar{E}_0)^*]}{(\bar{\bar{\Gamma}}\bar{E}_0)_2(\bar{\bar{\Gamma}}\bar{E}_0)_2^* + (\bar{\bar{\Gamma}}\bar{E}_0)_3(\bar{\bar{\Gamma}}\bar{E}_0)_3^*} (\bar{K}^T \bar{\bar{\Gamma}}\bar{E}_0) - \right. \tag{91}$$

$$- \frac{\overline{\overline{\Gamma}}\bar{E}_0 \times (\overline{\overline{\Gamma}}\bar{E}_0 \times \bar{G})_1 \bar{e}_1}{(\overline{\overline{\Gamma}}\bar{E}_0)_2 (\overline{\overline{\Gamma}}\bar{E}_0)_2^* + (\overline{\overline{\Gamma}}\bar{E}_0)_3 (\overline{\overline{\Gamma}}\bar{E}_0)_3^*} [\bar{K}^T (\overline{\overline{\Gamma}}\bar{E}_0)^*] \Bigg\} = 0 ,$$

where

$$\begin{aligned} \alpha &= \omega^2 \varepsilon_0 \mu_0 q N(\bar{r}) , \\ \beta &= (a - m\omega^2) + j \left(s\omega - \frac{13}{15} B \bar{K}^T \bar{G} \right) , \\ B &= \frac{q^2 \delta^2}{\varepsilon_0} N^{-2/3}(\bar{r}) , \\ \bar{G} &= \overline{\text{grad}}\, N(\bar{r}) , \\ \overline{\overline{\Gamma}} &= k_0^2 \overline{\overline{1}} + \overline{\overline{\Lambda}} = k_0^2 \overline{\overline{1}} + (\bar{K} \times \bar{K} \times \ldots). \end{aligned} \tag{92}$$

It can be seen that (91) is a linear, homogeneous equation in $| \bar{E}_0 |$.

The method of solution:

a) Let us first solve Equ. (91). The boundary conditions consist of the starting direction of $\bar{E}_0$ and the value of $\varphi(\bar{r})$ along a given surface. The unknowns to be determined are: the function $\varphi(\bar{r})$ and the complex "direction coefficients". The fourth — additional — equation presents itself from the internal connection of the complex direction coefficients, called the norm-equation.

b) After these from Maxwell's equations:

$$\frac{\bar{x}}{\bar{E}} = - \frac{1}{\alpha} \overline{\overline{\Gamma}},$$

that is

$$\overline{\overline{\varepsilon}}_{INH} = \overline{\overline{1}} - \frac{1}{k_0^2} \overline{\overline{\Gamma}} \tag{93}$$

$|\bar{E}_0|$ and $\bar{H}_0$ can be given from the primary-mode part of Maxwell's equations.

c) Finally, the complete wave pattern can be constructed by using the method of combining functions.

VII. Conclusions

All the above considerations made it possible to give a general theory for investigating the propagation in inhomogeneous media together with calculation (and "design") methods. It can be assumed that the numerous propagation versions can be investigated on computers applying the "literal algebra". The next task is to search for new phenomena based on the results of Chapters II—V, and it must in every case be completed by determining $\overline{\overline{\varepsilon}}_{INH}$, $\overline{\overline{\mu}}_{INH}$ in the different materials. Finally, in regard to the moving media the generalization of propagation in inhomogeneous, moving media must be given with the aid of relativistic electrodynamics.

*

Acknowledgements are due to Prof. Dr. K. SIMONYI, furthermore to Dr. Gy. TARCSAI geophysicist, Dr. A. CSURGAY electrical engineer and I. FERENCZ electrical engineer.

REFERENCES

1. FERENCZ, Cs.: Wave Propagation in Inhomogeneous, Anisotropic Time-Varying Medium. *Periodica Polytechnica* **12** (1968), 347—355.
2. MATTILA, P.: Wave Propagation in Anisotropic Media, Electromagnetic Wave Theory (Edited by J. Brown); Part I. Pergamon Press 1967; 155—156.
3. ALLIS, W. P.—BUCHSBAUM, S. J.—BERS, A.: Waves in Anisotropic Plasmas. M. I. T. Press 1963.
4. DRAHOS, D.—FERENCZ, Cs.—FERENCZ, I.—HORVÁTH, F.—TARCSAI, GY.: Some Theoretical Contributions Concerning the Doppler Geodetical Measurements. Paper presented at *COSPAR XII. Plenary Meeting* WG. I-a.8, Praha 1969 (to be published in *Space Research*).
5. FERENCZ, Cs.—FERENCZ, I.—TARCSAI, GY.: Refraction Problems and Wave Propagation in Doppler Geodetical Measurements. Paper presented at the conference on *Observation of Artificial Satellites of the Earth*, Varna 1969 (to be published in *Наблюдение ИСЗ*).
6. BIRKEMEIER, W. P.—MERRIL, H. S.—SARGEANT, D. H.—THOMSON, D. W.— BEAMER, C. M.—BERGEMANN, G. T.: Observation of Wind-Produced Doppler-Shifts in Tropospheric Propagation. *Radio Science* (New series) **3** (1968), No. 4.
7. NOVOBÁTZKY, K.: A relativitás elmélete (Theory of Relativity). Tankönyvkiadó, Budapest 1951.
8. UNZ, H.: Relativistic Magnetoionic Theory for Drifting Plasma. *Radio Science* (New series) **3** (1968), No. 3.
9. SYNGE, J. L.: Relativity, the Special Theory. North-Holland Publishing Co. 1965.
10. Special Issue on Ray-racing. *Radio Science* (New series) I (1968), No. 1.
11. SIMONYI, K.: Elektronfizika (Electronphysics). Tankönyvkiadó, Budapest 1965.
12. SIMONYI, K.: Foundations of Electrical Engineering. Pergamon Press 1963.

Wellenausbreitung in inhomogenen linearen Medien. In der Arbeit wird zuerst die Ausbreitung der elektromagnetischen Wellen in schwach inhomogenenen Medien untersucht, wenn das Medium stationär ist, mit der Zeit veränderliche Parameter aufweist und schließlich strömt. In Zusammenhang hiermit wird darauf hingewiesen, daß die Theorie die einheitliche Behandlung von vielen bekannten Ergebnissen ermöglicht und die exakte Untersuchung der Erscheinungen bei der Ausbreitung in strömenden Medien ermöglicht. Hiernach wird für beliebige Inhomogenitäten die Methode der Bestimmung des vollständigen Wellenbilds mittels Summierung der "inhomogenen Grundformen" gezeigt. Es wird angegeben, auf welche Weise das "vierfache und mehrfache Brechungs-Spiegelungsgesetz" gewonnen werden kann. Auf dieser Grundlage werden die ray-tracing Programme revidiert und das grundlegende Schema der "modifizierten ray-tracing" Programme wird angegeben. Schließlich wird nachgewiesen, daß die homogenen und die inhomogenen Kennwerte des Mediums nicht identisch sind und — beispielsweise — wird die inhomogene Permittivität des elektronen-polarisierten Mediums bestimmt. Die Methode für die Bestimmung des Wellenbilds, der "Wechselwirkungstensor" und beispielsweise die "modifizierte Eikonal-Gleichung" werden angegeben.

Распространение волн в негомогенных линейных средах *(Ч. Ференц)*. В статье сначала исследуется распространение электромагнитных волн в слабо негомогенных средах, если среда является стационарной, с изменяющимся во времени параметром и, наконец, если движется. В связи со сказанным указывается на то, что теория дает возможность единного рассмотрения ряда известных результатов и позволяет осуществить точное исследование явлений, возникающих при распространении в движущихся средах. После чего, суммируя «негомогенные основные модусы», для случая произвольных негомогенностей демонстрируется метод определения полной волновой картины. Указывается, каким путем можно получить «закон четырехкратного и многократного преламления — отражения». На основе этого пересматриваются программы ray-tracing и приводится основная схема «измененных ray-tracing» программ. Наконец показано, что показатели гомогенных и негомогенных сред не являются идентичными и, используя в качестве примера электронно-поляризационную среду, определяется негомогенная пермитивность. Указываaерся метод опеделения волновой картины, "тензор взаимодействия,, и для пимера приводится "измененное уравнение Ейконала".

Acta Technica Academiae Scientiarum Hungaricae; Tomus 68 (1—2), pp. 245—253 (1970)

PREPARATION AND PROPERTIES OF GaAs SINGLE CRYSTLS

E. PAPP DOCTOR OF CHEM. SC., S. ZSINDELY, T. LEGÁT
RESEARCH INSTITUTE FOR NON-FERROUS METALS, BUDAPEST
and
B. PŐDÖR
RESEARCH INSTITUTE FOR TECHNICAL PHYSICS OF THE HUNGARIAN ACADEMY OF SCIENCES, BUDAPEST

[Manuscript received June 23, 1969]

GaAs single crystals were prepared with the aid of a modified Bridgman method. Undoped crystals were of *n*-type with electron concentrations from 4×10^{16} cm^{-3} to 3×10^{18} cm^{-3}, and with a maximum room temperature electron mobility of 4200 cm^2/Vs. Chemical analysis showed that the main impurities of the crystals were S, Si, Se, Fe and Zn. Electrical conductivity, Hall coefficient and Hall mobility were measured on the crystals in the temperature range of 77—400 °K. From the measured mobilities the total impurity content was deduced with the aid of the Brooks–Herring formula.

I. Introduction

GaAs is one of the most important semiconducting materials belonging to the group of $A^{III}B^{V}$ intermetallic alloys. The significance of GaAs as a basic material for the electronic industry, and the fact that high-purity Ga was readily available, resulted in starting a research work at the *Research Institute for Non-Ferrous Metals* with the purpose of preparing GaAs single crystals [1, 2]. The main results of this work are reported in this paper.

Single crystals of GaAs were produced with the aid of a modified version of the well-known Bridgman method [3, 4]. Our procedure yielded GaAs single crystals with medium and high impurity content, the characteristics of which were similar to those of GaAs crystals described in the literature. Basic electrical parameters (conductivity type, electrical conductivity, carrier concentration and mobility) were determined at 77 and 300 °K temperatures. Results of magnetoresistance measurements on some of the GaAs single crystals performed by one of the authors have already been published [5, 6].

In this paper the preparation of the crystals and the results of the chemical analysis and of the electrical measurements are described and discussed.

II. Preparation of GaAs single crystals

The GaAs single crystals were prepared with the aid of the Bridgman method. The original procedure was modified, the synthesis of the GaAs crystal and the growth of the single crystal were accomplished in one step [3].

The GaAs was synthetized and the single crystal was grown in a quartz boat placed inside a quartz ampoule. The ampoule was sealed in vacuum. The starting material was 6*N* grade Ga and 5*N* grade As which were prefired in vacuum. The synthesis was carried out at about 1240 °C, while the other end of the ampoule was kept at about 605—607 °C temperature to maintain the proper vapour pressure of the As. The cooling down was accomplished by pulling the furnace off the quartz ampoule with a predetermined velocity. During the cooling down process proper precautions were taken to maintain the necessary As vapour pressure. Cooling down with adequate velocity resulted in the formation of a single crystalline GaAs ingot.

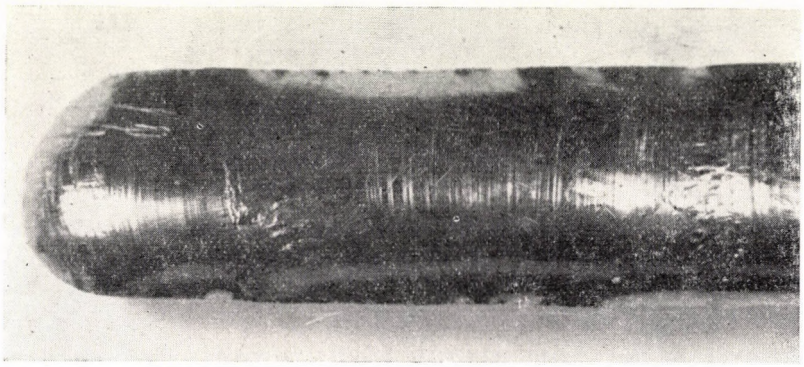

Fig. 1. Photograph of a typical GaAs single crystal grown by us

The main disadavantage of this simple method is that the growing crystal, the melt and the solid-liquid interface are in immediate contact with the walls of the crucible or boat. The melt may be contaminated by reactions between the melt and the crucible. Secondary nucleation may be caused by the crucible walls, and large stresses may be produced in the crystal during the cooling process. As crystallization according to the Bridgman method is spontaneous, it is very important to maintain a proper temperature gradient during the cooling down. Other important factors are the speed of the crystal growth, the purity of the boat or crucible, etc.

In two cases the crystals were lightly doped with Cr, and in one case the crystal was grown in oxygen atmosphere. The ingots prepared in this way were about 7 cm long, having an ellipsoidal cross-section, the diameter of which was about 1—1,5 cm. In Fig. 1 the photograph of a typical crystal is shown. In many cases the end of the ingot was polycrystalline. In some cases not one but two or three single crystals were formed, which were grown together. Some of the crystals were examined with the aid of X-ray methods.

The impurity content of the crystals was examined by activation analysis and by chemical (photometric) methods [2, 7]. Typical results of these analyses are shown in Table I.

Table I

Results of analyses

Impurity	Concentration, ppm	Method of determination
Fe	1—2	Activation analysis
Zn	$\approx$0,5	Activation analysis
Se	$\lesssim$1	Photometric analysis
S	4	Photometric analysis
Si	$\approx$1 (estimated)	Spectral analysis

III. Electrical measurements on the GaAs single crystals

The following physical and electrical parameters were measured on the GaAs single crystals: conductivity type, electrical conductivity, charge carrier concentration and mobility, concentrations of electrically active impurities and centres and impurity compensation degree. The conductivity type and the carrier concentration were determined with the measurement of the Hall effect. Carrier mobility, impurity concentration and compensation degree were determined by combining the results of the Hall effect and electrical conductivity measurements.

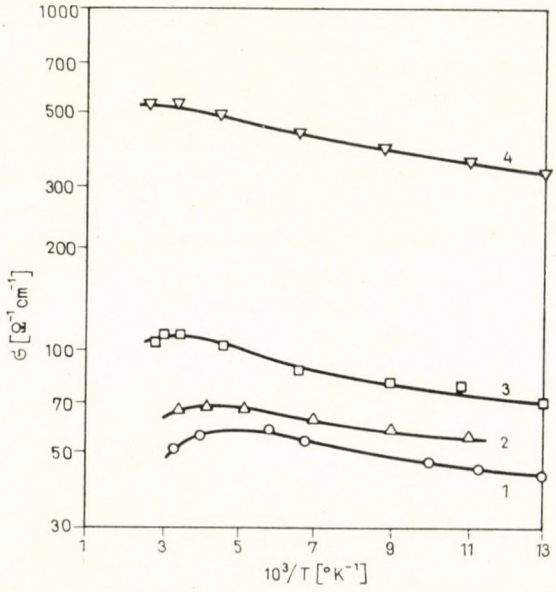

Fig. 2. Electrical conductivity of GaAs single crystals vs reciprocal temperature: *(1)* $n = 8{,}3 \times 10^{16}$ cm^{-3}; *(2)* $n = 1{,}8 \times 10^{17}$ cm^{-3}; *(3)* $n = 3{,}8 \times 10^{17}$ cm^{-3} (doped with Cr); *(4)* $n = 1{,}6 \times 10^{18}$ cm^{-3} (doped with O)

Electrical conductivity, Hall coefficient and Hall mobility were measured by the usual d.c. compensation method at 77° and 300 °K temperatures. On some of our samples these parameters were measured in the function of the temperature between 77° and 400 °K. As to details on sample preparation, measurement methods, etc., see [8].

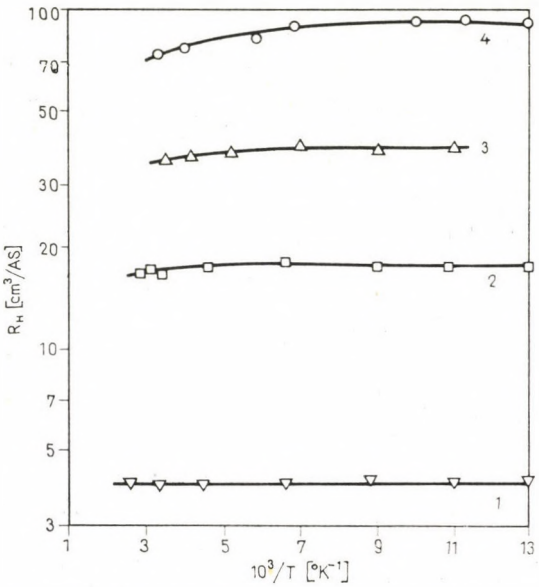

Fig. 3. Hall coefficient of GaAs single crystals vs reciprocal temperature (numbering of samples is the same as in Fig. 2)

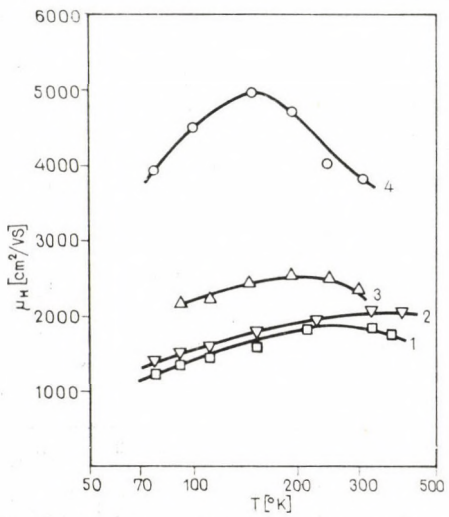

Fig. 4. Hall mobility of GaAs single crystals vs temperature (numbering of samples is the same as in Fig. 2)

Electrical conductivity and Hall coefficient in the function of the reciprocal temperature for some of our crystals are shown in Figs 2 and 3, Hall mobility versus temperature curves for the same crystals are presented in Fig. 4. Samples 1 and 2 were undoped, sample 3 was doped with Cr and sample 4 was doped with O. The results for the other crystals are similar to those presented here. All of our samples were of *n*-type, the electron concentrations measured at room temperature were between 4×10^{16} and 3×10^{18} cm^{-3}, the values of electrical conductivity were between 30 and 1000 Ω^{-1} cm^{-1} and the mobilities were between 1900 and 4200 cm^2/Vs.

IV. Discussion of the results of measurements

According to the literature [9], the simplest explanation for the fact that undoped GaAs crystals grown in quartz boats and ampoules are usually of *n*-type is that these crystals are contaminated with Si, due to the interaction of GaAs melt with the quartz walls. Si, in not too high concentrations, substitutes for Ga atoms in the crystal, and produces shallow donor levels, with an energy of 0,002 eV below the conduction band edge [10]. In our case most probably the S contamination (see Table I) plays an important role in determining the conductivity-type of the samples, because it produces shallow donor levels in GaAs, too. Typical results of chemical analyses presented in Table I show that our samples were contaminated with S and probably with Si and Se; the latter is a donor-type impurity, too. The concentrations of donor-type impurities shown in Table I correspond to $(4—6) \times 10^{17}$ cm^{-3}, which is in order of magnitude in agreement with the electron concentrations measured on our purer samples.

The temperature dependence of the electrical resistivity, the Hall coefficient and the Hall mobility correspond to the data published in the literature [11, 12]. The Hall coefficients and the electron concentrations are practically independent of the temperature in the temperature range of our measurements. The dependence of the mobility on the temperature is weak too, which can be explained by the assumption that the mobility limiting scattering mechanism, mainly below room temperature, is the scattering of electrons on the ionized impurities. In case of high electron concentrations this leads to weak temperature dependence of mobilities, as was observed in our crystals.

At room temperature and above it, besides the scattering by ionized impurities, the scattering of electrons by polarized optical phonons also plays an important role. The measured mobility can be approximately obtained by adding the reciprocal values of the mobilities determined separately by the two mechanisms. Because the scattering effect of the polarized optical phonons

decreases exponentially with decreasing temperature [11], their effect can be neglected below room temperature. At 300 °K the mobility limited by the scattering of electrons on the polarized optical phonons is 9300 cm²/Vs. This value is the result of H. EHRENREICH's calculations [14], but has recently been confirmed by the measurements of C. S. KANG and P. E. GREENE, too [15].

In Fig. 5 the electron mobilities measured at room temperature are plotted in the function of the electron concentration. It can be seen that with increasing electron concentration the electron mobility decreases. The wide scattering of the points belonging to the same value of electron concentrations

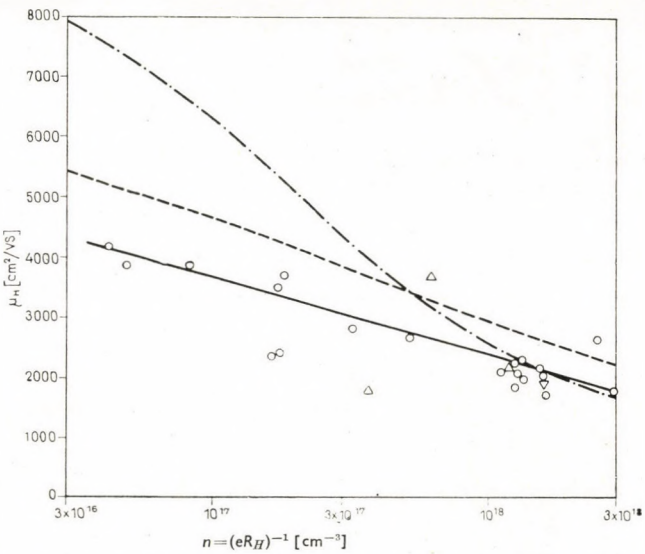

Fig. 5. Room temperature mobility of GaAs single crystals vs electron concentration: *(1)* undoped, *(2)* Cr-doped, *(3)* 0-doped crystals; curve *(a)* corresponds to the mean values of our measurements, curve *(b)* is the experimental curve from [10], curve *(c)* is calculated with the help of the Conwell—Weisskopf formula

Denotations: ——— *(a)* ○ *(1)*; ——— *(b)* △ *(2)*; —.— *(c)* ▽ *(3)*.

shows that the total impurity content was different in crystals having equal electron concentrations. Curve (*b*) in Fig. 5 is taken from the literature [10] and represents the average of mobilities measured on more than thousand samples. It runs appreciably higher than our experimental curve (*a*). Curve (*c*) in Fig. 5 was computed by us, taking into account the combined effect of ionized impurity and polar optical phonon scatterings.

The mobility of electrons due to the scattering by ionized impurities was estimated with the aid of the Conwell—Weisskopf formula [11], and the mobility due to the scattering of electrons by the polar optical phonons was assumed to be 9300 cm²/Vs [13, 14]. The resulting mobility was calculated by adding the reciprocal values of mobilities caused by the two scattering mecha-

nisms mentioned above. This approximation can appreciably overestimate the resulting mobility in the region where the effects of the two scattering mechanisms are comparable. As can be seen in Fig. 5, the calculated curve agrees with the measurements above 5×10^{17} cm^{-3} electron concentrations, but runs higher than the experimental curves in the region of lower electron concentrations. The cause of this discrepancy is possibly the fact that the Conwell—Weisskopf formula does not take into account the impurity compensation and that we have neglected other possible mobility reducing effects, i.e. inhomogeneities, neutral impurities, etc.

The mobility values measured by us are too low in comparison with other experimental results or with the theoretical predictions. A possible cause of this discrepancy is that our crystals were compensated, i.e. their impurity content was higher than the electron concentration, as determined from the Hall coefficient, and the scattering effect of excess impurities reduced the mobilities. The total concentration of electrically active centres was estimated using the mobility values measured at 77 and 300 °K temperatures [5, 15]. At liquid nitrogen temperature (77 °K) the mobility of electrons is limited only by the scattering on ionized impurities. From the measured Hall coefficient we can calculate the electron concentration, taking into account the value of scattering factor r in the expression $n = r/eR_H$. Knowing the electron concentration and the Hall mobility, the latter being converted to conductivity mobility with the aid of the formula $\mu = \mu_H/r$, the concentration of ionized impurities can be estimated with the aid of the Brooks—Herring formula, which also takes into account the impurity compensation [11]. Knowing the impurity concentration and the electron concentration, the calculation of the donor (N_d) and acceptor (N_a) concentrations is straightforward. The impurity compensation degree is given by $K_n = N_a/N_d$. This analysis for our crystals gave a compensation degree of roughly 0,5—0,6, i.e. the concentration of electrically active centres is about 4—5 times higher than the concentration of electrons as determined from the Hall coefficient.

The same analysis was applied to the results of measurements performed at room temperature. In this case the scattering factor was taken to be approximately 1. The mobility reducing effect of the scattering on polarized optical phonons was taken into account, too, in the way described above. The impurity concentrations determined by the two procedures agreed reasonably well with an accuracy of 20—30 per cent, a difference which is not significant, considering the different assumptions and approximations made during the analysis.

We should like to note that the impurity concentrations are possibly overestimated by this analysis because we have neglected other mobility reducing effects (i.e. the scattering by neutral impurities and crystalline defects, and the scattering by the space charge regions caused by the inhomogeneous distribution of impurities in the crystals). The neglect of these effects results

in an apparently greater impurity concentration than the actual one. Besides, the Brooks—Herring formula seems to overestimate the screening effects of the free charge carriers [16] and this results in the overestimation of the total impurity concentration too. This explains the fact that the impurity concentrations determined by this analysis are several times higher than those determined by the chemical methods. But this value gives a good estimation of the total concentration of electrically active centres in our crystals.

V. Conclusions

From the results presented above was can draw the following conclusions:

a) We have succeeded in producing GaAs single crystals with the aid of a modified Bridgman method;

b) the results of chemical and electrical analyses have shown that our undoped crystals were of *n*-type with medium or high impurity concentrations;

c) the impurities responsible for the observed *n*-type conductivity are presumably S and Si;

d) our samples are compensated and a method is described for the determination of the impurity compensation degree.

*

We wish to express our acknowledgement to Mr. I. Bertóti and to Mr. J. Hagyó for preparing the electrical contacts, and to Mr. K. Somogyi (all of the Research Institute for Technical Physics) for constructing the cryostat for the Hall effect and the conductivity measurements. The authors would like to express their acknowledgements to Dr. G. Gergely of the Research Institute for Technical Physics, for his constant interest during this work.

REFERENCES

1. Hungarian patent No. 148953.
2. Closing report an GaAs. Research Institute for Non-Ferrous Metals, Budapest 1968 (unpublished).
3. Hungarian patent application 2251/FE-645/5.
4. Papp, E.—Zsindely, S.—Legát, T.: *Neue Hütte* **13** (1968), 29.
5. Pődör, B.—Ivánka, C.: *Acta Phys. Hung.* **25** (1968), 115.
6. Pődőr, B.: *Phys. Stat. Sol.* **31** (1969), K 55.
7. Bujdosó, E.—Miskei, M.—Ormos, Gy.: Proc. Anal. Chem. Conf.; Budapest 1966, 262.
8. Papp, E.—Pődör, B.—Zsindely, S.—Legát, T.: *Híradástechnika* **20** (1969), 368.
9. Eckstrom, L.—Weisberg, L. R.: *J. El. Chem. Soc.* **109** (1962), 321.
10. Sze, S. M.—Irvin, J. C.: *Solid-State Electronics* **11** (1968), 599.
11. Madelung, O.: Physics of III—V Compounds. Wiley, New York 1964.
12. Fertin, J. L.—Lebailly, J.—Deyrs, F.: Proc. Symp. on GaAs; Reading 1966, 46.
13. Ehrenreich, H.: *Phys. Rev.* **120** (1960), 1951.
14. Kang, C. S.—Greene, P. E.: *Appl. Phys. Letters* **11** (1967), 171.
15. Pődör, B.: *Acta Phys. Hung.* **27** (1969), 449.
16. Amith, A.—Kudman, I.—Steigmeier, E. F.: *Phys. Rev.* **138** (1965), A 1270.

Herstellung und Eigenschaften von Galliumarsenid-Einkristallen. Es wurden GaAs-Einkristalle gemäß einem modifizierten Bridgman-Verfahren hergestellt. Die undotierten Kristalle des Typs *n* hatten eine Elektronenkonzentration von 4×10^{16} cm^{-3} bis 3×10^{18} cm^{-3} sowie

eine Elektronenbeweglichkeit von 4200 cm^2/Vs. In den Kristallen wurden Spuren von Verunreinigungen von S, Si, Ge, Fe and Zn durch chemische Analyse festgestellt. Die elektrische Leitfähigkeit, der Hall-Koeffizient und die Hall-Beweglichkeit wurden im Temperaturbereich zwischen 77 °K and 400 °K gemessen. Der totale Verunreiningungsgehalt wurde mit Hilfe der Brooks–Herringschen Formel aus den gemessenen Beweglichkeitswerten abgeschätzt.

Изготовление и свойства монокристаллов арсенида галлия *(Э. Папп, Б. Пе́дер Ш. Жиндей* и *Т. Легат)*. В данной работе описываются способ изготовления монокристаллов арсенида галлия и характеристики изготовленных кристаллов. Кристаллы были выращены при помощи видоизмененного метода Бриджмена. Кристаллы были анализированы химическими методами. Электропроводность, эффект Холла и холловская подвижность были измерены на монокристаллических образцах в температурном интервале от 77 до 400° К. Концентрация носителей тока, концентрация примесей и степень компенсации были определены на основе анализа результатов измерений.

Acta Technica Academiae Scientiarum Hungaricae; Tomus 68 (1—2), pp. 255—258 (1970)

THE CATHODE–PLASMA INTERACTION OF LOW-PRESSURE ARC DISCHARGES WITH OXIDE CATHODES

J. F. BITÓ

CAND. OF TECHN. SC.

RESEARCH INSTITUTE FOR ELECTRONICS, BUDAPEST

[Manuscript received July 17, 1969]

The author demonstrates by the analysis of the static and functional parameters of the oxide cathode and their influence upon the discharge spaces that the thermionic emission current of the cathode, being a complex cathode parameter, is suitable for the description of the connection between the potential and space characteristics of the cathode and cathode side. The coupling between the cathode and cathode space takes place with the aid of the emission current and by the ion current striking into the cathode.

I. Experimental conditions and methods

The experiments were carried out in case of a discharge, containing 3 mm Hg argon and about $6 \cdot 10^{-3}$ mm Hg mercury vapour. The function of the cathode was performed by a tungsten triplespiral and the oxide coating on it; the compound, weight, decomposition and activation processes have constantly been controlled. The internal diameter of the applied discharge tube was 36 mm. The previously developed diagnostic system on the cathode side served as an experimental method. It consists of the following elements: probe measurements, the determination of the axial length of the cathode spaces, measurement of the cathode spot temperature, measurement of the emission current, the determination of the work function (in gas), the observation of the cathode spot surface, interferometric measurements of electron concentration by laser beam, microwave transmissions measurements, measurement of cathode damage, oscillation and striction control with photomultipliers. The aim of our investigation was the dynamic characterization of the interaction between the cathode and the cathode space arising from the conditions mentioned above.

II. Results

The oxide cathode can be looked at as such a transformer which produces electrical energy by electron emission through the heat energy, arising in consequence of the electron current flowing through it, and in consequence of the ion current. In our case a spot of high temperature appears on the cathode which produces more than 60—70% of the emitted electrons.

In case of cold cathode resistance, heat up characteristics and work function, given for the functional and dynamic characterization of the cathode, its emission current, spot temperature and average temperature, and also the size of the cathode spot surface must be determined. The respective correlation system was published in previous papers [3—5]. In the following the most important characteristics of the cathode space were determined and the correlations between them were sought for [1—4]. The axial dimension of the cathode light and of the Faraday dark space were determined, and the character of the electron energy distribution to be found in them was measured [5].

At the same time we examined in what degree did the single discharge perturbations, as e.g. the change of the argon gas pressure, influence the macroscopic and microscopic characteristics of the spaces [1—5]. Thus we succeeded in forming a further system of correlations which offered an opportunity for the characterization of the behaviour of the cathode spaces and for the description of the basic processes in them. The connexion existing between the correlations in the cathode space characteristics and the functional parameters, the characterizing of the cathode function was determined by means of the ion and electron current connecting the cathode with the cathode spaces. We thoroughly investigated the changes to be expected in the energy balance of the cathode [6] and in the cathode spaces [7]. The proportion of the generation factor of the electron generation, occurring on the cathode and in the cathode space, that is to say, on the surface and in the discharge volume was analysed in detail.

It was established that if a cathode with a given work function is applied, in the case examined by us the emission current emerging from the cathode depends only on the cathode spot temperature. This is determined in case of a given spot surface by the intensity of the impact ion current component. The value of the ion current is determined on the other hand — in case of a given discharge current — by the primary, so-called static qualities of the cathode. These are the following: the work function, the cold resistance and structure of the cathode. This means, in other words, that in case of a cathode with a lower work function an essentially lower cathode temperature is needed for the securing of a given emission current than in the case of a cathode with a higher work function. For the setting up of a lower spot temperature this is also influenced by the static parameters of the cathode and in this way they determine the connexion between the cathode and cathode space.

The emission current of the cathode is determined in case of a given cathode temperature by the work function of the cathode. The emission current is a complex cathodic parameter, as its value beside the work function depends also on the spot temperature and on the spot surface. Consequently, for the

characterization of the cathode function and for the establishment of the influence of the cathodic parameters in the cathode space the use of the emission current is advisable.

With the application of this complex cathode parameter we sought for a double influence in the cathodic space: we examined the emission dependence of the cathode fall and cathode spaces [4, 5]. In other words, with the application of the emission current we tried to draw a conclusion about the volumetric electron generation and about the acceleration and energization of the electrons, produced in the cathode space. At the same time we wanted to define that part of space which cannot be characterized by the usual distribution functions and transforms the conventional electron energy distribution containing primary and secondary energy-peaks into Maxwell—Boltzmann distribution, that is to say, it performs an energetic homogenization. We have proved that the emission current has, through the influencing on the cathode fall, an effect on the volumetric electron generation in the cathode space. The existence of the cathode fall itself, its sign and value depend on this complex cathode parameter: on the emission current [5].

The axial length of the cathode light can be influenced by the change of the emission current [4]. This influence was explained by the size-adaptation of that part of space to the cathode properties, which was necessary for the electron generation and acceleration [5]. We found the axial length of the Faraday dark space independent of the emission current: the dimensions of this part of space can be altered by the change of the gas pressure, which has an influence on the interaction phenomena between the electrons and neutral atoms. From this the conclusion could be drawn that the Faraday dark space plays an important role in the energetic homogenization of the electrons. The latter could have been experimentally proved by carrying out a detection of axial distribution [6, 7].

Thus we succeeded in the characterization of the interaction between the emission current containing more cathode qualities, and the potential and field characteristics of the cathode side. In this sense the coupling between the cathode and cathode space is carried out by the ion current striking into the cathode, or by the emission current of the cathode.

REFERENCES

1. Bitó, J. F.: Ph. D. Thesis; Budapest 1968.
2. Bitó, J. F.: *Acta Techn. Hung.* (under publication).
3. Bitó, J. F.: Lecture held on the *VIII. Int. Conf. on Phen. in Ionized Gases* (contributed papers 83); Vienna 1967.
4. Winter, E.—Bitó, J. F.: Lecture held on the *VIII. Int. Conf. on Phen. in Ionized Gases* (contributed papers 82); Vienna 1967.
5. Bitó, J. F.: Physik und Technik des Plasmas (lecture); Eisenach 1968.
6. Bitó, J. F.: *Acta Techn. Hung.* **62** (1968), 409.
7. Bitó, J. F.: *Acta Techn. Hung.* **62** (1968), 317.

Die Kathode—Plasma Wechselwirkung der Niederdruck-Bogenentladungen mit Oxydkatode. Der Verfasser weist durch die Analyse der statischen und funktionellen Parameter der Oxydkatode und des Einflusses derselben auf die Entladungsräume nach, daß der thermionische Emissionsstrom der Katode — als komplexer Parameter der Katode — für die Beschreibung des Zusammenhanges zwischen der Katode und den potentiellen und Raum-Parametern der Katodenseite geeignet ist. Die Koppelung zwischen der Katode und dem Katodenraum wird durch den Emissionsstrom und den in die Katode einschlagenden Ionenstrom gesichert.

Взаимодействие катода и плазмы дугового разряда низкого давления оксидных катодов *(Я. Ф. Бито)*. Автор анализом статических и функциональных параметров оксидного катода и их влиянием на разрядные пространства доказывает, что термионический ток эмиссии катода (как комплексный показатель катода) пригоден для спецификации соотношения между катодом и потенциональными пространственными показателями катодной стороны. Двухстороннее соотношение между катодом и катодным пространством обеспечивает ток эмиссии и ток ионов, нападающие на катод.

Acta Technica Academiae Scientiarum Hungaricae; Tomus 68 (1—2), pp. 259—263 (1970)

RECENSIONES

Pál Selényi

COLLECTED WORKS

Ed. Prof. Zalán Bodó

Publishing House of the Hungarian Academy of Sciences. 1969

The comprehensive, many-sided life-work of Pál Selényi, the world-famous experimental physicist, performed by him despite the unfavourable circumstances and many difficulties, plays an important role in the history of science. It was an excellent idea to publish the collected works of Pál Selényi, with the help of which we get acquainted with his very precious life-work. The clear-cut and concise arrangement of the material must be underlined, which is the work of Prof. Zalán Bodó.

Pál Selényi was interested in many fields of science. Consequently his scientific research was carried out in different fields of experimental and applied physics. In this volume his publications are divided into the following groups:

optics
incandescent lamps
vacuum techniques
photocells
photometry
selenium rectifiers
photoelectric cells
electrography
the heavy and inert mass
publications, connected mostly with measuring techniques.

Before these publications, divided according to the different subjects, a short bibliography in Hungarian and German written by Mrs. Selényi, acquaints the reader with the human elements of the scientist. From this introduction and also from the subjects and treatment of these subjects it turns out that Pál Selényi attained outstanding results not only as a teacher, but he achieved a reputation as a pioneer of the Hungarian industrial and applied research and as a natural scientist of excellent experimental sense.

This volume proves the necessity of applied industrial research and the fact that such precise, persistent research brings useful results.

The words of Pál Selényi, quoted in the introduction, underline this conception: "... science in itself has the trend to become a technique earlier or later, that is to say, invention and the industrial researcher can only accelerate this process."

Selényi did not only proclaim the importance of industrial research, but he helped by his active research work and through his world-wide-known results to raise the industrial research to a convenient level also in Hungary.

The first chapter of the volume contains also the publication referring to the experiment with the wide-angle interference. The experiment, outlined in this chapter — which can also be easily demonstrated in secondary schools —, proves unambiguously that the atoms behave as Hertz-like dipoles when they emit visible light. This is a clear proof that the atoms emit spherical waves which travel further in space. The wave character of light is proved just as evidently by the Selényi experiment, as its photon-like character by the photoelectric effect. The wide-angle interference experiment of Pál Selényi defeated the presupposition, according to which between two beams, differing strongly in their direction, an interference is not possible at all.

The papers concerning incandescent lamps, vacuum techniques and thermionic electron emission arouse interest in vacuum physics and electron physics even to-day. Many more

such experimental methods are outlined here which were designed or worked out experimentally by him, with the aim to improve the production of incandescent lamps or the applied vacuum technique. Many patents were born from these experiments.

In the part dealing with photocells and photometry, the detailed description of the photometer, for which a patent application was submitted in 1934, is very remarkable. It does not require a special, separate electrical source and consists only of a photocell, containing one or more blocking layers. This very skilful, simple instrument is applied for the measurement of the illumination level throughout the world even to-day.

Chapter 4, containing the publications connected with selenium rectifiers and photocells, outlines in a well arranged form the experiments aiming at the improvement of the production of rectifiers, the sensibilizing methods, further the observations, evaluated but scarcely even in our days and which could not be overlooked even at that time by Pál Selényi, who performed his work with very simple instruments.

Chapter 5 contains the publications connected with electrography or as it is called to-day with xerography. The experiments outlined here served as a basis for the now widespread and useful xerographic method. The examination of the here outlined basic experiments and observations is very helpful.

Chapter 6 deals with the observations concerning the heavy and inert mass, with the elementary theory of the Eötvös torsion balance, further with the problems of gravitation.

Chapter7 deals with problems connected with the measuring technique and with making of models, with analogies, completing the sense of comprehension, further with the sensibilization of the galvanometer through photoelectric feedback.

The collected papers of Pál Selényi represent very precious scientific remains for us. It is worthwile and inspiring to study them. This well arranged, percise compilation is useful also for his successors, for the modern physicists.

J. F. Bitó

Siljak D. D.

NONLINEAR SYSTEMS

THE PARAMETER ANALYSIS AND DESIGN

John Wiley and Sons, Inc., New York, London, Sydney, Toronto 1969, 632 pages

Thi s book, written for engineers by an engineering professor, has the purpose to make the reader acquainted with a special tool for analysis and synthesis of nonlinear systems described by high-order differential equations. This tool is the parameter method, originally introduced by the Russian scientist Vishnegradsky at the end of the last century and generalized in the last decades by the Yugoslav professor Mitrovič. Recently the method of parameter analysis has been further generalized and applied to the investigation of nonlinear systems. The book yields a unified and self-contained exposition of the topic.

The book contains eight chapters of about four hundred pages and auxiliary material arranged in eight appendices of about two hundred pages.

Chapter one provides the fundamental notions and concepts of the parameter method, namely the definition and technique of the parameter mappings. The method is first applied to the root distribution of characteristic equations and to the root evaluation as the function of some adjustable parameters. The root sensitivity to parameter variations is also interpreted. Appendices A and B, closely connected to this chapter supply the basic theorems and derivations as well as the possible computer applications.

In the following chapter the parameter mapping method is employed to the analysis and design of linear control systems. Here a procedure for multiparameter mapping and design is also shown. Appendices C, D and E are related with this chapter. Appendix C gives the relations between the pole-zero locations and the corresponding time response. In Appendix D some stability criteria such as that of Hurwitz, Nyquist, Mikhailov and the D-decomposition method of Neumark are outlined. Appendix E contains a squared-error optimization procedure in the parameter plane for systems with stochastic input signals and stability constraints.

The third chapter is an introduction to the approximate analysis of nonlinear systems. Here the describing function method, and the asymptotic method of Krylov and Bogoliubov are presented. Appendix F gives some standard expressions, tables and diagrams relating to the harmonic linearization of some typical nonlinearities. Appendix G focuses attention on some accuracy considerations with respect to the describing function method.

The next chapter shows how the harmonic linearization and parameter mapping method can be used in the investigation of symmetric periodic oscillations as well as in testing of their stability. For the latter purpose the root sensitivity analysis is employed. Systems with two nonlinearities, multivalued nonlinearities and nonlinearities with frequency-dependent and variable-pole describing functions are also treated.

In chapter five the analysis of asymmetrical nonlinear oscillations can be found. Here also the parameter method and the describing function method are further applied.

The sixth chapter considers transient oscillations. First the Krylov–Bogoliubov method is extended for damped nonlinear oscillations, then this concept is generalized for high order nonlinear systems by means of the parameter analysis.

Chapter seven presents the analysis of forced nonlinear oscillations in the parameter plane. Mainly the phenomenon of jump resonance is considered in detail.

A very interesting and modern part of the book constitutes chapter eight presenting the parameter analysis of absolute stability in nonlinear systems. First the stability investigation method of Lyapunov is treated in some detail, then the concept of absolute stability is defined, thereafter the Lur'e problem is thrown into relief, finally, the frequency domain solution of the problem due to Popov is outlined. The results of Yakubovich giving a close connection between the time-domain and frequency-domain solutions are also presented. Then Aizerman's conjecture is mentioned. In the remainder of the chapter the parameter method is applied to the study of absolute stability and the stability conditions are interpreted in the parameter space. Appendix H yields the proofs of stability theorems discussed in the relevant chapter. Here also a survey of the newer results concerning absolute stability analysis is given.

Many examples and problems can be found within the text and at the end of the book.

Although this work is essentially a monograph, the organization ensures that the material can be also used by students as a textbook. This is realized by a successive approach from the fundamental concepts and notions to the more complicated ones. The first and the third chapters give the basis for the further reading, while the other subsequent chapters can be omitted or chosen at will.

The book is contemplated for a wide audience such as teachers, students, researchers and practicing engineers. This work can be regarded as the first systematic presentation of the parameter analysis and design method.

F. Csáki

Schlitt H.

THEORY OF CONTROLLED SYSTEMS

STOCHASTIC PROCESSES IN LINEAR AND NON-LINEAR CONTROL CIRCUITS*

Friedr. Vieweg & Sohn, Braunschweig, 1968, 324 pp., 223 figures

The statistical analysis and dimensioning has become in recent years one of the fundamental processes in control technique. The work in question is meant to give an introduction into the stochastic processes of linear and non-linear controls and the related statistic fundamental conceptions.

The work is divided into twenty chapters. The first ten chapters treat the linear systems having constant parameters, while the other ten chapters deal with the quasi-linear treatment of the non-linear systems.

The first chapter presents the fundamental conceptions of the stochastic processes. The second chapter is dedicated to the theoretical methods for the determination of the mean value in time, and of correlation functions. In the third chapter the basic concepts of spectrum functions are to be found. The fourth chapter describes the stochastic processes in the frequency domain. The fifth chapter discusses the power density spectrum. The sixth chapter contains some special correlation conceptions of linear systems. The eighth chapter treats the system theory of the stochastic signals. In the ninth chapter the stochastic signals are classified. The tenth chapter deals with noise filtration.

* Theorie geregelter Systeme. Stochastische Vorgänge in linearen und nichtlinearen Regelkreisen.

The eleventh chapter discusses the behaviour of the non-linear systems with respect to the sine signals and the descriptive functions. In the twelfth chapter figure descriptive functions of several characteristic non-linearities. The thirteenth chapter discusses the behaviour of the non-linear system in relation to the steady stochastic signals. The fourteenth chapter presents the statistic descriptive functions of some characteristic non-linearities. The fifteenth chapter shows a more general approximation method. In the sixteenth chapter optimum linear substitute systems are dealt with. The seventeenth chapter is dedicated to the series expansion of the non-linear function and to the relation between the correlation function and the power density spectrum. The eighteenth chapter discusses the closed control system containing a single statistic non-linearity. The following nineteenth chapter brings examples thereof. And finally the twentieth chapter deals with some features of the non-linear systems, in the first place with the generating of the multi-valued resonance curves.

An ample list of references completes the book, classifying 82 books and papers.

The usage of the book is facilitated by a table of contents and an index. It offers a very good introduction into the comprehension of statistic analysis and dimensioning of the control systems and the attaining of the most important methods. Many figures and a clear style make the material easy to understand. More specialized technical works may go deeper into the subject, but this book has the advantage that it presents a comprehensive picture of the discussed theme.

F. Csáki

C. J. Tranter

BESSEL FUNCTIONS WITH SOME PHYSICAL APPLICATIONS

Hart Publishing Company Inc., New York. 1969, 148, pp.

The classic work of G. N. Watson "Theory of Bessel Functions" which outlines with a unique exactness and accuracy the Bessel functions and their applications appeared in 1922. In the course of the last 47 years no such book has appeared which would have treated this very important group of functions. Therefore we usually meet in the references of scientific papers Watson's work — published by the Cambridge Press — and also the "Higher Transcendental Functions" edited by A. Erdélyi (Publ.: McGraw Hill, 1953) which partly deals with the Bessel functions. The latter book however describes only the mathematical behaviour of the functions, and does not cover the applications.

Watson's work is somewhat difficult for those who are interested in the application of the function, however it is excellent for research mathematicians. Such a book which would have described with mathematical exactness the Bessel functions and would have shown the most important applications, with reference to their advantages in the field of physics and by the solving of different technical problems, has not appeared so far.

Tranter's book, recently published, met a long-felt need. The aim of the author was evidently to supply the engineers and physicists with a book which conveys quick information, but at the same time outlines with mathematical exactness the Bessel functions and the more important fields of their application. The book does not contain detailed deductions or analyses, it indicates however the basic parameters and refers to some less important deductions and transformations giving the sources, where a more detailed description of them may be found. Consequently the remarkably logical book conveys up-to-date information about the functions and their fields of applications and also about the basic problems which may be served with their aid.

At the beginning the solution of the Bessel equation, the Bessel functions of 0 and 1 order, the Hankel functions, the recurrent formulae, the Bessel coefficients, the modified Bessel functions are dealt with.

Following this the indefinite integrals are introduced and characterized and the Bessel function series are treated in detail. The author shows, through a more detailed analysis of the multiplication theory and addition theory, how the representation in line form of the multiplication of two Bessel functions is performed. Several examples are given for the further characterization of the operation.

The integral representation and the asymptotic expansions are dealt with in a separate chapter. This part is dedicated to the more detailed characterization of the Bessel and Poisson integrals. and the representation of the thus gained formula. The theory of construction of asymptotic series suitable for the substitution of the different Bessel functions is also outlined

in this chapter. In physics mainly the values of the Bessel functions of great argument must often be approximated by some series. Taking this into consideration the author shows a great accuracy in the characterization of these approximations and in the thorough description of the applicability of this method as well.

Another chapter discusses the zeros of the Bessel functions for the different types of these functions. The description of the Stokes method which makes the relatively rapid definition of the zeros of these functions possible is also given in this chapter. The remarkably exact analysis of the Fourier—Bessel series, of the Hankel integral formula and of the Hankel transformations is partly connected with the here given analysis, on the other hand it introduces the subsequent discussions.

The author also deals with the Sonine finite integral and its expansion, further with the solubility and calculability of the Weber—Schaftlein integral and of other finite or infinite definite integrals, containing Bessel functions, restricting himself to the representation of the most important axioms and emphasizing the fields of application. This part ends with the summing up of the calculable criteria of the general integrals, containing Bessel functions.

We often meet, both in applied mathematics and in the field of physics, such double integrals, the expression of which in canonical form would be of a great aid for the performation of the calculations. A separate chapter deals with the methods applicable in case of Bessel functions and the same chapter also outlines and analyzes the Abel integral equation and the Fredholm integral equation. The solubility of the different double integral equations by series and their reducibility to the Fredholm integral equation are proved by an easily understandable deduction.

The book ends with the enumeration of the possible applications in mathematics, physics and engineering sciences. The Laplace and Hankel transformations and also the solubility by integral transformation of the more characteristic differential equations are presented.

In the Appendix the gamma function, the more important types of integrals, which may be expressed by its aid, the functional equation satisfied by gamma function and also the definite integrals expressible in gamma functions, the derivative of gamma functions are treated.

The book appeared as part of the "Applied Mathematics Series" and it offers, on account of its elegant style and logical arrangement, an easily understandable material for engineers and physicists. It is by its character a valuable, long-needed book which will be of great help for the scientists who apply mathematical methods.

J. F. Bitó

INDEX

RECENSIONES

Printed in Hungary

A kiadásért felel az Akadémiai Kiadó igazgatója — Műszaki szerkesztő: Farkas Sándor

A kézirat nyomdába érkezett: 1970. II. 9. — Terjedelem: 23,25 (A/5) ív, 88 ábra, 1 melléklet

70.69096 Akadémiai Nyomda, Budapest — Felelős vezető: Bernát György

Acta Techn. Hung. **68** (1970), 3—8

FONÓ, A.: *Peak Load Power Station Fed from Long Distance Gas Pipeline*

Peak load power station can be fed from gas stored in a long distance pipeline in which the gas is stored by increasing its average pressure by interconnecting a compressor in the last line section. The overpressure thus caused can be utilized at the end of the line for power production during offpeak periods. The thus produced energy is so much more than that needed for boosting the pressure that from the gain the necessary investsments can be amortised in a short time. By this means she storing oo the gas does not cost any money.

Acta Techn. Hung. **68** (1970), 9—14

CSÁKI, F.—FISCHER P.: *On the Spectrum-Factorization. Part II*

As a direct continuation of a previously published paper, the necessary and sufficient conditions as well as procedures of factorizing pulsed-data matrices are given here.

Acta Tech. Hung. **68** (1970), 15—28

D. HALÁSZ, K. SZENDY: *Improvement of the Process "High-Grade Ionization in Cold Gas"*

The authors and other contributors made several proposals for the non-equilibrium ionization in MHD generators which have been presented and discussed at various MHD symposiums. None of these suggestions so far have come up to expectations. In a new method propounded in the present paper, recombination is expected to impede the photons emitted by glowing grains introduced into the working gas. Numerical relations have still to be determined by further examinations and experiments. Any MHD generator, especially its open-cycle version, will only become feasible, if the working gas is kept at moderate temperatures (1200 to 1800° K), where the proposed ionization effect may be useful.

Acta Techn. Hung. **68** (1970), 29—49

J. F. BITÓ: *Dependence of Cathode Properties on Neon Doping and Discharge Current*

Up to the present time no experimental data have been published concerning the influence of neon-gas doping on the cathode properties of mercury vapour-argon discharges. In the course of our experiments it was possible to demonstrate the length of cathode side spaces, the field strength of the positive column, the voltage drop and power consumption of the discharge tube on the partial pressure of neon. Furthermore the dependence of cathode properties on the discharge current has also been determined. The relationships obtained in the experiments have been interpreted in terms of the known plasmaphysical data.

Acta Techn. Hung. **68** (1970), 51—72

SEITZ, K., FÜLÖP, J.: *Analytic Calculation of Direct or Counterflow Heating of Solid Charges*

The paper deals with the calculation of the heating of a solid charge by direct or counter current. The partial differential equation systems describing the physical processes examined in the paper are solved by the help of a new method called "non-orthogonal" extension. With the above outlined calculating method the mathematical description of such heating processes becomes possible in the course of which — owing to the interaction of the two media — the temperature of the heat transporting medium changes continuously.

Acta Techn. Hung. **68** (1970), 73—85

MIHALKOVICS, T.: *Determination of the Independent Restriking Voltage on Circuit Breaker Contacts by Operator Calculus, from Equations Calculated in Advance, for Networks with Distributed Parameters*

One method for calculating the restriking voltage arising in a given network point is the operator calculus based on Thévénin's theorem. In the case of networks containing elements with distributed parameters, not replaceable by elements with lumped constants (e.g. transmission lines), the characteristic equations forming the base of the calculation are rather complicated. To save plant engineers these calculations, HAMMARLUND [1] carried out the calculations for a considerable number of circuits. But the experience of the author has proved that over and above the circuits analyzed by HAMMARLUND, in certain cases it is necessary to carry out the calculations also for new, more complicated circuits. The author presents the new method and its application to a numerical example, and furthermore he tabulates results deduced for such new circuits, together with those for the circuits of HAMMARLUND.

Acta Techn. Hung. **68** (1970), 87—115

F. KOLONITS: *Stresses in the Vessel of aPressurized Water Reactor during Stopping*

The present work analyzes the stresses in the vessel of a pressurized water reactor in case of quick stoppage. The results obtained are evaluated numerically for the pressured vessel of a reactor of the "Voroniesh" type. This study is a part of the investigations made in 1967 by the author at the *Institute of Thermal Power Stations, Technical University, Budapest.*

Acta Techn. Hung. **68** (1970), 117—119

A. LŐRINCZY, T. NÉMETH, M. SALLAY-NÉMETH, J. SWIDERSKI: *On Microinhomogeneities in GaAs Crystals*

Microinhomogeneity was detected on GaAs crystals (mono- and polycrystals) by means of electrolytic etching and using the photovoltaic effect. The presence of microinhomogeneity going through without breaking grain boundaries of crystals cannot be explained by the well-known mechanisms of formation.

Acta Techn. Hung. **68** (1970), 121—130

J. F. BITÓ: *Diagnostic System for the Examination of the Cathode Side of Arc Discharges with Oxide Coated Cathodes*

For the dynamic characterization of the arc discharges with oxide coated cathode on the cathode side, a diagnostic system, containing 10 experimental methods, was worked out. The system was constructed so that the measuring methods constituting it should make possible a manifold control, a simultaneous measurement and a relatively small perturbation. The formation of the diagnostic system became necessary on account of the strong microphysical heterogeneity of the cathode side. With the application of the system of the briefly characterized measuring methods we succeeded e.g. in establishing the cathode side model of the arc discharges with oxide coated cathodes.

Acta Techn. Hung. **68** (1970), 131—144

S. KERESZTÉLY: *Stability Range of Feedback Control Systems*

The parameters of a controlled section may change within a given range. The criterium is determined which is to be satisfied by the loop amplifier of the nominal system, in order to keep the feedback control system stable over the whole range of the parameter changes. The calculation may be carried out with a computer. By generalizing the method the fulfilment of more exacting demands than stability may be prescribed with practically the same amount of calculation work.

Acta Techn. Hung. **68** (1970), 145—160

J. GYÜRKI: *Some Questions of Identification on the Basis of Frequency Response*

An iterative least-square approximation method is presumed in the article for the identification of linear, dynamical control systems on the basis of the frequency response. The main concept of the method is described and two special questions are intensively investigated, namely the weighting problem and the decision about the structure of the identified transfer function. To the background of the theoretical part the proposed method was programmed on a MINSK—22 digital computer and the results of the practical investigation are summarized. A numerical example is presented, too.

Acta Techn. Hung. **68** (1970), 161—178

J. F. BITÓ: *A Laser Beam Method for the Examination of Cathode Spaces*

With the cathode side application of the traditional experimental methods, adapted so far, the plasma microparameters of these spaces cannot be determined with a satisfactory accuracy. In this paper an interferometric method with laser beams is demonstrated, with the aid of which the value of the electron concentration in the cathode spaces, its time dependence and axial distribution can be determined in a simple way, with an accuracy of $\pm 10^{10}$ electron/cm^3. The highest time resolution which can be reached is 10^{-8} sec.

Acta Techn. Hung. **68** (1970), 179—189

KAMEL A. EL-DEHEMY: *Kinetics of the Last Recovery Stage in Cold Worked Tungsten*

The recovery of the dislocation network was investigated by means of electrical resistivity measurements on severely cold worked undoped powder metallurgical tungsten wires. The decrease of the dislocation density during annealing follows the same kinetics in doped and undoped samples. The activation energy in both cases is close to that of self-diffusion. The detailed mechanism of the decrease of the dislocation density is still unknown. The inhomogeneity of the samples makes it impossible to determine the activation energy without a detailed assumption of the annealing kinetics.

Acta Techn. Hung. **68** (1970), 195—197

J. F. BITÓ: *On the Time Dependence of the Parameters on the Cathode Side*

The time dependence of the cathode fall, anode fall and plasma potential of the a.c. oxide cathode discharge was experimentally determined by the author with the aid of an adequate diagnostic system. With the analysis of the time dependence of the cathode spaces he refers to an interesting and characteristic contraction of column in the vicinity of the plasma.

Acta Techn. Hung. **68** (1970), 199—213

RÓZSA, É., STEFÁNIAY, V.: *Investigations on the Damaged Surface Layer Structure of Semiconductor Single Crystals. Lapping Effect*

The report deals with the investigation of the structure and depth of the dagamed surface layer of semiconductor single crystals resulting from lapping and with the methods adapted for measuring. Applying X-ray diffraction methods the structure and the depth of the damaged layer of [111] oriented germanium and silicon wafers are investigated. The degree of the flexure of the bent wafers due to mechanical stresses is measured as well. A relation is shown between the radius of curvature and the quality of the lapping process.

Acta Techn. Hung. **68** (1970), 215—243

Cs. Ferencz: *Wave Propagation in Inhomogeneous Linear Media*

In the paper, first, the propagation of electromagnetic waves in slightly inhomogeneous media is examined, when the medium is stationary and its parameters change with time and when, finally, it is flowing. In this connection the author points out that the theory permits the uniform treatment of many known results and also permits the exact investigation of the propagation phenomena in flowing media. Afterwards the method for the determination of the complete wave form by the addition of the 'inhomogeneous basic modes' is shown for arbitrary inhomogeneities. The deduction of the "quadruple and multiple refraction-reflection law" is presented. On this basis the ray-tracing programs are revised and the basic scheme of the "modified ray-tracing" programs is given. Finally, it is shown that the homogeneous and the inhomogeneous characteristics of the medium are not identical, and using as an example the electron-polarized medium, the inhomogeneous permittivity is determined.

Acta Techn. Hung. **68** (1970), 245—253

E. Papp, S. Zsindely, T. Legát, B. Pődör: *Preparation and Properties of GaAs Single Crystals*

GaAs single crystals were prepared with the aid of a modified Bridgman method. Undoped crystals were of *n*-type with electron concentrations from 4×10^{16} cm^{-3} to 3×10^{18} cm^{-3}, and with a maximum room temperature electron mobility of 4200 cm^2/Vs. Chemical analysis showed that the main impurities of the crystals were S, Si, Se, Fe and Zn. Electrical conductivity, Hall coefficient and Hall mobility were measured on the crystals in the temperature range of 77—400°K. From the measured mobilities the total impurity content was deduced with the aid of the Brooks—Herring formula.

Acta Techn. Hung. **68** (1970), 255—258

J. F. Bitó: *The Cathode–Plasma Interaction of Low-Pressure Arc Discharges with Oxide Cathodes*

The author demonstrates by the analysis of the static and functional parameters of the oxide cathode and their influence upon the discharge spaces that the thermionic emission current of the cathode, being a complex cathode parameter, is suitable for the description of the connection between the potential and space characteristics of the cathode and cathode side. The coupling between the cathode and cathode space takes place with the aid of the emission current and by the ion current striking into the cathode.

The *Acta Technica* publish papers on technical subjects in English, French, German and Russian.

The *Acta Technica* appear in parts of varying size, making up volumes.

Manuscripts should be addressed to

Acta Technica
Münnich Ferenc u. 7.
Budapest V.,
Hungary

Correspondence with the editors and publishers should be sent to the same address.

The rate of subscription is $ 16.00 a volume. Orders may be placed with "Kultura" Foreign Trade Company for Books and Newspapers (Budapest I., Fő utca 32. Account No. 43-790-057-181) or with representatives abroad.

Les *Acta Technica* paraissent en français, allemand, anglais et russe et publient des travaux du domaine des sciences techniques.

Les *Acta Technica* sont publiés sous forme de fascicules qui seront réunis en volumes.

On est prié d'envoyer les manuscrits destinés à la rédaction à l'adresse suivante:

Acta Technica
Münnich Ferenc u. 7.
Budapest V.,
Hongrie

Toute correspondance doit être envoyée à cette même adresse.

Le prix de l'abonnement est de $ 16.00 par volume.

On peut s'abonner à l'Entreprise pour le Commerce Extérieur de Livres et Journaux »Kultura« (Budapest I., Fő utca 32. Compte courant No. 43-790-057-181) ou à l'étranger chez tous les représentants ou dépositaires.

«*Acta Technica*» публикуют трактаты из области технических наук на русском, английском, французском и немецком языках.

«*Acta Technica*» выходит отдельными выпусками разного объема. Несколько выпусков составляют один том.

Предназначенные для публикации рукописи следует направлять по адресу:

Acta Technica
Münnich Ferenc u. 7.
Budapest V.,
Венгрия

По этому же адресу направлять всякую корреспонденцию для редакции и администрации. Подписная цена — $ 16.00 за том.

Заказы принимает предприятие по внешней торговле книг и газет «Kultura» (Budapest I., Fő utca 32. Текущий счет № 43-790-057-181) или его заграничные представительства и уполномоченные.

Reviews of the Hungarian Academy of Sciences are obtainable at the following addresses:

ALBANIA

Drejtorija Qändrone e Pärhapjes dhe Propagandimit tä Librit
Kruga Konferenca e Päzes
Tirana

AUSTRALIA

A. Keesing
Box 4886, GPO
Sydney

AUSTRIA

GLOBUS
Höchstädtplatz 3
A-1200 Wien XX

BELGIUM

Office International de Librairie
30, Avenue Marnix
Bruxelles 5
Du Monde Entier
5, Place St. Jean
Bruxelles

BULGARIA

HEMUS
11 pl Slaveikov
Sofia

CANADA

Pannonia Books
2, Spadina Road
Toronto 4, Ont.

CHINA

Waiwen Shudian
Peking
P. O. B. 88

CZECHOSLOVAKIA

Artia
Ve Směčkách 30
Praha 2
Poštovní Novinová Služba
Dovoz tisku
Vinohradská 46
Praha 2
Mad'arská Kultura
Václavské nám. 2
Praha 1
SLOVART A. G.
Gorkého
Bratislava

DENMARK

Ejnar Munksgaard
Nörregade 6
Copenhagen

FINLAND

Akateeminen Kirjakauppa
Keskuskatu 2
Helsinki

FRANCE

Office International de Documentation et Librairie
48, rue Gay Lussac
Paris 5

GERMAN DEMOCRATIC REPUBLIC

Deutscher Buch-Export und Import
Leninstraße 16
Leipzig 701
Zeitungsvertriebsamt
Fruchtstraße 3—4
1004 Berlin

GERMAN FEDERAL REPUBLIC

Kunst und Wissen
Erich Bieber
Postfach 46
7 Stuttgart S.

GREAT BRITAIN

Blackwell's Periodicals
Oxenford House
Magdalen Street
Oxford
Collet's Subscription Import Department
Dennington Estate
Wellingsborough. Northants.
Robert Maxwell and Co. Ltd.
4—5 Fitzroy Square
London W. 1

HOLLAND

Swetz and Zeitlinger
Keizersgracht 471—487
Amsterdam C.
Martinus Nijhof
Lange Voorhout 9
The Hague

INDIA

Hind Book House
66 Babar Road
New Delhi 1

ITALY

Santo Vanasia
Via M. Macchi 71
Milano
Libreria Commissionaria Sansoni
Vie La Marmora 45
Firenze

JAPAN

Kinokuniya Book-Store Co. Ltd.
826 Tsunohazu 1-chome
Shinjuku-ku
Tokyo
Maruzen and Co. Ltd.
P. O. Box 605
Tokyo-Central

KOREA

Chulpanmul
Phenjan

NORWAY

Tanum-Cammermeyer
Karl Johansgt 41—43
Oslo 1

POLAND

RUCH
ul. Wronia 23
Warszawa

ROUMANIA

Cartimex
Str. Aristide Briand 14—18
Bucureşti

SOVIET UNION

Mezhdunarodnaya Kniga
Moscow G—200

EDEN

Almquist and Wiksell
Gamla Brogatan 26
S—101 20 Stockholm

USA

F. W. Faxon Co. Inc.
15 Southwest Park
Westwood Mass. 02090
Stechert Hafner Inc.
31. East 10th Street
New York, N. Y. 10003

VIETNAM

Xunhasaba
19, Tran Quoc Toan
Hanoi

YUGOSLAVIA

Forum
Vojvode Mišića broj 1
Novi Sad
Jugoslovenska Knjiga
Terazije 27
Beograd

10. VIII. 1970. Index: 26.025

ACTA TECHNICA

ACADEMIAE SCIENTIARUM HUNGARICAE

REDIGIT: M. MAJOR

TOMUS 68
FASCICULI 3—4

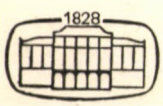

AKADÉMIAI KIADÓ, BUDAPEST 1970

ACTA TECHNICA

Az *Acta Technica* angol, francia, német és orosz nyelven közöl értekezéseket a műszaki tudományok köréből.

Az *Acta Technica* változó terjedelmű füzetekben jelenik meg, több füzet alkot egy kötetet.

A közlésre szánt kéziratok a következő címre küldendők:

Acta Technica
Budapest V., Münnich Ferenc u. 7.

Ugyanerre a címre küldendő minden szerkesztőségi és kiadóhivatali levelezés.

Megrendelhető a belföld számára az „Akadémiai Kiadó"-nál (Budapest V., Alkotmány utca 21. Bankszámla 05-915-111-46), a külföld számára pedig a „Kultúra" Könyv- és Hírlap Külkereskedelmi Vállalatnál (Budapest I., Fő utca 32. Bankszámla: 43-790-057-181) vagy annak külföldi képviseleteinél és bizományosainál.

Die *Acta Technica* veröffentlicht Abhandlungen aus dem Bereiche der technischen Wissenschaften in deutscher, englischer, französischer und russischer Sprache.

Die *Acta Technica* erscheint in Heften wechselnden Umfanges. Vier Hefte bilden einen Band.

Die zur Veröffentlichung bestimmten Manuskripte sind an folgende Adresse zu senden:

Acta Technica
Münnich Ferenc u. 7.
Budapest V.,
Ungarn

An die gleiche Anschrift ist auch jede für die Schriftleitung und den Verlag bestimmte Korrespondenz zu richten. Abonnementspreis pro Band: $ 16.00.

Bestellbar bei dem Buch- und Zeitungs-Außenhandels-Unternehmen »Kultura« (Budapest I., Fő utca 32. Bankkonto Nr. 43-790-057-181) oder bei seinen Auslandsvertretungen und Kommissionären.

Acta Technica Academiae Scientiarum Hungaricae, Tomus 68 (3—4), pp. 265—282 (1970)

REINFORCED CONCRETE FLAT SLABS AS REFLECTED BY THE VARIOUS SPECIFICATIONS

E. BÖLCSKEI*

CORRESPONDING MEMBER OF THE HUNGARIAN ACADEMY OF SCIENCES

[Manuscript received, Nov. 6, 1969]

A comparative study on the different specifications relating to the reinforced concrete flat slabs revealed significant divergences in the prescriptions of different countries and recommendations of the international committees, both in respect to the calculation and rules of construction. The physical entity is everywhere the same, therefore, it would be advisable to unify or at least to bring nearer to one another the different specifications.

1. Introduction

It is long time since the structural engineers have observed that the proportions of the flat slabs calculated according to the specifications of the different countries significantly differ. The purpose of this paper is to compare the divergences** in the specifications. In the following, our investigations and their results will be described in short. The problem is particularly timely because the revision of the Hungarian specification is at present in progress.

The flat slab is such a two-way reinforced concrete slab structure by which the applied load, commonly uniformly distributed, and of significant magnitude, is directly transmitted without beams to the columns rigidly jointed to the slabs.

The traditional reinforced concrete flat slabs are constructed by the application of columns with large capitals. The types applied are shown in Figs. 1a, 1b and 1c. In Fig. 1d a flat slab without column capital and drop panel (i.e. a flat plate) is illustrated.

Flat slabs were already employed in the early days of the reinforced concrete constructions, its rapid spread being due to its low structural depth, absence of beams and the relatively simple construction work.

The fields of its application in building construction are: floors of store houses and works (Fig. 2) of heavy loads; in civil engineering: deck plates for bridges (Fig. 3) and plates as well as supports for water reservoirs.

* Dr. techn. E. Bölcskei, Kovászna-u. 7, *Budapest XI*, Hungary

** The comparative calculations were carried out under the guideance of the writer, on the authority of the Panel for Engineering Mechanics of the Hungarian Academy of Sciences, by J. Almási, B. Gnädig, T. Kármán, I. Komlóssy, P. Lenkei and A. Windisch.

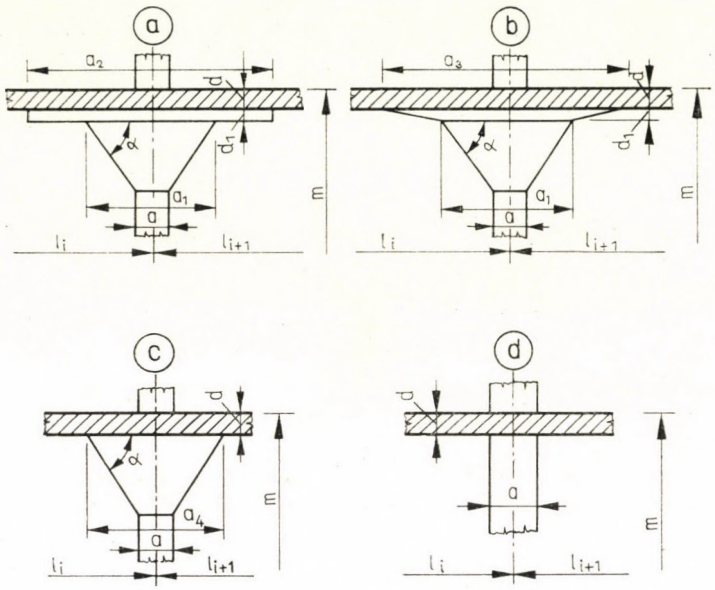

Fig. 1. Column-slab connection in the flat slab structure

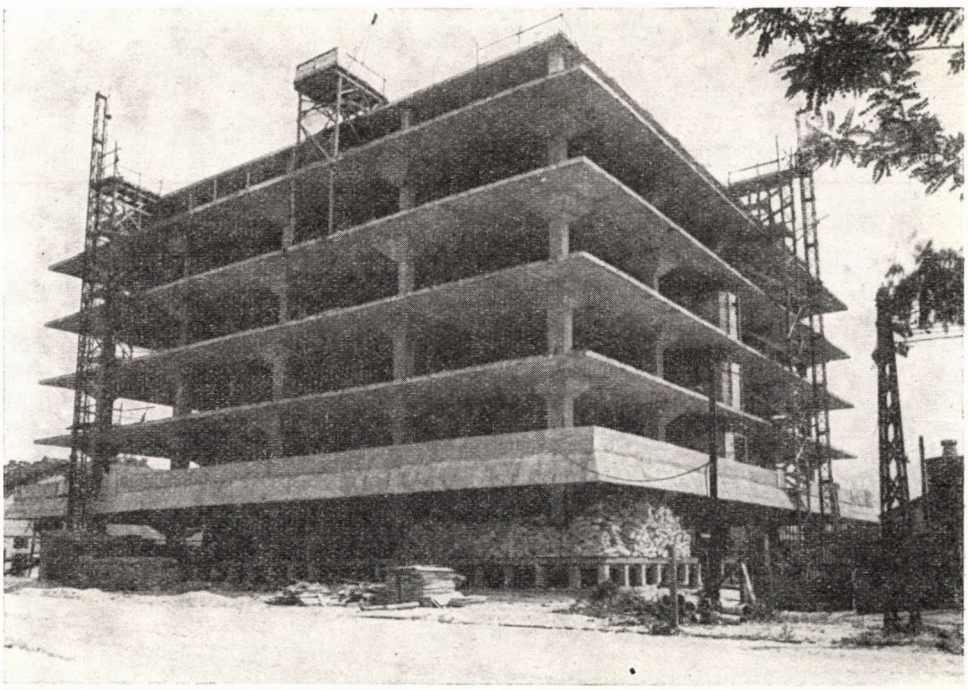

Fig. 2. Flat slab structure of a storehouse

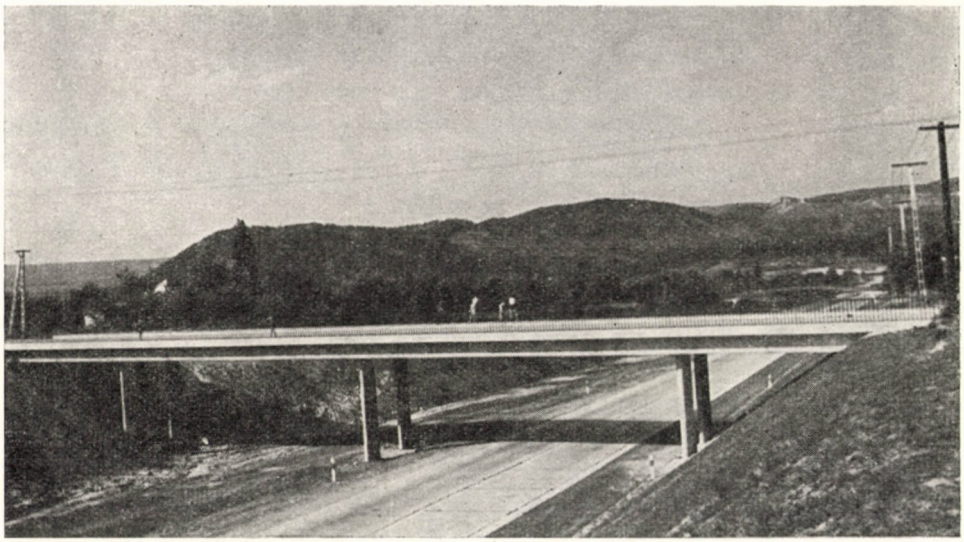

Fig. 3. Flat slab structure of a highway bridge

2. Short historical survey

The flat slab structure is one of the few forms really true to the material of reinforced concrete constructions. However, in the progress of development the structural engineers could hardly give up the traditional structures with ribs.

The idea of flat slabs had already occurred in America in the nineties of the last century, however, the first reliable evidence was a notice of the patent of O. W. NORCROSS from the year 1901. The public belief assigned the invention of this structure to C. A. P. TURNER who also applied for a patent in the United States in 1907. As a matter of curiosity, one of the drawings of the original patent is shown in Fig. 4. Anyhow, whosoever was the first, the merit of the development and spread of the structure belonged to TURNER who lived in Minneapolis. He published a paper dealing with this structure in connection with the construction of the local knitwear works in the year 1905.

In Europe, the falt slab structure was considered as a typical American invention. As far as one can make certain from sources available, first R. MAILLART from Switzerland made an attempt in 1908 to adopt this structure, and carried out extensive investigations at the plant of his firm in Zurich. In making use of the experiences for the first time the storehouse in Giesshübel of the Storing Company of Zurich was constructed in 1910. In the former Austro-Hungarian Monarchy, flat slabs were built during the Great War 1914—1918,

and in Hungary in 1922, in the town Karcag. They won a wide application at the beginning of the thirties by the hardy designs of B. ENYEDI.

The thought of the flat slab without column capitals (flat plates) already came up in the thirties, however, its use only became extensive in the recent two decades.

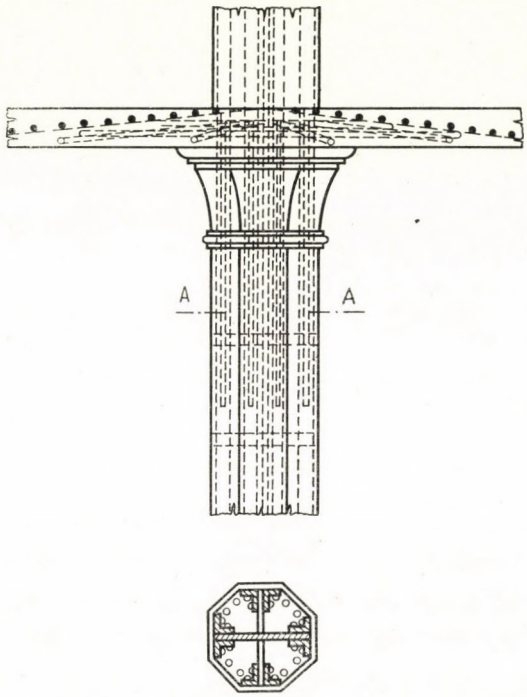

Fig. 4. One of the drawings of Turner's patent. Cross section A-A

3. Survey of the specifications

The investigations were first carried out on the specifications of the two great industrial powers, the United States and the Soviet Union. In both of these countries a series of full scale tests were conducted, and in establishing their specifications, the results obtained have been taken into account. The prescriptions of the German DIN also ought to be considered, for, among others, the Hungarian specifications relating to flat slabs were based on these latter, both between the two world wars, and in the fifties. The investigations have also been extended to the recommendations of the European Concrete Commission (CEB) recently prepared because they are now being applied in a number of European countries.

In the studies comparison has been made between those mentioned above and those used in Hungary:

— MSZ (Hungarian Standard) No 15022 published in 1953,

— domestic standard of the Design Institute for Industrial Buildings (IPARTERV),

— draft standard MSZ No 15022/1 published in 1968.

The latest prescriptions of the *Soviet SNIP* are positively based on the limit design method. In determining the stresses occurring in the exterior strip, they make a distinction according to the manmer of support. In respect to the calculations of the load carrying capacity, the investigations should be carried out with respect to

— the separate failures in the different strips perpendicular to one another

— the simultaneous failures of the strips crossing one another

— the perforation of the slabs by the columns.

The specification also includes prescriptions for the examination of the columns. It also gives complete formulas with the aid of which the designer can simply and rapidly find particulars relating to the reinforcement.

The examination in respect to freedom from, and restriction on, occurring cracks as well as of the stiffness is also prescribed, and there are measures relating to the arrangement of the reinforcement to the terminations and splices of bars.

No special rules exist for the calculation of flat plates and drop panels because the limit design method takes into account the way of modification of the crack pattern by the capital.

The *American specification ACI 318—63* permits the use of three design methods:

— the elastic

— the limit design method, and

— designing on the basis of test results.

The first two methods start from theoretical bases in determining the bending moments acting on the column and middle strips of the two-way frame system, as well as the stresses in the columns with capitals serving to support the floor slab. However, in practice, the empirical method is mainly applied, based on the results obtained from a great number of tests carried out on full size models of reinforced concrete structures.

The very same methods are applicable to the calculation of flat slabs supported by columns without capitals, with the only modification that the dimension c expressing the effect of the capital only designates the dimension of the column.

The prescriptions of the *German Standard DIN-1045* are based on the theory of elasticity. The stress pattern in the structure is determined by finding the internal forces of frames, assuming that each of the two-way systems of frames bears the entire load separately. It is specified how the stresses

in the slab obtained as described above, are distributed in the column strip and middle strip, in the midspan and the above support.

For the calculation of the flat plate supported by columns without capitals, in recent years a complementary specification has been prepared, the basic principles of which are the same as those above, but it reduces the width of the column strip on the account of that of the middle strip. At the same time the examination for perforation is also prescribed.

The recommendations of the *European Concrete Commission* (CEB), *Bulletin 67*, are also based on the limit design method starting from the lines of fracture. The recommendations, similarly to the Soviet specifications, assume two kinds of failure patterns. One of them is based on the system of positive lines of fractures, running in the centre lines, and on the system of negative lines of fracture developed along the drop panels, the other one on the nearly circular pattern formed all around the columns. On the basis of these assumptions not only the stresses in the slab can be found, but also those acting on the columns.

A special examination should be carried out with respect to the perforation. The responsible Commission of the CEB adopted for this purpose the suggestion of Prof. NYLANDER taking into account the shear surface in the load carrying capacity of both the concrete and the reinforcement.

The first of the *Hungarian Specifications* to be considered in the comparative study was the respective chapter of the Hungarian Standard MSZ 15022 published in 1953. In general, its prescriptions are the same as those of the reinforced concrete specification relating to this subject, and of the German DIN-1045 with the norms described above. Thus, in essence, this specification prescribes the examination of a twoway system of frames for the whole load in both directions with the aid of the theory of elasticity.

The constructions carried out in the fifties indicated that the Hungarian prescriptions led to the overdesign of flat slabs. In the Design Office IPARTERV Eng. I. KOMLÓSSY pursued comparative studies and suggested a calculation method which later became obligatory as a domestic specification in this Design Office. According to this suggestion the bending moments acting on the slab should be computed by using a reduction factor for the span determined in accordance with the dimensions of the capital. On certain conditions, this specification also prescribes the examination for perforation. The procedure may be extended to the flat plate structure.

The draft of the Hungarian Standard MSZ 15022/1 published in 1968, permits for the computation of flat slabs the application of an approximate procedure based in essence on the limit design method. In determining the stresses caused in the structure also the reduced span is taken into account. The value of the reduction factor depends on the proportions of the column capital. The method may be applied to the computation of flat plates, though, in this case, the reduction is rather small.

4. Comparison on the basis of stresses

In order to compare the different specifications, calculations were made with respect to existing intermediate floor slabs with and without column capitals, of commonly applied proportions and loads. The dimensions of the middle panel are 6.0×7.0 m, those of the exterior one, 5.0×7.0 m, supported at its longer side (Fig. 5).

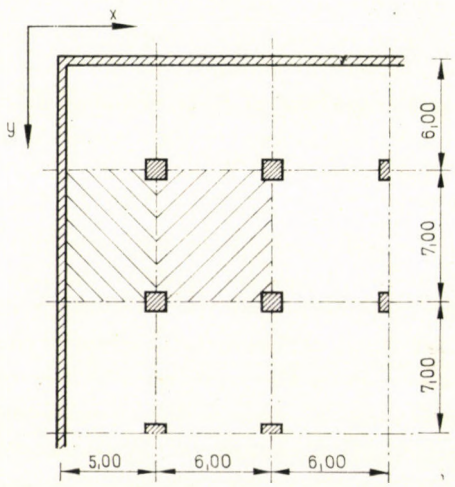

Fig. 5. Plan view of the examined flat slab. The panels examined are hatched

The calculations were carried out by applying the Soviet (SNIP), the American (ACI), the German (DIN) specifications and the recommendations of the European Concrete Commission (CEB). The same structure was examined by making use of the Hungarian standard MSZ 15022 (1953), the domestic specification of the Design Office IPARTERV and also the draft standard MSZ 15022/1 (1968).

The results obtained may also be used for the estimation of structures of other proportions, occurring in practice.

4.1 *Flat slab with column capital and drop panel*

A reinforced concrete flat slab, 18 cm thick, served as basis of the comparison, the live load at which it has been specified was 1200 kp/sq. metre.

Starting out from the data given above, the values of the moments acting on the middle and column strips of the flat slab structure have been determined. The specific moment per linear metre was expressed as ql^2/α, and Table 1 contains the α-divisors. In the fifth line of the table figure the divisors

characteristic of the mean total of the absolute values of the positive and negative moments acting on the strips.

In the sixth line of the table, taking up the average total moment as 100 per cent, calculated according to the prescriptions of the Hungarian Standard MSZ 15022 being at present in force, the index numbers characteristic of each specification are indicated.

Since according to the different specifications the reinforcements being in accordance with the moments are calculated in different ways, it seemed

Table 1

Name	No	SNIP	ACI	DIN	CEB	MSZ	IPAR-TERV	Suggested
Middle strip (+)	1	47,7	52,9	24,6	32,5	24,3	46,7	34,4
(−)	2	17,0	52,9	22,9	32,5	23,4	42,1	33,1
Column strip (+)	3	47,7	39,7	19,7	32,5	19,8	38,3	28,1
(−)	4	17,0	15,8	7,6	16,2	7,8	14,0	11,0
Mean divisor	5	12,5	15,8	7,5	13,0	7,6	14,0	10,8
Index number of the moment [%]	6	61	48	101	58	100	54	70
F_{steel} average [cm²/m]	7	6,67	9,36	23,14	11,91	12,95	6,94	8,52
Ratio of reinforcement [%]	8	51	72	179	92	100	54	66

to be reasonable to compare the reinforcements calculated. The average quantities of the reinforcement corresponding to the respective moments, are indicated in line 7 of the Table. In the eighth line, those index numbers are given which show what quantity of reinforcement is needed expressed in per cent, taking for 100 per cent the quantity of reinforcement to be applied according to the prescriptions of the Hungarian standard MSZ 15022 now in operation.

Similar calculations were also made in respect of the exterior strip. The different specifications make a distinction according to the manner of the exterior support which may be solved by applying half capitals, wall or beam. The fixed-end moment produced in the line of the exterior support is diversely weighted by the different specifications, for that very reason the comparison of the result of the calculations does not lead to a definite conclusion.

In order to clarify how much more advantageous the flat slabs are as considered by the different specifications in comparison with the ordinary floor slabs, comparative calculations have also been carried out. The load bearing capacity of the continuous slab produced with the reinforcement as

described above has been calculated according to each specification. The effective load bearing capacity of this reference beam was as indicated in Table 2.

In the second line of the table the quotients of the live load capacity of the continuous beam permitted by the specification in question and the assumed live load, 1200 kp/sq. metre, are indicated. These numbers characterize

Table 2

Name	SNIP	ACI	DIN	CEB	MSZ	IPAR-TERV	Suggested
Live load							
p_l [kp/sq·m]	562	355	1308	545	1280	575	723
p/p_l	2,14	3,38	0,92	2,20	0,93	2,08	1,66
Relative hardiness	2,30	3,62	0,99	2,36	1,0	2,23	1,78

the "hardiness" of the specification in question, in respect to the flat slab. Assuming the value obtained with the aid of the Hungarian standard as unit, then, in the third line of the table the values referring to this unit are indicated.

Finally, in order to compare the moments acting on the columns the average eccentricity of the forces acting on the columns were defined. By average eccentricity the arithmetic mean of the eccentricities in the x and y directions is meant. The respective results are shown in Table 3.

Table 3

Name	SNIP	ACI	DIN	CEB	MSZ	IPARTERV	Suggested
Eccentricity [cm]	17,9	7,7	15,3	0,0	16,9	11,9	13,4

4.2 *Flat slab structures without column capitals (Flat plate structures)*

In this case a structure with a reinforced concrete flat slab of a depth of 30 cm attacked by an effective load of 500 kp/sq.m served as basis for the comparative calculations.

By carrying out the calculations for the middle strip of the flat slab and for the reference beam, the results given in Tables 4 and 5 were obtained in respect to the flat plate. The Hungarian Standard MSZ (1953) is not mentioned

Table 4

Name	No	SNIP	ACI	DIN	CEB	IPARTERV	Suggested
Middle strip (+)	1	19,1	36,5	20,2	23,9	36,4	27,1
(−)	2	19,1	36,5	13,7	23,9	32,8	27,6
olumn strip (+)	3	19,1	26,6	17,9	23,9	29,8	22,2
(−)	4	19,1	12,7	5,5	12,0	10.9	9,2
Mean divisor	5	9,6	11,7	5,6	9,6	10.9	8,8
Index number of the moment [%]	6	58	48	100	58	51	64
F_{steel} [cm²/m]	7	4,77	6,80	10,61	6,06	6,68	5,13
Ratio of reinforcement [%]	8	45	64	100	57	63	48

Table 5

Name	SNIP	ACI	DIN	CEB	IPARTERV	Suggested
Live load p_l [kp/sq · m]	293	90	808	286	280	368
p/p_l	1,7	5,56	0,62	1,75	1,78	1,36
Relative hardiness	2,75	8,98	1,00	2,83	2,87	2,20

in the tables because by this time the flat plate structure was still unknown. This form of structure is relatively new. For this very reason, the specifications cannot depend on such an abundance of experiences than in the case of flat slab with column capitals, and in designing them great care should be taken. This holds especially for the examination of perforation.

Also in this connection comparative calculations were carried out in order to examine, that at the example in question, in case of the structure calculated according to the different specifications, how the limit force characteristic of the perforation of the plate by the column is related to the design force. It is important to notice that where the ratio P_{limit}/P_{design} is less than the unit, the concrete alone cannot withstand the shear stress; reinforcement or steel shear capital should be applied there. The results of the calculation are represented in Table 6.

Table 6

Name	SNIP	ACI	DIN	CEB	IPARTERV	Suggested
P_{limit}/P_{design}	0,78	1,11	1,24	0,95	1,02	1,05
Relative number [%]	0,63	0,90	1,00	0,77	0,82	0,85

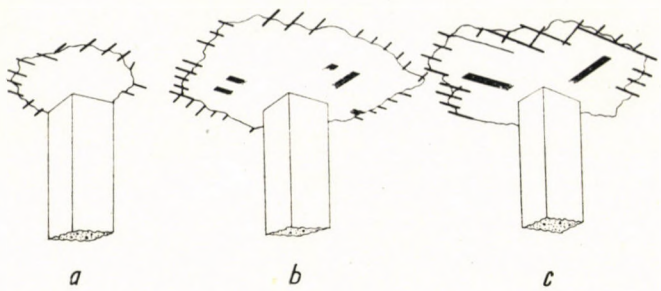

Fig. 6. Various forms of failure caused by perforation

Also for the examination in respect of the perforation extensive series of tests have been carried out. The failure pattern strongly depends on the shear reinforcement arranged in the capital. The manner of failure developed is represented in Fig. 6, i.e., in Fig. 6a in the case of the underreinforced, in Fig. 6b in the case of the ordinarily reinforced and in Fig. 6c in the case of the overreinforced floor structure.

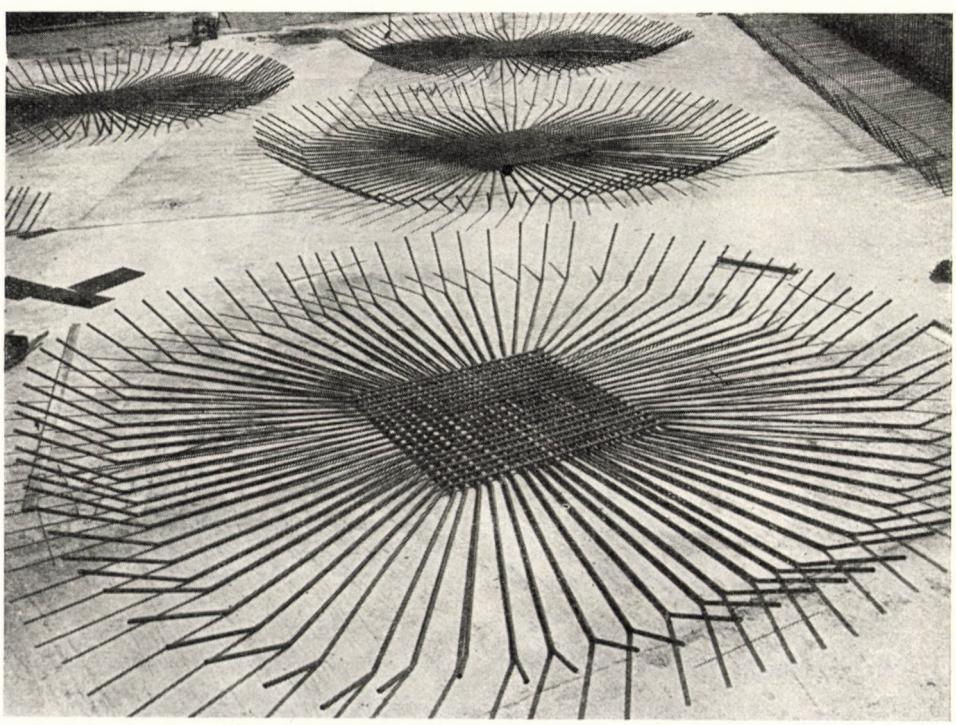

Fig. 7. Shear reinforcement of a base plate around the column capital

To withstand slab shear forces in a structure without column capital, in the neighbourhood of the column the following solutions may be applied:

— the concrete without shear reinforcement is sufficient in itself to withstand the shear stresses;

— shear stresses are withstood by suitably bent round bars (Fig. 7);

— in case of very high shear stresses special profiles serve to withstand shear forces (Fig. 8).

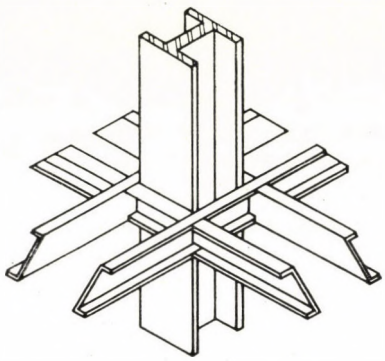

Fig. 8. Rigid reinforcement to withstand perforation stresses

4.3 *Conclusions*

The tables established for the flat slab structures with and without column capitals indicate the following results:

a) There is a wide dispersion in the *stress* values defined on the basis of the different foreign specifications. Between the maximum and minimum values there is a difference greater than 100 per cent. In the quantity of *reinforcement*, the differences are still greater. Here, the greatest value is 3.5 times that of the minimum. The characteristic index number of the "*hardiness*" varies between 1.0 and 3.62.

b) From among the foreign ones it is the German specification based on the theory of elasticity, which is the most cautious, the boldest being the American one based on the results of tests conducted on full scale models. The Soviet specification and the recommendations of the European Concrete Commission lie between these latter two. This conclusion holds for all three quantities mentioned in section a).

c) By making comparison between the Hungarian Specifications, it can be stated that the MSZ 15022 of 1953 is the most cautious one, the domestic standard of the Design Office IPARTERV is, in the opinion of the writer too daring, while the suggestion contained by the Hungarian standard MSZ 15022/1 published in the year 1968, represents the right middle way.

5. Comparison between the rules of construction

A comparison is also made between the rules of the Hungarian and foreign specifications of major importance relating to the construction of flat slab structures. All of the prescriptions which were of significance were examined in connection with the construction of flat slab structures. Such are the proportions of the column capital, the limiting values in respect to the thickness of the slab, the dimension of the columns, the side ratios of the panels and ratios of the adjacent spans.

5.1 *The column-slab connection in the flat slab structure*

The conventional flat slab structure is constructed with a column capital, and the specifications commonly deal with three types of capitals. On principle, the capitals may be rectangular or circular in plan. Recently, as has been mentioned, no capital is constructed at the joint of the slab and column. The arrangements of the different connections are represented in Fig. 1, whilst Table 7 indicates the minimum dimensions according to the prescriptions.

Table 7

Value	SNIP	ACI	DIN	CEB	MSZ	IPARTERV	Suggested
d_1	$d_1 \cong 1{,}0\ d \div 1{,}5\ d$	$\leq d/4$	$\leq d/2$	$\leq 0{,}6\ d$	$\leq d/2$	$\leq d/2$ $\leq 18\ \mathrm{cm} - d_1$	$\leq d/2$
a_1	$0{,}16\ l \leq a_1 \cong 0{,}24 l$	—	$0{,}2\ l$	$l/6 \leq a_1 \leq l/4$	$0{,}2\ l$	—	$0{,}2\ l$
a_2	$\leq a_1 + 0{,}18\ l\ d_1/d$	$l/3$	$0{,}4\ l$	$\leq a_1 + 0{,}36\ l\ d_1/d$	$0{,}4\ l$	formula	$0{,}4\ l$
a_3	$\leq a_1 + 0{,}18\ l\ d_1/d$	—	$0{,}4\ l$	$\leq a_1 + 0{,}36\ l\ d_1/d$	$0{,}4\ l$	formula	$0{,}4\ l$
a_4	—	—	—	—	$0{,}2\ l$	—	$0{,}2\ l$
α	$\leq 45°$	—	$\leq 45°$	$\leq 45°$	$\leq 45°$	$\leq 45°$	$\leq 45°$

5.2 *Slab thickness*

One of the most important problems in the construction of the flat slab is the selection of the slab thickness. Almost all the specifications only prescribe the minimum value of the thickness. The purpose of prescribing this value is

that no noticeable damaging deflection might occur which would limit the use of the structure even under the effect of relatively heavy live loads.

The Soviet specification does not comprise any limitations in respect to the slab thickness. The other specifications commonly prescribe the slab thickness independently of the type of capital. Exceptions are the American specification and the domestic standard of the IPARTERV based on this latter. In the American prescriptions the rules to be observed are too rigorous. Here, the slab thickness is affected by the span, shape of the column capital, load, and cube strength of the concrete. The domestic standard of the IPARTERV does not prescribe this requirement.

It is of interest to consider that in the case of the example treated, what limits are established in choosing the slab thickness by the different specifications. The respective specifications are indicated under the headings of Table 8, and the calculated thickness is shown below them. In determining the values in our example the selected value of c was 70 cm and for the capital the type "a" was applied. Further, it was assumed that the 28-day cube strength of the concrete of the structure was 200 kp/sq. cm, the ultimate strength of the reinforcing steel was 2700 kp/sq cm, and the safety factor 1.3.

From the preceding is to be seen that the rules of construction lay down strict limits to slab thickness. From this point of view, the German DIN is the most indulgent which only prescribes the lowest limit as 15 cm, whilst the ACI and CEB provide very strict rules. In these latter the slab thickness is directly influenced by the live load, shape of the capital, and grade of the concrete and steel applied. The Hungarian specifications follow, in the opinion of the writer, the right middle way.

5.3 *Dimensions of the supporting columns*

The traditional flat slab will fulfil its function as expected, if at the slab-column connection a significant effect of restraint is realized. Therefore, most of the specifications prescribe the minimum dimension for the columns either particularly in connection with the flat slabs or, in general. The respective prescriptions are indicated under the headings of Table 9, while below them the minimum dimensions of the columns are presented, calculated with the aid of the different specifications. It is also important to mention that in the calculations we started out from a column height of 4.0 m. In this respect, the specifications are as a rule, practically in agreement, with the only exception of the American one which is more rigorous than all the others.

Table 8

SNIP	ACI	DIN	CEB	MSZ	IPARTERV	Suggested
	$\geqq l/40$ $\quad \geqq l/36$ $\geqq 10{,}2$ cm $\quad \geqq 12{,}7$ cm $\geqq 4{,}0 + 0{,}024\,l \quad \geqq 2{,}5 + 0{,}028\,l$ $\left(1-\frac{2c}{3l}\right)\sqrt{\frac{250}{K_{28}}}\,q \quad \left(1-\frac{2c}{3l}\right)\sqrt{\frac{250}{K_{28}}}\,q$	$\geqq 15$ cm	$\geqq l_s/35$ wherein l_s = diagonal length $= \frac{\sigma_a^* l}{35\,000\,\gamma_s}\cdot\frac{p}{g+p}$	$\geqq 15$ cm $\geqq l/32$ (intermediate floor) $\geqq l/40$ (roof floor)	Intermediate floors $\geqq l/40 \mid = l/36$ $\geqq 12$ cm $\mid = 14$ cm at roof floors smaller by 20 %	$\geqq 14$ cm $\geqq l/32$ (interm. floor) $\geqq l/40$ (roof floor)
	17,5 cm 10,2 cm **26,0 cm**	**15 cm**	21,3 cm **28,4 cm**	15 cm **21,9 cm**	**17,5 cm** 12 cm	15 cm **21,9 cm**

Remarks

1. Dimension of all the lengths is *cm*.
2. Dimension of the uniformly distributed loads g, p and q = g + p is Mp/sq · m.
3. The value "*c*" in the ACI denotes the diameter (measured in the lower plane of the slab or drop panel) of an angle of vertex 90° which may be placed inside of the capital.
4. σ_a^* = ultimate strength of the reinforcing steel, γ_s = safety factor of the load.
5. By the length l commonly the largest span is meant.

Table 10

SNIP	SNIP	ACI	DIN	CEB	MSZ	IPARTERV	Suggested
$\frac{l_x}{l_y}$	$\frac{2}{3} \leqq \frac{l_x}{l_y} \leqq \frac{3}{2}$	$0{,}75 \leqq \frac{l_x}{l_y} \leqq 1{,}33$	–	$\frac{2}{3} \leqq \frac{l_x}{l_y} \leqq \frac{3}{2}$	$0{,}8 \leqq \frac{l_x}{l_y} \leqq 1{,}25$		
$\frac{l_{i+1}}{l_i}$	$\frac{3}{4} \leqq \frac{l_{i+1}}{l_i} \leqq \frac{4}{3}$	$0{,}8 \leqq \frac{l_{i+1}}{l_i} \leqq 1{,}25$	$\frac{l_{\min}}{l_{\max}} \geqq 0{,}8$	$\frac{3}{4} \leqq \frac{l_{i+1}}{l_i} \leqq \frac{4}{3}$	–	$\frac{l_{i+1}}{l_i} \cong 1$	–

Table 9

SNIP	ACI	DIN	CEB	MSZ	IPARTERV	Suggested
—	$\geqq 25$ cm	$\geqq 30$ cm	—	$\geqq 30$ cm	$\geqq 25$ cm	$\geqq 30$ cm
	$I \geqq 41\,600$ cm^4	$\geqq \frac{m}{15}$		$\geqq \frac{m}{15}$	$\geqq \frac{m}{15}$	$\geqq \frac{m}{15}$
	$I \geqq \frac{l}{12}$	$\geqq \frac{l}{20}$		$\geqq \frac{l}{20}$	$\geqq \frac{l}{20}$	$\geqq \frac{l}{20}$
	$\frac{md^3}{0{,}5+g/p}$					
	25 cm	30 cm		30 cm	25 cm	30 cm
	26,5 cm	26,6 cm		26,6 cm	26,6 cm	26,6 cm
	40 cm	30 cm		30 cm	30 cm	30 cm

Remarks

1. Dimension of all the lengths is *cm*.
2. Dimension of the uniformly distributed loads g and p is $Mp/sq \cdot m$.
3. m = height between floors.

5.4 *Side ratio of the panels and ratio of the adjecent spans*

In the different specifications, practically, almost the same side ratios are permitted for the panels in the strips of the flat slab structure except the DIN which does not provide any limitations. In the way, the specifications also make provision for avoiding great differences between the adjacent spans. Details in this connection are indicated in Table 10.

5.5 *Evaluation according to the construction rules*

It can be seen from the preceding that the construction rules of the different foreign specifications significantly differ.

Regarding the slab thickness of the flat slab structure the prescriptions of the American specification and the recommendations of the European Concrete Commission (CEB) are far more rigorous than those of the DIN, and especially those of the Soviet specification. This latter, as well as the Hungarian specification do not contain any particular limitations for the slab thickness of the flat slabs.

Thus, in the prescriptions relating to the calculation of flat slab's stresses an antagonistic trend is noticeable.

In essence, in the case of the minimum dimension of the columns supporting the flat slab, the situation is the same. In general, the specifications

provide the same limitations, except the American one which also in this respect is more rigorous.

There are also significant differences between the three Hungarian specifications. The MSZ published in 1953 and the draft of 1968 contain nearly the same rules, in turn, the domestic standard of the IPARTERV, especially in respect to the slab thickness, is extraordinarily concessive.

6. Summary and conclusions

Owing to the current revision of the Hungarian specifications relating to the load carrying structures of buildings, a thorough examination of the problems connected with the flat slabs became necessary. The conclusions may be derived as follows:

— The investigations in the manner of determing the stresses in the conventional flat slabs revealed significant divergences in the foreign specification. In the opinion of the writer, the DIN and the earlier Hungarian specifications based on this latter are too cautious, while the ACI seems to be too hardy. The Soviet specification and the recommendations of the European Concrete Commission follow a middle trend. It seems to be advisable to approach these latter by the new Hungarian prescriptions.

— In recent years flat plates increased in significance, therefore, it seemed to be necessary to provide prescriptions in the draft also for the calculation and construction of this form of structure. The examination of the foreign specifications have led to the same conclusion. The draft specification relating to the flat plate structures already takes these statements into account, however, in the reinforcement over the supports it requires an additional safety of 50 per cent.

— A comparison between the construction rules indicates that the specifications being hardier in the determination of the stresses, impose a precaution on the designer. The earlier Hungarian Specifications as well as the draft of 1968 follow a middle course.

*

The writer would greatly appreciate and consider it a success of this work if it would initiate an international discussion about the problem of flat slab structures, and would, therefore, look forward to any contributions on the subject.

Stahlbeton-Pilzdecken im Lichte der Vorschriften *(E. Bölcskei)*. Die Entgegenstellung von Vorschriften in bezug auf die Pilzdeckenkonstruktionen hat wesentliche Abweichungen entdeckt zwischen den diesbezüglichen Bestimmungen von einzelnen Ländern, bzw. den Vorschlägen der internationalen Ausschüsse. Diese Abweichungen zeigen sich sowohl in den Berechnungen, als auch in Zusammenhang mit den Konstruktionsregeln. Die physische Realität ist überall identisch, deshalb schlägt der Verfasser die Vereinheitlichung, oder wenigstens die Annäherung der verschiedenen Vorschriften vor.

Железобетонные безбалочные конструкции в зеркале технических условий *(Э. Бельчкеи)*. Сравнительное исследование технических условий, касающихся безбалочные конструкций, вскрыло значительные отклонения между техническими условими отдельных стран и предложениями международных комиссий. Эти отклонения наблюдаются как по методике расчета, так и правилами конструирования. Физическая действительность является идентичной и было бы целесообразным именно вследствие этого факта произвести унификацию этих технических условий, но хотя бы их приближение друг к другу. Инженерам-практикам уже давно бросилось в глаза, что между размерами железобетонных безбалочных конструкций, рассчитанных на основе технических условий, действительных в отдельных странах, существуют значительные отклонения. Сравнительные расчеты под руководством автора производились по поручению технико-механического коллектива Академии наук Венгрии Йожефом Альмаши, Бэла Гнедигом, Тамашем Карман, Иштваном Комлоши, Петером Ленкеи и Андором Виндиш. Вкратце дается изложение этих исследований и их результатов. Данный вопрос является особенно актуальным.

Acta Technica Academiae Scientiarum Hungaricae, Tomus 68 (3—4), pp. 283—291 (1970)

EINFLUSS VON ZUSATZMITTELN AUF DIE EIGENSCHAFTEN VON STABILISIERTEN BÖDEN

Á. KÉZDI*

KORRESPONDIERENDER MITGLIED DER UNG. AKADEMIE DER WISSENSCHAFTEN

und

B. NAGYVÁTI**

[Eingegangen: 21. Juni 1967]

Bei einigen traditionellen Stabilisierungsverfahren wird die Möglichkeit der Anwendung von ergänzenden, auf die Stabilisierung fördernd wirkenden Chemikalien und anderen Materialien erörtert. Ohne Anspruch auf Vollständigkeit, erstreckt sich der Aufsatz nur auf die Zusatzmittel, die wirtschaftlich benutzt werden und die die erforderlichen Eigenschaften des Erdstoffes wirksam verbessern können.

Unter Bodenstabilisierung versteht man bekanntlich die vorteilhafte Änderung einer Erdstoffeigenschaft und Festlegung des günstigen Wertes, um ein bestimmtes technisches Ziel zu erreichen. In Abhängigkeit von dem technischen Ziel, den Gegebenheiten des Erdstoffes und von den technisch-wirtschaftlichen Erwägungen können wir die Stabilisierung des Bodens auf verschiedene Arten erzielen; nach den Vorschriften der verschiedenen Verfahren mischt man dem Erdstoff eine ziemlich große Menge von Fremdmaterial zu, so z. B. im Falle von mechanischer Stabilisierung, zur Verbesserung der Kornverteilung, körnigen oder bindigen Erdstoff, bei anderen Verfahren Zement, Kalk, Bitumen oder andere chemische Materialien. Nach Vermischung dieser Materialien mit dem Grundstoff und nach gründlicher Verdichtung dieser Mischung erhalten wir den Erdstoff, der das Erreichen des gewünschten Zieles durch die auftretenden physikalischen und chemischen Prozesse sichert.

Außer den erwähnten wichtigsten Stabilisierungsstoffen wurden neuerlich Versuche angestellt mit der Absicht, den Einfluß von einigen Zusatzmitteln, d. h. zusammen mit den dem befestigenden Grundmaterial beigemischten Chemikalien, auf den stabilisierten Erdstoff zu untersuchen. Diese Zusatzmittel von geringer Menge verbessern oftmals sehr günstig einige Erdstoffeigenschaften; so z. B. kann durch deren Anwendung entweder die Festigkeit wesentlich erhöht oder die vorgeschriebene Festigkeit wirtschaftlicher, mit einer geringeren Stabilisatormenge erreicht werden.

Im folgenden werden wir einige Versuchsergebnisse über den Einfluß der in geringer Menge beigemischten Chemikalien vorlegen.

* Dr. techn. Á. KÉZDI, Logodi-u. 9, *Budapest I*, Ungarn
** B. NAGYVÁTI, Kuruclesi-út 9b, *Budapest II*, Ungarn

Zur Erhöhung der Festigkeit oder zur Verbesserung anderer Eigenschaften der *mit Zement stabilisierten Böden* wurden schon seit langem verschiedene chemische Verbindungen in geringer Menge angewendet. Mit der Beimengung von einigen Verbindungen der *Alkalimetalle* (Natrium, Kalium, Lithium) hat man sehr günstige Erfahrungen gemacht, doch auch mit Anwendung von anderen Chemikalien wurden Versuche vorgenommen.

Zugabe von Hydroxyden und zahlreichen Salzen der Alkalimetalle in 1 bis 4 Gewichtsprozent erhöht die Druckfestigkeit der mit Zement stabilisierten Böden in einer im Bild 1 dargestellten Weise. Die Diagramme stellen

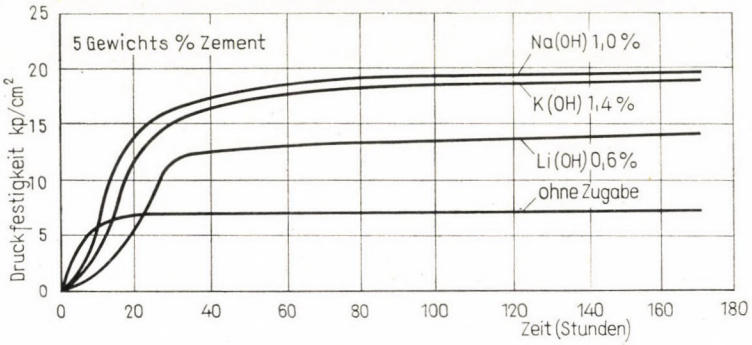

Bild 1. Einfluß von Alkali-Metallhydroxyden auf die Druckfestigkeit eines mit Zement stabilisierten Schluffes

die Druckfestigkeit eines Schluffes dar, im Falle von einer Zementzugabe von 5 Gewichtsprozent ($I_p = 16\%$). Im allgemeinen, je größer die Plastizitätszahl oder der organische Stoffgehalt des Bodens ist, um so kleiner wird der Befestigungseffekt. In Schluffen nimmt der Einfluß der Natriumverbindungen in der folgenden Reihenfolge ab: Sulfat-Aluminat—Metasilikat—Karbonat—Hydroxyd—Sulfit; die optimale Konzentration ist der Normalwert 1,0 des Alkalis in dem Mischwasser. Größere Konzentrationen ergeben zwar gleiche Endfestigkeiten, verlängern aber die Verfestigungsdauer. Die Wirksamkeit der Zusatzmittel hängt von der Menge der im Boden befindlichen, durch alkalischen Aufschluß ermittelbaren, reaktionsfähigen Silikate ab (Bild 2).

Die vorteilhaften Einflüsse können folgenderweise erklärt werden:

Wenn man Zement mit Erdstoff und Wasser vermischt, entstehen während des Hydratationsprozesses anfangs Kalk, Kalziumsilikat und Kalziumaluminat. Die Reaktion zwischen dem Kalk und den reaktionsfähigen Silikaten und Aluminaten des Bodens veranlaßt die Entstehung von adventivem Kalziumsilikat und Aluminat sowie eine Verminderung des pH-Wertes. Die Endprodukte der Reaktion des Erdstoffes und Zements sind hydratierte Aluminate und ein Kalziumsilikat-Gel.

Wenn der Abbindevorgang in der Anwesenheit irgendeiner Metallverbindung, z. B. von kaustischer Soda, Natriumsulfit, usw. verläuft, nimmt die Kalziumion-Konzentration in der Lösung stark ab, teils infolge des gewöhnlichen Ionenaustausches, teils der kaustischen Reaktion.

$$Na_2X + Ca(OH)_2 \rightarrow CaX + 2\,Na(OH)$$

Gleichzeitig nimmt die Wasserstoff-Ion-Konzentration, d. h. der pH-Wert stark ab. Die Verminderung der Kalziumkonzentration verzögert den Niederschlag des unlösbaren Kalziumsilikat-Gels, und die Zunahme des pH-Wertes

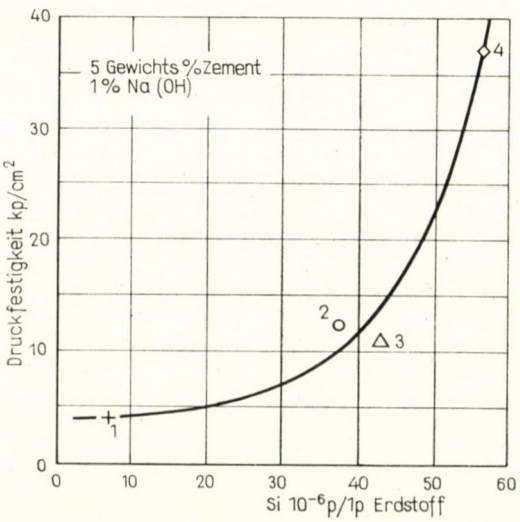

Bild 2. Einfluß des trennbaren Silikat-Gehaltes auf die Druckfestigkeit eines mit Zement stabilisierten und mit 1 vH Na (OH) behandelten Erdstoffes. 1 — Schluff; die Tonteilchen wurden ausgewaschen; 2 — nat. Schluff; 3 — Löß; 4 — toniger Schluff

beschleunigt die Bildung der lösbaren Alkalisilikate und Aluminate. Die Alkalisilikate werden mittels des Porenwassers in der ganzen Bodenmenge gleichmäßig verteilt, weshalb die Reaktion des freien Alkalis mit dem Erdstoff den pH-Wert herabsetzt, und auf diese Weise kann auch das Kalziumion in Lösung gehen. Die Reaktion des Kalziums mit den im Porenwasser gleichmäßig verteilten Alkalisilikaten und Aluminaten führt zur Bildung von gemischtem Kalzium-Natriumsilikat und eines Gels; die Menge dieser letzteren übertrifft aber die Menge, die im Falle von Zement allein sich ausbilden kann; dies erläutert schließlich den günstigen Einfluß der alkalischen Metallverbindungen.

In Bild 3 illustrieren einige Versuchsergebnisse des Verfassers den Einfluß des Natriumsulfits auf die Zunahme der Festigkeit.

Von den Zusatzmitteln der mit Zement stabilisierten Böden können noch das *Kalziumchlorid*, das *Bitumen* und die *Bitumenemulsion* erwähnt werden.

Die Beimengung von *Kalziumchlorid* kann auch den Wert der Druckfestigkeit bis zu einer bestimmten Grenze steigern, wie es aus Bild 4 ersichtlich ist. Die optimale Menge der Zugabe ist ungefähr 0,6 Prozent, wenn wir sowohl den sofortigen wie auch die in längerer Zeitdauer eintreffenden Einflüsse berücksichtigen. Das Kalziumchlorid hat in vielen Bodenarten keine solche Auswirkung; es beschleunigt bloß die Bindung des Zements.

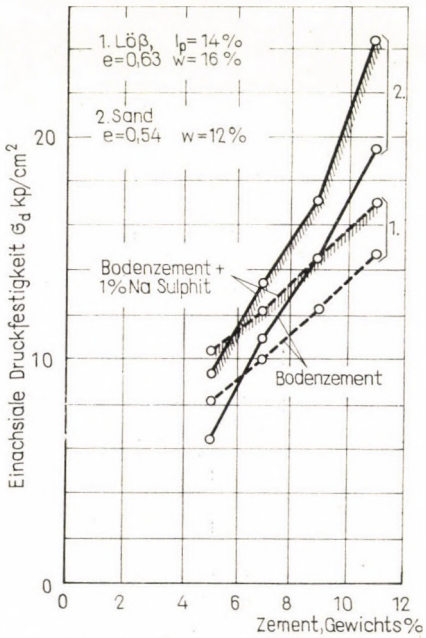

Bild 3. Einfluß von Na-Sulphit auf die Druckfestigkeit

Mit der Zugabe von *Bitumenemulsion* hat man in England Versuche vorgenommen. Die Emulsion, die eigens zu diesem Zwecke ausgearbeitet wurde, bleibt, wenn man sie dem feinkörnigen Erdstoff zumischt, eine kurze Weile stabil, folglich kann das Bitumen im Boden gut verteilt werden. Das nachher zugemischte Zement hat dreierlei Funktion: es bricht die Emulsion, adsorbiert einen Teil der frei gewordenen Feuchtigkeit durch Hydratation und erhöht die Festigkeit des behandelten und verdichteten Bodens. Um eine günstigere Wirkung zu erreichen, ist nach den Erfahrungen die Zugabe von 5 bis 7,5% Emulsion und 3 bis 5% Zement erforderlich. Das Endprodukt liegt zwischen dem mit Zement und mit Bitumen stabilisierten Böden; es ist ein wenig starr und ziemlich wasserdicht.

Mit der Beimengung von *Bitumen* wurden Versuche in der Sowjetunion (Bezruk—Knyazjuk 1951) und bei uns (Quirico 1954) angestellt. Die letz-

teren zeigten, daß die Zugabe von flüssigem Bitumen bis zu 6% vorteilhaft war; der Wert der Druckfestigkeit gestaltete sich in Abhängigkeit von der Zugabe des Zements und des Bitumens, gemäß Bild 5. Die Bindung des Zements wurde also durch das zugegebene Bitumen nicht verhindert.

Auch die Eigenschaften der mit Kalk stabilisierten Böden können durch Beimengung von Zusatzstoffen in geringer Menge wirtschaftlich verbessert werden.

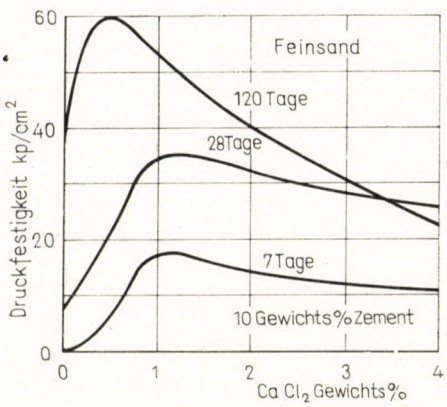

Bild 4. Einfluß van Ca Cl_2 auf die Druckfestigkeit eines mit Zement stabilisierten organischen Sandes

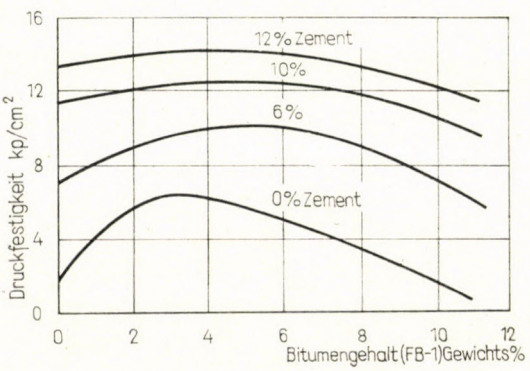

Bild 5. Druckfestigkeit von Löß als Funktion des Zement- bzw. Bitumengehaltes, w = $= w_{opt} = 9$ vH

Einige natürliche Stoffe, wie z. B. die vulkanische Asche, reagieren besser auf die Zugabe von Kalk als die gewöhnlichen Böden. Man nennt solche Materialien *Puzzolane*. Sie sind hauptsächlich vulkanischen Ursprungs, nicht kristallartiger, sondern ionartiger Struktur. Sie kommen in der Form von Vulkanasche, Tuff oder Traß (= Silikat-Trachyttuff) vor. Je niedriger der Entwicklungsgrad der Kristallisierung ist, um so größer wird ihre Aktivität. Durch die Beimengung zum Boden von so einem Material kann die Wirksamkeit der Stabilisierung mit Kalk gesteigert werden. Dagegen wäre die Zugabe von solchen natürlichen Materialien bei uns nicht wirtschaftlich; es gibt aber Kunststoffe, die eine gleiche Wirkung ausüben können. Solch ein Material ist vor allem die *Flugasche*, die sich hauptsächlich in der Nachbarschaft der Wärmekraftwerke in großen Mengen anhäuft und große Speicherungs- und Transportkosten verursacht. Dieses Material besteht überwiegend aus kugelförmigen, kristallartigen Silikat- und Aluminat- sowie aus abgerundeten Gammaeisenoxyd- (Fe_3O_4) Partikeln. Das Kalziumoxyd kommt nur in Kombination mit anderen Materialien vor, infolge der Kalzination des in der Kohle befindlichen Kalksteines. Die Menge der unverbrannten Kohlenteilchen — die sowohl vom Gesichtspunkt der Feuerung wie auch der Qualität der Flugasche aus schädlich

sind — ist stark veränderlich; sie hängt von der Wirksamkeit der Feuerung ab. Die Kohle verdünnt die Puzzolan-Körner, erhöht den Wasserbedarf und vermindert die größte trockene Dichte des stabilisierten Bodens. Die puzzolanartige Aktivität der Flugasche hängt von der Feinheit ihrer Kornverteilung ab; Zugabe von grobkörniger Flugasche ist nicht erfolgreich. Die Güte der Flugasche kann durch Mahlen verbessert werden, das ist aber nur selten wirtschaftlich.

Es kann vorkommen, daß die Körnchen der Flugasche elektrisch geladen sind, was vom Gesichtspunkt der Benutzung und Verdichtung schädlich ist und die Anwendung der Flugasche unmöglich macht.

Gegebenenfalls muß ein Entladungsverfahren ausgearbeitet werden.

Die größte Schwierigkeit der Anwendung der Flugasche liegt darin, daß ihre Güte, sogar in einem und demselben Werke stark veränderlich ist. Die Zusammensetzung der verbrannten Kohle, die Temperatur und Wirksamkeit der Feuerung sowie die Witterung stellen alle Änderungen herbeiführende Faktoren dar, und sie können nicht uniformisiert werden.

Folglich kann man einen ständigen, vorteilhaften Effekt kaum erhalten.

Der Einfluß der Flugasche auf die Stabilisierung ist, im Grunde genommen, von gleicher Art wie der des Kalkes; die Reaktionen sind dieselben.

Die Flugasche verstärkt von den erwähnten die puzzolanartige Reaktion am meisten. Die Erhärtung und die anderen Reaktionen finden im allgemeinen langsam statt, und es gibt Schluffe und Tonarten, die im Falle von Zugabe von Kalk + Flugasche keine besseren Resultate ergeben als im Falle von mit reinem Kalk durchgeführter Stabilisierung. Leider gibt es vorläufig keine Möglichkeit, den Effekt aufgrund von gesonderten Untersuchungen der Flugasche und des Erdstoffes im voraus abzuschätzen.

Außer der Flugasche wurde eine große Anzahl von verschiedenen Materialien zur Verbesserung der Eigenschaften des mit Kalk stabilisierten Bodens erprobt. Der Zweck der Anwendung der in kleinen Mengen beizumischenden Stoffe ist entweder die Erhöhung der Festigkeit oder die Abminderung der erforderlichen Qualität des Hauptstabilisators. Nur wenige von diesen Materialien brachten solche Ergebnisse, die zugleich auch wirtschaftlich angewendet werden können; es sind die Natriumverbindungen, die sich noch am allermeisten auch hier bewährt haben. Die Zunahme der Festigkeit infolge der Zugabe von Natriumverbindungen ist für den Fall eines Schluffes im Bild 6 dargestellt.

Neuerlich hat FÜLÖP (1967) einen umfassenden Versuch zur Erkenntnis der Stabilisationsfähigkeit der Flugasche angestellt.

In den letzten Jahren wurden ausführliche Untersuchungen vorgenommen (von MICHAELS und PUZINAUSKAS, 1956 und 1958), um die mit Bitumen durchgeführte Stabilisierung mit Hilfe von verschiedenen Zusatzmitteln zu verbessern. Die meistversprechenden Ergebnisse wurden mit der Zugabe von

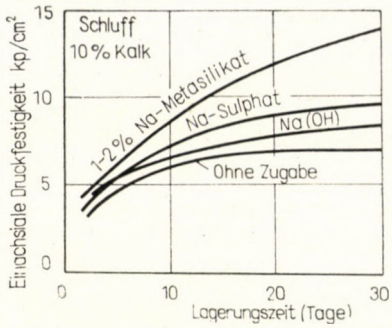

Bild 6. Zunahme der Druckfestigkeit bei der Zugabe von Na-Mischungen

Phosphorpentoxyd (P_2O_5) erzielt. Ein charakteristisches Ergebnis ist im Bild 7 dargestellt, wo die einachsige Druckfestigkeit eines Schluffes in Abhängigkeit von der Zeit, mit und ohne Zugabe von Phosphorpentoxyd angegeben wurde.

Der Effekt ist im Falle von Böden mit verhältnismäßig größeren Körnern stärker.

MICHAELS und PUZINAUSKAS erläutern diesen die Festigkeit in wesentlichem Masse erhöhenden Effekt auf die folgende Weise.

Wenn man einen nassen, bindigen Erdstoff mit verdünntem Bitumen in einer im allgemeinen üblichen Menge vermischt, dann ist die Menge der Flüssigkeit im Erdstoff in der Regel größer als die, die zum Ausfüllen der Poren

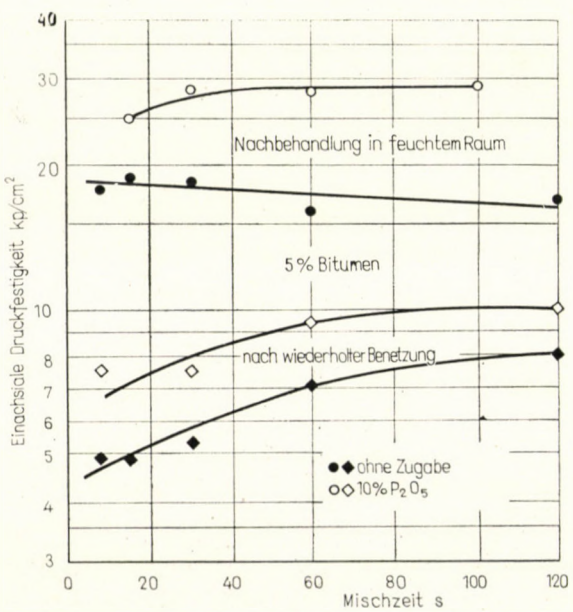

Bild 7. Einfluß der Mischzeit und der Menge von Phosphorpentoxyd auf die Druckfestigkeit

in dem verdichteten Boden erforderlich ist. Während der Mischung dispergiert die nicht benetzende -bituminöse Phase in der Form von kleinen Kugeln oder Fäden zwischen den Körnern oder den aneinander haftenden Körnerhaufen; der Vermischungsgrad (der durch den durchschnittlichen Durchmesser der Kügelchen und durch die Gleichförmigkeit der Verteilung charakterisiert werden kann) und das Zerbröckeln der anhaftenden Körnerhaufen hängt von der Zeitdauer und der Wirksamkeit der Mischung ab. Während der Verdichtung der Mischung vermindert sich der freie Hohlrauminhalt, ein Teil der flüchtigen Materialien (Wasser und Verdünnungsmittel) verdampft; die dispergierten Bitumenteilchen werden zu Fäden und Plättchen zusammengepreßt und füllen einen großen Teil des Hohlrauminhalts aus. Infolge der Kapillar-

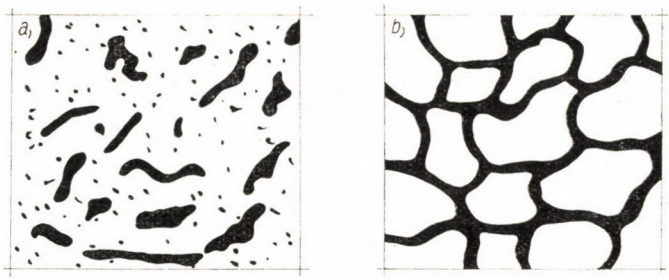

Bild 8. Bitumen im stabilisierten Erdstoff. a — ohne flächenaktive Beimengungen; b — mit flächenaktiven Beimengungen

kräfte beschränkt sich die Asphalt-Phase auf die größeren Poren und Kanäle, während das Wasser die Poren des Feinstoffes der Bodenmasse ausfüllt. Die Mischung ist in dieser Phase ein dichter Haufen von Körnern und Körnerklumpen, die mit Wasser befeuchtet sind und von mehr oder weniger zusammenhängenden Bitumenteilchen eingeschlossen sind (Siehe Bild 8). Nach der Trocknung der Mischung würde zwar die Schrumpfung eine weitere Dispersion herbeiführen, dieser Prozeß wird aber durch die gleichzeitige Erhöhung der Viskosität verhindert. Wenn der Boden keine eigene Kohäsion besitzt, ruft die Adhäsion des Bitumens zum Bodenteilchen in der Masse während der Evaporation des Wassers Kohäsion hervor. Die entstandene Festigkeit wird annähernd proportional dem Verhältnis aus den mit Bitumen ausgefüllten Poren und dem ganzen Porenanteil sein. Wenn wir dagegen zum bindigen Boden Bitumen mischen, dann wird es zwar an einen Teil der Körner haften, jedoch während des Trocknens verhindert es teils die Bindung zwischen den Bodenteilchen, und da die Festigkeit der Bindungen viel größer als die Adhäsion zwischen dem Bitumen und den Teilchen ist, wird die trockene Festigkeit der Mischung abnehmen.

SCHRIFTTUM

1. Безрук, В. М.—Князюк, К. А.: Устройство цементно-грунтовых оснований покрытий. Дфиздат, Москва. 1951.
2. Fülöp I.: Talajstabilizációs kísérletek bázikus hatású barnaszénpernyével. *Mélyépítéstudományi Szemle* (1967)
3. Gáspár L.: A cementes talajstabilizáció újabb hazai kísérletei. *Mélyépítéstudományi Szemle* (1964)
4. Kézdi, Á.: Über Bodenstabilisierung im Straßenbau. *Die Straße* (1963)
5. Kézdi Á.: Stabilizált földutak. Akadémiai Kiadó, Budapest 1967
6. Michaels, A. S.—Puzinauskas, V.: Additives as Aids to Asphalt Stabilization of Fine-Grained Soils. Highway Research Board, Bulletin 129. Washington D.C. (1956)
7. Michaels, A. S.—Puzinauskas, V.: Improvement or Asphalt-Stabilized Fine-Grained Soils with Chemical Additives. Highway Research Board, Bulletin 204. Washington D.C. (1958)
8. Quirico, D.: A cementstabilizáció kivitelezésével kapcsolatos újabb kísérletek és tapasztalatok. *Mélyépítéstudományi Szemle* (1953)

Effect of Additives on the Properties of Stabilized Soils. Besides the classical soil-stabilizing methods some complementary chemicals and other materials are presented which may be used for increasing the effects of stabilization. Without aiming at completeness, the paper only extends to materials which can be economically used and to those which effectively improve the required properties of the stabilized soil.

Влияние добавок на свойства стабилизированных грунтов *(А. Кезди, Б. Надвати).* В работе наряду с отдельными обычными методами стабилизации грунтов излагаются возможности применения нескольких химических и прочих дополнительных материалов, увеличивающих стабилизирующее действие. Не претендуя на полноту, автор занимается только экономично применяемыми материалами и теми, которые эффективно повышают желательные свойства стабилизированного грунта.

Acta Technica Academiae Scientiarum Hungaricae, Tomus 68 (3—4), pp. 293—310 (1970)

ESTIMATING MATRIX-DISPLACEMENT SOLUTIONS OF TWO-DIMENSIONAL PROBLEMS BY LARGE ELEMENT TECHNIQUE

R. SZILÁRD*

[Manuscript received: August 22, 1968]

Based on the general convergence criteria of the finite element solution of stress and displacement problems of continua, the concept of "large" discrete elements is introduced. For the derivation of the stiffness coefficients, no prescribed displacement pattern is forced upon the discrete elements; the node points are merely moved with unit motions. The compatibility of the stresses and strains within the element and at the edges of the adjoining elements is maintained by solving the pertinent differential equations of the theory of elasticity for unit nodal displacements utilizing the Method of Images. A symmetrical stiffness matrix is obtained by virtual work of the edge forces. Numerical examples compare the solutions of two-dimensional stress problems using small and large element approaches and analytical solutions. The convergence characteristics of the large element approach are markedly different from those of the small element approach; i.e., instead of an asymptotic convergence, the correct solution is at one "optimum" element number which can be determined by a simple graphical method. It is illustrated that by the use of large elements the order of the stiffness matrix can be considerably reduced, while the obtained accuracy is sufficient for estimating purposes. Techniques for improvement of the accuracy are outlined.

Symbols

The following symbols were adopted for use in this paper:

a, b	edge dimensions of flat discrete elements in X and Y directions, respectively
$\{d_j\}$	vector of edge displacements due to unit motion at node j
i, j, k, l	node points
h	thickness of the element
l	edge length
p_x, p_y	surface loads in local coordinate system
n_x, n_y, n_{xy}	membrane forces per unit length
t	time
u, v	displacement components in local coordinate system
$[B]$	matrix representing Hooke's law
E	Young's modulus of elasticity
$\{F_i\}$	vector of edge forces
$[K_{ij}]$	stiffness matrix of the total system in general reference coordinate system
$[N]$	matrix expressing Hooke's law
M_z	moment about Z axis in local coordinate system
P_x, P_y	concentrated loads in local coordinate system
$\{P_j\}$	vector of the forcing function in general reference coordinate system
U	potential energy
V	volume
X, Y, Z	axes of local coordinate system
X, Y, Z	axes of orthogonal general reference coordinate system
γ	shear strain
$\{\delta\}$	generalized vector of nodal displacement

* Dr. Ing. RUDOLPH SZILÁRD, Professor of Civil Engineering., University of Hawaii, *Honolulu*, Hawaii, U.S.A.

ε_x, ε_y	unit elongation in X and Y directions, respectively
θ	angle change
λ	finite difference mesh size for square grid
ν	Poisson's ratio
$[\varrho_{ij}]$	element stiffness matrix in local coordinate system
σ_x, σ_y	normal components of stress
$\{\sigma_x\}$, $\{\sigma_y\}$	stress vectors
τ	in-plane shearing stresses
$[M_{jk}]$	mass matrix of the total structure in general reference coordinate system

Subscripts

x, y	in the direction of X, Y axes
ij	reaction (motion, force) at point i due to cause (motion, force) at point j

Matrix Notations

$[\ ]$	rectangular matrix
$[\ ]^{-1}$	inverse matrix
$\{\ \}$	column matrix
$\{\ \}^T$	transposed column matrix (row)

1. Introduction

The Matrix Displacement Method [1, 2] based on the use of stiffness matrices is one of the most promising approaches to the economical solution of complex static and dynamic problems of continua. This method uses discrete elements and yields directly symmetric positive-definite stiffness or "dynamical" matrices which are heavily positioned along the principal diagonals. These properties of large matrices are of basic importance in inversion of large matrices and in other operations, such as obtaining eigenvalues and eigenvectors.

Because of the difficulty and expense involved in computer solutions with large matrices, the advantages of a reduction in the order of the stiffness matrix are obvious. In the analysis of actual stress problems, especially in shell structures, stiffness matrices in the order of 1500×1500 and larger are not uncommon even after the utilization of possibilities such as structural symmetry, coarse subdivision, reduction of the number of degrees of freedom, etc. On the other hand, in order to obtain acceptable results (± 5 percent discrepancy from the theoretical solutions) in cases of two- and three-dimensional stress problems by using discrete element method, a relatively fine subdivision is required. Thus, the requirements concerning the accuracy of the results and those of the applicability and economy of the conventional Matrix Dispacement Method are contradictory.

Furthermore, presently there is an acute need in matrix-displacement analysis of large systems to obtain an independent check to detect possible *machine errors*. For such checking or estimating purposes a considerably larger percentage of error (10 to 20 percent) than the ± 5 percent generally used in design, can be considered permissible. To satisfy these needs, the prime objec-

tive of this paper was to reduce the order of the stiffness matrix considerably, while maintaining for estimating purposes acceptable accuracy in the results.

These objectives have been achieved by introducing the Large Element concept in the derivation of the stiffness coefficients. Although the derivation of stiffness coefficients for "large" two-dimensional elements is treated in detail in the following discussion, the method introduced is general. That is, basically, the same approach can be used in the derivation of the bending stiffness coefficients of "large" shell elements and in the derivation of the stiffness coefficients of "large" three-dimensional discrete elements.

2. Large element versus small element approach

In the discrete element representation of continua, the continua are replaced by discontinua in the form of an assemblage of discrete elements joined at the node points, where continuity is expressed and where the statically and kinematically equivalent generalized forces act. Thus, the differential oquations of motion of a continuum can be written in matrix form using an erthogonal general reference coordinate system $\overline{X}$, $\overline{Y}$, $\overline{Z}$:

$$\{\delta_i(t)\}+[K_{ij}]^{-1}\{M_{jk}\ddot{\delta}_k(t)\}=[K_{ij}]^{-1}\{P_j(t)\} \tag{1}$$

where $\{\delta_i(t)\}$ represents the generalized vector of nodal displacement and $\{P_i(t)\}$ is the generalized time-dependent vector of the nodal forces. $[K_{ij}]$ is the square matrix of the stiffness coefficients of the assembled continuum expressed again in the general reference coordinate system, and $[M_{jk}]$ is the mass matrix. The dots in Eq. (1) indicate the derivatives of the displacements with respect to time.

Invariant (with respect to time) loads transform the dynamic problem described by Eq. (1) into a static problem; so we can write

$$\{\delta_i\}=[K_{ij}]^{-1}\{P_j\}. \tag{2}$$

Thus, the static problem of the continua can be considered a specific case of forced vibration. Consequently, the solution of dynamic problems automatically yields the static solution. The key to the solution of Eqs (1) and (2) is the stiffness matrix $[K_{ij}]$ assembled from the stiffness coefficients of corresponding elements.

In order to effectively represent the continuum by discontinua, i.e., the solution converges to the correct answer, certain requirements must be satisfied. Mathematically, the discrete element representation of the continuum strongly resembles the Ritz Method widely used in the solution of

various stress problems in the theory of elasticity. Thus, the most general criterion of the discrete element approach is:

1. The total energy of the substitute system, obtained by assembling discrete elements, must be equal to that of the original continuum. Hence, it follows that

$$U_{\text{real}} = \sum_{1}^{n} U_{\text{discrete}} \tag{3}$$

where U represents the potential energies.

Since the potential energy of the substitute system is expressed by the stiffness matrix, the following specific criteria are required concerning the stiffness matrices of the discrete elements:

2. The idealization of elements (such as replacing shells by a network of bars) should be avoided since the effect of idealization errors on the accuracy of the discrete element solution is disproportionate.

3. A close similarity between the final deformation region of the discrete elements and that of the corresponding region of the original continuum must be maintained.

4. The compatibility and continuity of all displacements and stresses within the finite elements must be maintained.

5. The compatibility and continuity of all displacements and stresses along the edges of adjoining elements must be maintained.

6. The macroscopic equilibrium of the element must be satisfied.

7. The generalized forces acting at the node points must be statically and kinematically equivalent to the distributed forces they replace.

The stiffness coefficients of "small" discrete elements are obtained by using a Displacement Model [2]. This is done by prescribing certain edge displacements, which result in a unit motion (one motion at a time) of the node point, while the other node points and edges are held fixed. The definition of the stiffness coefficients based on the potentials of the internal forces [3] is

$$\varrho_{ij}^{1} = \int_{V} \{\sigma_i\}^T \{\varepsilon_j\}\, dV \tag{4}$$

where ϱ_{ij} is the element stiffness coefficient expressed in a conveniently located local orthogonal coordinate system X, Y, Z; $\{\sigma_i\}$ represents the vector of the stress field due to the imposed unit motion of node i; and $\{\varepsilon_j\}$ is the compatible strain vector due to the unit motion of node j. The integration extends over the volume, V, of the discrete element.

The first critical phase in the derivation of the stiffness coefficients of small discrete elements is the selection of suitable edge displacement functions, which assures the monotonic convergence of the matrix solutions to the exact

solutions as the number of the small discrete elements is increased. In the case of two-dimensional continua considering only in-plane internal forces, the in-plane deflection curves in a small region can be well approximated by straight lines.

On the other hand, if in the derivation of element stiffness coefficients only unit motions of the nodes are introduced and the rest of the element (including the edges moved) is permitted to deform freely, then the element behaves as an assemblage of many small elements; therefore such a discrete

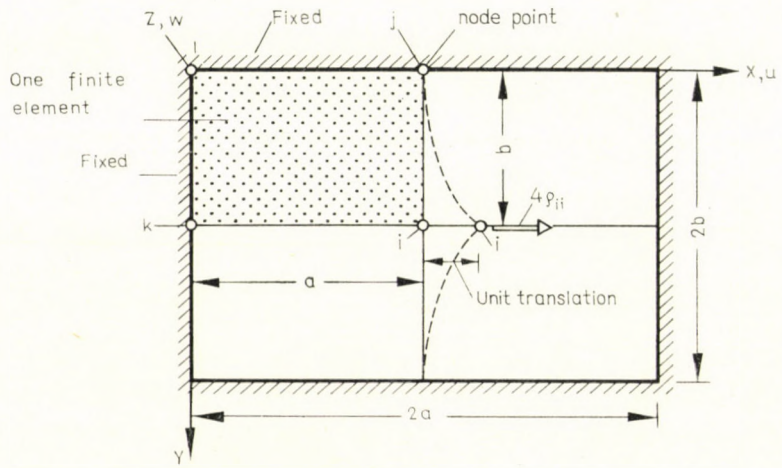

Fig. 1

element is called a "large" element. A large element can replace numerous small elements and thereby result in a marked reduction in the order of the stiffness matrix. As previously discussed, this requires that there be close similarity in the final deformation patterns of the original and substitute systems.

In order to achieve complete compatibility and continuity of displacements and stresses not only at the node points but also along the edges of the discrete elements, the Method of Images described by TIMOSHENKO [4] for solution of certain plate problems was extended to yield membrane and bending element stiffness coefficients for large elements. Instead of working with an element of size $a \times b$, a finite element of size $2a \times 2b$ was used as shown in Figure 1. Since four identical elements are involved, this approach yields four times the value of a stiffness coefficient that corresponds to one element. Continuity between the adjoining four elements is maintained as the node point located at the center of the assemblage is moved. Thus, the compatibility and continuity of the stresses and displacements are satisfied "ab ovo".

3. Derivation of membrane stiffness coefficients for large elements

In order to obtain the previously described large element behavior of the discrete elements used in the solution of two-dimensional stress problems, a unit translation in the X direction is introduced at node i (Figure 1) and the element is permitted to deform according to mathematical functions, which are the analytical solutions of the pertinent differential equations of the theory of elasticity. In the case of the problem under investigation, these differential equations are [5]:

$$\frac{\partial^2 u}{\partial x^2} + \frac{1-\nu}{2}\frac{\partial^2 u}{\partial y^2} + \frac{1+\nu}{2}\frac{\partial^2 v}{\partial x \partial y} = -\frac{1-\nu^2}{Eh} p_x \tag{5}$$

and

$$\frac{\partial^2 v}{\partial y^2} + \frac{1-\nu}{2}\frac{\partial^2 v}{\partial x^2} + \frac{1+\nu}{2}\frac{\partial^2 u}{\partial x \partial y} = -\frac{1-\nu^2}{Eh} p_y \tag{6}$$

where $u(x, y)$ and $v(x, y)$ are the displacement components in the X and Y directions, respectively, due to p_x and p_y, the external surface forces. The thickness of the element is h. Young's modulus of elasticity is E, and Poisson's ratio is represented by ν.

The conjugate generalized force producing unit displacement at node i is four times larger than the force required to induce unit translation of a node point of an element of size $a \times b$. Since both the load and the structural element are symmetrical in actual computation, the Method of Images is used only to determined the boundary conditions of the displacements along the adjoining edges $\overline{ij}$ and $\overline{ik}$ (Fig. 1).

The geometric boundary conditions of this two-dimensional stress problem are:

$$\text{at} \quad x = 0 \qquad u = v = 0\,, \qquad \frac{\partial u}{\partial y} = 0\,, \tag{7}$$

$$\text{at} \quad x = a \qquad \begin{matrix} u \neq 0\,, \\ v = 0\,, \end{matrix} \qquad \frac{\partial u}{\partial y} \neq 0\,, \tag{8}$$

$$\text{at} \quad y = 0 \qquad u = v = 0\,, \qquad \frac{\partial u}{\partial y} \neq 0\,, \tag{9}$$

$$\text{at} \quad y = b \qquad \begin{matrix} u \neq 0\,, \\ v = 0\,, \end{matrix} \qquad \frac{\partial u}{\partial y} \neq 0\,. \tag{10}$$

The graphical representation of these boundary conditions is given in Figure 2. Thus for u and v displacement components, the edges that moved due to the unit motion of node i behave as "guided", while the unmoved

edges are simply supported. The displacements within the "image" element resemble those of a corresponding network of cables (Fig. 2). The boundary conditions for unit translation of node i in the Y direction can be similarly obtained by substituting y for x and v for u.

The displacement coefficients (u, v) within the image element can be calculated either from the finite difference solution of Eqs (5) and (6) or from

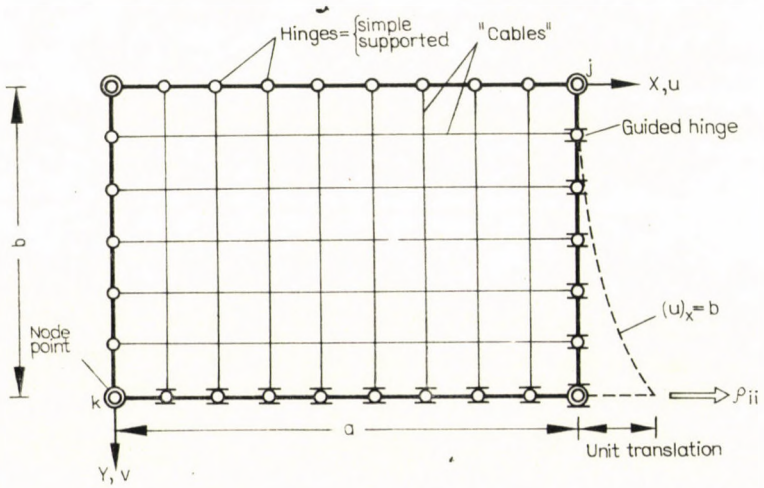

Fig. 2

Ritz's method based on the minimization of the total energy. Although this work uses the finite difference method to obtain higher accuracy, the application of Ritz's method is recommended.

The internal potential expressed by Eq. (4) is the scalar product of two vectors having the same direction. In case of stretching of flat elements, the stress vector can be written as

$$\{\sigma_i\} = \begin{Bmatrix} \sigma_x \\ \sigma_y \\ \tau \end{Bmatrix} = \frac{E}{1-\nu^2} \times \begin{bmatrix} 1 & \nu & 0 \\ \nu & 1 & 0 \\ 0 & 0 & \dfrac{1-\nu}{2} \end{bmatrix} \times \begin{Bmatrix} \dfrac{\partial u_i}{\partial x} \\ \dfrac{\partial v_i}{\partial y} \\ \dfrac{\partial u_i}{\partial y} + \dfrac{\partial v_i}{\partial x} \end{Bmatrix} \tag{11}$$

where σ_x and σ_y are the normal stresses, and τ is the shear stress acting in the plane of the element.

The compatible strain vector is obtained by introducing a unit motion at node point j, as shown in Fig. 3, and by determining the displacement components as described above. Thus, the strain matrix of the compatible displacement field is

$$\{\varepsilon_j\} = \begin{Bmatrix} \varepsilon_{xj} \\ \varepsilon_{yj} \\ \gamma_j \end{Bmatrix} = \begin{Bmatrix} \dfrac{\partial u_j}{\partial x} \\ \dfrac{\partial v_j}{\partial y} \\ \dfrac{\partial u_j}{\partial y} + \dfrac{\partial v_j}{\partial x} \end{Bmatrix} \tag{12}$$

where ε_x and ε_y are the strains in the X and Y directions, respectively, and γ represents the angular distortion.

The required macroscopic equilibrium of the element in the form of

$$\sum P_x \simeq 0 \qquad \sum P_y \simeq 0 \qquad \sum M_z \simeq 0 \tag{13}$$

can be satisfied only if the displacement field $\{\varepsilon_j\}$ is compatible with the stress field $\{\sigma_i\}$. Equation (13) gives a valuable intermediate check of accuracy of the stiffness coefficients. The use of such intermediate checks is highly recommended.

Since the virtual work expression of the stiffness coefficients given in Eq. (4) can be written in terms of either stresses or strains, the following equation can be written:

$$\varrho_{ij} = \int_V \{\sigma_i\}^T [N]\{\sigma_j\}\, dV = \int_l \{\varepsilon_i\}^T [B]\{\varepsilon_j\}\, dV \tag{14}$$

where $[N]$ and $[B]$ are symmetrical matrices representing the Hookean stress-strain relationship. Since both matrices are symmetrical

$$\varrho_{ij} = \varrho_{ji} \tag{15}$$

the resulting element stiffness matrix is also symmetrical.

Since the virtual work of the internal forces expressed by the right side of Eq. (4) must be equal to the virtual work of the edge forces, we can write

$$\varrho_{ij} = \int_V \{\sigma_i\}^T \{\varepsilon_j\}\, dV = \oint_l \{F_i\}^T \{d_j\}\, dl \tag{16}$$

where the matrices of the distributed edge forces and edge displacements are:

$$\{F_i\}^T = \{n_{xi}\, n_{yi}\, n_{xyi}\} \text{ and } \{d_j\} = \begin{Bmatrix} u_j \\ v_j \\ \theta_j \end{Bmatrix} \tag{17}$$

The notation of the edge forces and edge displacements in Eq. (17) conforms to the standard notation used in the pertinent literature and is illustrated in Figure 4. The resulting edge displacements are shown in Figure 3.

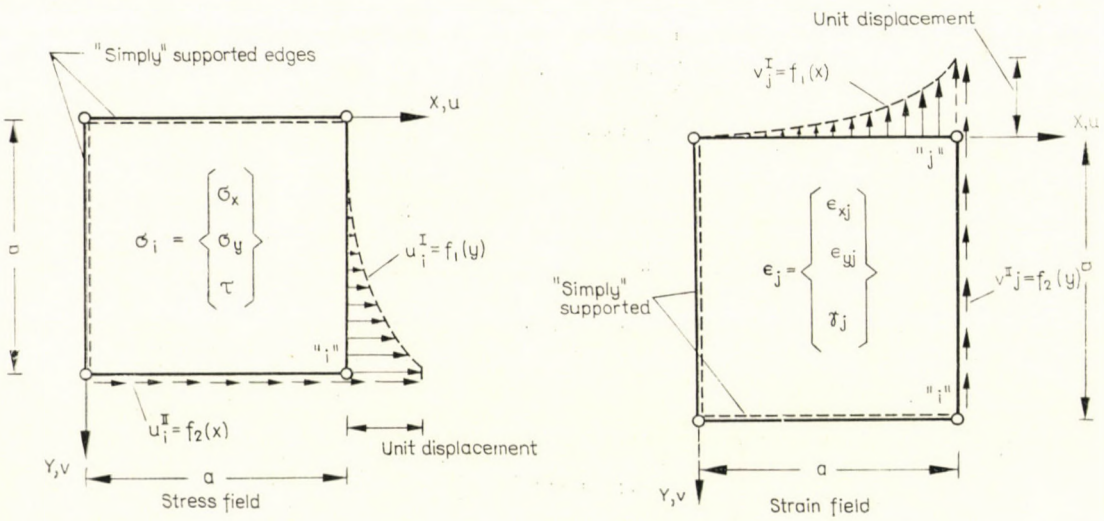

Fig. 3

A further check, which is recommended for elimination of numerical errors, is the pointwise satisfaction of Maxwell's law of reciprocity of forces and displacements.

Since the solution of static and dynamic problems of two- and three-dimensional continua by the Matrix Displacement Method is extremely sensitive to the correctness of the stiffness coefficients, it is considered mandatory that in addition to the intermediate checks mentioned above, the stiffness coefficients must be checked on test problems with known analytical solution before they are applied to actual problems. These tests must also include the investigation of convergence characteristics.

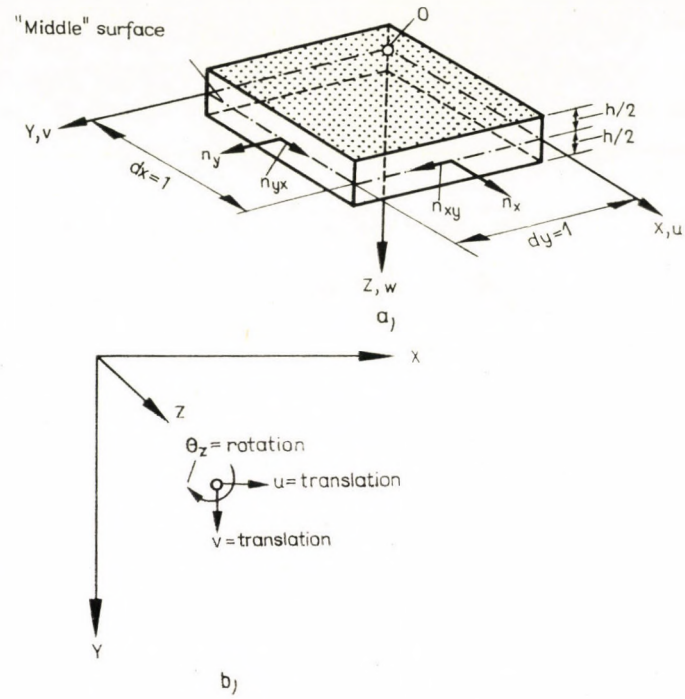

Fig. 4

4. Numerical values

Numerical values of stiffness coefficients of "large" square two-dimensional elements have been obtained utilizing ordinary (vs. improved) finite difference solutions. The deflection components $u(x, y)$ and $v(x, y)$ were calculated from the finite difference solution of Eqs (5) and (6) by introducing a unit translation of the node point and by assuming $\nu = 0.3$. The symbolic arrangement of this finite difference solution is illustrated in Fig. 5. The numerical results utilizing a 6×6 finite difference mesh is shown in Fig. 6. To check the result, the same problem was solved by 4×4 small discrete elements, using stiffness coefficients of good convergence characteristics (Fig. 7). Although coarse subdivisions were used in both methods, the two independent solutions show acceptable agreement.

The distributed edge forces along the edges $\overline{ij}$ and $\overline{ik}$ were obtained by finite difference method from the pertinent derivatives of the displacement components:

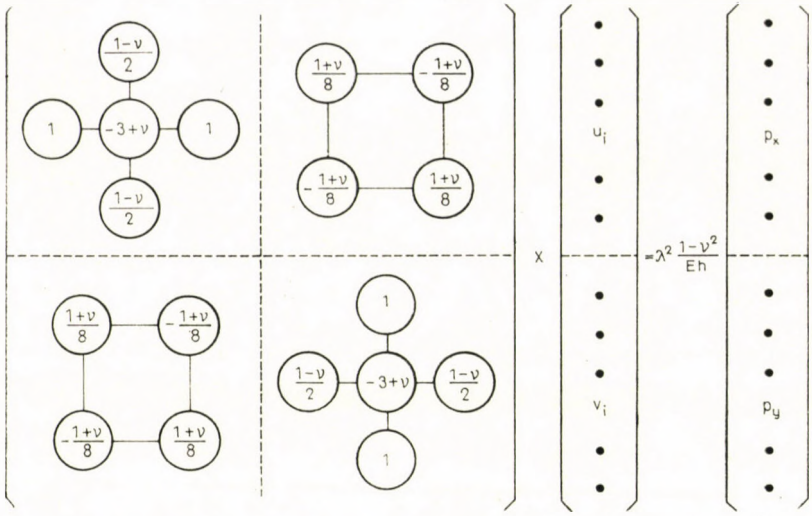

Fig. 5

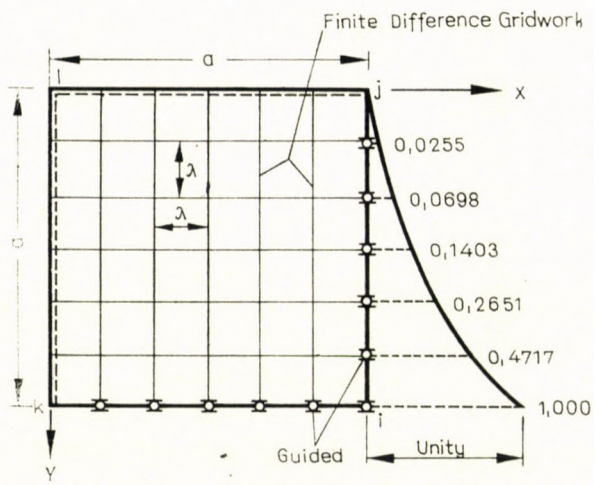

Fig. 6

$$n_x = \frac{Eh}{1-\nu^2}\left(\frac{\partial u}{\partial x} + \nu\frac{\partial v}{\partial y}\right) \qquad (a)$$

$$n_y = \frac{Eh}{1-\nu^2}\left(\frac{\partial v}{\partial y} + \frac{\partial u}{\partial x}\right) \qquad (b) \qquad (18)$$

$$n_{xy} = \frac{Eh}{2(1+\nu)}\left(\frac{\partial u}{\partial y} + \frac{\partial v}{\partial x}\right) \qquad (c)$$

The results of these computations are given in Fig. 8. The equilibrium check based on the edge forces and the pointwise satisfaction of Maxwell's reciprocity theorem yielded satisfactory results, indicating no numerical errors in the computation.

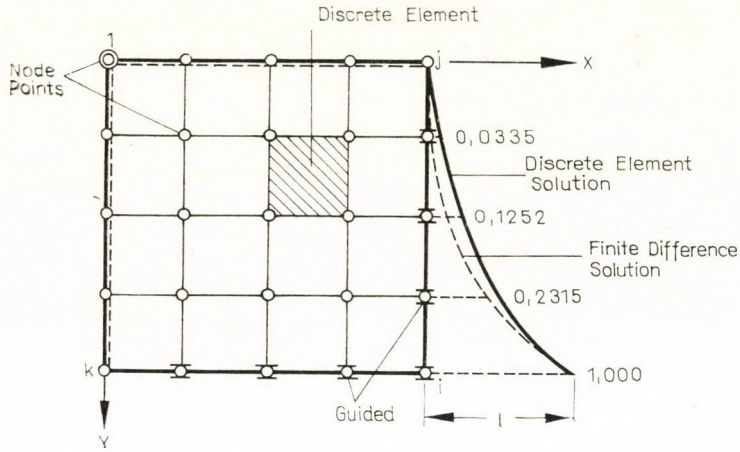
Discrete Element
1
Node Points
j
X
0,0335
Discrete Element Solution
0,1252
Finite Difference Solution
0,2315
1,000
k
Guided
l
Y

Fig. 7

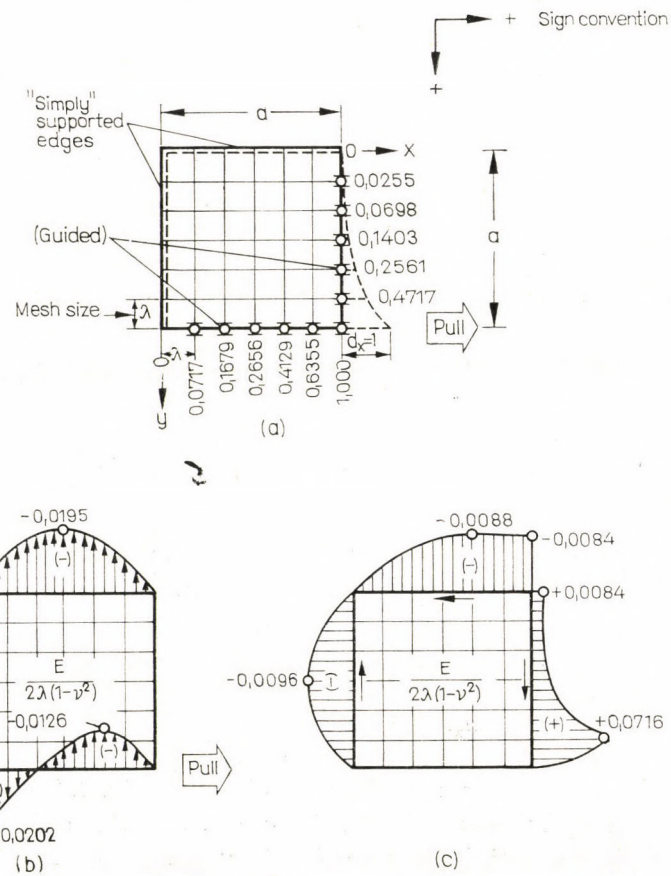
+ Sign convention
+
"Simply" supported edges
a
0
X
0,0255
0,0698
0,1403
0,2561
0,4717
(Guided)
Mesh size
λ
Pull
a
0
λ
0,0717
0,1679
0,2656
0,4129
0,6355
1,000
y
(a)
- 0,0195
(-)
E
2λ(1-ν²)
(-)
-0,0126
(-)
-0,0677
(+)
+0,0202
(b)
Pull
- 0,0088
- 0,0084
(-)
+0,0084
-0,0096
E
2λ(1-ν²)
(+)
+0,0716
(c)

Fig. 8

In assigning the distributed edge forces as equivalent concentrated forces to the nodes, the virtual work of the edge forces based on Eq. (16) was applied. The numbering system and sign convention are shown in Fig. 9. The resulting approximate stiffness matrix for a square two-dimensional large element is given in Table 1. The macroscopic equilibrium check based on Eq. (13) was satisfactory.

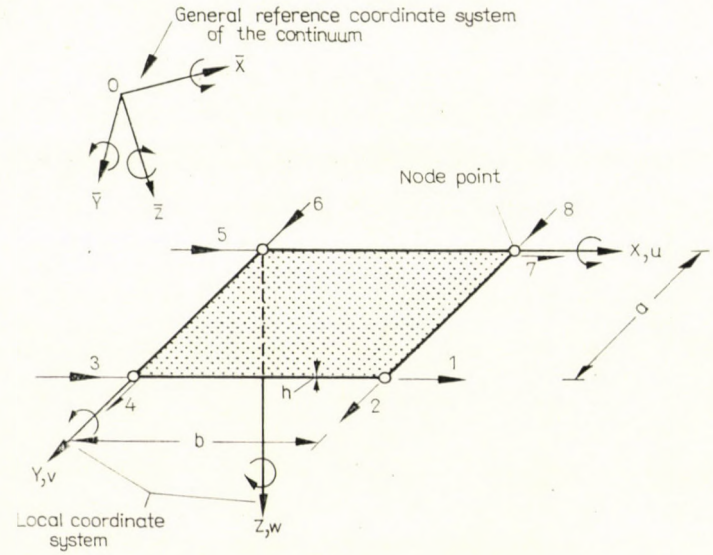

Fig. 9

Table 1

Approximate Stiffness Coefficients of a Large, Square, Two-Dimensional Element

$$[p_{ji}] = \frac{Eh}{1-0\cdot 3^2} \times$$

	1	2	3	4	5	6	7	8
1	0,2652							
2	0,0808	0,2652						
3	−0,1505	0,0339	0,2652			SYMMETRIC		
4	−0,0339	−0,0235	−0,0808	0,2652				
5	0,0912	0,0808	0,0235	0,0339	0,2652			
6	−0,0808	−0,0912	−0,0339	−0,1505	0,0808	0,2652		
7	−0,0235	−0,0339	−0,0912	0,0808	−0,1505	0,0339	0,2652	
8	0,0339	−0,1505	0,0808	−0,0912	−0,0339	−0,0235	−0,0808	0,2652

a) For numbering system and sign convention, see Figure 9.
b) If $\nu \neq 0.3$, approximate values can be obtained using $Eh/1 - \nu^2$ multiplicator.
c) $a = b$.

5. Convergence characteristics and accuracy

The accuracy and the convergence characteristics of the large element stiffness matrix were investigated using two test problems. The first of these is the deep beam problem. The solutions were tested against the centerline deflection of a deep cantilever beam loaded with concentrated load (Fig. 10), which was obtained from the theoretical solution of the problem [5]:

$$w(x) = \frac{Px^3}{6EI} - \frac{PL^2 x}{2EI} + \frac{PL_3}{3EI} + \frac{P\,(B/2)^2}{2IG}(L-x) \tag{19}$$

If $\nu = 0.3$, the maximum centerline deflection at $x = L$ is

$$w_{\max} = 39{,}8\,\frac{P}{Eh} \tag{20}$$

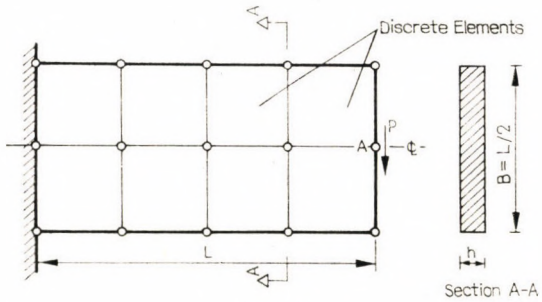

Fig. 10

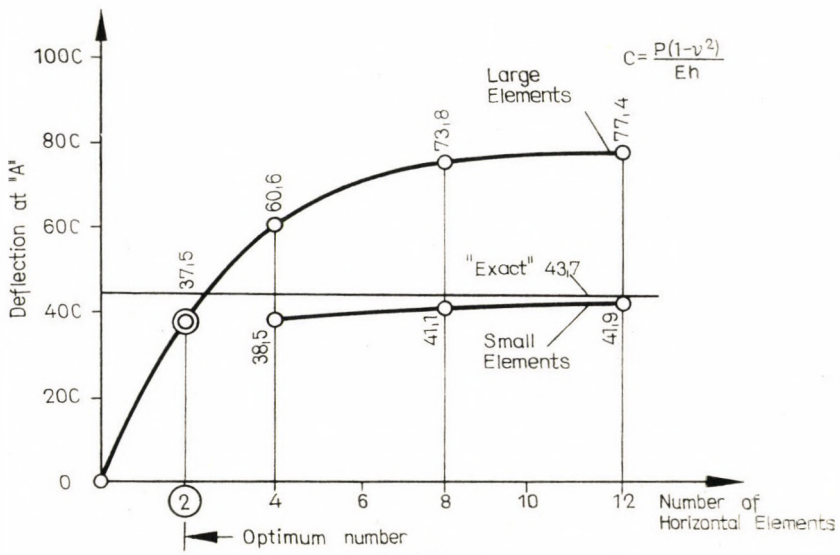

Fig. 11

This test problem was selected because of its sensitivity to the correctness of the in-plane stiffness coefficients. Fig. 11 shows the convergence characteristics for both small and large finite elements. As expected, the convergence tendency of large elements is opposite that of the small elements. That is, when a small number of large elements is used, the solution approaches the theoretical solution; but when the number of elements is increased, it asymptotically approaches approximately 1.8 times the theoretical solution,[1] which is consistent with the ratio of the work on the edge forces in a case of curved and straight line edge deflection

$$\frac{W_2}{W_1} \simeq 1{,}89\,. \tag{21}$$

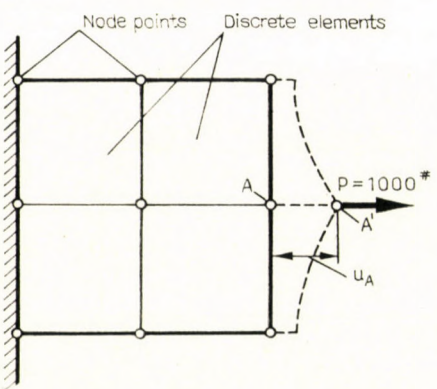

Fig. 12

There is an *optimum* number of large elements which results in a solution relatively close to the exact solution.

A second test case, stretching of a plate with concentrated load, as shown in Fig. 12, was also selected for testing these characteristics. Fig. 13 shows the edge deflections for this force for both large and small elements. The results are consistent with those of the deep beam problem discussed above.

The optimum large element number can be determined by a simple graphical approach illustrated in Fig. 14. Using limited, but sufficient number of large discrete elements the first part of the convergence curve can be plotted. Then the convergence curve is *extrapolated* with relative ease to obtain its asymptotic portion. Since the asymptote of the convergence curve is at 1.6 to 1.8 times the exact solution (21) the intersection of such a band with the convergence curve locates the optimum number of elements. The solution pertinent to the optimum number is the sought approximate value.

[1] Conforming stiffness coefficients such as those derived assure monotonic convergence characteristics.

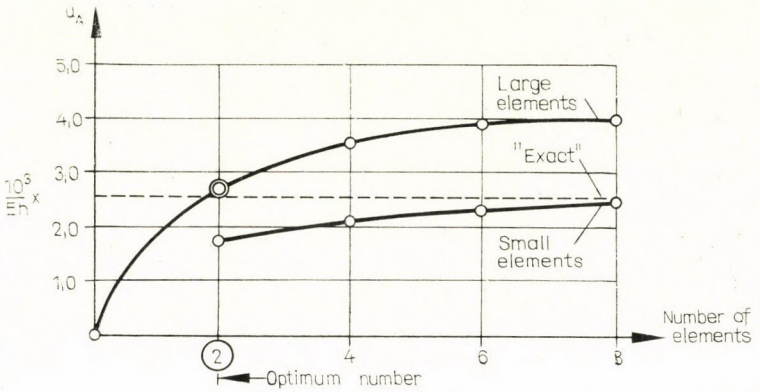

Fig. 13

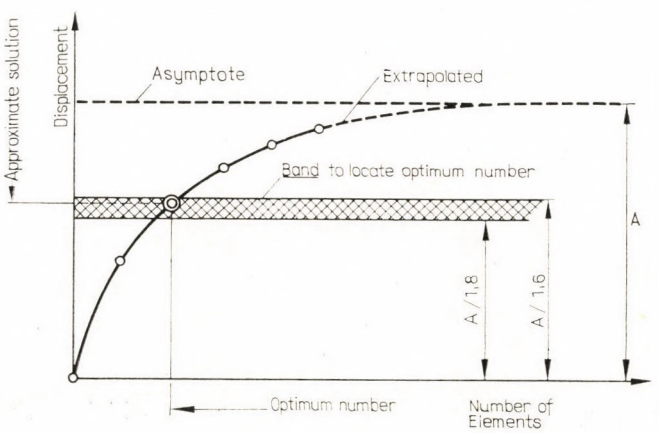

Fig. 14

6. Conclusions

Although neither the test problems nor the accuracy of the approximate stiffness coefficients have been favourable, the obtained results indicate the *potential* of the proposed Large Element Method for a considerable reduction in the order of the stiffness matrix.

The accuracy of the method, as presented, is acceptable only for checking or estimating purposes. Its accuracy, however, can be considerably improved by using

— finer subdivisions, coupled with an improved finite difference technique [6] to generate stiffness coefficients;

— improved displacement functions obtained through energy method;

— mathematical expressions for various convergence curves and for locating analytically the *optimum* number of elements;

— additional large elements with free edges.

Finally, there is a current need for a simple independent check of Matrix Displacement solutions involving large matrices to detect round-off errors and errors produced by ill-conditioned matrices, etc. The method, in its present form, provides for this need, and its demonstrated potential warrants further research in this field.

Acknowledgments

The author extends his appreciation to the Center for Engineering Research, University of Hawaii, for their assistance in the preparation of this manuscript.

REFERENCES

1. Argyris, T. H., Kelsey, S.: Modern Fuselage Analysis and the Elastic Aircraft, Butterworths, London 1960.
2. Zienkiewicz, O. C.—Cheung, Y. K.: The Finite Element Method in Structural and Continuum Mechanics, McGraw-Hill, London 1967.
3. Argyris, T. H.—Kelsey, S.: Energy Theorems of Structural Analysis, Butterworths, London 1963.
4. Timoshenko, S.—Woinowsky-Krieger, S.: Theory of Plates and Shells, 2nd ed., McGraw-Hill, New York 1959.
5. Timoshenko, S.—Goodier, T. N.: Theory of Elasticity, 2nd ed., McGraw-Hill, New York 1951.
6. Collatz, L.: The Numerical Treatment of Differential Equations, 3rd ed., Springer-Verlag, Berlin 1966.

Schätzung der Matrix-Verrückunglösungen von zweidimensionalen Aufgaben mit Hilfe des Großelementenverfahrens. Aufgrund der allgemeinen Konvergenzkriterien, die sich auf die Lösung der Spannungs- und Verrückungsaufgaben der Kontinua mit Hilfe von endlichen Elementen beziehen, leitet der Verfasser den Begriff der »Großelemente« ab. Bei der Ermittelung der Steifheitszahlen wird keine vorgeschriebene Verrückungsform den diskreten Elementen aufgezwungen; die Knotenpunkte führen nur Einheitsverrückungen durch. Die Kompatibilität der Spannungen und Verformungen die sich im inneren und an den Rändern der anschließenden Elemente entwickeln, wird mit Hilfe der Spiegelbildmethode durch auf die Einheitsverrückung des Knotenpunktes bezogene Lösung der betreffenden Differentialgleichungen der Theorie der Elastizität gesichert. Für die virtuelle Arbeit der Randkräfte erhalten wir eine symmetrische Steifheitsmatrix. Zur Vergleichung des zweierlei Verfahrens, d. h. Lösungen der zweidimensionalen Spannungsaufgaben mit Hilfe der Großelementenmethode und der analytischen Methode, werden Zahlenbeispiele mitgeteilt. Die Konvergenzkennwerte des Großelementen-Näherungsverfahrens weichen wesentlich von denen des Kleinelementen-Näherungsverfahrens ab; anstelle einer asymptotischen Konvergenz findet sich die exakte Lösung an einer optimalen Zahl der Elemente statt, die mit Hilfe eines einfachen graphischen Verfahrens ermittelt werden kann. Es wird nachgewiesen, daß durch Anwendung der Großelemente die Ordnung der Steifheitsmatrix wesentlich reduzierbar ist, jedoch bleibt die erreichbare Genauigkeit, vom Gesichtspunkt der Schätzung aus befriedigend. Einige, für Erhöhung der Genauigkeit dienende Verfahren werden dargestellt.

Приближенные решения с матричным сдвигом двумерных задач с помощью крупноэлементного метода. *(Р. Силард).* На основе общих критериев сходимости, касающихся решения с помощью конечных элементов задач напряжения и сдвига континуумов, автор выводит понятие «крупных» дискретных элементов. При выводе коэффициентов жесткости для дискретных элементов не предусматривается никаких заданных образов сдвига; узловые точки выполняют только единичный сдвиг. Компатибильность напряжения и деформации, имеющая место внутри элемента, а также на краях примыкающих элементов должна быть обеспечена применением метода зеркального отображения действительного для них дифференциального уравнения теории упругости, вернее путем решения, касающегося равновесного сдвига в узловой точке. Для виртуальной работы краевых усилий получается симметричная матрица жесткости. Автор для сревнения двух различных методов решения двумерных задач напряжения, а именно приближенного метода малых и крупных элементов, а также аналитического метода приводит числовые примеры. Характеристики сходимости крупноэлементного приближенного метода решения в значительной мере отличаются от характеристик сходимости малоэлементного приближенного метода решения; вместо асимптотической сходимости точное решение имеет место при некотором «оптимальном» числе элементов, которое можно определить при помощи простого графического метода. Автор доказывает, что применением крупных элементов можно значительно сократить порядок матрицы жесткости, но при этом достигнутая точность является достаточной для целей оценки; после чего схематически описываются некоторые методы, служащие для повышения точности.

Acta Technica Academiae Scientiarum Hungaricae, Tomus 68 (3—4), pp. 311—317 (1970)

ÜBER STABILISIERENDE UND DESTABILISIERENDE WIRKUNGEN

J. BARTA*

DOKTOR DER TECHNISCHEN WISSENSCHAFTEN

[Eingegangen: 15. Juli 1969]

Es werden Beispiele aus der Stabilitätstheorie der Ruhestellung eines elastischen Gebildes angeführt, um zu zeigen, daß die Wirkung der Dämpfung, der Versteifung und des auslenkunghindernden Zwanges nicht immer stabilisierend, sondern zuweilen destabilisierend ist.

Die vorliegende Arbeit bezieht sich auf die Stabilität der Ruhestellung eines elastischen Gebildes. Man ist geneigt zu vermuten, daß die Wirkung

a) der Dämpfung,

b) der Versteifung,

c) des auslenkunghindernden Zwanges

immer stabilisierend, d. h. günstig für die Stabilität der Ruhestellung des elastischen Gebildes sei.

Diese Vermutung wurde im Fall a) von ZIEGLER [1] widerlegt. Er hat nämlich nachgewiesen, daß eine geschwindigkeitsproportionale Dämpfungskraft, falls die an dem elastischen Gebilde angreifende Last nichtkonservativ ist, unter Umständen destabilisierend wirken kann.

Zugunsten der Vermutung im Fall b) liegt in der Literatur [2] ein Satz vor, der besagt: »Ist die an dem elastischen Gebilde angreifende Last konservativ, und wird an irgendwelchen Stellen des elastischen Gebildes die Steifigkeit erhöht und nirgends erniedrigt, so können sämtliche Eigenwerte (also auch der kleinste Eigenwert, d. h. die Knickkraft) nur größer oder wenigstens nicht kleiner werden; das Umgekehrte gilt bei Erniederigung der Steifigkeit.« Dieser Satz ist aber ohne nähere Umschreibung des elastischen Gebildes offenbar falsch. Denn z. B. bei dem in Bild 1 veranschaulichten elastischen Gebilde ruft der kritische Wert P_k der Last P die gestrichelt gezeichnete Knickung hervor. Wird die Steifigkeit des unteren Kragbalkens erhöht, so wird P_k kleiner, was dem zitierten Satz widerspricht. Damit hat sich die Vermutung auch im Fall b) als falsch erwiesen.

Die Vermutung im Fall c) zu widerlegen, ist der Zweck der nachfolgenden Erörterungen. Dazu wollen wir zeigen, daß im Falle einer nichtkonservativen

* Prof. Dr. techn. J. BARTA, József-körút 35, *Budapest VIII*, Ungarn.

Last der auslenkunghindernde Zwang unter Umständen destabilisierend wirken kann. Dies wird an Hand des unten angeführten ersten Beispiels geschehen. In einem zweiten Beispiel werden wir dagegen sehen, daß ein ähnlicher Zwang stabilisierend wirkt.

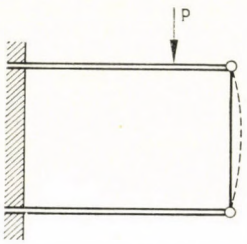

Bild 1. Der vertikale Stab des elastischen Gebildes erleidet eine Knickung

Erstes Beispiel

Das in Bild 2 veranschaulichte ebene elastische Gebilde besteht aus zwei gleichen homogenen starren Stäben und zwei gleichen elastischen Gelenken. Das eine Gelenk verbindet die zwei Stäbe, das andere Gelenk knüpft den

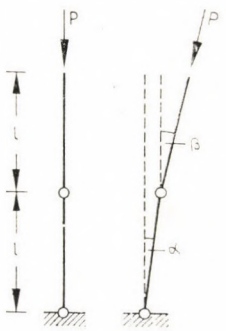

Bild 2. Die Ruhestellung und die ausgelenkte Stellung

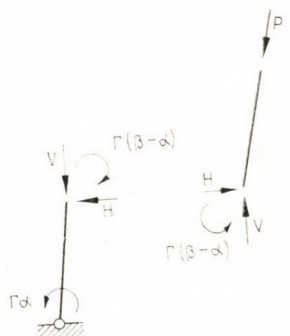

Bild 3. Kräftespiel während der Auslenkung

unteren Stab an den festen Untergrund. Jeder Stab hat die Masse m. Jedes Gelenk ist durch die Federkonstante Γ charakterisiert. Die Last besteht aus einer einzigen äußeren Kraft P, die am freien Ende des oberen Stabes stets in der Richtung des oberen Stabes angreift. Das Gewicht soll außer Acht gelassen werden. Man soll den kritischen Wert P_k berechnen.

Zur Lösung dieser Aufgabe sei die kinetische Methode verwendet, denn die Last ist nichtkonservativ. Es wird also der Bewegungsvorgang betrachtet, der durch eine hinreichend kleine Störung (Anfangsauslenkung und Anfangsgeschwindigkeit) hervorgerufen wird. Die Auslenkung aus der Ruhestellung ist durch die Winkel α und β charakterisiert. Das Kräftespiel ist in Bild 3

veranschaulicht. Dann lauten die kinetischen Gleichungen (Schwerpunktsatz und Momentensatz) für den oberen Stab

$$m\left(l\alpha+\frac{l}{2}\beta\right)^{\cdot\cdot}=-P\beta+H\,,$$

$$\frac{ml^2}{12}\beta^{\cdot\cdot}=-\frac{l}{2}H+\frac{l}{2}\beta V-\Gamma(\beta-\alpha)\,,$$

für den unteren Stab

$$\frac{ml^2}{3}\alpha^{\cdot\cdot}=-lH+l\alpha V+\Gamma(\beta-2\alpha)\,.$$

Eine weitere Gleichung, die hier nicht angeführt ist, liefert $V=P$. Aus diesen Gleichungen eliminiert man H und V, und erhält so das Differentialgleichungssystem

$$\begin{aligned}\frac{4}{3}ml\alpha^{\cdot\cdot}+\frac{1}{2}ml\beta^{\cdot\cdot}&=P\alpha-P\beta-2\frac{\Gamma}{l}\alpha+\frac{\Gamma}{l}\beta,\\ ml\alpha^{\cdot\cdot}+\frac{2}{3}ml\beta^{\cdot\cdot}&=2\frac{\Gamma}{l}\alpha-2\frac{\Gamma}{l}\beta.\end{aligned}\tag{1}$$

Unter einer Lösung des Systems (1) versteht man ein Funktionenpaar

$$\alpha(t)\,,\quad\beta(t)\,,\tag{2}$$

das dem System (1) genügt. Die Ruhestellung nach Bild 2 ist dann und nur dann stabil, wenn die Funktionen (2) bei jeden Anfangswerten $\alpha(0)$, $\beta(0)$, $\alpha^{\cdot}(0)$, $\beta^{\cdot}(0)$ für jedes t, auch für $t\to\infty$, endlich bleiben (Forderung F). Es fragt sich also, bei welchen Werten von P diese Forderung erfüllt ist. Um diese Frage zu beantworten, betrachten wir den Fall, wo die Lösung (2) die Form

$$\alpha=Ae^{\omega t},\quad\beta=Be^{\omega t}\tag{3}$$

hat. Wird (3) in (1) eingeführt, so entstehen die Gleichungen

$$\begin{aligned}\frac{4}{3}ml\omega^2A+\frac{1}{2}ml\omega^2B&=\left(P-2\frac{\Gamma}{l}\right)A-\left(P-\frac{\Gamma}{l}\right)B,\\ ml\omega^2A+\frac{2}{3}ml\omega^2B&=2\frac{\Gamma}{l}A-2\frac{\Gamma}{l}B.\end{aligned}$$

Diese sind homogen linear in bezug auf A und B. Die notwendige und hinreichende Bedingung dafür, daß sie nicht nur die Lösung $A = B = 0$ besitzen, ist

$$\begin{vmatrix} \frac{4}{3} ml\omega^2 - P + 2\frac{\Gamma}{2} & \frac{1}{2} ml\omega^2 + P - \frac{\Gamma}{l} \\ ml\omega^2 - 2\frac{\Gamma}{l} & \frac{2}{3} ml\omega^2 + 2\frac{\Gamma}{l} \end{vmatrix} = 0,$$

das heißt,

$$(ml\omega^2)^2 + \left(\frac{108}{7}\frac{\Gamma}{l} - \frac{30}{7}P\right) ml\omega^2 - \frac{36}{7}\frac{\Gamma^2}{l^2} = 0. \tag{4}$$

Dies ist eine algebraische Gleichung vierten Grades in ω (zweiten Grades in ω^2). Die Forderung F wird erfüllt sein, wenn keine der Wurzeln ω_1, ω_2, ω_3, ω_4 der Gleichung (4) einen positiven reellen Teil besitzt. Dies wird, wie sich durch eine leichte Überlegung zeigen läßt, eintreffen, wenn

$$\frac{108}{7}\frac{\Gamma}{l} - \frac{30}{7}P \geq 0, \left(\frac{108}{7}\frac{\Gamma}{l} - \frac{30}{7}P\right)^2 - 4\frac{36}{7}\frac{\Gamma^2}{l^2} \geq 0$$

ist, woraus sich

$$-\infty \leq P \leq \frac{2}{5}(9 - \sqrt{7})\frac{\Gamma}{l} \tag{5}$$

ergibt. Das Bestehen der Ungleichung (5) ist also notwendig zur Erfüllung der Forderung F, falls (2) die Form (3) hat.

Es soll noch abgeklärt werden, ob das System (1) auch eine Lösung (2) hat, die nicht von der Form (3) ist. Deshalb eliminieren wir $\alpha(t)$ bzw. $\beta(t)$ aus (1), wodurch eine Differentialgleichung für $\alpha(t)$ und eine für $\beta(t)$ entsteht:

$$m^2 l^2 \alpha'''' + \left(\frac{108}{7}\frac{\Gamma}{l} - \frac{30}{7}P\right) ml\alpha'' + \frac{36}{7}\frac{\Gamma^2}{l^2} = 0, \tag{6}$$

$$m^2 l^2 \beta'''' + \left(\frac{108}{7}\frac{\Gamma}{l} - \frac{30}{7}P\right) ml\beta'' + \frac{36}{7}\frac{\Gamma^2}{l^2} = 0. \tag{7}$$

Wenn man die zu (6) und (7) gehörigen charakteristischen Gleichungen ins Auge faßt, so findet man, daß sie mehrfache Wurzeln (das Kennzeichen dafür, daß (2) nicht nur von der Form (3) ist) dann und nur dann b sitzen, wenn

$$P = \frac{2}{5}(9 \pm \sqrt{7})\frac{\Gamma}{l}$$

ist. Das System (1) kann also eine Lösung, die nicht von der Form (3) ist, höchstens dann haben, wenn

$$P = \frac{2}{5}(9 \pm \sqrt{7})\frac{\Gamma}{l}$$

ist. Daraus und aus (5) folgt, daß in dem in Bild 2 veranschaulichten Fall

$$P_k = \frac{2}{5}(9 \pm \sqrt{7})\frac{\Gamma}{l} = 2{,}5417\,\frac{\Gamma}{l} \tag{8}$$

ist.

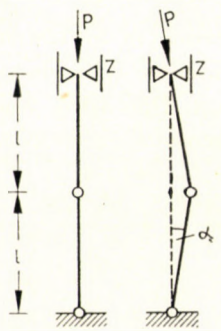

Bild 4. Die Ruhestellung und die ausgelenkte Stellung, wenn der auslenkunghindernde Zwang Z angewendet wird

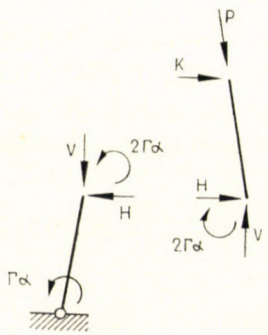

Bild 5. Kräftespiel während der Auslenkung

Betrachten wir nun den im Bild 4 veranschaulichten Fall. Dieser unterscheidet sich von dem in Bild 2 veranschaulichten Fall nur darin, daß am oberen Endpunkt des elastischen Gebildes ein auslenkunghindernder Zwang Z angewendet ist. Dieser besteht darin, daß der obere Endpunkt des elastischen Gebildes geradlinig vertikal geführt ist. Zur Ermittlung von P_k sei wieder die kinetische Methode verwendet. Unter der Benützung der Bezeichnungen der Bilder 4 und 5 lauten jetzt die kinetischen Gleichungen

$$m\left(\frac{l}{2}\alpha\right)^{\cdot\cdot} = P\alpha + H + K\,,$$

$$\frac{ml^2}{12}\alpha^{\cdot\cdot} = \frac{l}{2}H - \frac{l}{2}K + \frac{l}{2}\alpha V - 2\Gamma\alpha\,,$$

$$\frac{ml^2}{3}\alpha^{\cdot\cdot} = -lH + l\alpha V - 3\Gamma\alpha\,.$$

Nach Elimination von H und K und unter Berücksichtigung von $V = P$ ergibt sich

$$\alpha'' = \frac{P - 2{,}5\dfrac{\Gamma}{l}}{\dfrac{2}{3}ml}\,\alpha.$$

Aus dieser Differentialgleichung sieht man, daß in dem in Bild 4 veranschaulichten Fall

$$P_k = 2{,}5\frac{\Gamma}{l} \tag{9}$$

ist. Nebenbei sei bemerkt, daß das Resultat (9) auch mit der statischen Methode hergeleitet werden könnte.

Der Vergleich des Resultates (9) mit dem Resultat (8) führt zur Feststellung: *Die Wirkung des auslenkunghindernden Zwanges Z ist in diesem Beispiel destabilisierend.*

Allerdings ist das behandelte Beispiel nur aus prinzipiellen Gründen interessant. Denn die Differenz zwischen (8) und (9) ist klein, ja sogar praktisch unbedeutend. Ein Beispiel mit krasserer Differenz liegt zurzeit noch nicht vor.

Zweites Beispiel

Das ebene elastische Gebilde ist ein an einem Ende eingespannter schlanker Stab von konstantem Querschnitt. EI ist die Biegesteifigkeit. Der Stab ist durch eine an seinem freien Ende stets in der Richtung der Tangente angreifende Druckkraft P belastet (Bild 6). Das Gewicht soll außer Acht gelassen werden. Mann soll den kritischen Wert P_k berechnen. Die Berechnung wurde

Bild 6. Die Ruhestellung und die ausgelenkte Stellung

Bild 7. Die Ruhestellung und die ausgelenkte Stellung, wenn der auslenkunghindernde Zwang Z angewendet wird

unter Verwendung der kinetischen Methode von BECK durchgeführt [3]. Er fand, daß in dem in Bild 6 veranschaulichten Fall

$$P_k = 20{,}05 \frac{EI}{l^2} \tag{10}$$

ist.

Nun sei am oberen Ende dieses elastischen Gebildes der Zwang Z angewendet (Bild 7). In diesem Falle liefert die kinetische (und auch die statische) Methode das Resultat:

$$P_k = 20{,}19 \frac{EI}{l^2}, \tag{11}$$

wie es schon aus den Erörterungen von BECK unmittelbar hervorgeht [4].

Der Vergleich von (10) mit (11) führt zur Feststellung: *Die Wirkung des auslenkunghindernden Zwanges Z ist in diesem Beispiel stabilisierend.*

SCHRIFTTUM

1. ZIEGLER, H.: Die Stabilitätskriterien der Elastostatik. Ing.-Arch. **20** (1952), 49.
2. Siehe z. B.: PFLÜGER, A.: Stabilitätsprobleme der Elastostatik. Aufl. 1 (1950), 215, oder Aufl. 2 (1964), 226.
3. BECK, M.: Die Knicklast des eingespannten tangential gedrückten Stabes. *ZAMP*, **3** (1952), 225—228.
4. Ibidem, S. 226, Zeilen 9—11 und u. a.: SZABÓ, I.: Einführung in die technische Mechanik. Aufl. (1956), 168.

Stabilizing and Destabilizing Effects. This paper is concerned with the equilibrium stability of elastic structures. By means of examples, it shows that the effect of damping or stiffening or constraints applied against displacement are not always stabilizing but sometimes destabilizing.

О стабилизирующих и дестабилизирующих воздействиях *(Й. Барта)*. Приведены примеры из теории стабильности (устойчивости) при переведении упругой формы в стабильное состояние для доказательства того, что амортизация, придание жесткости и принуждение, предотвращающее элонгацию, не во всех случаях имеют стабилизирующее, а иногда дестабилизирующее действие.

Acta Technica Academiae Scientiarum Hungaricae, Tomus 68 (3—4), pp. 319—334 (1970)

PARABOLOID SHELLS OF REVOLUTION STAR-POLYGONAL IN PLAN

P. CSONKA*
DOCTOR OF TECHN. SC.

[Manuscript received, March 9 1970]

Paper deals with the statical analysis of paraboloid shells of revolution, the ground-plan figure of which resembles a regular polygon, but has sides curved inward instead of straight ones. It is presumed that the edge beam of the shell is supported by a wall or by vertical columns standing close to each other. A vertical force system equally distributed over the ground-plan area is assummed as being a loading. The arching of the shell's edge line is set up in such a way as to enable the calculation of the reduced inner forces by simple closed formulae. Paper also states the principal values of the reduced inner forces, moreover, it determines the equation of their trajectories. A numerical example is given to prove the simplicity of the calculation.

1. Introduction

Under *star polygon* a regular figure similar to regular polygons should be understood, the sides of which are curved inward (Fig. 1).

Paraboloid shells of revolution constructed over a star-polygonal ground-plan are relatively easy to analyze in case of vertical loads equally distributed over the ground-plan area. However, the analysis of such shells is simple only with the condition that the curved sides of the ground-plan figure are appro-

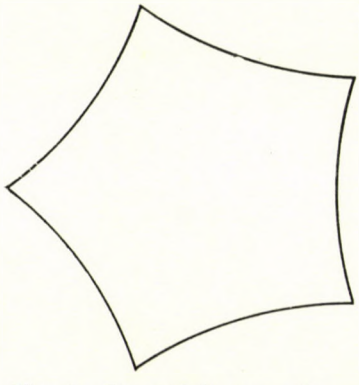

Fig. 1. Five-sided star-polygon

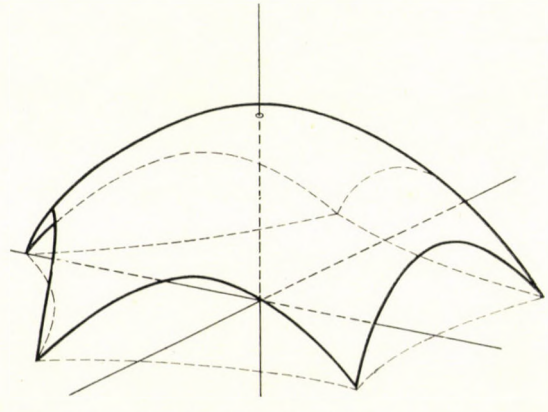

Fig. 2. Paraboloid shell of revolution constructed over a five-sided star-polygon

* Dr. PÁL CSONKA, Bartók B. út 31, *Budapest XI.*, Hungary.

priately chosen and the edge beam of the shell is supported by a wall or by vertical columns set close to each other (Fig. 2).

In the following, the analysis of paraboloid shells of star-polygonal ground-plan is based on the membrane theory of shells. Consequently, the bending and torsional forces of the shell wall as well as those arising in the vicinity of the shell edge, will be neglected. The bending and torsional forces to which the edge arches are subjected, as being insignificant, anyway may equally be left out.

2. The star-polygon

2.1. *Equation of the contour line*

The shape of the n-sided star-polygon may be characterized in the polar coordinate system $0(r, \varphi)$ by the equation

$$f(r, \varphi) = A \frac{r^2}{R^2} + B \frac{r^n}{R^n} \operatorname{cosn} \varphi + C = 0$$

in which A, B and C are constant values (Fig. 3). To the latter such values must be attached that the ground-plan figure should have corner points (double points) at the required places. In order to ensure this, it is necessary for f, $\partial f/\partial r$, $\partial f/\partial \varphi$ to have zero value at the mentioned points, further, that not

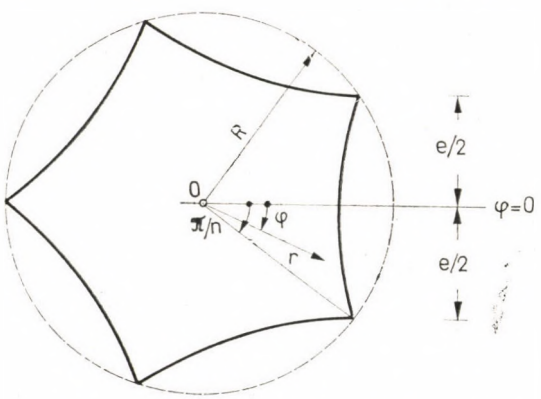

Fig. 3. Polar coordinate system 0 (r,φ)

all the second derivates of f should be equal to zero. All these requirements will be fulfilled, if

$$A = 1, \qquad B = \frac{2}{n}, \qquad C = -\frac{n-2}{n}.$$

In this case, equation

$$f(r, \varphi) = +\frac{r^2}{R^2} + \frac{2}{n} \cdot \frac{r^n}{R^n} \cos n\varphi - \frac{n-2}{n} = 0 \tag{1}$$

holds, which can also be expressed as

$$\varphi = \frac{1}{n} \arccos\left[\frac{n}{2} \cdot \frac{R^n}{r^n}\left(\frac{n-2}{n} - \frac{r^2}{R^2}\right)\right]. \tag{2}$$

2.2. *Case of* $n = 3$

If $n = 3$, equation (1) of the edge line of the star-polygon takes the simple form

$$\frac{r^2}{R^2} + \frac{2}{3} \cdot \frac{r^3}{R^3} \cos 3\varphi - \frac{1}{3} = 0 \tag{3}$$

which, after some transformation, may also be written as follows:

$$\left(1 - 2\frac{r}{R}\cos\varphi\right)\left(\frac{r}{R}\sin\varphi + \frac{1}{\sqrt{3}} \cdot \frac{r}{R}\cos\varphi + \frac{1}{\sqrt{3}}\right) \cdot \left(\frac{r}{R}\sin\varphi - \frac{1}{\sqrt{3}} \cdot \frac{r}{R}\cos\varphi + \frac{1}{\sqrt{3}}\right) = 0. \tag{4}$$

Above equation can be divided into three factors:

$$1 - 2\frac{r}{R}\cos\varphi = 0,$$

$$\frac{r}{R}\sin\varphi + \frac{1}{\sqrt{3}} \cdot \frac{r}{R}\cos\varphi + \frac{1}{\sqrt{3}} = 0, \tag{5}$$

$$\frac{r}{R}\sin\varphi - \frac{1}{\sqrt{3}} \cdot \frac{r}{R}\cos\varphi - \frac{1}{\sqrt{3}} = 0.$$

These are equations of three straights, intersecting each other at angles of 60 degrees, which means that in the given case the star-polygon degenerates into an equilateral triangle (Fig. 4).

2.3. *Case of* $n = 4$

If $n = 4$, equation (2) of the edge line of the star-polygon becomes

$$\frac{r^2}{R^2} + \frac{1}{2} \cdot \frac{r^4}{R^4} \cos 4\varphi - \frac{1}{2} = 0. \tag{6}$$

However,

$$\cos 4\varphi = 2\cos^2 2\varphi - 1,$$

so that the former equation may be modified as

$$\left(\frac{r^2}{R^2}\cos 2\varphi - \frac{1}{\sqrt{2}}\cdot\frac{r^2}{R^2} + \frac{1}{\sqrt{2}}\right)\cdot\left(\frac{r^2}{R^2}\cos 2\varphi + \frac{1}{\sqrt{2}}\cdot\frac{r^2}{R^2} - \frac{1}{\sqrt{2}}\right) = 0\,. \tag{7}$$

Dividing above equation into two factors we obtain the equations

$$\begin{aligned}\frac{r^2}{R^2}\cos 2\varphi - \frac{1}{\sqrt{2}}\cdot\frac{r^2}{R^2} + \frac{1}{\sqrt{2}} &= 0\,,\\ \frac{r^2}{R^2}\cos 2\varphi + \frac{1}{\sqrt{2}}\cdot\frac{r^2}{R^2} - \frac{1}{\sqrt{2}} &= 0\,,\end{aligned} \tag{8}$$

representing *two hyperboles*. Accordingly, in the present case, the star-polygon is bordered by hyperbolic arches (Fig. 5). The length of the real half-axis of these is

$$a = \frac{R}{\sqrt{\sqrt{2}+1}} \cong 0{,}643\,59\,R \tag{9}$$

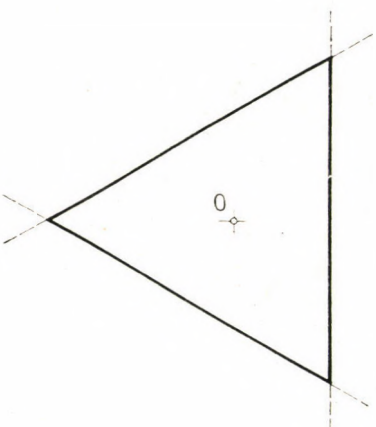

Fig. 4. Tringular star-polygon

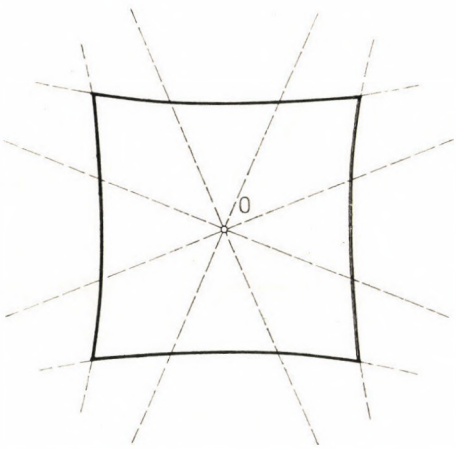

Fig. 5. Quadrangular star-polygon

and that of the imaginary half-axis is

$$b = \frac{R}{\sqrt{\sqrt{2}-1}} \cong 1{,}553\,77\,R. \tag{10}$$

2.4. *Geometrical representation of the star-polygon*

The polar angle φ of arbitrary point P of the edge line lying at a distance from origin 0 may be determined with aid of equation (2) and so the edge line of the star-polygon can be drawn with the desired exactitude.

However, instead of the above accurate method, for practical purposes it is quite sufficient to determine the edge arches of the star-polygon approximately, by fixing its five points and five tangents. Parabolic or circular arches may be drawn as substitutes for the arch sections between the known points. In order to facilitate this method of geometrical construction the data of star-

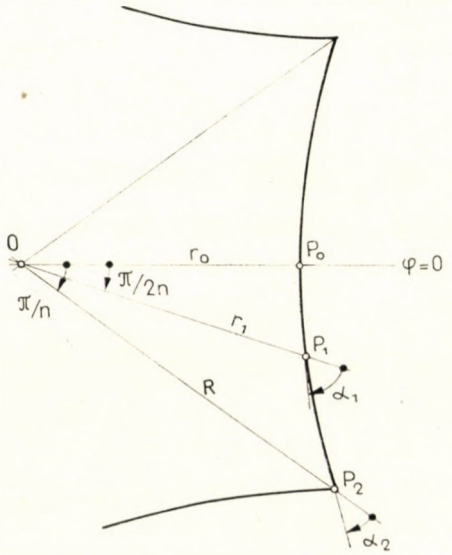

Fig. 6. Symbols

polygons with sides from $n = 5$ to $n = 10$ are compiled in Table I. Fig. 6 gives the explanation of symbols figuring in this Table.

The shape of star-polygons $5 \leq n \leq 10$ can be seen in Fig. 7.

Table I

Data for geometrical representation of star-polygons $3 \leq n \geq 10$

n	r_0	$r_1 = \left(\frac{n-2}{n}\right)^{1/2} R$	$\tan \alpha_1 = \left(\frac{n}{n-2}\right)^{(n-2)/2}$	$\tan \alpha_2 = \left(\frac{n-2}{n}\right)^{1/2}$
3	0,5000 R	0,5774 R	1,7321	0,5774
4	0,6436 R	0,7071 R	2,0000	0,7071
5	0,7221 R	0,7746 R	2,1552	0,7746
6	0,7721 R	0,8165 R	2,2500	0,8165
7	0,8098 R	0,8452 R	2,3250	0,8452
8	0,8322 R	0,8860 R	2,3704	0,8860
9	0,8515 R	0,8819 R	2,4225	0,8819
10	0,8670 R	0,8944 R	2,4414	0,8944

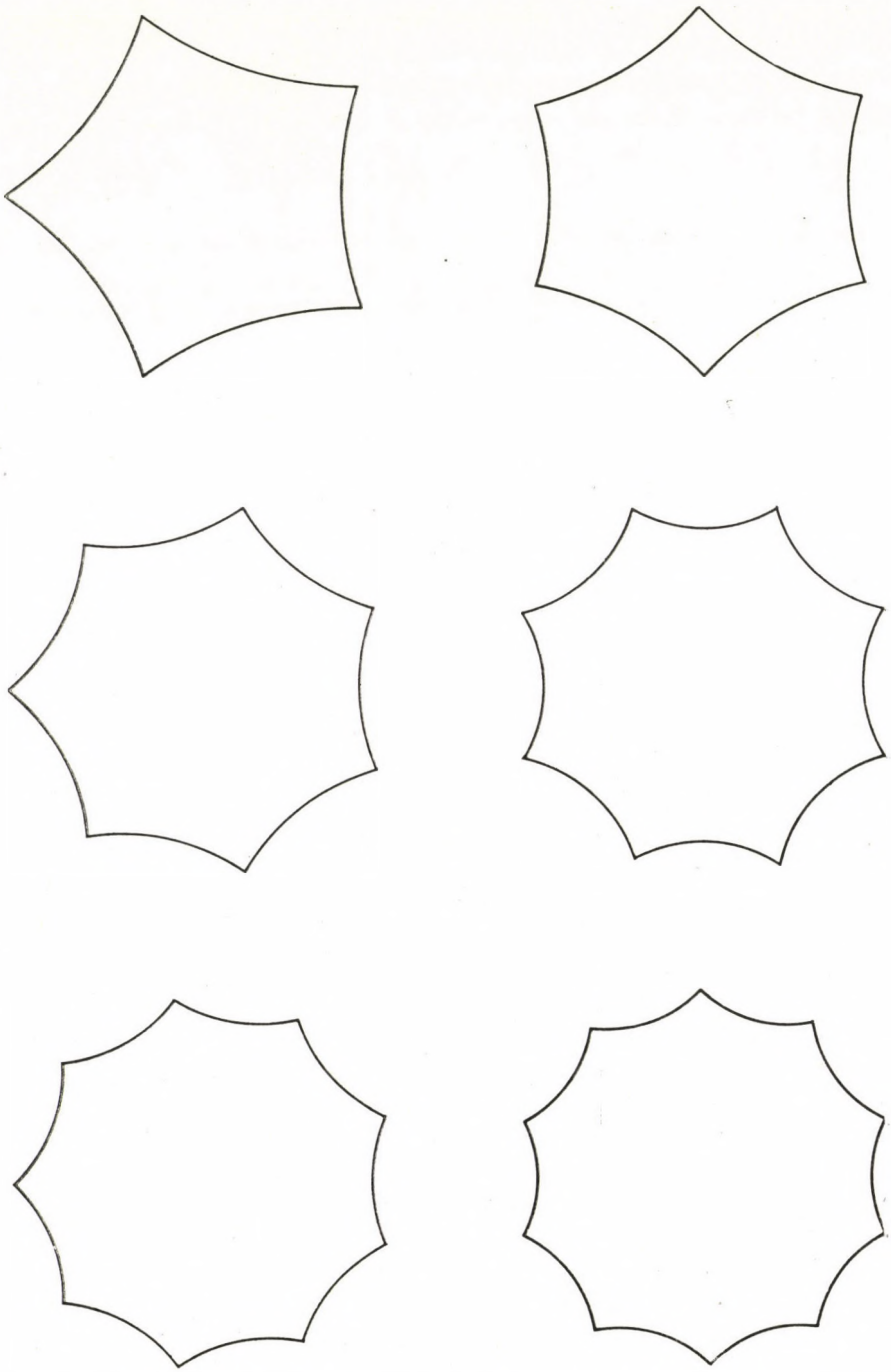

Fig. 7. Five to ten-sided star-polygons

3. Shape of the shell

Denoting the height of the shell by h, the middle surface's shape of the paraboloid shell of revolution over an n-sided star-polygon can be characterized in the cylindrical coordinate system $0(r, \varphi, z)$ shown in Fig. 8 by the equation

$$z = \frac{h}{R^2} r^2. \tag{11}$$

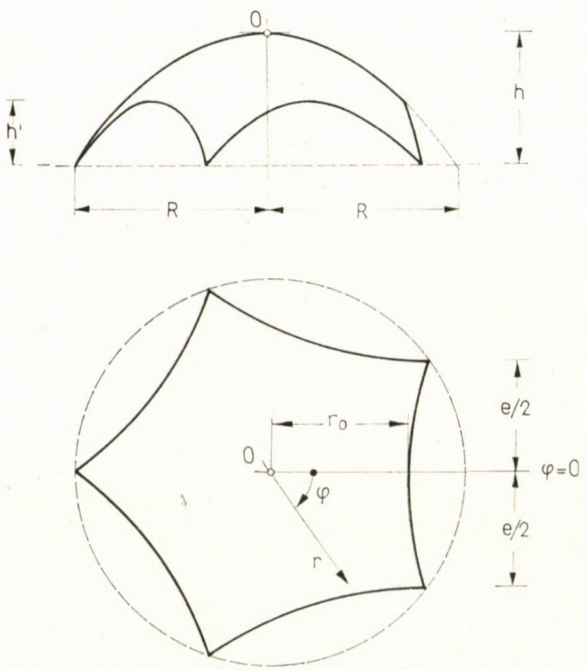

Fig. 8. Paraboloid shells of revolution constructed over star-polygonal ground-plans

The cylinder constructed over the boundary line of the ground-plan figure is intersected into arches by this surface. In case of $n > 3$, these arches are spatial curves, the rise of which is

$$h' = h\left(1 - \frac{r_0^2}{R^2}\right). \tag{12}$$

The rise h' of the edge arches of paraboloid shells of revolution over an $3 \leq n \leq 10$ sided starpolygon is given in Table II.

Fig. 9 shows the axonometrical view of paraboloid shells of revolution over ground-plans with $n = 4$, $n = 6$ and $n = 8$ sides.

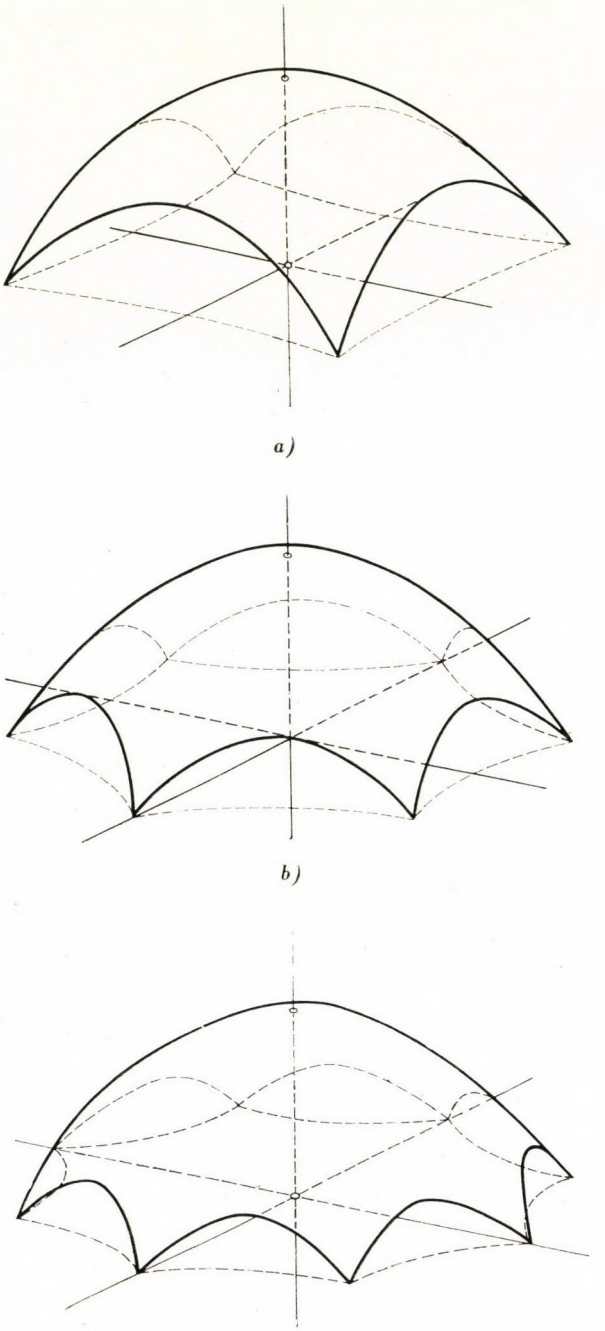

Fig. 9. Paraboloid shells of revolution constructed over four-, six- and eight-sided star-polygonal ground plans

Table II

The rise h′ of the edge arches of paraboloid shells of revolution over an n-sided star-polygon as ground-plan

n	h'
3	0,7500 h
4	0,5858 h
5	0,4786 h
6	0,4039 h
7	0,3442 h
8	0,3076 h
9	0,2750 h
10	0,2483 h

4. General solution of the problem

For the analysis of the stress state of shells it is expedient to establish the so-called *stress function* $F = F(r, \varphi)$. In the case of shells of revolution loaded by distributed vertical forces this function has to satisfy the differential equation

$$\frac{\partial^2 F}{\partial r^2} \cdot \frac{1}{r} \cdot \frac{dz}{dr} + \frac{1}{r} \cdot \frac{\partial F}{\partial r} \cdot \frac{d^2 z}{dr^2} + \frac{1}{r^2} \cdot \frac{\partial^2 F}{\partial \varphi^2} \cdot \frac{d^2 z}{dr^2} + g = 0 \quad (13)$$

where $g = g(r, \varphi)$ represents the specific value of the distributed vertical forces to which the shell is subjected, as related to the unit of the ground-plan area. In the present case this specific value is

$$g = g_0 = \text{const}, \quad (14)$$

and the following relations hold:

$$\frac{dz}{dr} = \frac{2h}{R^2} r, \qquad \frac{d^2 z}{dr^2} = \frac{2h}{R^2}.$$

Thus, differential equation (13) is simplified as:

$$\frac{\partial^2 F}{\partial r^2} + \frac{1}{r} \cdot \frac{\partial F}{\partial r} + \frac{1}{r^2} \cdot \frac{\partial^2 F}{\partial \varphi^2} + \frac{R^2}{2h} g_0 = 0. \quad (15)$$

Apart from differential equation (15) the unknown function F has also to satisfy the *boundary condition* of the problem. This condition can be expressed by equation

$$F_{edge} = \text{const}, \quad (16a)$$

if the edge beam is supported along its entire length by a wall, and by equation

$$F_{edge} \cong \text{const}, \tag{16b}$$

if the support consists of vertical columns close to each other.

If we succeed in establishing a function F satisfying both equations (15) and (16), the r and φ directed reduced inner forces can be determined by the following known formulae:

$$\begin{aligned} n_r &= \frac{1}{r} \cdot \frac{\partial F}{\partial r} + \frac{1}{r^2} \cdot \frac{\partial^2 F}{\partial \varphi^2}, \\ n_{r\varphi} &= -\frac{\partial}{\partial r}\left(\frac{1}{r} \cdot \frac{\partial F}{\partial \varphi}\right), \\ n_\varphi &= \frac{\partial^2 F}{\partial r^2}. \end{aligned} \tag{17}$$

5. Stress state of the shell

5.1. *Stress function of the problem*

It is easy to prove that in the case of vertical loads equally distributed over the ground-plan area the stress function $F = F(r, \varphi)$ of the problem can be established as

$$F(r, \varphi) = -\frac{R^4 g_0}{8h} f(r, \varphi). \tag{18}$$

In this formula $f(r, \varphi)$ denotes the equation (1) of the boundary line of the star-polygon reduced to zero. Written in detail, the stress function of a paraboloid shell of revolution with an n-sided star-polygon as a ground-plan, is

$$F = -\frac{R^4 g_0}{8h}\left(\frac{r^2}{R^2} + \frac{2}{n} \cdot \frac{r^n}{R^n} \cos n\varphi - \frac{n-2}{n}\right). \tag{19}$$

The stress function being known, the r and φ directed reduced inner forces can be determined by aid of formulae (17):

$$\begin{aligned} n_r &= -\frac{R^2 g_0}{4h}\left[1 - (n-1)\frac{r^{n-2}}{R^{n-2}} \cos n\varphi\right], \\ n_{r\varphi} &= -\frac{R^2 g_0}{4h}(n-1)\frac{r^{n-2}}{R^{n-2}} \sin n\varphi, \\ n_\varphi &= -\frac{R^2 g_0}{4h}\left[1 + (n-1)\frac{r^{n-2}}{R^{n-2}} \cos n\varphi\right]. \end{aligned} \tag{20}$$

5.2. *Principal values of the reduced inner forces*

The formula

$$n_{1,2} = \frac{1}{2}(n_r + n_t) \pm \frac{1}{2}\sqrt{(n_r - n_\varphi)^2 + 4n_{r\varphi}^2},$$

familiar in statics, can be used for calculating the principal values n_1 and n_2 of the inner forces. When substituting values (20) into this, it was found that

$$n_{1,2} = -\frac{R^2 g_0}{4h}\left[1 \pm (n-1)\frac{r^{n-2}}{R^{n-2}}\right]. \tag{21}$$

It may be noted that *the principal values of the reduced inner forces do not depend on the polar angle* φ, which means that every point of the shell lying

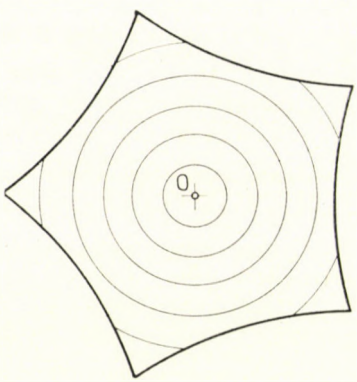

Fig. 10. The trajectories of points identically stressed

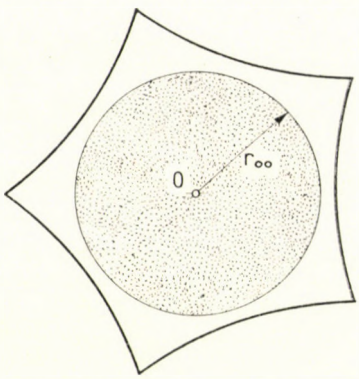

Fig. 11. The zone free from tensile forces (the dotted area)

at an equal distance from axis z is in the same stress state. In other words, the trajectories of the points in a similar stress state are concentric circles drawn round the central point 0 (Fig. 10).

Formula (21) also demonstrates that only a single circular zone of the shell is free from tensional forces. The radius r_{00} of this circular zone (Fig. 11) can be determined by equation

$$1 - (n-1)\frac{r_{00}^{n-2}}{R^{n-2}} = 0$$

from which it results that

$$r_{00} = \frac{1}{(n-1)^{1/(n-2)}} R. \tag{22}$$

Table III

Radius of the zone free from tangential forces

n	r_{00}
3	0,5000 R
4	0,5774 R
5	0,6300 R
6	0,6687 R
7	0,6988 R
8	0,7230 R
9	0,7430 R
10	0,7598 R

This value for shells of different n-sided star-polygonal ground-plan is compiled in Table III.

Formula (21) also shows us that the absolute value of the principal compressive force in the corner points of the ground-plan is three times greater than that in the centre point. On the other hand, the principal tensional force at the same points is $(n - 2)$ times greater than the absolute value of the compressive force acting on the middle point of the shell.

5.3. *Principal directions of the reduced inner forces*

According to the teaching of statical science the angular deviation α between principal directions in point P (Fig. 12) and the radius vector directed to point P can be determined by formula

$$\tan 2\alpha = \frac{2n_{r\varphi}}{n_r - n_\varphi} .$$

Substituting (20) into this formula, relationship

$$\tan 2\alpha = -\tan n\varphi$$

is arrived at. Hence

$$\alpha = \begin{cases} -n\varphi/2 , \\ -n\varphi/2 - \pi/2 . \end{cases} \tag{23}$$

Above formula proves that *the principal directions of the reduced inner forces do not depend on length r of the radius vector.* This means that all the tra-

jectories of the principal directions intersect the same radius vector at an identical angle α (Fig. 13). In short, all the trajectories are similar in shape and only differ in scale.

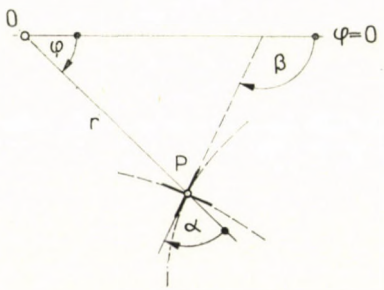

Fig. 12. Positon of the principal directions at point P

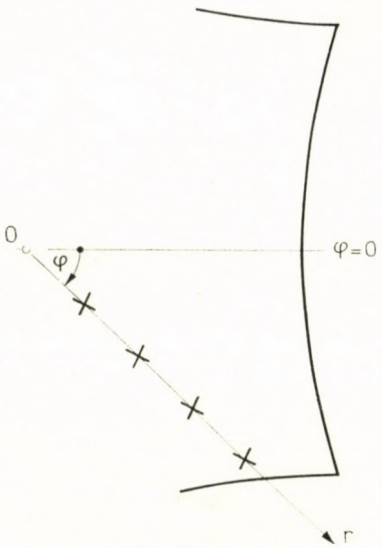

Fig. 13. The trajectories of the principal directions intersect the same radial line under the same angle

5.4. *Equation of the trajectories*

As is known from analytical geometry, the trajectories of the principal inner forces can be determined with aid of formula

$$\tan\alpha = \frac{r}{dr/d\varphi} .$$

According to this formula

$$\frac{dr}{d\varphi} = \frac{r}{\tan\alpha}$$

holds, respectively, taking (23) into consideration,

$$\frac{dr}{d\varphi} = \frac{r}{\begin{matrix}-\tan\\+\cot\end{matrix}(n\varphi/2)}$$

is valid. Hence, by separating the variables, the formula

$$\frac{1}{r}dr = \left[\pm\begin{matrix}\tan\\\cot\end{matrix}(n\varphi/2)\right]\cdot d\varphi$$

follows. Integrating both sides, the result will be

$$\ln c\, r = -\frac{2}{n} \ln \begin{matrix}\cos \\ \sin\end{matrix} (n\varphi/2) = \ln \left[\begin{matrix}\cos \\ \sin\end{matrix} (n\varphi/2)\right]^{-2/n}$$

where c denotes a constant of integration. Further

$$c\, r = \left[\begin{matrix}\cos \\ \sin\end{matrix} (n\varphi/2)\right]^{-2/n},$$

respectively,

$$r = \frac{1}{c} \left(\frac{1 \pm \cos n\varphi}{2}\right)^{-1/n}. \tag{24}$$

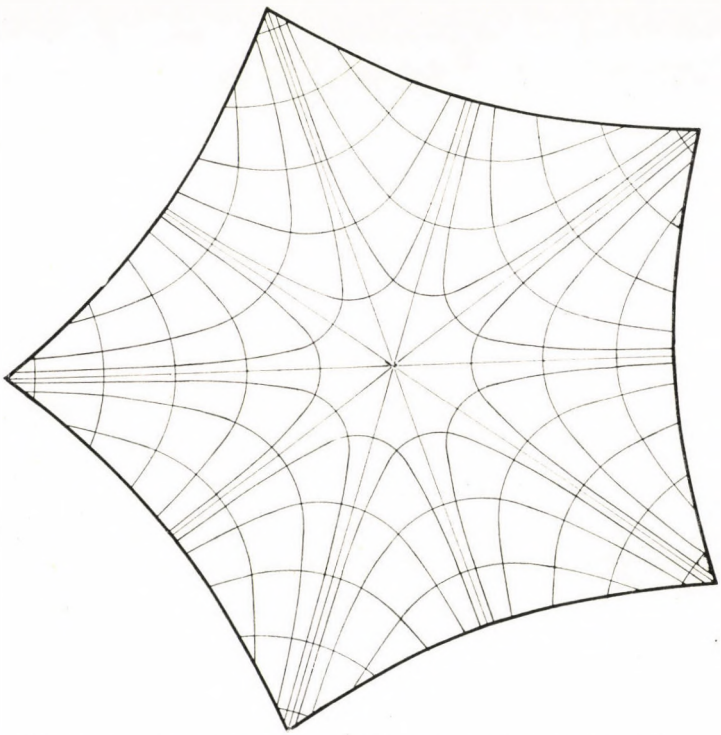

Fig. 14. Trajectories of the principal directions of the reduced inner forces

In case of the trajectory passing through point $P_1(r_1, \varphi_1)$ the value of the constant of integration c can be determined with aid of equation

$$r_1 = \frac{1}{c} \left(\frac{1 \pm \cos n\varphi_1}{2}\right)^{-1/n}$$

Calculating the value of c from the former equation and placing it into formula (24), the equation of the trajectory passing through the point $P_1(r_1, \varphi_1)$ will take the following form:

$$r = \left(\frac{1 \pm \cos n\varphi_1}{1 \pm \cos n\varphi}\right)^{1/n} \cdot r_1 \tag{25}$$

The trajectories of the principal directions of the reduced inner forces of a paraboloid shell of revolution constructed over a five-sided star-polygonal ground-plan are shown in Fig. 14.

6. Numerical example

Let us apply the calculating method expounded above to the paraboloid shell of revolution constructed over a five-sided star-polygonal ground-plan shown in Fig. 15. The shell under examination is subjected to a vertical load

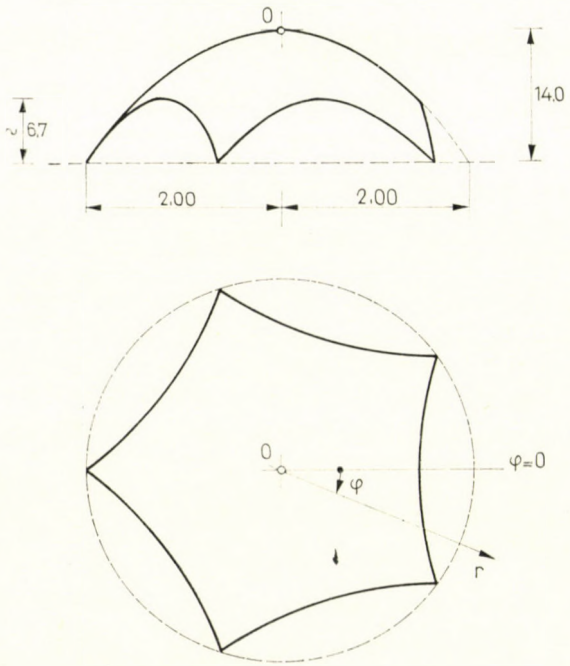

Fig. 15. Paraboloid shell of revolution constructed over a pentagonal star-polygon

system uniformly distributed over the ground-plan area of intensity:

$$g = g_0 = 280 \text{ kp/m}^2.$$

In the present case

$$R = 20{,}0 \text{ m}, \quad h = 14{,}0 \text{ m}, \quad h' = 6{,}7 \text{ m}$$

and thus, according to (20) the r and φ directed inner forces of the shell will be:

$$n_r = -\frac{20{,}0^2 \cdot 280}{4 \cdot 14{,}0}\left(1 - 4\frac{r^3}{20{,}0^3}\cos 5\varphi\right) = -2000\left(1 - \frac{r^3 \cos 5\varphi}{2000}\right)[\text{kp/m}],$$

$$n_{r\varphi} = -\frac{20{,}0^2 \cdot 280}{4 \cdot 14{,}0} 4\frac{r^3}{20{,}0^3}\sin 5\varphi = -r^3 \sin 5\varphi\,[\text{kp/m}],$$

$$n_\varphi = -\frac{20{,}0^2 \cdot 280}{4 \cdot 14{,}0}\left(1 + 4\frac{r^3}{R^3}\cos 5\varphi\right) = -2000\left(1 + \frac{r^3 \cos 5\varphi}{2000}\right)[\text{kp/m}],$$

As is to be seen from the above formulae, the shell is in a very favorable stress state, the reduced inner forces being relatively slight even at the corners of the shell: the highest reduced compressive force amounts to 10 000 kp/m, the highest reduced tensile force to 6000 kp/m.

An axonometric view of the shell analyzed above is shown in Fig. 1.

Rotationsparaboloidschalen über Sternpolygon-Grundrißen. Der Aufsatz behandelt die Berechnung von Rotationsparaboloidschalen, deren Grundriß einem regelmäßigen Vieleck ähnelt, dessen Seiten jedoch nach innen gebogen sind. Es wird angenommen, daß der Randbalken der Schale durch eine Wand, oder dicht aneinandergereihte Säulen unterstützt wird. Als Belastung wird ein auf der Grundrißfläche gleichmäßig verteiltes Kraftsystem in Rechnung gestellt und die Achsenlinie der Randbögen wird derart bestimmt, daß die reduzierten Spannkräfte der Schale durch einfache Formeln berechnet werden können. Der Aufsatz bestimmt auch die Hauptwerte der reduzierten Spannkräfte und stellt sogar die Gleichung der Trajektorien der Hauptrichtungen auf. Die Einfachheit der Bestimmung der reduzierten Spannkräfte wird durch ein numerisches Beispiel illustriert.

Оболочки — параболоиды вращения с планом в виде звездного многоугольника *(П. Чонка).* Работа занимается расчетом таких оболочек — параболоидов вращения, профиль плана которых представляет собою правильный многоугольник с направленными внутрь сторонами. Предполагается, что краевая балка оболочки опирается на стену или же на густо расположенные друг возле друга колонны. В качестве нагрузки предполагается перпендикулярная силовая система, равномерно распределяющаяся на площади плана, и профиль краевой линии оболочки определяется так, чтобы приведенные внутренние силы оболочки можно было бы вычислять при помощи простых замкнутых формул. В работе определяются также основные значения приведенных распирающих усилий, более того, выведено также уравнение траектории приведенных напряженных основных направлений. Простота вычисления приведенных распирающих усилий подверждается числовым примером.

Acta Technica Academiae Scientiarum Hungaricae, Tomus 68 (3—4), pp. 335—351 (1969)

UNTERSUCHUNG VON STATISCH UNBESTIMMTEN KONSTRUKTIONEN AUF GRUND DER VERALLGEMEINERUNG DES NIKOLSKIJSCHEN ALGORITHMUS

A. FEKETE*

[Eingegangen: 22. Nov. 1968]

Die Ermittelung der inneren Kräfte in den statisch vielfach unbestimmten Konstruktionen mit Hilfe des Kraftgrößenverfahrens erfordert unter den Verhältnissen des Konstruktionsbüros — wo im allgemeinen kein Rechenautomat dem Konstrukteur zur Verfügung steht — eine umfangreiche Rechenarbeit. Besonders viel Rechnen verlangt die Invertierung der Koeffizientenmatrix des Kompatibilitätsgleichungssystems. Die Verallgemeinerung des Iterationsverfahrens von Nikolskij erlaubt die Verringerung der umfangreichen Rechenarbeit. In der Abhandlung wird die Untersuchung der wichtigsten Probleme dieser Verallgemeinerung erörtert, die Gültigkeit des Algorithmus auf den Fall der n-mal unbestimmten Konstruktionen ausgedehnt und bestätigt.

1. Einleitung

Zur Untersuchung der inneren Kräfte statisch unbestimmter Konstruktionen sind zwei Methoden — das Kraftgrößenverfahren und die Deformationsmethode — bekannt. Der Unbestimmtheitsgrad der bei dem Kraftgrößenverfahren angewandten Grundsysteme ist immer niedriger, während der der bei der Deformationsmethode benutzten Grundsysteme immer höher ist, als derselbe der ursprünglichen Konstruktionen. Dementsprechend ist das Grundsystem des Kraftgrößenverfahrens »weicher« und das der Deformationsmethode »steifer« als die ursprüngliche Konstruktion. Die unbekannten Größen des Kraftgrößenverfahrens sind Kräfte, während die der Verformungsmethode Bewegungen sind. Demzufolge schreibt das Kraftgrößenverfahren die Lösung mit Hilfe der Kompatibilitätsgleichungen und die Verformungsmethode mit Hilfe der Gleichgewichtsgleichungen auf. Betrachtet man die tatsächlichen inneren Kräfte als Grundlage für einen Vergleich, so wird das Kräftespiel der steiferen Konstruktion eine obere und das der weicheren Konstruktion eine untere Näherung der tatsächlichen inneren Kräfte sein. Dies ist das Grundprinzip des Iterationsverfahrens, welches von E. N. NIKOLSKIJ [1] [2] zur Berechnung der statisch vielfach unbestimmten Eisenbahnwagen mit Gurtträger ausgearbeitet wurde. Nikolskij baute seine Methode auf das Kraftgrößenverfahren auf und illustrierte sie durch solch ein statisch unbestimmtes Modell, welches — ähnlich den Steifigkeitsverhältnissen der Gurtträger-Eisen-

* A. FEKETE, Akácfa-u. 6, *Budapest VII*, Ungarn.

bahnwagen — aus zwei Konstruktionsteilen mit sehr verschiedenen Steifigkeiten besteht (Bild 1). Die Eigenheit des Verfahrens ist, daß trotz der Anwendung des Kraftgrößenverfahrens als Ausgangstheorie, in den einzelnen Schritten der Iteration abwechselnd Kompatibilitäts- bzw. Gleichgewichtsbedingungen befriedigt werden. Es seien A, bzw. B zwei Konstruktionen von

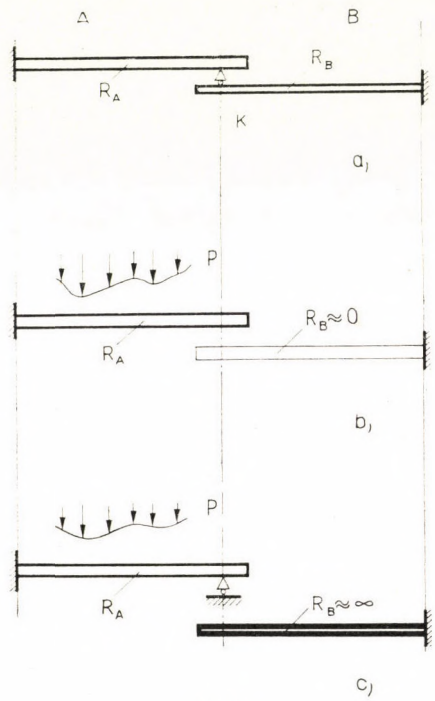

Bild 1

verschiedenen Steifigkeiten R_A bzw. R_B. Betrachtet man dies von der Anwendung des Nikolskijschen Verfahrens aus, so können drei mögliche Fälle unterschieden werden:

1. Fall: $R_A > R_B$

Die das Ausgangssystem kennzeichnenden Steifigkeitsverhältnisse sind: (Bild 1b) R_A = endlich, $R_B \approx 0$. Nach Beseitigung der Verbindung zwischen den Konstruktionsteilen A und B zerfällt das Ausgangssystem in die den charakteristischen Steifigkeiten entsprechenden zwei Teile:

a) der statisch bestimmte Konstruktionsteil von endlicher Steifigkeit (System A);

b) der statisch bestimmte Konstruktionsteil von Nullsteifigkeit (System B).

Das System B kann in sich selbst keine äußere Belastung tragen ($R_B \approx 0$), demzufolge kann die Methode nur im Falle von speziellen äußeren (im vor-

liegenden Falle nur auf das A System wirkenden) Belastungen angewendet werden. Unter der Einwirkung einer solchen äußeren Belastung erfährt das System A eine Verformung, die seiner tatsächlichen Steifigkeit entspricht.

Zwingt man die Verformung des Systems A an der Stelle des beseitigten Anschlusses (Bild 1, Punkt K) dem System B auf, so entsteht in diesem letztgenannten eine der tatsächlichen Steifigkeit (R_B = endlich) entsprechende innere Zwangskraft. Im zweiten Schritt muß man also das System B mit seiner tatsächlichen Steifigkeit berücksichtigen. Übt man die auf diese Weise entstehende innere Kraftwirkung als eine zusätzliche äußere Belastung auf das System A aus, so nimmt die im ersten Schritt erhaltene Verformung ab. Man zwingt die herabgeminderte Verformung wiederholt dem System B auf und setzt die Näherung fort, bis der Unterschied zwischen den in zwei aufeinander folgenden Schritten erhaltenen Kräften vernachlässigt werden kann. Die auf diese Weise erhaltene Kraft kann mit guter Annäherung als die der ursprünglichen Konstruktion entsprechende unbekannte innere Kraft betrachtet werden. Bei der vorliegenden, statisch einfach unbestimmten Konstruktion können die aufeinander folgenden Schritte durch eine unendliche geometrische Reihe beschrieben werden, deren Konvergenz durch die Steifigkeitsverhältnisse $R_A > R_B$ gesichert wird.

2. Fall: $R_A < R_B$

Die das Ausgangssystem (Bild 1c) kennzeichnenden Steifigkeitsverhältnisse sind: R_A = endlich, $R_B \approx 0$. Durch Abheben der Verbindung der Konstruktionsteile A und B wird das Ausgangssystem in zwei, den charakterisierenden Steifigkeitsverhältnissen entsprechende Teile zerlegt:

a) in einen statisch einfach unbestimmten Konstruktionsteil von endlicher Steifigkeit (System A);

b) in einen statisch bestimmten Konstruktionsteil von großer Steifigkeit (System B; $JE = \infty$).

Das System B kann keine Verformungen unter der Einwirkung irgendeiner äußeren Belastung erleiden ($R_B \approx \infty$), dementsprechend kann auch dieses Verfahren nur im Falle von speziellen (im vorliegenden Falle auf das System A wirkenden (äußeren) Kräften angewendet werden. Unter dem Einfluß einer solchen Belastung entsteht an der Auflagerstelle K des Systems A eine Reaktion, deren Wert NIKOLSKIJ mit Hilfe des Kraftgrößenverfahrens ermittelt. Übt man diese Kraftwirkung in demselben Sinne auf das System B aus, so wird in diesem letztgenannten eine der tatsächlichen Steifigkeit (R_B = endlich) entsprechende Verformung auftreten. Demnach muß auch hier das System B im zweiten Schritt mit seiner tatsächlichen Steifigkeit berücksichtigt werden. Läßt man die so erhaltene Verformung im System A sich entwickeln, so wird sich die im ersten Schritt erhaltene Stützkraft ver-

mindern. Man setzt die schrittweise Näherung fort, indem man die verringerte Kraftwirkung auf das System B anwendet, bis die Differenz zwischen den in zwei aufeinander folgenden Schritten erhaltenen Reaktionen vernachlässigt werden kann. Die auf diese Weise erhaltene Kraft kann mit guter Näherung als die den untersuchten Steifigkeitsverhältnissen entsprechende innere Kraft betrachtet werden. Auch hier kann der Algorithmus durch eine unendliche geometrische Reihe aufgeschrieben werden, deren Konvergenz durch die Steifigkeitsverhältnisse $R_A < R_B$ gesichert ist.

3. Fall: $R_A = R_B$

Bei diesen Steifigkeitsverhältnissen ist der Algorithmus nicht konvergent, das Verfahren kann also nicht angewendet werden.

Im allgemeinen, je kleiner der Unterschied zwischen den Steifigkeiten der zwei Konstruktionsteile ist, um so langsamer wird die Konvergenz, und im äußersten Fall ($R_A = R_B$) hört sie sogar auf. Jedoch, können nach NIKOLSKIJ, die in der Praxis vorkommenen Konstruktionen (hauptsächlich die statischen Konstruktionen der Fahrzeuge) immer in zwei Teile zerlegt werden, deren Steifigkeiten sich voneinander wesentlich unterscheiden; höchstens wird die Aufteilung nicht in natürlichen Teilungspunkten stattfinden.

NIKOLSKIJ hat in seiner grundlegenden Arbeit [1] mit dem Beispiel des vorerwähnten, statisch einfach unbestimmten Modell nachgewiesen, daß die untersuchten Näherungen einerseits konvergente Iterationen sind, andererseits im letzten Schritt des Algorithmus das richtige Ergebnis — die gesuchte, statisch unbestimmte innere Kraft — liefern. Er wendete das Verfahren in der Praxis im Zusammenhang mit verwickelteren, statisch vielfach unbestimmten Konstruktionen (Gurtträger-Eisenbahnwagen) an, ohne daß er dessen Gültigkeit für beliebig belastete, n-mal statisch unbestimmte Konstruktionen nachgewiesen und die Bedingungen der Konvergenz bestimmt hätte.

Der vorliegende Aufsatz beweist die Gültigkeit des Nikolskijschen Verfahrens für beliebig ausgebildete und belastete Konstruktion, und auf Grund der gezogenen Folgerungen ergänzt er das heute schon für traditionell betrachtete Kraftgrößenverfahren gemäß einem bisher noch nicht untersuchten Gesichtspunkt. Um die Vorteile der Matrizensymbolik auszunützen, wird die mathematische Behandlung mit Hilfe der Matrizenrechnung durchgeführt.

2. Verallgemeinerung des Nikolskijschen Verfahrens

2.0. *Lösung mit Hilfe des Kraftgrößenverfahrens*

Das untersuchte Modell ist das Rechnungsmodell der n-fach unbestimmten Konstruktion (Bild 2). Die Konstruktion besteht aus zwei, durch n überzählige Verbindungen aneinander verknüpften Teilen.

Die im folgenden benutzten Bezeichnungen und Begriffe entsprechen denselben des Kraftgrößenverfahrens (Bild 3):

— die Ausbildung des Grundsystems erfolgt durch die Auflösung von n Gelenken;

— der Vektor der unter dem Einfluß der äußeren Belastungen im System A auftretenden Verformungen ist:

$$\mathbf{a}^* = [\alpha_{10}, \ldots \alpha_{i0}, \alpha_{k0}, \ldots \alpha_{n0}]; \tag{1}$$

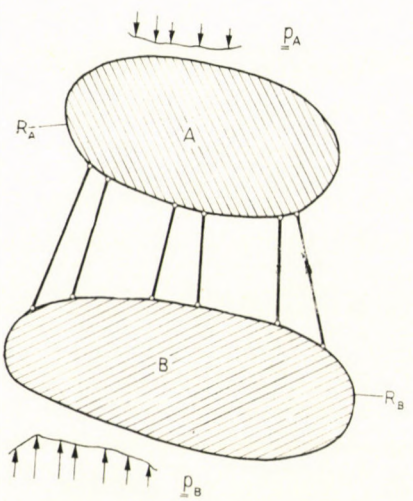

Bild 2

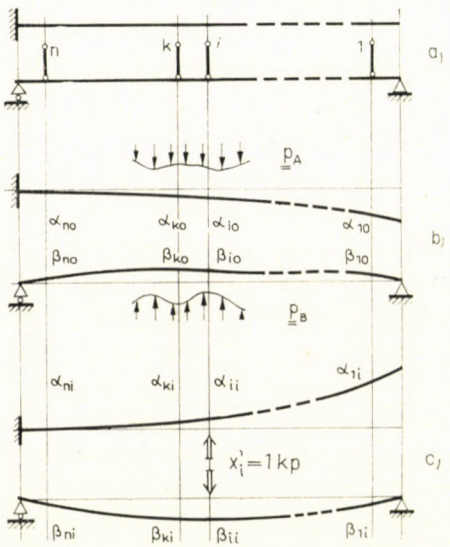

Bild 3

— der Vektor der unter dem Einfluß der äußeren Belastungen im System B auftretenden Verformungen ist:

$$\mathbf{b}^* = [\beta_{10}, \ldots \beta_{i0}, \beta_{k0}, \ldots \beta_{n0}]; \tag{2}$$

— die Relativverschiebungen der entsprechenden Punkte beider Systeme unter der Einwirkung der äußeren Belastungen sind:

$$\mathbf{d}^* = [\delta_{10}, \ldots \delta_{i0}, \delta_{k0}, \ldots \delta_{n0}] = \mathbf{a}^* + \mathbf{b}^*; \tag{3}$$

— die quadratische Matrix, die die von der Wirkung der Einheitsbelastungen hervorgerufene relative Entfernung der entsprechenden Punkte beider Systeme ausdrückt, ist:

$$\mathbf{D} = [\delta_{ik}]_{nxn} = [\alpha_{ik} + \beta_{ik}]_{nxn} = \mathbf{A} + \mathbf{B}, \tag{4}$$

worin — $\mathbf{A} = [\alpha_{ik}]_{nxn}$, und α_{ik} — die Verschiebung der einzelnen Punkte des Systems A unter der Wirkung der Einheitsbelastungen im Vergleich mit der Ausgangsstelle;

— $\mathbf{B} = [\beta_{ik}]_{nxn}$ und β_{ik} — die Verschiebung der einzelnen Punkte des Systems B unter der Wirkung der Einheitsbelastungen im Vergleich mit der Ausgangsstelle;

— der Vektor der auf den Anschlußstellen entstehenden inneren Kräfte:

$$\mathbf{x}^* = [X_1, .. X_i, X_k, .. X_n]; \tag{5}$$

— das Gleichungssystem, das die Lösung der statisch unbestimmten Aufgabe liefert, ist:

$$\mathbf{Dx} = \mathbf{d} \tag{1}$$

$$\mathbf{x} = \mathbf{D}^{-1}\,\mathbf{d} = (\mathbf{A}+\mathbf{B})^{-1}(\mathbf{a}+\mathbf{b}). \tag{1a}$$

Wenn die äußeren Belastungen voneinander unabhängig auf die zwei Teile des Grundsystems wirken, ergibt sich:

$$\mathbf{x}_A = \mathbf{D}^{-1}\,\mathbf{a}, \tag{2a}$$

$$\mathbf{x}_B = \mathbf{D}^{-1}\,\mathbf{b}, \tag{2b}$$

$$\mathbf{x} = \mathbf{x}_A+\mathbf{x}_B. \tag{1b}$$

2.1. *Lösung mit Hilfe des Nikolskijschen Verfahrens im Falle, wenn das System A steifer als das System B ist*

2.11. *Die äußere Belastung wirkt nur auf das System A.* Die das Ausgangssystem kennzeichnenden Steifigkeitsverhältnisse sind nach Nikolskij $R_A =$

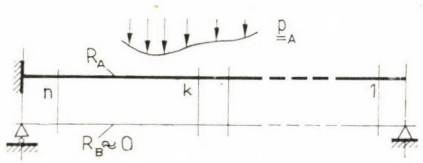

Bild 4

endlich, $R_B = 0$ (Bild 4), d. h., nur das System A ist belastungsfähig. Demnach verhält sich das Ausgangssystem als ein *labiles Grundsystem*, ausgewählt gemäß dem Kraftgrößenverfahren [9].

Die Iterationsschritte verlaufen wie folgt:

1. Unter der Wirkung der äußeren Kräfte $\mathbf{p}_A$ erhält das System A den Verformungszustand (das Verschiebungssystem) **a** (Bild 5a) und die Gleichgewichtsbedingungen werden in den Anschlußpunkten befriedigt.

Läßt man das Verschiebungssystem **a** in das die tatsächliche Steifigkeit besitzende System B sich entwickeln, so entsteht in diesem letzteren ein System $\mathbf{n}_1$ der Innenkräfte (Bild 5b):

$$\mathbf{a} = \mathbf{B}\mathbf{n}_1 \rightarrow \mathbf{n}_1 = \mathbf{B}^{-1}\mathbf{a}\,; \quad \text{wenn } \det(\mathbf{B}) \neq 0 \tag{6}$$

und

$$\mathbf{n}_1^* = [N_1^1, \ldots N_1^i, N_1^k, \ldots N_1^n]. \tag{7}$$

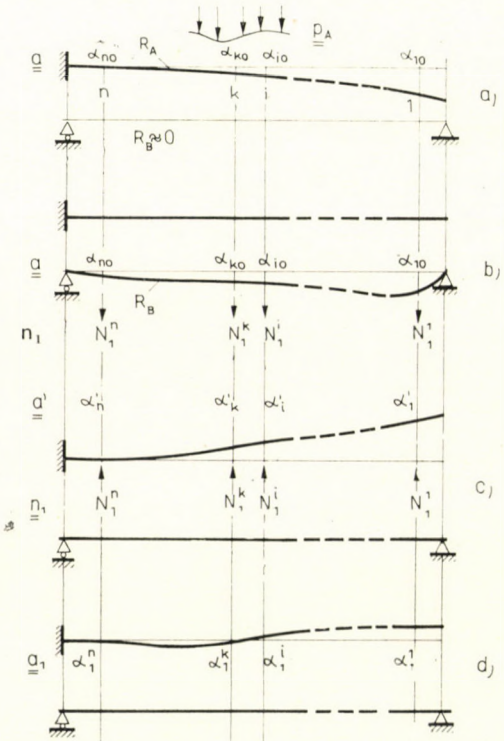

Bild 5

Die Kompatibilitätsbedingungen werden zwar befriedigt, das Gleichgewicht hört aber auf.

Legt man das Kraftsystem $\mathbf{n}_1$ auf das System A zurück, so entsteht ein Verschiebungssystem $\mathbf{a}'$ (Bild 5c), das das Ausgangssystem **a** vermindert:

$$\mathbf{a}' = \mathbf{A}\mathbf{n}_1 = \mathbf{A}\mathbf{B}^{-1}\mathbf{a}. \tag{8}$$

Wenn $\mathbf{a}_1 = \mathbf{a} - \mathbf{a}' < \mathbf{a}$, d. h., wenn die Absolutwerte aller Elemente von **a** größer als die der entsprechenden Elemente von $\mathbf{a}_1$ sind, so wird das verminderte Verschiebungssystem (Bild 5d):

$$\mathbf{a}_1 = \mathbf{a} - \mathbf{a}' = \mathbf{a} - \mathbf{A}\mathbf{B}^{-1}\mathbf{a} = (\mathbf{E} - \mathbf{A}\mathbf{B}^{-1})\mathbf{a}. \tag{9}$$

Die Gleichgewichtsbedingungen werden also wiederum befriedigt, auf Kosten der Kompatibilität.

2. Das Verschiebungssystem $\mathbf{a}_1$ bringt auf dem System B dem ersten Schritt entsprechend ein Kraftsystem $\mathbf{n}_2$ zustande:

$$\mathbf{n}_2 = \mathbf{B}^{-1}\,\mathbf{a}_1\,.$$

Das im System A unter der Wirkung von $\mathbf{n}_2$ entstehende Verrückungssystem wird:

$$\mathbf{a}_1' = \mathbf{A}\mathbf{n}_2 = \mathbf{A}\mathbf{B}^{-1}\,\mathbf{a}_1 = \mathbf{A}\mathbf{B}^{-1}(\mathbf{E} - \mathbf{A}\mathbf{B}^{-1})\,\mathbf{a}\,, \tag{10}$$

und das reduzierte Verschiebungssystem:

$$\mathbf{a}_2 = \mathbf{a} - \mathbf{a}_1' = \mathbf{a} - \mathbf{A}\mathbf{B}^{-1}(\mathbf{E} - \mathbf{A}\mathbf{B}^{-1})\,\mathbf{a} = [\mathbf{E} - \mathbf{A}\mathbf{B}^{-1} + (\mathbf{A}\mathbf{B}^{-1})^2]\,\mathbf{a}\,. \tag{11}$$

Setzt man die Iteration fort, so wird das Endresultat des $(m-1)$-ten Schrittes das *gemeinsame* Verschiebungssystem der Anschlußpunkte der beiden Systeme (d. h. die Kompatibilität):

$$\mathbf{a}_{m-1} = \mathbf{a} - \mathbf{a}_{m-2}' = [\mathbf{E} - \mathbf{A}\mathbf{B}^{-1} + (\mathbf{A}\mathbf{B}^{-1})^2 - + \ldots (-1)^{m-1}(\mathbf{A}\mathbf{B}^{-1})^{m-1}]\,\mathbf{a}\,. \tag{12}$$

Dieses Verschiebungssystem wird durch das Kraftsystem $\mathbf{n}_{m-1}$ hervorgerufen. Bei einer konvergenten Iteration, wenn $m \to \infty$:

$$\mathbf{n}_m - \mathbf{n}_{m-1} = \mathbf{o}\,; \tag{13}$$

demzufolge werden in diesem Schritt auch die Gleichgewichtsbedingungen befriedigt. Das endgültige Kraftsystem wird auf Grund von

$$\mathbf{n}_m = \mathbf{B}^{-1}\,\mathbf{a}_{m-1}\,:$$

$$\lim_{m\to\infty} \mathbf{n}_m = \mathbf{B}^{-1}[\mathbf{E} - \mathbf{A}\mathbf{B}^{-1} + (\mathbf{A}\mathbf{B}^{-1})^2 - + \ldots]\mathbf{a} = \mathbf{B}^{-1}\,\mathbf{S}_1\,\mathbf{a}\,. \tag{3}$$

Die Inverse der Koeffizientenmatrix des Kraftgrößenverfahrens ($\mathbf{D}^{-1}$) kann in vier Formen in Potenzreihe entwickelt werden. Die erste von diesen kann durch das Herausheben der Matrix $\mathbf{B}$ als rechtseitigen Faktors gewonnen werden (die anderen Formen werden weiter unten besprochen):

$$\begin{aligned}\mathbf{D}^{-1} = (\mathbf{A}+\mathbf{B})^{-1} = [(\mathbf{A}\mathbf{B}^{-1}+\mathbf{E})\mathbf{B}]^{-1} = \mathbf{B}^{-1}(\mathbf{A}\mathbf{B}^{-1}+\mathbf{E})^{-1} = \\ = \mathbf{B}^{-1}[\mathbf{E} - \mathbf{A}\mathbf{B}^{-1} + (\mathbf{A}\mathbf{B}^{-1})^2 - + \ldots] = \mathbf{B}^{-1}\,\mathbf{S}_1.\end{aligned} \tag{4}$$

Die nach (4) hergestellte Matrizenpotenzreihe $\mathbf{S}_1$ ist gleich der im $(m-1)$-ten Schritt $(m \to \infty)$ des Nikolskijschen Verfahrens gewonnenen Potenzreihe (3). Aus dem Vergleich der Beziehungen (2a), (3) und (4) ist ersichtlich, *daß das Nikolskijsche Verfahren, ausgegangen von dem steiferen Konstruktionsteil, im Schritt* $m = \infty$ *die Lösung* des statisch n-fach unbestimmten Problems *nach dem Kraftgrößenverfahren* bei der angenommenen äußeren Belastung *liefert.* Demnach, wenn die Potenzreihe der physikalischen Bedingung $(\mathbf{a} - \mathbf{a}' < \mathbf{a})$ des Nikolskijschen Verfahrens entsprechend konvergent ist, d. h.,

$$\lim_{m\to\infty} (\mathbf{AB}^{-1})^m = \mathbf{o},$$

dann ergibt sich:

$$\underset{m\to\infty}{\mathbf{n}_m} = \mathbf{B}^{-1}\,\mathbf{S}_1\,\mathbf{a} = (\mathbf{A}+\mathbf{B})^{-1}\,\mathbf{a} = \mathbf{D}^{-1}\,\mathbf{a} = \mathbf{x}_A. \tag{3a}$$

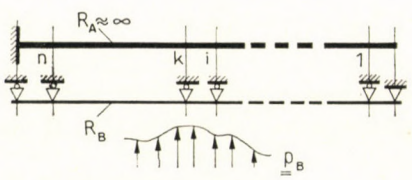

Bild 6

2.1.2. *Nur das System B wird durch äußere Belastung angegriffen.* Die das Ausgangssystem kennzeichnenden Steifigkeitsverhältnisse sind nach Nikolskij: R_B = endlich, $R_A = \infty$ (Bild 6), d. h., das System A kann eine beliebige äußere Belastung ohne Verformung tragen. Demnach verhält sich der *Ausgangsträger* als ein nach dem Kraftgrößenverfahren ausgewähltes, *statisch unbestimmtes Grundsystem* [9]. Die Iterationsschritte sind wie folgt:

1. Unter der Wirkung der äußeren Belastungen p_B erregt sich an den Auflagerstellen des Systems B ein Kraftsystem $\bar{\mathbf{n}}$ (Bild 7), und die *Kompatibilitätsbedingungen* werden an den Anschlußstellen *erfüllt.* Das Kraftsystem

$$\bar{\mathbf{n}}^* = [\overline{N}_1, \ldots \overline{N}_i, \overline{N}_k, \ldots \overline{N}_n]$$

kann mit Hilfe des Kraftgrößenverfahrens ermittelt werden.

Wird das System A durch das Kraftsystem $\bar{\mathbf{n}}$ angegriffen, so wird auf dem letztgenannten ein seiner ursprünglichen Steifigkeit entsprechender Verformungszustand (d. h. entsprechendes Verschiebungssystem) $\bar{\mathbf{a}}_1$ hervorgerufen (Bild 7b):

$$\bar{\mathbf{a}}_1 = \mathbf{A}\bar{\mathbf{n}},$$

und

$$\bar{\mathbf{a}}_1^* = [\bar{\alpha}_1^1, \ldots, \bar{\alpha}_1^i, \bar{\alpha}_1^k, \ldots \bar{\alpha}_1^n]. \tag{14}$$

Die Gleichgewichtsbedingungen sind zwar befriedigt, die Kompatibilität wird aber ausgelöscht.

Läßt man das Verschiebungssystem $\bar{\mathbf{a}}_1$ im System B sich entwickeln, so entsteht ein Kraftsystem $\bar{\mathbf{n}}'$ (Bild 7c), das das Ausgangssystem $\bar{\mathbf{n}}$ reduziert:

$$\bar{\mathbf{a}}_1 = \mathbf{B}\bar{\mathbf{n}}' \rightarrow \bar{\mathbf{n}}' = \mathbf{B}^{-1}\bar{\mathbf{a}}_1; \quad \text{wenn } \det(\mathbf{B}) \neq 0. \tag{15}$$

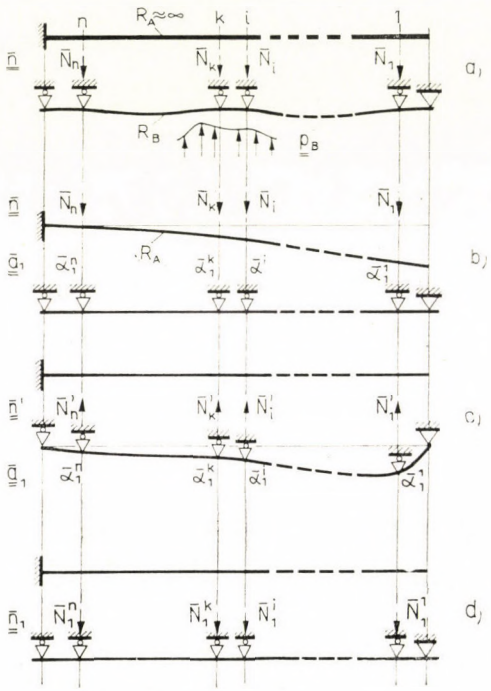

Bild 7

Wenn $\bar{\mathbf{n}}_1 = \bar{\mathbf{n}} - \bar{\mathbf{n}}' < \bar{\mathbf{n}}$, d. h., wenn die Absolutwerte aller Elemente von $\bar{\mathbf{n}}$ größer als die der entsprechenden Elemente von $\bar{\mathbf{n}}_1$ sind:

$$\bar{\mathbf{n}}_1 = \bar{\mathbf{n}} - \bar{\mathbf{n}}' = \bar{\mathbf{n}} - \mathbf{B}^{-1}\bar{\mathbf{a}} = \bar{\mathbf{n}} - \mathbf{B}^{-1}\mathbf{A}\bar{\mathbf{n}} = (\mathbf{E} - \mathbf{B}^{-1}\mathbf{A})\bar{\mathbf{n}}. \tag{16}$$

Die Kompatibilitätsbedingungen sind nochmals erfüllt, wenn auch auf Kosten des Gleichgewichts.

2. Das Kraftsystem ruft im System A dem ersten Schritt entsprechend ein Verschiebungssystem $\bar{\mathbf{a}}_2$ hervor:

$$\bar{\mathbf{a}}_2 = \mathbf{A}\bar{\mathbf{n}}_1 = \mathbf{A}(\mathbf{E} - \mathbf{B}^{-1}\mathbf{A})\bar{\mathbf{n}}. \tag{17}$$

Unter der Wirkung von $\bar{\mathbf{a}}_2$ entsteht im System B auf Grund von

das Kraftsystem $$\bar{\mathbf{a}}_2 = \mathbf{B}\bar{\mathbf{n}}_1' \tag{18}$$

$$\bar{\mathbf{n}}_1' = \mathbf{B}^{-1}\bar{\mathbf{a}}_2 = \mathbf{B}^{-1}\mathbf{A}(\mathbf{E} - \mathbf{B}^{-1}\mathbf{A})\bar{\mathbf{n}} = [\mathbf{B}^{-1}\mathbf{A} - (\mathbf{B}^{-1}\mathbf{A})^2]\bar{\mathbf{n}}. \tag{19}$$

Das verminderte Kraftsystem wird:

$$\bar{\mathbf{n}}_2 = \bar{\mathbf{n}} - \bar{\mathbf{n}}_1' = \bar{\mathbf{n}} - [\mathbf{B}^{-1}\mathbf{A} - (\mathbf{B}^{-1}\mathbf{A})^2]\bar{\mathbf{n}} = [\mathbf{E} - \mathbf{B}^{-1}\mathbf{A} + (\mathbf{B}^{-1}\mathbf{A})^2]\bar{\mathbf{n}}. \tag{20}$$

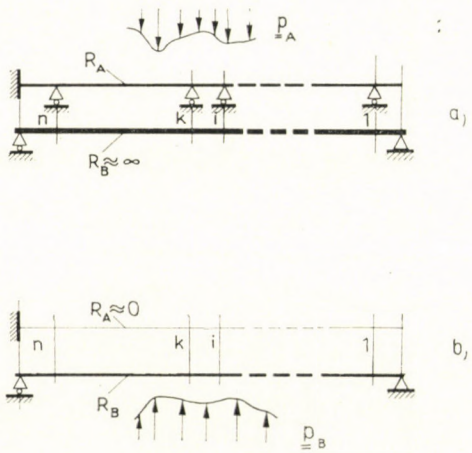

Bild 8

Setzt man die Iteration fort, so wird das Endresultat des m-ten Schrittes das die beiden Kraftsysteme verknüpfende System der inneren Kräfte (d. h. das Gleichgewicht):

$$\underset{m\to\infty}{\bar{\mathbf{n}}_m} = \bar{\mathbf{n}} - \bar{\mathbf{n}}'_{m-1} = [\mathbf{E} - \mathbf{B}^{-1}\mathbf{A} + (\mathbf{B}^{-1}\mathbf{A})^2 - + \ldots (-1)^m(\mathbf{B}^{-1}\mathbf{A})^m]\bar{\mathbf{n}}. \tag{21}$$

Das Ausgangskraftsystem $\bar{\mathbf{n}}$ gemäß dem Kraftgrößenverfahrens wird:

$$\bar{\mathbf{n}} = \mathbf{B}^{-1}\mathbf{b}; \quad \det(\mathbf{B}) \neq 0. \tag{21}$$

Demnach ist im Schritt $m = \infty$ das letzte Kraftsystem:

$$\underset{m\to\infty}{\bar{\mathbf{n}}_m} = [\mathbf{E} - \mathbf{B}^{-1}\mathbf{A} + (\mathbf{B}^{-1}\mathbf{A})^2 - + \ldots]\mathbf{B}^{-1}\mathbf{b} = \mathbf{S}_2\mathbf{B}^{-1}\mathbf{b}. \tag{5}$$

Die der Gl. (4) ähnliche, entwickelte Form der Inversen der im Kraftgrößenverfahren vorkommenden Koeffizientmatrix (die Matrix $\mathbf{B}$ als rechtseitigen Multiplikator heraushebend) wird:

$$\begin{aligned}\mathbf{D}^{-1} = (\mathbf{A}+\mathbf{B})^{-1} = [\mathbf{B}(\mathbf{B}^{-1}\mathbf{A}+\mathbf{E})]^{-1} = (\mathbf{B}^{-1}\mathbf{A}+\mathbf{E})^{-1}\mathbf{B}^{-1} = \\ = [\mathbf{E} - \mathbf{B}^{-1}\mathbf{A} + (\mathbf{B}^{-1}\mathbf{A})^2 - + \ldots]\mathbf{B}^{-1} = \mathbf{S}_2\mathbf{B}^{-1}.\end{aligned} \tag{6}$$

Die nach (6) hergestellte Matrizenpotenzreihe $\mathbf{S}_2$ ist gleich der im m-ten Schritt des Nikolskijschen Verfahrens ($m \to \infty$) erhaltenen Potenzreihe (5). Auf Grund der Vergleichung der Beziehungen (2b), (5) und (6) ist ersichtlich, daß *das Nikolskijsche Verfahren, von dem weicheren Konstruktionsteil ausgehend, im Schritte* $m = \infty$ *die Lösung gemäß dem Kraftgrößenverfahren* des betrachteten, statisch n-mal unbestimmten Problems, im Falle der vorausgesetzten äußeren Belastung liefert. Demzufolge, wenn die Potenzreihe den physikalischen Bedingungen des Nikolskijschen Verfahrens ($\bar{\mathbf{n}} - \bar{\mathbf{n}}' < \bar{\mathbf{n}}$) entsprechend konvergent ist, d. h.,

$$\lim_{m\to\infty} (\mathbf{B}^{-1}\mathbf{A})^m = \mathbf{o}, \tag{22}$$

so ergibt sich:

$$\lim_{m\to\infty} \bar{\mathbf{n}}_m = \mathbf{S}_2 \mathbf{B}^{-1}\mathbf{b} = (\mathbf{A}+\mathbf{B})^{-1}\mathbf{b} = \mathbf{D}^{-1}\mathbf{b} = \mathbf{x}_B. \tag{5a}$$

Auf gleiche Weise kann die Gültigkeit des Nikolskijschen Verfahrens auch für den Fall nachgewiesen werden, wenn *das System A weicher als System B ist.*

Das zu den Ausgangssystemen gehörige Endresultat kann nämlich mit Hilfe der Beziehungen (3a) und (5a) durch Vertauschung der Symbole $A \rightleftarrows B$ und $a \rightleftarrows b$ unmittelbar aufgeschrieben werden. Zum Nachweis benutzen wir die dritte bzw. die vierte entwickelte Form der Inversmatrix $\mathbf{D}^{-1}$, wo die Matrix $\mathbf{A}$ als rechts-, bzw. linksseitiger Multiplikator herausgehoben werden soll.

3. Untersuchung der Konvergenzbedingungen des Nikolskijschen Verfahrens

Im vorausgehenden Abschnitt haben wir nachgewiesen, daß die unbekannten Verbindungskräfte einer gegebenen, statisch unbestimmten Konstruktion mit Hilfe des verallgemeinerten Nikolskijschen Verfahrens in vier unendlichen geometrischen Matrizenpotenzreihen aufgeschrieben werden können:

$$\begin{aligned}
\mathbf{S}_1 &= \mathbf{E} - \mathbf{A}\mathbf{B}^{-1} + (\mathbf{A}\mathbf{B}^{-1})^2 - + \ldots = \mathbf{E} - \mathbf{Q}_1 + \mathbf{Q}_1^2 - + \ldots, \\
\mathbf{S}_2 &= \mathbf{E} - \mathbf{B}^{-1}\mathbf{A} + (\mathbf{B}^{-1}\mathbf{A})^2 - + \ldots = \mathbf{E} - \mathbf{Q}_2 + \mathbf{Q}_2^2 - + \ldots, \\
\mathbf{S}_3 &= \mathbf{E} - \mathbf{A}^{-1}\mathbf{B} + (\mathbf{A}^{-1}\mathbf{B})^2 - + \ldots = \mathbf{E} - \mathbf{Q}_3 + \mathbf{Q}_3^2 - + \ldots, \\
\mathbf{S}_4 &= \mathbf{E} - \mathbf{B}\mathbf{A}^{-1} + (\mathbf{B}\mathbf{A}^{-1})^2 - + \ldots = \mathbf{E} - \mathbf{Q}_4 + \mathbf{Q}_4^2 - + \ldots .
\end{aligned} \tag{7}$$

Diese Potenzreihen befinden sich in einer wechselseitigen engen Beziehung, da sie zu den verschieden aufgeschriebenen Formen der Inverse derselben Matrix $\mathbf{D}$ gehören. Die *notwendige und ausreichende Bedingung* ihrer

Konvergenz — und zugleich derselben des Nikolskijschen Verfahrens — ist, daß alle absoluten Eigenwerte $|\lambda_i|$ der zu den Reihen gehörigen Quotientmatrizen $\mathbf{Q}_i$ kleiner als die Einheit seien [3], [5], [7], [8]:

$$\max |\lambda_i| < 1. \tag{8}$$

Jedoch, alle der in (7) befindlichen und zu derselben Aufgabe (Koeffizientmatrix) gehörigen vier möglichen Potenzreihen können nicht simultan konvergent sein. Da nämlich, die in den Quotienten befindlichen Matrizen **A** und **B** symmetrisch sind, bestehen die Gleichungen:

$$\begin{aligned} \mathbf{Q}_1^* &= \mathbf{Q}_2 \quad \text{und} \quad \mathbf{Q}_3^* = \mathbf{Q}_4, \\ \mathbf{Q}_1^{-1} &= \mathbf{Q}_4 \quad \text{und} \quad \mathbf{Q}_3^{-1} = \mathbf{Q}_2. \end{aligned} \tag{9}$$

Die Eigenwerte der miteinander in transponierter Beziehung befindlichen Matrizen sind bekanntlich gleich, und die der miteinander in reziproker Beziehung befindlichen Matrizen sind die Inversen von einander [7], [8]. Deshalb kann auf Grund von (9) aufgeschrieben werden:

$$\begin{aligned} \lambda_{1,i} &= \lambda_{2,i} \quad \text{und} \quad \lambda_{3,i} = \lambda_{4,i}, \\ \lambda_{1,i}^{-1} &= \lambda_{4,i} \quad \text{und} \quad \lambda_{3,i}^{-1} = \lambda_{2,i}. \end{aligned} \tag{10}$$

Ferner, mit Rücksicht darauf, daß die Konvergenz der Potenzreichen (7) gemäß (8) von den Eigenwerten der Quotientmatrix $\mathbf{Q}_i$ abhängt, ist auf Grund von (10) ersichtlich, daß:

a) die Potenzreihen $\mathbf{S}_1$ und $\mathbf{S}_2$ bzw. $\mathbf{S}_3$ und $\mathbf{S}_4$ unter gleichen Bedingungen *simultan konvergent* sind,

b) die Potenzreihen $\mathbf{S}_1$ und $\mathbf{S}_4$ bzw. $\mathbf{S}_3$ und $\mathbf{S}_2$ unter gleichen Bedingungen *nicht simultan konvergent sein können:* jedoch, wenn z. B. $\max |\lambda_{1,i}| > 1$, d. h. $\mathbf{S}_1$ nicht konvergent ist, dann, gemäß (10) $\max |\lambda_{4,i}| < 1$, also wird $\mathbf{S}_4$ jedenfalls konvergent,

c) keine der Potenzreihen kann konvergent sein, wenn $\mathbf{A} = \mathbf{B}$, d. h. $Q_i \equiv E$ ist.

Es gibt mehrere Methoden zur algorithmischen Invertierung der besonders großen Matrizen. Von diesen — besonders in Zusammenhang mit statischen Berechnungen — benutzt man gerne zur nachträglichen Korrektion von Rechnungsfehlern oder früherer Vernachlässigungen die geometrische Reihendarstellung der zu invertierenden Matrix, worin die in den durch Entwicklung der Inversmatrix von der Form $\mathbf{D}^{-1} = (\mathbf{A} + \mathbf{B})^{-1}$ erhaltenen Potenzreihen — z. B. in $\mathbf{S}_3$ oder $\mathbf{S}_4$ — befindliche Inverse $\mathbf{A}^{-1}$ schon bekannt, und **B** die »Fehlermatrix« ist.

Es kann jedoch vorkommen, daß diese Potenzreihen infolge der geometrischen- und Steifigkeitsverhältnisse der Konstruktion nicht konvergent sind. In diesem Falle können die durch die Entwicklung der $\mathbf{D}^{-1}$ erhaltenen zwei anderen Matrizen ($\mathbf{S}_1$ und $\mathbf{S}_2$) konvergent werden. Ihre Quotienten enthalten aber schon $\mathbf{B}^{-1}$, d. h., zur Lösung muß man die »Vernachlässigungen« enthaltende, bzw. »Fehlermatrix« invertieren. Es versteht sich von selbst, daß die Anwendung des Nikolskijschen Verfahrens nur in dem Falle zweckmäßig ist, wo $\mathbf{B}$ leichter als $\mathbf{D}$ invertiert werden kann, z. B. wenn $\mathbf{B}$ eine Diagonal-, bzw. Kontinuantenmatrix ist [10].

Im Falle eines statisch n-mal unbestimmten Problems erfordert die Ermittelung des Eigenwertes (d. h. die Entscheidung der Konvergenz) die Lösung eines Gleichungssystems n-ten Grades, oder mindestens umfangreiche Iterationsrechnungen. Im vorliegenden Falle genügt es, allein die dominanten Eigenwerte zu ermitteln. Von den zahlreichen Methoden scheint das Collatzsche Iterationsverfahren [5], [8] das vorteilhafteste zu sein, da schon nach dem zweiten Iterationsschritt entschieden werden kann, ob der Absolutwert des gesuchten größten Eigenwertes gegen eine Zahl, die kleiner oder größer als die Einheit ist, konvergiert.

Für die Praxis ist es oftmals genügend, nur eine hinreichende Bedingung der Konvergenz zu untersuchen. Nachdem das Aufschreiben der Potenzreihen $\mathbf{S}_i$ ohnehin die Bildung der Quotienten $\mathbf{Q}_i$ erfordert, ist es zweckmäßig, eine solche hinreichende Bedingung zu suchen, die sich auf $\mathbf{Q}_i$ bezieht. Eine solche bekannte, ausreichende Bedingung besteht darin, daß die Reihen- oder Spaltensummen der mit den Absolutwerten von $\mathbf{Q}_i$ gebildeten Matrix $\tilde{\mathbf{Q}}_i$ immer noch kleiner als die Einheit werden müssen, also

$$\mathbf{i}^* > \mathbf{i}^* \tilde{\mathbf{Q}}_i ,$$

oder

$$\mathbf{i} > \tilde{\mathbf{Q}}_i \mathbf{i} . \tag{11}$$

Diese zwei Bedingungen entsprechen den Bedingungen, die sich auf die Identität der Eigenwerte der miteinander in transponiertem Zusammenhang befindlichen Matrizen beziehen.

Die notwendige Bedingung der Durchführung der aufeinander folgenden Iterationsschritte bei der Verallgemeinerung des Nikolskijschen Algorithmus ist

nach 2.11

$$\mathbf{a} - \mathbf{a}' < \mathbf{a} , \tag{12}$$

nach 2.12

$$\bar{\mathbf{n}} - \bar{\mathbf{n}}' < \bar{\mathbf{n}} . \tag{12a}$$

Die Bedingung (12) bezieht sich auf die Absolutwerte der Elemente des Differenzenvektors $\mathbf{a} - \mathbf{a}'$, also

$$|\alpha_{i0} - \alpha_i'| < |\alpha_{i0}|$$

Diese Ungleichheit besteht, wenn

$$1)\quad |\alpha_{i0}| > |\alpha_i'|\,,$$

in diesem Falle

$$|\alpha_{i0}| - |\alpha_i'| < |\alpha_{i0}|\,,$$

$$\text{d.h.}\quad 0 < |\alpha_i'|\,;$$

$$2)\quad |\alpha_{i0}| < |\alpha_i'|\,,$$

in diesem Falle

$$|\alpha_i'| - |\alpha_{i0}| < |\alpha_{i0}|\,,$$

$$\text{d.h.}\quad |\alpha_i'| < 2\,|\alpha_{i0}|\,.$$

Die notwendige physikalische Bedingung der Konvergenz ist also

$$0 < |\alpha_i'| < 2\,|\alpha_{i0}|\,. \tag{13}$$

Es leuchtet ähnlicherweise ein, daß

$$0 < |\overline{N}_i'| < 2\,|\overline{N}_{i0}|\,. \tag{13a}$$

Ferner kann bewiesen werden, daß diese physikalischen Bedingungen auch die ausreichenden Bedingungen nach (11) enthalten. Demzufolge ist *die notwendige und ausreichende Bedingung der Konvergenz des Nikolskijschen Algorithmus die Befriedigung der Beziehungen (13), bzw. (13a).*

4. Schlußfolgerungen

Auf Grund der Verallgemeinerung des Nikolskijschen Verfahrens kann nachgewiesen werden, daß das Verfahren auch im Falle eines statisch n-mal unbestimmten Trägers (der also n überzählige Verbindungen besitzt) ein richtiges Ergebnis liefert.

Das Nikolskijsche Verfahren enthält in seinem originalen Konzept gewisse Grenzen für die äußeren Belastungen (nämlich, keine äußere Last kann die Konstruktionsteile, die als absolut weich oder als unendlich steif betrachtet werden, angreifen). Eine beliebige Lastsystem kann aber immer in zwei Belastungsgruppen zerlegt werden, die die von Nikolskij für die äußeren Belastungen vorgeschriebenen Bedingungen einzeln befriedigen. Das Verfahren kann in zwei Iterationsschritten auch für beliebige Belastungen angewendet werden. Superponiert man die auf diese Weise erhaltenen, voneinander unabhängigen zwei inneren Kraftsysteme (Verbindungskräfte $\mathbf{x}_A$ und $\mathbf{x}_B$), so erhalten wir das der ursprünglichen äußeren Belastung entsprechende innere Kraftsystem **(x)** [1b], [2a], [2b].

Besteht eine beliebig belastete, n-mal unbestimmte Konstruktion aus zwei, vom Gesichtspunkt der Steifigkeit aus betrachtet, sehr verschiedenen Konstruktionsteilen, so kann das Ausgangssystem des Nikolskijschen Verfahrens physikalisch als ein Grundsystem betrachtet werden, das aus einem nach dem Nikolskijschen Verfahren ausgewählten statisch unbestimmten und aus einem labilen Grundsystem aufgebaut worden ist.

Die Inverse einer beliebig aufgelösten Matrix $\mathbf{D} = (\mathbf{A} + \mathbf{B})$ kann in vier mögliche Potenzreihen entwickelt werden. Zwei davon sind immer konvergent unter gleichen Bedingungen, wenn sie dabei die notwendige und ausreichende Bedingung der Konvergenz befriedigen. Im Falle von statischen Problemen sind im allgemeinen jene Potenzreihen konvergent, in denen sich die Inverse der Koeffizientenmatrix der »weicheren« Konstruktion befindet ($\mathbf{A}^{-1}$ oder $\mathbf{B}^{-1}$).

Eine Näherungsmethode, im wesentlichen identisch mit dem Nikolskijschen Verfahren, wurde von A. MINA [11], von Nikolskij unabhängig, zur Berechnung von Seitanwänden der Eisenbahnwagen mit schlanken Pfosten ausgearbeitet. Diese unterscheidet sich von dem Nikolskijschen Verfahren nur darin, daß sie anstatt der analytischen Methode, abwechselnd analytische und grafische Schritte anwendet. Der vorliegende Aufsatz kann zugleich auch als Nachweis des Mina—Bognárschen Verfahrens betrachtet werden.

BIBLIOGRAPHIE

1. Никольский Е. Н.: О работе хребтогой балки в цельнометаллических вагонах. (Канд. дисс.) Бежица 1945
2. Никольский, Е. Н.: Расчёт вагонов на прочность. Москва 1960
3. SZABÓ, J.: Die Matrizenrechnung und ihre technische Anwendungen. Handschrift. Fortbildungskurs für Ingenieure, Budapest 1959
4. SZABÓ, J.: Gleichung des dreidimensionalen Trägerrostes. Publikationen des Bauwissenschaftlichen Instituts, Band 34. Budapest 1964
5. ZURMÜHL, R.: Matrizen. Springer-Verlag 1950
6. Фаддеев, Д. И.: Вычислительные методы линейной алгебры. Физматгиз. Москва 1963
7. GÁSPÁR, GY.: Matrizenrechnung. Technische Verlaganstalt, Budapest 1963
8. KREKÓ, B.: Matrizenrechnung. Technische Verlaganstalt, Budapest 1966
9. MICHELBERGER, P.: Basic Systems for Statically Indeterminate Structures. *Proceedings on the Third Conference on Dimensioning.* Ung. Akad. der Wissenschaften, Budapest 1968
10. MICHELBERGER, P.—FEKETE, A.: Analysis of Spatially Loaded Frame Rows with Longitudinal Symmetry. *Proceedings on the Third Conference on Dimensioning.* Ung. Akad. der Wissenschaften, Budapest 1968
11. MINA A.: Berechnungsprinzipien der selbstragenden Eisenbahnwagenkasten. Fortbildungskurs für Ingenieure, Budapest 1953

Analysis of Statically Undetermined Structures on the Basis of the General Extending of Nikolskij's Algorithm. The analysis of the stress pattern of the many times hyperstatic structures with the aid of the energy theorem requires, under the conditions of the design bureaus — where no computer is at hand commonly — much calculation work. Especially much labour is needed for the inversion of the coefficient matrix of the set of compatibility equations. The extension of the trial-and-error method of Nikolskij permits the reduction of the amount of calculation work. The paper deals with the analysis of the most significant

problems of this generalization. It extends and proves the validity of the algorithm to the statically n-times undertermined structures, defines the convergence criteria and eliminates the original load-dependence of the procedure. Besides, on the one hand, the algorithm is a procedure easy to be treated by itself and, on the other, on the basis of conclusions to be derived from the result of the extension, the earlier neglects can be corrected within the same problem to a desired exactitude without a lengthy inversion.

Анализ статически неопределенных конструкций на основе обобщения алгоритма Никольского *(А. Фекете)*. Определение работы статически многократно неопределенных конструкций методом усилий в производственных условиях или же в условиях проектных бюро (где обычно не имеются в распоряжении проектантов вычислительные машины) требует трудоемкой вычислительной работы. Особенно трудоемкой является инверсирование параметрической матрицы системы уравнений компатибильности. Обобщение итерационного метода Никольского позволяет сократить трудоемкую вычислительную работу. Работа содержит анализ важнейших вопросов этого обобщения. Автор расширяет и доказывает действительность этого алгоритма для статически n-кратно неопределенных конструкций, далее определяет критерии сходимости и устраняет зависимость метода от нагрузки. В то же время алгоритм, с одной стороны, и сам собою является легким в обращении методом, а с другой стороны, на основе заключений, которые можно сделать из обобщенного результата, пренебрежения, сделанные ранее в рамках одной и той же задачи, без широкой по масштабу инверсии могут быть скорректированы до произвольной точности.

Acta Technica Academiae Scientiarum Hungaricae, Tomus 68 (3—4), pp. 353—358 (1970)

SOLUTION OF THE FIRST BASIC PROBLEM OF THE THEORY OF ELASTICITY WITH REAL POTENTIALS

K. SZMODITS*

DR. OF TECHN. SC.

[Manuscript received, March 31 1969]

The first boundary-value problem of the theory of elasticity consists of the establishment of the biharmonic stress function relating to the rim loads. According to Goursat's theorem this function may be expressed with the aid of two harmonic functions to be solved by means of the logarithmic potentials of the simple-layer and double-layer edge curves. The density functions of these potentials may be determined from the boundary conditions, consequently, the biharmonic problem may be reduced to two independent Dirichlet problems. The solution in numerical form consists in the solution of two independent sets of equations written to the discrete points of the rim curve.

The first basic problem of the theory of elasticity is the determination of the internal stresses in a disc of elastic material subject to a given load at its edge. This problem is the perimeter-value problem of the homogeneous, biharmonic differential equation where the stress function ($F(x, y)$ is the desired function; the boundary conditions are defined by the given edge loads.

In practice, this problem will commonly be solved in such a way that F will be expressed by an infinite series composed of biharmonic terms, and the unknown constants of the terms of this series will be determined from the boundary conditions. Since the few biharmonic expressions at hand are not sufficient to establish the general solution of the biharmonic differential equation, the boundary conditions and edge loads may only approximately be taken into account. This solution is, first of all, applicable for the analysis of rectangular discs, however, consideration of the unloaded edge section is also here intricate and involves difficulties in calculations.

The general solution of the biharmonic differential equations may be carried out by presenting the biharmonic function in an integral form and thereby, the boundary conditions may theoretically be satisfied in an exact way. The integral forms define the values of a harmonic function within a range from the function given at the boundary of the range (this being not identic with the boundary values). Such integrals are: in the complex domain the Cauchy integral; in the real domain the logarithmic potential of the simple or of the double-layer boundary curve. Since both the complex and

* Dr. techn. K. Szmodits, Hőgyes E. út 1, *Budapest IX*, Hungary.

the real potentials define harmonic functions, the establishment of the desired biharmonic F-function should be traced back to the determination of harmonic functions. This is feasible by making use of the *Goursat* formula

$$F = x\,u + v$$

in which $u(x, y)$, $v(x, y)$ are harmonic functions, and the edge curve may be intersected only at two points by all of the straight lines being parallel to the x-axis. With the aid of this expression, in all of the domains, inside the edg curve, every F-function may be set up.

The load acting at the edge S defines the boundary values of the derivative $\partial F/\partial n$ with respect to the stress function F and the n normal of the edge curve. These edge values unambiguously determine the desired F function.

If the boundary conditions are expressed by the stress function F given in the above form, and we determine the edge values of the harmonic functions u and v from it, the problem is reduced to the usual solution of the first boundary value problem of the potential theory.

This train of thought is followed by the solution according to MUSZHELISVILI who uses complex potentials in calculating the edge values of the u-function, written in a complex form, from an integral equation.

With the aid of this procedure a number of elasticity problems have been solved in a closed form.

In the first volume of his book, FRANK-MISES solves the boundary-value problem of the biharmonic differential equations, similarly to the first perimeter-value problem of the potential theory, with the aid of real potentials, with two simultane integral equations.

With the aid of these methods, the problems, analytically unsolvable, may also be solved numerically by replacing the integral equations by finite quantities and then numerically solving the set of equations thus obtained.

Such a transformation of the usual analytic methods into numerical procedures attaches to every segment of the boundary curve subdivided into finite segments two unknown edge values, consequently, the number of equations of the set of equations defining the unknowns is twice the number of the edge segments. The method described, as follows, determines the edge values of the harmonic functions u and v independently of each other, from a set of equations of the same number as the edge segments.

Let the edge of the disc examined be a closed curve with continuous curvature within each segment, that is, it should consist at most of continuous arches of finite number between break points.

Let us decompose the load acting at the edge segment s into components X and Y parallel to the axes x and y, respectively. At a point S of the edge,

the edge values F and $\partial F/\partial n$ are connected to the forces X and Y (Fig. 1).

$$F_s = \int_0^s X(y_s - y)\,ds + \int_0^s Y(x - x_s)\,ds, \tag{1}$$

$$\left(\frac{\partial F}{\partial n}\right)_s = -\cos\alpha \int_0^s Y\,ds + \sin\alpha \int_0^s X\,ds. \tag{2}$$

The right-hand side of formula (1) is the moment of the edge forces about the point S acting on the segment s of the curve; the first and second terms of

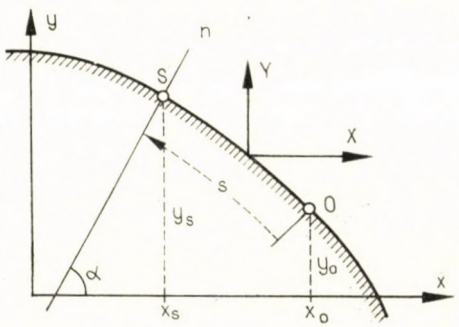

Fig. 1

the right-hand side of formula (2) are the projections of the same forces at the axes x and y, respectively. The problem can statically be solved only if the edge forces are in equilibrium. This is subject to the condition that by integration along the whole boundary, the right-hand sides of Eqs (1) and (2) are zero at a point $O \equiv S$.

This condition is only satisfied if at the points $O \equiv S$ at the coinciding lower and upper limits of the integrals $F_0 \equiv F_s$ and $(\partial F/\partial n)_0 \equiv (\partial F/\partial n)_s$, that is, the edge functions F, $\partial F/\partial n$ are continuous.

The edge values F and $\partial F/\partial n$ calculated from the given loads are connected to the unknown edge values u, v as follows:

$$F = xu + v, \tag{3}$$

$$\frac{\partial F}{\partial n} = u\cos\varphi + x\frac{\partial u}{\partial n} + \frac{\partial v}{\partial n}. \tag{4}$$

The relation between one of the edge values v_σ of the harmonic function v and the rest of v-s as well as the edge value $\partial v/\partial n$ is, according to the Green formula

$$v_\sigma = \frac{1}{\pi}\oint \left(v\frac{\cos(r,n)}{r} - \ln\frac{1}{r}\frac{\partial v}{\partial n}\right) ds \tag{5}$$

in which σ is a fixed point of the edge; r is the distance between the edge points σ and s.

Expressing v from Eq. (3) and $\partial v/\partial n$ from Eq. (4), and substituting them into (5) give:

$$F - xu = \frac{1}{\pi} \oint \left[(F - xu) \frac{\cos(r, n)}{r} - \right.$$
$$\left. - \ln \frac{1}{r} \left(\frac{\partial F}{\partial n} - u \cos \varphi - x \frac{\partial u}{\partial n} \right) \right] ds . \tag{6}$$

Since u is a harmonic function, and the edge values u and $\partial u/\partial n$ may be expressed by the logarithmic potentials of the simple-layer edge curve:

$$u_\sigma = \oint v \ln \frac{1}{r} ds ; \left(\frac{\partial u}{\partial n} \right)_\sigma = \oint v \frac{\cos(r, n)}{r} ds - \pi v_\sigma \tag{7}$$

in which v is the density function of the simple layer.

By substituting the expressions (7) into (6) we obtain

$$F - x \oint v \ln \frac{1}{r} ds = \frac{1}{\pi} \oint_s \left\{ \left(F - x \oint v \ln \frac{1}{r} ds \right) \frac{\cos(r, n)}{r} - \right.$$
$$\left. - \ln \frac{1}{r} \left[\frac{\partial F}{\partial n} - \cos \varphi \oint v \ln \frac{1}{r} ds - x \left(\oint v \frac{\cos(r, n)}{r} ds - \pi v_\sigma \right) \right] \right\} ds . \tag{8}$$

In relation (8) only the density function v defining the function u is unknown. From this, we determine the density function v at the point σ at the edge of the range, and at point P within the range

$$u_\sigma = \oint v \ln \frac{1}{r} ds \quad \text{and} \quad u_P = \oint v \ln \frac{1}{r} ds \tag{9}$$

in which r is the distance of the points σ and P from the boundary points s.

We find the edge values of the function v from the formula (3) by placing in the edge values of u_σ:

$$v_\sigma = F - x u_\sigma . \tag{10}$$

Inside the range at a point P, v may be found by solving the integral equation of the first boundary problem of the potential theory

$$\mu_\sigma = \frac{v_\sigma}{\pi} - \oint \mu \frac{\cos(r, n)}{r} ds \tag{11}$$

for the double-layer density-function u, then

$$v_p = \oint \mu \frac{\cos(r, n)}{r} ds. \tag{12}$$

The described procedure should be brought to numerical form by dividing the edge curve into n segments of a length Δs and we replace the perimeter values of these segments by the mean values taken in their centre and the integral of the formulas by finite quantities.

The formulas (8), (9), (11) and (12) are:

$$F_s - x_\sigma \sum_s \nu_s \ln \frac{1}{r_{s\sigma}} \Delta s =$$

$$= \frac{1}{\pi} \sum_\sigma \left\{ \left(F_\sigma - x_\sigma \sum_s \nu_s \ln \frac{1}{r_{s\sigma}} \Delta s \right) \frac{\cos(r_{s\sigma} n_s)}{r_{s\sigma}} - \right.$$

$$- \ln \frac{1}{r_{s\sigma}} \left[\left(\frac{\partial F}{\partial n} \right)_\sigma - \cos \varphi_\sigma \sum_s \nu_s \ln \frac{1}{r_{s\sigma}} \Delta s - \right.$$

$$\left. \left. - x_\sigma \left(\sum_s \nu_s \frac{\cos(r_{s\sigma} n_s)}{r_{s\sigma}} \Delta s - \pi \nu_\sigma \right) \right] \right\} \Delta \sigma . \tag{13}$$

$$u_\sigma = \sum_s \nu_s \ln \frac{1}{r_{\sigma s}} \Delta s , \tag{14}$$

$$u_p = \sum_s \nu_s \ln \frac{1}{r_{ps}} \Delta s , \tag{15}$$

$$\mu_\sigma = \frac{v_\sigma}{\pi} - \sum_s \mu_s \frac{\cos(r_{s\sigma} n_s)}{r_{s\sigma}} \Delta s . \tag{16}$$

$$v_p = \sum_s \mu_s \frac{\cos(r_{ps} n_s)}{r_{ps}} \Delta_s \tag{17}$$

in which $\sigma = 1, 2, 3, \ldots, n$.

In carrying out the numerical calculations we solve the set of equations (13) for the unknowns $\nu_1, \nu_2, \ldots \nu_n$ and with their aid we determine from the formulas (14) and (15) the u_σ and u_p values of the edge points σ and the internal points P, respectively. From formula (10) we determine the edge values v_σ and by substituting them into the set of equations (16), we solve this latter for the unknowns $\mu_1, \mu_2, \ldots \mu_n$, then we use them to determine the v_p values of the internal points P from formula (17). With the values u_p and v_p of the internal points P we establish the stress function F, the derivatives of which formed numerically give the internal stresses.

The advantage of the method presented is that it reduces the solution of the boundary value problem of the biharmonic differential equation to two solutions, independent of each other, of the Dirichlet problem, and it is well applicable to electronic computation.

REFERENCES

STENBERG: Potentialtheorie. Sammlung Göschen
MICHLIN, Sz. G.: Integrálegyenletek. Akadémiai Kiadó Budapest 1953.

Lösung des ersten Grundproblems der Elastizitätstheorie mit Hilfe von reellen Potentialen. Das erste Randwertproblem der Elastizitätstheorie besteht in der Ermittelung der den Randbelastungen zugehörigen biharmonischen Spannungsfunktion. Dem Goursatschen Satz gemäß kann diese Funktion durch zwei harmonische Funktionen ausgedrückt werden, die mit Hilfe des logarithmischen Potentials von doppel- und einfach belegten Randkurven angegeben werden können. Die Dichtefunktionen dieser Potentiale können aus den Randbedingungen ermittelt werden, folglich läßt sich die biharmonische Aufgabe auf zwei, voneinander unabhängige Dirichletsche Probleme zurückführen. Die numerische Lösung besteht in der Lösung von zwei, auf die diskreten Punkte der Randkurve aufgeschriebenen, voneinander unabhängigen Gleichungssystemen.

Решение первой основной задачи теории упругости с помощью вещественных потенциалов *(К. Смодич).* Первая задача краевых значений теории упругости состоит в определении бигармонической функции напряжений, соответствующей краевым нагрузкам. По теореме Goursat эта функция может быть выражена двумя гармоническими фуикциями, которые могут быть даны логарифмическими потенциалами краевых кривых с двойным и одинарным слоем. Функции плотности этих потенциалов могут быть определены на основе краевых условий и, таким образом, бигармоническую задачу можно свести к двум независимым друг от друга проблемам Dirichlet. Решение в числовой форме состоит из решения двух независимых друг от друга систем уравнений, записанных для дискретных точек краевой кривой.

Acta Technica Academiae Scientiarum Hungaricae, Tomus 68 (3—4), pp. 359—361 (1970)

D'UNE GÉNÉRALISATION IMPORTANTE DE LA MÉTHODE DES DIFFÉRENCES FINIES

D. HOLNAPY*

[Manuscrit présenté le 25 janvier 1968]

La solution du problème de la valeur au contour des équations différentielles partielles par la méthode des différences finies est généralisée par l'auteur à des systèmes d'équations. De cette façon, il reçoit une méthode numérique facilement utilisable pour la solution de méthodes mathématiques complexes. Un exemple d'application concret est donné pour les voiles plats.

Introduction

L'incessant progrès de la technique soulève de nos jours des problèmes toujours plus complexes, qui nécessitent plus d'une fois la solution du problème de la valeur au contour de systèmes d'équations différentielles partielles. Comme exemple, citons la détermination des forces intérieures chez les voiles minces. Mais l'application d'une méthode est rendue plus difficile du fait que la littérature n'offre aucun procédé numérique sûr et simple pour ce modèle mathématique nécessitant des calculs relativement compliqués.

Dans le présent article, nous présentons un procédé grâce auquel la solution d'équations différentielles partielles par la méthode des différences finies peut être généralisée à des systèmes d'équations différentielles partielles, ce qui permettra, par exemple, d'élargir le champ d'application des voiles minces.

2. Généralisation du problème

Soient $L_{ij}(x)$ $i, j = 1, 2 \ldots n$ des opérateurs différentiels linéaires définis dans chaque point $x \in T$ [4] et $\varphi_1, \varphi_2 \ldots \varphi_n$ des fonctions définies dans le domaine T. De ces dernières, on suppose qu'elles peuvent être continuellement dérivées le nombre de fois voulu, suivant les opérateurs différentiels utilisés.

Considérons le système d'équations différentielles partielles

$$\sum_{i=1}^{n} \mathbf{L}_{ij}(x)\varphi_i(x) = f_j(x), \quad j = 1, \ldots n. \tag{1}$$

* D. HOLNAPY, Öv-u. 150, *Budapest XIV*, Hongrie.

C'est à ce système que nous voulons généraliser la méthode des différences finies.

Si dans un réseau déterminé, un opérateur différentiel linéaire est remplacé par un opérateur aux différences, la valeur de la fonction dans un nœud donné et les valeurs des fonctions dans les nœuds voisins (valeurs dont le nombre dépend de l'ordre de l'opérateur) forment une expression algébrique linéaire. Dans l'équation (1), nous appliquons l'opérateur différentiel linéaire à plusieurs fonctions et ces fonctions doivent être additionnées, de sorte que — en cas de calcul aux différences finies — l'ensemble de l'expression continue à rester linéaire.

Sans vouloir l'étudier dans le détail, rappelons ici un cas spécial connu de la littérature [1], [3], qui examine les critères de la solution pour le cas d'une fonction inconnue unique.

Dans notre problème, il figure plusieurs fonctions inconnues. Dans un tel cas, le critère de la solution est qu'avec un nombre de nœuds l on puisse résoudre le système d'équations à $l \cdot n$ inconnues écrit pour le réseau entier [3].

Le système d'équations ainsi reçu peut être résolu par toutes les méthodes connues. Un mode de solution frappant — bien qu'inapplicable dans certains cas pratiques — consiste à utiliser la relaxation de bloc de Southwell [6] et de corriger simultanément, dans le système d'équations, celles des valeurs des fonctions inconnues qui correspondent au même nœud. On choisit un vecteur initial $\varphi^{\circ},(x)$ puis en allant d'un nœud à l'autre on résout un système d'équations à autant d'inconnues qu'il y a de valeurs de fonctions inconnues dans le point donné.

Si les $f(x_k)$ calculés des $\varphi(x_k)$ obtenus par approximations successives ne diffèrent des côtés droits cherchés que dans la limite admise, on a réussi à avoir une solution d'exactitude suffisante dans la pratique.

3. Application

Considérons le système d'équations partielles des voiles plats [2], [5]:

$$\begin{aligned} C_{11}\,\mathbf{L}_1\,w(x,y)+C_{12}\,\mathbf{L}_2\,\Phi(x,y) &= p(x,y) \\ C_{21}\,\mathbf{L}_2\,w(x,y)+C_{22}\,\mathbf{L}_1\,\Phi(x,y) &= 0 \end{aligned} \tag{2}$$

où

C_{ij} = constantes

$\mathbf{L}_1 = \Delta\Delta$ = opérateur différentiel biharmonique

$$\mathbf{L}_2 = \frac{\partial^2 z}{\partial x^2}\cdot\frac{\partial^2}{\partial y^2} - 2\,\frac{\partial^2 z}{\partial x \partial y}\cdot\frac{\partial^2}{\partial x \partial y} + \frac{\partial^2 z}{\partial y^2}\,\frac{\partial^2}{\partial x^2}$$

$w(x, y)$ = fonction de déplacement vertical

$\Phi(x, y)$ = fonction de contraintes

$p(x, y)$ = fonction de charge

$z\ (x, y)$ = forme de la surface.

Soient données, au contour, les valeurs des deux fonctions de solution et les expressions linéaires formées des dérivées supérieures de ces fonctions. De la sorte, il n'y aura de valeurs de fonction inconnues que dans les nœuds intérieurs et toujours deux dans chaque nœud.

L'exemple ci-dessus est le cas spécial du problème général, pour $n = 2$.

La solution de l'équation de plaque

$$\Delta\Delta w(x, y) = cp(x, y) \tag{3}$$

par la méthode des différences finies est généralement connue.

L'équation (3) correspond en somme au cas spécial $n = 1$ de l'équation (1). La solution de (2) présente avec elle cette différence qu'au lieu d'une seule valeur de fonction (w) correspondant à chaque point donné dans l'équation différentielle partielle de l'équation de plaque, en cas de voile mince deux valeurs de fonctions (w, Φ) correspondent à ces mêmes points.

En cas d'utilisation de la méthode de relaxation, la valeur de fonction satisfaisant l'équation aux différences a été obtenue, pour les plaques, d'une équation à une inconnue. Pour les voiles minces, par contre, un système d'équations linéaires à deux inconnues doit être résolu en chaque point.

LITTÉRATURE

1. I. S. Berezin—N. P. Zhidkov: Computing Methods. Pergamon Press, Oxford 1965
2. W. Flügge: Statik und Dynamik der Schalen (3. Auflage) Springer Verlag, Berlin 1962
3. L. V. Kantorovics—V. I. Krülov: A felsőbb analyzis közelítő módszerei. Akadémiai Kiadó, Budapest 1953
4. J. Mikusiński: Operátorszámítás. Műszaki Kiadó, Budapest 1961
5. W. S. Wlassow: Allgemeine Schalentheorie und ihre Anwendung in der Technik. Akademie-Verlag, Berlin 1958
6. E. Bálint: Numerikus és grafikus közelítő módszerek. Tankönyvkiadó, Budapest 1965

On a Significant Generalization of the Lattice Point Method from the Engineering Viewpoint. The solution of the problem of the boundary value of the partial differential equations with the aid of the lattice-work point method (i.e. finite difference method) has been generalized into systems. By this a numerical procedure, easy to handle, for the solution of intricate mathematical models was established which is shown by a specified example of shallow shell structures.

Eine vom technischen Gesichtspunkt wichtige Verallgemeinerung der Gitterpunktmethode. Die Lösung des Randwertproblems von partiellen Differentialgleichungen mit Hilfe der Gitterpunktmethode (d.h. der endlichen Differenzenmethode) wird auf Systeme verallgemeinert, wodurch zur Lösung von verwickelten mathematischen Modellen eine leicht behandelbare rechnerische Methode hergestellt wird. Das Verfahren wird für den Fall von konkreten Flachtragwerken angewendet.

О важном с технической точки зрения обобщении метода конечной разности *(Д. Хольнапи)*. Автор обобщает решение проблемы окружного значения парциальных дифференциальных уравнений методом конечной разности для систем; вследствие этого для решения сложных математических моделей он получает легкий в обращении числовой метод, который демонстрируется им в конкретном случае плоских оболочек.

Acta Technica Academiae Scientiarum Hungaricae, Tomus 68 (3—4), pp. 363—382 (1970)

NATURAL FREQUENCY OF THE HORIZONTAL VIBRATIONS OF MULTI-STOREY BUILDINGS WITH BEARING WALLS

GY. VÉRTES*
CAND. OF TECHN. SCI.

[Manuscript received: July 5, 1968]

In multi-storey buildings with bearing walls, if no two-way symmetry exists, the horizontal free vibrations present themselves in a so-called "coupled" form. This means that, at the same time, flexural and torsional vibrations take place. The determination of the momentum characteristics of the mentioned vibration is detailed and after establishing the set of differential equations, an approximate method of solution for a simple calculation, and an exact method adaptable for electronic computation are described.

1. Introduction

In buildings constructed with bearing walls the floor loads are supported, instead of the traditional brick walls, by reinforced concrete slabs of vertical plane. Multi-storey houses constructed on this system have been widely spread for the last decade, owing to the economicalness of their structure or even more on the building technique connected with this system. There are a number of questions in connection with the statical and strength analysis of slab carcasses which should be cleared up, and it would not be stretching things to suggest that theoretical investigation in this field falls far behind the claims of practice. This is true even more emphatically in connection with problems of dynamic character, a number of which are not solved at all, or only unsatisfactorily. Also the determination of the natural frequency of the horizontal vibration of multi-storey buildings having slab skeleton, is a problem of this character. Namely, in most cases, the load bearing slab walls are not symmetrically arranged, and thence, from the viewpoint of the theory of vibration, it follows that the building cannot be brought into vibration by pure flexural or pure torsional character.

In case of a simple beam, if its cross section is not symmetrical and its gravity centre does not coincide with the shear centre, the pattern of the free vibration will be composed of simultaneous flexural and torsional vibrations. A vibration of such a character is called "coupled" vibration. The coupled vibration of a beam may be represented by a set of three simultaneous fourth

* Dr. techn. GY. VÉRTES, Madách I.-tér 6, *Budapest VII*, Hungary.

order partial differential equations [1], [4], [11], the solution of which is, even in case of simple types of beams, very complicated.

In analyzing the horizontal vibrations of buildings with slab skeletons, it can easily be seen that also here we have to do with "coupled" vibrations which are similar to those of the beam mentioned, however, owing to the different forms of structure, they cannot be treated on the same basis. Regarded from the structural viewpoint the most significant difference between them is that while every point of the cross section of the beam, in conformity with the theory based on the Bernouilli—Navier hypothesis, can perform only such movements which are conform with the given geometrical conditions, and cannot be independent of the adjacent points, the bearing walls forming the slab skeleton, in most cases, are composed of members in planes inclined to each other, and therefore they can make some movements only in dependence, and some independently of each other. All of this show that the vibration system in question is very intricate, accordingly, the methods used so far, are not suitable for the solution of problems of this character.

In the following, for the determination of the natural frequency of the horizontal vibrations of tower houses with slab skeleton, a computation method will be presented which, in case of fulfilment of certain symplifying assumptions, may also be applied in general cases related to the buildings mentioned.

2. Principles and pattern of computation

The structure of the buildings in question consists of horizontal floors, and vertical bearing walls between the floors. The diagrammatic cross-section of such a building is shown in Fig. 1. The wall members strengthened together and inclined at oblique angles to each other, form a single wall unit, but if they are not rigidly connected, then each of the wall members should be considered as a separate unit.

For our calculations we have made the following assumptions:

a) the walls behave as elastic bodies under the effect of vibration;

b) the mass of the structure belonging to each floor, also including the mass of the floor, walls and other equipments, will be taken up at the level of the respective storey, but as to the distribution of the mass, no reservations will be made;

c) the effect of damping on the variation of the natural frequency is ignored;

d) each floor forms in its own plane a disc considered as infinitely rigid, but perpendicularly to its plane it is perfectly elastic. This means that all of the wall members are forced to perform the very same displacement and

rotation in the plane of the floors, however, perpendicularly to their plane they may be deformed independently of each other;

e) the arrangement in plan of the wall members and their thickness may be arbitrarily chosen but it should be identical at each storey. The coaction of the wall members of each storey being in the same vertical plane, and with the foundation by the rigid connections is ensured at their joinings. Thus, the wall members in the same vertical plane form a vertical cantilever;

f) in calculating the deformations, the torsional stiffness of each wall member which, in comparison with the flexural stiffness, is very small, may be neglected.

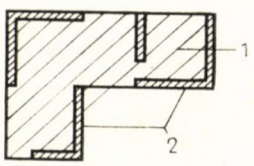

Fig. 1. Floor, all members

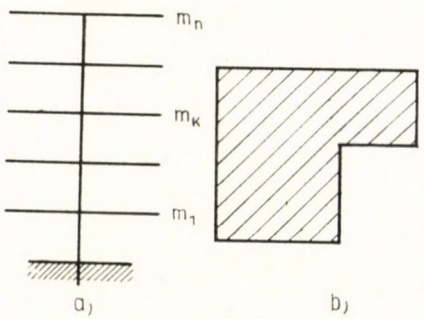

Fig. 2. Side elevation, cross-section

The pattern serving as basis for the calculation is shown in Fig. 2. As the cross-section, which is obtained by cutting the building in question with a horizontal plane directly above one of the floors, only the floor is to be considered as a rigid disc in its own plane, represented without drawing the supporting wall members. In the following, this cut will be called the *cross-section of the building*. This significantly differs from the cross-section of the simple flexural beams, consequently the usual characteristics of the former should be defined accordingly.

In the following, by the *centre of gravity* (S) *of the cross-section of the building*, the common centre of gravity of the intersecting plane of the wall members figuring in the cross-section is meant which, in general, differs from the *gravity centre of the mass of the cross-section* (S_M); this latter meaning the centre of gravity of the mass concentrated in the floor plane and evenly distributed in the horizontal plane.

Similarly to the cross-section of the beam, also the cross-section of the building possesses such a point which is characterized by the horizontal external force acting on the building in the plane of the floor, the cross section (the floor) is subject to a torsional moment, the rotation takes place around this point. This point, in the following, will be called the *centre of rotation* (O) *of the cross-section of the building*.

Thus, under the effect of the horizontal force intersecting the centre of rotation, the floor will be displaced only in its own plane, however, the direction of the displacement is not the same as that of the force. As we shall see in the following, among the directions of an infinite number, there are two directions perpendicular to each other, the active force in which only displacement in the direction of the force is induced, and these two directions will be called the *principal directions.*

Symbols of major importance used in the formulas and deductions are as follows:

F — cross-sectional area of the wall member
J_1, J_2 — principal moments of inertia of the cross section of the wall members
E — modulus of elasticity
s — coefficient serving for taking into account the weakening of the wall slab members
S — centre of gravity of the cross-sectional plane figure
S_M — centre of gravity of the mass
0 — centre of shear or rotation
p_{xx}, p_{yy}, $p_{xy} = p_{yz}$ — stiffness factors of the wall members

$$A = \sum_{i=1}^{m} p_{ixx}\,; \quad B = \sum_{i=1}^{m} p_{iyy}\,; \quad C = \sum_{i=1}^{m} p_{ixy} = \sum_{i=1}^{m} p_{iyx}\,,$$

$K = AB - C^2$
x, y — system of coordinates in the planes of the floors
z — coordinate axis perpendicular to the planes of the floors
u, v — system of coordinates corresponding to the principal directions of the cross-section of the building, and magnitude of the displacement taking place along these axes
u_M, v_M — coordinates of the centre of gravity of the mass in the system of coordinates u, v
Φ — angle of rotation around the centre of rotation of the cross-section of the building
E_h — potential energy
E_m — kinetic energy
J_0 — Moment of mass inertia related of the axis intersecting the centre of rotation
M_i — value of the twisting moment causing the unit rotation of the cross-section of the building
m_i — mass of the floor concentrated in the level of a storey
p_u, p_v — value of the force causing the unit displacement, acting in the principal directions

3. Determination of the characteristics of the cross-section

Determination of the centre of gravity and centre of gravity of the mass of the cross-section of the building, defined in the foregoing, takes place according to the commonly known method of calculation of the centres of gravity of plane figures and masses. New notions are the principal directions and the centre of rotation which are the functions of the stiffness of the cross-section, and are connected with the stiffness of the wall members as cantilevers fixed at one of their ends. In the following, first determination of these latter will be dealt with.

3.1. *Determination of the stiffness factors of the wall members*

The principal directions of inertia of the beam are of the same properties as those of the cross-section of the building in respect, that is, if the external is parallel with one of them, also the displacement of the cross-section will be parallel with the direction of the force. Since the principal directions (1, 2) and principal moments of inertia (J_1, J_2) of the cross-section may easily be determined by means of the relations well known from the theory of strength of materials [7], in the following they will be considered as known values.

Calculation of the stiffness factors of the wall members is well known from the literature [7], [9], therefore they will be dealt with only very shortly.

If we want to displace the cross-section denoted by "i" of a homogeneous prismatic bar stiffly fixed at one of its ends, and the material which follows Hooke's law, being at a distance "z" from the fixed end of the beam, parallel with the principal directions 1 and 2, of a magnitude of Δ_1 and Δ_2 respectively, in the shear centre of the cross-section denoted by "k" being at a distance c ($c \geq z$) from the fixed end of the beam, parallel with the respective displacement P_1 and P_2 forces should be applied. Magnitudes of the forces are in conformity with the well-known relation of the elementery theory of strength of materials

$$P_1 = \frac{I_2}{H} \Delta_{1ik} \tag{1}$$

and

$$P_2 = \frac{I_2}{H} \Delta_{2ik}\,, \tag{2}$$

respectively.

In the above formulas

$$H = \frac{s}{E}\left(c\frac{z^2}{2} - \frac{z^3}{6}\right)$$

where E is the modulus of elasticity of the material of the bar and s is a coefficient expressing the effect of the gaps (opening for doors and windows) in the wall.

Now let us determine in a system of a coordinate with the axes x, y, assumed also to be at a distance "z" from the fixed extremity of the bar, what is the value of an external force which should act on the cross-section "k" to cause a unit displacement in the x direction of the shear centre of the cross-section. If the axis x is not a principal direction, the force causing the displacement is not parallel with the axis x itself, but it can be characterized by the components p_{xx} and p_{xy} of the directions x and y respectively, which can be calculated as follows. The components in the principal directions *1* and *2* of the mentioned unit, the displacement following the direction x and inclining at

an angle α to the principal direction 1, as can be seen in Fig. 3, are equal to $1 \cdot \cos\alpha$ and $-1 \cdot \sin\alpha$, respectively. To create these components, according to formulas (1) and (2), forces of magnitudes

$$Q_1 = \frac{I_2}{H} \cos\alpha \tag{3}$$

and

$$Q_2 = \frac{I_1}{H} \sin\alpha \tag{4}$$

acting in the directions of the axes 1 and 2 are needed.

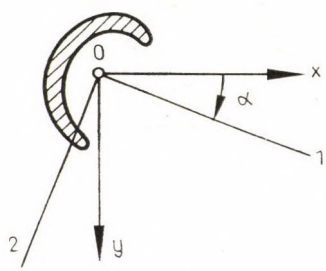

Fig. 3

The force components p_{xx} and p_{xy} which are to be found are given by the sum of the projections in the directions of x and y of (3) and (4), thus

$$p_{xx} = Q_1 \cos\alpha - Q_2 \sin\alpha = \frac{1}{H}(I_1 \sin^2\alpha + I_2 \cos^2\alpha), \tag{5}$$

$$p_{xy} = Q_1 \sin\alpha + Q_2 \cos\alpha = -\cos\alpha \sin\alpha \left(\frac{I_1 - I_2}{H}\right). \tag{6}$$

For provoking the unit displacement in the direction of y of the cross-section investigated, the forces p_{yy} and p_{yx} should be applied in the directions of y and x, respectively. These forces may be determined in the same way as has been shown above, and we will find the following results:

$$p_{yy} = \frac{1}{H}(I_1 \cos^2\alpha + I_2 \sin^2\alpha), \tag{7}$$

$$p_{yx} = -\frac{1}{H} \cos\alpha \sin\alpha (I_1 - I_2) = p_{xy}. \tag{8}$$

In the following, the quantities p_{xx}, p_{yy} and $p_{xy} = p_{yx}$, found in this way will be called the *stiffness factors of the wall member.*

3.2. *Determination of the principal directions, centre of rotation of the cross section of the building, and the dynames provoking its unit displacements*

The principal directions of the cross-sections of the building may be determined starting out from the condition that the displacement, caused by the force intersecting the centre of rotation and acting parallel with the principal direction, will also be parallel with the direction of the force. This is also true inversely, viz., the straight of the so-called restoring force created by the effect of the displacement in the principal direction, also coincides with the principal direction. If the centre of rotation, the place which is so far unknown of the cross-section of the building outlined in Fig. 4, we assumed

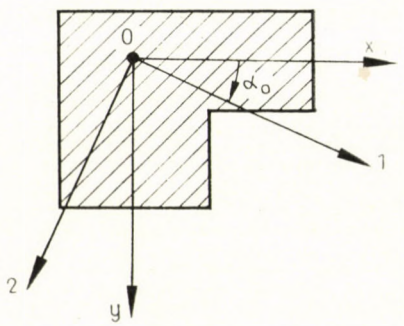

Fig. 4

an optional system of coordinates x, y, and denoted the angle between the principal direction and the axis z, with α_0. Then we displaced the cross-section supported by wall members of a number of "n" along the principal direction by an amount of Δ. The straight of the force (R) needed for causing the displacement, coincides accordingly with the principal direction. The components of the displacement Δ in the directions of x and y are equal to $\Delta \cos \alpha_0$ and $\Delta \sin \alpha_0$, respectively, and the forces causing these displacements are the same as the components in the respective directions of R. Between the forces needed for creating the components of the displacement and the respective components R, the following relations may be established with the aid of the stiffness factors of the wall members:

$$\begin{aligned} \Delta \cos \alpha_0 \sum_{i=1}^{m} p_{ixx} + \Delta \sin \alpha_0 \sum_{i=1}^{m} p_{ixy} &= R \cos \alpha_0 \\ \Delta \sin \alpha_0 \sum p_{iyy} + \Delta \cos \alpha_0 \sum p_{ixy} &= R \sin \alpha_0 \end{aligned} \tag{9}$$

In these equations p_{ixx}, p_{iyy} and $p_{ixy} = p_{iyx}$ represent the stiffness factors of the ith wall member. Introducing the terms

$$A = \sum_{i=1}^{m} p_{ixx}\,, \quad B = \sum_{i=1}^{m} p_{iy,y}\,, \quad C = \sum_{i=1}^{m} p_{ixy} \tag{9a}$$

and solving the set of equations, we have the relation

$$\tan 2\,\alpha_0 = \frac{2C}{A - B}\,. \tag{10}$$

From this relation, in conformity with the problems of similar character, it is evident that for the value of α_0 two solutions may be obtained. Namely, if a value α_0' satisfies the equation, then the value $\alpha_0'' = \alpha_0' + \pi/2$ will satisfy it, too, because $\tan 2\,\alpha_0'' = \tan (2\alpha_0' + \pi) = \tan 2\,\alpha_0'$. This means that we find two directions perpendicular to each other with respect to which the determination of the principal direction is true, and by that, also the existence of the principal directions is verified.

As can be seen, the distance between the cross-section examined and the fixed end is not included in the expression of α_0, thus, relation (10) may be equally used to every cross-section examined, in each storey of the building.

In the following we shall also need the value of the force causing the unit displacement in the principal direction, therefore, we shall now treat its determination. Let us denote the force causing a displacement as $\Delta = 1$ in the principal direction inclined at an angle α_0 to the axis x, by p. The Equations (9) may then be written as follows:

$$\begin{aligned} A\cos\alpha_0 + C\sin\alpha_0 &= p\cos\alpha_0\,, \\ B\sin\alpha_0 + C\cos\alpha_0 &= p\sin\alpha_0\,. \end{aligned} \tag{11}$$

The solution of the equation will not be detailed, because this also is similar to that of the set of equations serving for the determination of the principal stresses, and in this respect, it is well-known from the literature. The final result of the calculation is

$$p = \frac{A+B}{2} + \sqrt{\left(\frac{A-B}{2}\right)^2 + C^2}\,. \tag{12}$$

The relation obtained, considering the two signs before the square root, gives two values corresponding to the two principal directions. The greater one (which, in the following, will be denoted by p_u) may be found by applying the positive sign, and the smaller one by considering the negative sign in front of the square root. Thus, by applying the symbols of Fig. 4, the forces causing

the unit displacement in the principal directions may be calculated by means of the following formulas:

$$p_u = \frac{A+B}{2} + \left[\left(\frac{A-B}{2}\right)^2 + C^2\right]^{1/2},$$
$$p_v = \frac{A+B}{2} - \left[\left(\frac{A-B}{2}\right)^2 + C^2\right]^{1/2}. \tag{13}$$

Now, let us analyse the method of determining the centre of rotation of the cross-section of the building according to [7] and [9]. Let us assume that on the floor at a distance z from a fixed end and parallel with the axis z shown in Fig. 4, in the centre of rotation, the place which is not yet known, a horizontal force $R_x = 1$ Mp is acting. According to the definition no rotation of the floor will occur, only its displacement of Δ_{xx} and Δ_{xy} in the directions x and y, respectively. Similarly to the method applied for the calculation of the principal directions, we can write down the following projection equations:

$$\Delta_{xx} A + \Delta_{xy} C = 1\,,$$
$$\Delta_{xx} C + \Delta_{xy} B = 0\,. \tag{14}$$

Introducing the abbreviation $K = AB - C^2$, from the obtained set of equations for the displacements of the floor we have

$$\Delta_{xx} = \frac{B}{K}, \quad \Delta_{xy} = -\frac{C}{K}\,. \tag{14a}$$

In the light of the displacements, the forces of the directions of x and y, applied on the wall members can easily be calculated from the external force $R_x = 1$ Mp. Thus, in the direction of x and y, on the ith wall member the forces

$$r_{ixx} = \Delta_{xx} p_{ixx} + \Delta_{xy} p_{ixy} = \frac{1}{K}(B p_{ixx} - C p_{ixy}) \tag{15}$$

and

$$r_{ixy} = \Delta_{xx} p_{ixy} + \Delta_{xy} p_{iyy} = \frac{1}{K}(B p_{ixy} - C p_{iyy}), \tag{16}$$

respectively, are acting. Since the external force is the resultant of these forces, we can write down that the moment of the resultant force related to a point (in this case to the origo $0'$ of the system of coordinates x', y' to be seen in Fig. 5) is equal to the sum of the moments of the forces acting on the wall members, related to the same point. Thus,

$$\sum_{i=1}^{m} (x'_i r_{ixy} - y'_i r_{ixx}) = y'_0 \cdot 1\,. \tag{16a}$$

Here, x_i' and y_i' are the distances of the centre of rotation of the ith wall member from the axes y' and x' respectively, and y_0' is the distance of the centre of rotation from the axis x'. By making use of the results of Equations (15) and (16) the magnitude of this latter may be found with the aid of the equation

$$y_0' = \frac{B}{K}\left[\sum_{i=1}^{m} y_i' p_{ixx} - \sum_{i=1}^{m} x_i' p_{ixy}\right] + \frac{C}{K}\left[\sum_{i=1}^{m} x_i' p_{iyy} - \sum_{i=1}^{m} y_i^1 p_{ixy}\right]. \tag{17}$$

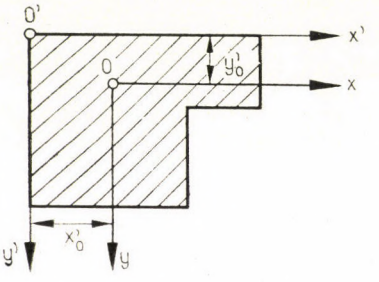

Fig. 5

Almost similarly to what has been presented in the foregoing, in investigating the effect of the force $R_y = 1$ Mp of the direction of y, the distance of the centre of rotation from the axis y' may be deducted, which is

$$x_0' = \frac{A}{K}\left[\sum_{i=1}^{m} x_i' p_{iyy} - \sum_{i=1}^{m} y_i' p_{ixy}\right] + \frac{C}{K}\left[\sum_{i=1}^{m} y_i' p_{ixx} - \sum_{i=1}^{m} x_i' p_{iyx}\right]. \tag{18}$$

Finally we shall determine the value of the moment to be applied in the centre of rotation of the cross-section of the building inducing the unit rotation of the cross-section. Let us assume that the floor belonging to the cross-section investigated undergoes the unit rotation. Then the shear centre of the ith wall member will be displaced in the directions of x and y by the lengths of x_i and y_i, respectively, and for inducing the displacement, in the centre of rotation forces of values

$$r_{i\varphi x} = (z_i p_{ixy} - y_i p_{ixx}), \tag{19}$$

and

$$r_{i\varphi y} = (x_i p_{yy} - y_i p_{ixy}) \tag{20}$$

should be applied in the directions of x and y, respectively. In these formulas, $x_i = x_i' - x_0'$ and $y_i = y_i' - y_0'$, i.e., they are the distances, respectively, of the centre of rotation of the ith wall member from the axes of the system of coordinates assumed in the centre of rotation. The sum of the moments of the

forces induced by the effect of the rotation related to the centre of rotation should be equal to the turning moment of the couple causing the rotation, i.e.,

$$M_i = \sum_{i=1}^{m} (x_i \, r_{i\varphi x} - y_i \, r_{i\varphi y}) = \\ = \left[\sum_{i=1}^{m} y_i^2 \, p_{ixx} - 2 \sum_{i=1}^{m} x_i y_{i\,xy} + \sum_{i=1}^{m} x_i^2 \, p_{iyy} \right]. \tag{21}$$

4. Set of differential equations serving to represent the vibration and its solution

The differential equation of a complex vibration system may be directly written down in many cases with the aid of the Lagrange equation. In determining the natural of vibration of tower houses of slab skeleton, we chose the

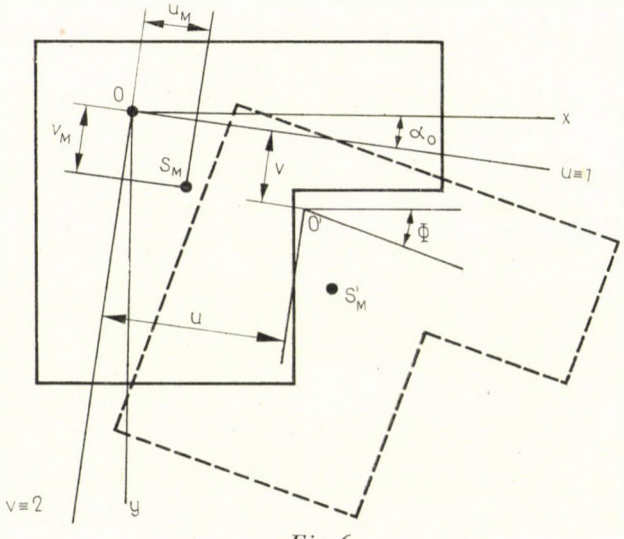

Fig. 6

very same way, and first set out from the displacements of the ith floor of the building examined. As was referred to above, the motion of the floor induced by the vibration may be characterized by the rotation around the centre of rotation and the simultaneous displacement. In the following, in lieu of the displacement we shall take into account its components in the principal directions and, accordingly, the displacement of the centre of rotation of the floor will be denoted by the components u and v and its rotation by Φ, as is shown in Fig. 6.

Under the effect of the displacement, as is to be seen in the figure, the centre of rotation of the floor will be transferred to 0′, and its centre of gravity

of mass in S'_M. Its kinetic energy in a given moment, as the impetus of a rigid body, subject to rotation and translation movements, may be found as follows (the point above the character denoting the derivative of the movement in respect with time).

The kinetic energy of the whole building written in the form of a matrix is

$$E_m = \frac{1}{2}\dot{\mathbf{u}}^*\mathbf{M}\dot{\mathbf{u}} + \frac{1}{2}\dot{\mathbf{v}}^*\mathbf{M}\dot{\mathbf{v}} + \frac{1}{2}\dot{\boldsymbol{\Phi}}^*\mathbf{M}\dot{\boldsymbol{\Phi}} + \mathbf{M}\dot{\boldsymbol{\Phi}}(u_M\dot{\mathbf{v}} - v_M\dot{\mathbf{u}}) \tag{22}$$

$$\dot{\mathbf{u}} = \begin{bmatrix} \dot{\mathbf{u}}_1 \\ \vdots \\ \dot{\mathbf{u}}_i \\ \vdots \\ \dot{\mathbf{u}}_n \end{bmatrix}, \qquad \dot{\mathbf{v}} = \begin{bmatrix} \dot{\mathbf{v}}_1 \\ \vdots \\ \dot{\mathbf{v}}_i \\ \vdots \\ \dot{\mathbf{v}}_n \end{bmatrix}, \qquad \dot{\boldsymbol{\Phi}} = \begin{bmatrix} \dot{\boldsymbol{\Phi}}_1 \\ \vdots \\ \dot{\boldsymbol{\Phi}}_i \\ \vdots \\ \dot{\boldsymbol{\Phi}}_n \end{bmatrix}$$

vectors and $\mathbf{M} = \langle m_1, m_2 \ldots m_n \rangle$; $J_0 = \langle J_{01}, . J_{0i}, \ldots J_n \rangle$ diagonal matrices.

The potential energy of the floor at the very same moment will be

$$\frac{d}{dt}\frac{\partial E_m}{\partial \dot{\mathbf{q}}} - \frac{\partial E_m}{\partial \mathbf{q}} + \frac{\partial E_h}{\partial \mathbf{q}} = \mathbf{f}. \tag{23}$$

In the equation by $\mathbf{q}(\mathbf{u}, \mathbf{v}, \boldsymbol{\Phi})$ the vectors of the so-called generalized coordinates characterizing the motion of the centre of gravity of the mass of the floor, and by $\mathbf{f}$ the active dyname vectors are denoted which, in this case, as free vibrations are dealt with equal to zero.

Let us now determine the derivatives of the Lagrange equation. These are

$$\begin{aligned}
\frac{d}{dt}\frac{\partial E_m}{\partial \dot{\mathbf{u}}} &= \mathbf{M}\ddot{\mathbf{u}} - v_M\mathbf{M}\ddot{\boldsymbol{\Phi}}, \\
\frac{d}{dt}\frac{\partial E_m}{\partial \dot{\mathbf{v}}} &= \mathbf{M}\ddot{\mathbf{v}} + u_M\mathbf{M}\ddot{\boldsymbol{\Phi}}, \\
\frac{d}{dt}\frac{\partial E_m}{\partial \dot{\boldsymbol{\Phi}}} &= -v_M\mathbf{M}\ddot{\mathbf{u}} + u_M\mathbf{M}\ddot{\mathbf{v}} + \mathbf{I}_0\ddot{\boldsymbol{\Phi}}, \\
\frac{\partial E_m}{\partial \mathbf{u}} &= \frac{\partial E_m}{\partial \mathbf{v}} = \frac{\partial E_m}{\partial \boldsymbol{\Phi}} = 0,
\end{aligned} \tag{23a}$$

further

$$\begin{aligned}
\frac{\partial E_h}{\partial \mathbf{u}} &= \mathbf{K}_u\mathbf{u}, \\
\frac{\partial E_h}{\partial v} &= \mathbf{K}_v\mathbf{v}, \\
\frac{\partial E_h}{\partial \Phi} &= \mathbf{K}_\Phi\boldsymbol{\Phi}.
\end{aligned} \tag{23b}$$

Examining the three derivatives written down on the basis of $\partial E_h/\partial q$, we can see that they actually present the magnitudes of the restoring force related to the respective floor taking place during vibration, and of the moment exerted by the elastic support of the floor. In case of a system of a unique mass and one degree of freedom they can easily be determined, but, in our case, there being several masses in question, the magnitudes of the restoring dynames acting on a certain mass are influenced by the displacement of the

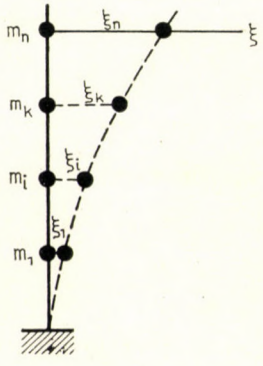

Fig. 7

other masses, namely, under the effect of the displacement of one of the masses, the other mass will also be displaced, and vice versa. Let us investigate the manner of calculation for the dynames in these cases.

On a beam fixed at one of its extremities shown in Fig. 7 concentrated loads are applied. Let us denote the displacements of the direction of ξ induced by the horizontal unit force applied at the place of the ith mass by a_{ii}, and at the place of an other mass, by a_{ik}. Similarly, under the effect of the horizontal unit force applied at the point of the mass denoted by "k", at the points "k" and "i" displacements a_{kk} and a_{ki}, respectively, are taking place. As is known, in conformity with Maxwell's principles of reciprocal displacements, $a_{ki} = a_{ik}$. According to what has been said above, the forces R may be calculated which jointly cause a displacement ξ at the place of the mass denoted by "i". In turn, these forces give in addition that in the displacement ξ, which takes place simultaneously, what the value of the elastic restoring force is which acts on the mass denoted by m_i.

The elastic restoring forces acting on each of the masses may be determined by the application of the principle of superposition in the following

set of equations.

$$\begin{aligned} a_{11}R_1+a_{12}R_2+\ldots a_{1n}R_n &= \xi_1, \\ a_{21}R_1+a_{22}R_2+\ldots a_{2h}R_n &= \xi_2, \\ \text{- - - - - - - - - - - - - - - - - -} & \\ a_{n1}R_1+a_{n2}R_2+\ldots a_{nn}R_n &= \xi n. \end{aligned} \tag{23c}$$

The set of equations written in the form of matrix is

$$\mathbf{Nr} = \xi. \tag{24}$$

Here

$$\mathbf{r} = \begin{bmatrix} R_1 \\ R_2 \\ \vdots \\ R_n \end{bmatrix}, \qquad \xi = \begin{bmatrix} \xi_1 \\ \xi_2 \\ \vdots \\ \xi_n \end{bmatrix} \tag{24a}$$

and

$$\mathbf{N} = \begin{bmatrix} a_{11} & a_{12} & \ldots & a_{1n} \\ a_{21} & a_{22} & \ldots & a_{2n} \\ \text{- - - - - - - - - - - - - - - - - -} & & & \\ an_1 & a_{n2} & \ldots & a_{nn} \end{bmatrix}. \tag{24b}$$

The solution of the matrix equation is

$$\mathbf{r} = \mathbf{N}^{-1}\xi \tag{25}$$

where $\mathbf{N}^{-1}$ is the so-called inverse matrix of **N**. Considering that matrix **N** is symmetrical, its inverse is symmetrical too, accordingly $a'_{ij} = a'_{ji}$. On the basis of the above the derivatives of the potential energy with respect to the generalized coordinates are as follows:

$$\begin{aligned} \frac{\partial E_h}{\partial \mathbf{u}} &= \mathbf{r}_n = \mathbf{N}_u^{-1}\mathbf{u}, \\ \frac{\partial E_h}{\partial \mathbf{v}} &= \mathbf{r}_v = \mathbf{N}_r^{-1}\mathbf{v}, \\ \frac{\partial E_h}{\partial \boldsymbol{\Phi}} &= r_\Phi = \mathbf{N}_\Phi^{-1}\boldsymbol{\Phi}. \end{aligned} \tag{25a}$$

These derivatives at the same time give the restoring dynames acting on the floors.

In the above formulas

$$\mathbf{r}_u = \mathbf{N}_u^{-1}\,\mathbf{u} = \begin{bmatrix} a'_{u,11}\,u_1 + a'_{u,12}\,u_2 + \ldots + a'_{u,1n}\,u_n \\ a'_{u,21}\,u_1 + a'_{u,22}\,u_2 + \ldots + a'_{u,2n}\,u_n \\ \vdots \\ a'_{u,n1}\,u_1 + a'_{u,n2}\,u_2 + \ldots + a'_{u,nn}\,u_n \end{bmatrix},$$

$$\mathbf{r}_v = \mathbf{N}_v^{-1}\,\mathbf{v} = \begin{bmatrix} a'_{v,11}\,v_1 + a'_{v,12}\,v_2 + \ldots + a'_{v,1n}\,v_n \\ a'_{v,21}\,v_1 + a'_{v,22}\,v_2 + \ldots + a'_{v,2n}\,v_n \\ \vdots \\ a'_{v,n1}\,v_1 + a'_{v,n2}\,v_2 + \ldots + a'_{v,nn,}\,v_n \end{bmatrix}, \tag{25b}$$

$$\mathbf{r}_\Phi = \mathbf{N}_\Phi^{-1}\,\boldsymbol{\Phi} = \begin{bmatrix} a'_{\Phi,11}\,\Phi_1 + a'_{\Phi,12}\,\Phi_2 + \ldots + a'_{\Phi,1n}\,\Phi_x \\ a'_{\Phi,21}\,\Phi_1 + a'_{\Phi,22}\,\Phi_2 + \ldots + a'_{\Phi,2n}\,\Phi_n \\ \vdots \\ a'_{\Phi,n1}\,\Phi_1 + a'_{\Phi,n2}\,\Phi_2 + \ldots + a'_{\Phi,nn}\,\Phi_n \end{bmatrix}.$$

(Members marked with primes represent those associated with the inverse $\mathbf{N}^{-1}$ of the matrix $\mathbf{N}$.)

Then the set of differential equations expressing the motion will be

$$\begin{aligned} \mathbf{M}\ddot{\mathbf{u}} - v_M\,\mathbf{M}\ddot{\boldsymbol{\Phi}} + \mathbf{N}_u^{-1}\,\mathbf{u} &= 0\,, \\ \mathbf{M}\ddot{\mathbf{v}} + u_M\,\mathbf{M}\ddot{\boldsymbol{\Phi}} + \mathbf{N}_v^{-1}\,\mathbf{v} &= 0\,, \\ -v_M\,\mathbf{M}\ddot{\mathbf{u}} + u_M\,\mathbf{M}\ddot{\mathbf{v}} + \mathbf{I}_0\ddot{\boldsymbol{\Phi}} + \mathbf{N}_\Phi^{-1}\,\Phi &= 0. \end{aligned} \tag{26}$$

Before treating the solution of the set of differential equations we should compute the coefficients (load factors) of the sets of equations serving to determine the restoring dynames. These may easily be found on the basis of what has been said in Chapter 2.

Namely, the relation (13) contains the forces p_1 and p_2 causing the unit displacement in the directions u and v, respectively. The coefficients of the sets of equations serving to calculation of $\mathbf{r}_u$ and $\mathbf{r}_v$, which represent the displacement induced by the effect of the unit forces, may be obtained simply as the inverse values of these latters, i.e.,

$$a_{u,ik} = \frac{1}{p_{u,ik}} \quad \text{and} \quad a_{v,ik} = \frac{1}{p_{r,ik}} \tag{27}$$

where p_{ik} represents the force applied at point "k" causing the unit displacement at the ith place. Relation (13) suitably applied may be used for the determination of all of the p_{ik}'s, only the distance associated to the points "i"

and "k" should be substituted into the formula of H, figuring in the formulas (5), (6), (7), (8).

The rotation of the cross-section of the building induced by the unit couple is equal to the inverse of the numerical value of the couple acting in the plane of the floor causing unit rotation, i.e.,

$$a_{\Phi ik} = \frac{1}{M} . \tag{28}$$

The value of M included in this formula may be calculated by means of Equation (21).

Having dealt with the system rigidly fixed at one of its ends and without support at the other, if we allow the ith cross section of the building at an angle Φ to rotate, then all the cross sections "k" being between this and the free end carry out rotations at the same angle. Therefore, we can write down:

$$a_{\Phi ii} = a_{\Phi ik}. \tag{29}$$

In solving the set of equations we proceed in conformity with the usual method applied in the case of the multiple-mass oscillation system. Assuming that the free oscillation of the system is a harmonic one, then it may be characterized by the functions

$$\begin{aligned} \mathbf{u} &= \mathbf{u}_0 \sin \omega t , \\ \mathbf{v} &= \mathbf{v}_0 \sin \omega t , \\ \boldsymbol{\Phi} &= \boldsymbol{\Phi}_0 \sin \omega t \end{aligned} \tag{29a}$$

and

$$\begin{aligned} \ddot{\mathbf{u}} &= -\omega^2 \mathbf{u}_0 \sin \omega t , \\ \ddot{\mathbf{v}} &= -\omega^2 \mathrm{v}_0 \sin \omega t , \\ \ddot{\boldsymbol{\Phi}} &= -\omega^2 \boldsymbol{\Phi}^0 \sin \omega t . \end{aligned} \tag{29b}$$

On substituting these into the set of equations (28) and dividing them by $\sin \omega t$, we have

$$\begin{aligned} (\mathbf{N}_u^{-1} - \omega^2 \mathbf{M})\, \mathbf{u}_0 + \mathbf{0}\, \mathbf{v}_0 + \omega^2 v_M \mathbf{M} \boldsymbol{\Phi}_0 &= 0 , \\ \mathbf{0} \qquad \mathbf{u}_0 + (\mathbf{N}_v^{-1} - \omega^2 \mathbf{M})\, \mathbf{v}_0 \omega^2 u_M \mathbf{M} \boldsymbol{\Phi}_0 &= 0 , \\ \omega^2 v_M \mathbf{M}\, \mathbf{u}_0 - \omega^2 u_M \mathbf{M} v_0 + (\mathbf{N}_{\Phi}^{-1} - \mathbf{I}_0 \omega^2)\, \boldsymbol{\Phi}_0 &= 0 . \end{aligned} \tag{30}$$

Here $\mathbf{0}$ represents the zero matrix of the nth order.

Further introducing the notations

$$
\begin{aligned}
&(\mathbf{N}_u^{-1} - \omega^2 \mathbf{M}) = \mathbf{P}\,, \\
&\omega^2 v_M \mathbf{M} = \mathbf{Q}\,, \qquad \text{(diagonal matrix)} \\
&(\mathbf{N}_v^{-1} - \omega^2 \mathbf{M}) = \mathbf{R}\,, \\
&-\omega^2 v_M \mathbf{M} = \mathbf{S}\,, \qquad \text{(diagonal matrix)} \\
&(\mathbf{N}_\Phi^{-1} - \omega^2 \mathbf{I}_0) = \mathbf{T}\,,
\end{aligned}
$$

the set of equation becomes

$$
\begin{aligned}
&\mathbf{P}\,\mathbf{u}_) + \mathbf{O}\,\mathbf{v}_0 + \mathbf{Q}\,\boldsymbol{\Phi}_0 = 0\,, \\
&\mathbf{O}\,\mathbf{u}_0 + \mathbf{R}\,\mathbf{v}_0 + \mathbf{S}\,\boldsymbol{\Phi}_0 = 0\,, \\
&\mathbf{Q}\,\mathbf{u}_0 + \mathbf{S}\,\mathbf{v}_0 + \mathbf{T}\,\boldsymbol{\Phi}_0 = 0\,.
\end{aligned} \tag{31}
$$

The homogeneous set of equations obtained has a solution other than zero only in that case if the determinant formed from the coefficients is equal to zero. In our case the coefficient matrix is given by the following hypermatrix

$$
\mathbf{W} = \begin{bmatrix} \mathbf{P} & \mathbf{O} & \mathbf{Q} \\ \mathbf{O} & \mathbf{R} & \mathbf{S} \\ \mathbf{Q} & \mathbf{S} & \mathbf{T} \end{bmatrix}. \tag{32}
$$

Finally, the equation for the determination of the natural angular frequency of vibration is

$$
\det \mathbf{W} = (\det \mathbf{P})\,(\det \mathbf{R} \det \mathbf{T} - \det \mathbf{S}^2) - \det \mathbf{Q}^2 \det \mathbf{R} = 0\,. \tag{33}
$$

This equation is with respect to ω^2 of the $3n$-th degree, having $3n$ roots. Considering that the matrices included in the characteristic equation are symmetrical, and so is the hypermatrix $\mathbf{W}$ itself, the roots of the equation are real, accordingly, we obtain for ω real or pure imaginary values. It follows from the physical condition of motion that pure imaginary or real negative values for the roots cannot be taken into account, and so, in fact, for ω only values of n number might be considered. Among these it is the smallest one which gives the fundamental angular frequency of the natural oscillation the rest of them represent the angular frequencies associated with the vibrations of more complex forms. Thus, the fundamental natural angular frequency of the building is $\omega = \omega_{\min}$, and the fundamental frequency of vibration of the building is

$$
N = \frac{\omega_{\min}}{2\pi}\,. \tag{34}
$$

Since the solution of the set of equations (32) involves cumbersome calculation work and in case of a multistorey building it is unimaginable without using an electronic computer, the method adaptable to computer will also be presented.

Separating the terms of the set of equations (30) according to including ω or not, yields

$$(\mathbf{A}^{-1} - \omega^2 \mathbf{B})\,\mathbf{q} = 0 \tag{34a}$$

where

$$\mathbf{A}^{-1} = \begin{vmatrix} \mathbf{N}_u^{-1} & \mathbf{0} & \mathbf{0} \\ \mathbf{0} & \mathbf{N}_v^{-1} & \mathbf{0} \\ \mathbf{0} & \mathbf{0} & \mathbf{N}_\Phi^{-1} \end{vmatrix}, \quad \text{(hypermatrix)} \tag{34b}$$

$$\mathbf{B}^{-1} = \begin{vmatrix} \mathbf{M} & \mathbf{0} & -v_M\mathbf{M} \\ \mathbf{0} & \mathbf{M} & \mu_M\mathbf{M} \\ -v_M\mathbf{M} & u_M\mathbf{M} & \mathbf{I}_0 \end{vmatrix} \quad \text{(hypermatrix)} \tag{34c}$$

and $\mathbf{q}$ is the hypervector including the coordinates of the displacement $(\mathbf{u}, \mathbf{v}, \boldsymbol{\Phi})$.

This directly yields

$$\mathbf{Eq} = \omega^2 \mathbf{ABq}\,.$$

(Here $\mathbf{E}$ is the unit hypermatrix and $\mathbf{A}$ is the inverse of the hypermatrix $\mathbf{A}^{-1}$. Thus the inversion of the matrices $\mathbf{N}_u$, $\mathbf{N}_v$, $\mathbf{N}$ may be evitable.)

Introducing further the expressions $\mathbf{A} \cdot \mathbf{B} = \mathbf{C}$ hypermatrix and $\lambda = 1/\omega^2$ (since the computer presents the results on the basis of the root of maximum value of the equation, but from the viewpoint of the theory of vibration, the vibration of the smallest frequency and the associated roots are of interest) we obtain

$$(\mathbf{C} - \mathbf{E}\lambda)\,\mathbf{q} = 0\,.$$

From this the eigenvalue of $\mathbf{C}$ may be calculated.

5. Approximate method for the determination of natural frequency

According to the method described above the natural frequency of the buildings of slab skeleton may be calculated without any implications, but in case of multistorey buildings, owing to the great number of equations and unknown values, the problem may be economically solved only by computer. To eliminate this inconvenience an approximate calculation will be described by means of which even in case of a number of storeys a good approximate

value may be found without any implications in the calculation. The calculation is carried out by means of the Dunkerley equation [11] which, in lieu of determining the natural frequency of an oscillating system containing masses of "n" number, simplifies the problem for the determination of the natural frequency of systems of "n" number, each containing only one single mass. According to the relation

$$\frac{1}{\omega^2} = \sum_{i=1}^{n} \frac{1}{\omega^2} . \tag{35}$$

Here, ω_i is the imaginary natural angular frequency of the beam of the negligible mass, in that case, if only the ith mass is acting on the beam. The result obtained is smaller by 5 to 15 per cent than the exact value.

In our case we should proceed by calculating the natural angular frequency for a building having only a single storey and this storey changes according to the actual storeys of the building. Namely, in this case we have always to do with a system of a single mass performing a coupled vibration, to which we can apply the set of equations, but written in an appearance significantly simpler, because in a single-mass system the restoring dyname is given by the product of the spring constant and displacement. In turn, the spring constant is equal to the numerical value of the dyname causing the unit rotation which has already been determined in Chapter 2; this is in the case of the displacement p_v or p_ν (see Formula 13) and in the case of rotation H (see Formula 21).

On the grounds of the above stated, for the free vibration of the single-mass system we can write down the following set of equations

$$\begin{aligned}
&(p_{ui} - m_i \omega^2) u_i + \omega^2 v_M m_i \Phi_i = 0 , \\
&(p_{vi} - m_i \omega^2) v_i + \omega^2 v_M m_i \Phi_i = 0 , \\
&\omega^2 v_M m_i u_i - \omega^2 u_M m_i v_i + (M_i - I_{0i} \omega^2) \Phi_i = 0 .
\end{aligned} \tag{36}$$

The homogeneous set of equation has a solution other than zero only in that case if the determinant formed of its coefficients is equal to zero, thus

$$\begin{vmatrix}
(p_{ui} - m_i \omega^2) & 0 & \omega^2 v_M m_i \\
0 & (p_{vi} - m_i \omega^2) & -\omega^2 u_M m_i \\
\omega^2 v_M m_i & -\omega^2 u_M m_i & (M_i - I_{0i} \omega^2)
\end{vmatrix} = 0 . \tag{36a}$$

Expanding the determinant we obtain for ω^2 the following equation of the third degree

$$a\omega^6 + b\omega^4 + c\omega^2 + d = 0 \tag{37}$$

where

$$a = m_i (u_M^2 m_i + v_M^2 m_i - I_{0i}),$$
$$b = m_i [I_{0i}(p_{ui} + p_{vi}) - m_i (p_{ui} u_M^2 + p_{vi} v_M^2) + m_i M_i],$$
$$c = -[m_i M_i (p_{ui} + p_{vi}) + p_{ui} p_{vi} I_0], \tag{37a}$$
$$d = p_{ui} p_{vi} M_i .$$

It follows from the symmetry of the determinant that the roots of the equations are real values. For us, only the angular frequency associated with the fundamental vibration, $\omega_{\min}$ is of interest and thus in case of storeys of a number of n', n different from $\omega_{\min}$'s are obtained, from which the natural angular frequency of the building may be determined with the aid of Equation (35).

REFERENCES

1. Bosznay, Á.: Technical Theory of Vibration (in Hungarian). Műszaki Könyvkiadó, Budapest 1962.
2. Egupov, V. K.: Raszcset zdanij na procsnoszt' usztojcsivoszt' i koljebanija (Design Calculation of Strength, Stability and Vibration of Buildings), Kiev 1965
3. Forbat, N.: Analytische Mechanik der Schwingungen, Berlin 1966
4. Gere, J. M.—Lin, Y. K.: Coupled Vibrations of Thin Walled Beam of Open Cross-Section. *Journal of Applied Mechanics* (1958), Vol. 25, No. 3. 373—378
5. Harris, C. M.—Cred, Ch. E.: Shock and Vibration Handbook. McGraw-Hill Book Comp.
6. Hildebrand, F. B.: Methods of Applied Mathematics. New York, 1952
7. Kaliszky, S.: Calculation of Buildings of Bearing Walls Subject to Horizontal Forces (in Hungarian). *Magyar Építőipar* (1962) 12. 541—548.
8. Major, S.: Design and Calculation of Foundations of Machines and Turbines (in Hungarian) Műszaki Könyvkiadó Budapest, 1956
9. Petur, A.: Theory of Strength of Aeroplanes. Tankönyvkiadó (in Hungarian), Budapest 1952
10. Rosman, R.: Beitrag zur Untersuchung des Zusammenwirkens von waagerecht belasteten Wänden und Stockwerkrahmen bei Hochbauten. *Beton- und Stahlbetonbau.* (1963) 6. 272—279
11. Timoshenko, S. P.—Young, D. H.: Vibration Problems in Engineering. New York, 1955
12. Timoshenko, S. P.—Young, D. H.: Advanced Dynamics, New York 1948
13. Vértes, Gy.: Theory of Vibration. Lecture Notes (in Hungarian). Engineering Retraining Course, Budapest 1965.

Eigenfrequenz der horizontalen Schwingungen von Hochgebäuden mit Plattenrahmen. Bei Hochgebäuden mit Plattenskelett treten, wenn keine zweifache Symmetrie besteht, die horizontalen freien Schwingungen in der Form der sog. »wilden« Schwingungen auf. Dies bedeutet, daß gleichzeitig Biege- und Torsionsschwingungen entstehen. Die Abhandlung behandelt ausführlich die Ermittelung der Bewegungsmerkmale der erwähnten Schwingung und nach der Aufstellung des Differentialgleichungsystems beschreibt sie eine exakte Lösungsmethode, die auch für Maschinenkalkül anwendbar ist, und ein Näherungsverfahren, das einfachere Berechnungen erfordert.

Число собственных горизонтальных колебаний высотных зданий пластинчатого каркаса *(Д. Вертеш).* У высотных зданий пластинчатого каркаса без двунаправленной симметрии горизонтальные по своему направлению свободные колебания проявляются в виде т. н. «связанной» форме. Это означает то, что одновременно возникают изгибающие крутящие колебания. В работе детально рассматривается определение характеристик движения указанных колебаний и после выведения системы дифференциальных уравнений для его решения описывается приближенный метод, пригодный для машинного вычисления и являющийся точным и проще вычислимым.

Acta Technica Academiae Scientiarum Hungaricae, Tomus 68 (3—4), pp. 383—402 (1970

VERDICHTUNGSTECHNISCHE BEITRÄGE ZUR ENTWURFSTHEORIE DER KIESBETONE

J. CSUTOR*

[Eingegangen am 26. Sept. 1968]

Aufgrund der Versuche, die zur numerischen Ermittelung der Arbeitsmethode des Nadelrüttlers und der Kennwerte der mit diesem Letztgenannten durchgeführten Verdichtung angestellt worden waren wurde festgestellt, daß man eine physikalische Größe finden kann, die als Ergänzung der Betonentwurfes zur Regelung der Betonverdichtung eine Niederlegung von Grundprinzipien ermöglicht. Diese physikalische Größe ist die *spezifische Verdichtungsarbeit.* Kennt man schon die spezifische Verdichtungsarbeit, so können die Bedingungen der Reproduzierbarkeit für alle Rüttelmethoden festgestellt werden, wenn man bei der Herstellung der Probekörper der optimalen Betonfestigkeit die spezifischen Verdichtungsarbeit zuordnet.

1. Einleitung

Der Beton ist ein aus Zement, Wasser, Sand und Grobzuschlagstoff, aus Luft und eventuell aus Zusatzmitteln zusammengesetztes heterogenes Material, dessen Zusammensetzung den vorgeschriebenen Eigenschaften (z. B. Druckfestigkeit, Wasserdichte) entsprechend — mit Hilfe von Formeln, Diagrammen, Rechenschieber und Tabellen — nach allgemein bekannten Verfahren entworfen werden kann.

Die Eigenschaften des Betons werden — außer seiner Zusammensetzung — durch die Mischung, Beförderung, Verdichtung, Erhärtung und Nachbehandlung beeinflußt. Die Entwurfsbehelfe ziehen die Einflüsse dieser Faktoren entweder gar nicht, oder nur indirekt in Betracht, indem sie einen porenfreien Beton oder einen bestimmten Luftinhalt annehmen (die Feretsche, Bolomey—Palotás'sche Formel). Das ist aber vielmehr eine Umgehung der tatsächlichen Berücksichtigung der Verdichtung. Daß die gegenwärtige Regeln des Betonentwurfes keine Anleitungen für den Verdichtungsprozeß geben konnten, kann durch verschiedene Gründe erklärt werden, die wir im folgenden zusammenfassen können:

a) Sowohl die Komponenten des Betons wie auch die Parameter der Schwingungen können sich in einem so breitem Intervall ändern, daß die eindeutige Feststellung einer Beziehung zwischen den Parametern des Betons und des die erregenden Schwingungen herstellenden Verdichtungsgerätes sehr schwierig wird.

* J. Csutor, Villányi-u. 55—65, *Budapest XI*, Ungarn.

b) Die Betontechnik behandelte das Problem nur von der Betonseite her, und deshalb hat die Rolle der erregenden Schwingungen sowie die der sehr verschiedenen Betriebsarten in den Untersuchungen nur eine untergeordnete Bedeutung erhalten.

c) Es wurde versucht, eine Beziehung zwischen einigen beliebig ausgewählten Schwingungskennwerten und den Parametern des Betons herzustellen.

In der vorliegenden Abhandlung wird aufgrund einer konkreten Messungsserie und durch folgerichtige Anwendung von einigen Grundprinzipien ein gangbarer Weg vorgeführt, einerseits zur Ergänzung des unvollständigen Betonentwurfes, andererseits zur Beseitigung der bisherigen Widersprüche.

2. Beschreibung des Versuches

Ein Gestell (Bild 1) hält den Rüttelkopf des Nadelrüttlers HV11 mit Hilfe der biegsamen Antriebswelle in vertikaler Lage. Die wichtigsten Betriebskennwerte des Rüttelkopfes sind in der Tafel 1 angegeben. Der Rüttel-

Tafel 1

Betriebskennwerte des Rüttelkopfes des Rüttlers HV11

Rüttelkopf-durchmesser $2R_1$ cm	Länge des Rüttelkopfes H cm	Drehzahl n min^{-1}	Winkelgeschwindigkeit ω s^{-1}	Kinetisches Moment $M = G_0 \cdot e$ cmkp	Zentrifugalkraft C_0 kp	Leerlaufamplitude A_{il} cm
6,8	$3{,}2 \cdot 10$	$6{,}5 \cdot 10^3$	$6{,}8 \cdot 10^2$	$7{,}54 \cdot 10^{-1}$	$3{,}5 \cdot 10^2$	$5{,}15 \cdot 10^{-2}$

kopf befindet sich in der geometrischen Mittellinie einer hölzernen Kiste, deren obere Kante und das obere Ende des Rüttelkopfes in gleichem Niveau liegen. Die Kiste wird mit Beton gefüllt, der Beton abgeflächt und der Rüttler in Bewegung gesetzt. In dieser Anordnung war der Versuch eine erweiterte Fortsetzung eines früheren Versuches, der sich allein auf die Ermittelung der Änderungstendenz der Parameter beschränken konnte. Unter der Wirkung der Rüttelung entsteht ein dichter, mit der Achse des Rüttelkopfes konzentrischer, kreiszylindrischer Betonkörper.

Mit Hilfe der Versuche wollten wir feststellen

a) die Gestaltung der den Verdichtungsgrad kennzeichnenden Betonparameter und deren Änderungstendenz (die betreffenden Parameter sind: das Frischbetonraumgewicht γ, der Verdichtungskoeffizient β und die zur meßbaren Volumänderung notwendige Zeit),

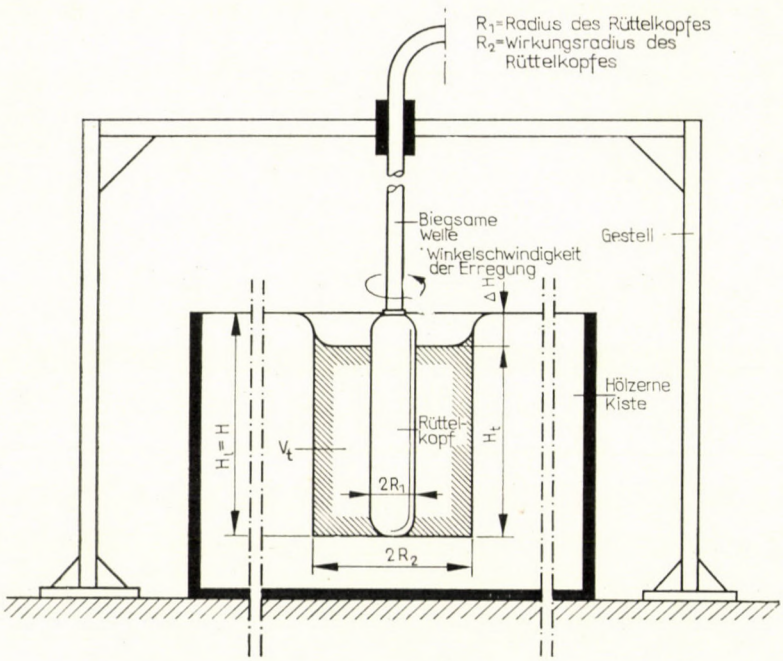

Bild. 1. Versuchsanordnung

b) die Änderungen dieser Größen in Abhängigkeit von den verschiedenen Betongüten,

c) einen die Verdichtung zahlenmäßig kennzeichnenden etwaigen Kennwert.

Der Zementgehalt Z der in Ungarn üblichen Kiesbetonarten beträgt

$$250\ \text{kpm}^{-3} \leq Z \leq 500\ \text{kpm}^{-3}; \tag{1}$$

deshalb haben wir zu den Versuchsbetonen einheitlich 350 kp Zement dosiert. Dieses Mischungsverhältnis kann als Mittelwert betrachtet werden, und sichert zur Extrapolation eine sehr vorteilhafte Basis. Der Zementgehalt spielt auch vom Gesichtspunkt der Verdichtungstechnik aus eine wichtige Rolle, da er den Wassergehalt des Betons entscheidend beeinflußt.

Wir haben den Beton in drei — in der Praxis am häufigsten benutzten — Güteklassen untersucht, die im folgenden mit den *maximalen Korngrößen* bezeichnet werden; die entsprechenden Zusammensetzungen sind in den Bildern 2, 3 und 4 wiedergegeben. Der Wasserzementwert wurde in jeder Kategorie zwischen breiten Grenzen variiert, und dem gesetzten Ziele entsprechend haben wir die vom verdichtungstechnischen Gesichtspunkt aus wichtigen Parameter gemessen und danach gerechnet.

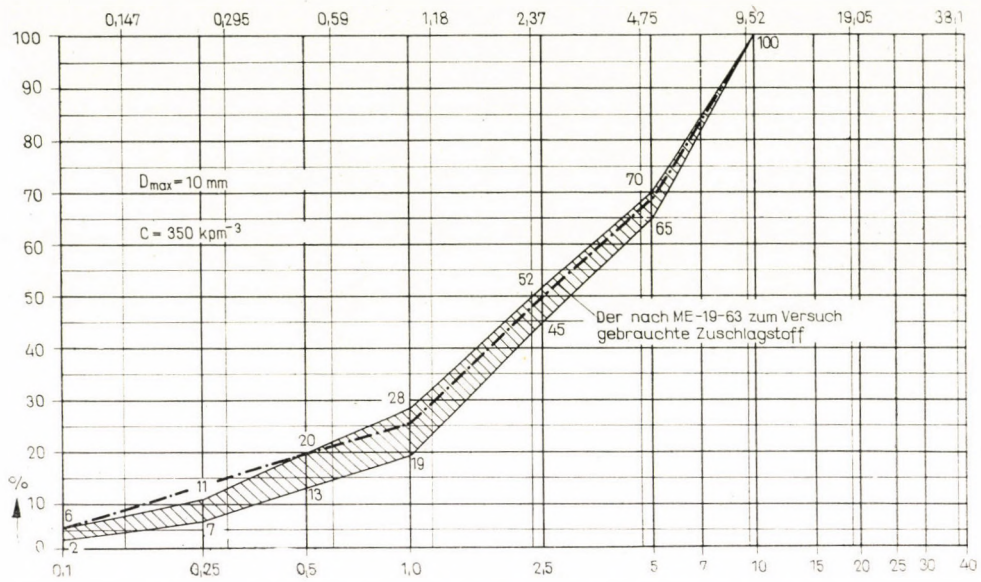

Bild 2. Der nach ME—19—63 zum Versuch gebrauchte Zuschlagstoff

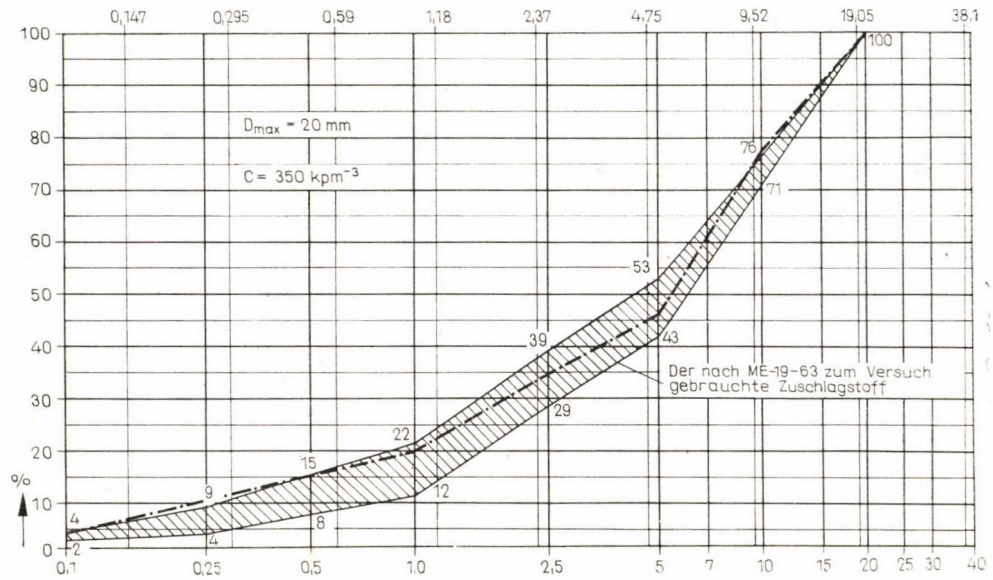

Bild 3. Der nach ME—19—63 zum Versuch gebrauchte Zuschlagstoff

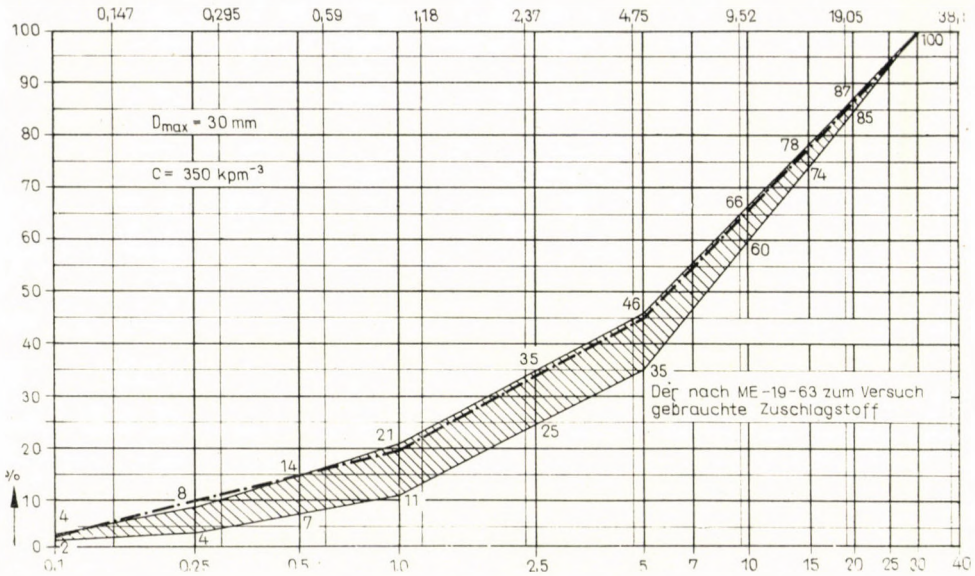

Bild 4. Der nach ME—19—63 zum Versuch gebrauchte Zuschlagstoff

3. Die gemessenen und die gerechneten Kennwerte

3.1. *Das lose Betonvolumen und der Verdichtungskoeffizient*

Für unsere Erörterungen ist es erforderlich, den Begriff des losen Volumens zu definieren. Zwischen der Betonmischmaschine und dem Bauplatz gibt es immer eine bestimmte Entfernung, die durch eine Beförderungsanlage überbrückt werden muß. Die Beförderung kann den aus dem Mischer in losem Zustand erhaltenen Beton weiter auflockern, oder verdichten oder gar keinen Einfluß auf die Dichte des Betons ausüben. Demnach werden wir unter dem Ausdruck »loser Zustand« die Dichte verstehen, die im Mischer in dem Moment gemessen wird, wenn die Frischbetonmischung den homogenen Zustand erreicht. Wir betrachten die Betonmischung für homogen, wenn in der durch beliebige Koordinaten bestimmten Raumeinheit das Verhältnis der Betonkomponenten im statistischen Sinne konstant ist.

Nach Ermittelung des losen Volumens des Frischbetons wollen wir nun den Begriff des Verdichtungskoeffizienten auslegen, den wir als Quotienten des losen und des dichten Betonvolumens, bzw. der denselben zugehörigen und proportionalen Höhenwerte angeben:

$$\beta = \frac{V_l}{V_d} = \frac{H_l}{H_d} > 1 \,. \tag{2}$$

In unseren Versuchen ist es zweckmäßig, die Höhe (in cm) als lose Schichthöhe des Betons anzunehmen, d. h. (Bild 1),

$$H = H_l$$

Nach Deutung des losen Zustandes und des Verdichtungskoeffizienten haben wir das Oberflächeneinsinken ΔH (Bild 1) gemessen, wonach wir die Verdichtungskoeffizienten berechnen konnten. Die gefundenen Werte sind in Tafel 2 wiedergegeben.

Tafel 2

Werte der Verdichtungskoeffizienten in Abhängigkeit vom Wasserzementwert

D_m mm	Wasserzementwerte							
	0,32	0,36	0,40	0,44	0,48	0,52	0,56	0,60
10			1,379	1,269	1,212	1,111		
20		1,355	1,290	1,166	1,066	1,1025		
30	1,292	1,212	1,142					

3.2. *Das benutzte Maßsystem*

Da wir den Verdichtungseffekt zahlenmäßig nur dann charakterisieren können, wenn die kennzeichnende Größe sowohl die wichtigen Parameter des verdichteten Betons als auch die des Rüttlers enthält, müssen zugleich maschinelle und betontechnische Größen in denselben Formeln vorkommen. Dabei ist es der Einfachheit halber erforderlich, daß die numerischen Ergebnisse aus den Formeln leicht erhalten werden können; deshalb ist es zweckmäßig, das Gewicht immer in kp, die Länge in cm und die Zeit immer in Sekunden zu messen. Die Masse ist also eine aus dem Gewicht (= Kraft) und der Schwerkraftbeschleunigung, als deren Quotient abgeleitete Größe.

3.3. *Die zur meßbaren Volumänderung erforderliche Zeitdauer*

Der Prozeß der Verdichtung kann in zwei große Phasen zerlegt werden. Diese sind: die Phase der *meßbaren* (= bleibenden) und die der *nicht meßbaren* (= elastischen) Volumänderungen. Hier ist zu bemerken, daß das Kriterium »nicht meßbar« derart gedeutet werden soll, daß wir die Meßverfahren, die die elastischen Verformungen registrieren können, ausschließen, da sie einerseits vom Gesichtspunkt der Praxis aus betrachtet keine Bedeutung haben, andererseits, außerordentlich kostspielig und kompliziert sind. Es sei

t^* die auf die meßbaren, t_1 auf die elastischen Verformungen angewandte Zeit, dann gilt für die ganze Dauer der Verdichtung, daß

$$t = t^* + t_1 = t^* + \xi_1 \cdot t^* = t^*(1+\xi),$$

worin ξ_1 ein Faktor ist, dessen Wert nur im Laufe der Verfertigung der Probekörper bestimmt werden kann.

Der Zweck unserer Versuche war nur die Ermittelung der vorerwähnten Zeiträume t^*. Die für dieselben erhaltenen Werte sind in Tafel 3 angeführt.

Tafel 3

Die zur meßbaren Volumänderung notwendigen t^* Zeiträume als Funktion des Wasserzementwertes

D_m mm	Wasserzementwerte							
	0,32	0,36	0,40	0,44	0,48	0,52	0,56	0,60
10			$1 \cdot 10^2$	$3 \cdot 10$	$1{,}6 \cdot 10$	6,5		
20		$4{,}5 \cdot 10$	$2{,}8 \cdot 10$	$1{,}4 \cdot 10$	$1{,}05 \cdot 10$	6		
30	$1{,}2 \cdot 10^2$	$2 \cdot 10$	$1 \cdot 10$					

3.4. *Raumgewicht des Betons*

Aus dem sich um den Nadelrüttler ausgebildeten dichten Betonzylinder haben wir mit einem unten verschärften Rohrstück einen Betonblock von 1 dm^3 herausgenommen und aus diesem das Raumgewicht des verdichteten Frischbetons ermittelt. Im unseren Maßsystem ist dessen Einheit $kpcm^{-3}$. Tafel 4 zeigt die gewonnenen Werte.

Tafel 4

Raumgewicht des verdichteten Frischbetone $\gamma(kpcm^{-3})$ als Funktion des Wasserzementwertes

D_m mm	Wasserzementwert							
	0,32	0,36	0,40	0,44	0,48	0,52	0,56	0,60
	$\cdot 10^{-3}$							
10			2,36	2,32	2,27	2,24		
20		2,41	2,39	2,35	2,30	2,25		
30	2,48	2,44	2,40					

3.5. *Wirkungsradius des Rüttelkopfes*

Nach Ingangsetzen des Rüttlers beginnt der Beton auf einer gut abgrenzbaren Kreisfläche einzusinken, er verdichtet sich allmählich, und auf diese

Fläche scheidet sich Wasser aus, die Fläche wird glänzend. Unter dem Wirkungsradius des Rüttelkopfes versteht man die Entfernung R_2 von der Mittellinie des Rüttelkopfes, über die der Beton auch noch nach beliebig langer Zeit nicht verdichtet wird. Diese Entfernung *wächst* im allgemeinen *nicht* nach der Beendigung der meßbaren Volumänderung, d. h., der Wirkungsradius ist gleich dem, der sich unter der zur meßbaren Volumänderung notwendigen Zeitdauer ausgebildet hat. Die Wirkungsradien sind in Tafel 5 angegeben.

Tafel 5

Die Wirkungsradien R_2 (cm) als Funktion des Wasserzementwertes

D_m mm	Wasserzementwert							
	0,32	0,36	0,40	0,44	0,48	0,52	0,56	0,60
10			7	$1{,}6 \cdot 10$	$2{,}3 \cdot 10$	$2{,}9 \cdot 10$		
20		$1{,}2 \cdot 10$	$1{,}8 \cdot 10$	$3{,}0 \cdot 10$	$4{,}2 \cdot 10$			
30	4	$1{,}4 \cdot 10$	$3{,}0 \cdot 10$					

4. Folgerungen

4.1. *Der Verdichtungskoeffizient und das Raumgewicht des Betons*

Untersucht man die erhaltenen Werte eingehend, so können wir feststellen, daß

a) die Werte der Verdichtungskoeffizienten — ähnlich den Raumgewichtswerten — durch ein lineares Funktionsdiagramm sehr gut, mit sehr geringem Fehler angenähert werden können. Diese den verschiedenen Werten von D_m zugehörigen Geraden sind gleichlaufend (parallel);

b) im Falle eines Zuschlagstoffes von kontinuierlicher Kornverteilung der zu demselben Wasserzementwert gehörige Verdichtungskoeffizient mit der Zunahme von D_m abnimmt,

c) im Falle der Zunahme von D_m der Wasserzementwert, wo $\beta = 1$, abnimmt; d. h., die obere Grenze der Verdichtbarkeit herabgesetzt wird. Wenn nämlich

$$H_l = H_d$$

dann ist gemäß unserer Definition $\beta = 1$, und *der Beton kann auf Kosten der Volumänderung nicht verdichtet werden.*

d) Im Falle eines Nadelrüttlers — jedoch auch irgendeines Rüttelgerätes — gibt es ein Minimum des Wasserzementwertes, worunter der Beton mit dem gegebenen Rüttler (im vorliegenden Falle mit dem Nadelrüttler) wirt-

schaftlich nicht verdichtet werden kann. Diese untere Grenze zeigt sich derart, daß der Rüttelkopf um sich einen Hohlraum ohne Verdichtung erzeugt.

e) Die obere und untere Grenzen bestimmen den *Bereich der Verdichtbarkeit.* Aufgrund unserer Versuche können wir feststellen, daß dieser Bereich, von dem Wasserzementwert abhängig, sich gegen den niedrigeren Wert desselben verschiebt, wenn D_m zunimmt.

f) Nimmt D_m zu, so nimmt der lose Absolutrauminhalt des Betons ab.

g) Mit der Zunahme des Wasserzementwertes, vermindert sich der Rauminhalt des Frischbetons.

Aufgrund dieser Folgerungen können wir sowohl analytisch als auch graphisch die Geradenscharen der Verdichtungskoeffizienten und Raumgewichte erstellen. Für die Verdichtungskoeffizienten erhalten wir

$$[\beta]_{D_m=10} = 2{,}1 - 1{,}96\, w/z\,, \tag{4}$$

$$[\beta]_{D_m=20} = 2{,}01 - 1{,}96\, w/z \tag{5}$$

und

$$[\beta]_{D_m=30} = 1{,}9 - 1{,}96\, w/z \tag{6}$$

und für die Raumgewichte

$$[\gamma]_{D_m=10} = (2{,}740 - 0{,}982\, w/z)\cdot 10^{-3} \tag{7}$$

$$[\gamma]_{D_m=20} = (2{,}765 - 0{,}982\, w/z)\cdot 10^{-3} \tag{8}$$

und

$$[\gamma]_{D_m=30} = (2{,}780 - 0{,}982\, w/z)\cdot 10^{-3}. \tag{9}$$

Die erhaltenen Geradenscharen wurden in einem Nomogramm (Bild 5) aufgetragen. Diese Geradentafel gibt einerseits der Wirklichkeit sehr naheliegende Werte, andererseits erstellt sie die zur Regelung der Verdichtung unerläßlich erforderlichen zwei Werte in einer leicht behandelbaren Form.

4.2. *Die zur meßbaren Volumänderung notwendige Zeit und der Wirkungsradius des Rüttelkopfes*

Diese Parameter sind als zusammengehörige Wertepaare im Bild 6 dargestellt. Hier fügen wir die folgende, allgemeine Bemerkung hinzu:

a) Verdichtet man lose Betone von gleichem Zementgehalt und Wasserzementwert, und bereitet man diese mit Anwendung von Zuschlagstoffen kontinuierlicher Kornverteilung zu, so wird der Wirkungsradius des Rüttelkopfes mit der Zunahme von D_m zunehmen und die zur meßbaren Volumänderung erforderliche Zeit sich verkürzen.

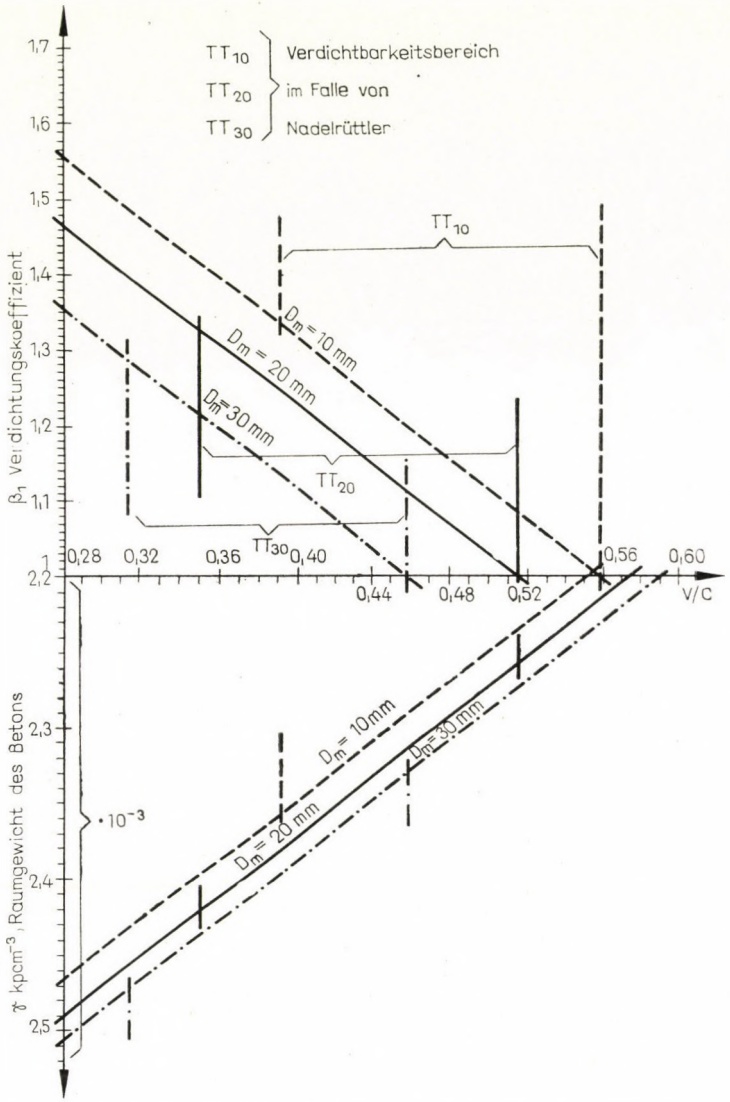

Bild 5. **Die zusammengehörigen Werte des Verdichtungskoeffizienten und des Raumgewichtes als Funktion des Wasserzementwertes**

β_1: **Verdichtungskoeffizient,**
γkpcm^{-3}, **Raumgewicht des Betons**

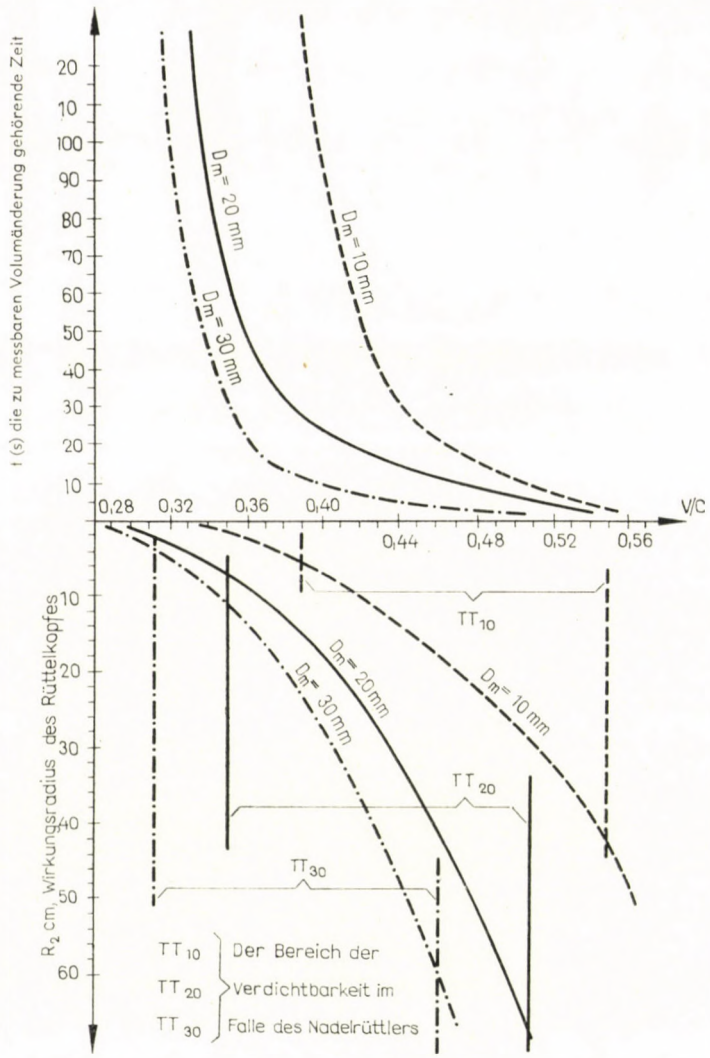

Bild 6. Die zusammengehörigen Werte der zur meßbaren Volumänderung erforderlichen Zeit und des Wirkungsradius des Rüttelkopfes in Abhängigkeit vom Wasserzementwert

$\overset{*}{t}$ (s) die zur meßbaren Volumänderung erforderliche Zeit, R_2 cm, Wirkungsradius des Rüttelkopfes,

5. Die spezifische Verdichtungsarbeit

In unseren Bestrebungen, den Verlauf der Verdichtung zahlenmäßig zu bestimmen, können wir von folgenden Feststellungen ausgehen:

a) Die Verdichtung ist ein Arbeitsaufwand, im Laufe dessen eine gegebene lose Betonmenge sich in eine gegebene dichte Betonmenge umwandelt.

b) Für die Dichte und damit auch für die Betonfestigkeit gibt es einen Grenzwert, worüber hinaus sie auf Kosten von keinem weiteren Arbeitsaufwand gesteigert werden können.

c) Sind zwei Betonklassen den betontechnischen Regeln gemäß identisch, so erfordern beide — unabhängig von den geometrischen Dimensionen — die gleiche spezifische Verdichtungsarbeit.

d) Der Grenzwert der Dichte kann mit den verschiedensten Schwingungsparametern bei verändlicher Zeitdauer erreicht werden, während der spezifische Arbeitsaufwand gleich bleibt. Es muß aber vorausgesetzt werden, daß es für die Schwingungsparameter solche untere Grenzwerte gibt, worunter die Zunahme der anderen Parameter schon keine Kompensationswirkung ausübt: die Verdichtung findet nicht statt.

Wenn wir den spezifischen Arbeitsaufwand der Verdichtung kennzeichnen können, dann kann einerseits entschieden werden, ob der zur erreichenden Festigkeit verwendete Arbeitsaufwand genügt, andererseits, ob infolge der Feststellung unter a) im Zusammenhang mit der Identität die Bedingungen der Reproduktion hergestellt werden können.

Es kann nachgewiesen werden [1, 4], daß der Arbeitsaufwand des erregten Rüttelkopfes des Nadelrüttlers (im allgemeinen, der von jeder lotrechtachsigen und in der horizontalen Ebene wirkenden Erregung) durch den Ausdruck

$$\lambda = 10^{-1} \frac{C_0 \, v_0 \, t\beta}{V_l(\beta - 1)}, \tag{10}$$

gekennzeichnet werden kann,

worin

λ [Ws/cm³ Volumenverminderung]	=	der zur Verdichtung des Betons erforderliche Arbeitsaufwand.
C_0 [kp]	=	die resultierende Erregungskraft (= Zentrifugalkraft)
v_0 [cms^{-1}]	=	die maßgebende Maximalgeschwindigkeit des für einmassig betrachteten erregten Systems
t [s]	=	Verdichtungsdauer
β	=	das Verdichtungsverhältnis des Betons nach (2)
V_l [cm³]	=	der lose Betonrauminhalt.

Es kann einfach nachgewiesen werden [2], daß der Ausdruck (10) in seinem Inhalt gleich der folgenden Beziehung ist:

$$p_d = \frac{C_0 v_0 t\beta}{V_l(\beta-1)} \text{ kpcm}^{-2}, \tag{11}$$

die wir infolge ihrer Maßeinheit mit dem Namen »dynamischer Druck« benennen können. Die Beziehung (11) ist vorteilhafter als die Formel (10), denn einerseits ist sie einfacher zu behandeln, andererseits mißt auch p_d — wie schon bemerkt wurde — Arbeitsaufwand. Sie ist also erstens eine Wirkung messende Größe, und kein Zustandskennwert. Dies ist auch daraus ersichtlich, daß sie der Zeit proportional ist und infolgedessen zur Kennzeichnung eines in der Zeit konstanten Zustandes (z. B. der Raumspannung) nur eine beschränkte Gültigkeit haben kann.

Nun ist zu erklären, was wir unter maßgebender Maximalgeschwindigkeit eines einmassigen erregten Systems verstehen. Betrachtet man außer der Frequenz die Amplitude als Energieträger der Erregung, so können wir die Tatsache, daß ein wohlbestimmter Wirkungskreis um den Rüttelkopf ausgebildet werden kann, nur in dem Sinne verstehen, daß die sich in Form einer Wellenbewegung fortpflanzende Energie über diesen Wirkungskreis nicht mehr hinaus gelangen kann: an der durch den Wirkungskreis bestimmten Grenze ist die Amplitude das *zur Verdichtung des Betons erforderliche Minimum.* Vom Gesichtspunkt der Verdichtung aus ist also der Rauminhalt des durch den Wirkungsradius und die Rüttelkopflänge definierten Zylinders maßgebend. Innerhalb dieses Zylinders ergibt die Bewegung des Rüttelkopfes eine Wellenbewegung von longitudinalem Charakter, deren Amplitude sich von der Mittellinie des Rüttelkopfes bis zum Maximum des Wirkungsradius allmählich vermindert. Die Verminderung der Amplitude kann mit Hilfe einer Exponentialfunktion ausgedrückt werden, also können wir die das System kennzeichnende Mittelamplitude mit ausreichender Genauigkeit ermitteln.

Der Einfachheit halber betrachten wir für diesen Mittelwert die Amplitude, die derart berechnet wird, daß wir den dichten, sich innerhalb des Wirkungsradius befindlichen Betonzylinder als einen *mit dem Rüttelkopf synchron mitschwingenden steifen Körper annehmen.* Mit Hilfe der gemessenen Wirkungsradien und aufgrund des Prinzips der Mitschwingung, unter Berücksichtigung von (11) können einfach zu jeder Betonkategorie die dynamischen Drücke, die den zur Verdichtung (im vorliegenden Falle: nur zur meßbaren Volumänderung) erforderlichen spezifischen Arbeitsaufwand messen, berechnet werden. Die dynamischen Drücke sind im Bild 7 dargestellt, woraus wir die folgenden Gesetzmäßigkeiten ersehen können:

a) Mit der Zunahme des Wasserzementwertes nimmt der dynamische Druck, d. h. der spezifische Arbeitsaufwand für die Verdichtung des Betons ab.

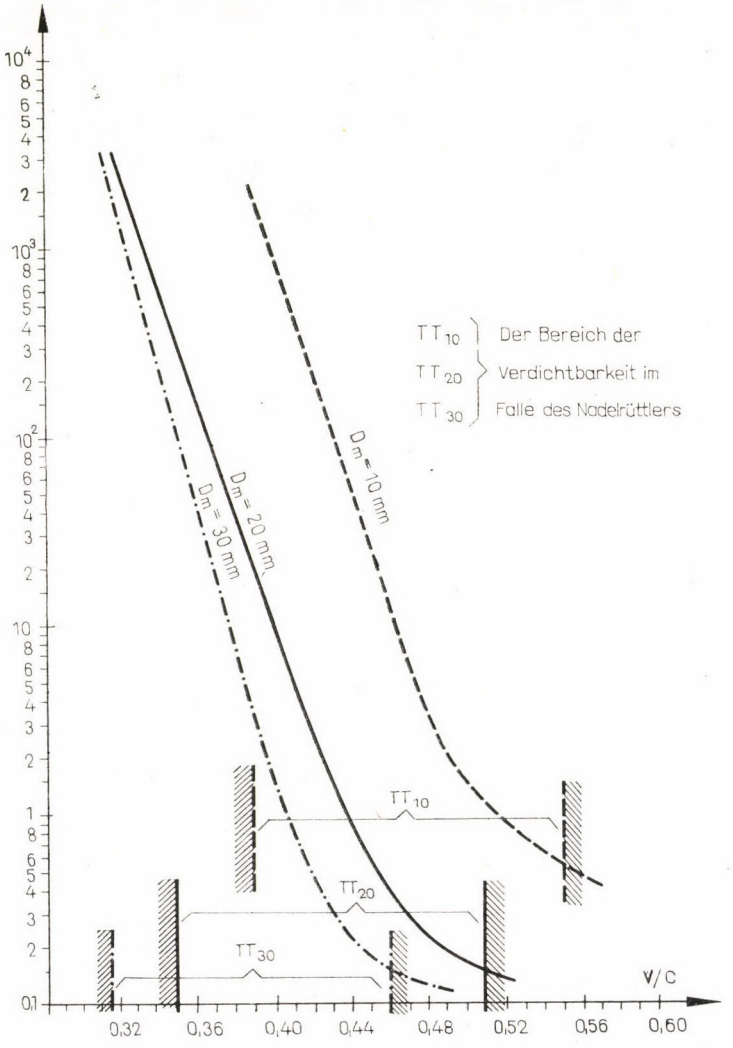

Bild 7. Die den spezifischen Arbeitsaufwand messenden dynamischen Drücke als Funktion des Wasserzementwertes

b) Mit der Zunahme der maximalen Korngröße des Zuschlagstoffes weist der spezifische Arbeitsaufwand für die Verdichtung des Betons eine fallende Tendenz auf.

6. Anwendungen

Wir behaupten also, daß (11) den spezifischen Arbeitsbedarf der Betonverdichtung charakterisiert, der als ein Materialkennwert des untersuchten Betons betrachtet werden kann. Aufgrund der unter den Abschnitten 5a und b im Zusammenhang mit dem spezifischen Arbeitsbedarf gemachten Fetstellungen können wir aus den beschriebenen Versuchsergebnissen die folgende dreifache Folgerung ziehen:

a) Wir können die wichtigsten Betriebskennwerte eines beliebigen Rüttelkopfes für dieselben Betone ermitteln, und damit nachweisen, daß einige konkrete Werte der unmittelbaren Schwingungskennzahlen vom Gesichtspunkt des Verdichtungserfolgs aus nicht ausschließlichen (ausgezeichneten) Charakters sind. Wenn wir nämlich, jeden wichtigen Kennwert des Rüttelkopfes sowie die sich auf dieselben Betone beziehenden Werte p_d, γ und β kennen, dann bleiben in (11) nur R_2 und t unbekannt. Die zu beantwortende Frage kann daher auf zweierlei Art gestellt werden: entweder fragt man (innerhalb welchen Wertes von R_2) in einer im voraus gegebenen Zeitdauer der erforderliche dynamische Druck p_d ermittelt werden kann, und dann kann die Antwort aufgrund von (11) durch die Umwandlung

$$R_2 = R_2(t) \tag{12}$$

einfach erhalten werden. Oder kann man auch fragen, in welcher Zeit innerhalb eines gegebenen R_2 der erforderliche p_d erreicht werden kann (vorausgesetzt, daß wir innerhalb des Bereiches der Verdichtbarkeit bleiben), und in diesem Falle kann die Antwort aufgrund von (11) durch eine Umwandlung nach

$$t = t(R_2) \tag{13}$$

gegeben werden.

b) Es besteht die Möglichkeit, die Betriebswerte eines anderen — beliebigen — Verdichtungsgeräts (Schwingtisch, Schalungs- oder Oberflächenrüttler) derart zu bestimmen, daß wir zu denselben Betonen dieselben p_d-Werte und damit denselben spezifischen Arbeitsaufwand koordinieren können. Dazu bringen wir ein willkürliches Beispiel, und zwar den Betriebsfall einer auf dem Schwingtisch frei aufliegenden Fertigungsform. Die Formel des dynamischen Druckes für diesen Betriebsfall ist

$$p_d = \frac{\gamma v_0 \cdot t}{\beta - 1} . \tag{14}$$

Wenn wir p_d, γ und β kennen, dann kann im Falle von gleichen Betonklassen die Umformung

$$v_0 = v_0(t) \tag{15}$$

mit Annahme der zur Verdichtung erforderlichen Zeit einfach durchgeführt werden. Betrachtet man die untersuchte Betriebsart für ein einmassiges System, so können aufgrund der Beziehungen

$$v_0 = v_0(M);\ v_0 = v_0(G_t) \quad \text{und} \quad v_0 = v_0(t) \tag{16}$$

die Kennwerte des Schwingtisches und der Verdichtung eindeutig ermittelt werden.

In diesen Beziehungen:

M [cmkp] = kinetisches Moment der Erregung des Schwingtisches,
G_t [kp] = das zu erregende Totalgewicht.

c) Wir sind in der Lage, zur Vervollständigung dem Betonentwurf im Zusammenhang mit der Verdichtung eindeutige Instruktionen geben zu können. Nach Feststellung der Dosierung der Betonkomponenten verfertigt man wie bekannt, die Probekörper (Würfel, oder Zylinder), und durch deren Zerstörung stellt man fest, ob die Zusammensetzung des untersuchten Betons die erwünschte Betonfestigkeit sichert. Im Falle von verneinendem Ergebnis wird die Dosierung korrigiert und es werden neue Probekörper unter Bruchversuch gezogen. Die ungarischen Normen schreiben das Stampfen zur Verdichtung der Probekörper vor. Doch kann diese Verdichtungsart durch die fünf verschiedenen Betriebsarten der Rüttelung *nicht reproduziert werden*.

Da wir den zur Verdichtung erforderlichen Arbeitsbetrag für alle Betriebsarten bestimmen, und die als Materialkennwert betrachteten p_d-Werte dem Bild 7 analog für beliebige Betriebsarten festsetzen können, leuchtet die Logik der nachstehenden Reihenfolge leicht ein:

1. Zum Abschluß des Betonentwurfes verdichtet man den Probekörper auf einem Schwingtisch, dessen wichtigste Verdichtungsparameter ein für allemal konstant sind; infolgedessen kann dieser Schwingtisch als Verdichtungsetalon betrachtet werden.

2. Verdichtet man die Probekörper mit $\lambda_1 < \lambda_2 < \lambda_3 \ldots$ zunehmenden spezifischen Arbeitsaufwänden, und wählt man nach dem Bruchversuch den Arbeitsaufwand, der schon die vorgeschriebene Betonfestigkeit liefert, d. h., die Funktionenreihen

$$p_d = p_d(\lambda_{\min})$$

und (17)

$$p_d = p_d(\sigma_0)$$

sollen ermittelbar werden. Bestimmen wir dabei die Betonkennwerte γ und β, so können wir Tabellen zusammenstellen, die mit den in dem Betonentwurf bisher gebrauchten Entwurfsbehelfen benutzt werden können und die Reihenfolge der Entwurfsschritte abschließen, indem sie die bisherigen Widersprüche beseitigen.

7. Prinzip der Mitschwingung und die Desowsche Formel

Unserer Meinung nach ist die Amplitude ein sehr wichtiger Schwingungskennwert vom Gesichtspunkt der Verdichtung aus betrachtet. Diese Tatsache wird auch durch die Desowsche Formel ausgedrückt, die zur Beschreibung des Betriebs von Nadelrüttlern auf der ganzen Welt gebraucht wird:

$$\frac{A_2}{A_1}\sqrt{\frac{R_1}{R_2}}\cdot\exp\left[-\frac{k}{2}(R_2-R_1)\right], \tag{18}$$

worin

R_1 [cm] = Radius des Rüttelkopfes,
R_2 [cm] = Wirkungsradius des Rüttelkopfes,
A_1 [cm] = Leerlaufamplitude (= Eigenamplitude) des Rüttelkopfes,
A_2 [cm] = Grenzamplitude, die in der dem Wirkungsradius entsprechenden Entfernung nachgewiesen werden kann,
e = Grundzahl des Napierschen Logarithmus,
k [cm^{-1}] = Dämpfungskoeffizient.

Für die Dämpfungskoeffizienten gibt Desow die in Tabelle 6 vorgeführten Werte.

(18) ist eine Beziehung von allgemeiner Gültigkeit, worin die Buchstabenbezeichnung auch derart — und richtig — erklärt werden kann, daß A_1 und A_2 die in den Entfernungen R_1 bzw. R_2 von der Achse des Rüttelkopfes auftretenden Amplituden sind. Trotzdem ist auch diese Formel nur eine Näherung der Wirklichkeit, da der Dämpfungskoeffizient k sich auf einen breiten Konsistenzbereich bezieht, innerhalb dessen sein Wert sich schon ändern kann. Die Desowsche Formel beweist aber auch die Tatsache, daß die Verdichtungsschwingungen sich auch in der von uns untersuchten *Etalon-Lage* des Nadelrüttlers (Bild 1) in der Form von gedämpften Longitudinalwellen fortpflanzen, wie es schon im Abschnitt 5 festgestellt worden ist. Daraus folgt, daß die um den Rüttelkopf ausgebildete dichte Betonmenge durch die Tatsache bestimmt ist, daß am Ende des Wirkungsradius die Amplitude unter den gegebenen Umständen sich auf jenen Minimalwert (= Grenzwert) vermindert, bei dem der gegebene Beton noch überhaupt verdichtet werden kann.

In dieser Deutung ermöglicht die Desowsche Formel, aufgrund der gemessenen Wirkungsradien Grenzamplituden zu berechnen. Dazu können die in Tafel 6 gegebenen Angaben verwendet werden. Die Tatsache, daß die Schwingungszahl des Nadelrüttlers um 8 Prozent größer als die in der letzten Rubrik der Tafel 6 ist, spielt augensichtlich keine Rolle: den Wert von k müssen wir mit Extrapolation nicht korrigieren. Die in der Tabelle befindlichen und die Konsistenz untersuchenden Kegeleindringwerte sind praktisch gleich dem von uns gemessenen Dichtbarkeitsbereiche.

Nach unserer Meinung muß man in der praktischen Anwendung der Theorie der Vibrationsverdichtung des Betons der wesentlichen Vereinfachung

Tafel 6

Die Dämpfungskoeffizienten k nach Desow

Minuten-schwingungs-zahl	Portlandzement Beton, wenn die Kegeleindringtiefe (cm)		
	0—1	2—4	4—6
$3 \cdot 10^3$	$1{,}3 \cdot 10^{-1}$	$1{,}1 \cdot 10^{-1}$	$7 \cdot 10^{-1}$
$4{,}5 \cdot 10^3$	$1{,}2 \cdot 10^{-1}$	$9 \cdot 10^{-2}$	$6 \cdot 10^{-2}$
$6 \cdot 10^{-3}$	$1{,}1 \cdot 10^{-1}$	$8 \cdot 10^{-2}$	$5 \cdot 10^{-2}$

Tafel 7

Die mit Hilfe der Desowschen Formel (D) und aufgrund der Mitschwingung berechneten Grenzamplituden (cm) (M)

D_m mm	Wasserzementwert				
	0,32	0,36	0,40	0,44	0,48
10 D			$3{,}45 \cdot 10^{-2}$	$1{,}91 \cdot 10^{-2}$	$1{,}52 \cdot 10^{-2}$
10 M			$5{,}15 \cdot 10^{-2}$	$1{,}88 \cdot 10^{-2}$	$7{,}32 \cdot 10^{-3}$
20 D		$2{,}31 \cdot 10^{-2}$	$1{,}29 \cdot 10^{-2}$	$1{,}30 \cdot 10^{-2}$	
20 M		$2{,}95 \cdot 10^{-2}$	$1{,}07 \cdot 10^{-2}$	$3{,}38 \cdot 10^{-3}$	
30 D	$3{,}45 \cdot 10^{-2}$	$1{,}91 \cdot 10^{-2}$	$1{,}52 \cdot 10^{-2}$		
30 M	$5{,}15 \cdot 10^{-2}$	$1{,}80 \cdot 10^{-2}$	$7{,}32 \cdot 10^{-3}$		

Tafel 8

Die arithmetischen Durchschnittswerte (cm), die mit Hilfe der Desowschen Formel (D) und nach dem Prinzip der Mitschwingung aus den Grenzamplituden und den Eigenamplituden des Rüttelkopfes berechnet wurden

D_m mm	Wasserzementwert				
	0,32	0,36	0,40	0,44	0,48
10 D			$4{,}3 \cdot 10^{-2}$	$3{,}53 \cdot 10^{-2}$	$3{,}33 \cdot 10^{-2}$
10 M			$5{,}15 \cdot 10^{-2}$	$3{,}40 \cdot 10^{-2}$	$2{,}92 \cdot 10^{-2}$
20 D		$3{,}73 \cdot 10^{-2}$	$3{,}22 \cdot 10^{-2}$	$3{,}27 - 10^{-2}$	
20 M		$4{,}05 \cdot 10^{-2}$	$3{,}11 \cdot 10^{-2}$	$2{,}74 \cdot 10^{-2}$	
30 D	$4{,}30 \cdot 10^{-2}$	$3{,}53 \cdot 10^{-2}$	$3{,}33 \cdot 10^{-2}$		
30 M	$5{,}15 \cdot 10^{-2}$	$3{,}51 \cdot 10^{-2}$	$2{,}92 \cdot 10^{-2}$		

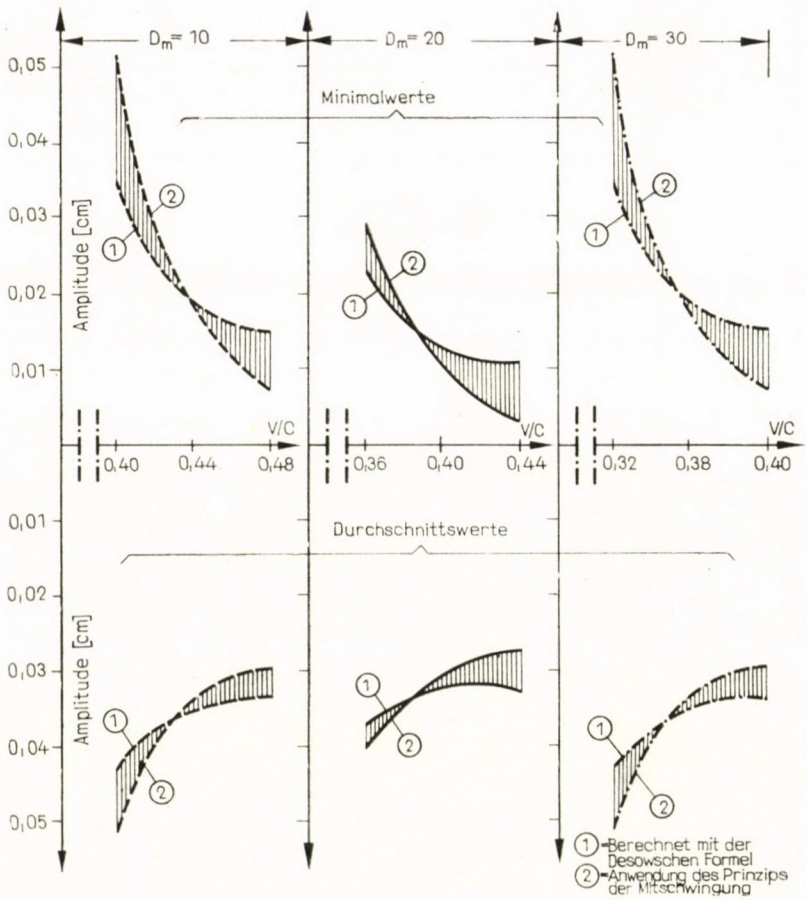

Bild 8. Grenzamplituden

zustreben, da übrigens die Theorie sich von der Praxis notwendigerweise trennt; wir können gegen die Desowsche Formel nur eine einzige Einwendung erheben, daß sie nämlich für praktische Berechnungen verhältnismäßig kompliziert ist. Eine einfachere und die Wirklichkeit gut annähernde Lösung gibt das im Abschnitt 5 behandelte Prinzip der Mitschwingung. Dies wird bestätigt durch die Tafeln 7 und 8. Tafel 7 faßt die Grenzamplituden (als Minimalamplituden) zusammen. Tafel 8 führt die arithmetischen Mittel vor, die aus den Grenzamplituden und den Eigenamplituden des Rüttelkopfes berechnet

werden können. Eine graphische Darstellung dieser Tabellen ist im Bild 8 wiedergegeben.

Aufgrund des Vorangehenden können wir feststellen:

a) Das Prinzip der Mitschwingung bildet eine annehmbare Näherung im Vergleich mit der exakten Desowschen Formel.

b) Das arithmetische Mittel der aus der Mitschwingung berechneten Amplituden und der Eigenamplituden des Rüttelkopfes gibt einen solchen Durchschnittswert, der größer als der mit Hilfe der Desowschen Formel erhaltene ist, welcher als der notwendige absolute Minimalwert betrachtet werden kann; demnach kann die Anwendung dieses Mittelwertes als gerechtfertigt betrachtet werden.

SCHRIFTTUM

1. CSUTOR, J.: Die Betonverdichtung, Műszaki Könyvkiadó, Budapest, 1967
2. CSUTOR, J.: Theorie zur Regelung des Betriebs des Oberflächenrüttlers für die Betonverdichtung, mit besonderer Rücksicht auf den Kiesbeton. Ungarische Akademie der Wissenschaften, *Műszaki Tudományok Osztályának Közleményei*, 1968/40
3. CSUTOR, J.: Einheitliche Theorie zur Regelung der Vibrationsverdichtung des Betons, mit besonderer Rücksicht auf den Kiesbeton. Ungarische Akademie der Wissenschaften, *Műszaki Tudományok Osztályának Közleményei*, 1968/41
4. CSUTOR, J.: Die Schalungsrüttelung, *Magyar Építőipar*, 1966/10
5. CSUTOR, J.: Der Nadelrüttler, *Magyar Építőipar* 1967/9
6. CSUTOR, J.: Betonverdichtung in Batterieschalungen der Hausbauwerke. *Magyar Építőipar*, 1968/11—12
7. CSUTOR, J.: Einige Probleme der modernen Betonplanung, *Építőanyag*, 1969/5
8. DESOW—MIKLASCHEWSKIJ—GERSBERG—SCHESTOPEROV: Handbuch für Betonverarbeitung mit Rüttlergeräten. Dorizdat, Moskau 1950
9. DESOW: Mit Rüttler verdichteter Beton, Stroizdat, Moskau 1950
10. TÓTH, F.: Serienfertigung von Bauelementen, Műszaki Könyvkiadó, Budapest 1962
11. STORK, J.: Theorie der Betonverarbeitung, Vydavatelstvo Slovenskej. Akadémie Vied, Bratislava, 1964

Contributions of Compaction Technique to the Theory of Concrete Designing. On the basis of compaction tests carried out with vibrators for internal vibration, to determine the methods to be followed and the characteristics of compaction, the statements has been made that a physical quantity may be found which, in finishing the designing of concrete, permits to establish instructions for controlling compaction operations. This physical quantity is the *specific compaction work*. Knowledge of the specific compaction work permits to establish the conditions of reproduction in connection with all of the compaction methods, if, in preparing the test pieces, the specific compaction work will be coordinated to the optimal concrete strength.

Данные по технике уплотнения к теории проектирования гравийных бетонов *(Я. Чутор)*. На основе экспериментальных опытов, проводившихся с целью числового определения параметров уплотнения и режима работы стержневого вибратора, можно сделать следующие выводы.

а. Можно найти такое физическое количество, которое в завершение проектирования бетона позволяет разработать инструкции по урегулированию уплотнения. Этим физическим количеством является *удельная работа уплотнения*.

б. Если известна удельная работа уплотнения, тогда возможно получить условия воспроизводимости для всех вибрационных режимов уплотнения, если при изготовлении образцов для оптимальной прочности бетона придать удельную работу уплотнения.

Acta Technica Academiae Scientiarum Hungaricae, Tomus 68 (3—4), pp. 403—413 (1970)

A METHOD OF APPROXIMATION IN THE LARGE DEFLECTION ANALYSIS OF IMPULSIVELY LOADED RIGID-PLASTIC STRUCTURES

T. WIERZBICKI*

[Manuscript received: 28 May 1969]

The paper is concerned with a method of approximation for impulsively loaded rigid-plastic structures. A method is presented for the determination of permanent deformation for circular plates and rotationally symmetric shells in the range of moderately large deflections. For the application of the theory three important boundary value problems were solved. Simple formulas were derived which compare favourably with known exact solutions and recent experimental data.

1. Symbols

W	transverse deflection
U	displacement in the tangential direction
W_0	central deflection
δ	permanent central deflection
$\dot{K}_1$, $\dot{K}_2$	curvature rates
$\dot{\lambda}_1$, $\dot{\lambda}_2$	extension rates
Q_i	generalized stress vector
$\dot{q}_i$	generalized strain rate vector
$M_0 = \sigma_0 h^2$	full plastic moment
$N_0 = 2\sigma_0 h$	full membrane force
P_0	initial value of limit load
P	limit load
I	impulse for unit area of structure
M	mass of the projectile
V_0	velocity of the projectile
E	kinetic energy imput
σ_0	yield stress in simple tension
μ	mass density per unit area of structure
x	axial coordinate
r	radial coordinate
ϱ	dimensionless radial coordinate
t	time
t_f	duration time of the deformation process
R	radius of the plate of shell
L	length of the cylindrical shell
h	half thickness of the structure
S	integration area
V	volume of the body
$\dot{D}$	rate of plastic work
β	mass ratio
$\psi_n(\lambda_n, \varrho)$	eigenfunction
λ_n	eigenvalue
P_n	normal component of loading
P_t	tangential component of loading
$(\ )'$	$= \partial/\partial x$ or $\partial/\partial r$
$(\dot{.})$	$= \partial/\partial t$

* Institute of Basic Technical Research, Swiętokrzyska 21, *Warsaw*, Poland.

2. Introduction

Recent theoretical and experimental investigations on dynamic plastic deformations of structural elements and structures have demonstrated the good applicability of the rigid-perfectly plastic model of the material in the analysis of permanent deflections of beams and plates [1, 2, 3]. In spite of the high strain rate attained in all impact and impulsive loading problems the viscous properties of the material were found to be of less importance than the geometry changes and a resulting strengthening of the structure. The latter effect becomes a decisive factor in the response of the structure for moderately large deflection and can reduce by half the value of permanent deformation of impulsively loaded simply supported plate as compared with the solution of small deflection theory [4, 5]. A complete theory which takes into account all the inertia terms, bending moments, membrane forces and changes in geometry usually leads to a very complicated and non-linear mathematical problem [6, 7]. It is, therefore, of interest to develop a certain approximate method of solution which takes all factors mentioned above into account but leads to simple and straightforward calculations.

The solution of a dynamic problem will be considerably simplified by imposing certain pattern of deformation on the structure. Such an approach, based on mode approximation, will be developed herein.

3. Basic assumptions

We introduce the following assumptions concerning the mechanical and geometrical parameters of the structure, conditions of loading and kinematics of the solution.

1. The structure is made of rigid-perfectly plastic material obeying either Tresca or Mises yield conditions and the associated flow rule.

2. Structures with only one spatial coordinate are considered (beams and rotationally symmetric plates and shells).

3. The external loading is axi-symmetrical and acts normally on the undeformed surface of the structure.

4. The velocity and displacement fields are taken from the solution of the associated static problem.

5. Only such static problems are considered for which the velocity field in the transverse direction is given in the separable form

$$\dot{W}(x, t) = \dot{W}_0(t) \cdot f(x) ,$$

where x is a single space coordinate for rotationally symmetric problems, t denotes time and $\dot{W}_0(t)$ is the central velocity of a given structure.

The deformation process of a dynamically loaded structure is characterized by a transient motion, which means that the relevent velocity field is subjected to considerable changes as time proceeds. For example, in the circular plate struck by a rigid mass centrally there is initially a discontinuous velocity profile where the centre of the plate is moving with prescribed velocity, while the remainder of the plate is at rest. This velocity profile is gradually smoothed out and can be described by a continuous function $f(x, t)$. A somewhat similar situation arises for impulsively loaded plate with the single difference that the initial discontinuity takes place not at the center but at the simply supported or clamped edges. The rigid-plastic analysis with the concept of travelling plastic hinges has proved very useful in the description of transient motion of beams, plates and shells. Usually the entire process was subdivided into two stages, the first one being the transient [3, 8]. The advantage of such a method is that using simple ideas of linearized yield condition a pattern of deformation is obtained which is physically quite realistic. A further insight into this problem provided the method of linearization of governing equations which is based upon the Huber—Mises yield condition. It was shown that the motion of rigid-viscoplastic plates and shells could be conveniently analysed on the basis of Fourier synthesis [9, 10]. The deflection and velocity profiles can be represented as an infinite sum of modal functions with time variable coefficients. The series is rapidly convergent except for the early stage of the deformation process. In many instances, for dynamically loaded plates and shells, the dominant role in the response of these structures plays only the first mode [9, 11, 12]. This would suggest that a good approximation to the solution of a dynamic problem is a single mode solution. Of course, such a velocity field would never satisfy the discontinuous initial condition but the resulting over-all permanent deflection which usually comes close to both an exact solution and recorded experimental data [9,12]. The present paper is mainly concerned with the determination of permanent plastic deformation of dynamically loaded plates and shells rather than with a detailed description of the entire deformation process. For this purpose the introduction of a separable form of the velocity field seems to be a reasonable approximation. In general, we can think of any kinematically admissible velocity field. As the single mode velocity field we choose the velocity field of the corresponding quasi-static problem. It was shown in the example of impulsively loaded simply supported circular plate and impacted clamped plate that the static velocity field was a very good approximation to the exact dynamical solution [9, 11]. The resulting deflection field was shown to adequately reproduce the experimentally measured shape of the deformed plate even when large deflections were permitted [4]. The determination of the velocity field is thus reduced to the proper choice of the quasi-static problem associated with the dynamic one. The term "associated problem" requires additional

explanation. Usually the above mentioned correspondence is not unique and there are many static problems with kinematics similar to the dynamic solution. The conditions how the load is applied to the structure give indication as to the choice of the associated state. If, for example, the plate is loaded by a uniformly distributed impulse, then the corresponding static problem would be the uniformly distributed pressure acting on the plate surface. The same applies for pulses of finite duration. If the plate or shell is impacted by a projectile of the Mass M moving with velocity V, then the corresponding static problem would be a point force acting on the point of impact, and so on.

4. Solution of the problem

Let us consider the class of problems with zero initial conditions for velocity and deflection. Assuming further that at $t = 0$ the load is suddenly applied and then suddenly removed so that each particle of the structures is first accelerated and then decelerated and at the instant t_f the structure is brought to rest. The entire energy E introduced to the system is dissipated nto the plastic work

$$E = \int_0^{t_f} \left(\int_V Q_i(t)\, \dot{q}_i(t) \cdot dV \right) dt, \tag{1}$$

where Q_i and $\dot{q}_i$ are, respectively, generalized stresses and strain rates. The integration is extended over the whole volume of structure V. In the case of plates and rotationally symmetric shells the generalized stresses are bending moments and membrane forces $Q_i = (M_\alpha, N_\alpha)$ and generalized strain rates are extension rates and curvature rates $\dot{q}_i = (\dot{\lambda}_\alpha, \dot{K}_\alpha)$, $\alpha = 1, 2$. The yield condition is represented in the four-dimensional space by a closed hypersurface $\psi(M_\alpha, N_\alpha) = 0$. The strain rate vector is at each point perpendicular to that surface. According to assumptions 2 and 3 the displacement vector has two components, vertical W and horizontal U.

Let us now consider the associated static problem and denote by $\bar{Q}_i$, $\bar{\dot{q}}_i$, $\bar{P}$ and $\bar{\dot{W}}$ the complete solution at moderately large deflections. We shall now apply the principle of virtual work by equating the internal and external energy dissipation rates

$$\int_V \bar{Q}_i\, \bar{\dot{q}}_i\, dV = \int_S \bar{P}(\bar{W})\, \bar{\dot{W}} \cdot dS. \tag{2}$$

The contribution of the horizontal component of the velocity on the right hand side of Eq. (2) is zero in view of the assumption 3, since the component of external loading vanishes in that direction.

The quasi-static flow of the structure is possible when the external load P reaches the limit value known as the load-carrying capacity of the structure P_0. This value is constant if changes in geometry and strain hardening are neglected. For moderately large deflections the limit load is an increasing function of the permanent deflection of the structure $P(W_0)$. The rise in external loading is accompanied by the redistribution of stresses, $\bar{Q}_i = \bar{Q}_i(W_0)$.

If the velocity and displacement profiles of the static and dynamic problem are identical (assumptions 4 and 5), the corresponding strain rate vectors in (1) and (2) would be identical $\bar{\dot{q}} = \dot{q}$. Using the associate flow rule with each strain rate vector we can uniquely associate certain stress vectors. Consequently the internal energy dissipation rates in static and dynamic problems are the same. Hence, substituting (2) into (1) we obtain

$$E = \int_0^{t_f} \left(\int_S P(x,t)\, \dot{W}(x,t) \cdot dS \right) dt. \tag{3}$$

In the theory of time, independent plasticity time can be replaced by any monotonously increasing function of time. Assuming that central deflection $W_0(t)$ is such a function, let us denote by $\delta = W_0(t_f)$ the permanent central deflection of the structure. Assuming next that the limit load $P(x, t) = P(W_0)$ does not depend upon the space coordinate i.e., it is either uniformly distributed or concentrated. Using assumption 4 the right hand side of (3) can be transformed to

$$\int_0^{t_f} \left(\int_S P(W_0)\, \dot{W}_0 \cdot f(x) \cdot dS \right) dt = \int_S f(x) \left[\int_0^{\delta} P(W_0) \cdot dW_0 \right] dS. \tag{4}$$

The estimate for the characteristic deflection of the structure δ can be found by combining (3) and (4)

$$E = \int_S f(x) \left[\int_0^{\delta} P(W_0) \cdot dW_0 \right] dS. \tag{5}$$

In particular, for small deflection $P(W_0) = P_0 = \text{const}$ and Eq. (3) is reduced to

$$E = P_0\, \delta \int_S f(x) \cdot dS. \tag{6}$$

The value of the energy input E is, of course, a known quantity.

The determination of the permanent deflection of a given structure has been reduced to a single decision which consists of the proper choice of the quasi-static problem associated with the dynamic one. We utilize next the complete solution of the load-carrying capacity problem at large deflections.

The proposed procedure permits to give immediate estimates on dynamic plastic deformations of structures for which the corresponding solution of the load-carrying capacity problem is known. Note, that in the above presentation of the theory nothing is said about the internal forces, i.e. generalized stresses and corresponding strain rates. In that respect the present theory considerably differs from all previous work on that subject [13, 16, 17, 18].

5. Applications

5.1. *Simply supported plate under a uniformly distributed impulse*

Let us consider the Wang problem [3] of a thin circular plate simply supported on the outer edge and subjected to the uniform ideal impulse of intensity I. This is equivalent to prescribing a constant initial velocity $V = I/\mu$ over the plate, where μ is the mass density per unit area of the plate middle surface. The amount of the kinetic energy introduced to the system is equal to

$$E = 2\pi \cdot \frac{1}{2} \mu_0 \int_0^R V^2 \, r \cdot dr = \frac{\pi R^2 I^2}{2\mu} . \tag{7}$$

Alternatively the value of energy E can be related to the amount of explosive used in the impulse loading problem. The complete solution of the associated static problem, based on the Tresca yield condition is known to be

$$P_0 = 6 \frac{M_0}{R^2} , \quad f(x) = 1 - \frac{r}{R} , \tag{8}$$

where $M_0 = \sigma_0 h^2$ is a full plastic moment and R denotes the outer radius of the plate. Substituting (8) and (8) into (4) and integrating over the plate area we obtain

$$\delta = \frac{I^2 R^2}{4 \mu M_0} . \tag{9}$$

In the exact result of WANG [3] obtained by considering two-phase motion (the first phase was a transient one) in place of the numerical constant 4 stands 8.

A result similar to (9) is obtained for a Huber—Mises yield condition. In that instant $P_0 = 6.51 \; M_0/R^2$ and a good analytical approximation [19] to the numerical computation by EASON [20] is the following velocity field

$$f(r) = \frac{1}{5} (r^4 - 6 r^2 + 5) .$$

At that instant the numerical constant 4 is replaced by 5.1.

LANCE and ONAT [21] and recently CALLEDINE [22] computed a limit load associated with a conical deformation pattern (8) taking into account changes in the geometry of an originally flat simply supported plate. The resulting solution accounting for the membrane forces bending moments interaction is

$$P(W_0) = P_0\left[1+\frac{1}{3}\left(\frac{W_0}{2h}\right)^2\right]. \tag{10}$$

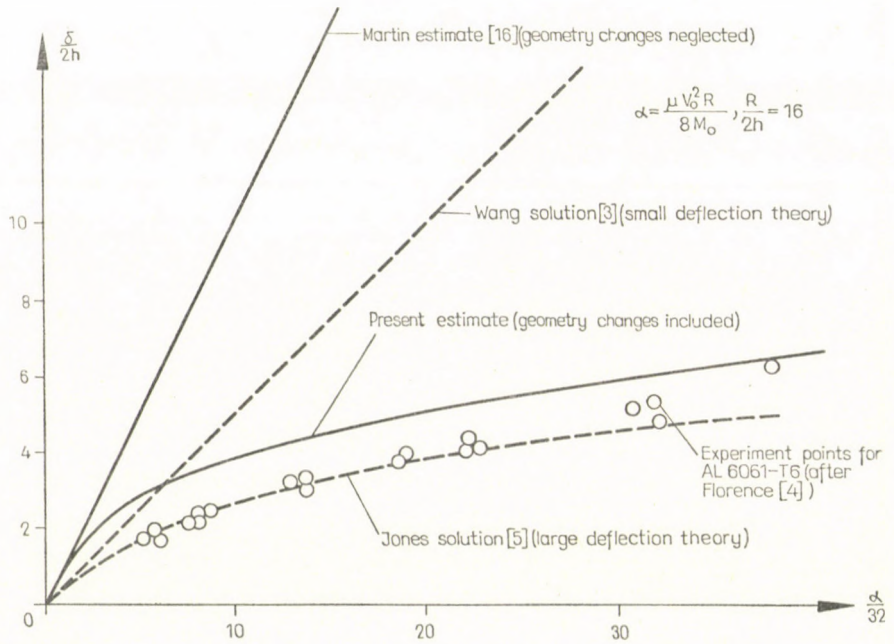

Fig. 1

Introducing this result into (5) and integrating, we found an improved approximation for permanent plate deflection

$$\delta+\frac{1}{36\,h^2}\delta^3 = \frac{I^2\,R^2}{H\mu M_0}\,. \tag{11}$$

The above formula is formally analogous to Symonds solution for an impulsively loaded beam with an axial constrain [8].

A comparison of large deflection solution (11) and small deflection solution (9) with Florence experimental data [4] is presented in Fig. 1. A considerable improvement of the approximate solution due to the consideration of membrane action and geometry changes, Eq. (11) is evident.

5.2. *Impact of a rigid mass on a clamped plate*

Motion of a circular viscoplastic plate subjected to projectile impact was analysed in [11, 12]. The corresponding quasi-static problem to the considered dynamical one is that of concentrated point force, which for the Huber—Mises yield condition has the value

$$P_0 = \frac{4\pi M_0}{\sqrt{3}} . \tag{12}$$

The velocity field associated with the above load is known to be

$$f(\varrho) = 1 - \varrho^2 (1 - 2\log\varrho) , \quad \varrho = \frac{r}{R} . \tag{13}$$

It should be noted that in case of a point force acting on the centre of the plate the integration area S in (6) is reduced to zero and the final solution does not depend on the velocity field.

Introducing (12) into (6) and noting that the kinetic energy of the striking mass is $E = \frac{1}{2} MV_0^2$ we compute the permanent central deflection

$$\frac{4\pi M_0}{\sqrt{3}} \delta = \frac{1}{2} MV_0^2 , \tag{14}$$

while in a more complete analysis of the same problem [12, 13] the solution depends upon the plate and projectile mass ratio β,

$$\frac{4\pi M_0}{\sqrt{3}} \delta = \frac{1}{1 - \dfrac{\pi}{6\beta}} \cdot \frac{1}{1 + \dfrac{4}{10\beta}} \cdot \frac{1}{2} MV_0^2 . \tag{15}$$

It is easy to see that the solution (15) converges to the present approximation (14) for large values of the parameter β. This corresponds to the case of heavy projectiles impacting light plates where we can expect the one-degree of freedom approximation becoming a more realistic hypothesis. Indeed, Fig. 2, taken from [11] shows that for $\beta \to \infty$ the first term $\psi_1(\lambda_1, \varrho)$ in the eigenvalue expansion of the exact velocity field for a considered dynamic problem coincides with the velocity field corresponding to the quasi-static problem (13). It should be noted that the second term $\psi_2(\lambda_2, \varrho)$, except for the early stage of the process, is small as compared with ψ_1 and it can be neglected. From Fig. 2 it is also clear that the static velocity field $f(\varrho)$ provides

a fairly good approximation to the true velocity field in the entire range of the mass ratio β, thus constituting the proof of the correctness of the basic hypothesis introduced in the present paper.

CALLEDINE [22] gave an approximate formula for the load-carrying capacity of the clamped plate for large deflections

$$P(W_0) = P\left[1 + \frac{5}{12}\left(\frac{W_0}{2h}\right)^2\right]. \tag{16}$$

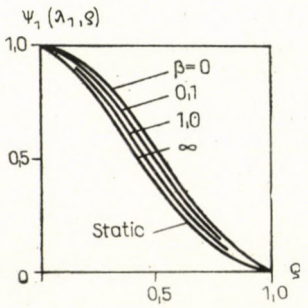

Fig. 2

Using (16) instead of (12) we find

$$\delta + \frac{5}{4}\frac{1}{36h^2}\delta^3 = \frac{\sqrt{3}}{4\pi M_0}\frac{1}{2}MV_0^2, \tag{17}$$

which is similar to the result derived in [11].

5.3. *Impulsive loading of a simply supported cylindrical shell*

As a last example let us consider a simply supported cylindrical shell free to move in an axial direction subjected to the uniformly distributed ideal impulse of internal pressure. Because of the assumed condition of support (zero axial force) no strengthening of the shell due to geometry changes is predicted by the theory of moderate deflections. The fact that the static limit load is constant over the range of deflection of several thicknesses of the uniform shell has been experimentally conformed by DEMIR and ONAT [23]. Thus, the approximate solution to be found will be valid both in the ranges of small and moderately large deflections. The complete solution for a rigid-perfectly plastic shell was derived by HODGE [24], while a similar problem for a rigid-viscoplastic shell was recently solved by PABIANEK [10]. The static load carrying capacity of the shell and the associated velocity field depends upon the choice of the yield condition. For the linearized Tresca yield condition

the required static solution is [24]

$$P_0 = \frac{1 - \frac{1}{2}\cos c}{1 - \cos c}, \quad c = \frac{L}{\sqrt{Rh}} \quad \text{for } c > \frac{\pi}{2}, \tag{18}$$

where L is the length of the shell and R denotes the shell radius.

On substitution of (18) into (6) the permanent central deflection of the shell is found to be

$$\delta = \frac{\pi}{2} \frac{I^2}{\mu P_0}, \tag{19}$$

which differs from the exact result derived in [10] only by a constant multiplier $2/\pi$.

6. Conclusion

The solutions of three important boundary value problems obtained by means of very simple and straightforward calculations were shown to give a good correlation with recent experimental data and known exact solutions of the same problem. Since nothing can be said about the accuracy of the proposed method, the obtained solution should be regarded merely as an approximation to the exact solution.

In the present approach it was assumed that all energy introduced to the system went into the first mode. In actual facts only a part of the energy E is transmitted to the first mode, the remainder goes into the higher modes and is rapidly dissipated in the first, transient stage of motion. Since the value of the energy associated with the prescribed kinematics is overestimated by the present theory, the obtained solution would clearly be an upper boundary on the transverse displacements.

The present method, unlike all previous work on this subject, is not restricted to small deflections and it takes care of such important effects as changes in geometry and resulting moment — membrane forces interaction.

There are no conceptional difficulties to extend the present theory to the structures other than circular plates and rotationally symmetric shells.

REFERENCES

1. Bodner, S. R.—Symonds, P. S.: Experimental and Theoretical Investigation of the Plastic Deformation of Cantilever Beams Subjected to Impulsive Loading. *Journal of Applied Mechanics*, ASME, **29** (1962), 719
2. Florence, A. L.—Firth, R. D.: Rigid-plastic Beams under Uniformly Distributed Impulses. *Journal of Applied Mechanics*, ASME, **32** (1965), 481
3. Wang, A. J.: The Permanent Deflection of a Plastics Plate under Blast Loading. *Journal of Applied Mechanics*, **22** (1955), 375
4. Florence, A. L.: Circular Plate under a Uniformly Distributed Impulse. *International Journal of Solids and Structures* **2** (1966), 37

5. JONES, N.: Impulsive Loading of a Simply Supported Rigidplastic Circular Plate. *Journal of Applied Mechanics*, ASME, **35** (1968), 59
6. JONES, N.: Finite Deflections of a Rigid-Viscoplastic Strain-Hardening Plate Loaded Impulsively. *Journal of Applied Mechanics*, ASME, Paper No 68 — APM — 24
7. WIERZBICKI, T.: Large Deflections of Strain Rate Sensitive Plate Loaded Impulsively. *Archiwum Mechaniki Stosowanej*, **20** (1968) 67
8. SYMONDS, P. S.: Large Plastic Deformations of Beams under Blast Loading. *Proceedings 2nd U. S. Natl. Congress on Applied Mechanics*, ASME (1954), 505
9. WIERZBICKI, T.: Impulsive Loading of Rigid-viscoplastic Plates. *International Journal of Solids and Structures* **3** (1967), 635
10. PABIANEK: Dynamic Loading of Rigid-viscoplastic Cylindrical Shell. *Archiwum Mechaniki Stosowanej* (to be published)
11. KELLY, J. M.—WIERZBICKI, T.: Motion of a Circular Viscoplastic Plate Subject to Projectile Impact. *Journal of Applied Mathematics and Physics* **18** (1967), 236
12. KELLY, J. M.—WIERZBICKI, T.: Finite Deflection of a Circular Viscoplastic Plate Subjected to Projectile Impact. *International Journal of Solids and Structures*, **4** (1968), 1081
13. HAYTHORNTHWAITE, R. M.: Mode Change during the Plastic Collapse of Beams and Plates. *Proceedings of the Seventh Midwestern Mechanics Conference*, Michigan State University, Michigan, 1961 Ed. LAY. J. E., MALVERN, L. E., 203—215
14. DUSZEK, M.: Plastic Analysis of Shallow Spherical Shells at Moderately Large Deflections. *Proceedings of the I.U.T. A.M. Symposium*, Copenhagen 1967.
15. HODGE, P. G.: The Mises Yield Condition for Rotationally Symmetric Shells. *Quarterly of Applied Mathematics* **18** (1961), 305
16. MARTIN, J. B.: A Displacement Bound Principle for Inelastic Continua, Subjected to Certain Class of Dynamic Loading. *Journal of Applied Mechanics*, ASME, **32** (1965),
17. MARTIN, J. B.—SYMONDS, P. S.: Mode Approximations for Impulsively Loaded Rigid-Plastic Structures. *Journal of the Engineering Mechanics Division*, **92** (1966), 43
18. MELVIN, L. B.—BLEICH, H. H.—WEIDLINGER, P.: Dynamic Elastic Plastic Analysis of Structures. *Journal of the Engineering Mechanics Division*, **87** (1961), 23
19. WIERZBICKI, T.: A Method for Approximate Solution of Boundary Value Problems for Rigid, Viscoplastic Structures. *Acta Mechanica*, **3** (1967), 56
20. EASON, G.: Velocity Fields for Circular Plates with the von Mises Yield Condition. *Journal of the Mechanics and Physics of Solids*, **6**, 1958, p. 231
21. LANCE, R. H.—ONAT, E. T.: A Comparison of Experiments and Theory in the Plastic Bending of Circular Plates. *Journal of the Mechanics and Physics of Solids*, **10** (1962), 301
22. CALLEDINE, C. R.: Simple Ideas in the Large-deflection Plastic Theory of Plates and Slabes, Engineering Plasticity. Ed. HEYMAN J. and LECKI, F. A., Cambridge University Press, 1968
23. DEMIR, H. H.—DRUCKER, D. C.: An Experimental Study of Cylindrical Shells under Ring Loading. Progress in Applied Mechanics, The Prager Anniversary Volume, The Macmillan Co., New York, N. Y. 1963, 205—220
24. HODGE, P. G., Jr.—PAUL, B.: Approximate Yield Conditions in Dynamic Plasticity. Third Midwestern Conference on Solid Mechanics, 1957, 29—47

Schwingungsgebilde-Näherung in der Analyse der großen Durchbiegungen von dynamisch belasteten steif-plastischen Konstruktionen. Es werden Schwingungsgebilde-Näherungen der dynamisch belasteten steif-plastischen Konstruktionen behandelt. Ein Verfahren zur Bestimmung der bleibenden Formänderungen von Kresiplatten und rotationssymmetrischen Flächentragwerken im Bereich der Durchbiegungen mäßiger Größe wird beschrieben. Als Anwendung der Theorie werden drei wichtige Randwertprobleme gelöst. Einfache Formeln wurden abgeleitet, deren Ergebnisse in guter Übereinstimmung mit denen der exakten Lösungen und neuesten Experimente sind.

Приближение картины колебаний при исследовании большой деформации нагруженных импульсами жесткопластичныхконструкций *(T. Виерзбицки)*. Излагается метод приближения модуса при расчете жесткопластичных конструкций динамической нагрузки. Метод, служащий для определения остаточных деформаций круглых пластин и оболочек с симметрий вращения в области умеренно больших деформаций. Для демонстрации применения теории сообщается решение задачи с тремя важными краевыми значениями. Дается вывод простых формул, результаты которых очень хорошо совпадают с результатами известных точных методов и с результатами проводившихся недавно экспериментальных опытов.

Acta Technica Academiae Scientiarum Hungaricae, Tomus 68 (3—4), pp. 415—429 (1970)

FLEXURE OF PRISMATIC BEAMS (1)

M. GOPALA KRISHNA MURTHY*

[Manuscript received 27 Aug 1969]

A formal solution is given to the problem of flexure in the case, when the mapping function which maps conformally the semi-cross section of the beam on to a *semi-unit circle*, is known in power series. The method is illustrated by applying it to the problem of flexure of a prismatic beam whose cross section is one half of Pascal's limacon. The cases of beams whose cross sections are one half of a cardioid and one half of a circle are derived as particular cases.

1. Introduction

DEUTSCH in his paper [1] has solved the problem of flexure of beams whose cross sections can be conformally mapped on to the unit semi-circle. The method is further simplified in case of mapping functions which can analytically be continued. In the present paper, the problem is solved when the mapping function is in the form of power series. The solutions of various problems are derived as particular cases.

2. Nomenclature

We consider a prismatic beam made of isotropic homogeneous material bounded by planes perpendicular to the generating lines. The beam is fixed at one end and is in equilibrium under the action of forces acting upon it in the plane of the other end. Body forces are assumed to be absent and the lateral surface of the beam free from applied forces. We adopt the following notation [2]:

O (O, O, O) = Origin in the plane of the fixed end
Ox, Oy, OZ = Mutually axes, Oz being parallel to the generating lines of the beam

L = Length of the beam
S = Section of the free end $Z = L$
z_G = $x_G + i\, y_G$
Ω = Area of S
C = Boundary of S
O' = (O, O, L)

* Department of Mathematics, Regional Engineering College, *Warangal-4 (A. P.)*, India.

G = (x_G, y_G, L) C. G. of S

A = $\iint_S (y-y_G)^2\, dS$ Second moments of area with reference to axes through the centroid of the section parallel to the x, y axes.

B = $\iint_S (x-x_G)^2\, ds$

H = $\iint_S (x-x_G)\,(y-y_G)\, dS$

W = Total load of a distribution of shear stresses applied over the plane end $Z = L$

W_x, W_y = Forces acting at O' parallel to x and y axes — statically equivalent to the shear system W

M = Moment about OZ

P = $W_x + i\, W_y$

α_x = $(A\, W_x - H\, W_y)/E\Delta$

α_y = $(B\, W_y - H\, W_x)/E\Delta$

Δ = $A\, B - H^2$

β = $\alpha_x + i\,\alpha_y = [(A + B)\, P - (B - A + 2iH)\bar{P}]/2E\Delta$

E = Young's modulus

μ = Shear modulus

ν = Poisson's ratio

σ_{xx}, σ_{yy}, σ_{zz} = normal stress components,

τ_{xy}, τ_{yz}, τ_{zx} = Shearing stress components

$I_{m,n}$ = $\iint_S x^m y^n\, dS$

I = Polar moment of Inertia = $I_{0,2} + I_{2,0}$

I' = $I_{2,0} - I_{0,2} + 2\, i\, I_{1,1}$

The non-vanishing stress components are

$$\tau_{xz} - i\,\tau_{yz} = \mu\,[\Phi(z) - p\bar{z} - q\bar{z}^2 - rz\bar{z}] \tag{1}$$

$$\sigma_{zz} = E(Z-L)[\alpha_x(x-x_G) + \alpha_y(y-y_G)] \tag{2}$$

where

$$p = i\tau - 1/2(1+\nu)(\beta\bar{z}_G + \bar{\beta}z_G) \tag{3}$$

$$q = 1/4\,(1+2\nu)\,\beta,\quad r = 1/2\,\bar{\beta} \tag{4}$$

$\Phi(z)$ is the flexure function, τ is a real constant whose value is determined by (6). $\Phi(z)$ is holomorphic over S and on C. We have [3],

$$\Phi(z)\frac{\partial z}{\partial S_1} - \bar{\Phi}(\bar{z})\frac{\partial \bar{z}}{\partial S_1} = (p + q\bar{z} + rz)\,\bar{z}\frac{\partial z}{\partial S_1} - (\bar{p} + \bar{q}z + \bar{r}\bar{z})\,z\frac{\partial \bar{z}}{\partial S_1} \tag{5}$$

at the boundary C of S.

$$\frac{2M}{\mu} = \frac{1}{2}(K + \bar{K}) + 2\tau I + \frac{1}{24}(1-2\nu)(\beta J + \bar{\beta}\bar{J}) \tag{6}$$

with

$$I = -\frac{1}{4}\int_C z\bar{z}^2\, dz \tag{7}$$

$$J = \int_c z\bar{z}^3\, dz \tag{8}$$

$$K = \int_c z\bar{z}\Phi(z)\, dz \tag{9}$$

$$\bar{Z}_c = 2i\, \partial M_0/\partial P \tag{10}$$

where M_0 denotes the value of M which corresponds to

$$\tau = \frac{1}{2}\, iv(\beta\bar{Z}_G - \bar{\beta}Z_G). \tag{11}$$

The condition (5) is sufficient to determine uniquely the function $\Phi(z)$ whenever the cross section can be conformally mapped on a unit semi-circle. Thus, once $\Phi(z)$ is known, the flexure problem is completely solved.

3. The mapping function

$$z = \omega(s) \tag{12}$$

maps the region S on to the unit semi-circle $|\, s\,| \leq 1$, $\eta \geqslant 0$ in the $s = \xi + i\,\eta$ plane.

Let

$$\Phi(z) = \Phi[w(s)] = \psi(s) \tag{13}$$

Γ = semi circumference $|\, s\,| = 1$, $\eta \geqslant 0$,
δ = diameter $\eta = 0$, $-1 \leq \xi \leq 1$,
$\sigma = e^{i\Theta}$ is a point on Γ and ξ is a point on δ.

For the points on Γ

$$z = \omega(\sigma)\,,\ \bar{z} = \bar{\omega}(\bar{\sigma})\,,$$

$$\frac{\partial z}{\partial S_1} = \omega'(\sigma)\frac{d\sigma}{dS_1}\,,\quad \frac{d\bar{z}}{dS_1} = \frac{-1}{\sigma^2}\,\bar{\omega}'(\bar{\sigma})\frac{d\sigma}{dS_1}$$

(5) takes the form

$$\psi(\sigma)\,\omega'(\sigma) + \frac{1}{\sigma^2}\,\bar{\omega}'(\bar{\sigma})\,\bar{\psi}(\bar{\sigma}) = \bar{\omega}(\bar{\sigma})\,\omega'(\sigma)\,[p + q\,\bar{\omega}(\bar{\sigma}) + r\omega(\sigma)] + \tag{14}$$

$$+ \frac{1}{\sigma^2}\,\omega(\sigma)\,\bar{\omega}'(\bar{\sigma})\,[\bar{p} + \bar{q}\,\omega(\sigma) + \bar{r}\,\bar{\omega}(\bar{\sigma})]\,.$$

For points on δ

$$z = \omega(\xi), \qquad \bar{z} = \bar{\omega}(\xi),$$

$$\frac{\partial z}{\partial S} = \omega'(\xi)\frac{d\xi}{dS}, \qquad \frac{\partial \bar{z}}{\partial S} = \bar{\omega}'(\xi)\frac{d\xi}{dS},$$

(5) takes the form

$$\begin{aligned}\psi(\xi)\,\omega'(\xi) - \bar{\psi}(\xi)\,\bar{\omega}'(\xi) = \bar{\omega}(\xi)\,\omega'(\xi)[p + q\bar{\omega}(\xi) + r\omega(\xi)] \\ - \omega(\xi)\,\bar{\omega}'(\xi)[\bar{p} + \bar{q}\omega(\xi) + \bar{r}\bar{\omega}(\xi)].\end{aligned} \tag{15}$$

Let

$$\varkappa_1(s) = s\psi(s)\,\omega'(s). \tag{16}$$

The boundary conditions (14) and (15) give

$$\varkappa_1(s) + \overline{\varkappa_1(s)} = U(\sigma) \text{ on } \Gamma \tag{17}$$

$$\varkappa_1(s) - \overline{\varkappa_1(s)} = V(\xi) \text{ on } \delta \tag{18}$$

with

$$U(\sigma) = \sigma\,\overline{\omega(\sigma)}\,\omega'(\sigma)[p + q\,\overline{\omega(\sigma)} + r\omega(\sigma)] + \frac{1}{\sigma}\omega(\sigma)\omega'(\sigma)[\bar{p} + \bar{q}\omega(\sigma) + \bar{r}\bar{\omega}(\bar{\sigma})] \tag{19}$$

$$V(\xi) = \xi\,\bar{\omega}(\xi)\,\omega'(\xi)[p + q\bar{\omega}(\xi) + r\omega(\xi)] - \xi\omega(\xi)\,\bar{\omega}'(\xi)[\bar{p} + \bar{q}\omega(\xi) + \bar{r}\bar{\omega}(\xi)] \tag{20}$$

clearly

$$\bar{\omega}(s) = \overline{\omega(s)}.$$

The flexure problem is reduced to the task of finding a function $\chi_1(s)$ holomorphic in and on the semi-circle $|s| \leq 1$, $\eta \geq 0$ whose real part takes the value $1/2\ U(\sigma)$ on Γ and whose imaginary part takes the value $1/2i\ V(\xi)$ on δ. If the mapping function can be continued analytically into the semi-circle $|s| \leq 1$, $\eta < 0$, the expressions for $\chi_1(s)$, I, J, K as given in [1] are

$$s\psi(s)\omega'(s) = V(s) + \frac{1}{2\pi i}\int_\Gamma [U(\sigma) - V(\sigma)]\left[\frac{1}{\sigma - s} - \frac{1}{\sigma - 1/s}\right]d\sigma \tag{21}$$

$$I = -\frac{i}{4}\int_\Gamma [\bar{\omega}(\bar{\sigma})^2 - \bar{\omega}^2(\sigma)]\,\omega(\sigma)\,\omega'(\sigma)\,d\sigma \tag{22}$$

$$J = \int_\Gamma [\bar{\omega}(\bar{\sigma})^3 - \bar{\omega}^3(\sigma)]\,\omega(\sigma)\,\omega'(\sigma)\,d\sigma \tag{23}$$

$$K = \int_\Gamma \omega(\sigma)\,\omega'(\sigma)\,\psi(\sigma)[\bar{\omega}(\bar{\sigma}) - \bar{\omega}(\sigma)]\,d\sigma. \tag{24}$$

4. Torsion

In the case of torsion we have

$$W_x = 0 = W_y, \quad M \neq 0, \quad \beta = 0,$$
$$p = i\tau, \quad q = r = 0. \tag{25}$$

$\psi(s)$ is given by (21) with

$$U(s) = i\tau\left[\bar{\omega}\left(\frac{1}{s}\right)\omega'(s) - \frac{1}{s}\,\omega(s)\,\bar{\omega}'(s)\right],$$
$$V(s) = i\tau\,[s\bar{\omega}(s)\,\omega'(s) + s\omega(s)\,\bar{\omega}'(s)]. \tag{26}$$

The flexure function $\Phi(z)$ and the complex torsion function $F(z)$ are related by

$$\Phi(z) = \tau F'(z). \tag{27}$$

Further from (1) we find, for the stresses

$$\tau_{xz} - i\tau_{yz} = \mu\,[\Phi(z) - i\tau\bar{z}]$$

on putting

$$\Phi(z) = \tau F'(z)$$

we have

$$\tau_{xz} - i\tau_{yz} = \mu\tau[F'(z) - i\bar{z}].$$

5. Results

Let the mapping function (12) be written in the form

$$z = \omega(\sigma) = \sum_0^\infty a_n\,\sigma^n, \tag{12}$$

a_n ($n = 0, 1, 2, \ldots$) being, in general, complex coefficients.

After some algebraic manipulations we find

$$\omega(\sigma)\,\omega'(\sigma) = \sum_0^\infty \beta_n\,\sigma^n, \quad \bar{\omega}^2(\sigma) = \sum_0^\infty \alpha_n\,\sigma^n,$$
$$\bar{\omega}(\bar{\sigma})^2 = \sum_0^\infty \alpha_n\,\sigma^{-n}, \quad \bar{\omega}(\bar{\sigma})^2\,\omega(\sigma)\,\omega'(\sigma) = \sum_0^\infty \nu_n\,\sigma^n + \sum_1^\infty \nu_n'\,\sigma^{-n} \tag{28}$$
$$\bar{\omega}^2(\sigma)\,\omega(\sigma)\,\omega'(\sigma) = \sum_0^\infty \delta_n\,\sigma^n,$$

where

$$\beta_n = \sum_{r=0}^{\infty} (n-r+1)\, a_r\, a_{n-r+1}\,,$$

$$\alpha_n = \sum_{r=0}^{\infty} \bar{a}_{n-r}\, \bar{a}_r\,,$$

$$\nu_n = \sum_{r=0}^{\infty} \beta_{n+r}\, \alpha_r,\ \nu'_n = \sum_{0}^{\infty} \beta_n\, \alpha_{n+r}\,, \tag{29}$$

$$\delta_n = \sum_{r=0}^{\infty} \alpha_{n-r}\, \beta_r\,.$$

Substituting in (22) and making use of the integrals given in the Appendix, we have

$$I = \frac{-i}{4}\left[\sum_{0,2,4\ldots}^{\infty} \frac{-2H_n}{n+1} + \sum_{2,4,6\ldots}^{\infty} \frac{2\nu'_n}{n-1} + i\pi\nu'_1\right] \tag{30}$$

where

$$H_n = \nu_n - \delta_n\,.$$

Now

$$\bar{\omega}(\bar{\sigma})^3\, \omega(\sigma)\, \omega'(\sigma) = \sum_{0}^{\infty} F_n\, \sigma^n + \sum_{1}^{\infty} F'_n\, \sigma^{-n}\,,$$

$$\bar{\omega}^3(\sigma)\, \omega(\sigma)\, \omega'(\sigma) = \sum_{0}^{\infty} G_n\, \sigma^n \tag{31}$$

where

$$F_n = \sum_{r=0}^{\infty} \nu_{n+r}\, \bar{a}_r\,,$$

$$F'_n = \sum_{r=0}^{\infty} \nu_r\, \bar{a}_{n+r}\,, \tag{32}$$

$$G_n = \sum_{r=0}^{\infty} \delta_{n-r}\, \bar{a}_r\,.$$

Substituting these results in (23) and evaluating the integrals we have

$$J = \sum_{0,2,4\ldots}^{\infty} \frac{-2G'_n}{n+1} + \sum_{2,4,6\ldots}^{\infty} \frac{2F'_n}{n-1} + i\pi F'_1 \tag{33}$$

where

$$G'_n = F_n - G_n$$

and we have from (21)

$$s\psi(s)\omega'(s) = \sum_0^\infty B_n s^n + \frac{1}{2\pi}\int_\Gamma \left[\sum_0^\infty D_n \sigma^n + \sum_1^\infty A'_n \sigma^{-n}\right] \times \times \left[\frac{1}{\sigma - s} - \frac{1}{\sigma - 1/s}\right] d\sigma \tag{34}$$

where

$$D_n = A_n - B_n ,$$

and

$$\begin{aligned} A_n &= pb_n + qc_n + r(d_n + d'_n) + \bar{p}\, e_n + \bar{q} f_n + \bar{r} g_n , \\ A'_n &= pb'_n + qc'_n + rd''_n + \bar{p} e'_n + \bar{q} f'_n + \bar{r}(g'_n + g''_n) , \\ B_n &= ph_n + qh'_n + rh''_n - \bar{p} l_n - \bar{q} l'_n - \bar{r} l''_n , \end{aligned} \tag{34}$$

where

$$b_n = \sum_{r=0}^\infty (n+r)\, a_{n+r}\, \bar{a}_r , \qquad b'_n = \sum_{r=1}^\infty r a_r\, \bar{a}_{n+r} ,$$

$$d_n = \sum_{r=0}^\infty b_{n-r}\, a_r , \qquad d'_n = \sum_{r=1}^\infty a_{n+r}\, b'_r ,$$

$$d''_n = \sum_{r=0}^\infty a_r\, b'_{n+r} , \qquad c_n = \sum_{r=0}^\infty (n+r)\, a_{n+r}\, \alpha_r ,$$

$$c'_n = \sum_{r=1}^\infty r a_r\, \alpha_{n+r} , \qquad e_n = \sum_{r=1}^\infty r a_{n+r}\, \bar{a}_r ,$$

$$e'_n = \sum_{r=0}^\infty (n+r)\, a_r\, \bar{a}_{n+r} , \qquad \bar{\alpha}_n = \sum_{r=0}^\infty a_{n-r}\, a_r ,$$

$$f_n = \sum_{r=1}^\infty \bar{\alpha}_{n+r}\, \bar{a}_r , \qquad f'_n = \sum_{r=0}^\infty (n+r)\, \bar{\alpha}_r\, \bar{a}_{n+r} ,$$

$$g_n = \sum_{r=0}^\infty e_{n+r}\, \bar{a}_r , \qquad g'_n = \sum_{r=0}^\infty e_r\, \bar{a}_{n+r} ,$$

$$g''_n = \sum_{r=1}^\infty e'_n\, \bar{a}_{n-r} , \qquad h_n = \sum_{r=0}^\infty (n-r)\, \bar{a}_r\, a_{n-r} , \quad h_0 = 0 ,$$

$$h'_n = \sum_{r=0}^\infty (n-r)\, \alpha_r\, a_{n-r} \qquad \text{with } h'_0 = 0 , \tag{35}$$

$$h''_n = \sum_{r=0}^\infty b''_r\, a_{n-r} , \qquad b''_n = \sum_{r=0}^\infty a_{n-r}\, \bar{a}_r \text{ with } h''_0 = 0 ,$$

$$l_n = \sum_{r=0}^\infty (n-r)\, a_r\, \bar{a}_{n-r} \qquad \text{with } l_0 = 0 ,$$

$$l'_n = \sum_{r=0}^\infty (n-r)\, \bar{\alpha}'_r\, \bar{a}_{n-r} \qquad \text{with } l'_0 = 0 ,$$

$$l''_n = \sum_{r=0}^\infty (n-r)\, \alpha'_r\, \bar{a}_{n-r} \qquad \text{with } l''_0 = 0 ,$$

and

$$\alpha'_n = \sum_{r=0}^{\infty} a_r \bar{a}_{n-r} .$$

Evaluating the integral in (34), we have finally

$$s\psi(s)\,\omega'(s) = \sum_{0}^{\infty} \lambda_n s^n + \sum_{1}^{\infty} \lambda'_n s^{-n} + \frac{1}{2\pi i} \sum_{1}^{\infty} \lambda''_n (s^n - s^{-n}) \log \frac{1+s}{1-s} \tag{36}$$

with

$$\lambda_n = B_n + \frac{1}{2} D_n + \frac{1}{2} A'_n + 2 (E'_n - E_n)$$

$$\lambda'_n = 2 (E_n - E'_n)$$

$$\lambda''_n = D_n - A'_n \quad \text{with} \quad A'_0 = 0$$

and

$$E_n = \sum_{r=0}^{\infty} \frac{1}{2r-1} D_{n+2r-1} , \quad E'_n = \sum_{r=1}^{\infty} \frac{1}{2r-1} A'_{n+2r-1} .$$

From (24) we have

$$K = \int_{\Gamma} \frac{1}{\sigma} \left[\sum_{0}^{\infty} T_n \sigma^n + \sum_{n=1}^{\infty} T'_n \sigma^{-n} + \right.$$

$$\left. + \frac{1}{2\pi i} \left\{ \sum_{0}^{\infty} S_n \sigma^n + \sum_{0}^{\infty} S'_n \sigma^{-n} \right\} \log \frac{1+\sigma}{1-\sigma} \right] d\sigma \tag{37}$$

where

$$T_n = L_n + L'_n + Q_n + N_n + N'_n ,$$

$$T'_n = L''_n + Q'_n + Q''_n + N''_n \text{ with } Q''_1 = 0 ,$$

$$S_n = M_n + P_n - M'_n - P'_n + R_n \text{ with } M_0 = 0 = P_0 ,$$

$$S'_n = R'_n - R''_n - M''_n - P''_n \text{ with } R''_1 = 0 ,$$

and

$$L_n = \sum_{r=0}^{\infty} K_{n-r} \lambda_r , \qquad L'_n = \sum_{r=1}^{\infty} K_{n+r} \lambda'_r ,$$

$$L''_n = \sum_{r=0}^{\infty} K_r \lambda'_{n+r} , \qquad K'_n = \sum_{r=0}^{\infty} a_{n+r} \bar{a}_r ,$$

$$K'_n = \sum_{r=0}^{\infty} a_{n-r} \bar{a}_r , \qquad N_n = \sum_{r=0}^{\infty} K'_{n-r} \lambda_r ,$$

$$N'_n = \sum_{r=1}^{\infty} K'_{n+r} \lambda'_r , \qquad N''_n = \sum_{r=0}^{\infty} K'_r \lambda'_{n+r} ,$$

$$M'_n = \sum_{r=1}^{\infty} K_{n+r}\,\lambda''_r\,, \qquad M_n = \sum_{r=0}^{\infty} K_r\,\lambda''_{n-r}\,,$$

$$M''_n = \sum_{r=0}^{\infty} K_r\,\lambda''_{n+r}\,, \qquad P_n = \sum_{r=0}^{\infty} K'_r\,\lambda''_{n-r}\,,$$

$$P'_n = \sum_{r=1}^{\infty} K'_{n+r}\,\lambda''_r\,, \qquad P''_n = \sum_{r=0}^{\infty} K'_r\,\lambda''_{n+r}\,,$$

$$Q_n = \sum_{r=1}^{\infty} \lambda_{n+r}\,\bar{K}_r\,, \qquad Q'_n = \sum_{r=0}^{\infty} \lambda_r\,\bar{K}_{n+r}\,,$$

$$Q''_n = \sum_{r=1}^{\infty} \bar{K}_r\,\lambda'_{n-r}\,, \qquad R_n = \sum_{r=1}^{\infty} \lambda''_{n+r}\,\bar{K}_r\,,$$

$$R'_n = \sum_{r=1}^{\infty} \lambda''_r\,\bar{K}_{n+r}\,, \qquad R''_n = \sum_{r=1}^{\infty} \bar{K}_r\,\lambda'_{n-r}\,.$$

Performing the integration in (36) with the help of the integrals in the Appendix, we have

$$K = T_0\,i\pi - 2\sum_{n=1}^{\infty}\frac{T_{2n-1}-T'_{2n-1}}{2n-1} + \frac{1}{2\pi i}\left[\sum_{n=1}^{\infty} S_{2n}\,\widetilde{H}_{2n-1} - \frac{\pi^2}{2}\,S_0 + \right.$$
$$\left. + 2\,i\pi\sum_{n=1}^{\infty}\frac{S'_{2n-1}}{2n-1} + \sum_{n=1}^{\infty} S'_{2n}\,\widetilde{H}'_{2n+1}\right] \tag{38}$$

where $\widetilde{H}$'s are the values of the corresponding integrals for $n = 1, 2, \ldots$, i.e.

$$\widetilde{H}_{2n-1} = \int_\Gamma \sigma^{2n-1}\log\frac{1+\sigma}{1-\sigma}\,d\sigma\,,$$

$$\widetilde{H}'_{2n+1} = \int_\Gamma \sigma^{-2n-1}\log\frac{1+\sigma}{1-\sigma}\,d\sigma\,.$$

The values of Ω, Z_G, A, B, H, Δ depend only on the geometry of the cross-section. They may be calculated either directly for each problem or with the aid of the coefficients of the mapping function in (12).

Calculating with the help of the mapping function, we have

$$\Omega = \frac{1}{2i}\int_\Gamma\left[\bar{\omega}\left(\frac{1}{\sigma}\right) - \bar{\omega}(\sigma)\right]\omega'(\sigma)\,d\sigma$$
$$= \frac{\pi}{2}\,Q_1^{(1)} \quad \text{where} \quad Q_1^{(1)} = \sum_{r=1}^{\infty} r\bar{a}_r\,a_r \tag{39}$$

$$z_G\,\Omega = \frac{1}{2i}\int_\Gamma [\bar{\omega}(\bar{\sigma}) - \bar{\omega}(\sigma)]\,\omega(\sigma)\omega'(\sigma)\,d\sigma$$
$$= \frac{1}{2i}\left[\sum_{0,2,4\ldots}^{\infty} \frac{2(Q_n^{(4)} - Q_n^{(2)})}{n+1} + Q_1^{(3)}\,i\pi + \sum_{2,4,6\ldots}^{\infty} \frac{2Q_n^{(3)}}{n-1}\right] \tag{40}$$

where

$$Q_n^{(2)} = \sum_{r=0}^{\infty} \beta_{n+r}\,\bar{a}_r\,, \quad Q_n^{(3)} = \sum_{r=0}^{\infty} \beta_r\,\bar{a}_{n+r}$$

$$Q_n^{(4)} = \sum_{r=0}^{\infty} \bar{a}_{n-r}\,\beta_r$$

$$A + B = I - z_G\,\bar{z}_G\,\Omega \tag{41}$$

$$I' = \frac{1}{2i}\int_\Gamma [\bar{\omega}(\bar{\sigma}) - \bar{\omega}(\sigma)]\,\omega^2(\sigma)\,\omega'(\sigma)\,d\sigma$$
$$= \frac{1}{2i}\left[\sum_{0,2,4\ldots}^{\infty} \frac{2\,(Q_n^{(8)} - Q_n^{(5)} - Q_n^{(6)})}{n+1} + Q_1^{(7)} i\pi + \sum_{2,4,6\ldots}^{\infty} \frac{2Q_n^{(7)}}{n-1}\right] \tag{42}$$

where

$$Q_n^{(5)} = \sum_{r=0}^{\infty} \bar{\alpha}_{n+r}\,Q_r^{(9)}$$

$$Q_n^{(6)} = \sum_{r=0}^{\infty} \bar{\alpha}_{n+r}\,Q_r^{(1)}, \qquad Q_n^{(7)} = \sum_{r=0}^{\infty} \bar{\alpha}_r\,Q_{n+r}^{(1)}\,,$$

$$Q_n^{(8)} = \sum_{r=0}^{\infty} \bar{\alpha}_{n-r}\,Q_r^{(2)} \qquad Q_n^{(9)} = \sum_{r=0}^{\infty} (n+r+1)\,a_{n+r+1}\,\bar{a}_r\,,$$

$$Q_n^{(1)} = \sum_{r=1}^{\infty} r a_r\,\bar{a}_{n+r+1} \quad \text{with } Q_0^{(1)} = 0\,,$$

$$B - A - 2iH = I' - z_G^2\,\Omega\,.$$

Substituting for K, $\bar{K}$, I, β and J in (6) we get M. From (11) we get the centre of flexure.

6. Example

Flexure of a beam whose cross-section is one half of Pascal's limacon. The mapping function is

$$z = w(\varrho) = R(\varrho + m\varrho^2)$$
$$R > 0\,,\ 0 \leqslant m < \frac{1}{2}\,.$$

From (22), (23) and (21) we get

$$I = \frac{\pi R^4}{4}(1+6m^2+2m^4),$$

$$J = R^5\left[(3m+6m^3)\,i\pi + \frac{12}{5} + 20m^2+16m^4\right],$$

$$(1+2m\varrho)\,\psi(\varrho) = \frac{R}{2}(p-\bar{p})(\varrho+3m^2\varrho^2+2m^2\varrho^3) + \frac{R^2}{2}(q+r+\bar{q}+\bar{r})\times$$

$$(\varrho^2+4m\varrho^3+5m^2\varrho^4+2m^3\varrho^5) + \frac{R}{2}\left(\frac{a_0}{\varrho} + a_1 + a_2\varrho + a_3\varrho^2\right) +$$

$$\frac{R}{\pi i}\left[a_4(1-\varrho^{-2}) + a_5(\varrho-\varrho^{-3}) + a_6(\varrho^2-\varrho^{-4}) + a_7(\varrho^3-\varrho^{-5}) + \right.$$

$$+ a_8(\varrho^4-\varrho^{-6}) + \frac{1}{2}\{a_9(1-\varrho^{-2}) + a_{10}(\varrho-\varrho^{-3}) +$$

$$+ a_{11}(\varrho^2-\varrho^{-4}) - a_{12}(\varrho^3-\varrho^{-5}) - a_7(\varrho^4-\varrho^{-6}) -$$

$$\left. - a_8(\varrho^5-\varrho^7)\}\log\frac{1+\varrho}{1-\varrho}\right]$$

where

$$a_0 = (1+2m^2)(p+\bar{p}) + mR(2q+2\bar{q}+r+\bar{r}),$$

$$a_1 = 3m(p+\bar{p}) + R\{(1+4m^2)(q+\bar{q}) + (1+3m^2)(r+\bar{r})\},$$

$$a_2 = mR\{2(1+m^2)(q+\bar{q}) + (3+2m^2)(r+\bar{r})\},$$

$$a_3 = m^2R(q+\bar{q}+2r+2\bar{r}),$$

$$a_4 = (p-\bar{p}) - mR\{(3+2m^2)(r-\bar{r}) - 2(1+m^2)(q-\bar{q})\} +$$

$$+ \frac{4mR(q+r-\bar{q}-\bar{r}) + 2m^2(p-\bar{p})}{3} + \frac{2mR^3}{5}(q+r-\bar{q}-\bar{r}).$$

$$a_5 = R(q+r-\bar{q}-\bar{r}) + 3m(p-\bar{p}) - m^2R(2r-2r-q+\bar{q}) +$$

$$+ \frac{5m^2R}{3}(q+r-\bar{q}-\bar{r}),$$

$$a_6 = 2m^2(p-\bar{p}) + \frac{2R}{3}(m^3+6m)(q+r-\bar{q}-\bar{r}),$$

$$a_7 = 5m^2R(q+r-\bar{q}-\bar{r}),$$

$$a_8 = 2m^3R(q+r-\bar{q}-\bar{r}),$$

$$a_9 = m(p-\bar{p}) + R\{(1+3m^2)(r-\bar{r}) - (1+4m^2)(q-\bar{q})\},$$

$$a_{10} = mR\{(3+2m^2)(r-\bar{r}) - 2(1+m^2)(q-\bar{q})\} - (p-\bar{p}),$$

$$a_{11} = m^2 R\{2r - 2\bar{r} - q + \bar{q}\} - 3m(p - \bar{p}) - R(q + r - \bar{q} - \bar{r}),$$
$$a_{12} = 4mR(q + r - \bar{q} - \bar{r}) + 2m^2(p - \bar{p}).$$

From (24), we have

$$\frac{K + \bar{K}}{2R^4} = \frac{\pi\tau}{2}(1 + 6m^2 + 2m^4) - \frac{4\tau}{9\pi}(18 + 112m^2 + 32m^4) -$$
$$- \frac{(20m + 16m^3)(p + \bar{p})}{15} - \frac{R}{105}[(70 + 434m^2 + 552m^4) \times$$
$$\times (q + \bar{q}) + (70 + 546m^2 + 488m^4)(r + \bar{r})] +$$
$$+ \frac{R}{\pi i}\left[(q - \bar{q})\left\{m(1 + 2m^2)\pi^2 - \frac{136m}{9} - \frac{1216m^3}{45} - \frac{8064m^5}{1575}\right\} -\right.$$
$$\left. - (r - \bar{r})\left\{m(1 + 2m^2)\frac{\pi^2}{4} + \frac{4m}{9} + \frac{32m^3}{15} - \frac{448m^5}{225}\right\}\right].$$

The quantities depending on the geometry of the section are given by

$$\Omega = \frac{\pi R^2}{2}(1 + 2m^2),$$

$$\Omega z_G = \frac{iR^3}{2}\left(\frac{4 + 16m^2}{3} - mi\pi\right),$$

$$A + B = \frac{\pi R^4}{4}(1 + 6m^2 + 2m^4) - \frac{R^4}{2\pi(1 + 2m^2)}\left[m^2\pi^2 + \frac{16(1 + 4m^2)^2}{9}\right],$$

$$B - A + 2iH = \frac{iR^4}{15}(20m + 16m^3) + \frac{R^4}{2\pi(1 + 2m^2)}\left[mi\pi - \frac{4(1 + 4m^2)}{3}\right]^2.$$

From the above relations, we get

$$A = \frac{\pi R^4}{8}(1 + 6m^2 + 2m^4) - \frac{8R^4}{9\pi(1 + 2m^2)}(1 + 4m^2)^2,$$

$$B = \frac{\pi R^4}{8}(1 + 6m^2 + 2m^4) - \frac{\pi m^2 R^4}{2(1 + 2m^2)},$$

$$H = \frac{2R^4}{15}(5m + 4m^3) - \frac{2m R^4(1 + 4m^2)}{3(1 + 2m^2)}.$$

Substituting for K, $\bar{K}$, I, J and Z_G, we get

$$2M/\mu = \pi\tau R^4(1+6m^2+2m^4) - \frac{4\tau R^4}{9\pi}(18+112m^2+32m^4) -$$

$$- \frac{R^4(20m+16m^3)(p+\bar{p})}{15} - \frac{R^5}{105}\{(70+434m^2+552m^4)(q+\bar{q}) +$$

$$+ (70+546m^2+488m^4)(r+\bar{r})\} + \frac{R^5}{\pi i}\left[\left\{m(1+2m^2)\pi^2 - \frac{136m}{9} -\right.\right.$$

$$\left.\left. - \frac{1216m^3}{225} - \frac{8064m^5}{1575}\right\}(q-\bar{q}) - \left\{m(1+2m^2)\frac{\pi^2}{4} + \frac{4m}{9} + \frac{32m^3}{15} -\right.\right.$$

$$\left.\left. - \frac{448m^5}{225}\right\}(r-\bar{r})\right] + \frac{R^5}{24}(1-2\nu) \times$$

$$\times \left\{\left(\frac{12}{5} + 20m^2+16m^4\right)(\beta+\bar{\beta}) + 3mi\pi(1+2m^2)(\beta-\bar{\beta})\right\}.$$

Substituting for τ, we get the expression for M_0, given by

$$\frac{2M_0}{\mu R^5} = (\beta+\bar{\beta})\left\{\frac{14+336m^6+732m^4-276m^6)\nu}{105(1+2m^2)} -\right.$$

$$\left. - \frac{49+158m^2+856m^4+800m^6}{210(1+2m^2)} - \frac{8(1+4m^2)(18+112m^2+32m^4)}{27\pi^2(1+2m^2)}\right\} -$$

$$- i(\beta-\bar{\beta})\left\{\frac{m(1+2m^2)\pi}{4} - \frac{16(25+60m^2+112m^4+64m^6)}{225\pi(1+2m^2)} +\right.$$

$$\left. + \nu\left[\frac{1+8m^4}{4(1+2m^2)} + \frac{4m(65+376m^2+144m^4)}{45\pi(1+2m^2)} -\right.\right.$$

$$\left.\left. - \frac{1}{\pi}\left(\frac{68m}{9} + \frac{608m^3}{45} + \frac{4032m^5}{1575}\right)\right]\right\}.$$

The centre of flexure is given by

$$\bar{z}_c = \frac{2i\mu R^5(A+iH)}{E\Delta}\left\{\frac{\nu(14+336m^2+732m^4-276m^6)}{105(1+2m^2)} -\right.$$

$$\left. - \frac{49+158m^2+856m^4+800m^6}{210(1+2m^2)} - \frac{8(1+4m^2)(18+112m^2+32m^4)}{27\pi^2(1+2m^2)}\right\} +$$

$$+ \frac{2\mu R^5(B-iH)}{E\Delta}\left\{\frac{m(1+2m^2)\pi}{4} -\right.$$

$$\left. - \frac{16m(25+60m^2+112m^4+64m^6)}{225(1+2m^2)\pi} +\right.$$

$$+\nu\left\{\frac{1+8m^4}{4\,(1+2m^2)}+\frac{4m(65+376m^2+144m^4)}{45\,\pi\,(1+2m^2)}-\right.$$
$$\left.-\frac{1}{\pi}\left(\frac{68m}{9}+\frac{608\,m^3}{45}+\frac{4032m^5}{1575}\right)\right\}.$$

Substituting $m = 0$ in the above results, we get the results for the flexure of a beam whose cross-section is one half of a circle. These results agree with those given by DEUTSCH [1]. Putting $m = 1/2$, we get the results for the beam whose cross-section is one half of a cardiod.

Achnowledgements

The author wishes to thank Prof. John JEWITT, Chairman, Department of Mathematics, Oklahoma State University, Stillwater, U.S.A., for the Post-doctoral fellowship and Prof. E. K. MACLACHLAN of the same department for the useful discussion the author had on this paper.

REFERENCES

1. DEUTSCH, E.: *Q.J.M.A.M.* **14** (1961), 471—79
2. DEUTSCH, E.: *Q.J.M.A.M.* **15** (1962), 303—315
3. MILNE-THOMSON, L. M.: *Trans. Amer. Soc.* **90** (1959), 143—60
4. MUSKHELISHVILI, N. I.: Some Basic Problems on the Mathematical Theory of Elasticity, 1953
5. SOKOLNIKOFF, I. S.: Mathematical Theory of Elasticity, 1956
6. DEUTSCH, E.: *Bulletin De L'Académie Polonaise Des Sciences*, Vol. X, No. 2 (1962), 85
7. MURTHY, M. G. K.: Torsion of Prismatic beams. *Acta Techn. Hung.* (1967)

APPENDIX

Use has been made of the following integrals:

1. $\int_\Gamma \sigma^{2n-1}\, d\sigma = 0\,, \qquad n \neq 0\,,$
$= i\pi\,, \qquad n = 0\,,$

2. $\int_\Gamma \sigma^{2n}\, d\sigma = \frac{-2}{2n+1}\,, n = 0,\ \pm 1, \pm 2, \pm 3, \ldots$

3. $\int_\Gamma \sigma^n \log\frac{1+\sigma}{1-\sigma}\, d\sigma = \quad = 0\,,\ n = 0, 2, 4, \ldots$
$= \frac{-4}{n+1}\left(1+\frac{1}{3}+\frac{1}{5}+\frac{1}{7}+\ldots+\frac{1}{n}\right).$
$n = 1,3,5,\ldots$
$= -\frac{\pi^2}{2}\,, \quad n = -1$
$= -\frac{2\,i\pi}{n+1}\,, \quad n = -2, -4, -6, \ldots$

$$= -\frac{4}{n+1}\left(1+\frac{1}{3}+\ldots+\frac{1}{-(n+2)}\right),$$

$$n = -3, -5, -7, \ldots$$

$$4.\ \int_\Gamma \sigma^n\left(\frac{1}{\sigma-\varrho}-\frac{1}{\sigma-1/\varrho}\right)d\sigma = -\frac{2}{n-1}\left(\varrho-\frac{1}{\varrho}\right)-\frac{2}{n-3}\left(\varrho^3-\frac{1}{\varrho^3}\right)-\ldots+i\pi\varrho^n+$$

$$+(\varrho^n-\varrho^{-n})\log\frac{1+\varrho}{1-\varrho},\quad n = 2, 4, 6, \ldots$$

$$= -\frac{2}{n-2}(\varrho^2-\varrho^{-2})-\frac{2}{n-4}(\varrho^4-\varrho^{-4})-\ldots+i\pi\varrho^n+(\varrho^n-\varrho^{-n})\frac{1+\varrho}{1-\varrho}$$

$$n = 3, 5, 7, \ldots$$

$$= i\pi,\quad n = 0$$

$$= i\pi\varrho+(\varrho-\varrho^{-1})\log\frac{1+\varrho}{1-\varrho},\quad n = 1.$$

$$5.\ \int_\Gamma \sigma^{-n}\left(\frac{1}{\sigma-\varrho}-\frac{1}{\sigma-1/\varrho}\right)d\sigma = \frac{2}{n-1}(\varrho-\varrho^{-1})+\frac{2}{n-3}(\varrho^3-\varrho^{-3})++.+i\pi\varrho^n-$$

$$-(\varrho^n-\varrho^{-n})\log\frac{1+\varrho}{1-\varrho},$$

$$n = 2, 4, 6, \ldots$$

$$= \frac{2}{n-2}(\varrho^2-\varrho^{-2})+\frac{2}{n-4}(\varrho^4-\varrho^4)+\ldots+i\pi\varrho^n-(\varrho^n-\varrho^{-n})\log\frac{1+\varrho}{1-\varrho}$$

$$= i\pi,\ n = 0 \qquad n = 3, 5, 7, \ldots$$

$$= i\pi\varrho-(\varrho-\varrho^{-1})\log\frac{1+\varrho}{1-\varrho},\quad n = 1.$$

Biegung prismatischer Stäbe. Eine exakte mathematische Lösung des Biegungsproblems mit Hilfe einer Potenzreihe ist bekannt im Falle, wo die Bildfunktion den Querschnitt eines Stabes auf der Hälfte eines Einheitskreises konform abbildet. Die Methode wird durch Anwendung zur Lösung des Biegeproblems eines prismatischen Stabes dargelegt, dessen Querschnitt eine halbe Pascalsche Kreisconchoide ist. Als partikuläre Fälle sind Stäbe von Halbkardioid- oder Halbkreisquerschnitt behandelt.

Изгиб балок призматического сечения *(Г. К. Мурти)*. Излагается математическое решение степенного ряда задачи изгиба в случае функции конформного отображения до круга с полуединичным радиусом получения балки. Автор дает описание метода для его использования такой балки призматического сечения, поперечное сечение которой соответствует полуконхоиде Паскаля. В качестве специального случая рассматривается случай таких балок, которые имеют сечение в виде полукардиоиды и полукруга.

RECENSIONES

BETONTECHNISCHE BERICHTE 1968

Betonverlag, Düsseldorf 1968, 175 Seiten

Die Abhandlung umfaßt die Ergebnisse von acht Forschungsarbeiten.

1. Die Neufassung der Zementnorm DIN 1164 wird in acht Abschnitten erläutert, in denen der Entwurf des Portland-, Essenportland-, Hochofen- und Traßzementes eingeschlossen ist.

In dem Entwurf sind außer den Begriffen noch die Prüfmethode und Qualitätsförderungen angegeben.

Die Zahl der Festigkeitsklassen wurde von drei auf vier erhöht.

2. In dieser Arbeit ist die Untersuchung der Betonblöcke aus den Jahren 1916 und 1938 beschrieben, die als Wellenbrecher vor der Mole von Helgoland liegen. Um die Wirkung des Meerwasserangriffes zu beurteilen, wurde der Beton chemisch, mikroskopisch und röntgenographisch untersucht. Dabei ergab sich, daß der Beton von 1916 zwischen 210 und 290 kp Zement je m^3 enthält, mit der Festigkeit von 240—360 kp/cm^2. Der Beton von 1938 enthält demgegenüber zwischen 360 und 420 kp Zement je m^3 mit der Festigkeit von 660—750 kp/cm^2. Die Ergebnisse zeigten, daß die Betone dem Meerwasser gegenüber beständig sind. Chloridionen sind in den Beton von 1916 mindestens bis zu 5 cm, in den Beton von 1938 höchstens bis zu 3 cm tief eingedrungen.

3. Die Schlagfestigkeit des Betons für Rammpfähle wurde durch wiederholte Schläge eines 50 kp Fallbären aus der Fallhöhe von 80 cm geprüft. Die Versuche bestätigten, daß die Eigenschaften des zu den Rammpfählen verwendeten günstigen Betons wie folgt sind:

— Elastizitätsmodul: $E = 300—350\,000$ kp/cm^2,
— Zylinderdruckfestigkeit 450 kp/cm^2, Spaltzugfestigkeit von mindestens 35 kp/cm^2,
— Wasserzementwert 0,45
— Zementgehalt 400 kp/m^3,
— Körnung: $d_{max} = 30$ mm, 0/7 — Zuschlag mindestens 60%.

4. Der Entwurf der DIN 1045 enthält die technologischen Bestimmungen für unbewehrten Beton, für Stahlbeton, für Transportbeton und Stahlbeton-Fertigteile. Im Zusammenhang mit der Herstellverfahren und Qualitätsbedingungen teilt die Neufassung der DIN 1045 die Betone in zwei Güteklassen ein: Beton I und Beton II. Für die Gewährleistung der verlangten Druckfestigkeit und für den Schutz der Bewehrung gegen Korrosion sowie Widerstand gegen Frost, Hitze, chemische Angriffe und mechanische Abnutzung sind besonders eingehende Bestimmungen aufgenommen worden.

5. Das vorläufige Merkblatt I legt Einzelheiten der Überwachungsprüfung des Leichtzuschlagbetons fest. Die Anforderungen sind in der Tafel I zusammengefaßt.

6—7. Diese beiden Arbeiten befassen die Untersuchungsergebnisse über den Einfluß der Feuchtigkeit des Betons auf seine Druckfestigkeit und über das Angriffsvermögen von betonschädlichen Wässern, Böden und Gasen.

8. Besonders wertvolle Ergebnisse für die Praxis sind in den Bemerkungen zu den Blättern E der DIN 4030 und DIN 1045 zusammengefaßt. Die meist 1 bis 2 m dicken Bauwerke erwärmen sich durch die bei der Hydration des Zementes freiwerdende Wärme. Die von den Fundamenten behinderten Formänderungen führen zu vertikalen Temperaturrissen. Man hat bedeutende durchgehende Spaltrisse bei den Widerlager- und Flügelmauern aus Beton beobachtet. Das Rißbild und die Verteilung der Risse kann durch eine sehr starke Flächenbewehrung geregelt werden. Durch Anordnung von Dehnungsfugen kann man die Temperaturrisse abfangen. Die Fugen sind im allgemeinen *gespärt*, der Abstand ist von der Dicke der Mauer abhängig. Die Arbeit stellt Bemessungsrichtlinien und konsultative Vorschläge vor.

B. Goschy

P. Conil:

LE VOILE AUTOPORTANT
CONCEPTION – TRACÉ – CONSTRUCTION

Édition Eyrolles, Paris 1967. 202 pages, 160 figures, 16 photos

Les premiers chapitres s'occupent des notions fondamentales, de la classification des voiles et surtout de la création de formes nouvelles. Des explications sont données en premier lieu sur les formes déterminées par un plan de base et deux courbes génératrices situées en des plans intersectés. Les intersections de ces surfaces parallèles aux plans des génératrices sont des courbes affines aux génératrices. Le plan d'affinité est identique au plan de base. L'auteur donne un procédé de construction pour déterminer les sections intermédiaires, ainsi qu'un procédé pour la construction des profils verticaux déterminés par deux génératrices à plans parallèles et une ligne droite. Il présente ensuite des méthodes pour construire les sections verticales de voiles à base triangulaire.

Par la suite, le livre présente des formules approchées pour le calcul rapide de quelques types de voile simples et donne des conseils pratiques pour leur exécution.

Une objection qui pourrait être faite à l'auteur est qu'il ne définit pas assez la notion de «voile autoportant». De même, il néglige de remarquer que les voiles dont la surface moyenne possède un point plan (par ex. les points S sur les figures 3,14, 3,57 et les points 0 sur les figures 3,15 et 3,39) ne peuvent pas être équilibrés dans le voisinage de ce point par les seules forces de membrane. (La même remarque est valable pour le voisinage des bords de voiles ayant des plans tangents tout le long de leur bord. Voir figures 3,11, 3.12 et 3,38.)

A part ces objections, le livre se proposant de rapproches les points de vue de l'ingénieur et de l'architecte mérite d'être hautement apprécié par les spécialistes, pour l'intéressant exposé de sujet propre à éveiller bien des idées nouvelles.

P. Csonka

PROCEEDINGS OF THE THIRD CONFERENCE ON DIMENSIONING AND STRENGTH CALCULATIONS

Publisher: Akadémiai Kiadó, Budapest 1968, 778 pages

This international conference dealt with problems of fatigue and brittle fracture, though topical interest was extended to other questions of dimensioning as well. A number of papers were devoted to phenomena of brittle fracture and fatigue, aiming at a better understanding of the relevant problems by the most thoroughly possible evaluation of recent results available in the literature. The presentation of the problems not yet solved along with those which have recently obtained their answers or still under study constitutes the main merit of this conference. This mighty volume is excellently printed on the finest paper. Authors and topics of lecture are as follows:

M. F. Abdel-Gaber (The effect of welding sequence and cooling rate on residual stresses in built-up I section), I. M. Allison (An application of three dimensional photoelasticity to design for short life fatigue loading), J. H. Argyris—D. W. Scharpf—J. B. Spooner (The elasto-plastic calculation of general structures and continua), B. Biró, N. Párducz (The scatter of the reliability factor of roller bearing dimensioning and its practical aspects), J. G. Bouwkamp (Tubular joints under alternating loads), S. L. Bussa—J. Der Hovanesian (Cumulative damage analysis of random stresses), Gh. Buzdugan (Fatigue coefficient in machine foundation design), R. M. Caddel—J. L. Duncan—W. Johnson (Fracture and limit strains in annealed and cold rolled brass and aluminium sheet), S. E. Chukwujekwu—C. Ruiz (Plastic failure under internal pressure of aluminium spherical shells with nozzle reinforced openings), H. C. van Elst (Notch-sensitivity to fracture initiation in a medium high strength pressure vessel steel), J. Farkas,—J. Cselényi—A. Vass—G. Farkas—G. Zolnay (Rotating beding fatigue limit of welded spline shafts), T. Fekete (Stress calculation and measurements of rubber-cored railway wheels), J. W. Fischer (Effect of weldings on the fatigue strength of steel beams), G. Galgóczy (Recent experiments on the application of high strength friction grip bolted joints in structural steelwork), V. N. Geminov (The secondary curves as a method of determining fatigue life under unstationary loading), L. F. Gillemot (The influence of tensile testing machine hardness on the flow curve), M. M. Hanna—

A. F. YACOUB (Magnification factors of stresses in reinforced concrete flexural members due to curvature of the axis), V. HORÁK (Inverse variational principles of the nonlinear mechanics of solids), I. HUSZÁR (Calculation of the force play of arch bound commutators), J. G. ILLESY (Dynamic behaviour of structures and dynamic simulation), V. S. IVANOVA (Dislocation-energetical hypothesis of ductile and brittle fracture), G. JACOBY (Comparison of fatigue life estimation processes for irregularly varying loads), K. KÁLNA (Investigation of the size effect in brittle failure), W. J. KIPPOLA—J. Der HOVANESIAN (An experimental study of a cumulative fatigue damage indicator), S. KOCANDA—A. KRUKOWSKI (Torsional fatigue limit of heavy press-fitted assemblies), A. KOCHENDÖRFER—K. E. HAGEDORN—D. KRIEGER (Evaluation of proper strain and stress quantities for bent rectangular bars), M. KOZAROV (Thermostability of layered glassplastic cylindrical shells), H. KREISKORTE (Servo-hydraulic test equipment for strength and vibration testing), I. V. KUDRYAVTZEV—I. N. SHKANOV (Fatigue resistance of mild steels under sharp cycle asymmetry and the influence of boiling water), H. de LEIRIS (Fatigue factures in welded constructions, after the collection of the International Institute of Welding), G. Z. LIBERTINY (The use of short life fatigue data in design), M. G. LOZINSKY —A. N. ROMANOV (Certain peculiarities of dislocational structure, appearing in high-temperature fatigue tested silicon iron), M. MATOLCSY (Coefficients determining the fracture and the service life of vehicle-frames), P. MICHELBERGER (Basic systems for statically indeterminate structures), P. MICHELBERGER—A. FEKETE (Spatially loaded frame row with longitudinal symmetry), E. MISTÉTH (Dimensioning for fatigue of engineering steel structures on the basis of probability theory), A. J. MOE (On the safety against fracture in firm standing static structures as seen from an engineer's point of view), G. NASSAR (Stability problems of continuous plating in steel structures), H. A. OSMAN (Stress and strain distribution on notched members under cyclic loading), S. V. PINEGIN—A. V. ORLOV (Influence on the form of contact area and element size on the contact strength on rolling), P. RAABE—G. POMEY (Comparison of fatigue limits obtained under various loading conditions, using several statistical methods), J. C. RADON—J. R. CROSBY (Fracture toughness of an Al-alloy in the biaxial stress field), U. ROSETTI (Application of the cumulative damage theory to the endurance test of wire-ropes, by the progressive load method), G. RUDNAI—G. PETRÓCZY (Full-scale fatigue of a forged vehicle component), S. A. SAAFAN (Analytical and empirical determination of failure load of structural frames), B. I. SANDOR —J. MORROW (Alleviation of fatigue damage), S. V. SERENSEN—R. M. SCHNEIDEROVITCH (Design of construction elements under low-cycle loading), S. V. SERENSEN—M. N. STEPNOV (Statistical evaluation of the fatigue properties of light alloys in connection with strength calculations), G. C. SIH (Propagation of elastic waves around a crack), T. SOBIEPANEK (On the role of microcracks in brittle fractures of mild steel), S. SORETZ (Influence of geometrical discontinuities on the fatigue strength of reinforced concrete), R. SPIERS—M. S. G. CULLIMORE (Geometrical factors influencing the fatigue of friction grip bolted joints), L. I. STEINWOLF (Calculation of frictional self-oscillation in the mechanical transmission of power units), H. P. STÜVE (On the theory of unstable deformation), W. SWITEK—A. BUCH (The problem of maximum notch effect in case of flat element with transverse holes), C. C. TEODORESCU (Repeated Loading and strain-hardening curve used for the calculation of long welded rails), D. D. VÁSÁRHELYI (Experimental study of the fatigue of thin steel plates due to cyclic shear buckling), I. VÖRÖS (Dimensioning of gears for cantilever beam stress with up-to-date strength factors), T. YOKOBORI—M. NANBU—N. TAKEUCHI (On the initiation and propagation of fatigue crack), Á. ZSÁRY (Photoelasticity testing of the stress-gradient factor on notched tensile specimen).

As this list indicates, the volume is useful for theoreticians of metallurgy and for practical working engineers engaged in testing of material or in design of structures.

J. Barta

Heinrich Engel:

TRAGSYSTEME. STRUCTURE SYSTEMS

Deutsche Verlags-Anstalt. Stuttgart, 280 Seiten

Die Einführung zu diesem zweisprachigen Werk großen Formats (22×23 cm) schrieb Ralph RAPSON, Leiter der School of Architecture University Minnesota und der Text wird durch eine kurze Abhandlung aus der Feder von Hanskarl BANDEL ergänzt, die die neuen Wege in der Planung von Tragkonstruktionen auseinandersetzt.

Das Buch selbst, das aus einer Sammlung von Konstruktionsfiguren besteht, ist in fünf Teile geteilt.

Das *erste Kapitel* (formaktive Tragsysteme, Formactive Structure Systems) befaßt sich mit Tragwerken, in denen unter Einwirkungen der Belastung nur gleichsinnige Normalkräfte (Zug- bzw. Druckkräfte) entstehen, d.h. daß sie ihrem Wesen nach frei von Biege- und Torsionskräften sind. Der Materialbedarf dieser Konstruktionen ist minimal, somit sind sie geeignet, große Spannweiten zu überbrücken. Im Rahmen dieser Konstruktionsgruppe werden von dem Verfasser die verschiedenen Typen der Hängedächer, der Zeltdächer, die pneumatischen Dächer (Innendruck- und Doppelmembransysteme), sowie die Bogensysteme ausführlich erörtert. Die behandelten Tragwerke werden teils durch orthogonale, bzw. klinogonale Projektionen, teils durch Modellfotos dargestellt. Die Abbildungen werden durch kurzgefaßte, aber charakteristische Unterschriften erklärt.

Das zweite Kapitel (Vectoraktive Tragsysteme, Vector-active Structure Systems) beschäftigt sich mit verschiedenen Typen der Fachwerke, wobei außer den ebenen und Raumfachwerken auch die auf gekrümmte Flächen angepaßten Flechtwerke behandelt werden. Auch hier werden die verschiedenen Tragwerke und deren Konstruktionsprinzipien durch klare und anschauliche Abbildungen und Modellfotos erklärt.

Das *dritte Kapitel* (Massenaktive Tragsysteme — Bulk-active Structure Systems) befaßt sich mit auf Biegung beanspruchten Konstruktionen. Es werden die verschiedenen Typen der einfachen Kragträger und Durchlaufträger, Zweigelenk- und Dreigelenk-Rahmensysteme, horizontale und vertikale Rahmensysteme, Systeme, für Voll- und Mehrfeldrahmen, Mehrgeschoßrahmensysteme, Trägerraster- und Tragplattensysteme dargestellt. Im Gegensatz zu den vorangehenden Kapiteln ist das Bildmaterial nicht überall anschaulich.

Das *vierte Kapitel* (Flächenaktive Tragsysteme — Surface-active Structure Systems) ist eine sehr ausführliche Sammlung von Abbildungen über Flächentragwerke. Es werden die Grundtypen der Faltwerke, ihre verschiedenartigen Kombinationen, sowie die aus gleichförmigen und zweiförmigen ebenen Flächenelementen errichtbaren Polyeder behandelt. Hier gelangen einfache und zusammengesetzte Zylinderschalen, Kreuz- und Sektorialschalen, Kugel- und Kappenschalen, Rotationsschalen und die Kombinationen all dieser zur Darstellung. Die verschiedenen Arten der hyperbolischen Paraboloidschalen, sowie zahlreiche Beispiele der aus solchen Elementen zusammengesetzten Schalen werden wom Verfasser mit großer Ausführlichkeit veranschaulicht. Die Zeichnungen (Phototypien) sind äußerst demonstrativ, was von den Photos (Autotypien) nicht immer behauptet werden kann.

Das *fünfte Kapitel* (Senkrechte Tragsysteme — Vertical Structure Systems) veranschaulicht die verschiedenen Möglichkeiten von Aufbau und Versteifung der Gebäudegerippen.

Im allgemeinen kann festgestellt werden, daß das Buch, dessen Inhalt zu 80% aus lehrreichen, mit größter Sorgfalt verfertigten, überaus schönen Abbildungen besteht, einen erfolgreichen Versuch bildet, um die verschiedenen Tragwerke in ein einheitliches System einzuordnen und die Prinzipien ihrer Wirkungsweise zu demonstrieren. Der didaktische Aufbau des Werkes ist tadellos: es führt stufenweise von den einfachern Tragsystemen zu den komplizierteren und versäumt es auch nicht, durch die Bildunterschriften instruktive und das Verständnis fördernde, das Wesen und Kräftespiel der betreffenden Tragwerke erläuternde Bemerkungen zu machen.

Das mit großer Phantasie entworfene Buch kann Bauingenieuren und Architekten und allen jenen wärmstens empfohlen werden, die den Formenreichtum der Tragwerke und die sich in ihrem Kräftespiel äußernde Schönheit liebevoll studieren.

P. Csonka

S. Falk:

LEHRBUCH DER TECHNISCHEN MECHANIK

ZWEITER BAND. MECHANIK DES STARREN KÖRPERS

Springer Verlag, Berlin—Heidelberg—New York 1968. 468 Seiten

Der erste Band des vorliegenden Werkes wurde bereits in dieser Zeitschrift besprochen. Der jetzt erschienene Band behandelt jenen Teil der Mechanik starrer Körper, der an den Fakultäten für Maschinen- und Bauingenieure der technischen Hochschulen der ganzen Welt fast einheitlich vorgetragen wird. Dieser Band umfaßt die Statik, die Kinematik und Kinetik der starren Körper, des besseren Verständnisses halber erst in bezug auf Flächen, dann in bezug auf dreidimensionale starre Körper. Von zahlreichen gut verfaßten Kapiteln sind die Abschnitte 14.1 und 25.1 besonders hervorzuheben, die den Begriff der Schnittkräfte erörtern. Didaktisch gesehen müssen alle Kapitel, die die Theorie

des Kreisels behandeln, als sehr gelungen angesprochen werden. Dieses, als »Lehrbuch« bezeichnete Buch können alle Leser gut gebrauchen, denen der Stoff bereits aus Vorträgen oder aus sonstigen Quellen, mehr oder weniger bekannt ist. Das Buch scheint für das erste Studium dieses Gegenstandes etwas schwer verständlich zu sein.

J. Barta

J. H. Joiner:

ESSENTIALS OF THE THEORY OF STRUCTURES

Hart Publishing Company Inc., New York City 1968. 262 pages, 150 figures

This book was destined by the author to be a textbook for university students, as well as a manual for practicing engineers. It is devided into 18 chapters and comprises in general the knowledge conveyed by faculties of moderate standard.

Titles of the single chapters are: Frame Works, Framework Deflection and Strain Energy in Frames, Shear Force and Shear Stress, Bending of Beams, Beam Deflection, Travelling Loads, Compound Stresses, Struts and Columns, Dams, Retaining Walls and Foundations, Statically Indeterminate Structures, Area-Moment Theorems, Theory of Three Moments, Slope Deflection Method of Analysis, Moment Distribution, Flexural Strain Energy, Arches, Suspension Cables and Bridges, Plastic Design of Beams.

The book is written in a concise, clear and precise styl, the material treated is logically grouped and easy to oversee. Comprehension is promoted by simple figures and a large amount of numerical examples. It can be objected, however, that the table on fixed moments for beams only comprises a part of the often occurring loading cases.

Although the book does not contain anything beyond costumary textbooks and raises no claim for a higher level of its content, it will make useful reading during university studies and is an appropriate help for the practising engineer to refresh his memory on basic formulae and methods and principals of analysis.

P. Csonka

MITTEILUNGEN DES INSTITUTS FÜR LEICHTE FLÄCHENTRAGWERKE (IL) — INFORMATION OF THE INSTITUTE FOR LEIGHT WEIGHT STRUCTURES (IL)

Universität Stuttgart — University Stuttgart

Das Institut für Leichte Flächentragwerke — verkürzt IL genannt — dessen Zielsetzung die Erforschung von anpassungsfähigen, weitgespannten Bauten ist, wurde vom Professor der Stuttgarter Technischen Universität F. LEONHARDT in 1964 gegründet. Das Institut gehört zur Bauingenieur-Fakultät der Stuttgarter Universität, ihr Leiter ist OTTO, Frei, der mit dem Perret-Preis der UIA ausgezeichneter statischer Sachverständiger des deutschen Pavillons auf der Weltausstellung Montréal ist.

Eine Reihe von zweisprachigen — deutschen und englischen — Mitteilungen wird fortlaufend vom Institut herausgegeben, die den Plänen gemäß 3 bis 4mal im Jahre erscheinen sollen. Das erste Heft dieser Reihe — IL1 benannt — ist kürzlich erschienen.

Aus dem Inhalt des ersten Heftes ist vor allem der Aufsatz von MINKE, G.—SCHÖFL, G. über Minimalnetze herauszuheben. Hierin handelt es sich unter andern um die experimentelle Lösung des Minimalwegproblems, d. h. um die Feststellung dessen, wie eine beliebige Zahl von Punkten, die in der Ebene verteilt sind, durch einen — eventuell verzweigten — Linienzug geringster Gesamtlänge miteinander verbunden werden können.

Die vom Institut entwickelte experimentelle Einrichtung besteht dem Wesen nach aus einem Glasgefäß, in welches eine glatte Glasplatte mit genau waagerechter Oberfläche eingehängt ist. In das Gefäß wird eine besondere Seifenlösung (Pustefix) gegossen, so daß sie auch die Glasplatte bedeckt. Wenn das Niveau der Seifenlösung langsam stufenweise gesenkt wird, gerät etwas Luft unter die Glasplatte, doch trennt sich die Seifenlösung nicht sofort von ihr, sondern bleibt durch die Einwirkung der adhäsiven und kohäsiven Kräfte in Kreiszylindergestalt an der Platte haften. Wird das Niveau weitergesenkt, verengt sich der Durchmesser des haftengebliebenen Flüssigkeitszylinders allmählich, bis er sich endlich vollständig von der Glasplatte trennt.

Anders ist die Lage, wenn von unten aus sich bis zur Glasplatte erstreckende senkrechte Nadeln angebracht werden. In diesem Fall bleibt der der Glasplatte anhaftender Teil der Seifenlösung nur so lange kreiszylinderförmig, bis der Rand dieses Zylinders die erwähnten Nadeln nicht erreicht. Von hier an werden auch die Nadeln in die Aufrechterhaltung des Gleichgeweichtes des haftenden Flüssigkeitsteils herangezogen. Wird das Niveau der Flüssigkeit weiter langsam gesenkt, verengt sich die Konfiguration des haftenden Flüssigkeitteils immer weiter, bis endlich die die Lösung der Minimalaufgabe ergebende Konfiguration entsteht, die photographisch fixiert wird.

Der Aufsatz stellt zahlreiche interessante Minimalkonfigurationen dar. Die Oberflächen dieser sind senkrechte Ebenen, die in den inneren dreifachen Verzweigunspunkten einen Winkel von 120° miteinander bilden.

Bemerkenswert ist, daß die Minimal-Konfigurationen, außer ihrem theoretischen Interesse, auch eine praktische Bedeutung besitzen, sie zind z. B. bei Planen von Straßennetzen zweckmäßig zu verwerten.

Das Heft enthält auch zahlreiche Bilder von verschiedenen Hängedächern und Ausstellungszelten. Die Erforschung der Konstruktionsprinzipien solcher Bauten gehört ebenfalls in den Wirkungskreis des Instituts für Leichte Flächentragwerke.

Die weiteren Nummern der Mitteilungen erwarten wir mit lebhaftem Interesse.

P. Csonka

Árpád Kézdi—Iván Markó

ERDBAUTEN

Gemeinschaftsausgabe des Akadémiai Kiadó, Budapest, und des Werner-Verlages, Düsseldorf, 1969; 403 Seiten

Das in deutscher Sprache erschienene Werk enthält eigentlich die zusammengefaßte und neu bearbeitete Thematik des früher in ungarischer Sprache erschienenen Werkes der Verfasser »Földművek védelme és víztelenítése« (Schutz und Entwässerung der Erdbauten) sowie des Werkes ÁRPÁD KÉZDI—MIHÁLY PÓCZY: »Földművek« (Erdbauten). Das Buch besteht aus folgenden 11 Kapiteln:

1. Aufschluß der Bodenverhältnisse (Á. KÉZDI)
2. Standsicherheit der Böschungen (Á. KÉZDI)
3. Gründung von Dämmen (Á. KÉZDI)
4. Erddruck, Stützmauern (Á. KÉZDI)
5. Entwässerung des Geländes (I. MARKÓ)
6. Sicherung von Ufererdbauten (I. MARKÓ)
7. Regulierung kleiner Wasserläufe (I. MARKÓ)
8. Entwässerung des Untergrundes, Grundwasserabsenkung (Á. KÉZDI und I. MARKÓ)
9. Wasserhaltung und Grundwasserabsenkung (Á. KÉZDI und I. MARKÓ)
10. Entwässerung der Verkehrswege (I. MARKÓ)
11. Entwässerung der Terrainregulierungen (I. MARKÓ)

Das Buch verfolgt — wie dies die Autoren im Vorwort betonen — nicht den Zweck, theoretische Fragen zu behandeln, sondern dem praktisch tätigen Ingenieur anhand der erörterten Verfahren und angeführten Beispiele die Lösung der sich auf diesem Fachgebiet ergebenden Probleme zu erleichtern. Im Interesse dieses Zieles behandelt das Buch nur vollkommen durchgearbeitete und in der Praxis bewährte Verfahren und erläutert diese mit Hilfe zahlreicher und ausführlicher Strichfiguren und Bilder.

Diesen Zielsetzungen wurde das Buch vollauf gerecht. Das gut gewählte Bildermaterial, die Abbildungen, die stets das Wesen ausdrücken und eine gute Darstellung der konkreten Lösungen bieten, sowie die durch ihre originelle Technik die Aufmerksamkeit erweckenden Skizzen, veranschaulichen sehr gut den Text. Es verdient besonders die bereits in der ungarischen Ausgabe gebrauchte Darstellungsart erwähnt zu werden, wo die schwarz gezeichneten Abbildungen mit einem durchsichtigen Papier überdeckt werden, auf welchem mit auffallenden Farben der Plan der durchzuführenden Arbeiten, bzw. deren voraussichtliches Ergebnis dargestellt ist.

In den einzelnen Kapiteln ist das dem gesetzten Ziel entsprechende, praktische und anschauliche Element vorherrschend. Die jeweils erforderlichen Planungs- und Bauarbeiten werden kurz in ihrem Wesen erfaßt und ihrer Reihenfolge entsprechend angeführt, doch sind auch die wesentlichen Faktoren und Vergleiche dieser Arbeiten nicht vernachlässigt.

Bezüglich der einzelnen Kapitel können folgende Feststellungen gemacht werden:

ad 1. Das Kapitel »Aufschluß der Bodenverhältnisse« befaßt sich, ohne die diesbezüglichen Verfahren und die gebräuchlichen Geräte zu behandeln, nur mit deren Anwendungsmöglichkeiten bei der Planung der verschiedenen Erdbauten, zwecks Bestimmung der erforderlichen Daten. Es gibt die Reihenfolge der auf der Baustelle vorzunehmenden, die Identifizierung des Bodens bezweckenden einfachen Untersuchungen an und faßt deren Ergebnisse tabellarisch zusammen.

ad 2.—3. Das der Standsicherheit der Böschungen gewidmete 2. Kapitel enthält die auf Grund der neuesten Theorien zusammengestellten Tafeln und die auf praktischen Erfahrungen beruhenden Prinzipien der Planung von Böschungen sowie die diesbezüglichen praktischen Regeln im Zusammenhang mit den verschiedenen Bodenarten. Anhand von Beispielen und Vergleichen zeigt der Autor die möglichen Fehler der Planung und Bauausführung und gibt Hinweise zu deren Beseitigung. Das Problem ist im Zusammenhang mit verschiedenen Bodenarten und Schichtungen behandelt. Es darf vielleicht als ein Mangel erwähnt werden, daß der den Dammböschungen gewidmete Teil (z. B. die Beremen) etwas kurz gefaßt ist. Im 3. Kapitel wird die Gründung von Dämmen, vornehmlich im Zusammenhang mit der Dammsetzung und des Grundbruches unter den Dämmen besprochen.

ad 4. Dieses Kapitel, das sich mit den Stützmauern beschäftigt, schließt sich logisch an die vorhergehenden an. Von den auf die Stützmauern wirkenden Lasten und Kräften ausgehend, ist in diesem Kapitel — unter Berücksichtigung aller Planungsmöglichkeiten — die Wirksamkeit der verschiedenen Stützmauerprofile, der neuesten, aus vorgefertigten Elementen erbauten Winkelstützmauern mit Rippenversteifung, der Pfeilerstützmauern mit vorgefertigten bogenförmigen Stützelementen und der Kastenwände sehr anschaulich dargestellt. Das Kapitel erstreckt sich auch auf die Behandlung des Prinzips der verankerten Mauertypen sowie auf die Probleme der Dehnfugen, der Hinterfüllung und der Entwässerung.

ad 5. Dieses Kapitel, das der Entwässerung des Geländes bzw. der Ableitung des Außenwassers gewidmet ist, ist verhältnismäßig umfangreicher, als es die vorhergehenden Kapitel sind. Vor allem behandelt es sehr ausführlich die Theorien der Berechnung der Abflußmenge des von der Geländeoberfläche abfließenden Wassers und die Ausgestaltung der Wasserläufe auf der Geländeoberfläche. Auch die Hydraulik und die Planung von der Entwässerung von Erdbauten dienenden offenen Kanälen und Gräben sind ausführlich behandelt. Im Zusammenhang mit der Bauausführung dieser Gerinne ist auch der Materialbedarf der verschiedenen Bekleidungen ausführlich angegeben und die Bekleidungsarten selbst an Vergleichen und an praktischen Beispielen eingehend erläutert.

ad 6. Dieses Kapitel befaßt sich mit den konstruktiven und baulichen Problemen der dem Hochwasserschutz dienenden Deiche sowie mit jenen der Uferschutzbauten, es widmet den in der Sowjetunion gebräuchlichen Konstruktionen zum Schutz der Uferböschungen besondere Aufmerksamkeit, behandelt die die Dämme abschließenden Steinkegel sowie die Wellenschutzbauten.

ad 7. Ein besonderes Kapitel des Werkes ist der Regulierung kleiner Wasserläufe gewidmet, ein Problem das in Ungarn mit dem Schutz der durch die Erosion gefährdeten Gebiete zusammenhängt und deshalb besonders wichtig ist. Auch dieses Kapitel scheint ausführlicher zu sein als die Kapitel 2—4.

ad 8. Dieses Kapitel, das die Entwässerung des Untergrundes zum Gegenstand hat, ist ein recht ausgeglichener Teil des Buches. Nach einer kurzen Zusammenfassung der mechanischen Erscheinungen sind die praktischen Regeln und die hydraulischen Berechnungen der Sickergräben angegeben, dann anhand konkreter Lösungen die Regeln für die Planung, Anwendung und Ausführung dieser Gräben festgelegt. Auch die wichtige Frage der Instandhaltung, die Entwässerungsstollen und Sickermatten sind ausführlich besprochen.

ad 9. Die Wasserhaltung und Grundwasserabsenkung bilden den Inhalt dieses Kapitels, das sich aber außer mit der Entwässerung von Erdbauten (Einschnitten) sowohl theoretisch als auch praktisch mit der Entwässerung von Baugruben befaßt.

ad 10. Dieses Kapitel umfaßt die Probleme der Entwässerung der Verkehrswege, behandelt die Planung und konstruktive Ausgestaltung der Seitengräben der Straßen und der Bahnkörper von Eisenbahnen. Die zulässigen Gefälle, die Absturzschächte und Sohlenstufen sind eingehend erörtert und für ihre Bemessung sind Diagramme angegeben. Ein besonderer Abschnitt ist der Entwässerung der Autobahnen und der Straßen in Siedlungen, den Straßeneinläufen und Schächten sowie der Entwässerung von Bahnhöfen und Flugplätzen gewidmet und enthält bis ins einzelne gehende Läsungen einschlägiger Aufgaben.

ad 11. Das letzte Kapitel behandelt die mit der Entwässerung der Terrainregulierungen zusammenhängenden Probleme und im Rahmen dieser die konstruktiven Lösungen sowie die hydraulische Bemessung der Leitungen und Durchlässe.

Wie aus obigem ersichtlich, behandelt des Buch eingehend und zusammenfassend alle Probleme und Aufgaben, die mit der Standfestigkeit und Entwässerung von Erdbauten zusammenhängen, sowohl vom Gesichtspunkt des Konstrukteurs als auch von dem des Bauingenieurs aus und bietet diesen unentbehrliche Hilfe bei ihrer täglichen Arbeit.

K. Széchy

A. Paduart:

VOILES MINCES EN BÉTON ARMÉ

Presses Universitaires de Bruxelles—Brusselles—Eyrolles Éditeurs, Paris 1969, 149 pages, 74 figures

Ce livre de l'illustre auteur est l'édition entièrement refondue de son ouvrage paru en 1961 sous le titre «*Introduction au calcul et à l'exécution des voiles minces en béton armé*» et dont la traduction anglaise intitulée «*Shell Roof Analysis*» a été publiée en 1966 par la C. R. Books Ltd. Présentant les problèmes théoriques et pratiques de la construction des voiles minces et les possibilités de leur solution, il peut servir dans l'enseignement universitaire aussi bien que dans la pratique de l'ingénieur.

Les premiers chapitres du livre contiennent les connaissances générales se rapportant à la construction des voiles minces. Ils présentent la classification des formes, traitent les diverses conditions d'appui, les questions d'éclairage, d'écoulement des eaux pluviales, d'isolation thermique, ainsi que les possibilités de précontrainte et de préfabrication. Le coffrage, le ferraillage, le bétonnage et le décoffrage des voiles minces en béton armé y sont également traités en détail.

Dans les chapitres suivants, les différents modes de calcul des voiles prismatiques et le calcul des membranes sont exposés. En dehors de la théorie des membranes cylindriques et de révolution, sont également étudiées les calottes sphériques, les paraboloïdes elliptiques et hyperboliques, les conoïdes et les voiles à surface de translation.

Le livre étudie ensuite en détail la théorie des coques et présente l'application de méthodes générales de résolution pour les coques cylindriques et de révolution et pour les coques surbaissées. L'auteur traite enfin des problèmes d'instabilité d'équilibre.

L'auteur présente les problèmes clairement groupés, sans jamais perdre de vue les buts pratiques. Outre les procédés de résolution exacte, il offre aussi différentes méthodes approximatives d'une manière fort instructive pour le lecteur. L'explication se limite, en plusieurs cas, à un bref exposé des principes essentiels sans s'étendre aux détails du procédé, l'auteur pouvant ainsi embrasser une matière très vaste dans un cadre relativement étroit.

La maîtrise avec laquelle l'auteur traite son sujet et la claire logique à laquelle il fait appel pour appuyer ses observations critiques sont des qualités majeures ajoutant encore à la valeur de l'excellent livre du Professeur Paduart.

P. Csonka

Gyula Sebestyén:

GROSSTAFELBAUWEISE IM WOHNUNGSBAU

Gemeinschaftsausgabe des Verlages der Ungarischen Akademie der Wissenschaften und des Werner-Verlags, Budapest 1969. 549 Seiten, 359 Bilder, 44 Tafeln

Das Buch wurde bisher in ungarischer Sprache in zwei Auflagen und in englischer Sprache mit dem Titel »*Large-Panel Buildings*« ausgegeben. Die bisherigen Ausgaben fanden sowohl in ungarischen als auch in ausländischen Fachkreisen günstige Aufnahme.

Das Werk analysiert auf Grund einer komplexen Betrachtungsweise die Grundsätze des Entwurfes, behandelt die Fundamentkonstruktionen und ihre Verbindungen, die Bau- Ausbau- und Installationskonstruktionen, die Bemessungsverfahren, Bauvorschriften und vermittelt auch die einschlägigen technischen Daten. Es befaßt sich eingehend mit stoffkund-

lichen und statischen, ferner mit Wärme- und dampftechnischen Problemen sowie mit dem Lärm- und Feuerschutz und dem Schutz gegen Schlagregen. Auch die Fragen der Fertigungs- und Bautechnologie sind im erforderlichen Maße erörtert und die wirtschaftliche Wirksamkeit der Großtafelbauweise erläutert.

Der ausgedehnte Kreis wissenschaftlicher Erkenntnisse ist im Buch vortrefflich systematisiert. Die sich ergebenden Probleme sind in einer modernen, die wissenschaftlichen Ansprüche befriedigenden Weise analysiert und mit Berücksichtigung der in- und ausländischen Erfahrungen zusammengefaßt.

Sehr wertvoll sind die der ausländischen Baupraxis entnommenen Informationen, die das Buch bezüglich der Großblock-, der Tafelbauweise, der Montagebauweise mit vorgefertigten Elementen bzw. Raumelementen bietet. Natürlich enthält die deutsche Ausgabe zahlreiche, in den früheren Ausgaben nicht angeführte deutsche Beispiele.

Besondere Erwähnung verdient die seitens des Verfassers mit richtigem Verständnis zusammengestellte reiche Bilderauswahl, die bei Werken dieser Art unentbehrlich ist.

Die geschmackvolle Ausstattung des Buches zeugt nicht nur von dem ästhetischen Anspruch des Verfassers, sondern auch für die sorgfältige Arbeit des Verlages.

Der Großteil in- und ausländischer Fachleute ist übereinstimmend der Meinung, daß der immer dringender auftretende Bedarf an Wohnungen mit Hilfe der herkömmlichen Bauweisen — denen auch der monolithische Stahlbetonskelettbau zuzuzählen ist — nicht gut befriedigt werden kann. Dies ist der Grund, weshalb sich in den letzten Jahrzehnten die Anwendung von Großelementen — so auch die der »Großtafeln« — im Bauwesen nicht nur in den sozialistischen Ländern, darunter auch in Ungarn, sondern auch in zahlreichen west- und nordeuropäischen Ländern stark verbreitet hat. Der Verfasser hat als gründlicher Kenner dieses Fachgebietes mit der neuen und jetzigen deutschen Ausgabe seines Werkes den auf diesem Gebiet tätigen Fachleuten einen großen Dienst erwiesen.

L. Széll

DEUXIEME RENCONTRE DE L'ASSOCIATION INTERNATIONALE CONSTRUCTION ET HUMANISME

La Deuxième Semaine de Rencontres Internationales *Construction et Humanisme* aura lieu à Cannes du 11 au 17 Mars 1970 et sera placée sous le signe de la compétence.

De la recherche même utopique exposée par les 14 équipes sélectionnées pour le Grand Prix International d'Urbanisme et d'Architecture 70, sur le thème des villes nouvelles et leur développement contrôlé, aux projets, expérimentations ou réalisations majeures recensées dans le monde, chacun, selon son niveau d'intervention et de responsabilité, devra justifier ses choix, ses orientations, son action dans l'un des domaines les plus préoccupants: l'environnement construit.

Des délégations étrangères comportant non seulement architectes et urbanistes, mais aussi entreprises, industries et représentants des «usagers», viendront présenter, et mettre en discussion des thèmes vivants qui permettront d'aller au delà de la recherche fondamentale pour explorer des cas concrets et en tirer des enseignements.

A la suite d'un débat général «Priorité à la Compétence», cinq journées lourdes d'expériences permettront d'aborder successivement:

1. L'Université
2. L'Urbanisation des grandes villes
3. Les villes nouvelles
4. L'habitat individuel
5. Transports et communications

Renseignements et inscriptions:

CONSTRUCTION ET HUMANISME

10 Place Vendôme, P A R I S, 1er

INTERNATIONAL SYMPOSIUM ON ICE AND ITS ACTION ON HYDRAULIC STRUCTURES

The International Association for Hydraulic Research — IAHR — is organizing its 1st Symposium

in Reykjavik, Iceland, September 7—10, 1970.

The topic of this Symposium is :

"Ice and its Action on Hydraulic Structures"

The purpose of the Symposium is to unite, for the first time, under the auspices of the IAHR, engineers and scientists interested in furthering the field of ice engineering by providing a forum for reporting and discussing recent original research from the laboratory and the field.

For invitations and particulars apply to
Mr. S. FREYSTEINSSON
Chairman of the Organizing Committee,
IAHR Ice Symposium 1970,
Verkfraedistofa,
Sigurdur Thoroddsen Sf.
ARMULA 4, Reykjavik, Iceland

INDEX

RECENSIONES

Printed in Hungary

A kiadásért felel az Akadémiai Kiadó igazgatója — Műszaki szerkesztő: Farkas Sándor

A kézirat nyomdába érkezett: 1970. III. 31. — Terjedelem: 15,50 (A/5) ív, 80 ábra, 4 melléklet

70.69453 Akadémiai Nyomda, Budapest — Felelős vezető: Bernát György

Acta Techn. Hung. **68** (1970), 265—282

BÖLCSKEI, E.: *Reinforced Concrete Flat Slabs as Reflected by the Various Specifications*

A comparative study on the different specifications relating to the reinforced concerte flat slads revealed significant divergences in the prescriptions of different countries and recommendations of the international committees, both in respect to the calculation and rules of construction. The physical entity everywhere is the same, therefore, it would be advisable to unify or at least to bring nearer to one another the different specifications.

Acta Techn. Hung. **68** (1970), 283—291

KÉZDI, Á.—NAGYVÁTI, B.: *Effect of Additives on the Properties of Stabilized Soils*

Besides the classical soil-stabilizing methods some complemetary chemicals and other materials are presented which may be used for increasing the effect of stabilization. Without aiming at completeness, the paper only extends to materials which can be economically used and to those which effectively improve the required properties of the stabilized soil.

Acta Techn. Hung. **68** (1970), 293—310

SZILÁRD, R.: *Estimating Matrix-Displacement Solutions of Two-Dimensional Problems by Large Element Technique*

Based on the general convergence criteria of the finite element solution of stress and displacement problems of continua, the concept of "large" discrete elements is introduced. For the derivation of the stiffness coefficients, no prescribed displacement pattern is forced upon the discrete elements; the node points are merely moved with unit motions. The compatibility of the stresses and strains within the element and at the edges of the adjoining elements is maintained by solving the pertinent differential equations of the theory of elasticity for unit nodal displacements utilizing the Method of Images. A symmetrical stiffness matrix is obtained by virtual work of the edge forces. Numerical examples compare the solutions of two-dimensional stress problems using small and large element approaches and analytical solutions. The convergence characteristics of the large element approach are markedly different from those of the small element approach.

Acta Techn. Hung. **68** (1970), 311—317

BARTA, J.: *Stabilizing and Destabilizing Effects*

This paper is concerned with the equilibrium stability of elastic structures. By means of examples, it shows that the effect of damping or stiffening or constraints applied against displacement are not always stabilizing but sometimes destabilizing.

Acta Techn. Hung. **68** (1970), 319—334

CSONKA, P.: *Paraboloid Shells of Revolution Star-Polygonal in Plan*

Paper deals with the statical analysis of paraboloid shells of revolution, the ground-plan figure of which resembles a regular polygon, but has sides curved inward instead of straight ones. It is presumed that the edge beam of the shell is supported by a wall or by vertical columns standing close to each other. A vertical force system equally distributed over the ground-plan area is assumed as being a loading. The arching of the shell's edge line is set up in such a way as to enable the calculation of the reduced inner forces by simple closed formulae. Paper also states the principal values of the reduced inner forces, moreover, it determines the equation of their trajectories. A numerical example is given to prove the simplicity of the calculation.

Acta Techn. Hung. **68** (1970), 335—351

FEKETE, A.: *Analysis of Statically Undetermined Structures on the Basis of the General Extending of Nikolskij's Algorithm*

The analysis of the stress pattern of the many times hyperstatic structures with the aid of the energy theorem requires under the conditions of the design bureaus — where no computer is at hand commonly — much calculation work. Especially much labour is needed for the inversion of the coefficient matrix of the set of compatibility equations. The extension of the trial-and-error method of Nikolskij permits the reduction of the amount of calculation work. The paper deals with the analysis of the most significant problems of this generalization. It extends and proves the validity of the algorithm to the statically n-times undetermined structures, defines the convergence criteria and eliminates the original load-dependence of the procedure. Besides, on the one hand, the algorithm is a procedure easy to be treated by to be derived from the result of the extension, the earlier neglects can be corrected within the same problem to a desired exactitude without a lengthy inversion.

Acta Techn. Hung. **68** (1970), 353—358

SZMODITS, K.: *Solution of the First Basic Problem of the Theory of Elasticity with Real Potentials*

The first boundary-value problem of the theory of elasticity consists of the establishment of the biharmonic stress function relating to the rim loads. According to Goursat's theorem this function may be expressed with the aid of two harmonic functions to be solved by means of the logarithmic potentials of one and two-course rim-curves. The density functions of these potentials may be determined from the boundary conditions, consequently, the biharmonic problem may be reduced to two independent Dirichlet problems. The solution in numerical form consists in the solution of two independent sets of equations written to the discrete points of the rim curve.

Acta Techn. Hung. **68** (1970), 359—361

HOLNAPY, D.: *On a Significant Generalization of the Lattice Point Method from the Engineering Viewpoint*

The solution of the problem of the boundary value of the partial differential equations with the aid of the lattice-work point method (i.e. finite difference method) has been generalized in to systems. By this a numerical procedure, easy to handle, for the solution of intricate mathematical models was established which is shown by a specified example of shallow shell structures.

Acta Techn. Hung. **68** (1970), 363—382

VÉRTES, GY.: *Natural Frequency of the Horizontal Vibrations of Multi-Storey Buildings with Bearing Walls*

In multi-storey buildings with bearing walls if no two-way symmetry exists, the horizontal free vibrations present themselves in a so-called "coupled" form. This means that, at the same time, flexural and torsional vibrations take place. The determination of the momentum characteristics of the mentioned vibration is detailed and after establishing the set of differential equations, an approximate method of solution for a simple calculation, and an exact method adaptable for electronic computation are described.

Acta Techn. Hung. **68** (1970), 383—402

CSUTOR, J.: *Contribution of Compaction Technique to the Theory of Concrete Designing*

On the basis of compaction tests carried out with vibrators for internal vibration, to determine the methods to be followed and the characteristics of compaction, the statement has been made that a physical quantity may be found which, in finishing the designing of concrete permits to establish instructions for controlling compaction operations. This physical quantity is the specific compaction work. Knowledge of the specific compaction work permits to establish the conditions of reproduction in connection with all of the compaction methods if, in preparing the test pieces, to the optimal concrete strength the specific compaction work will be coordinated.

Acta Techn. Hung. **68** (1970), 403—413

WIERZBICKI, T.: *A Method of Approximation in the Large Deflection Analysis of Impulsively Loaded Rigid-Plastic Structures*

The paper is concerned with method approximations for impulsively loaded rigid-plastic structures. A method is presented for the determination of permanent deformation for circular plates and rotationally symmetric shells in the range of moderately large deflections. For the application of the theory three important boundary value problems were solved. Simple formulas were derived which compare favourably with known exact solutions and recent experimental data.

Acta Techn. Hung. **68** (1970), 415—429

M. GOPALA KRISHNA MURTHY: *Flexure of Prismatic Beams (1)*

A formal solution is given to the problem of flexure in the case, when the mapping function which maps conformally the semi-cross sections of the beam on to a semi-unit circle, is known in power series. The method is illustrated by applying it to the problem of flexure of a prismatic beam whose cross-section is one half of Pascal's limaçon. The cases of beams whose cross-sections are one half of a cardiod and one half of a circle are derived as particular cases.

The *Acta Technica* publish papers on technical subjects in English, Freneh, German and Russian.

The *Acta Technica* appear in parts of varying size, making up volumes.

Manuscripts should be addressed to

Acta Technica
Münnich Ferenc u. 7.
Budapest V.,
Hungary

Correspondence with the editors and publishers should be sent to the same address.

The rate of subscription is $ 16.00 a volume. Orders may be placed with "Kultura" Foreign Trade Company for Books and Newspapers (Budapest I., Fő utca 32. Account No. 43-790-057-181) or with representatives abroad.

Les *Acta Technica* paraissent en français, allemand, anglais et russe et publient des travaux du domaine des sciences techniques.

Les *Acta Technica* sont publiés sous forme de fascicules qui seront réunis en volumes.

On est prié d'envoyer les manuscrits destinés à la rédaction à l'adresse suivante:

Acta Technica
Münnich Ferenc u. 7.
Budapest V.,
Hongrie

Toute correspondance doit être envoyée à cette même adresse.

Le prix de l'abonnement est de $ 16.00 par volume.

On peut s'abonner à l'Entreprise pour le Commerce Extérieur de Livres et Journaux »Kultura« (Budapest I., Fő utca 32. Compte courant No. 43-790-057-181) ou à l'étranger chez tous les représentants ou dépositaires.

«*Acta Technica*» публикуют трактаты из области технических наук на русском, английском, французском и немецком языках.

«*Acta Technica*» выходит отдельными выпусками разного объема. Несколько выпусков составляют один том.

Предназначенные для публикации рукописи следует направлять по адресу:

Acta Technica
Münnich Ferenc u. 7.
Budapest V.,
Венгрия

По этому же адресу направлять всякую корреспонденцию для редакции и администрации.

Подписная цена — $ 16.00 за том. Заказы принимает предприятие по внешней торговле книг и газет «Kultura» (Budapest I., Fő utca 32. Текущий счет № 43-790-057-181) или его заграничные представительства и уполномоченные.

Reviews of the Hungarian Academy of Sciences are obtainable at the following addresses:

ALBANIA
Drejtorija Qändrone e Pärhapjes dhe Propagandimit të Librit
Kruga Konferenca e Päzes
Tirana

AUSTRALIA
A. Keesing
Box 4886, GPO
Sydney

AUSTRIA
GLOBUS
Höchstädtplatz 3
A-1200 Wien XX

BELGIUM
Office International de Librairie
30, Avenue Marnix
Bruxelles 5
Du Monde Entier
5, Place St. Jean
Bruxelles

BULGARIA
HEMUS
11 pl Slaveikov
Sofia

CANADA
Pannonia Books
2, Spadina Road
Toronto 4, Ont.

CHINA
Waiwen Shudian
Peking
P. O. B. 88

CZECHOSLOVAKIA
Artia
Ve Směčkách 30
Praha 2
Poštovní Novinová Služba
Dovoz tisku
Vinohradská 46
Praha 2
Mad'arská Kultura
Václavské nám. 2
Praha 1
SLOVART A. G.
Gorkého
Bratislava

DENMARK
Ejnar Munksgaard
Nörregade 6
Copenhagen

FINLAND
Akateeminen Kirjakauppa
Keskuskatu 2
Helsinki

FRANCE
Office International de Documentation et Librairie
48, rue Gay Lussac
Paris 5

GERMAN DEMOCRATIC REPUBLIC
Deutscher Buch-Export und Import
Leninstraße 16
Leipzig 701
Zeitungsvertriebsamt
Fruchtstraße 3—4
1004 Berlin

GERMAN FEDERAL REPUBLIC
Kunst und Wissen
Erich Bieber
Postfach 46
7 Stuttgart S.

GREAT BRITAIN
Blackwell's Periodicals
Oxenford House
Magdalen Street
Oxford
Collet's Subscription Import Department
Dennington Estate
Wellingsborough. Northants.
Robert Maxwell and Co. Ltd.
4—5 Fitzroy Square
London W. 1

HOLLAND
Swetz and Zeitlinger
Keizersgracht 471—487
Amsterdam C.
Martinus Nijhof
Lange Voorhout 9
The Hague

INDIA
Hind Book House
66 Babar Road
New Delhi 1

ITALY
Santo Vanasia
Via M. Macchi 71
Milano
Libreria Commissionaria Sansoni
Vie La Marmora 45
Firenze

JAPAN
Kinokuniya Book-Store Co. Ltd.
826 Tsunohazu 1-chome
Shinjuku-ku
Tokyo
Maruzen and Co. Ltd.
P. O. Box 605
Tokyo-Central

KOREA
Chulpanmul
Phenjan

NORWAY
Tanum-Cammermeyer
Karl Johansgt 41—43
Oslo 1

POLAND
RUCH
ul. Wronia 23
Warszawa

ROUMANIA
Cartimex
Str. Aristide Briand 14—18
Bucureşti

SOVIET UNION
Mezhdunarodnaya Kniga
Moscow G—200

SWEDEN
Almquist and Wiksell
Gamla Brogatan 26
S—101 20 Stockholm

USA
F. W. Faxon Co. Inc.
15 Southwest Park
Westwood Mass. 02090
Stechert Hafner Inc.
31. East 10th Street
New York, N. Y. 10003

VIETNAM
Xunhasaba
19, Tran Quoc Toan
Hanoi

YUGOSLAVIA
Forum
Vojvode Mišića broj 1
Novi Sad
Jugoslovenska Knjiga
Terazije 27
Beograd

15. IX. 1970. Index: 26.025